UNIL | Université de Lausanne
Faculté des géosciences et de l'environnement
Institut de géologie et de paléontologie

Trace-element and phosphorus contents in sediments associated with Cretaceous oceanic anoxic events

Thèse de doctorat

présentée à la Faculté des géosciences et de l'environnement
de l'Université de Lausanne par

Stéphane Westermann,

diplômé en géologie de l'Université de Strasbourg

Jury:
Prof. Torsten Vennemann, Université de Lausanne (Président du jury)
Prof. Karl B. Föllmi, Université de Lausanne (Directeur de thèse)
Dr. Thierry Adatte, Université de Lausanne (Expert interne)
Dr. Virginie Matera, Université de Neuchâtel (Expert externe)
Prof. Nicolas P. Tribovillard, Université de Lille (Expert externe)

Lausanne 2010

UNIL | Université de Lausanne
Faculté des géosciences et de l'environnement
Institut de géologie et de paléontologie

Trace-element and phosphorus contents in sediments associated with Cretaceous oceanic anoxic events

Thèse de doctorat

présentée à la Faculté des géosciences et de l'environnement
de l'Université de Lausanne par

Stéphane Westermann,

diplômé en géologie de l'Université de Strasbourg

Jury:

Prof. Torsten Vennemann, Université de Lausanne (Président du jury)
Prof. Karl B. Föllmi, Université de Lausanne (Directeur de thèse)
Dr. Thierry Adatte, Université de Lausanne (Expert interne)
Dr. Virginie Matera, Université de Neuchâtel (Expert externe)
Prof. Nicolas P. Tribovillard, Université de Lille (Expert externe)

Lausanne 2010

UNIL | Faculté des géosciences
et de l'environnement

Imprimatur

Vu le rapport présenté par le jury d'examen composé de

Président du jury : M. le Professeur Torsten Vennemann
Directeur de thèse : M. le Professeur Karl Föllmi
Expert externe : Mme le Docteur Virginie Matera
Expert externe : M. le Professeur Nicolas P. Tribovillard
Expert interne : M. le Docteur Thierry Adatte

le Conseil de Faculté autorise l'impression de la thèse de

Monsieur Stéphane Westermann

Titulaire d'un Diplôme d'études approfondies Terre: Dynamique, Ressources et Environnement" délivré en 2004 par l'Université "Louis-Pasteur" (Strasbourg I)

intitulée

Trace-element and phosphorus contents in sediments associated with Cretaceous anoxic events

Lausanne, le 5 février 2010

Pour le Doyen de la Faculté des géosciences et de l'environnement

Prof. Torsten Vennemann, Vice-doyen

Table of Contents

CHAPTER C:

CHAPTER D:

CHAPTER E:

CHAPTER F:

CHAPTER G:

Remerciements

-

Acknowledgements

Cette première partie, seule partie écrite en français, est pour moi l'occasion de remercier toutes les personnes qui m'ont soutenu de près comme de loin dans cette aventure helvétique tant sur le plan académique que personnel…

Je voudrais tout d'abord remercier Prof. Karl Föllmi pour avoir cru en moi et m'avoir engagé dans son équipe de recherche, il y a maintenant un peu plus de quatre ans à Neuchâtel. Il a toujours été là pour répondre à mes interrogations et m'a permis d'acquérir un esprit plus critique vis-à-vis de mes résultats. Enfin il a toujours accepté de corriger dans de brefs délais les résumés de congrès, les posters, les présentations et les différentes parties du manuscrit de thèse malgré son emploi du temps chargé. Karl, merci pour avoir consacré beaucoup de ton temps à corriger mes fautes « *westermanniennes* »… *Märsi fer àlles, Karl !*

Je voudrais ensuite dire un grand merci au Dr Virginie Matera, pour toute l'aide qu'elle m'a apportée que ce soit pour des « pré-corrections » avant d'aller voir Karl, ou pour prendre le temps d'écouter les premières versions de mes présentations. Elle a toujours répondu présente avec plus ou moins de patience (*good moon* ou *bad moon, today ?*) pour aiguiller mes recherches, m'aider dans les analyses ICP MS et poser les bonnes questions *(d'ailleurs, ça veut dire quoi ICP MS ?)*. J'ai beaucoup apprécié son soutien lors de la manipulation d'acides dangereux effectuée à l'université de Berne et son investissement même pendant ses vacances… Un grand merci super cheffe !

Je souhaiterais également remercier Dr Thierry Adatte pour les nombreuses discussions et commentaires éclairés pour l'amélioration des manuscrits et pour l'aide apportée durant l'échantillonnage sur le terrain. J'ai beaucoup appris à ses côtés lors des discussions, pas toujours scientifiques d'ailleurs. Je pense notamment aux soirées GEA, avec un souvenir tout particulier pour le four à pizza d'Enges et la « Ken mobile ».

Pour finir, je voudrais exprimer ma gratitude au Prof. Nicolas Tribovillard (Université de Lille) pour avoir accepté de juger ce travail et d'avoir ainsi contribué à améliorer le manuscrit final et ma compréhension des événements anoxiques. Un grand merci également au Prof. Torsten Vennemann pour avoir présidé le comité de thèse.

Après cette partie plutôt officielle, j'aimerais maintenant remercier toutes les personnes qui ont rendu très agréables les moments passés en Suisse.

Je tiens tout d'abord à remercier mes collègues de bureau, Christina, à Neuchâtel pour m'avoir donné l'occasion de travailler un peu mon allemand, et Melody, à Neuchâtel et Lausanne pour sa bonne humeur (*« c'est moi qui l'ai fait ! »*) et les discussions scientifiques sur les coupes de Gorgo a Cerbara et Cassis/La Bédoule. Et parce qu'une thèse ne se résume pas que dans le travail, je voudrais aussi la remercier pour son enthousiasme lors des différentes sorties ski et soirées. Merci Gigi !

Je voudrais ensuite remercier l'équipe des « anciens de Neuchâtel », avec une pensée particulière pour la team « *IGH Prod. »* et la faction neuchâteloise de la *« CF »*. Un grand merci à Charles, Beni, Mary-Alix, Alexis, Stéphane, Haydon, Pascal, Laurette, Flurin, Guillaume, Olivier, Laurent, Cyril, Isabelle, Christophe, Raoul, Erwan (Desiles), François, Ivan, Laure, Saskia, Dmitry, Natalia, Brahim, Anne-Lise, Pierre-André et Roberto.

Je ne pourrais pas continuer les remerciements sans faire un crochet par l'université de Lausanne où l'équipe des transfuges neuchâtelois a été accueillie à bras ouverts. Merci à Chloé, James, Laurent, Pierre, Hassan, Denise, Alex, Julien, Loraine, Philippe, Gilles, Luc, Antoine, Mathias et Guillaume pour les « pauses Banane ».

Acknowledgments

On ne peut imaginer un travail de thèse sans un soutien du personnel technique. J'aimerais donc exprimer mes meilleurs sentiments à Tiffany et André (*Balaye Dédé !!*) pour leur aide lors la préparation des échantillons et des lames minces ainsi qu'à Gianfranca, Sabine, Eli, Anne-Marie et Pariza pour m'avoir rendu les tâches administratives plus faciles à gérer.

Ma vie en Suisse ne se résume pas uniquement aux nombreuses heures passées à l'université. Ainsi j'aimerais remercier toutes les personnes du groupe Capoeiragem de Neuchâtel, avec un « special thank » pour Olivier, Nadia, Serpente, Pedro, Andreas, Daniel, Helena et Papa.

Je voudrais également remercier tous mes amis d'Alsace avec qui j'ai passé de nombreux moments à faire la fête. Greg, Tom, Denis, Virginie et Arnaud, Tali, Fabien, Arnaud, Etienne, Jérôme, Hélène, Pierre, Jessica, Hélène et Eric, Cornélie et Greg. Merci à tous pour avoir été là pour moi.
Pour continuer en Alsace, je souhaiterais aussi remercier mes anciens collègues du Rond Point Geispolsheim qui ont permis de rendre un peu moins pénible les week-ends passés au magasin pendant mes études à Strasbourg. Merci à toute l'équipe de la caisse et de la station-service.

Rien de tout cela n'aurait été possible sans la confiance et les conseils de mes parents, Danièle et Bernard, dans les différents choix que j'ai été amené à faire au cours de ces 28 dernières années. Ils m'ont toujours soutenu dans mes décisions et étaient là pour m'encourager à aller toujours plus loin, même s'ils ne comprenaient pas toujours ce que je faisais. Merci aussi à mon frère, Olivier, pour avoir toujours répondu présent quand le moral était au plus bas. Rien n'aurait été possible sans vous…

Un grand Merci à Michelle et Henri pour les discussions du dimanche soir et pour m'avoir offert mon premier marteau de géologue.

Enfin, j'aimerais remercier Sandrine (*the last but not least)* pour avoir passé ces quelques années à mes côtés. Elle a toujours cru en moi (même quand moi, je n'y croyais plus) et m'a apporté soutien et réconfort au quotidien tout au long de cette aventure. Elle m'a également permis de m'ouvrir à différentes choses comme les joies des sports d'hiver ou l'envie de voyager. Merci aussi pour m'avoir supporté durant les derniers mois de cette thèse (ce qui ne devait pas être évident).

Encore merci à tous...

Stéphane

Abstract
-
Résumé

Abstract

During my SNSF-funded Ph.D. thesis project, I studied the evolution of redox conditions and organic-carbon preservation in the western Tethyan realm during three major positive excursions in the Cretaceous $\delta^{13}C$ record, corresponding to the Valanginian, Early Aptian and Late Cenomanian. These periods were characterized by important global environmental and climate change, which was associated with perturbations in the carbon cycle.

For the period of the Valanginian $\delta^{13}C$ excursion, total organic carbon (TOC) contents and the quality of preserved organic matter are typical of oxic pelagic settings in the western Tethys. This is confirmed by the absence of major excursions in the stratigraphic distribution of RSTE during the $\delta^{13}C$ shift. Published TOC data from other parts of the Valanginian oceans indicate that dys- to anaerobic zones were restricted to marginal seas within the Atlantic and Southern Ocean, and to the Pacific. Phosphorus (P) and mineralogical contents suggest a stepwise climatic evolution during the Valanginian, with a humid and warm climate prior to the $\delta^{13}C$ shift leading to an increase in continental runoff. During the $\delta^{13}C$ shift, a decrease in detrital input and P contents suggests a change in the climate towards more arid conditions.

During the early Aptian oceanic anoxic event (OAE 1a), a general increase followed by a rapid decrease in P contents suggests enhanced nutrient input at the beginning of OAE 1a. The return to lower values during OAE 1a, associated with an increase in RSTE contents, may have been related to the weakened capacity to retain P in the sedimentary reservoir due to bottom-water oxygen depletion. In basinal settings, the RSTE distribution indicates well-developed anoxic conditions during OAE 1a, whereas in the shallower-water environments, conditions were oxic to suboxic, rather than anoxic. Furthermore, in the deeper part of the Tethys, two distinct enrichments have been observed, indicating fluctuations in the intensity of water column anoxia during the $\delta^{13}C$ excursion.

We also studied the effect of the end-Cenomanian oceanic anoxic event (OAE 2) on an expanded section in the Chrummflueschlucht (E of Euthal, Ct Switzerland). The goal here was to identify paleoceanographic and paleoenvironmental conditions during OAE 2 in this part of the northern Tethyan margin. The results show that this section is one of the most complete sections for the Cenomanian-Turonian boundary interval known from the Helvetic realm, despite a small hiatus between sediments corresponding to peaks 1 and 2 in the $\delta^{13}C$ record. The evolution of P contents points to an increase in the input of this nutrient at the onset of OAE 2. The trends in RSTE contents show, however, that this part of the Helvetic realm was not affected by a strong depletion in oxygen conditions during OAE 2, despite its hemipelagic position.

A further goal of this project was to submit the samples to a total extraction method (a combined $HF/HNO_3/HCl$ acid digestion) and compare the results obtained by the partial HNO_3 acid extraction in order to standardize the analytical procedures in the extraction of RSTE. The obtained results for samples of OAE 1a suggest that RSTE trends using the partial HNO_3 digestion are very comparable to those obtained by the total digestion method and subsequently normalized with regards to Al contents.

Keywords

oceanic anxoic event (OAE), Valanginian, Aptian, Cenonamian-Turonian, western Tethys paleoceanographic change, redox-sensitive trace-element, phosphorus, $\delta^{13}C$, acid extraction methods.

Résumé

Durant ce projet de thèse, financé par le Swiss National Science Funding (SNSF), j'ai étudié l'évolution des conditions redox et de la préservation de carbone organique dans le domnaine ouest-téthysien pendant trois excursions majeures du $\delta^{13}C$ au Crétacé correspondant au Valanginien, à l'Aptien inférieur et à la limite Cénomanien-Turonien. Ces périodes sont caractérisées par des changements climatiques et environnementaux globaux associés à des perturbations dans le cylce du carbone.

Pour L'excursion positive en $\delta^{13}C$ du Valanginien, les analyses du carbone organique total (COT) et les observations palynologiques du domaine téthysien ont présenté des indications d'environnement pélagique relativementbienoxygéné.L'absenced'enrichissements en éléments traces sensibles aux conditions redox (TE) pendant l'excursion positive en $\delta^{13}C$ confirme ces interprétations. Les données publiées de COT dans d'autres partie du globe indiquent cependant l'existence de conditions dys- à anaérobiques dans certains bassins restreints de l'Atlantique, l'Océan Austral et du Pacifique. L'évolution du phosphore (P) et la composition minéralogique des sédiments semblent indiquer un climat relativement chaud et humide avant l'excursion en $\delta^{13}C$ entraînant une augmentation de l'altération continentale. Pendant le shift isotopique, une diminution des apports détritiques et du P suggèrent une transition vers des conditions plus arides.
À l'Aptien Inférieur, le début de l'événement anoxique (OAE 1a) est marqué par une augmentation générale du P dans les sédiments indiquant une augmentation du niveau trophique à la base de l'excursion isotopique. Durant l'événement anoxique, les sédiments sont relativement appauvris en P. Cette diminution rapide associée à des enrichissements en TE est probablement liée à une remobilisation plus importante du P lors de la mise en place de conditions anoxiques dans les eaux de fond. Dans les environnements de bassin, le comportement des TE (enrichissements bien marqués) attestent de conditions réductrices bien marquées alors que dans les environnements moins profonds, les conditions semblent plutôt oxiques à dysoxiques. De plus, deux niveaux d'enrichissement en TE ont été observés dans la partie plus profonde de la Téthys, indiquant des fluctuations assez rapides dans l'intensité de l'anoxie de la colonne d'eau.
Nous avons ensuite étudié les effets de l'événement anoxique de la fin du Cenomanien (OAE 2) dans un basin marginal de la marge nord de la Téthys avec la coupe de Chrummflueschlucht (à l'est de Euthal, Ct Schwyz). Les résultats ont montré que cette coupe présente un des enregistrements sédimentaires des plus complets de l'OAE 2 dans le domaine helvétique malgré un hiatus entre le pic 1 et 2 de l'excursion en $\delta^{13}C$. L'évolution du P montre une augmentation au début de l'OAE 2. Cependant, la distribution des TE indique que cette région n'a pas été affectée par des conditions réductrices trop importantes.

Un second aspect de ce travail a été l'étude des différentes méthodes sur l'analyse de la distribution des TE. Des échantillons de l'OAE 1a ont été soumis à deux types d'extractions, l'une dite « totale » (attaque combinée d'acides $HF/HNO_3/HCl$) et l'autre dite « partielle » (HNO_3). Les résultats obtenus suggèrent que les courbes de tendances des TE acquises par extraction partielle sont semblables à celle obtenues par extraction totale et normalisées par l'Al.

Mots-Clés

événement océanique anoxique, Valanginien, Aptien, Cenomanien-Turonien, domaine ouest-téthysien changements paléocéanographiques, redox-sensitive éléments traces reodx-sensibles, phosphore, $\delta^{13}C$, méthode d'attaque acide.

CHAPTER A:
Introduction

View on the Alps from the Pilatus

-A-
General Introduction

A.1 Introduction: Understanding global change

Globally speaking, the last 30 years were unusually warm and have in fact been the warmest since accurate records started a little over 100 years ago. In face of anthropogenically induced global environmental change and the impact of human activity on the Earth system, Earth scientists have begun to investigate the past in order to understand mechanisms and processes that control global climate. Earth history presents a wide range of climatic and oceanographic conditions and thus records case histories of how climate systems operate and react to change. An understanding of the mechanisms and interactions, which are involved in these different periods, is important as we attempt to predict the consequences of modern global warming. The basic principle of the Earth climate system can be understood by considering the radiation energy from the Sun that warms the Earth's surface and the thermal radiation from the Earth and the atmosphere that is radiated out to space. Water vapour, carbon dioxide, methane and additional gases in minor quantities present in the atmosphere partially absorb the thermal radiation leaving the surface and act as a blanket causing the actual average surface temperature on the Earth of about 15°C. This blanketing is known as the greenhouse effect and the gases are known as greenhouse gases. Without the greenhouse effect, the surface of the Earth would be covered in ice.

To understand how modifications in the greenhouse effect worked in the past and what the future holds for us in our own warming environment, one of the most important questions is how the carbon (C) cycle affects climate on geological time scales. The chemistry of C appears to have played a key role in the history of Earth (Fig. A.1). It is the primary component of the biosphere and, in its gaseous forms (CO_2 and CH_4), it is closely involved in the greenhouse effect, which sufficiently warms the Earth surface to support life. A large part

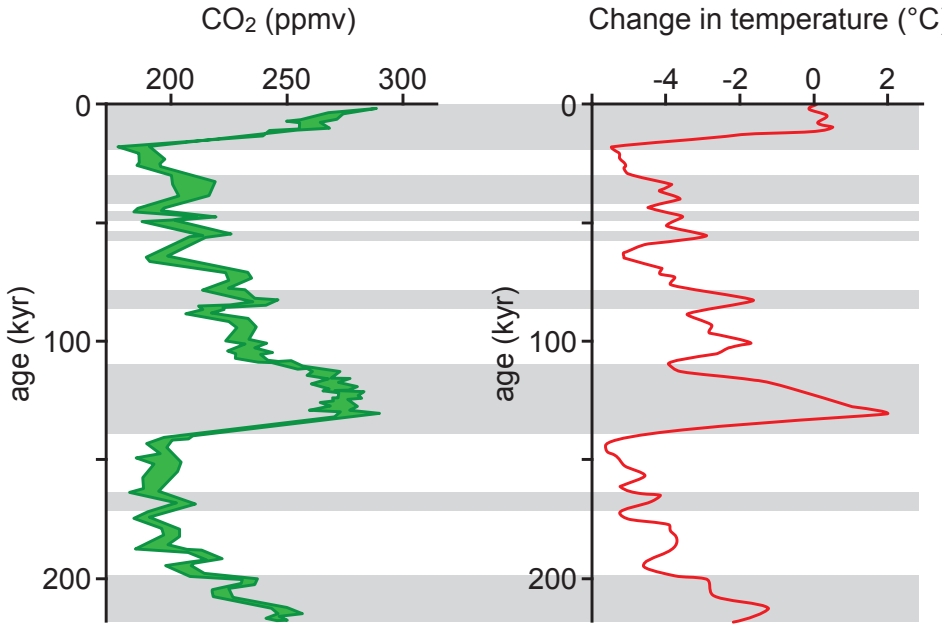

Fig. A.1: Evolution of pCO_2 (in ppmv) and temperature (°C) from the Vostok ice core. The CO_2 and temperature trends show similar variations and indicate a generally warm period around 140 and 18 kyrs ago (adapted from Skelton et al., 2003).

of the science of climate and environmental change, therefore, equates to investigations of the variations in the biogeochemistry of carbon.

The carbon cycle can be viewed at three interrelated time scales. The short and intermediate-term carbon cycles (the terrestrial and marine carbon cycle) are mainly governed by the biosphere and the very large marine reservoir. The long-term cycle (the geological carbon cycle) is controlled by the interactions between atmospheric CO_2, chemical weathering and organic-carbon production. The terrestrial C cycle is mainly driven by biological activity, which controls formation, decomposition and recycling of organic material. Unlike the terrestrial C cycle, the marine C cycle is dominated by the chemistry of inorganic carbon and is closely related to the atmospheric CO_2. Indeed, the marine carbon reservoir is linked to the atmosphere by a constant exchange of gases across the air/ocean interface. Physical processes (upwelling, sink of cold water mass in high latitudes) and biological activity (surface productivity, bacterial and algal photosynthesis) are the main mechanisms that determine the proportion of CO_2 gas and the different forms of dissolved inorganic carbon in the ocean (i.e. H_2CO_3, HCO_3^- and CO_3^{2-}). The equilibrium between all these chemical species is known as the carbonate system. The formation and the preservation of carbonate rock constitute, then, a major sink for C. In the geological C cycle, the long-term stability of the C cycle is controlled by positive and negative feedback loops acting on several time scales. Volcanism, carbonate weathering and organic matter oxidation will return C into the system, whereas continental weathering, carbonate formation and deposition and preservation of organic carbon will act as a sink for atmospheric C.

As shown above, the ocean and climate systems are closely linked and oceans act on climate by several feedback loops. Firstly, oceans play a key role in the C cycle during the Earth history. Secondly, with warmer temperatures more evaporation occurs in the ocean and from wetland surfaces, implying a general wetter climate with more water vapour (a greenhouse gas) in atmosphere and consequently more precipitations. This acts as a positive feedback on the greenhouse effect. Thirdly, ocean possesses a large heat capacity compared to the atmosphere. That means that the oceans warm much more slowly than the atmosphere and exert, therefore, a dominant control on the distribution of the heat on the Earth and thus, on global climate change. And finally, through their internal circulation, the oceans redistribute heats throughout the climate system. Thus, oceans and oceanic sediments provide very sensitive recorders of climate and global environmental change. The red line of this PhD thesis is the change in ocean chemistry and its impact on the global carbon cycle during key periods of the history of Earth where rapid climatic changes occurred.

A.2 The Cretaceous world

A.2.1. The Cretaceous, a greenhouse world

The Cretaceous is a special episode in the history of Earth. The geological record reveals a world that experienced extreme climatic warmth (Fig. A.2, Hallam, 1984; Francis & Frakes, 1993) resulting in a more equable climate between high and low latitudes (Sloan & Barron, 1990). The widespread occurrence of coals at high paleolatitudes (>60°) demonstrates that temperatures were high enough there for plant life to flourish and that large volumes of glacial ice were absent. At low paleolatitudes (<30°), the extent of evaporites (especially in the northern hemisphere) shows that large areas were predominantly arid, with evaporation exceeding precipitation. The warmer climate was a reflection of higher atmospheric levels of greenhouses gases, CO_2 and possible CH_4, reinforced by higher water vapour content in response to the warmer temperatures (e.g. Hay, 2008 and references therein). Despite this overall warmer climate, some authors argued that there may have been extensive ice at certain times during the Early and the Late Cretaceous based on sediments, sea-level curves and oxygen isotopes (Kemper, 1987, Frakes & Francis, 1988; Frakes et al., 1992; Ahlberg et al., 2002; Immenhauser, 2005). However, only sparse and controversial evidence exists for the presence of ice on lands. If indeed polar ice would have occurred, it was only for short time intervals, and during most of the Cretaceous, the polar regions were ice free (Hay, 2008).

Another noticeable feature of the Cretaceous world is that the individual landmasses are smaller in extent than those of today: there are no corresponding areas of land as large as modern Eurasia for example. The reason for this is twofold: firstly, the paleogeography of the Cretaceous was a product of the rifting of the supercontinent Pangea; secondly, Cretaceous sea levels were, at times, a few tens to hundred meters

higher than at present, so that large areas of the continents were covered by shallow seas. These shallow seas were important to the world climate in that they were a source of moisture in what otherwise would have been dry land areas, warmed and cooled more slowly than the surrounding land, and acted as conduits for heat as water currents flowed from one ocean to another.

The Cretaceous appears to be a unique laboratory for understanding how the climate system operates when one or both polar regions are ice free (Hay, 2008). Facing the global rise of temperature, the icecap retreat in the Arctic and the spreading of vegetation covers in alpine and subpolar regions (Grace et al., 2002), greater knowledge and understanding of the Cretaceous appears critical in predicting future changes in the ocean-climate system.

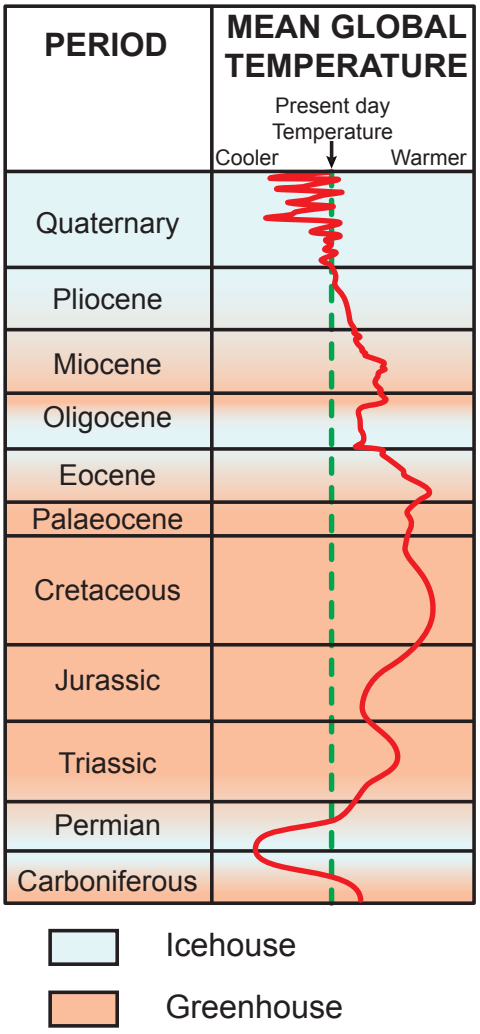

Fig. A.2: Climate through the late Paleozoic, Mesozoic and Cenozoic: curve of estimated global temperature (adapted from Skeleton et al, 2003; data for the Paleozoic and the Mesozoic from Frakes (1979 and 1999) and for the Cenozoic from Zachos et al. (2001)).

A.2.2. Paleogeography and paleoceanography

During the Cretaceous period, the configuration of the continents changed from the prevailing Early Mesozoic pattern of two supercontinents (Laurasia and Gondwana) separated by an equatorial ocean (Tethys) to one with several continents separated by oceans, which extended into high latitudes, thereby anticipating the present-day continental configuration. In the Early Cretaceous, the North Atlantic started to extend northwards. The South Atlantic, initially opened as a discrete basin between South America and Africa, achieved a connection with the Central Atlantic in the latest Albian, creating a narrow seaway between the northern and the southern continental masses. A hallmark of the Cretaceous was the presence of a continuous equatorial seaway between Laurasia and Gondwana, which allowed ocean currents to flow between the two. However, microcontinental fragments and platforms offer some obstruction to this flow in the western part of the Tethys. Paleoceanographic currents were mostly oriented east-west (Pucéat et al., 2005). The Pacific was probably characterized by two giant gyres (Barron and Peterson, 1989; Stille et al., 1996). This is however still under debate. Connections between the Tethys and the Boreal realm were possible during sea-level high stand and led to the influx of cooler water into the Tethyan realm through the Polish Furrow and the Moscou platform (e.g., van de Schootbrugge, 2001).

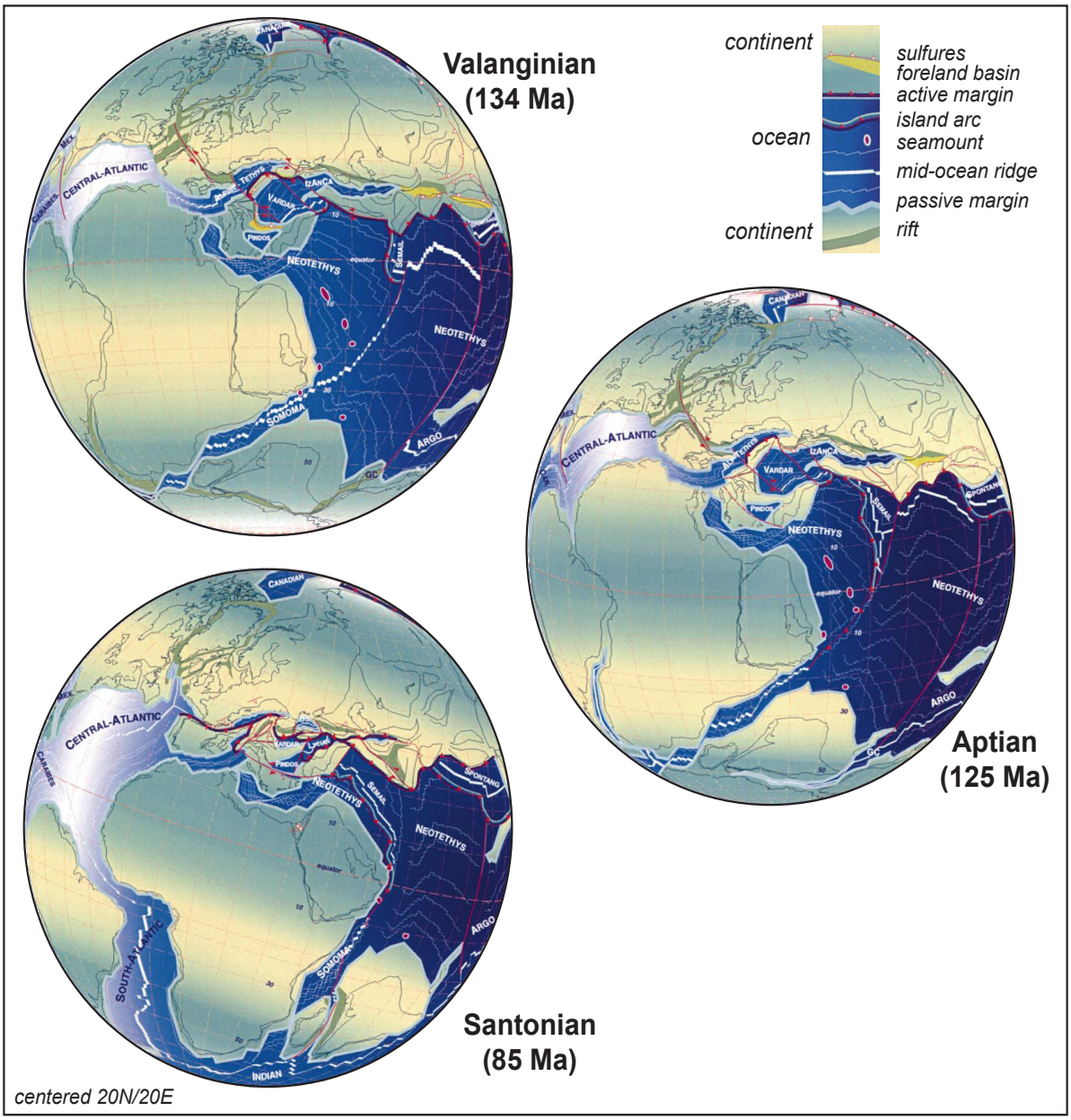

Fig. A.3: General arrangement and evolution of continents and ocean for lower (Valanginian), mid- (Aptian) and upper Cretaceous (Santonian) based on plate reconstructions (Stampfli & Borel, 2002).

A.2.3. Oceanic anoxic events and black shales

Throughout this relatively warm period, several positive shifts in the C isotopic compositions have been observed in marine sediments. These perturbations are coeval with the widespread deposition of black-shale horizons, which are attributed to oceanic anoxic events (OAEs, Schlanger & Jenkyns, 1976). During the Cretaceous (Fig. A.4), OAEs have been identified during the Early Aptian (OAE 1a or Selli Event, e.g., Erba et al., 1999), the Aptian-Albian transition (OAE 1b; e.g., Herrle et al., 2004), the Late Albian (OAE 1c and OAE 1d; Arthur et al., 1990), the end Cenomanian (OAE 2) and the transition of the Coniacian-Santonian (OAE 3; Arthur et al., 1990). In addition, during the Valanginian, a major excursion in the $\delta^{13}C$ signal is reported and assumed to signal the earliest OAE of the Cretaceous (Lini et al., 1992; Erba et al., 2004).

Even though each OAE may have its own triggering mechanism, a general scheme involving eutrophisation of seawater and a slowdown of carbonate production relative to organic carbon production can be put forward (e.g. Meyers, 2006). Jenkyns (2003) showed the good relationship between the formation of large igneous provinces (LIPs) leading to an excess of volcanogenic CO_2 supplied to the ocean and the atmosphere, and the occurrence of OAEs in the Phanerozoic,. This may trigger perturbations in the carbon cycle, inducing an enhanced greenhouse effect and global environmental change (accelerated hydrological cycle, increased continental fluxes into the oceans, change in deep-

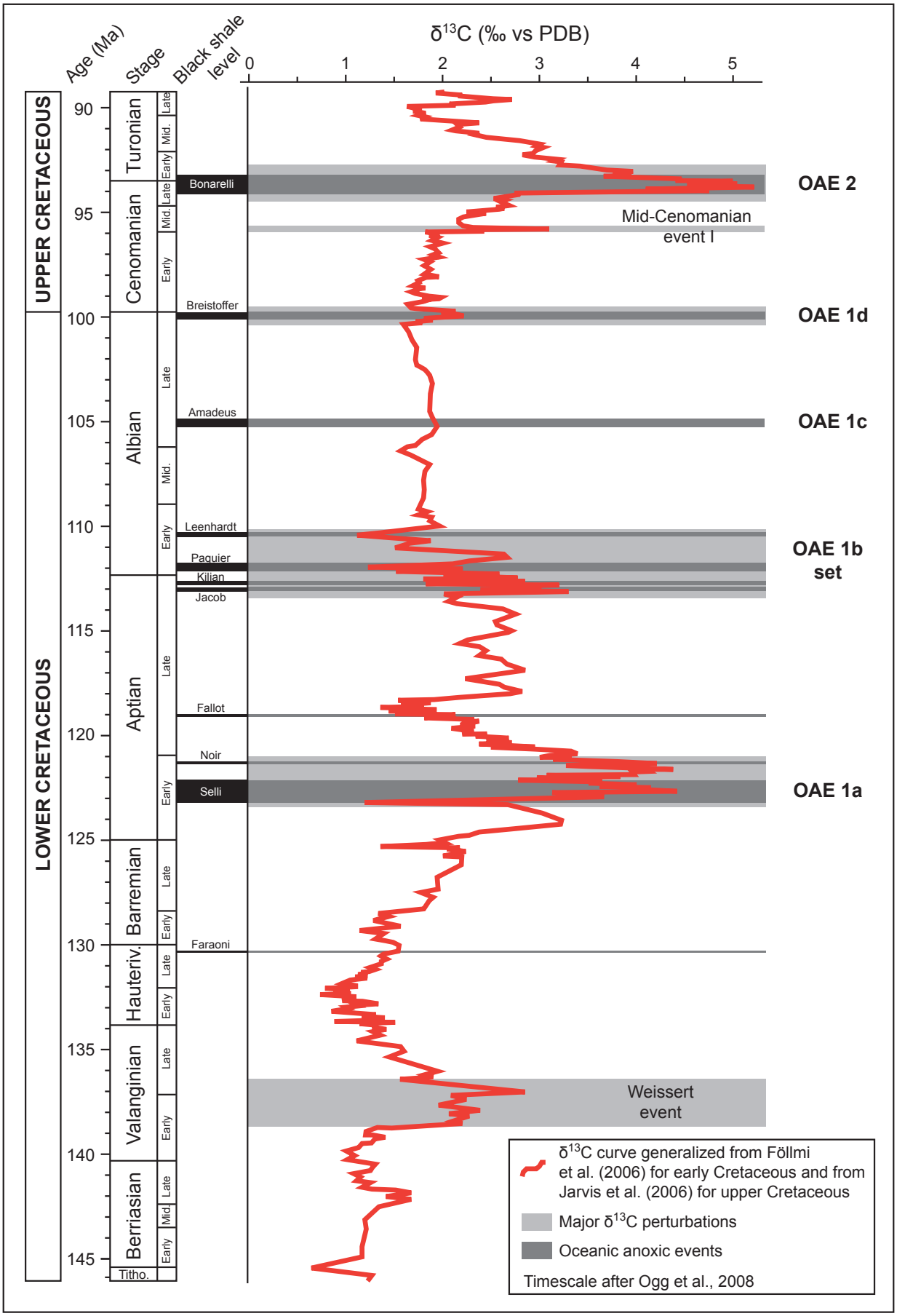

Fig. A.4: Composite $\delta^{13}C$ record adapted from Föllmi et al. (2006), Jarvis et al. (2006) and Föllmi et al. (in prep.) through the Berriasian to the Turonian. The curve highlights the major oceanographic and environmental events and the correlation between positive shifts in carbon isotopic composition and the occurrence of black-shale levels.

water circulation). Surface productivity became enhanced and led to an increase in organic matter burial due to oxygen-depleted bottom water. Elevated organic matter deposition marks the onset of the OAEs. Finally, increased weathering and organic matter deposition (driven by increased productivity and/or better preservation) led to a drawdown of atmospheric CO_2, resulting in the decrease in nutrient fluxes into the ocean and cooling, and ending the OAEs.

In this general scheme, two processes play a key role in the occurrence of large black-shale deposits. Derived from these mechanisms, two distinct models have been proposed: the expanded oxygen minimum zone (OMZ) model versus the stagnant ocean model. The first model is a productivity-driven model, in which black shales are the result of high primary productivity in the photic zone of the ocean. This increase in organic matter production can be related to several factors, such as an increase in the nutrient flux to the oceans, as a consequence of volcanic forcing of the climate, increased humidity and precipitation (Larson, 1991; Larson & Erba, 1999; Hasegawa, 2003). The enhanced supply of organic matter to the deeper part of the ocean depletes oxygen throughout the water column and causes the expansion of the OMZ. In the second model - a preservation-driven model, the burial of organic matter, as evidenced by the black shales, is sensitive towards oxidative destruction on the path through the water column to sediments (Rullkötter, 2000). As a result, the concentration of free oxygen at the water-sediment interface is the most important factor determining the amount of organic matter stored in sediments. Thus, ocean stratification is regarded as the most important factor, leading to variations in the advection of oxygen-laden surface to bottom water. In reality, both productivity and preservation play a crucial role in forming black-shale deposits (e.g. Mort et al., 2007). Understanding and studying both processes is important because they directly influence the oceanic nutrient and carbon cycle, which in turn affect the climate of the Earth.

A.3 Tracing change in the redox change of the ocean

A.3.1. The redox-sensitive trace-element (RSTE) behaviour

In the last two decades, variations in trace-element abundances in sediment and sedimentary rock have been widely investigated to reconstruct paleodepositional conditions (Calvert & Pedersen, 1993; Jones & Manning, 1994; Crusius et al., 1996; Dean et al., 1997; Yarincik et al., 2000; Morford et al., 2001; Algeo & Maynard, 2004; Algeo & Lyons, 2006; Bodin et al., 2006; Tribovillard et al., 2006). Redox-sensitive trace elements (RSTE) commonly exhibit considerable enrichments in laminated, organic-rich sediments, especially those deposited under euxinic conditions. Such a pattern exists because many RSTE have multiple valence states, and the reduced forms that exist under low-oxygen conditions are more readily complexed with organic acids, incorporated into solid solution in authigenic sulfides, or precipitated as insoluble oxyhydroxides. Because the behaviour of RSTE in the water column and during early diagenesis and their sensitivity to redox conditions is rather element-specific, it is generally recommended that a suite of RSTE be used for reconstructing paleo-redox conditions rather than a single element (Tribovillard et al., 2006). Moreover, by using the distribution of a suite of RSTE, it is not only possible to distinguish oxic from suboxic or anoxic, but also suboxic/anoxic from euxinic conditions (Fig. A.5, Algeo & Maynard, 2004; Tribovillard et al., 2006).

In the following, the behaviour of some of the most specific RSTE (chosen because of their different behaviour under anoxic and euxinic conditions) is described:

- Vanadium (V): In oxygenated waters, V occurs as V^{5+} in vanadate ionic species such as HVO_4^{2-} and H_2VO^{4-}, which are absorbed onto manganese and iron oxyhydroxides. Under weakly reducing conditions, V is reduced to V^{4+} in vanadyl, VO^{2+}, which binds even more strongly to metal oxyhydroxides and organic matter. Under more strongly reducing conditions, V is further reduced to V^{3+}, which is absorbed onto geoporphyrins or is precipitated as particulate oxide or hydroxide. This two-step behavior leads to a concentration of V in organic matter and to a lesser amount in sulfides during the non-sulfidic anoxic diagenetic stage, whereas under sulfidic anoxic diagenesis, V is mainly associated with sulfides (e,g., Morford & Emerson, 1999; Algeo & Maynard, 2004).
- Uranium (U): In oxygenated waters, U is

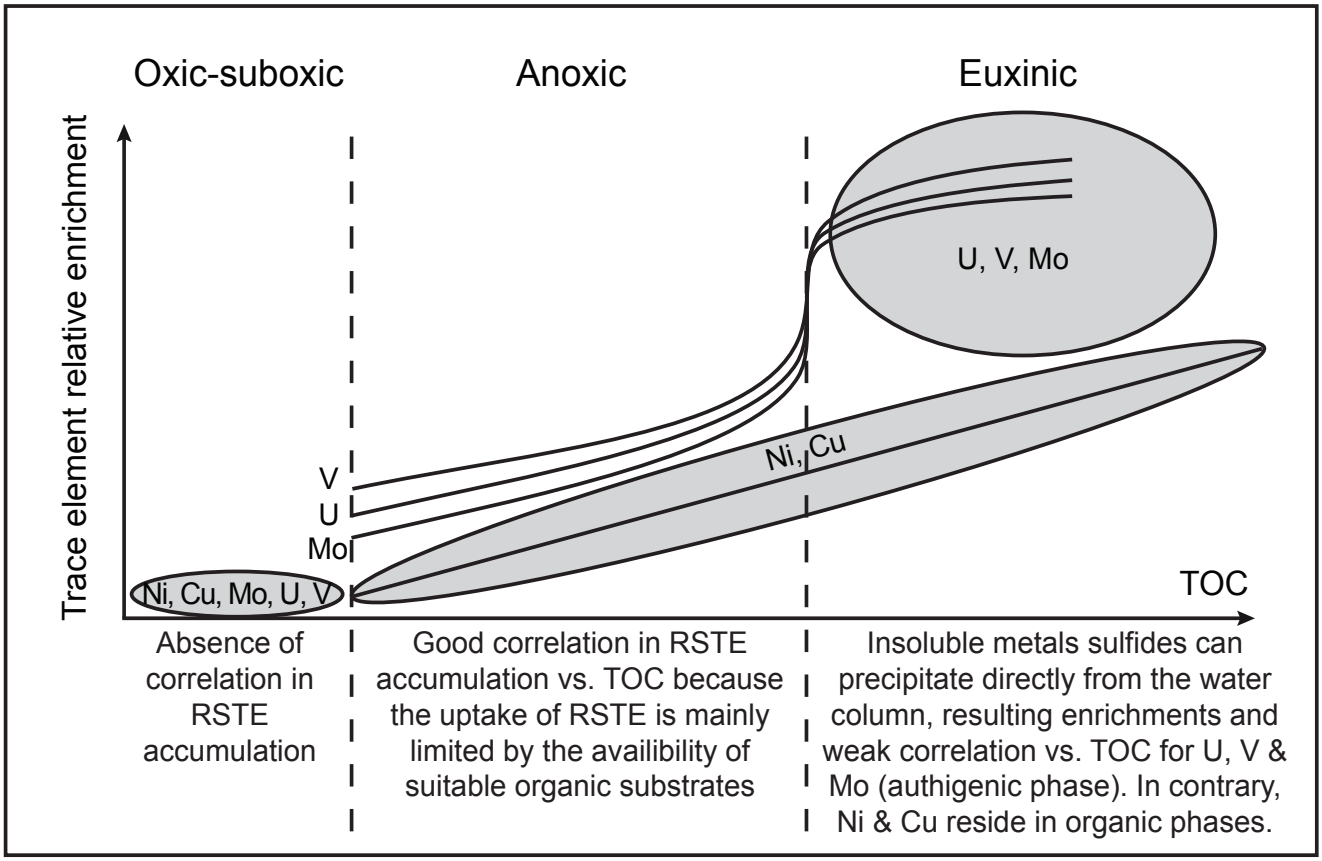

Fig. A.5: Schematic diagram of the behaviour of redox-sensitive trace elements as a function of TOC accumulation (adapted from Tribovillard et al., 2006).

stable as soluble U^{6+}, which forms complexes with carbonate ions, which are stable and dominate natural oxygenated waters. Under anoxic conditions, U is removed from the water column as U^{4+} by the formation of organic-metal ligands in humic acids and by the precipitation of uraninite UO_2 (Calvert & Pederson, 1993; Algeo & Maynard, 2004)

- Molybdenum (Mo): M o occurs as Mo^{6+} in MoO_4^{2-} in oxygenated waters, and can as such be absorbed onto manganese oxyhydroxides and absorbed on or complexed with humic substances and organic matter in general. Under anoxic conditions, Mo is reduced to Mo^{4+}, which is less soluble and authigenically precipitated in the anoxic diagenetic environment, where it can be complexed with sulfurized organic matter (Tribovillard et al., 2004). There, a Mo transfer is also observed from organic matter into a sulfidic mineral phase under progressively anoxic conditions (Brumsack, 1989; Calvert & Pederson, 1993; Morford & Emerson, 1999).
- Manganese (Mn): Under oxidizing conditions Mn^{4+} is precipitated as MnOOH or in the form of other Mn phases (e.g., Hem, 1972). Under reducing conditions, manganese oxyhydroxides are dissolved and Mn occurs as Mn^{2+} ions. The concentration of dissolved Mn in anoxic waters is up to 1000 times higher (max. 1000 ppb) than that in oxic environments (Martin & Knauer, 1983). Because of that, anoxic water bodies act as transport paths of Mn in the ocean. The most important sinks of dissolved Mn in the ocean are (1) adsorption onto sinking detrital and biogenic particles and (2) hydrogenous and hydrothermal precipitation of Mn oxyhydroxides either in the sediments or in the water column (Martin & Knauer, 1983).

A.3.2. The behaviour of phosphorus under anoxic conditions

Phosphorus (P) is an important and often limiting element in ocean primary productivity. It is closely linked to the carbon (C) cycle by two processes: (1) weathering of continental rocks (the transformation of atmospheric CO_2 into the weak acid H_2CO_3 is the driving factor in chemical weathering processes during which P is mobilized); and (2) photosynthesis during which CO_2 is transformed into organic C (P is an essential nutrient and implied in photosynthetic processes). The only significant source of P to the ocean is via rivers (continental weathering) and atmospheric transport (Föllmi, 1996; Delaney, 1998). The efficiency of P storage in the sedimentary reservoir is redox dependent. P regeneration becomes more important in oxygen-depleted bottom waters (Ingall and Jahnke, 1994; Van Cappellen and Ingall, 1996; Colman and Holland, 2000; Emeis et al., 2000; Tamburini et al. 2002; Bodin et al., 2006; Mort et al., 2007; Slomp & Van Cappellen, 2007). In the last two decades, a sequential extraction technique (known as SEDEX) has been developed to measure the different types of P (i.e. organic-P, Fe-bounded P, authigenic-P and detrital-P; Fig. A.6) (Ruttenberg, 1992; Anderson & Delaney, 2000; Tamburini, 2002; Mort et al., 2007). Changes in the different types of P are related to changes in the mode of deposition. For example, the increased accumulation of authigenic-P is indicative of oxic conditions at the time of deposition. On the other side, an increase in organic-P may be explained by higher productivity and organic matter burial, or by the reduction of oxygen content at the water-sediment interface, reducing the rate of organic matter oxidation and preferential release of organic-P. Thus, P is suitable proxy to understand the role of productivity and preservation during Cretaceous OAEs.

A reconstruction of changes in the P cycle trough the end-Cenomanian anoxic event recently provided evidence of nutrient regeneration during OAE 2, characterized by high accumulation rates of reactive P at the onset of the anoxic event followed by an increase of P recycling due to anoxic conditions (Mort et al., 2007). In this case, a switch in marine sediments occurred during the anoxic event - from a P sink to a P source, thereby acting as a positive feedback on surface productivity.

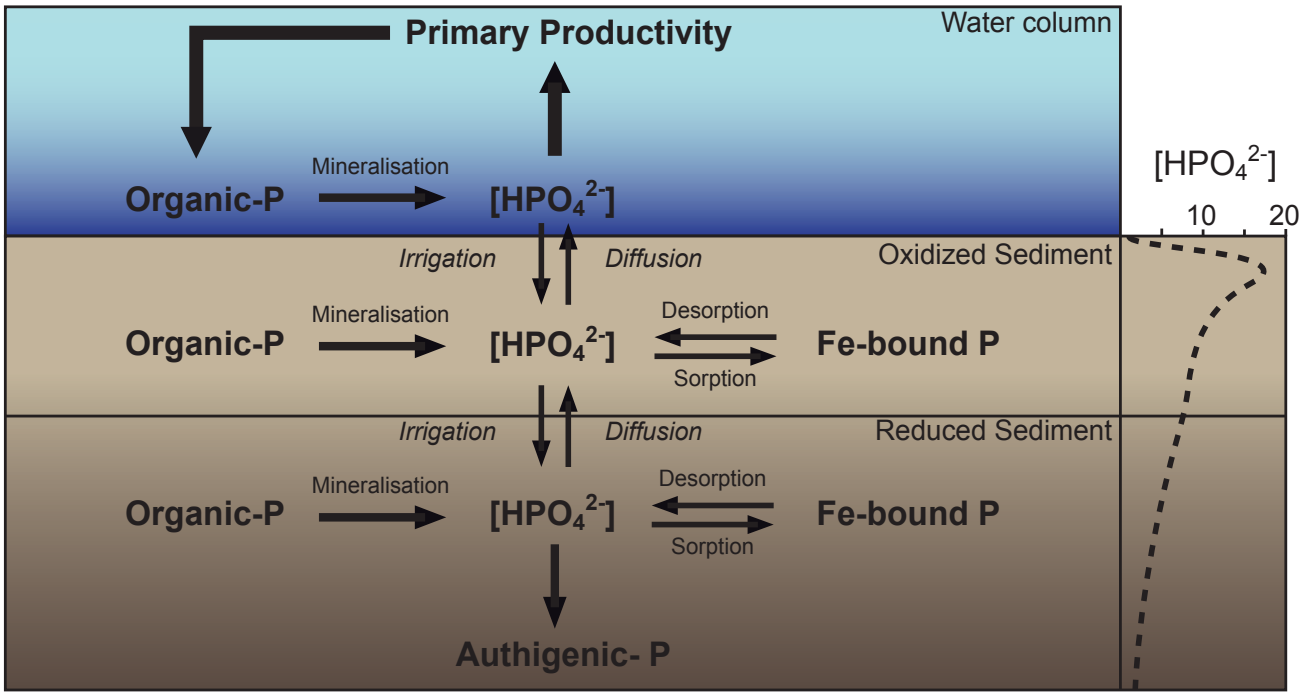

Fig. A.6: Behaviour of the different types of P in the ocean and marine sediments. The phosphate molecule progresses though a series of redox states, which is dependent on oxygen abundance in the water. Redrawn from Mort (2007) and Slomp et al. (1996).

A.4 Introduction to Thesis

The aim of this PhD project is to better understand the interactions between paleoceanographic change, oxygen-depletion in the water column and organic-carbon preservation in the Tethyan realm during three major positive carbon-isotope excursions, which are observed during the Early to early Late Cretaceous (Valanginian, early Aptian and end Cenomanian). These periods correspond to oceanic anoxic events (OAEs, see above) and are characterized by a positive shift in $\delta^{13}C$ record and by carbonate-platform drowning. However, whereas the Early Aptian and the end-Cenomanian OAEs are characterized by the widespread occurrence of organic-rich sediments, for the Valanginian, only a few organic-rich deposits are known.

The project covers three themes, which partly overlap. The first theme is the exploration of the evolution of the intensity of redox conditions and general paleoceanographic change in time and in space. We employed redox-sensitive trace elements (RSTE) and phosphorus contents as proxies. These data are complemented by the analysis of stable carbon and oxygen isotopes, organic carbon and mineral contents. A further goal is to estimate the importance of preservation and productivity as driving factors of organic matter accumulation and to test the different models proposed for OAEs. Furthermore, we propose to standardize the analytical process by submitting the samples to different types of acid attacks.

This thesis is presented in six parts:

A. This general introduction

B. A comparison of partial and total extraction methods used in the analysis of redox-sensitive trace metals

C. The Valanginian carbon excursion

D. The early Aptian OAE 1a

E. The expression of the end-Cenomanian OAE 2 in the Helvetic realm

F. General conclusions

G.Annexes (raw data, affiliated paper, conference abstracts, etc)

References

Ahlberg, A., Herman, A. B., Raikevich, M., Rees, A. and Spicer, R. A. [2002]. Enigmatic Late Cretaceous high palaeo-latitude lonestones in Chukotka, northeasternmost Asia. GFF (Geologiska Föreningens i Stockholm Förhandlingar) 124, 197-199.

Algeo, T. J. and Lyons, T. [2006]. Mo–total organic carbon covariation in modern anoxic marine environments: Implications for analysis of paleoredox and paleohydrographic conditions. Paleoceanography 21 (PA1016).

Algeo, T. J. and Maynard, J. B. [2004]. Trace-element behavior and redox facies in core shales of Upper Pennsylvanian Kansas-type cyclothems. Chemical Geology 206, 289-318.

Anderson, D. L. and Delaney, M. L. [2000]. Sequential extraction and analysis of phosphorus in marine sediments: streamliming of the SEDEX procedure, Limnology and Oceanography, 45, 509-515.

Arthur, M. A., Jenkyns, H. C., Brumsack, H.-J. and Schlanger, S. O. [1990]. Stratigraphy, geochemistry, and paleoceanography of organic-carbon rich Cretaceous sequences, in R. N. Ginsburg and B. Beaudoin: Cretaceous Research, Events and Rhythms, Kluwer Acad., Norwell, 75-119.

Barron, E. J. and Peterson, W. H. [1989]. Model Simulation of the Cretaceous ocean circulation. Science 244, 684-686.

Bodin, S., Godet, A., Matera, V., Steinmann, P., Vermeulen, J., Gardin, S., Adatte, T., Coccioni, R. and Föllmi, K. B. [2006]. Enrichment of redox-sensitive trace metals (U, V, Mo, As) associated with the late Hauterivian Faraoni oceanic anoxic event. International Journal of Earth Sciences 96, 327-341.

Brumsack, H.J. [1989]. Geochemistry of recent TOC-rich sediments from the Gulf of California and the Black Sea. Geol. Rundsch. 78, 851–882.

Calvert, S. E. and Pedersen, T. F. [1993]. Geochemistry of recent oxic and anoxic marine sediments: Implications for the geological record. Marine Geology 113, 67-88.

Crusius, J., Calvert, S. E., Pedersen, T. F. and Sage, D. [1996]. Rhenium and molybdenum enrichments in sediments as indicators of oxic, suboxic

and sulfidic conditions of deposition Earth and Planetary Science Letters 145, 65-78.

Colman, A.S. and Holland, H.D. [2000]. The global diagenetic flux of phosphorus from marine sediments to the oceans; redox sensitivity and the control of atmospheric oxygen levels. In: Glenn, C.R., Prévôt-Lucas, L., Lucas, J. (Eds.), Marine Authigenesis; From Global to Microbial, SEPM Special Publication, vol. 66, pp. 53–75.

Dean, W. E., Gardner, J. V. and Piper, D. Z. [1997]. Inorganic geochemical indicators of glacial-interglacial changes in productivity and anoxia on the California continental margin. Geochimica et Cosmochimica Acta 61, 4507-4518.

Delaney, M.L. [1998]. Phosphorus accumulation in marine sediments and the oceanic phosphorus cycle. Glob. Geochem. Cycles 12, 563-572.

Emeis, K.-C., Stuck, U., Leipe, T., Pollehne, F., Kunzendorf, H. and Christiansen, C. [2000]. Changes in the C, N, P burial rates in some Baltic Sea sediments over the last 150 years - relevance to P regeneration rates and the phosphorus cycle. Marine Geology 167, 43-59.

Erba, E., Bartolini, A. and Larson, R. L. [2004]. Valanginian Weissert oceanic anoxic event. Geology 32, 146-152.

Erba, E., Channel, J. E. T., Claps, M., Jones, C. E., Larson, R. L., Opdyke, B., Premoli Silva, I., Riva, A., Salvini, G. and Torriceli, S. [1999]. Integrated stratigraphy of the Cismon Apticore (southern Alps, Italy); a “reference section” for the Barremian-Aptian interval at low latitudes. Journal of Foraminiferal Research 29, 371-391.

Föllmi, K. B. [1996.] The phosphorus cycle, phosphogenesis and marine phosphate-rich deposits. Earth-Science Reviews 40, 55-124.

Föllmi, K. B., Godet, A., Bodin, S. and Linder, P. [2006]. Interactions between environmental change and shallow water carbonate buildup along the nothern Tethyan margin and their impact on the Early Cretaceous carbon isotope record. Paleoceanography 21 (PA4211, doi:10.1029/2006PA001313), 1-16.

Föllmi, K. B., Delamette, M. and Ouwehand, P. J. Aptian to Cenomanian deeper-water hiatal stromatolites from the northern Tethyan margin. *In*: Seckbach, J. and Tewari, V. (Eds), The Stromatolites: Interactions of Microbes with Sediments. Springer-Verlag (in preparation).

Frakes, L. A. [1979]. Climates throughout geologic time. Elsevier, 322 p.

Frakes, L. A. [1999]. Estimating the global thermal state from the Cretaceous sea surface and continental temperature data. *In:* Barrera, E. and Johnson, C. C. (Eds.), Evolution of the Cretaceous Ocean-Climate System, Geological Society of America Special Paper, 332, 49-57.

Frakes, L. A. and Bolton, B. [1992]. Effects of ocean chemistry, sea level, and climate on the formation of primary manganese ore deposits. Economic Geology 87, 1207-1217.

Frakes, L. A. and Francis, J. E. [1988]. A guide to Phanerozoic cold polar climates from high-latitudes ice-rafting in the Cretaceous. Nature 333, 547-549.

Francis, J. E. and Frakes, L. A. [1993]. Cretaceous climates. Sedimentology Review 1, 17-30.

Hallam, A. [1984]. Pre-Quaternary Sea-Level Changes. Annual Review of Earth and Planetary Sciences 12, 205-243.

Hasegawa, T. [2003]. Cretaceous terrestrial paleoenvironments of northeastern Asia suggested from carbon isotope stratigraphy: Increased atmospheric pCO_2-induced climate. Journal of Asian Earth Sciences, 21, 849-859.

Hay, W. W. [2008]. Evolving ideas about the Cretaceous climate and ocean circulation. Cretaceous Research 29, 725-753.

Hem, J. D., [1972]. Chemical factors that influence the availability of iron and manganese in aqueous systems. Geological Society of America Bulletin 83, 443-450.

Herrle, J. O., Kössler, P., Friedrich, O., Erlenkeuser, H. and Hembelen, C. [2004]. High-resolution carbon isotope records of the Aptian to Lower Albian from SE France and the Mazagan Plateau (DSDP Site 545): a stratigraphic tool for paleoceanographic and paleobiologic reconstruction. Earth and Planetary Science Letters 218, 148-161.

Immenhauser, A., Hillgärtner, H. and Van Bentum, E. [2005]. Microbial-foraminiferal episodes in the Ealry Aptian of the southern Tethyan margin: ecological significance and possible relation to oceanic anoxic event 1a. Sedimentology 52, 77-99.

Ingall, E. D. and Jahnke, R. [1994]. Evidence for enhanced phosphorus regeneration from marine sediments overlain by oxygen depleted waters.

Geochimica et Cosmochimica Acta 58, 2571-2575.

Jarvis, I., Gale, A. S., Jenkyns, H. C. and Pearce, M. A. [2006]. Secular variation in the Late Cretaceous carbon isotopes: a new $\delta^{13}C$ carbonate reference curve for the Cenomanian-Campanian (99.6-70.6Ma). Geol. Mag. 143, 561-608.

Jenkyns, H. C. [2003]. Evidence for rapid climate change in the Mesozoic-Palaeogene greenhouse world. Phil. Trans. R. Soc. Lond. A 361, 1885-1916.

Jones, B. and Manning, A. C. [1994]. Comparison of geochemical indices used for the interpretation of palaeoredox conditions in ancient mudstones. Chemical Geology 111, 111-129.

Kemper, E. [1987]. Das Klima der Kreide-Zeit. Geologisches Jahrbuch, Reihe A, 96, 5-185.

Larson, R. L. [1991]. Geological consequences of superplumes. Geology 19, 963-966.

Larson, R. L. and Erba, E. [1999]. Onset of the Mid-Cretaceous Greenhouse in the Barremian-Aptian: igneous events and the biological, sedimentary, and geochemical responses. Paleoceanography 14, 663-678.

Lini, A., Weissert, H. and Erba, E. [1992]. The Valanginian carbon isotope event: a first episode of greenhouse climate condition during the Cretaceous. Terra Nova 4, 374-384.

Martin, J. H., and Knauer, G. A. [1983]. VERTEX: Manganese transport with $CaCO_3$. Deep Sea Research, 30, 411-425.

Meyers, P. A. [2006]. Paleoceanographic and paleoclimatic similarities between Mediterranean saporpels and Cretaceous black shales. Palaeogeography, Palaeoclimatology, Palaeoecology 235, 305-320.

Morford, J. L. and Emerson, S. R. [1999]. The geochemistry of redox sensitive trace metal in sediments. Geochimica et Cosmochimica Acta 63, 1735-1750.

Mort, M., Adatte, T., Föllmi, K. B., Keller, G., Steinmann, P., Matera, V., Berner, Z. and Stüben, D. [2007]. Phosphorus and the roles of productivity and nutrient recycling during oceanic anoxic event 2. Geology 35, 483-486.

Pucéat, E., Lécuyer, C. and Reisberg, L. [2005]. Neodymium isotope evolution of NW Tethyan upper ocean waters throughout the Cretaceous. Earth and Planetary Science Letters 236, 705-720.

Rullkötter, R. [2000]. Organic matter: The driving force for early diagenesis. In: Schulz, H. D. and Zabel, M. (Eds), Marine Geochemistry. Springer, 129-172.

Ruttenberg, K.C. [1992]. Development of a sequential extraction method for different forms of phosphorus in marine sediments: Limnology and Oceanography, 37, 1460-1482.

Schlanger, S. O. and Jenkyns, H. C. [1976]. Cretaceous oceanic anoxic event: causes and consequences. Geologie en Mijnbouw 55, 179-188.

Sloan, L. C. and Barron, E. J. [1990]. “Equable” climates during Earth history? Geology 18, 489-492.

Slomp, C. P. and Van Cappellen, P. [2007]. The global marine phosphorus cycle: sensitivity to oceanic circulation. BIogeosciences 4, 155-171.

Stampfli, G. M. and Borel, G. D. [2002]. A plate tectonic model for the Paleozoic and Mesozoic constrained by dynamic plate boundaries and restored synthetic oceanic isochrons. Earth and Planetary Science Letters 196, 17-33.

Stille, P., Steinmann, M. and Riggs, S. R. [1996]. Nd isotope evidence for the evolution of the paleocurrents in the Atlantic and Tethys Oceans during the past 180 Ma Earth and Planetary Science Letters 144, 9-19.

Tamburini, F. [2002]. Phosphorus in marine sediments during the last 150’000 years : exploring relations between continental weathering, productivity and climate. Unpublished PhD thesis, Université de Neuchâtel, 219 pp.

Tamburini, F., Huon, S., Steinmann, P., Grousset, F.E., Adatte, T. and Föllmi, K.B. [2002]. Dysaerobic conditions during Heinrich events 4 and 5: evidence from phosphorus distribution in a North Atlantic deep-sea core. Geochimica et Cosmochimica Acta 66, 4069– 4083.

Tribovillard, N., Algeo, T. J., Lyons, T. W. and Riboulleau, A. [2006]. Trace metals as paleoredox and paleoproductivity proxies : An update. Chemical Geology 232, 12-32.

Tribovillard, N., Riboulleau, A., Lyons, T. and Baudin, F. [2004]. Enhanced trapping of molybdenum by sulfurized marine organic matter of marine origin in Mesozoic limestones and shales. Chemical Geology 213, 385-401.

Van Cappellen, P. and Ingall, E. D. [1996]. Redox stabilization of the atmosphere and oceans by phosphorus-limited marine productivity. Science

271, 493-496.

Van de Schootbrugge, B. [2001]. Influence of paleoenvironmental changes during the Hauterivian (early Cretaceous) on carbonate deposition along the northern margin of the Tethys: Evidence from geochemical records (C, O, and Sr-isotopes, P, Fe, Mn). Unpublished PhD Thesis, University of Neuchâtel, 291 p.

Yarincik, K. M., Murray, R. W. and Peterson, L. C. [2000]. Climatically sensitive eolian and hemipelagic deposition in the Cariaco Basin, Venezuela, Over the Past 578,000 Years: Results From Al/Ti and K/Al. Paleoceanography 15, 210-228.

Zachos, J. C., Pagani, M., Sloan, L. C., Thomas, E. and Billups, K. [2001]. Trends, rhythms, and aberrations in global climate 65 Ma to Present. Science, 292, 686-693.

CHAPTER B: Comparison of two acid extraction methods

The Glaise section, France

The following chapter presents redox-sensitive trace-elements trends obtained by two different extractions methods. We submitted samples of the early Aptian OAE interval to a total extraction method (a combined HF/HNO_3/HCl acid digestion) and compared the results with the data we obtained by the HNO_3 digestion.

-B-

A Comparison of Partial and Total Extraction Methods used in the Analysis of Redox-Sensitive Trace Metal from Oxic, Dysoxic and Anoxic Sediments

Stéphane Westermann[1], Virginie Matera[2], Thierry Adatte[1] and Karl B. Föllmi[1]

[1]Institute of Geology and Paleontology, University of Lausanne, Anthropôle, 1015 Lausanne, Switzerland.
[2]Institute of Geology, University of Neuchâtel, Emile Argand 11, CP 158, 2009 Neuchâtel, Switzerland.

Manuscript in preparation for submission in Chemical geology

Abstract

In this study, we analysed three representative sections covering the Early Aptian Oceanic Anoxic Event 1a (OAE 1a) of the western Tethys for their redox-sensitive trace-element (RSTE) contents. The three sections (Gorgo a Cerbara, central Italy; Glaise, SE France; Cassis/La Bédoule, SE France) represent the full spectrum of euxinic, anoxic, dysoxic and oxic conditions, which prevailed during OAE 1a. We used a partial and a total extraction method in order to compare the results and test the viability and efficiency of the partial extraction method on different lithology. For the partial extraction method, we selected a digestion procedure by suprapur HNO_3 because of the good dissolution percentages obtained on carbonate samples (close to 95%, n=190), the rapidity of sample preparation and the relatively low degree of hazard. For the total extraction method, we selected an extraction procedure by $HF/HNO_3/HCl$. The both digestion methods also differ by the heating procedure, using a microwave oven and a heating-plate for the partial and total extraction methods, respectively.

The RSTE contents and stratigraphic trends obtained by HNO_3 digestion for the sections of Gorgo a Cerbara and Glaise, which are characterized by euxinic to dysoxic conditions, are well correlated with the Al-normalized data obtained by the total extraction method. In Cassis/La Bédoule, the correlation is less clear, likely because of the absence of RSTE enrichments along the section. These results suggest that partial digestion by HNO_3 viably trace all RSTE enrichment intervals within the OAE-1a sediments, even in the case they contain less than 10% $CaCO_3$. The HNO_3 extraction method provides therefore a valuable alternative for accessing changes in paleoredox conditions in the OAE-1a related sediments. This is especially valid for RSTE, which precipitate in the sediment as authigenic phase under anoxic conditions (U, V, Mo). For RSTE, which are supplied to the sediment in association with organic matter (i.e. Ni, Cu), the HNO_3 digestion appears to transfer a representative RSTE fraction into solution and the trends show similarities with non-Al-normalized data obtained by total extraction. However, for these elements, the contents obtained by the nitric acid extraction should be evaluated with care. Overall, the partial digestion method provides a good approximation of RSTE contents in the analysed OAE-1a-related sediments, especially if stratigraphic variations are evaluated.

***Keywords**: Aptian, Oceanic Anoxic Event 1a, redox conditions, redox-sensitive trace elements H_2NO_3 extraction, $HF/HNO_3/HCl$ extraction, comparison*

B.1 Introduction

Redox-sensitive trace element (RSTE) contents or ratios have been widely used as an indicator of redox conditions in modern and ancient sedimentary systems (Calvert and Pedersen, 1993; Jones and Manning, 1994; Crusius et al., 1996; Dean et al., 1997; Yarincik et al., 2000; Morford et al., 2001; Algeo and Maynard, 2004;

Algeo and Lyons, 2006; Bodin et al., 2006; Tribovillard et al., 2006; Bodin et al., 2006; Algeo and Maynard, 2008; Westermann et al., in prep.). RSTE commonly exhibit considerable enrichments in laminated, organic-rich sediments, especially in those, which were deposited under euxinic conditions. This is related to the presence of multiple valence states. The reduced forms that exist under low-oxygen conditions are more readily complexed with organic acids, incorporated in authigenic sulfides, or precipitated as insoluble oxyhydroxides. As such, RSTE provide a valuable proxy for redox conditions in sedimentary rocks, which is most widely used (e.g. Algeo and Maynard, 2004). Despite its common application, a uniform approach for the extraction of RSTE is not always given and results of different studies are not always comparable. In most studies, an acid digestion is employed to extract RSTE contents. A combination of different acids (type and proportion) is generally recommended to completely digest the samples consisting of 1) hydrofluoric (HF), nitric (HNO_3) and perchloric ($HClO_4$) acids (Bayon et al., 2002; Lipinsi et al., 2003; Böning et al., 2004; Snow et al., 2005; Abanda and Hannigan, 2006; Annaboldi and Meyers, 2007); 2) HF, HNO_3 and hydrochloric (HCl) acids (Barling et al., 2001; Kolonic et al., 2005; Siebert et al., 2006; McKay et al., 2007) or 3) HF and HNO_3 acids (Morford and Emerson, 1999; Morford et al., 2001; Morford et al., 2005). The choice of these different acid mixtures is mostly dependent on the type of instrumental tools used to measure RSTE contents: ICP MS (Morford et al., 1999; Barling et al., 2001; Lipinski et al., 2003; Böning et al., 2004; Tribovillard et al., 2004; Snow et al., 2005; Abanda and Hannigan, 2006; Turgeon and Brusack, 2006), ICP AES (Tribovillard et al., 2004; Kolonic et al., 2005; Lyons et al., 2006; Riquier et al., 2006; Annaboldi and Meyers, 2007) or atomic absorption spectrometry (Huerta Diaz et al., 1992). The partial extraction method applies HNO_3 as the extracting acid and is especially used for the analysis of carbonates rocks and sediments (Soon and Abboud, 1993; Bodin et al., 2006; Quezada-Hinojosa et al., 2009).

In this contribution, we investigate three representative sections through the Early Aptian Oceanic Anoxic Event (OAE) 1a from the western Tethys (Gorgo a Cerbara, central Italy; Glaise, Vocontian Through, southeastern France; Cassis/La Bédoule, southeastern France). These sediments cover a wide spectrum of bottom-water oxygenation levels ranging between euxinic and fully oxygenated (Westermann, 2009; Westermann et al., in prep.). They offer favourable conditions for studying the geochemical signatures of redox facies in function of the lithology and the type of acid extraction, because of 1) OAE 1a is one of the most significant and widespread black-shale events of the Cretaceous (e.g., Arthur et al., 1990; Jenkyns, 1999; Robinson et al., 2004); (2) the black-shale member in the type locality of Gorgo a Cerbara is composed of a lower bioturbated green interval and an upper laminated black interval, representing a range of redox conditions from mildly dysoxic to strongly anoxic, and, possibly, euxinic (Robinson et al., 2004; Pancost et al., 2004; Westermann et al., in prep); (3) the sections of Glaise and Cassis/La Bédoule include centimetric levels enriched in organic carbon showing higher RSTE contents, which are embedded in organic-carbon lean segments with low RSTE contents, suggesting variations in the intensity of redox conditions (Westermann et al., in prep); (4) the OAE 1a sections analysed here include different types of sedimentary rocks (limestone, marl, shale, radiolarite); (5) general paleoceanographic conditions have been well studied for the western Tethys.

We tested two different protocols for the extraction of RSTE on these sediments, in order to evaluate the validity of the partial extraction method in this type of sediments. For the partial extraction method, we selected a suprapur HNO_3 digestion method because of the good dissolution percentages obtained on carbonate samples (close to 95%, n=190), the rapidity in the sample preparation procedure and the relative low degree of hazard for safety. For the total extraction method, we selected a combined $HF/HNO_3/HCl$ acids extraction method adapted from Böning et al. (2004). We choosed to avoid the use of $HClO_4$ because of enhanced safety problems due to high organic carbon concentrations.

B.2 Geological Settings

The three sections selected here are part of a depth transect across the western Tethys and include the Livello Selli (in Italy) or its French equivalent, the Goguel level (Fig. B.1).

B.2.1 Gorgo a Cerbara, Italy

The section of Gorgo a Cerbara crops out in the Umbria Marche Basin, central Italy (Coccioni et al., 1992) and has been proposed as the type section

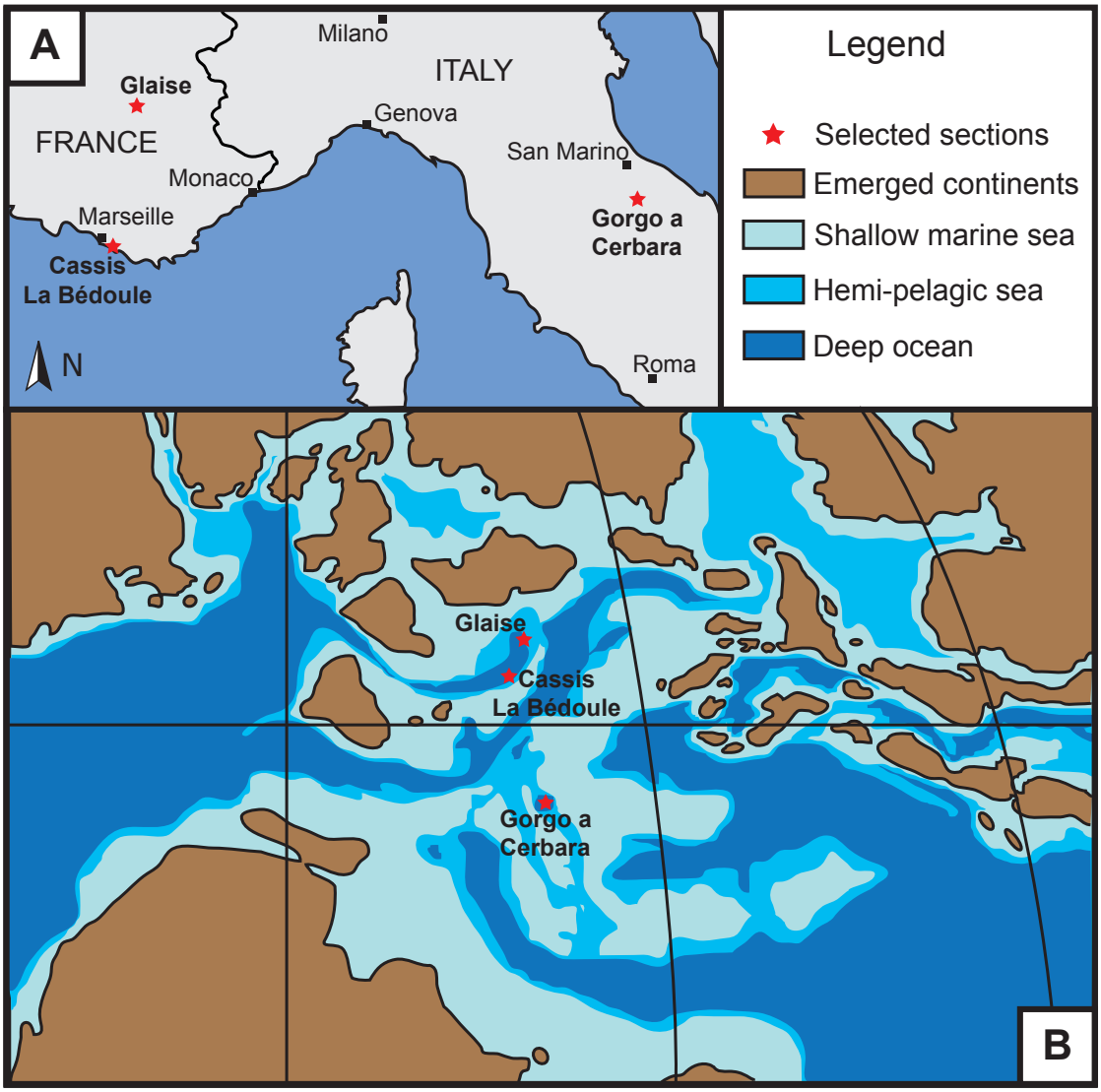

Fig. B.1: A. Localisation of the sections analysed in this study. B. Aptian paleogeographic map of the western Tethys (Redrawn after Scotese et al., 2001). Modified after Westermann et al., in prep.

for the Aptian stage. The lower part of the section is composed of white to grey micritic limestone (Maiolica Formation), which is intercalated with siliceous layers and thin marly and shaly, organic-rich intervals. On top of the Maiolica Formation, a 1.5 meter-thick dark interval of organic-rich shale is present - the Livello Selli -, which corresponds to OAE 1a. The Livello Selli is stratigraphically located at the base of the Marne a Fucoidi Formation (Early Aptian to Late Albian; Coccioni et al., 1992). The sediments of the Marne a Fucoidi Formation following the Livello Selli consist of a greenish to reddish alternation of decimetric limestone and marly limestone with marly intervals.

B.2.2 Glaise, France

The Glaise section is situated near Gap (SE France) in the Vocontian Trough. In this area, the Early Aptian is documented by the hemipelagic sediments of the "Marnes Bleues" Formation (Aptian to Albian in age; e.g., Bréhéret, 1997). The segment analysed here consists of a marly succession, which is interrupted by centimetric turbiditic layers. The Goguel level, which is considered to be time equivalent to the Livello Selli, includes six laminated layers noted Go 1 to Go 6 (Bréhéret, 1997). The section ends with the occurrence of marly limestone beds.

B.2.3 The section of Cassis/La Bédoule

The section of Cassis/La Bédoule (SE France) is located in an intracratonic basin (Masse and Philip, 1976; Moullade, 1998). In this composite section, the Lower Aptian (Bedoulian) sediments reach a thickness of 115 m. The lower part of the section is located in an abandoned quarry near the Cassis/La Bédoule railway station and consists of a marly whitish to grayish limestone succession with marly intervals. The upper

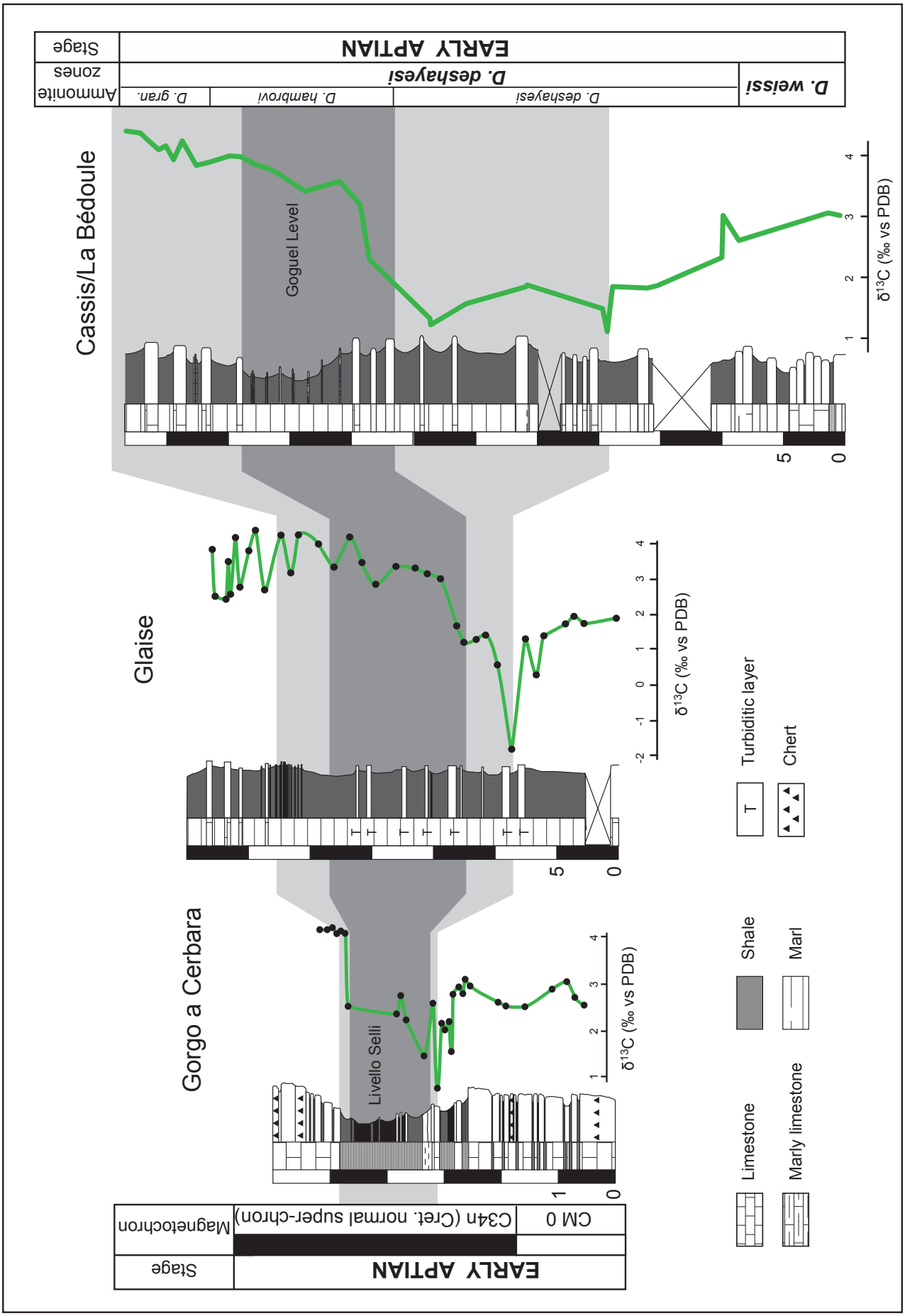

Fig. B.2: Chemostratigraphic correlations between the section of Gorgo a Cerabra, Glaise and Cassis/La Béboule. The light grey box indicates the stratigraphic extention of OAE 1a based on the definition given in Méhay et al. (2009). The dark grey band shows the position of the black shale interval (Livello Selli and its equivalent).

part of the section crops out behind a camping area near La Bédoule. This latter interval is constituted by a rather thick and well-preserved marly succession. The top becomes more calcareous with the occurrence of thick limestone banks.

B.3 Methods

B.3.1 Organic-matter contents

The content and the type of organic matter were determined using Rock Eval pyrolysis (Rock-Eval™6; Behar et al., 2001). Total organic carbon contents (TOC, in weight %) was obtained using the standard temperature cycle. Samples were calibrated with both IFP 160000 (a standard from the Institut Français du Pétrole, Paris, France) and an internal standard with an instrumental precision of <2% (Espitalié et al., 1985).

B.3.2 Redox-sensitive trace-elements

Redox-sensitive trace-element (RSTE) analyses were performed on bulk rock and were determined by a quadrupole ICP-MS (ELAN 6100, Perkin Elmer) using a semi-quantitative mode (TotalQuant™, TQ) at the University of Neuchâtel. TQ is a simple, rapid and accurate panoramic method based on full mass-spectra scan methods and was successfully applied to the analysis of various biological and environmental samples (Jitaru et al. 2003) like, for instance, in sediments (Bayon et al. 1998). TQ enables spectral interpretation of a full mass spectrum by comparison with an internal response table which includes assignment of element intensities based on internal response factors and an interpretation of interferences based on implemented algorithms for numerical calculation of interference corrections. The response table is usually updated before analysis by determination of a blank and one standard solution. The calibration is based on two certified reference materials (CRM): LKSD-1 lake sediment and USGS Cody Shale SCo-1.

Here, two methods of acid extraction were used to measure the RSTE distribution along the studied sections.

B.3.2.1 The partial nitric acid extraction

10 mL of suprapur nitric acid (HNO_3) were added to 250 mg of sample powder. The samples were then heated at 175°C in closed Perfluoroalkoxy (PFA) Teflon bombs during 10 minutes using a microwave oven (MSL-Ethos plus, Milestone) following three steps as described in the USEPA 3051 Method: in step 1, the PFA bombs were heated from ambient temperature to 120 °C during 1 minute; the step 2 corresponds to a second phase of heating from 120 to 175 °C during 4 minutes 30; in the step, heating temperature is maintained at 175 °C during 4 minutes 30. After cooling, the solution was filtered (0.45µm) and diluted to 100 mL with ultrapure water. Dissolution percentages determined after filtration were about 47±27% (n=74) for the Gorgo a Cerbara samples (73±16% for limestone and 36±23% for marl samples), 33±24% (n= 36) for the Glaise samples (77±7% for limestone and 29±20% for marl samples) and 75±9% (n=28) for the Cassis/La Bédoule samples (74±15% for limestone and 75±9% for marl samples).

B.3.2.2 The total hydrofluoric acid extraction

The protocols by Lipinsky et al. (2003) and Böning et al. (2004) were adapted for the analytical procedure used here. 50 mg of sample material were pre-oxidized with 1mL of suprapur nitric acid (HNO_3 65%) in 20-mL PFA vessels (Savilex©) overnight. The PFA vessels were placed into graphite racks and the samples were then heated in the closed Savilex© for 6h at 120°C with 3 mL of suprapur HF and 3 mL of suprapur HNO_3 on a hot plate. After digestion, the acids were evaporated at 180°C to incipient dryness. Afterwards, three times 3 mL of 6N HCl aliquots were added and evaporated. The wet residue was, then, dissolved in 1 mL of suprapur HNO_3 and diluted to 50 mL with ultrapure water. No residual fraction has been observed after this last dissolution.

B.3.3 Data treatment

The RSTE concentrations obtained by nitric acid digestion are reported in ppm. For carbonate, this partial extraction method is normally sufficient to transfer a representative fraction (above 95%) of trace metals into solution, whereas for samples with significant siliciclastic contents the transfer of a representative RSTE fraction is less obvious. Despite the low dissolution percentages for some samples of the sections of Gorgo a Cerbara and Glaise, no correlation was observed between the concentration of the different analysed elements and the dissolution percentage obtained during the partial digestion procedure (e.g., V in Fig. B.3). This suggests that the elements studied here are present in the soluble authigenic phase and are not due to partial leaching of the detrital insoluble fraction (e.g., Bodin et al., 2006).

For the data obtained by the hydrofluoric acid

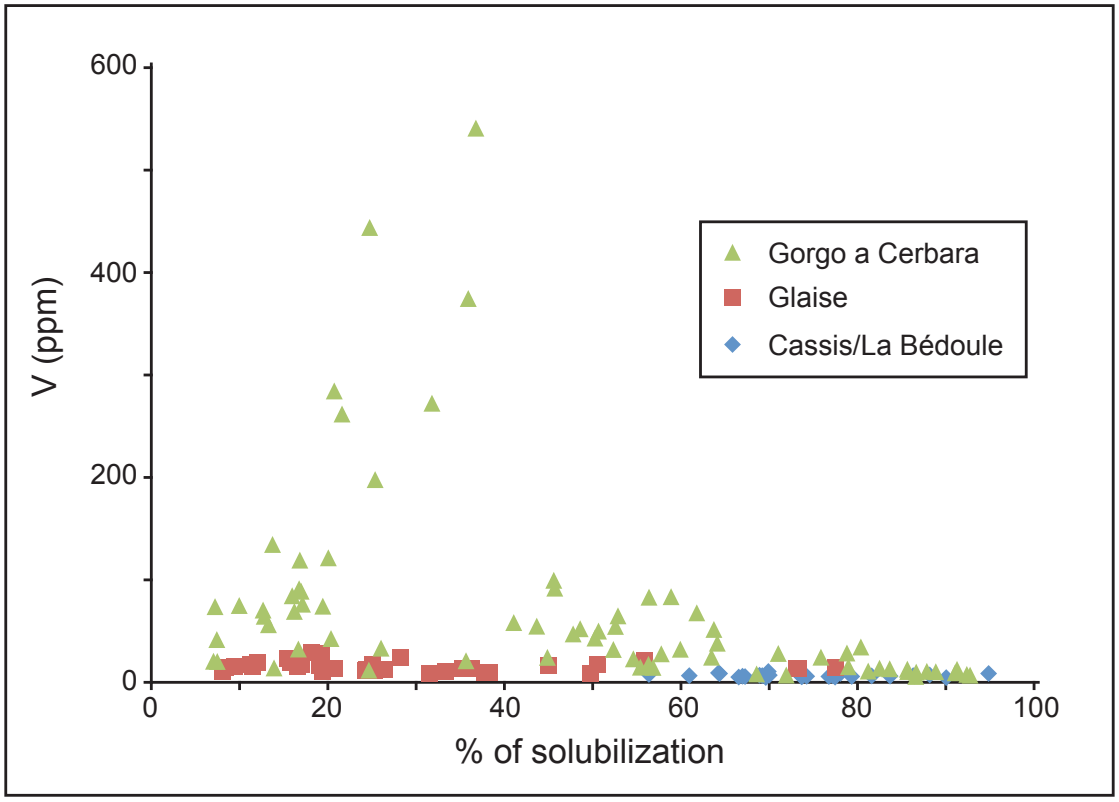

Fig. B.3: V contents (in ppm) obtained by the nitric acid digestion versus percentage of dissolution in the three studied sections. No correlation is observed.

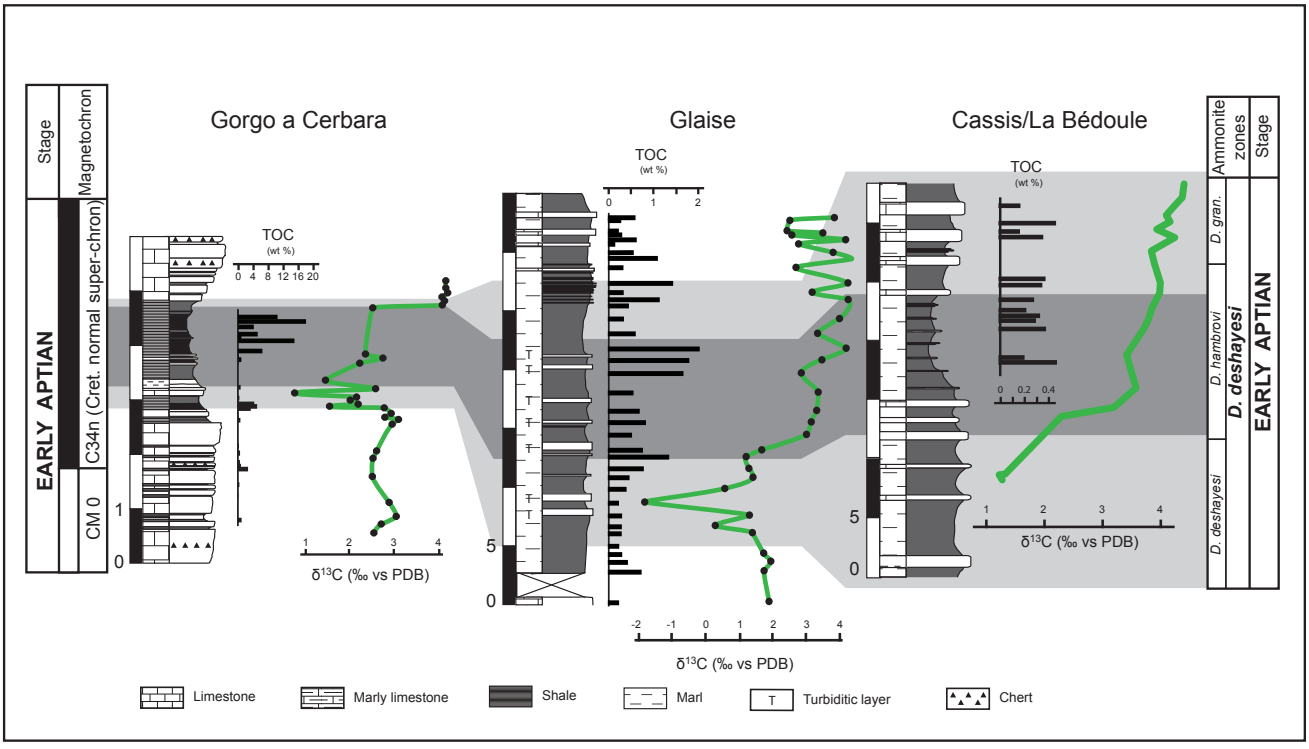

Fig. B.4: Total organic carbon (TOC) contents in the three studied sections.

digestion, we report RSTE concentrations in ppm in order to compare the absolute values obtained by both extraction methods. RSTE concentrations are commonly normalized to Al to correct for detrital dilution (Arthur et al., 1990; Calvert and Pederson, 1993; Morford et al., 2001). This normalisation procedure is valid if Al principally resides in the siliciclastic phase and is immobile during diagenesis (Brumsack, 1989; Calvert and Pedersen, 1993; Morford and Emerson, 1999; Piper and Perkins, 2004). In our study, we also report RSTE concentrations as Al-normalized values with a unit of 10^{-4} to estimate the proportion of detrital influence on RSTE behaviour in the studied intervals.

B.4 Results

B.4.1 Total organic carbon

In the limestone samples, measured TOC values are lower than 0.1 wt%. We will therefore restrict our discussion to the results obtained from marl samples (Fig. B.4). In Gorgo a Cerbara, a first maximum of 5.05 wt% is measured in layers corresponding to the negative spike in $\delta^{13}C$. Within the Livello Selli, the average value of TOC is close to 5.65 wt% and is marked by two maxima of 14.94 and 18.01 wt%. The section of Glaise shows low TOC contents with an average value close to 0.60 wt%. The base and the top of the Goguel level are characterized by two maxima with values of 1.27 and 1.94 wt%, respectively. A third increase, reaching 1.11 wt%, is observed during the $\delta^{13}C$ plateau at the top of the section. For Cassis/La Bédoule, TOC contents show rather low values fluctuating around the average value of 0.26 wt%.

B.4.2 Redox-sensitive trace element recovery

B.4.2.1 Standard reference materials LKSD-1 lake sediment and Cody Shale S-Co1

Samples with significant clay and siliciclastic contents show the lowest dissolution rates following HNO_3 digestion relative to carbonate-rich sediments. We therefore test the HNO_3 digestion of the Canadian LKSD-1 standard to evaluate the RSTE recovery in carbonate sediments, and both extraction methods on the USGS standard material Cody Shale, SCo-1 to evaluate and compare the RSTE recovery rates on siliciclastic sediments. LKSD-1 corresponds to composite lake sediment from lake Joe and lake Brady in Ontario with quite high carbonate contents. SCo-1 is an Upper Cretaceous silty marine shale, intermediate between fine-grained offshore shale and coarser nearshore marine siltstone (Flanagan, 1976).

Results and recovery ratios are presented in Table 1a and 1b for LKSD-1 and SCo-1, respectively. For the LKSD-1 CRM, mean recovery rate (n=12) were 103% for U, 90% for V, 105% for Co, 110% for Cu and 89% for Mo. For the total extraction method, our results show recovery rates (n=4) for the analysed trace elements, except for Mo, with values between 99 and 109% (Table B.1). For the HNO_3 extraction, the analysed elements show systematically lower values than the recommended values. Only Co, Cu and As show higher mean recovery values between 94 and 103%.

The quantification limit for the analysed RSTE were determined by using LKSD-1 CRM and are 5×10^{-4} ppb for U, 2.9×10^{-1} ppb for V, 8×10^{-2} ppb for Co, 10.89 ppb for Cu, 1.13 ppb for Ni and 1.4×10^{-1} ppb for Mo.

B.4.2.2 RSTE variations along the studied sections

The raw data for U, V, Mo, As, Co, Cu, Ni and Cr obtained by both extraction methods are shown in Tables B.2 and B.3 for the three studied sections. Al-normalized data are presented in Table B.4. In the following, we will describe and compare the results obtained for three RSTE (Cu, V and Mo, Fig. B.5) in more detail. These elements were selected according to the following criteria:

- Their specific behaviour under oxic, anoxic and euxinic conditions: under oxic conditions, Cu, V and Mo show no correlation and overall links are present with detrital input. Under anoxic conditions, Cu is associated with organic matter and shows good correlation with TOC contents. V is diffused into the sediment, precipitates as an authigenic phase and shows a relative good correlation with TOC. Mo shows rather low enrichments. Under euxinic conditions, V and Mo precipitate directly from the water column and show relatively weak correlations with TOC, contrary to Cu, which resides in organic phases (Algeo and Maynard, 2004; Tribovillard et al., 2006).
- The difference in abundance in the marine environment. In the water column, Cu and V contents are generally higher than Mo contents.
- The difference in recovery as a function of the extraction method. Cu shows relatively high recovery rates using both digestion

methods (94.4% and 100.3% for the HNO_3 and HF digestion, respectively) whereas V and Mo which show much better recovery using the HF extraction.

The Gorgo a Cerbara section

The data obtained for Cu, V and Mo contents show comparable variations independently of the extraction method used. Cu, V and Mo distributions are consistently characterized by low background levels, which are contrasted by higher concentrations within the Livello Selli. V contents show a first maximum just before the black-shale interval. Within the Livello Selli, Cu, V and Mo show two marked increases with very high concentrations relative to the background level. For Mo, the second peak shows much higher values than the first using both extraction methods. The average values for the background level correspond to approximately 63.9, 7.2 and 1.5 ppm and the maximum values to 312.2, 64.8 and 7.1 ppm for Cu, V and Mo using the nitric acid extraction method. For the HF digestion, the average values fluctuate around 53.7, 71.5 and 5.0 ppm with maximum values of 242.2, 540.5 and 94.0 ppm for Cu, V and Mo, respectively.

For Al-normalized data, the three RSTE show the same behaviour as described above (Fig. 5.). Cu, V and Mo distributions display low background values with two marked maxima within the Livello Selli.

The Glaise section

In this section, no correlation enrichment is observed for the RSTE targeted here. Moreover, it appears that each RSTE shows a different trend as a function of the extraction method employed. Using the HNO_3 extraction, Cu contents show a maximum at the onset of the Goguel level with values reaching 73.9 ppm (background level of 38.8 ppm). V shows a rather constant trend with values fluctuating around 16 ppm. Two weak peaks are observed at 12 and 19 m above the base of the sections with maximal values of 28.4 and 29.5 ppm, respectively. Mo contents are rather low along the section with an average value of 0.3 ppm. At the top of the Goguel level (approximately 20 m above the base of the section) an increase in Mo concentration is observed reaching 1 ppm. For the concentrations obtained by the total extraction method, Cu and Mo show trends comparable to those obtained by the nitric acid digestion method with an average value of 38.6 and 0.7 ppm and with maxima of 75.9 and 4.2 ppm for Cu and Mo, respectively. Contrary to the data obtained by the HNO_3 digestion, V contents are characterized by a decreasing trend.

For Al-normalized data, no change in the global trend is observed for Cu and Mo (Fig. B.5). However, when normalized to Al, the trend in V contents obtained by the total extraction method shows more or less the

a. Recovery for LKSD-1 using the nitric acid extraction

Elements	Recommended values	HNO_3 extraction	% Recovery
V	50	45.0	90.0
Co	11	11.6	105.0
Cu	44	48.4	110.0
As	40	44.0	110.0
Mo	5	4.5	89.0

b. Recovery for SCo-1 using both acid extractions

Elements	Recommended values	HF extraction	% Recovery	HNO_3 extraction	% Recovery
Al	72525	86532.7	119.3	77133.3	106.4
Ti	7554	4717.8	62.5	54.7	0.7
V	130	131.3	101.0	55.1	42.4
Cr	68	68.7	101.1	28.3	41.6
Co	11	10.9	99.5	10.3	93.6
Ni	27	29.0	107.5	23.5	87.0
Cu	29	29.1	100.3	27.4	94.5
As	12	13.1	109.3	10.9	90.8
Mo	1.4	1.7	119.4	0.1	7.1

Table 1: Results (in ppm) and recovery (in %) of the two studied acid digestion methods on the USGS Cody Shale SCo-1 standard.

same behaviour as the one observed for the nitric acid digestion method, with two weak increases at the base and the top of the Goguel level, respectively.

The Cassis/La Bédoule section

In the Cassis/La Bédoule section, the presented RSTE show rather low values along the section. Similar trends are observed between the data obtained by HNO_3 and HF digestion methods. Cu displays an increasing trend in the first part of the section reaching a maximum of 9.7 and 13.4 ppm for the HNO_3 and HF extraction methods, respectively. V contents indicate rather constant values fluctuating around 4.8 and 33.8 ppm for the two digestion methods, respectively. Mo behaves in the same way and remains more or less constant with relatively low values.

In this section, the RSTE behaviours are preserved when Al-normalized as shown in Fig. B.5. No correlations are observed between the presented RSTE.

B.5 Discussion

B.5.1 Comparison between the three sections

The RSTE show different distributions in the three time-equivalent sections. In Gorgo a Cerbara, pronounced peaks in RSTE contents characterize the Livello Selli. These RSTE enrichments are coeval with the highest TOC values measured along the section (Fig. 4). In contrast, in the other two sections, Cu, V and Mo do not show significant enrichments and correlatable trends during the positive carbon-isotope excursion, except for a short-lived increase in Cu and V contents at the base of the Goguel level in Glaise. In these sections, TOC values are generally low, with an average value of approximately 0.5 wt%. The Goguel level at Glaise is characterized by somewhat higher TOC contents with values reaching ~2 wt%. (Fig. B.4).

The different pattern in RSTE distribution in the sections representing different paleogeographic settings suggests different redox conditions during the OAE 1a interval. This is discussed in more details in Westermann et al. (in prep) and is summarized here in the following. In the deep basin (Gorgo a Cerbara), the strong enrichments in RSTE are well correlated with high TOC values and the presence of laminated layers. This is related to phases of strong oxygen depletion in the bottom water. In the shallower settings (Glaise and Cassis/La Bédoule), the absence of RSTE enrichments is explained by the presence of rather well oxygenated environments, characterized by oxic/dysoxic conditions (Westermann et al., in prep.). In Glaise, the weak increase at the base and the top of the Goguel level may be related to a rapid switch to more oxygen-depleted conditions at the onset and the end of the OAE 1a interval. But given the overall low TOC values along the two French sections, the reducing conditions did not exceed the dysoxic/anoxic threshold (Algeo and Maynard, 2004; Tribovillard et al., 2006).

B.5.2 Comparison of the two extraction methods

Cu, V and Mo contents obtained by two acid-extraction methods are compared to test the feasibility of the partial extraction method (HNO_3) relatively to the total extraction method (HF) applied to siliciclastic sediments. In the following, we will compare the general trends and provide an overview of the differences and similarities in RSTE behaviour.

In the Gorgo a Cerbara section, HNO_3 extracted Cu, V and Mo contents exhibit, as a whole, the same trends as Al-normalized HF extracted data. This especially true for V and Mo, and confirms that these HNO_3 extracted elements trace changes in redox conditions, independent of changes in the lithology (i.e., independent of the dissolution rate). The correlation between Cu_{HNO3} and Cu_{HF}/Al_{HF} is less clear, which may be related to the higher recovery rate of Cu by HNO_3 extraction (94.4%) and the possibility that Cu includes a significant detrital component. Al-normalized and unmodified Cu_{HF} contents show also a good correlation. This suggests that the HNO_3 extraction method provides a good approximation of Al-normalized data obtained by total acid digestion in sediments deposited under anoxic conditions.

In the Glaise section, the HNO_3-derived raw RSTE contents and the Al-normalized, HF-derived RSTE contents show comparable stratigraphic trends. However, in contrast to the Gorgo a Cerbara section, differences are observed in the trends of the raw data obtained by HF digestion. For example, HF-derived V contents show an overall decreasing trend along the section, whereas the HNO_3-derived V contents display two peaks (Fig. B.5). On the other hand, similarities in the stratigraphic evolution of V are observed, if we compare the HF-derived Al-normalized data with the HNO_3-derived raw data. Thus, as for anoxic environments, in sediments formed under dysoxic conditions, the HNO_3 extraction method appears to approximate redox-dependent variations in authigenic RSTE.

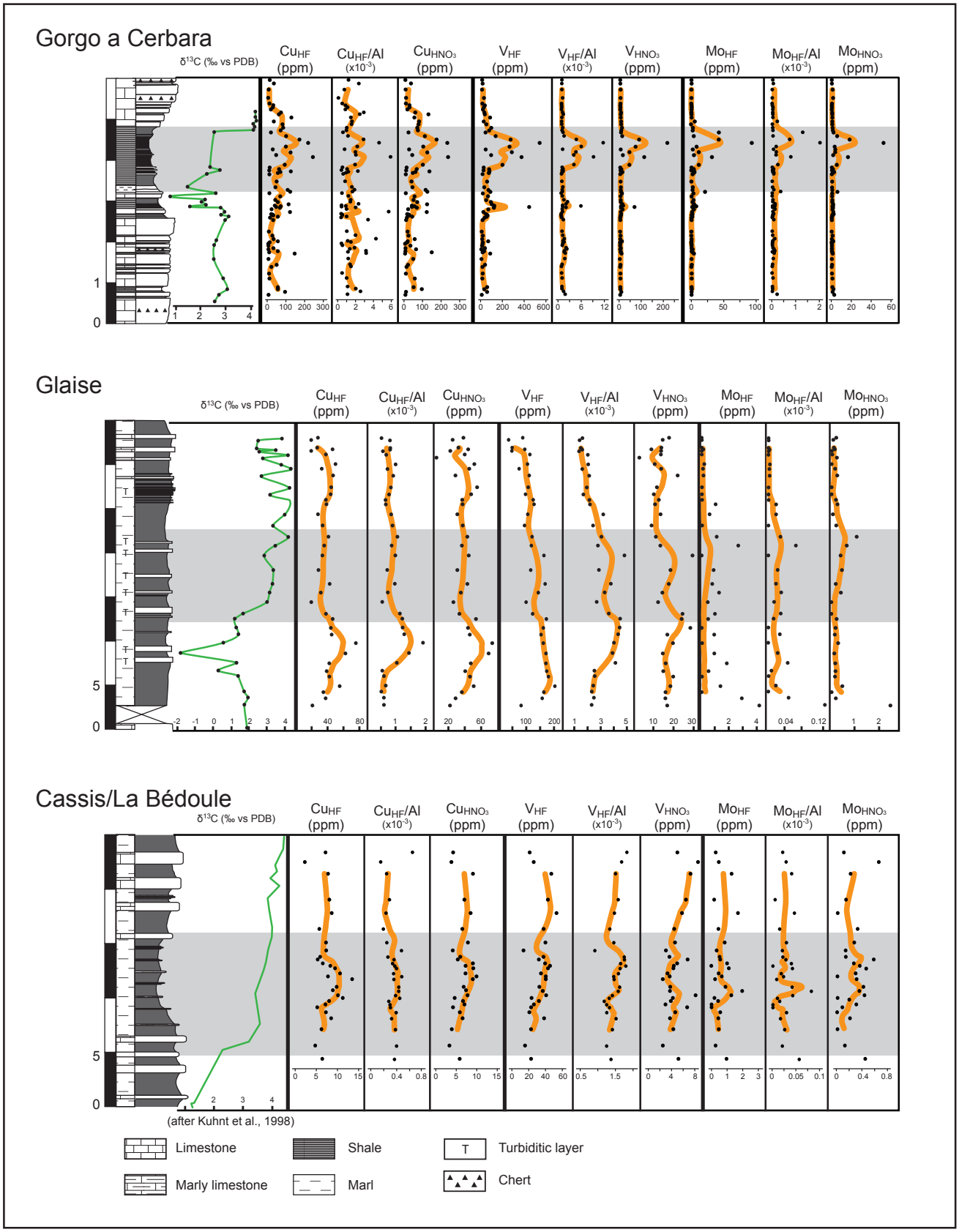

Fig. B.5: Distribution of Cu, V and Mo contents for the sections of Gorgo a Cerbara, Glaise and Cassis/La Bédoule. Unmodified data obtained by the HNO_3 and HF extraction methods are expressed in ppm. Al-normalized data are presented in units of 10^{-3}. The grey band indicates the positions of the Livello Selli and the Goguel level or its equivalent for each section.

In Cassis/La Bédoule, correlations between the trends obtained by both digestion methods and Al-normalized data are less clear. One explanation may be related to the general control of redox conditions on RSTE accumulation. The OAE 1a-related sediments of the Cassis/La Bédoule section apear to have experienced rather well oxygenated conditions in comparison to the other two sections. RSTE are highly insoluble under oxic conditions and tend to stay in the water column (Calvert and Perderson, 1993; Algeo and Maynard, 2004; Tribovillard et al., 2006), which may explain the much lower values in Cassis/La Bédoule in comparison to the sections of Gorgo a Cerbara and Glaise. In the range of these low values, the partial dissolution of siliciclastic material and the related recovery of RSTE by the HNO_3 digestion method may impact the total quantities measured, whereas in the section of Gorgo a Cerbara, the presence of RSTE enrichments with values up to 100 times higher than the average background level minimizes the importance of small background variations.

Similar observations are made for RSTE presented in Tables B.2 and B.3. U and Co appear to behave in the same way as V and Mo, whereas Ni, As and Cr contents follow the evolution of Cu. In summary, RSTE behaviour obtained by the nitric acid extraction method appears to provide a valid first approximation of Al-normalized data obtained by total extraction.

B.5.3 Al-normalization versus partial extraction

The major problem in using RSTE concentrations as paleoenvironmental proxy is to determine whether they are enriched or depleted. Commonly, the degree of RSTE enrichment or depletion is evaluated relative to its concentration in a reference material, which usually is average shale (Wedepohl, 1971, 1991: McLennan, 2001; Tribovillard et al., 2006). In addition to that, sediments and sedimentary rocks may have variable proportions of mineral phases that may dilute the RSTE abundance. In the marine environment, these phases are often represented by biogenic calcium carbonate and opal. In order to compare samples with variable carbonate and opal contents, normalization of RSTE with respect to Al is commonly performed, because in sedimentary systems Al is considered as an indicator of the aluminosilicate fraction, which remains largely immobile during diagenesis (Calvert and Perdersen, 1993; Morford and Emerson, 1999; Piper and Perkins, 2004; Tribovillard et al, 2006). Al-normalization is also useful to determine RSTE enrichment factors relative to the concentrations in average shale.

However, Van der Weijden (2002) demonstrated that Al-normalization may modify the RSTE distribution pattern by creating, increasing, decreasing or blurring correlations. This is most likely to occur when the variation coefficient (the standard deviation divided by the mean) of Al is large in comparison to other elements (Van der Weijden, 2002) and in sediments with very low amounts of detrital components (Kryc et al., 2003). This is, however, not the case in our study. In each section, the variation coefficient of Al shows low values relative to the other elements (Table 5). We also compare Al variations through the studied sections with Ti, which is another terrigenous element (Boyle, 1983; Shimmield et al., 1990; Shimmield and Mowhay, 1991; Yarincik et al., 2000). A good correlation between these two elements is observed at Gorgo a Cerbara (r^2 of 0.8, n=74) and Cassis/La Bédoule (r^2 close to 0.9, n=28). However, at Glaise, a discrepancy between Al and Ti is observed (r^2 of 0.4, n=34). This may be related a preferential removal of Ti as function of organic particulate removal processes under low reducing conditions (Kryc et al., 2003). This seems, therefore, to confirm that Al is mainly of terrigenous origin in the sections studied here.

If our interpretation is correct, then the nitric acid extraction method would provide a valid alternative to the total extraction method and Al-normalization for the study of redox variations in the marine environment. Despite variable dissolution rates throughout the studied sections, RSTE trends obtained by this extraction method show good correlations with Al-normalized RSTE trends obtained by HF extraction. All RSTE-enriched intervals were identified and the amplitudes of the RSTE enrichments were coherent with the Al-normalized HF-extracted data. However, the absolute values of HNO_3-derived RSTE contents cannot be compared to those obtained by HF-extracted RSTE contents, as is shown by our analysis of identical samples of the three OAE 1a-related sediments and of international standards. The interest of this simple, rapid, and low-risk method lies, therefore, in tracing stratigraphic variations in RSTE contents rather than in obtaining absolute RSTE values. The HNO_3 extraction works especially well for elements, which are directly precipitated in authigenic phases under anoxic conditions (i.e., U, V, Mo). For RSTE supplied by organic matter (e.g., Ni, Cu), the HNO_3 extraction method is sufficient to dissolve a representative fraction

(recovery rate of 94.4% on USGS standard SCo-1). In this case, however, the raw content data are not always reliable as is shown in Fig. B.5.

B.6 Conclusion

In this contribution, we analyzed RSTE contents in three representative sections covering the Early Aptian OAE 1a (Gorgo a Cerbara, central Italy; Glaise, Vocontian Through, SE France; Cassis/La Bédoule, SE France). We used two different RSTE extraction methods: the partial HNO_3 and the total HF/HNO_3/HCl extraction methods, in order to test the viability of the first method. We observe a rather poor correlation between the RSTE absolute quantities obtained by the two methods on the same samples, and a positive correlation between HNO_3–derived RSTE raw contents and HF-derived Al-normalized RSTE contents.

With the partial HNO_3 extraction method, we were able to retrace all RSTE enrichments detected by HF extraction. Therefore, with the partial HNO_3 extraction method, a valuable method is given for the assessment of paleoredox changes in marine environments, which is simple, rapid and less hazardous. This is especially true for elements, which precipitate in sediments as authigenic phases under anoxic conditions (e.g., U, V, Mo). For RSTE supplied win association with organic matter, the partial HNO_3 extraction method appears to transfer a representative fraction into solution and the thus obtained trends show similarities with unmodified data obtained by HF extraction. For these elements, normalization may then be required.

To complete our observations, a statistic analyse of each elemental behaviour obtained by both extraction methods under the different redox conditions will be done. Some samples will also be analysed with a “direct” method using X-ray fluorescence coupled with Laser Ablation ICP MS.

Acknowledgements

We thank Jean-Pierre Masse for having guided us through the Cassis/La Bédoule composite section, Stéphane Bodin and Alexis Godet for their help in the field and Tiffany Monnier for laboratory assistance on ICP MS measurements. We also thank Dr Niklaus Waber and Ruth Mäder for their advices and help in the laboratory during the hydrofluoric acid extraction. This research is supported by the Swiss National Science Foundation (Grants 200021-109514/1, 200020-121600).

	Al	Ti	V	Cr	Co	Ni	Cu	As	Mo	U
Gorgo a Cerbara	0.676	0.733	1.380	0.727	1.005	1.017	0.915	0.900	2.642	1.440
Glaise	0.370	0.404	0.412	0.373	0.366	0.305	0.365	0.600	1.507	0.335
Cassis/La Bédoule	0.267	0.221	0.300	0.278	0.335	0.230	0.282	0.420	0.796	0.218

Table B.5: Variation coefficients of for the studied elements in the sections of Gorgo a Cerbara, Glaise and Cassis/La Bédoule. The variation coefficient of Al shows low values relative to the other elements indicating that Al-normalization can be used in our study to avoid detrital dilution.

References

Abanda, P. A. and Hannigan, R. E. [2006] Effect of diagenesis on trace element partitioning in shales. Chemical Geology 230, 42-59.

Algeo, T. J. and Lyons, T. [2006] Mo–total organic carbon covariation in modern anoxic marine environments: Implications for analysis of paleoredox and paleohydrographic conditions. Paleoceanography 21(PA1016).

Algeo, T. J. and Maynard, J. B. [2004] Trace-element behavior and redox facies in core shales of Upper Pennsylvanian Kansas-type cyclothems. Chemical Geology 206, 289-318.

Algeo, T. J. and Maynard, J. B. [2008] Trace-metal covariation as a guide to water-mass conditions in ancient anoxic marine environments Geosphere 5, 872-887.

Anarboldi, M. and Meyers, P. A. [2007] Trace element indicators of increased primary production and decreased water-column ventilation during deposition of latest Pliocene sapropels at five locations across the Mediterranean Sea. Palaeogeography, Palaeoclimatology, Palaeoecology 249, 425-443.

Arthur, M. A., Jenkyns, H. C., Brumsack, H.-J. and Schlanger, S. O., [1990] Stratgraphy, geochemistry, and paleoceanography of organic-carbon rich Cretaceous sequences, *in* R. N. Ginsburg and B. Beaudoin: Cretaceous Research, Events and Rhythms, Kluwer Acad., Norwell, 75-119.

Barling, J., Arnold, G. L. and Anbar, A. D. [2001] Natural mass-dependent variations in the isotopic composition of molybdenum. Earth and Planetary Science Letters 193, 447-457.

Bayon, G., German, C.R., Boella, R. M., Milton, J. A., Taylor, R. N. and Nesbitt, R. W. [2006] An improved method for extracting marine sediment fractions and its application to Sr and Nd isotopic analysis. Chemical Geology, 187, 179-199.

Bayon, M. M., Alonso, J. I. G., Medel, A. S. [1998] Enhanced semiquantitative multi-analysis of trace elements in environmental samples using inductively coupled plasma mass spectrometry. Journal of Analitical Atomic Spectrometry 13, 277-282.

Behar F., Beaumont V. and Penteado H. L. D. [2001] Rock-Eval 6 technology: performances and developments. Oil Gas Science Technology 56, 111–134

Bodin, S., Godet, A., Matera, V., Steinmann, P., Vermeulen, J., Gardin, S., Adatte, T., Coccioni, R. and Föllmi, K. B. [2006] Enrichment of redox-sensitive trace metals (U, V, Mo, As) associated with the late Hauterivian Faraoni oceanic anoxic event. International Journal of Earth Sciences 96, 327-341.

Böning, P., Brumsack, H.-J., Böttcher, M. E., Schnetger, B., Kriete, C., Kallmeyer, J. and Borchers, S. L. [2004] Geochemistry of Peruvian near-surface sediments. Geochimica et Cosmochimica Acta 68, 4429-4451.

Bréhéret, J.-G. [1997] L'Aptien et l'Albien de la Fosse vocontienne (des bordures au bassin). Evolution de la sédimentation et enseignements sur les événements anoxiques. Société géologique du Nord, 614 p.

Brumsack, H.J. [1989] Geochemistry of recent TOC-rich sediments from the Gulf of California and the Black Sea. Geol. Rundsch. 78, 851–882.

Calvert, S. E. and Pedersen, T. F. [1993] Geochemistry of recent oxic and anoxic marine sediments: Implications for the geological record. Marine Geology 113, 67-88.

Coccioni, R., Erba, E. and Premoli-Silva, I. [1992] Barremian-Aptian calcareous plankton biostratigraphy from the Gorgo a Cerbara section (Marche, central Italy) and implications for plankton evolution. Cretaceous Research 13, 517-537.

Crusius, J., Calvert, S. E., Pedersen, T. F. and Sage, D. [1996] Rhenium and molybdenum enrichments in sediments as indicators of oxic, suboxic and sulfidic conditions of deposition Earth and Planetary Science Letters 144, 65-78.

Dean, W. E., Gardner, J. V. and Piper, D. Z. [1997] Inorganic geochemical indicators of glacial-interglacial changes in productivity and anoxia on the California continental margin. Geochimica et Cosmochimica Acta 61, 4507-4518.

Espitalié, J., Deroo, G. and Marquis, F. [1985] La pyrolyse Rock-Eval et ses applications. Revue de l'Institut Français du Pérole 40, 563-579.

Flanagan, F.J. [1976] Descriptions and Analyses of Eight New USGS Rock Standards, U.S. Geological Survey Professional Paper 840, 192p.

Huerta-Diaz, M. A. and Morse, J. W. [1992] Pyritization of trace metals in anoxic marine sediments. Geochimica et Cosmochimica Acta 56, 2681-

2702.

Jenkyns, H. C. and Wilson, P. A. [1999] Stratigraphy, paleoceanography, and evolution of Cretaceous pacific guyots: Relics from a greenhouse earth. American Journal of Science 299, 341-392.

Jitaru, P., Tirez, K. and De Brucker, N. [2003] Panoramic analysis for monitoring trace metals in natural waters by ICP-MS. Atomic Spectrometry 24, 1-10.

Jones, B. and Manning, A. C. [1994] Comparison of geochemical indices used for the interpretation of palaeoredox conditions in ancient mudstones. Chemical Geology 111, 111-129.

Kolonic, S., Wagner, T., Forster, A., Sinnighe Damsté, J. S., Walsworth-Bell, B., Erba, E., Turgeon, S., Brumsack, H.-J., Chellai, E. H., Tsikos, H., Kuhnt, W. and Kuypers, M. M. M. [2005] Black shale deposition on the northwest African Shelf during the Cenomanian/Turonian oceanic anoxic event: Climate coupling and global organic carbon burial. Paleoceanography 20(PA1006).

Kryc, K. A., Murray, R. W. and Murray, D. W. [2003] Al-to-oxide and Ti-to-organic linkages in biogenic sediment: relationships to paleo-export production and bulk Al/Ti Earth and Planetary Science Letters 211, 125-141.

Lipinski, M., Warning, B. and Brumsack, H.-J. [2003] Trace metal signatures of Jurassic/Cretaceous black shales from the Norwegian Shelf and the Barents Sea. Palaeogeography, Palaeoclimatology, Palaeoecology 190, 459-475.

McKay, J. L., Pederson, T. F. and Mucci, A. [2007] Sedimentary redox conditions in continental margin sediments (N.E. Pacific) — Influence on the accumulation of redox-sensitive trace metals. Chemical Geology 238, 180-196.

McLennan, S.M. [2001] Relationships between the trace element composition of sedimentary rocks and upper continental crust. Geochemistry Geophysics Geosystems 2 (paper # 2000GC000109).

Méhay, S., Keller, C.E., Bernasconi, S.M., Weissert, H., Erba, E., Bottini, C. and Hochuli, P.A. [2009] A volcanic CO_2 pulse triggered the Cretaceous oceanic anoxiv event 1a and a biocalcification crisis. Geology 37, 819-822.

Morford, J. L. and Emerson, S. R. [1999] The geochemistry of redsox sensitive trace metal in sediments. Geochimica et Cosmochimica Acta 63, 1735-1750.

Morford, J. L., Emerson, S. R., Breckel, E. J. and Kim, S. H. [2005] Diagenesis of oxyanions (V, U, Re, and Mo) in pore waters and sediments from a continental margin. Geochimica et Cosmochimica Acta 69, 5021-5032.

Morford, J. L., Ruffell, A. D. and Emerson, S. R. [2001] Trace metal evidence for changes in the redox environment associated with the transition from terrigenous clay to diatomaceous sediment, Saanich Inlet, BC. Marine Geology 174, 355-369.

Moullade, M., Kuhnt, W., Bergen, J. A., Masse, J.-P. and Tronchetti, G. [1998] Correlation of biostratigraphic and stable isotope events in the Aptian historical stratotype of La Bédoule (SE France). C. R. Académie des sciences, Paris, Sciences de la terre et des planètes 327, 693-698.

Pancost, R. D., Crawford, N., Magness, S., Turner, A., Jenkyns, H. C. and Maxwell, J. R. [2004] Further evidence for the development of photic-zone euxinic conditions during mesozoic oceanic anoxic events. Jounal of the geological Society of London 161, 353-364.

Piper, D.Z. and Perkins, R.B. [2004] A modern vs. Permian black shale - the hydrography, primary productivity, and water-column chemistry of deposition. Chemical Geology 206, 177–197.

Quezada-Hinojosa, R., Matera, V., Adatte, T., Rambeau, C. and Föllmi, K. B. [2009] Cadium distribution in soils covering Jurassic oolitic limestone with high Cd contents in the Swiss Jura. Geoderma, 150, 287-301.

Riquier, L., Tribovillard, N., Averbuch, O., Devleeschouwer, X. and Riboulleau, A. [2006] The late Frasnian Kellwasser horizons of the Harz Mountains (Germany): Two oxygen-deficient periods resulting from different mechanisms. Chemical Geology 233, 137-155.

Robinson, S. A., Williams, T. and Bown, P. R. [2004] Fluctuations in biosiliceous production and the generation of Early Cretaceous oceanic anoxic events in th ePacific Ocean (Shatsky Rise, Ocean Drilling Program Leg 198). Paleoceanography 19 (doi:10.1029/2004PA001010).

Siebert, C., McManus, J., Bice, A., Poulson, R. L. and Berelson, W. M. [2006] Molybdenum isotope signatures in continental margin marine sediments. Earth and Planetary Science Letters 241, 723-733.

Shimmield, G.B. and Pedersen, T.F. [1990] The

geochemistry of reactive trace metals and halogenes in hemipelagic continental margin sediments. Aquatic Science 3, 255–279.

Snow, L. J., Duncan, R. A. and Bralower, T. J. [1976] Trace element abundances in the Rock Canyon Anticline, Pueblo, Colorado, marine sedimentary section and their relationship to Caribbean plateau construction and ocean anoxic event 2. Paleoceanography 20, PA3005.

Soon, Y. K. and Abboud, S. [1993] Cadmium, chromium, lead, and nickel. In: M.R. Carter, Editor, Soil Sampling and Methods of Analysis, Canadian Society of Soil Science, 101–107.

Tribovillard, N., Riboulleau, A., Lyons, T. and Baudin, F. [2004] Enhanced trapping of molybdenum by sulfurized marine organic matter of marine origin Mesozoic limestones and shales. Chemical Geology, 213, 385-401.

Tribovillard, N., Algeo, T. J., Lyons, T. W. and Riboulleau, A. [2006] Trace metals as paleoredox and paleoproductivity proxies : An update. Chemical Geology 232, 12-32.

Van der Weijden, C. [2002] Pifalls of normalization of marine geochemical data using a common divisor. Marine Geology 184, 167-187.

Wedepohl, K.H. [1971] Environmental influences on the chemical composition of shales and clays. In: Ahrens, L.H., Press, F., Runcorn, S.K., Urey, H.C. (Eds.), Physics and Chemistry of the Earth. Pergamon, Oxford, pp. 305–333.

Wedepohl, K.H. [1991] The composition of the upper Earth's crust and the natural cycles of selected metals. In: Merian, E. (Ed.), Metals and their Compounds in the Environment. VCH-Verlagsgesellschaft, Weinheim, pp. 3–17.

Westermann, S., Matera, V., Fiet, N., Fleitmann, D., Stein M., Adatte, T. and Föllmi K. B. The evolution of redox conditions during the Early Aptian oceanic anoxic event (OAE 1a) in the Western Tethys, *in preparation for submission in Palaeogeography, Palaeoclimatology, Palaeoecology*.

Yarincik, K. M., Murray, R. W. and Peterson, L. C. [2000] Climatically Sensitive Eolian and Hemipelagic Deposition in the Cariaco Basin, Venezuela, Over the Past 578,000 Years: Results From Al/Ti and K/Al. Paleoceanography 15, 210-228.

Table B.2: RSTE contents (in ppm) in the three studied sections obtained by the nitric acid extraction method.

Gorgo a Cerbara

Samples ID	Sol(%)	Al	V	Cr	Co	Ni	Cu	As	Mo	U
GC 110	91.03	121 1.3	3.1	5.9	4.1	20.9	6.5	4.1	0.2	0.5
GC 111	63.69	12833.4	10.1	31.3	9.3	54.2	100.7	5.4	0.2	0.5
GC 112	70.99	4023.3	3.5	7.7	8.5	39.4	54.3	1.5		0.2
GC 113	52.54	11678.0	3.9	16.6	10.2	54.3	60.8	1.8		0.3
GC 114	85.65	1957.8	3.2	7.4	2.0	14.8	7.8	2.7		0.2
GC 115	78.93	2138.5	2.2	4.9	2.1	16.7	10.0	0.2		0.2
GC 116	83.61	2358.7	2.9	6.3	2.4	17.4	22.7	1.1		0.3
GC 117	64.08	9636.3	5.4	12.9	12.9	33.7	52.2	1.9		0.5
GC 118	92.35	718.5	1.4	3.4	2.4	14.1	4.5	0.2	0.1	0.5
GC 119	58.84	10494.6	11.4	20.3	47.3	128.6	150.2	12.4	0.4	1.3
GC 120	91.24	1933.4	5.1	5.7	3.7	19.3	8.3	0.5	0.1	0.9
GC 121	78.77	2807.0	6.3	10.7	8.8	55.6	66.1	4.0	0.1	0.9
GC 122	92.72	731.4	2.2	3.3	2.4	15.6	5.7	0.0		1.2
GC 123	80.34	2825.2	8.1	7.2	7.5	27.8	38.7	1.6		0.7
GC 124	86.62	1754.6	3.1	5.0	2.4	18.9	6.4	0.0		1.2
GC 125	85.61	1917.5	2.9	4.4	1.9	16.8	7.5	0.4		0.6
GC 126	88.84	983.1	2.6	3.6	3.6	16.2	14.2	0.2		0.3
GC 127	52.83	18434.9	12.6	28.0	15.9	54.9	58.3	2.0		1.0
GC 128	87.82	1446.2	3.6	5.0	15.9	41.9	33.4	1.5		0.4
GC 129	82.46	3210.5	4.3	8.3	1.8	16.0	23.7	0.9		0.3
GC 130	86.57	1165.5	1.5	2.5	1.5	15.5	7.9	0.4		0.2
GC 131	81.18	1614.6	2.6	3.3	7.9	28.1	34.9	1.2		0.2
GC 132	59.89	9597.6	3.6	9.1	6.4	44.9	14.5	1.8		0.3
GC 133	48.54	15223.1	4.2	17.0	8.5	43.2	51.8	1.8		0.3
GC 134	41.02	17386.0	3.8	16.3	9.3	44.9	31.6	3.2		0.4
GC 135	43.62	12620.0	3.5	14.1	8.4	44.5	29.0	2.2		0.4
GC 136	47.74	13176.2	3.3	13.1	4.4	30.6	21.0	1.8		0.4
GC 137	63.43	5132.4	5.8	10.1	21.8	53.2	127.2	2.2	0.8	0.5
GC 138	44.83	3188.3	2.7	5.6	7.5	16.5	23.0	1.2	0.1	0.6
GC 139	61.75	11280.3	13.5	19.6	46.4	118.6	72.0	7.9	0.8	1.1
GC 140	16.78	28690.8	7.7	17.9	17.4	52.2	43.1	2.3	0.0	1.8
GC 141	24.69	22570.5	69.5	41.6	46.3	180.1	72.1	14.0	1.5	3.3
GC 142	20.01	24026.2	6.5	15.0	9.5	46.0	39.2	2.3	0.1	2.0
GC 143	45.55	17309.2	23.1	32.5	45.2	165.3	125.6	11.4	1.3	2.0
GC 144	45.67	14636.3	22.5	23.4	47.7	146.5	68.4	10.4	1.0	1.4
GC 145	50.22	9564.6	7.8	11.0	12.8	42.5	51.5	3.2	0.1	0.5
GC 146	12.74	23286.8	8.8	15.6	10.2	36.7	72.8	2.8	0.7	0.5
GC 147	13.86	5412.6	3.9	3.6	3.3	15.8	11.2	1.1	0.1	0.1
GC 148	15.91	40520.9	15.6	45.0	12.6	46.5	124.0	1.3	0.2	0.5
GC 149	16.16	20202.7	8.1	12.0	9.7	30.0	119.9	3.1	5.9	1.7
GC 150	16.61	11023.5	6.8	7.1	2.8	10.7	45.2	2.0	0.4	0.2
GC 151	13.22	21962.5	7.6	14.2	5.2	33.6	50.7	0.6	0.2	0.3
GC 152	24.60	3589.6	3.5	1.5	1.4	8.7	9.8	0.7	0.1	0.1
GC 153	12.61	27434.5	10.6	19.6	6.9	33.8	60.5	1.5	0.4	0.4
GC 154	7.17	34470.9	19.3	25.0	11.2	77.2	77.0	3.4	1.6	0.4
GC 155	17.08	20514.6	10.7	16.7	11.0	48.2	138.9	4.8	1.3	0.6
GC 156	7.00	2663.3	2.6	3.1	8.8	17.0	9.8	2.3	0.1	0.1
GC 157	9.91	13640.7	6.6	10.2	11.0	40.4	63.6	3.1	0.8	0.4
GC 158	7.43	2464.0	2.1	2.1	9.5	23.0	11.6	2.4	0.1	0.2
GC 159	25.31	16495.6	45.4	27.7	48.0	157.0	100.3	12.1	6.1	3.5
GC 160	35.86	12890.4	115.7	27.0	21.9	186.0	245.0	14.3	16.2	13.6
GC 161	16.93	7096.8	14.8	3.5	10.4	44.6	47.9	3.7	0.7	0.5
GC 162	20.68	14004.4	46.7	24.6	24.9	114.6	126.9	7.9	2.6	2.6
GC 163	20.31	7853.3	4.0	6.9	2.2	9.5	27.0	4.7	0.1	0.5
GC 164	21.56	16684.2	72.7	41.4	10.6	92.8	101.5	6.9	3.1	3.6
GC 165	36.73	21507.2	216.9	44.3	82.1	397.6	236.2	23.5	51.6	14.7
GC 166	31.75	25129.5	86.9	35.7	42.0	169.2	175.9	20.1	17.3	8.2
GC 167	13.69	2441 1.5	10.8	19.6	23.5	55.5	107.9	4.7	0.1	1.2
GC 168	7.37	10543.3	5.7	7.2	7.4	24.7	19.7	3.6		0.4
GC 169	19.38	21186.3	6.5	15.7	9.4	42.8	71.9	3.6		0.7
GC 170	16.70	30547.2	8.7	24.8	25.1	120.6	86.6	5.1		0.6
GC 171	50.62	12661.2	7.0	10.6	14.7	48.8	77.7	4.4		0.3
GC 172	35.61	19697.9	6.4	15.2	15.6	52.7	86.2	10.6		0.5
GC 173	56.34	10838.4	4.2	8.3	30.9	69.1	51.3	9.8	0.1	0.5
GC 174	25.98	28325.9	4.3	12.4	50.7	173.6	133.7	10.7		0.4
GC 175	57.73	12487.5	6.0	6.7	4.9	28.3	66.8	3.4		0.2
GC 176	56.28	4865.8	2.1	4.8	3.9	24.5	18.0	1.9		0.2
GC 177	54.57	13358.2	4.0	7.6	4.6	31.3	27.6	1.9		0.2
GC 178	52.30	12061.6	2.9	5.4	4.3	30.7	28.6	3.1		0.2
GC 179	56.79	4803.6	2.8	4.6	3.6	18.8	9.7	0.8		0.2
GC 180	75.82	2312.6	1.8	3.8	1.8	12.1	6.7	0.0		0.1
GC 181	71.90	10268.7	3.5	5.5	21.8	41.7	39.7	0.1		0.3
GC 182	55.36	4352.6	2.4	2.7	13.0	17.7	7.9	2.8	0.1	0.6
GC 183	68.53	5779.1	2.8	3.5	3.9	16.9	13.4	0.6		0.2

Table B.2 (continued): RSTE contents (in ppm) in the three studied sections obtained by the nitric acid extraction method.

Glaise

Samples ID	Sol(%)	Al	V	Cr	Co	Ni	Cu	As	Mo	U
GL 2	44.97	6018.6	17.0	9.8	8.7	40.9	18.8	6.8	2.5	0.9
GL 3	16.55	7617.9	16.0	13.7	9.6	37.5	25.5	5.0	0.2	0.4
GL 4	11.37	8350.9	16.1	18.0	10.0	43.6	34.0	3.7	0.0	0.3
GL 5	11.18	9016.5	18.5	19.4	12.8	36.0	49.2	4.7	0.5	0.1
GL 6	15.77	9201.7	19.9	18.2	12.7	55.6	45.2	5.5	0.2	0.2
GL 7	8.33	8658.3	15.0	18.0	8.1	41.2	38.7	4.4	0.2	0.2
GL 8	9.38	8626.4	16.2	17.3	12.4	48.5	46.0	5.7	0.2	0.1
GL 9	8.28	8210.0	14.8	15.9	7.9	38.3	69.2	3.1	0.1	0.2
GL 10	11.95	10255.0	19.8	21.9	9.4	41.9	73.9	3.7	0.3	0.2
GL 11	18.97	8059.9	17.1	17.8	11.9	63.7	44.9	4.0	0.2	0.4
GL 12	19.24	10322.4	28.4	23.2	14.3	72.0	42.0	10.0	0.2	0.6
GL 13	15.43	9309.6	24.2	20.9	10.7	68.6	52.8	4.8	0.2	1.0
GL 14	28.20	11069.2	24.6	22.7	10.3	44.1	31.4	6.6		0.8
GL 15	25.19	8904.0	12.5	16.8	10.1	31.4	23.2	3.7		0.3
GL 16	20.76	8048.6	14.5	14.3	9.2	38.7	32.7	7.1	0.4	0.4
GL 17	17.01	8259.4	17.7	18.4	8.8	47.6	41.5	5.3	0.2	0.3
GL 18	24.99	10578.2	18.6	19.9	13.4	48.2	28.1	6.7	0.4	0.5
GL 19	18.13	10727.9	29.6	23.0	8.5	53.5	43.1	5.6	0.4	0.6
GL 20	24.32	7495.3	13.6	15.8	6.8	58.3	34.2	5.5	0.7	0.6
GL 21	19.30	7379.5	11.3	12.0	13.8	75.3	41.4	9.8	1.1	0.4
GL 22	31.43	6580.3	9.3	11.8	7.0	33.2	35.7	2.3	0.2	0.5
GL 23	26.40	8307.4	13.6	16.2	4.1	27.6	28.2	1.7		0.3
GL 24	8.03	6306.9	10.9	11.0	7.4	32.0	35.2	3.9	0.3	0.4
GL 25	24.17	7010.8	12.8	14.4	8.7	55.1	34.7	3.5	0.2	0.3
GL 26	38.32	6299.7	10.2	13.4	6.3	31.7	46.2	1.1		0.4
GL 27	33.28	7101.8	11.8	12.3	14.1	79.7	54.2	7.2		0.7
GL 28	55.80	8650.5	22.2	17.9	6.4	33.5	26.0	3.1	0.3	0.7
GL 29	36.28	7057.7	14.0	14.4	8.9	53.2	44.2	3.9	0.2	0.6
GL 30	37.72	6016.6	10.8	12.6	9.1	38.6	50.7	3.6		0.5
GL 32	35.20	7442.9	13.8	14.1	6.5	36.6	37.8	2.1	0.0	0.4
GL 33	73.07	5808.0	13.8	9.9	4.4	27.9	19.2	0.9		0.5
GL 34	49.70	5008.4	9.2	9.2	9.9	49.8	42.6	2.9	0.2	0.8
GL 35	73.23	5200.3	14.1	8.7	5.4	34.1	29.8	2.0	0.1	0.7
GL 36	77.52	5268.3	14.8	9.5	2.7	27.0	22.3	1.6		0.5
GL 37	50.52	8446.9	18.4	16.7	7.7	46.3	36.3	3.1	0.2	0.6

Cassis/La Bédoule

Samples ID	Sol(%)	Al	V	Cr	Co	Ni	Cu	As	Mo	U
BE 147*	88.14	2699.9	5.2	5.5	5.3	26.3	5.9	3.9	0.4	2.0
BE 149	90.02	1227.5	2.6	4.0	3.5	17.8	3.5	1.4	0.1	1.8
BE 151	86.42	1817.9	4.2	4.0	2.3	19.9	4.0	2.7		1.7
BE 152a1	79.31	2277.0	3.8	4.7	1.8	24.8	6.2	3.0	0.2	2.2
BE 152a2	86.27	2167.3	4.5	4.3	2.6	19.0	5.9	2.1		1.7
BE 152a3	94.82	3068.8	6.6	7.0	1.2	16.7	4.2	2.4	0.1	1.9
BE 152b1	66.51	1893.3	3.2	3.7	3.0	26.8	7.1	3.7	0.3	2.2
BE 152b2	66.93	2847.3	4.0	5.1	3.8	38.9	6.7	4.0	0.2	1.9
BE 152b3	83.65	2072.0	4.1	3.5	3.3	24.2	4.8	1.5		1.7
BE 153a1	73.65	5211.4	8.1	10.2	4.9	35.4	7.7	4.4	0.4	1.9
BE 153a2	74.21	2849.8	3.9	5.7	3.8	23.8	7.4	2.6	0.4	1.6
BE 153b1	76.72	2314.1	3.7	4.5	3.5	22.5	6.9	3.3	0.4	1.7
BE 153b2	69.58	3273.2	2.7	4.4	4.5	21.7	9.1	1.5	0.3	1.6
BE 153b3	67.23	3914.1	3.7	5.5	4.7	23.3	9.7	3.6		1.3
BE 154a	73.66	2530.4	3.4	4.0	4.5	25.6	7.3	4.1	0.3	1.0
BE 154b	81.57	3434.8	4.3	5.4	6.4	30.3	9.2	5.2	0.5	1.1
BE 155a	77.16	3358.2	4.5	6.3	5.2	26.7	7.4	3.1	0.4	1.3
BE 155b	69.97	3830.8	5.0	7.2	5.0	26.8	9.0	3.6	0.3	1.0
BE 156a	78.04	3635.3	6.8	8.1	3.9	28.0	5.4	3.8	0.6	1.1
BE 156b	73.61	2102.8	3.7	5.2	3.9	31.0	6.1	3.9	0.1	1.7
BE 156e	77.43	1993.9	3.1	4.3	3.2	18.2	4.2	2.7	0.1	1.0
BE 157c	69.17	2232.4	4.6	4.7	3.3	29.9	7.8	3.0	0.3	1.7
BE158a	60.90	2602.9	4.5	5.3	2.8	24.8	6.5	2.7	0.3	1.7
BE 159b	56.33	2829.5	5.7	6.8	3.6	34.5	8.5	3.6		1.8
BE 161a	64.34	2953.1	6.6	6.9	2.8	40.5	7.0	2.9	0.1	1.9
BE 163a	64.21	3627.2	7.2	7.6	4.0	42.6	9.1	3.2	0.2	1.5
BE 164a	69.86	2372.1	8.6	6.0	1.8	18.9	3.8	3.6	0.7	1.6
BE 164c	68.86	1343.9	4.9	4.6	1.2	14.8	4.3	1.2	0.1	1.7

Table B.3: RSTE contents (in ppm) in the three studied sections obtained by the hydrofluoric acid extraction method.

Gorgo a Cerbara

Samples ID	Al	Ti	V	Cr	Co	Ni	Cu	As	Mo	U
GC 110	3933.9	538.5	7.3	6.6	3.9	18.1	4.4	0.9	0.9	0.6
GC 111	36016.6	1795.8	52.3	79.7	11.6	57.4	92.9	2.1	0.9	0.9
GC 112	27193.5	1356.8	28.9	32.2	9.5	40.0	55.6	2.5	0.5	0.6
GC 113	52161.3	2341.6	55.3	65.7	13.6	61.3	59.4	1.9	0.7	1.2
GC 114	9862.7	750.8	11.3	11.8	2.2	14.7	10.1	0.3	0.4	0.4
GC 115	16254.0	890.8	15.9	20.3	3.2	20.1	8.4	0.7	0.2	0.5
GC 116	14345.6	893.0	14.0	15.5	3.2	18.9	21.5	1.0	0.4	0.7
GC 117	35172.1	1732.6	38.9	46.4	14.8	41.0	49.5	3.2	1.0	1.6
GC 118	3309.7	603.4	5.8	7.8	2.1	13.9	3.9	0.4	0.2	0.6
GC 119	45162.6	2163.4	84.2	70.1	50.0	133.1	145.2	10.1	4.0	3.0
GC 120	8111.1	653.5	13.4	10.1	4.1	21.0	9.5	0.7	0.3	1.0
GC 121	17311.2	1064.9	29.3	28.7	9.1	53.6	55.0	5.0	2.0	1.4
GC 122	3322.6	581.7	7.8	6.4	2.4	15.4	4.6	0.7	0.3	1.2
GC 123	16794.3	969.7	35.2	23.7	7.3	28.0	31.8	1.9	0.6	1.0
GC 124	9645.4	711.9	10.7	8.2	2.5	14.8	5.2	0.7	0.2	1.2
GC 125	10389.0	664.7	13.6	31.8	2.2	20.6	4.7	0.5	0.3	0.7
GC 126	7338.5	615.2	11.1	5.9	3.9	17.0	11.0	0.8	0.2	0.5
GC 127	47687.5	2423.8	65.5	62.7	17.2	54.5	55.4	1.7	0.5	2.0
GC 128	7082.4	628.1	11.5	19.6	14.9	42.2	30.5	1.6	0.9	0.5
GC 129	12184.7	828.8	14.5	17.8	2.2	16.7	24.5	0.8	0.1	0.5
GC 130	5985.6	607.4	6.5	6.6	1.7	15.0	6.2	0.5	0.0	0.4
GC 131	8805.3	640.1	11.7	9.7	7.6	27.6	30.1	1.7	0.6	0.3
GC 132	33870.6	1624.4	33.0	39.1	8.7	49.2	13.9	2.7	0.5	0.9
GC 133	54448.6	2512.6	53.0	66.0	12.4	54.3	54.5	2.4	0.9	1.3
GC 134	64948.2	4403.5	59.0	67.1	14.0	54.2	33.8	5.6	1.0	1.6
GC 135	59933.5	2510.4	55.5	69.5	11.8	51.2	28.6	3.3	1.4	1.4
GC 136	53881.5	2364.3	47.9	53.9	7.7	38.1	20.5	2.7	0.5	1.4
GC 137	21026.0	1055.5	25.3	27.3	21.8	55.8	120.2	3.1	1.2	1.0
GC 138	21262.0	975.2	25.1	25.5	8.4	20.5	21.7	3.1	0.8	1.2
GC 139	32294.9	1564.6	68.5	71.6	44.7	121.1	64.8	8.7	4.4	2.2
GC 140	99792.7	6599.8	119.8	86.1	20.7	61.1	45.4	5.3	2.4	4.9
GC 141	74820.9	3231.2	443.7	152.9	48.4	184.3	70.6	16.6	8.0	5.7
GC 142	97775.4	6293.2	122.1	81.0	12.8	57.2	40.1	5.1	3.4	5.2
GC 143	47640.5	1915.2	100.2	84.1	42.3	149.8	112.3	11.4	6.3	3.1
GC 144	38949.2	1700.1	92.5	59.5	39.7	124.5	55.6	8.9	4.5	2.5
GC 145	28848.4	1374.9	43.9	31.2	11.6	36.1	42.7	4.7	1.6	1.2
GC 146	57071.6	2157.2	65.1	51.0	10.4	38.2	68.3	3.3	2.7	1.5
GC 147	17223.6	548.1	14.8	12.7	3.1	15.0	8.7	2.1	0.6	0.5
GC 148	73366.6	4023.2	85.1	93.8	13.8	51.1	120.2	2.4	3.0	1.6
GC 149	57138.6	2110.6	69.9	48.0	11.5	35.8	108.1	4.8	21.6	2.7
GC 150	26535.4	1038.1	33.2	21.7	3.0	11.6	42.5	3.5	1.9	0.7
GC 151	55660.4	2008.8	56.9	46.1	6.5	39.2	49.0	2.6	1.8	1.2
GC 152	12213.4	403.6	12.7	9.1	1.6	8.3	7.7	2.3	0.6	0.4
GC 153	62190.5	2322.1	71.2	60.1	8.0	38.7	57.5	3.0	3.7	1.6
GC 154	59450.4	3195.5	74.5	52.1	11.2	77.8	69.7	4.1	5.3	1.6
GC 155	54333.5	1985.2	76.9	47.7	10.4	48.2	123.5	4.0	4.8	1.5
GC 156	18754.8	579.3	21.3	12.4	6.8	15.9	8.4	3.3	0.8	0.5
GC 157	57985.0	3164.2	75.6	48.1	11.8	45.6	61.8	3.7	4.5	1.7
GC 158	18967.8	638.8	21.1	14.2	9.4	27.1	10.5	3.4	0.5	0.6
GC 159	47806.3	1921.0	198.2	78.1	43.6	157.5	93.5	8.3	11.5	4.7
GC 160	40705.2	1666.4	374.6	77.7	21.6	195.7	242.2	11.2	31.9	16.5
GC 161	21781.6	626.4	89.5	35.5	10.2	51.6	44.8	4.5	3.7	1.2
GC 162	61627.3	2446.7	284.5	103.1	23.4	114.9	123.9	6.9	11.9	4.7
GC 163	35344.6	1168.2	43.5	31.8	2.8	12.1	27.3	5.1	2.1	1.6
GC 164	43290.3	1660.8	262.1	107.7	10.4	87.6	95.8	6.5	7.9	5.2
GC 165	46196.5	1701.3	540.5	93.3	72.5	370.9	214.2	17.0	94.0	17.1
GC 166	57913.2	2060.4	272.6	86.0	42.8	160.9	169.5	16.6	42.9	10.2
GC 167	84216.0	2969.2	135.1	78.5	25.0	58.2	99.3	6.7	3.7	4.1
GC 168	32434.7	1031.8	42.5	28.4	8.4	26.8	19.7	4.5	42.5	1.5
GC 169	70760.8	2400.9	75.0	57.9	11.3	47.7	71.1	4.4	1.9	2.4
GC 170	80440.5	2721.9	91.9	78.1	27.7	116.5	83.1	5.9	2.8	2.0
GC 171	50813.1	1926.6	50.7	45.3	17.0	52.8	79.8	11.3	0.7	1.5
GC 172	21964.3	950.5	21.8	21.0	30.9	65.3	35.2	7.4	4.9	0.7
GC 173	85717.8	4422.5	83.7	65.9	55.1	179.1	128.0	13.0	1.1	1.8
GC 174	24729.1	1024.6	34.1	20.3	5.7	30.5	61.7	4.2	0.2	0.6
GC 175	24209.1	987.8	28.6	22.9	14.6	48.6	71.0	4.3		0.9
GC 176	20380.6	915.9	18.3	17.1	4.8	26.8	17.8	2.1	0.7	0.5
GC 177	24602.2	1074.2	23.7	21.5	5.6	34.0	27.6	2.5	0.7	0.6
GC 178	33175.2	1403.6	32.8	26.2	6.0	36.3	28.8	3.4	0.4	0.8
GC 179	16410.2	759.2	15.4	13.1	3.9	21.5	8.5	1.4		0.5
GC 180	21923.9	1174.3	25.3	19.3	3.1	14.9	2.4	2.4	0.2	1.5
GC 181	7955.4	537.4	7.9	7.2	2.1	13.7	6.0	0.7		0.4
GC 182	15260.6	871.2	15.6	16.0	20.0	42.7	36.5	1.1	0.8	0.6
GC 183	8913.0	522.3	8.9	7.2	12.3	16.7	10.9	1.2	0.4	0.4

Table B.3 (continued): RSTE contents (in ppm) in the three studied sections obtained by the hydrofluoric acid extraction method.

Glaise

Samples ID	Al	Ti	V	Cr	Co	Ni	Cu	As	Mo	U
GL 2	34489.5	2777.5	79.9	55.3	8.5	49.9	20.8	9.4	4.2	2.0
GL 3	63014.4	5375.4	156.5	101.2	9.4	55.0	37.6	7.3	2.9	2.3
GL 4	68989.6	5581.0	161.5	113.9	9.9	49.6	35.0	8.4	0.0	3.3
GL 5	82578.4	6016.1	201.7	131.3	12.8	59.9	55.3	4.2	1.4	3.5
GL 6	69940.6	5859.0	178.8	116.6	13.0	66.2	42.2	4.1		2.4
GL 7	68858.6	5872.8	173.8	116.4	8.8	61.8	38.9	6.1	0.5	2.3
GL 8	40875.1	5246.5	168.8	103.6	11.8	62.9	42.5	7.6	1.8	2.0
GL 9	43415.3	4990.1	169.5	103.2	8.4	55.9	62.8	4.8	0.9	2.4
GL 10	39571.0	4530.1	159.2	96.0	8.9	59.7	75.9	3.2		2.5
GL 11	35009.5	3897.5	151.6	94.6	12.2	72.6	45.2	1.7	0.9	2.5
GL 12	35877.0	3932.6	159.6	95.8	13.8	65.2	44.3	8.2		2.9
GL 13	38097.5	3976.0	170.9	96.6	10.8	65.5	46.8	5.5	0.5	3.5
GL 14	33333.3	3832.3	120.7	78.0	11.0	50.1	38.0	5.7	1.0	2.7
GL 15	35458.1	3479.5	95.6	70.6	9.8	36.1	19.6	4.9	0.5	2.0
GL 16	42854.3	4086.1	141.6	93.2	8.6	38.6	31.5	5.1	1.3	2.1
GL 17	44010.2	4246.2	166.2	103.8	9.4	52.7	42.7	1.8	0.8	2.4
GL 18	40251.0	3725.6	114.6	79.7	13.1	44.3	28.7	3.9	0.9	2.3
GL 19	33731.4	3549.9	162.5	90.6	7.2	44.5	33.5	3.3		1.9
GL 20	41532.5	3253.6	116.2	82.8	6.6	59.2	35.8	9.5	2.7	2.3
GL 21	38898.2	3537.5	119.3	79.9	12.0	77.5	41.2	7.3	1.1	2.3
GL 22	37653.1	2956.2	91.4	62.7	7.9	40.2	33.7	2.7		1.5
GL 23	32548.9	3460.6	104.2	74.1	5.6	25.7	27.7	0.9	0.6	1.5
GL 24	57762.0	3708.1	126.1	82.6	7.6	37.3	38.7	4.8	1.1	2.8
GL 25	57502.6	3803.8	123.3	97.0	10.3	60.4	38.0	3.6		2.5
GL 26	56872.6	3016.3	95.6	69.0	6.9	30.5	44.1	0.9		1.9
GL 27	53219.8	3212.2	103.7	82.6	16.4	85.4	44.6	5.8		2.2
GL 28	51227.2	3254.3	109.3	84.9	9.2	60.4	47.1	5.5	0.1	2.4
GL 29	45018.7	2199.8	71.7	51.5	6.0	32.3	32.7	5.4	0.1	1.3
GL 30	50323.2	3243.3	103.5	82.9	11.0	50.1	50.1	3.9	0.2	1.9
GL 32	55197.5	3337.2	111.2	76.4	7.0	45.1	37.9	3.9		2.0
GL 33	33661.2	1399.0	45.5	30.8	4.3	33.5	19.1	2.9		1.0
GL 34	57113.2	2499.0	91.3	64.8	10.0	57.7	46.5	4.5	0.1	1.7
GL 35	31571.8	1341.8	47.1	31.7	5.5	30.2	26.0	6.5		1.1
GL 36	23928.7	1044.2	33.5	23.8	2.4	30.3	19.3	0.3		0.7
GL 37	52516.4	2421.1	84.2	57.4	6.9	44.2	27.6	1.9		1.8

Cassis/La Bédoule

Samples ID	Al	Ti	V	Cr	Co	Ni	Cu	As	Mo	U
BE 147*	16800.5	1014.7	23.2	14.3	5.5	27.0	6.2	3.8	1.0	2.1
BE 149	12204.3	787.3	15.4	15.2	3.1	19.7	4.8	2.7	0.3	1.8
BE 151	16555.5	946.4	23.7	20.1	2.3	19.5	6.2	4.9	0.4	2.1
BE 152a1	25409.5	1397.6	38.6	29.6	2.0	30.3	8.4	4.2	0.4	2.5
BE 152a2	18174.4	1061.2	23.2	17.9	3.5	25.1	7.1	1.0	0.5	1.8
BE 152a3	18212.3	1062.5	24.2	18.7	1.8	26.9	5.7	4.9		2.1
BE 152b1	20781.7	1144.7	26.5	22.3	3.5	26.5	6.2	3.1		2.4
BE 152b2	26698.7	1337.6	31.9	26.1	4.7	37.0	7.5	5.2	0.4	2.4
BE 152b3	18481.1	1084.4	24.8	21.6	4.1	26.4	8.1	3.1	0.2	1.5
BE 153a1	29129.1	1465.1	41.5	32.0	4.5	34.7	11.3	4.2	1.3	2.3
BE 153a2	23734.0	1452.6	37.6	29.0	5.7	39.6	10.1	2.8	2.0	1.9
BE 153b1	20924.3	1413.4	34.1	25.9	4.8	36.7	9.0	3.3	0.9	1.7
BE 153b2	27695.8	1695.3	40.9	34.2	4.2	29.1	9.8	3.9	0.3	2.1
BE 153b3	27866.0	1745.7	40.6	31.6	6.1	35.4	13.4	6.0	0.7	1.9
BE 154a	22150.0	1262.7	35.4	29.6	6.1	32.9	7.8	8.8	0.4	1.6
BE 154b	26643.1	1578.8	43.7	30.6	6.9	30.2	10.4	6.8	1.1	1.6
BE 155a	25518.5	1565.8	46.0	33.4	6.3	41.7	9.2	6.3		1.6
BE 155b	24146.9	1445.2	40.0	30.9	5.0	36.0	8.2	2.8	1.0	1.3
BE 156a	18477.4	1151.7	32.3	26.3	4.2	36.8	6.5	2.5	0.5	1.5
BE 156b	21396.6	1288.7	37.5	25.1	4.1	30.7	5.6	5.3	0.5	2.2
BE 156e	15317.4	852.9	14.1	18.2	2.6	16.4	7.3	0.7	0.3	0.5
BE 157c	27686.9	1466.9	40.3	30.6	4.4	30.0	6.9	3.9	0.8	2.1
BE158a	28779.3	1593.2	38.8	31.1	4.2	30.5	5.7	3.4	0.5	2.1
BE 159b	36205.3	1809.1	53.8	44.0	4.8	37.2	8.6	4.4	1.7	2.2
BE 161a	27780.5	1441.5	44.1	34.1	3.4	36.4	8.1	4.0	0.2	2.3
BE 163a	31204.3	1566.6	47.2	35.2	4.8	41.1	7.7	4.2	1.3	2.0
BE 164a	15480.8	1026.8	26.1	18.7	2.6	23.5	2.4	4.3	0.5	2.3
BE 164c	11219.6	826.7	20.6	15.1	1.8	18.0	7.2	2.3	0.3	1.9

Table B.4: Al-normalized RSTE contents (units of 10^{-3}) in the three studied sections obtained by the hydrofluoric acid extraction method.

Gorgo a Cerbara

Samples ID	Ti	V	Cr	Co	Ni	Cu	As	Mo	U
GC 110	0.137	1.864	1.689	0.990	4.589	1.113	0.239	0.227	0.143
GC 111	0.050	1.453	2.212	0.322	1.594	2.579	0.059	0.026	0.026
GC 112	0.050	1.063	1.185	0.350	1.470	2.044	0.091	0.019	0.023
GC 113	0.045	1.059	1.260	0.260	1.176	1.139	0.036	0.014	0.023
GC 114	0.076	1.149	1.194	0.225	1.494	1.029	0.026	0.042	0.042
GC 115	0.055	0.981	1.246	0.200	1.235	0.516	0.042	0.015	0.032
GC 116	0.062	0.976	1.079	0.221	1.319	1.502	0.073	0.028	0.046
GC 117	0.049	1.106	1.319	0.421	1.166	1.408	0.091	0.027	0.045
GC 118	0.182	1.741	2.371	0.643	4.214	1.183	0.119	0.056	0.196
GC 119	0.048	1.864	1.552	1.107	2.947	3.214	0.224	0.088	0.067
GC 120	0.081	1.652	1.250	0.505	2.593	1.170	0.082	0.034	0.129
GC 121	0.062	1.695	1.657	0.528	3.097	3.177	0.287	0.118	0.082
GC 122	0.175	2.336	1.940	0.720	4.644	1.374	0.214	0.082	0.347
GC 123	0.058	2.096	1.411	0.436	1.665	1.895	0.116	0.035	0.057
GC 124	0.074	1.109	0.846	0.260	1.530	0.539	0.076	0.024	0.124
GC 125	0.064	1.310	3.057	0.208	1.985	0.448	0.049	0.025	0.068
GC 126	0.084	1.515	0.807	0.535	2.310	1.498	0.109	0.030	0.066
GC 127	0.051	1.374	1.316	0.362	1.142	1.161	0.036	0.010	0.042
GC 128	0.089	1.621	2.763	2.108	5.965	4.300	0.233	0.127	0.067
GC 129	0.068	1.192	1.457	0.184	1.371	2.014	0.062	0.007	0.044
GC 130	0.101	1.091	1.098	0.292	2.511	1.036	0.088	0.003	0.061
GC 131	0.073	1.334	1.103	0.863	3.130	3.415	0.194	0.066	0.038
GC 132	0.048	0.976	1.155	0.257	1.452	0.412	0.079	0.016	0.026
GC 133	0.046	0.973	1.212	0.228	0.998	1.001	0.044	0.017	0.024
GC 134	0.068	0.908	1.033	0.216	0.835	0.521	0.087	0.016	0.024
GC 135	0.042	0.926	1.160	0.198	0.854	0.477	0.055	0.023	0.023
GC 136	0.044	0.890	1.000	0.143	0.707	0.381	0.050	0.009	0.026
GC 137	0.050	1.202	1.300	1.039	2.652	5.718	0.150	0.057	0.046
GC 138	0.046	1.180	1.199	0.395	0.966	1.019	0.144	0.038	0.058
GC 139	0.048	2.120	2.218	1.383	3.750	2.007	0.270	0.136	0.067
GC 140	0.066	1.201	0.862	0.208	0.612	0.455	0.053	0.024	0.049
GC 141	0.043	5.931	2.044	0.647	2.463	0.943	0.221	0.107	0.076
GC 142	0.064	1.248	0.829	0.131	0.585	0.410	0.052	0.034	0.054
GC 143	0.040	2.103	1.766	0.888	3.144	2.358	0.239	0.133	0.065
GC 144	0.044	2.375	1.527	1.020	3.197	1.427	0.229	0.115	0.063
GC 145	0.048	1.522	1.081	0.403	1.251	1.480	0.163	0.057	0.041
GC 146	0.038	1.141	0.893	0.182	0.669	1.197	0.058	0.048	0.027
GC 147	0.032	0.860	0.736	0.182	0.872	0.505	0.119	0.037	0.029
GC 148	0.055	1.160	1.279	0.188	0.697	1.638	0.032	0.041	0.022
GC 149	0.037	1.223	0.840	0.201	0.627	1.892	0.083	0.379	0.047
GC 150	0.039	1.252	0.818	0.113	0.437	1.601	0.130	0.071	0.028
GC 151	0.036	1.022	0.829	0.116	0.704	0.880	0.046	0.033	0.022
GC 152	0.033	1.036	0.743	0.134	0.680	0.631	0.188	0.045	0.036
GC 153	0.037	1.144	0.966	0.129	0.622	0.925	0.048	0.059	0.026
GC 154	0.054	1.253	0.876	0.188	1.308	1.172	0.069	0.090	0.026
GC 155	0.037	1.415	0.879	0.191	0.886	2.274	0.074	0.089	0.028
GC 156	0.031	1.136	0.664	0.360	0.846	0.445	0.176	0.044	0.027
GC 157	0.055	1.304	0.829	0.204	0.787	1.065	0.064	0.077	0.029
GC 158	0.034	1.112	0.747	0.496	1.427	0.552	0.179	0.028	0.031
GC 159	0.040	4.146	1.634	0.911	3.295	1.956	0.174	0.240	0.099
GC 160	0.041	9.202	1.908	0.530	4.807	5.951	0.276	0.785	0.406
GC 161	0.029	4.110	1.632	0.470	2.369	2.056	0.206	0.170	0.053
GC 162	0.040	4.617	1.673	0.379	1.864	2.011	0.112	0.193	0.076
GC 163	0.033	1.229	0.901	0.078	0.343	0.773	0.145	0.058	0.046
GC 164	0.038	6.054	2.489	0.241	2.023	2.212	0.151	0.182	0.121
GC 165	0.037	11.699	2.020	1.570	8.028	4.636	0.367	2.035	0.371
GC 166	0.036	4.707	1.485	0.739	2.778	2.926	0.287	0.741	0.176
GC 167	0.035	1.604	0.932	0.297	0.691	1.179	0.079	0.044	0.049
GC 168	0.032	1.309	0.876	0.258	0.827	0.607	0.140	1.309	0.046
GC 169	0.034	1.059	0.818	0.160	0.674	1.004	0.062	0.027	0.033
GC 170	0.034	1.143	0.971	0.345	1.449	1.033	0.073	0.035	0.024
GC 171	0.038	0.998	0.892	0.334	1.040	1.571	0.223	0.014	0.030
GC 172	0.043	0.992	0.958	1.408	2.973	1.605	0.336	0.222	0.032
GC 173	0.052	0.977	0.769	0.642	2.090	1.494	0.152	0.012	0.021
GC 174	0.041	1.378	0.823	0.230	1.235	2.495	0.171	0.008	0.023
GC 175	0.041	1.180	0.946	0.603	2.006	2.934	0.180		0.037
GC 176	0.045	0.897	0.838	0.235	1.315	0.871	0.105	0.035	0.025
GC 177	0.044	0.962	0.875	0.228	1.383	1.121	0.102	0.030	0.026
GC 178	0.042	0.988	0.790	0.181	1.095	0.868	0.103	0.014	0.024
GC 179	0.046	0.936	0.798	0.237	1.313	0.516	0.086		0.031
GC 180	0.054	1.153	0.878	0.141	0.679	0.110	0.112	0.007	0.067
GC 181	0.068	0.994	0.900	0.267	1.721	0.756	0.088		0.046
GC 182	0.057	1.020	1.051	1.313	2.801	2.389	0.074	0.054	0.038
GC 183	0.059	1.004	0.810	1.383	1.871	1.225	0.136	0.046	0.040

Table B.4 (continued): Al-normalized RSTE contents (units of 10^{-3}) in the three studied sections obtained by the hydrofluoric acid extraction method.

Glaise

Samples ID	Ti	V	Cr	Co	Ni	Cu	As	Mo	U
GL 2	0.081	2.316	1.603	0.248	1.446	0.603	0.274	0.122	0.058
GL 3	0.085	2.483	1.606	0.149	0.874	0.597	0.116	0.047	0.036
GL 4	0.081	2.341	1.651	0.143	0.719	0.507	0.121	0.000	0.048
GL 5	0.073	2.442	1.589	0.155	0.725	0.670	0.051	0.017	0.043
GL 6	0.084	2.557	1.668	0.186	0.947	0.603	0.058		0.034
GL 7	0.085	2.524	1.690	0.128	0.898	0.564	0.088	0.008	0.034
GL 8	0.128	4.129	2.534	0.289	1.539	1.040	0.185	0.045	0.049
GL 9	0.115	3.905	2.377	0.192	1.287	1.448	0.109	0.022	0.056
GL 10	0.114	4.022	2.426	0.226	1.509	1.919	0.081		0.064
GL 11	0.111	4.331	2.702	0.348	2.073	1.291	0.050	0.027	0.072
GL 12	0.110	4.448	2.669	0.384	1.818	1.235	0.227		0.080
GL 13	0.104	4.485	2.535	0.284	1.720	1.228	0.144	0.012	0.091
GL 14	0.115	3.621	2.341	0.329	1.504	1.141	0.171	0.029	0.081
GL 15	0.098	2.696	1.990	0.275	1.019	0.554	0.139	0.013	0.057
GL 16	0.095	3.304	2.174	0.201	0.901	0.736	0.120	0.029	0.049
GL 17	0.096	3.776	2.358	0.214	1.198	0.971	0.041	0.018	0.055
GL 18	0.093	2.847	1.980	0.326	1.101	0.712	0.098	0.022	0.057
GL 19	0.105	4.817	2.686	0.215	1.319	0.994	0.099		0.055
GL 20	0.078	2.797	1.993	0.159	1.426	0.863	0.229	0.064	0.056
GL 21	0.091	3.067	2.054	0.309	1.992	1.058	0.187	0.028	0.058
GL 22	0.079	2.429	1.666	0.209	1.068	0.895	0.072	0.000	0.039
GL 23	0.106	3.202	2.277	0.173	0.790	0.852	0.028	0.018	0.046
GL 24	0.064	2.184	1.431	0.132	0.646	0.671	0.083	0.018	0.049
GL 25	0.066	2.144	1.686	0.180	1.051	0.662	0.063		0.043
GL 26	0.053	1.681	1.212	0.121	0.536	0.776	0.015		0.033
GL 27	0.060	1.949	1.552	0.308	1.605	0.838	0.110		0.041
GL 28	0.064	2.134	1.657	0.180	1.179	0.918	0.108	0.003	0.047
GL 29	0.049	1.592	1.145	0.134	0.717	0.727	0.119	0.002	0.030
GL 30	0.064	2.057	1.648	0.219	0.996	0.996	0.077	0.004	0.038
GL 32	0.060	2.014	1.383	0.126	0.817	0.687	0.070		0.036
GL 33	0.042	1.353	0.916	0.127	0.995	0.568	0.086		0.031
GL 34	0.044	1.598	1.134	0.176	1.011	0.814	0.079	0.002	0.030
GL 35	0.042	1.493	1.004	0.174	0.957	0.822	0.206		0.036
GL 36	0.044	1.400	0.996	0.101	1.266	0.808	0.014		0.027
GL 37	0.046	1.603	1.092	0.132	0.842	0.526	0.037		0.035

Cassis/La Bédoule

Samples ID	Ti	V	Cr	Co	Ni	Cu	As	Mo	U
BE 147*	0.060	1.380	0.850	0.330	1.607	0.367	0.225	0.057	0.125
BE 149	0.065	1.265	1.247	0.252	1.612	0.396	0.225	0.022	0.148
BE 151	0.057	1.430	1.214	0.139	1.180	0.377	0.294	0.026	0.126
BE 152a1	0.055	1.519	1.164	0.080	1.194	0.329	0.165	0.017	0.100
BE 152a2	0.058	1.275	0.984	0.190	1.379	0.392	0.058	0.030	0.098
BE 152a3	0.058	1.328	1.024	0.099	1.479	0.311	0.268		0.115
BE 152b1	0.055	1.274	1.072	0.170	1.273	0.297	0.149		0.115
BE 152b2	0.050	1.196	0.976	0.177	1.388	0.280	0.195	0.016	0.090
BE 152b3	0.059	1.343	1.171	0.221	1.426	0.440	0.170	0.012	0.084
BE 153a1	0.050	1.425	1.100	0.155	1.191	0.386	0.143	0.044	0.080
BE 153a2	0.061	1.582	1.223	0.240	1.668	0.425	0.118	0.083	0.081
BE 153b1	0.068	1.628	1.239	0.231	1.753	0.429	0.158	0.042	0.083
BE 153b2	0.061	1.477	1.233	0.151	1.049	0.355	0.140	0.010	0.077
BE 153b3	0.063	1.455	1.133	0.218	1.270	0.480	0.216	0.024	0.068
BE 154a	0.057	1.597	1.336	0.275	1.483	0.353	0.396	0.020	0.074
BE 154b	0.059	1.642	1.147	0.259	1.132	0.390	0.255	0.042	0.060
BE 155a	0.061	1.801	1.309	0.246	1.635	0.362	0.247		0.062
BE 155b	0.060	1.657	1.280	0.205	1.493	0.341	0.117	0.041	0.054
BE 156a	0.062	1.749	1.423	0.226	1.991	0.354	0.133	0.030	0.079
BE 156b	0.060	1.752	1.172	0.190	1.436	0.264	0.249	0.023	0.102
BE 156e	0.056	0.921	1.187	0.169	1.070	0.476	0.046	0.022	0.033
BE 157c	0.053	1.457	1.104	0.158	1.085	0.248	0.139	0.030	0.074
BE158a	0.055	1.349	1.082	0.145	1.059	0.197	0.117	0.016	0.073
BE 159b	0.050	1.485	1.214	0.133	1.028	0.236	0.122	0.047	0.062
BE 161a	0.052	1.588	1.229	0.124	1.310	0.292	0.143	0.007	0.082
BE 163a	0.050	1.513	1.128	0.155	1.317	0.247	0.135	0.041	0.065
BE 164a	0.066	1.686	1.206	0.167	1.519	0.155	0.279	0.030	0.147
BE 164c	0.074	1.835	1.343	0.158	1.605	0.641	0.202	0.023	0.168

CHAPTER C: The Valanginian $\delta^{13}C$ positive excursion

The Alvier section, Switzerland

In order to better understand temporal changes at the Valanginian carbon-isotope excursion, redox-sensitive trace-elements, phosphorus and organic matter contents have been investigated on key sections from the western Tethys. Two papers resulted from these studies:

- The Valanginian $\delta^{13}C$ excursion may not be an expression of a global oceanic anoxic event (accepted for publication with moderate revisions in Earth and Planetray Science Letters)

- Paleoceanographic change along a tethyan shelf-basin transect during the Valanginian carbon-isotope excursion (in preparation for publication in Swiss Journal of Geosciences)

-C1-

The Valanginian $\delta^{13}C$ Excursion may not be an Expression of a Global Oceanic Anoxic Event

Stéphane Westermann[1], Karl B. Föllmi[1], Thierry Adatte[1], Virginie Matera[2], Johann Schnyder[3], Dominik Fleitmann[4], Nicolas Fiet[5,6], Izabela Ploch[7] and Stéphanie Duchamp-Alphonse[5]

[1]Institute of geology and paleontology, University of Lausanne, Anthropôle, 1015 Lausanne, Switzerland.
[2]Institute of geology, University of Neuchâtel, Emile Argand 11, CP 158, 2009 Neuchâtel, Switzerland.
[3]UPMC Univ. Paris 6, CNRS, UMR 7193, ISTEP, case 117, 4, pl. Jussieu, 75252 Paris Cedex 05, France.
[4]Institute of Geological Sciences, University of Bern, Baltzerstrasse 1-3, 3012 Bern, Switzerland.
[5]UMR 8148 – I.D.E.S., Bât. 504, University of Paris XI Orsay, 91405 Orsay Cedex, France.
[6]AREVA, 33 rue La Fayette, 75009 Paris, France.
[7]Polish Geological Institute, 4 Rakowiecka, 00-975 Warsaw, Poland.

Published in Earth and Planetary Science Letters, 2010, volume 290, pages 118-131.

Abstract

Marine and terrestrial sediments of the Valanginian age display a distinct positive $\delta^{13}C$ excursion, which has recently been interpreted as the expression of an oceanic anoxic episode (OAE) of global importance. Here we evaluate the extent of anaerobic conditions in marine bottom waters and explore the mechanisms involved in changing carbon storage on a global scale during this time interval. We assess redox-sensitive trace-element distributions (RSTE; uranium, vanadium, cobalt, arsenic and molybdenum) and the quality and quantity of preserved organic matter (OM) in representative sections along a shelf-basin transect in the western Tethys, in the Polish Basin and on Shatsky Rise. OM-rich layers corresponding in time to the $\delta^{13}C$ shift are generally rare in the Tethyan sections and if present, the layers are not thicker than several centimetres and total organic carbon (TOC) contents do not surpass 1.68 wt%. Palynological observations and geochemical properties of the preserved OM suggest a mixed marine and terrestrial origin and deposition in an oxic environment. In the Polish Basin, OM-rich layers show evidence for an important continental component. RSTE exhibit no major enrichments during the $\delta^{13}C$ excursion in all studied Tethyan sections. RSTE enrichments are, however, observed in the pre-$\delta^{13}C$ excursion OM-rich "Barrande" levels of the Vocontian Trough. In addition, all Tethyan sections record higher Mn contents during the $\delta^{13}C$ shift, indicating rather well-oxygenated bottom waters in the western Tethys and the presence of anoxic basins elsewhere, such as the restricted basins of the North Atlantic and Weddell Sea. We propose that the Valanginian $\delta^{13}C$ shift is the consequence of a combination of increased OM storage in marginal seas and on continents (as a sink of ^{12}C-enriched organic carbon), coupled with the demise of shallow-water carbonate platforms (diminishing the storage capacity of ^{13}C-enriched carbonate carbon). As such the Valanginian provides a more faithful natural analogue to present-day environmental change than most other Mesozoic OAEs, which are characterized by the development of ocean-wide dysaerobic to anaerobic conditions.

***Keywords**: Valanginian, oceanic anoxic event (OAE), $\delta^{13}C$, continental and marine organic carbon, redox-sensitive trace-elements, ocean drilling program (ODP)*

C1.1 Introduction

Global oceanic anoxic events (OAEs) represent exceptional episodes in Earth's history, which are marked by widespread dysoxic to anoxic conditions in the world oceans. These events are characterized by extensive organic carbon deposition in marine sediments and associated perturbations in the global

Table C1.1: Characteristics of the studied sections

Section	Localisation	Paleogeography	Paleoenvironment	Lithology	Age	Numbers of samples[1]	Ref[2]
Capriolo	Northern Italy (45°38'40" N; 09°57'26" E)	Lombardian basin	Open ocean, pelagic setting	Micritic limestone, some chert and marl	Valanginian (CM 14 to CM 10n)	88, (22)	1, 2, 3
Breggia	Southern Switzerland (45°52'43" N; 09°01'53" E)	Lombardian basin	Open ocean, pelagic setting	Micritic limestone with chert	Valanginian (CM 11n to CM 10n)	60, (10)	4, 5
Angles	SE France (43°58' N; 6°37' E)	Vocontian Trough	Epicontinental sea, hemipelagic setting	Marl-limestone succession	Valanginian (Pertransiens to Furcilata zone)	(10)	6
Vergol	SE France (44°13' N; 5°32' E)	Vocontian Trough	Epicontinental sea, hemipelagic setting	Marl-limestone succession	Valanginian (Campylotoxus zone)	20, (20)	7
Malleval	E France (45°08'55" N; 05°27'13" E)	Northern Tethyan shelf	Outer shelf	Limestone	Valanginian (Camplyotoxus to Verrucosum zone)	80	8
Alvier	E Switzerland (47°06'46" N; 09°24'56" E)	Northern Tethyan shelf	Outer shelf	Limestone and marly limestone	Valanginian	85	9, 10
Wawal	Central Poland (51°30'00" N; 20°04'21" E)	Poland basin	Shallow epicontinental sea environment	Silty clay with phosphate nodules	Valanginian (Verrucosum zone)	(7)	11
Hole 6814/04-U02	Ribban Basin (68°09'45" N; 14°09'47" E)	Norwegian-Greenland Seaway	Shallow seaway	Calcareous siltstone	Valanginian	(2)*	12, 13
Hole 6307/07-U02	Hitra Basin (63°27'54" N; 07°14'44" E)	Norwegian-Greenland Seaway	Shallow seaway	Red and grey marl	Valanginian	(2)*	12, 13
Poykin	Siberia (60°45' N; 71°22' E)	Western Siberian basin	Hemipelagic setting	Clayey mudstone and sandstone	Valanginian	(2)*	14, 15
Leg 198, site 1213B	Shatsky Rise (Pacific Ocean, 31°34.64' N; 157°17.86' W)	Pacific	Open marine pelagic environment (> 1000 m)	Micritic limestone with chert	Valanginian	10, (10)	16
Leg 93, site 603	Hatteras Rise (35°29.71'N; 70°01.71' W)	North Atlantic	Pelagic setting	Micritic limestone	Valanginian	(5)*	17
Leg 44, site 391C	Blake-Bahama Basin (28°13.61' N; 75°37.00' W)	North Atlantic	Pelagic setting	Calcareous claystone, nannofossil chalk	Valanginian	(2)*	18
Leg 76, site 534A	Blake-Bahama Basin (28°20.6' N;75°22.9' W)	North Atlantic	Pelagic setting	Bioturbated nannofossil-radiolarian limestone	Valanginian	(8)*	18
Leg 77, site 535	Gulf of Mexico (23°42.48' N; 84°30.97' W)	North Atlantic	Pelagic setting	Limestone and marly limestone	Valanginian	(12)*	19
Leg 101, site 638B	Galician Margin (42°09.2' N;12°11.8' W)	North Atlantic	Pelagic setting	Sandstone and claystone	Late Valanginian	(2)*	20
Leg 113, site 692B	Weddell Sea (70°43.43' S; 13°49.19' W)	Southern Ocean	Open ocean, pelagic setting	Clayey mudstone	Valanginian/Hauterivian	(29)*	21

[1]Number of samples analysed by ICP-MS; the numbers of samples analyses for organic matter determination are indicated in parentheses; numbers with * correspond to published data

[2]References: 1 = Lini et al., 1992, 2 = Channel et al., 1987, 3 = Channel & Erba, 1992, 4 = Bersezio et al., 2002, 5 = Channel et al., 1993, 6 = Duchamp-Alphonse, 2006, 7 = Reboulet et al., 2003, 8 = Blanc, 1996, 9 = Briegel, 1972, 10 = Föllmi et al., 1994, 11 = Lesniak et al., 2003, 12 = Langrock et al., 2003, 13 = Mutterlose et al., 2003, 14 = Peters et al., 1993, 15 = Vyssotski, et al., 2006, 16 = Bralower et al., 2002, 17 = van Hinte et al., 1987, 18 = Katz, 1983, 19 = Herbin et al., 1983, 20 = Stein and Rullkötter, 1988, 21 = O'Connell, 1990.

carbon cycle. The Valanginian stage is considered to include the oldest Cretaceous OAE ("Weissert" anoxic event; Erba et al., 2004) and effectively, it witnessed a pronounced excursion in marine carbonate- and marine and terrestrial organic carbon-isotope records with amplitudes of 1.5 ‰ and 4-5 ‰, respectively (Lini et al., 1992; Föllmi et al., 1994; Weissert et al., 1998; Hennig, 2003; Erba et al., 2004; Gröcke et al., 2005). However, in contrast to other Cretaceous OAEs, such as the Early Aptian OAE1a and the end-Cenomanian OAE2 (Schlanger and Jenkyns, 1976; Jenkyns, 1980; Jenkyns et al., 1994; Leckie et al., 2002; Bersezio et al., 2002; Erba, 2004; Kuypers et al., 2004; Mort et al., 2007), marine sediments deposited during the Valanginian carbon-isotope event lack the widespread occurrence of well-developed organic carbon rich levels (van de Schootbrugge et al., 2003; Reboulet et al., 2003; Gröcke et al., 2005), and the presence of centimetric organic-rich deposits is limited to a few localities (Erba et al., 2004).

The Valanginian positive-isotope excursion has been interpreted as the expression of a global perturbation of the carbon cycle, which was related to paleo-environmental change and resulted in a crisis of carbonate-producing biota (Lini et al., 1992; Erba et al., 2004; Duchamp-Alphonse et al., 2007). Along the northern Tethyan margin and elsewhere, these changes are coeval with the demise of shallow-water carbonate platforms (Schlager, 1981; Föllmi et al., 1994, 2006). The climate may have become cooler during the Valanginian $\delta^{13}C$ shift (Price, 1999; Price et al., 2000; McArthur et al., 2007).

Many triggering processes have been proposed to explain this change in the carbon cycle, such as an increase in CO_2 input into the atmosphere due to the emissions of the Paraña-Etendeka flood-basalt volcanism (Lini et al., 1992; Weissert et al., 1998), followed by general warming. This is supposed to have led to enhanced continental weathering and phosphorus delivery to the marine realm, which again increased marine primary productivity and storage rates of organic matter. This may have led to the drawdown of atmospheric CO_2 and subsequent cooling (Föllmi et al., 1994).

With the help of precise ammonite biostratigraphy, the $\delta^{13}C$ excursion is now dated as late Early to Late Valanginian (Hennig et al., 1999; Föllmi et al., 2006; Duchamp-Alphonse et al., 2007; Ogg et al., 2008). This is older than in earlier propositions based on magneto- and nannofossil stratigraphy, where the onset of the excursion was dated as Late Valanginian (Channel and Erba, 1992; Lini et al., 1992; Erba et al., 2004).

In this study, we investigate redox-sensitive trace-element (RSTE) and organic matter (OM) contents in a selection of representative sections along a shelf-basin transect in the Tethys, in order to improve our understanding of potential changes in redox conditions during the Valanginian $\delta^{13}C$ shift. In addition, we analysed samples of the Polish Basin and Shatsky Rise (northwestern Pacific). These data have been compared and correlated with published data from different localities, in order to complement our data and, thus, obtain a more complete view on global change during the Valanginian.

C1.2 Geological settings

The studied sections were chosen according to the following two criteria: (1) presence of organic-rich levels, and (2) representative of a specific paleogeographic setting within the studied transect. Here we briefly present the selected sections starting with basinal settings (Table C1.1).

C1.2.1 The Central Tethyan realm

The section of Capriolo (Lombardian Basin, northern Italy; Fig. C1.1) is situated in an abandoned quarry near the village of Capriolo. This basinal section belongs to the Maiolica formation (Late Tithonian to Early Aptian; Lini et al., 1992) and consists of a monotonous pelagic limestone succession with repetitive chert and marl layers. The temporal framework is given by nannofossil biostratigraphy and magnetostratigraphy (Channel et al., 1987; Channel and Erba, 1992), and the whole-rock and organic carbon $\delta^{13}C$ records were analysed by Lini et al. (1992).

The Breggia section is equally composed of pelagic limestone (Maiolica formation) and situated in the Mt Generoso half graben (southern Switzerland; Fig. C1.1), close to the Breggia River (Weissert, 1979; Bersezio et al., 2002). This section was selected in addition to the Capriolo section because of published data on organic matter (Bersezio et al., 2002) and, as in Capriolo, the calibration of the positive $\delta^{13}C$ shift by nannofossil biostratigraphy and magnetostratigraphy (Channel et al., 1993; Bersezio et al., 2002 and references therein).

C1.2.2 The northern Tethyan margin

The section of Vergol outcrops along a secondary road between Montbrun-Les-Bains and Vergol (SE France), and is located in the central part of Vocontian Trough, which represents a basinal setting indenting the northern Tethyan margin (Reboulet et al., 2003). This section is characterized by the presence of limestone-marl alternations. The biostratigraphy is based on ammonoids and is well constrained for the Valanginian (Reboulet & Atrops, 1999; Reboulet et al., 2003). We focused on a two-meter interval within sediments attributed to the *Campylotoxus* zone (situated between the banks 86 and 88, after Reboulet et al., 2003), which is characterized by the presence of four centimetric organic-rich layers (B1, B2 B3 and B4), named “Barrande” layers (Reboulet et al., 2003).

C1.2.3 The northern Tethyan shelf

Two sections were selected in order to characterize the shallow-water environment of the northern Tethyan margin. The first section is located along a road between Malleval and the Inn of Lombardière (Vercors, eastern France; Fig. C1.1). This section (Fig. C1.2) is divided into three parts: (1) the lower part consists of the “Calcaires des Ecouges” Formation (thick limestone beds dated as late Berriasian); (2) the middle part is composed of a succession of light-coloured decimetric limestone beds and variable marl levels (late Berriasian to early Valanginian); and (3) the upper part is formed by a monotonous succession of thick and often bioturbated limestone beds (Blanc, 1996). The biostratigraphy is not well constrained and chemostratigraphic data (e.g., $\delta^{13}C$) are lacking.

The section of Alvier (near Sargans and Buchs, eastern Switzerland; Fig. C1.1) represents the outer part of the northern Tethyan shelf. The section is composed of a monotone limestone and marly-limestone succession (Fig. C1.2). The base of the section belongs to the Diphyoides Formation (Valanginian) and the top to the Kieselkalk Formation (Hauterivian; Briegel, 1972). The stratigraphic framework is given by the $\delta^{13}C$ curve (Föllmi et al., 1994).

We complement our data by the study of samples from the Angles section (Vocontian trough; Duchamp-Alphonse et al., 2007), the Wawal section (central Poland, representing a shallow strait connecting the Boreal and Tethyan realms; Lesniak et al., 2003) and Shatsky Rise (ODP Leg 198, site 1213b; Bralower et al., 2002) (Table C1.1).

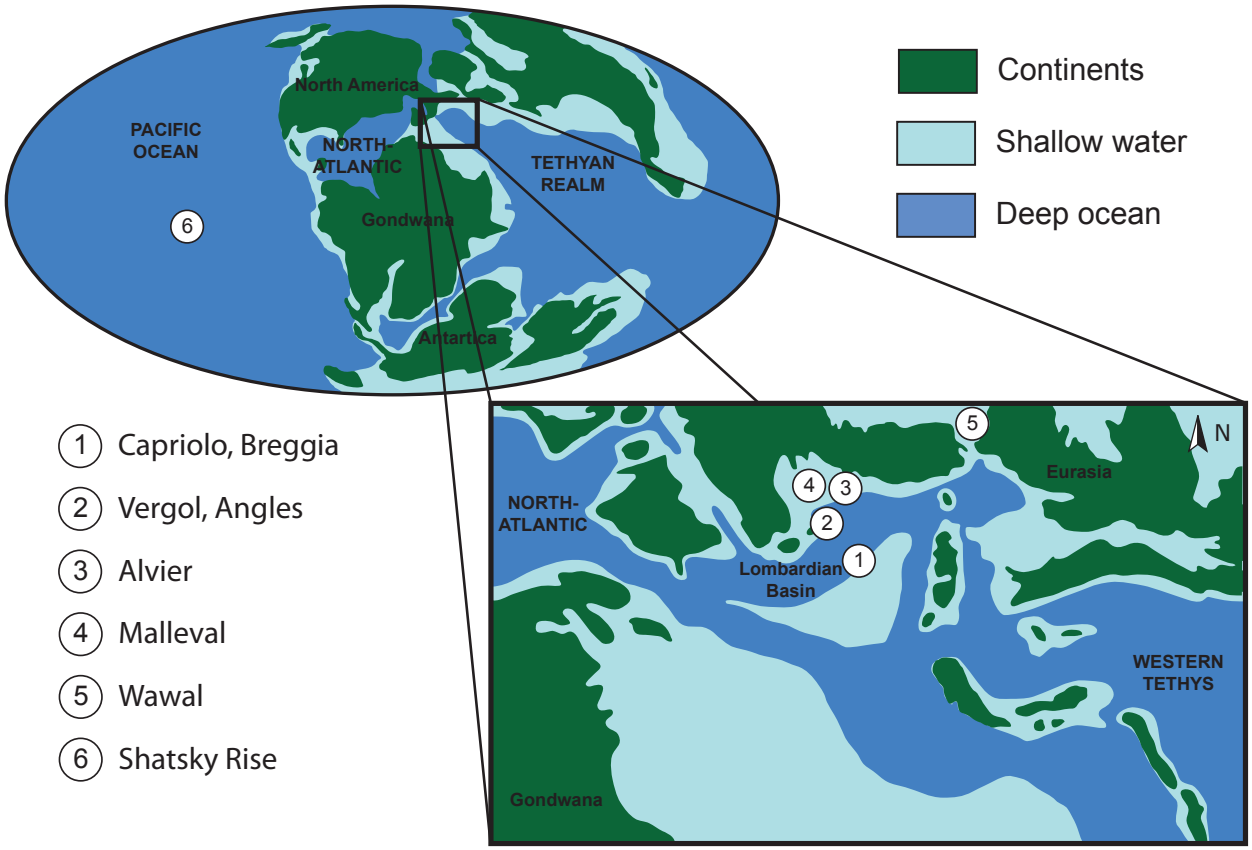

Fig. C1.1: Paleogeographic recontruction and localization of the studied sections (world map redrawn after Smith et al., 1994 and map of the western Tethys after Blakey, 2005: http://jan.ucc.nau.edu/~rcb7/).

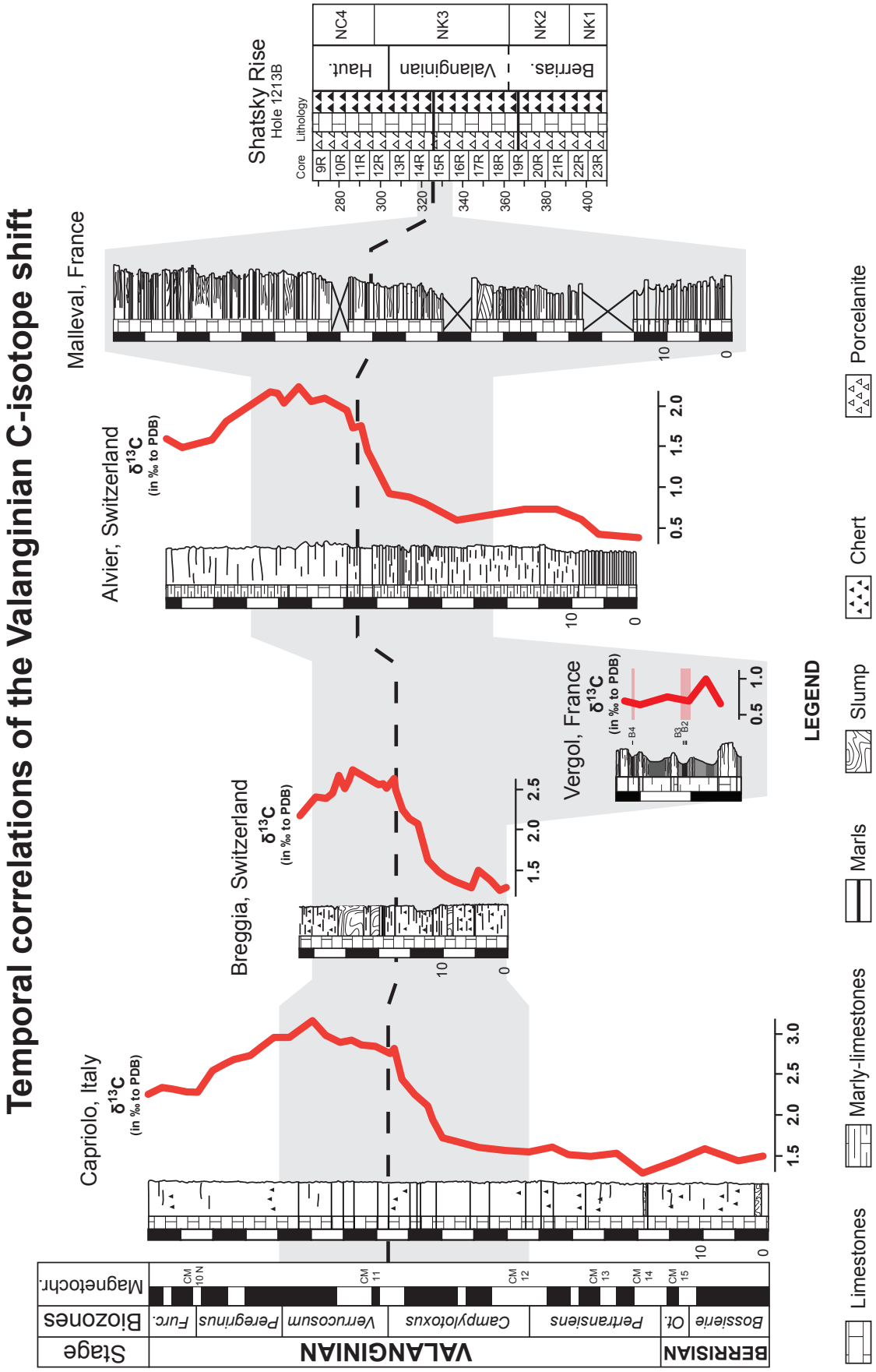

Fig. C1.2: Lithology and stratigraphic correlation of the Tethyan sections and Shatsky Rise. The temporal framework is based on the chemostratigraphic correlation of the $\delta^{13}C$ record for Capriolo (Lini et al., 1992), Breggia (Bersezio et al., 2002), and Alvier (Föllmi et al., 1994), ammonite biostratigraphy for Malleval (Blanc, 1996) and Vergol (this study), and nannofossil, foraminiferal and radiolarian biostratigraphy Shatsky Rise (Bralower et al., 2002).

C1.3 Methods

C1.3.1 Stratigraphic correlation and sediment-accumulation rates

Stratigraphic correlation between the studied sections of the western Tethys is mainly based on the $\delta^{13}C$ record. For absolute age assignments, the $\delta^{13}C$ curve was calibrated with the timescale of Ogg et al. (2008). The temporal framework of the DSDP and ODP legs is obtained by the calcareous nannofossil, radiolarian and planktonic foraminiferal biostratigraphy.

Sediment-accumulation rates were calculated by using the duration of ammonite biozones for the Vergol section and of magnetochrons for the sections of Capriolo and Breggia. At Shatsky Rise, the sediment-accumulation rate has been estimated based on the first and last occurrences of microfaunes (Bralower et al., 2002).

C1.3.2 Organic matter characterization

Total organic carbon (TOC) contents and maturity of preserved OM (hydrogen and oxygen indices: HI and OI) were determined using a Rock Eval™6 (Espitalié et al., 1985) with an instrumental precision of <2%. HI and OI represent the H/C and O/C ratios of organic matter, respectively, and are used to classify organic matter in a Van Krevelen-type diagram (Espitalié et al., 1985). Two standards (IFP 160000 and VP143h) were used to calibrate the measurements.

In order to complement our data sets on organic matter, we also performed elemental analyses on selected samples using a Carlo Erba CHN EA1108 - Elemental Analyzer. The quantification of nitrogen contents was conducted after carbonate removal with hydrochloric acid. The carbon/nitrogen (C/N) ratio was calculated as the weight ratio of TOC and nitrogen.

Palynofacies observations were performed on a selection of samples. After drying, bulk sediment samples were digested in HCl-HF acids in order to concentrate the OM. The OM residues were prepared using Microscope glass slides. Qualitative observations were obtained using a Zeiss Axioskop 40 microscope under transmitted light, in order to recognize and estimate the relative abundances of the following major organic components (Tyson, 1995): amorphous organic matter (AOM), dinoflagellate cysts, foraminifer linings, spores and pollen, and opaque to translucent vascular plant fragments.

C1.3.3 Geochemistry

Redox-sensitive trace-element (RSTE) analyses were performed on bulk limestone samples. 250 mg of powder was treated in 10 mL of suprapur nitric acid (HNO_3) in a PFA vessel. The samples were digested in a microwave oven (MSL-Ethos plus, Milestone) using the heating program EPA 3051. After cooling, the solution was filtered (0.45µm) and diluted to 100 mL with ultrapure water (cf. Bodin et al., 2006, for more details). Dissolution percentages determined after filtration were about 94% for the Capriolo samples, 86% for the Breggia samples, 67% for the Vergol samples, 76% for the Alvier samples and 95% for the Malleval samples. Despite the low dissolution percentages for some samples of the Vergol section, no correlation was observed between the concentration of the different analysed samples and the dissolution percentage obtained during digestion procedure (e.g., uranium in Fig. C1.3). This suggests that the elements studied here are present in the soluble authigenic phase and are not due to partial leaching of the detrital insoluble fraction. We additionally analyzed a selection of samples with a total extraction method using a combination of suprapur hydrochloric, nitric and hydrofluoric acids, and observed a positive correlation between HNO_3–derived RSTE raw contents and HF-derived Al-normalized RSTE contents. These findings are detailed in Westermann (2010) and will be the subject of a separate publication.

RSTE contents were determined by a quadrupole ICP-MS (ELAN 6100, Perkin Elmer) using a semi-quantitative mode (totalQuant™), with a precision of 5%. The calibration is based on two certified reference materials (CRM): LKSD-1 lake sediment and NIST-1640 natural water. We studied the contents of uranium (U), vanadium (V), cobalt (Co), molybdenum (Mo), arsenic (As), manganese (Mn), chromium (Cr), copper (Cu), zinc (Zn) and iron (Fe). The RSTE contents are expressed in ppm. The mean recovery rates (n=12 digestions) and quantification limit for the analysed RSTE were determined by using LKSD-1 CRM and are 103% and 5×10^{-4} ppb for U, 90% and 2.9×10^{-1} ppb for V, 105% and 8×10^{-2} ppb for Co, 110% and 2×10^{-2} ppb for As, 89% and 1.4×10^{-1} ppb for Mo and 111% and 1.82 ppb for Mn.

C1.4 Results

C1.4.1 Rock-Eval analyses

We analysed TOC contents of dark marly layers and laminae present in the sections of Capriolo, Vergol, Angles, Wawal and Shatsky Rise. In samples with TOC

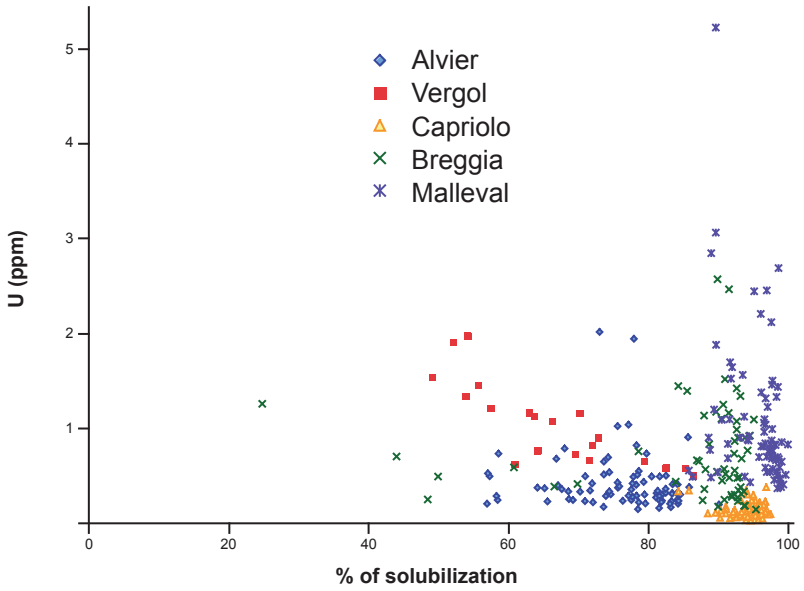

Fig. C1.3: U (ppm) versus percentage of solubilization in the studied sections.

values <0.3 wt.%, T_{max} and HI parameters are difficult to interpret (Espitalié et al., 1985). We therefore only present the results of samples with TOC values ≥ 0.3%.

In the Capriolo section, the average TOC value is close to 0.50 wt% (Fig. C1.4). A maximum TOC value of 1.68% has been measured in sediments below the carbon-isotope shift. A second peak in TOC values (1.48%) is observed in sediments corresponding to the positive shift in $\delta^{13}C$. The HI and OI parameters (n=22), indicate a Type-II organic matter. The samples plot close to the Type-III boundary with the exception of one sample, which plots well within the Type-II area. Bersezio et al (2002) observed the same evolution for the section of Breggia (average TOC value of approximately 0.80 wt%). Two marl layers present in sediments 15-20 m below the onset of the $\delta^{13}C$ shift show the highest values (2.03 and 1.99 wt%) in the section. In sediments deposited during the carbon-isotope shift, a second maximum of 1.53 wt% is observed. HI and OI parameters plot all into the Type-III area (Bersezio et al., 2002).

In the section of Vergol, the marly intervals below and above the “Barrande” layers display low TOC values fluctuating around 0.32 wt%. Within the “Barrande” layers, organic matter contents show maxima close to 4.00 wt%. The four “Barrande” levels are characterized by high HI (~350 mg HC/g TOC) and low OI (~30 mg HC/g TOC), indicating Type-II organic matter.

In the Angles section, TOC values are quite low in comparison to the Capriolo and Breggia sections. The average value is around 0.24 wt%. HI values are low and plot within the Type-III area.

In the Wawal section, the samples (n=7) show TOC values ranging from 0.28 to 2.94 wt%. The HI and OI values (HI: ~5-10 mg HC/g TOC; OI: ~50-250 mg HC/g TOC) suggest a Type-III signature for preserved organic matter (Tyson, 1995).

At Shatsky Rise, 10 samples were analysed. Three of them display high TOC values (>1 wt%) with a maximum value of 4.58 wt% (Fig. C1.4). The other show TOC values < 0.1 wt%. The high HI (~200-450 mg HC/g TOC) and the low OI (~65-136 mg HC/g TOC) indicate a Type-II or slightly altered signature for the preserved organic matter.

C1.4.2 C/N and palynofacies

When using the C/N ratio of preserved organic matter, one may consider the possibility that in organic-poor sediments the amount of inorganic nitrogen fixed as ammonium ions in the interlayers of clay minerals may present a major fraction of total nitrogen, causing a lowering of the C/N ratio (e.g., Stein, 1991). We therefore only show the results for samples with TOC values higher than 0.5 wt%.

The TOC/N ratios in the Capriolo samples range between 3 and 20. Only two samples show ratios higher than 10. These samples were taken from sediments older than the $\delta^{13}C$ shift. The other samples present values around 10, which are characteristic for marine planktonic organic matter (16; Redfield, 1958). In Wawal, the TOC/N ratios range between 0.4 and 34.5. For the samples with higher TOC values (up to 1 wt%), only one shows a TOC/N below 10. The other samples

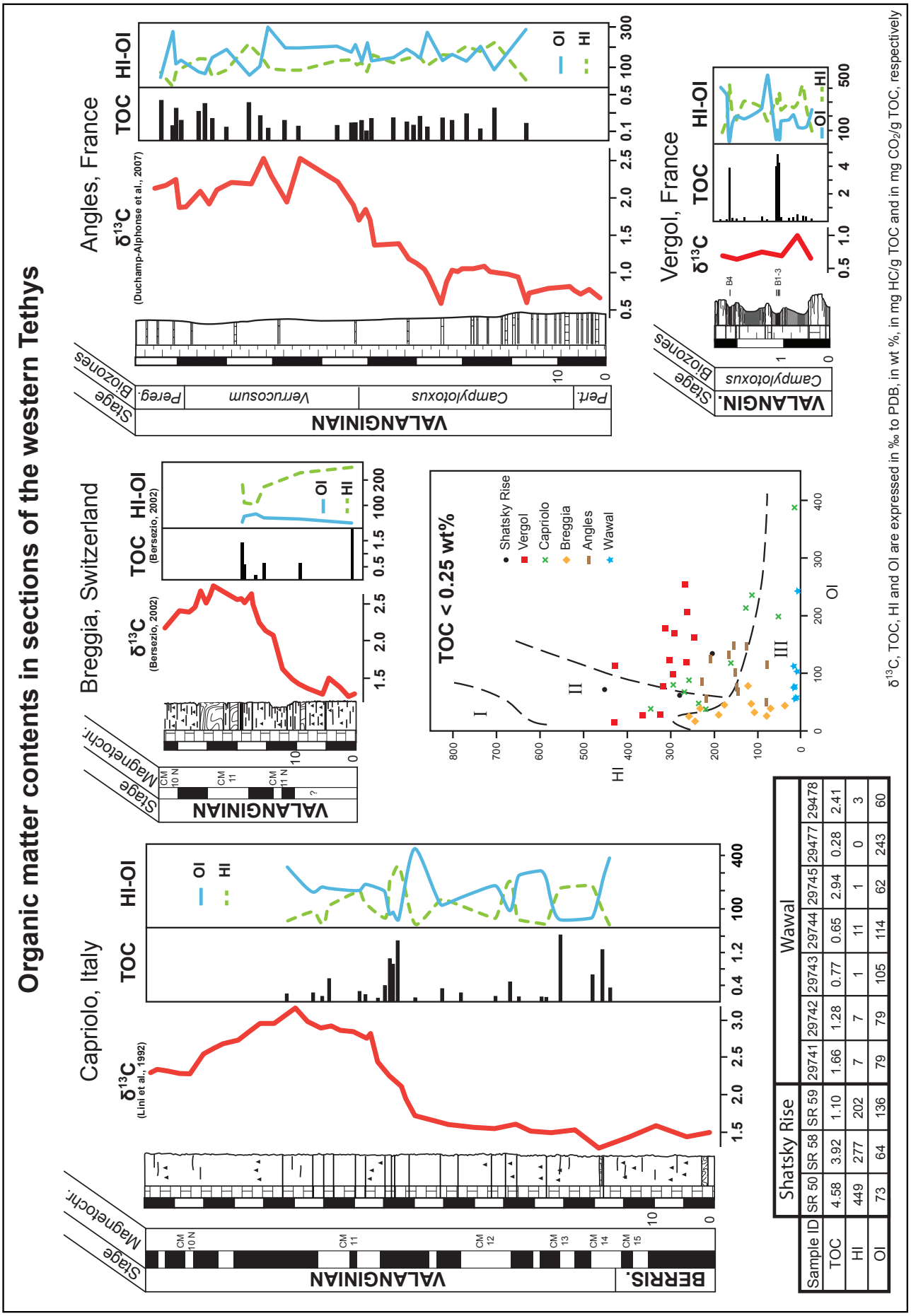

Shatsky Rise				Wawal						
Sample ID	SR 50	SR 58	SR 59	29741	29742	29743	29744	29745	29477	29478
TOC	4.58	3.92	1.10	1.66	1.28	0.77	0.65	2.94	0.28	2.41
HI	449	277	202	7	7	1	11	1	0	3
OI	73	64	136	79	79	105	114	62	243	60

Fig. C1.4: Evolution of the C_{org} content during the Valanginian positive $\delta^{13}C$ (in ‰ to PDB) excursion. TOC is expressed in wt%, hydrogen indices (HI) in mg HC/g TOC and oxygen indices (OI) in mg CO_2/g TOC.

indicate ratios up to 15. Raw TOC/N data are available in Appendix A.

In Capriolo, all analysed samples (n=7) show a dominance of amorphous organic matter (AOM). In addition, a minor terrestrial component is observed consisting of spores, pollen and ligno-cellulosic debris. Good correlation exists between the aspect of a given AOM flake in transmitted light and its preservation state (Tyson, 1995). In Capriolo, the samples with a more orange and more gelled AOM are well preserved and show higher HI values. The samples with a greyish and flocculent AOM show lower HI values. In the samples from Wawal, AOM dominates the non-filtered glass slides. As in Capriolo, we notice the presence of vascular plant debris and pyrite as a minor component but in higher proportions than in the samples of Capriolo. In filtered preparations (> 20 μm), the Polish samples show a higher proportion of palynomorphs, whereas in the Italian samples AOM still dominates the assemblage. Altered AOM is mostly lacking in filtered preparations, whereas pristine AOM may remain (see Tyson, 1995).

C1.4.3 Redox-sensitive trace elements

The data of the RSTE studied here (U, V, Co, As, Mo, Cu, Zn, Fe and Mn) are shown in Fig. C1.5 for the different sections.

C1.4.3.1 The Capriolo section

In samples of the Capriolo section, RSTE values are quite low. U shows a slight enrichment during the onset of the $\delta^{13}C$ shift. V, Co and As contents are quite stable throughout the section and fluctuate around mean values of 1.70, 0.15 and 1.90 ppm, respectively. Mo contents display more or less constant base values of around 0.06 ppm, which are superimposed by a series of pronounced peaks along the section. Cr, Zn and Cu contents show similar variations (Fig. C1.5) with no significant enrichment along the section. In contrast to the others elements, Mn show three intervals of increased concentrations along the section. The average concentration is close to 560 ppm. The first enrichment occurs approximately 20 m above the base of the section with a maximum of 2500 ppm. In sediments corresponding to the onset of the $\delta^{13}C$ shift and the shift itself, two further peaks occur with values close to 600 ppm. Coeval with the second increase in Mn contents, an increase in Fe contents is observed with a maximum of approximately 3750 ppm in sediments corresponding to the $\delta^{13}C$ shift (Fig. C1.5).

C1.4.3.2 The Breggia section

U shows no significant variations along the entire Breggia section (average value of 0.3 ppm). V and Co contents display minor peaks (~ 7 and 6 ppm, respectively) in sediments corresponding to the onset of the $\delta^{13}C$ shift whereas the As and Mo contents show a peak in sediments documenting the end of the increase in $\delta^{13}C$ values. The elements Cu and Zn show a slight increase in sediments deposited during the onset of the $\delta^{13}C$ shift. In sediments below the $\delta^{13}C$ shift, Mn contents are more or less constant, with an average value fluctuating around 460 ppm. In sediments corresponding to the onset of $\delta^{13}C$ excursion, Mn concentrations reach a maximum of 777 ppm. This peak is coeval with the Mo peak, which itself is followed by an increase in Fe contents (close to 15 000 ppm).

C1.4.3.3 The Vergol section

The majority of the studied RSTE shows comparable trends along the section of Vergol, with two intervals of higher contents corresponding to the “Barrande” layers. We therefore restrict the description of the results to the more characteristic elements. The average background RSTE content is rather low with values around 1.0, 11.8, 5.5, 3.8 and 0.6 ppm for U, V, Co, As and Mo, respectively (Fig. C1.5). The first enrichment zone corresponds to the “Barrande” layers B1, B2 and B3 with maximal values of 1.9, 23.5, 12.8 11.5 and 2.0 ppm for U, V, Co, As and Mo, respectively. All RSTE show a second maximum in the interval corresponding to layer B4 of the “Barrande” layers, except for Mo. The maximal values are lower than for the first enrichment interval. The Mn contents behave in a way, which is opposite to the other studied elements, with a high average value of 145 ppm and negative shifts within the two intervals including the “Barrande” layers.

C1.4.3.4 The Alvier section

The average content for U, V, Co, As and Mo corresponds to approximately 0.5, 8.3, 3.5, 1.3 and 0.1, respectively. In sediments below and above the increase in $\delta^{13}C$ values, concentrations are quite stable. During the $\delta^{13}C$ shift, V, Co and As contents show comparable variations with an increase reaching a maximum of 18.3, 6.3 and 3.5 ppm, respectively. Mo contents present differences in its stratigraphic behaviour relative to the other RSTE studied here. A first peak (0.3 ppm) is observed in sediments corresponding to the onset of the $\delta^{13}C$ shift, a second one in sediments documenting

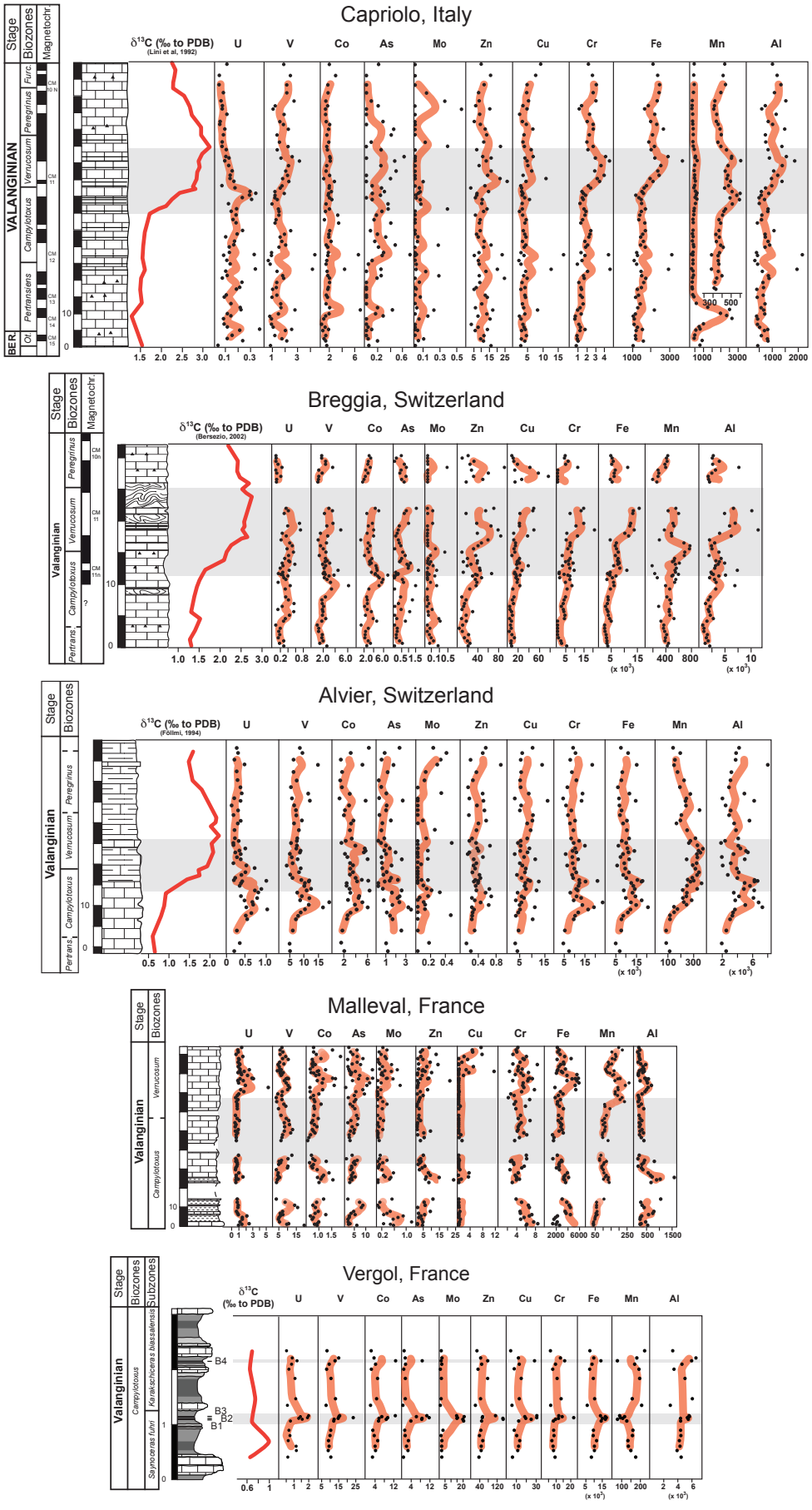

Fig. C1.5: Redox-sensitive trace elements (RSTE) expressed in ppm for the studied sections. Al (in ppm) has also been plotted to compare the behaviour of RSTE with detrital input.

the $\delta^{13}C$ plateau, and in sediments deposited during the end of the $\delta^{13}C$ excursion, a long-term increase is observed. The other RSTE (Cr, Zn, Cu and Fe) show a positive shift in sediments at the onset of the positive $\delta^{13}C$ excursion. Mn contents display a maximum of 371 ppm (mean value ~195 ppm) in sediments deposited during the $\delta^{13}C$ shift.

C1.4.3.5 The Malleval section

The values for the average RSTE contents are quite low (Fig. C1.5). U and V show comparable general trends with an increase in sediments of the *verrucosum* zone (maximum value of ~ 5 and 19.5 ppm, respectively). Co, As and Mo contents display coeval increases in an interval approximately 5 m above the increase in U and V contents, with maximal values of 1.8, 28.2 and 1.1 ppm, respectively. Ni and Cr contents remain more or less constant along the section with an average value of 13 and 4.9 ppm, respectively. Cu contents are below the detection limit for almost all analysed samples. Fe and Mn contents show maxima in sediments at the base of the *verrucosum* zone (corresponding to the $\delta^{13}C$ positive excursion) with values ranging around 6000 and 250 ppm, respectively.

C1.4.3.6 Leg ODP 198, Shatsky Rise

RSTE analyses on two dark layers at Shatsky Rise (cores 1213B-015R and 1213B-019R) show higher values in U, V, Co, As and Mo (maximal values of 1.7, 64.2, 13.3, 23.9 and 4.2 ppm, respectively) relative to other samples of the same core. Raw concentrations are available in Appendix B.

C1.5 Discussion

C1.5.1 Organic matter

C1.5.1.1 Pristine versus diagenetically altered organic matter

The T_{max} value obtained by Rock-Eval analyses corresponds to the maximum temperature needed to crack preserved OM during pyrolysis. For Type-II OM, T_{max} values higher than 435°C indicate a high degree of maturity and alteration (Espitalié et al., 1985). At Vergol and Shatsky Rise, the OM-rich samples display T_{max} values close to 425°C indicating rather good OM preservation (Fig. C1.6). For the samples of Capriolo, T_{max} values fluctuate around 430°C suggesting a well-preserved OM, even if they indicate a small diagenetic and/or a matrix effect. This is particularly true for low TOC values (Espitalié et al., 1985). Samples with higher TOC contents show lower T_{max} values, which plot in the field of immature OM in a HI/T_{max} diagram indicating a relatively high degree of OM preservation (Fig. C1.6). The samples of Angles show T_{max} values around 440°C. This suggests that its preserved OM experienced a higher degree of burial and thermal alteration and/or a matrix effect (Deconinck, 1987; Godet et al., 2008).

C1.5.1.2 Origin of organic matter in the Tethyan realm

Organic-rich layers corresponding to the Valanginian positive $\delta^{13}C$ excursion are only known from a few localities. Their maximal thickness is never more than a few centimetres and the maximum TOC content are not over 1.68 wt%. In pelagic settings of the western Tethys, our data show that preserved OM is of marine origin with variable terrestrial admixtures. In the section of Capriolo, the organic-rich layers show low HI values, which plot mainly in the Type-II and Type-III areas in a HI/OI diagram (Fig. C1.4). In sediments corresponding to the increase in $\delta^{13}C$ values, one sample displays a better preservation of the marine OM (higher HI, Type-II origin). The preserved OM is typical of a well-oxygenated marine setting with minor inputs of continental OM. Its marine origin is also shown by the low TOC/N ratio, ranging between ~1 and 10, which is characteristic for marine zoo- and phytoplankton (Stein, 1991). In the Angles section, despite the more pronounced alteration of OM suggested by HI/OI and HI/Tmax diagrams (Figs. C1.4 and C1.5), the preserved OM appears to have a marine origin. An increase in TOC is observed in sediments in the upper part of the *verrucosum* zone, corresponding to higher $\delta^{13}C$ values. In Wawal, the low HI and high OI suggest a terrestrial origin of OM, whereas observations of its palynofacies indicate a high proportion of marine OM (presence of AOM). AOM is generally interpreted as the product of marine phyto- and/or zooplankton degradation. However, in some cases, AOM may also derive from the degradation of continental OM (Tyson, 1995). In Wawal, AOM shows a rather good preservation despite its low HI. Moreover, the high TOC and low OI and T_{max} values suggest an absence of post-depositional thermal alteration. In addition, the TOC/N ratios are characteristic of terrestrial plants (Stein, 1991 and references therein). In Wawal, the OM appears, therefore, to bear a higher continental component, which is probably due to the proximal position of the section. At Vergol, the preserved OM in

the "Barrande" layers is pristine and shows an explicit marine origin (Type II field in the HI/OI diagram with high HI and low OI).

We compared TOC contents with sedimentation rates (SR) during the $\delta^{13}C$ shift. TOC/SR ratios have been used as a parameter for distinguishing oxic from anoxic depositional environments (Müller and Suess, 1979; Stein, 1991; Langrock et al., 2003; Langrock and Stein, 2004). By plotting the samples in a TOC/SR diagram (Fig. C1.7), it appears that the relatively organic-rich samples of Capriolo and Breggia were deposited under mainly oxic conditions. In both sections, only one sample indicates more oxygen-depleted conditions. In contrast, the samples of the "Barrande" intervals at Vergol plot in the anoxic realm (Fig. C1.7), as is also suggested by the presence of dark laminated layers.

In the sections of Capriolo, Breggia and Angles, the rather low maxima in TOC values occur in sediments deposited during the $\delta^{13}C$ positive excursion during the late *campylotoxus* zone. The time interval of the $\delta^{13}C$ positive excursion coincides with a period of high phosphorus (P) burial rates in ocean sediments (Föllmi, 1995). This suggests that higher flux rates of P may have triggered an increase in marine planktonic production rates, such as is indicated by the higher HI in Capriolo during the rise in $\delta^{13}C$. This hypothesized

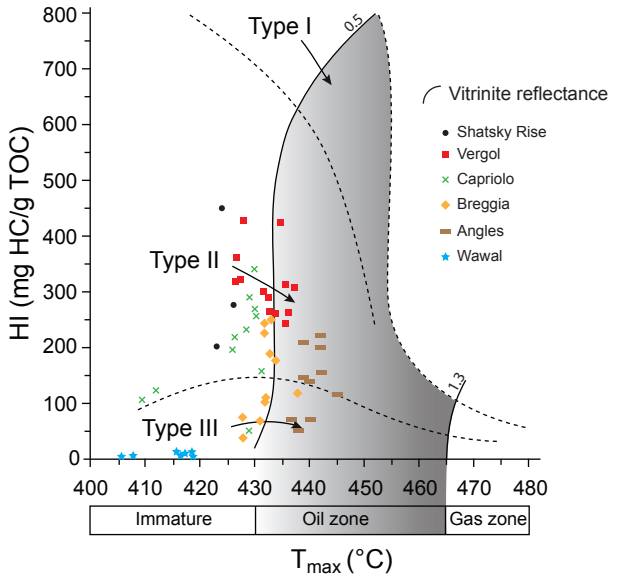

Fig. C1.6: HI/T_{max} diagram for preserved organic matter (OM) in the Tethyan sections. OM shows a good degree of immaturity for all the sections (except for Angles) and indicates a predominantly marine origin for Carpiolo, Vergol, Angles and Shatsky Rise and a terrestrial origin for Wawal. In Breggia a phase of higher terrestrial input is observed.

increase in marine productivity did, however, not lead to the deposition of widespread and important organic-rich layers in the western Tethys, and evidence for bottom-water anoxia is lacking.

C1.5.1.3 Origin of organic matter in other basins

Published TOC, HI and OI data from Valanginian sediments suggest a palaeogeographic pattern in the quality of preserved OM (Fig. C1.7). Under the premise that those sediments are coeval with the Valanginian positive $\delta^{13}C$ excursion, the Boreal realm and the Atlantic Ocean provides an OM signature similar to the western Tethys (except for Site 535); i.e., OM of marine origin with probable terrestrial admixtures deposited in oxygenated waters (Katz, 1983; Herbin et al., 1987). Additional information based on a palynological study from Site 534 (Habib, 1983) and solvent extraction from Sites 415 and 416 (Morocco Basin; Claypool and Baysinger, 1980) confirms the observed pattern. In contrast, in the marginal seas of North Atlantic, Pacific and Weddell Sea, the HI and OI indicate a clear marine origin (cf. Gulf of Mexico and Shatsky Rise). In the Weddell Sea, the average TOC value is close to 8.60 wt% for Site 692b. In the core attributed to the Valanginian, TOC shows the highest values ranging from 9 to 18 wt%. These values are in favour of dysaerobic to anaerobic conditions in these basins during the Valanginian (Barker et al., 1990).

With regards to the TOC/SR ratio, the organic-rich samples of Shatsky Rise point to deposition under anaerobic conditions (Fig. C1.7).

This implies that in the northern Atlantic, the Weddell Sea and at Shatsky Rise, preserved OM shows a clear marine origin possibly deposited under anoxic conditions.

C1.5.2 Palaeo-redox changes during the Valanginian carbon-isotope excursion

Enrichments in RSTE are well known from sediments deposited under anoxic conditions (Calvert and Pedersen, 1993; Lipinski et al., 2003; Böning et al., 2004; Tribovillard et al., 2004; Kolonic et al., 2005; Baudin et al., 2006; Bodin et al., 2006; Brumsack, 2006; Turgeon and Brumsack, 2006). Because the behaviour of RSTE in the water column and during early diagenesis, and their sensitivity to redox conditions is rather element-specific, it is generally recommended to use a suite of RSTE (here: U, V, Co, As and Mo) rather than single elements for reconstructing paleo-redox conditions. Moreover, by using the distribution of this

suite of RSTE, it is not only possible to distinguish oxic from anoxic, but also anoxic from euxinic conditions (Algeo and Maynard, 2004; Tribovillard et al., 2006).

The stratigraphic distribution of RSTE in the sections of Capriolo, Breggia, Alvier and Malleval does not show significant enrichments and correlatable trends in sediments deposited during the carbon-isotope excursion (Fig. C1.5). Most of the short-term variations appears to be due to the specific behaviour of each element rather than to general changes in redox conditions. For example, the increase in V during the $\delta^{13}C$ shift may be related to the increase in Fe contents to which V may be adsorbed (Morford and Emerson, 1999). In Capriolo, a series of shorted-lived peaks in the contents of U, V, Co, As and Mo appear partly correlated in sediments below the $\delta^{13}C$ shift. This may indicate small variations in redox conditions, which eventually correlate with the "Barrande" levels of the Vergol section. These intervals do, however, not coincide with the presence of organic-rich laminae. In the shallower settings analysed here, the general pattern of RSTE is following the Al content, which is indicative of a relationship between detrital input and RSTE distributions, and as such of aerobic conditions

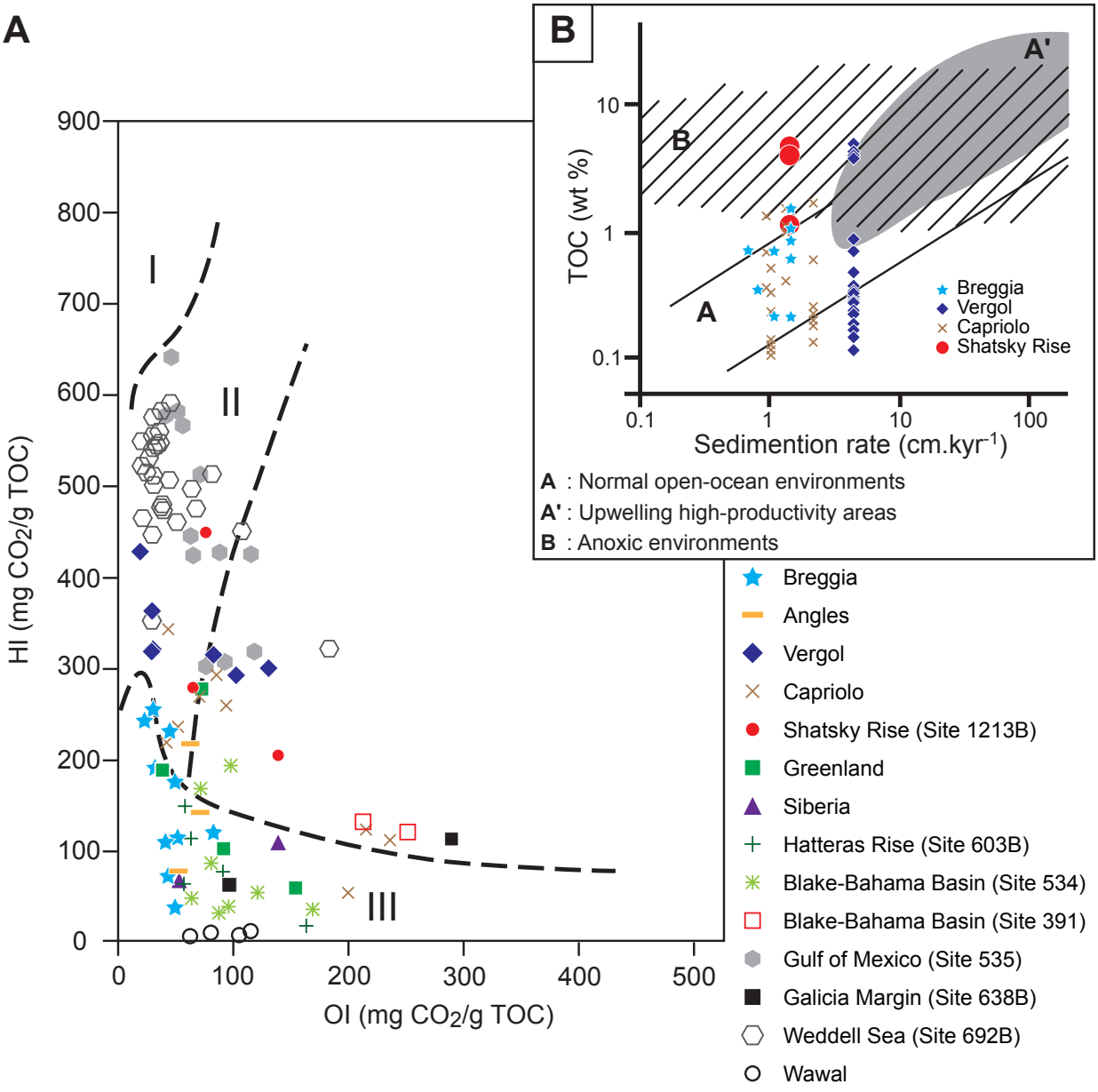

Fig. C1.7: A. HI/OI diagram characterising the origin of organic matter for a suite of Valanginian sections: Breggia (Bersezio et al., 2002), western Siberia (Peters et al., 1993), Greenland (Langrock et al., 2003; Mütterlose et al., 2003), Hatteras Rise (Meyers, 1987; Herbin et al., 1987), Blake-Bahama Basin (site 391 and 534; Katz, 1983), Gulf of Mexico (Herbin et al., 1983), Galicia Margin (Stein and Rullkötter, 1988), Weddell Sea (O'Connell, 1990). Only sediments with TOC contents > 0.4 w% were considered.

B. Sedimentation rate versus TOC contents in the studied Tethyan sections.

(Tribovillard et al., 2006).

In the section of Vergol, RSTE show enrichments in the intervals, in which the "Barrande" layers occur. The comparable behaviour of U, V, As and Mo in these intervals indicates anoxic conditions. This is also supported by the TOC values, which show maxima within these levels. As already stated, the occurrence of the "Barrande" layers clearly predates the $\delta^{13}C$ shift (Fig. C1.5). At Shatsky Rise, the RSTE contents of the centimetric dark levels are characterized by higher values compared to other samples within the same cores suggesting deposition under anoxic conditions.

All the sections studied record an increase in Mn contents during the $\delta^{13}C$ excursion, indicating an event of global importance. Most Mn entering the oceanic reservoir is mobilised on continents (Kuhn et al., 2005) and its concentration in ocean water and in deposited sediments is mainly controlled by redox cycling (Frakes and Bolton, 1992). In aerobic environments, Mn forms highly insoluble Mn(III) or Mn(IV) oxyhydroxides (Calvert and Pedersen, 1993) whereas in anaerobic environments Mn is reduced to Mn(II) - a soluble cation. Consequently, Mn recycling is enhanced under anoxic conditions. As such, an enrichment in Mn may be interpreted as a diagenetic redistribution of Mn from anoxic environments, with high Mn-recycling rates to oxic environments where increased deposition of Mn may occur (Morford and Emerson, 1999; Kuhn et al., 2005). Alternatively, an increase in continental weathering may accelerate the transfer of Mn into oceans and its deposition in oxic environments (Kuhn et al., 2005). Fe and Mn exhibit similar behaviour in aqueous environments, except for its mean residence time. Due to a rapid fixation in the sediments (Force and Cannon, 1988), Fe contents decrease as a function of the distance to the continental source. In our study, in the basinal settings Mn enrichments predate the increase in Fe contents, whereas in more proximal settings Mn enrichments are coeval with Fe enrichments. This indicates that Mn redox-recycling was combined with the accelerated transfer of Mn from continents to the oceans. Mn redox-recycling implies that anoxic conditions may have prevailed in certain parts of the world oceans, such as in the North Atlantic and Weddell Sea.

To summarize, the RSTE distributions in the analysed sections with the absence of correlative enrichments and a generalized increase in Mn contents indicate the absence of generalized anoxic conditions in the Tethyan realm. This interpretation goes along with the observation that organic-rich layers are rare and never thicker than a few centimetres.

The only organic-rich layers of Early Valanginian age in the Tethyan realm, which appear to have been formed under anaerobic depositional conditions are the "Barrande" levels at Vergol, and predate the carbon-isotope excursion.

It is also not clear to what extent the postulated anoxic conditions of Shatsky Rise can be extrapolated to the entire Valanginian Pacific Ocean, because of the scarcity of coeval sections from other parts of this ocean, most of the Valanginian Pacific being subducted.

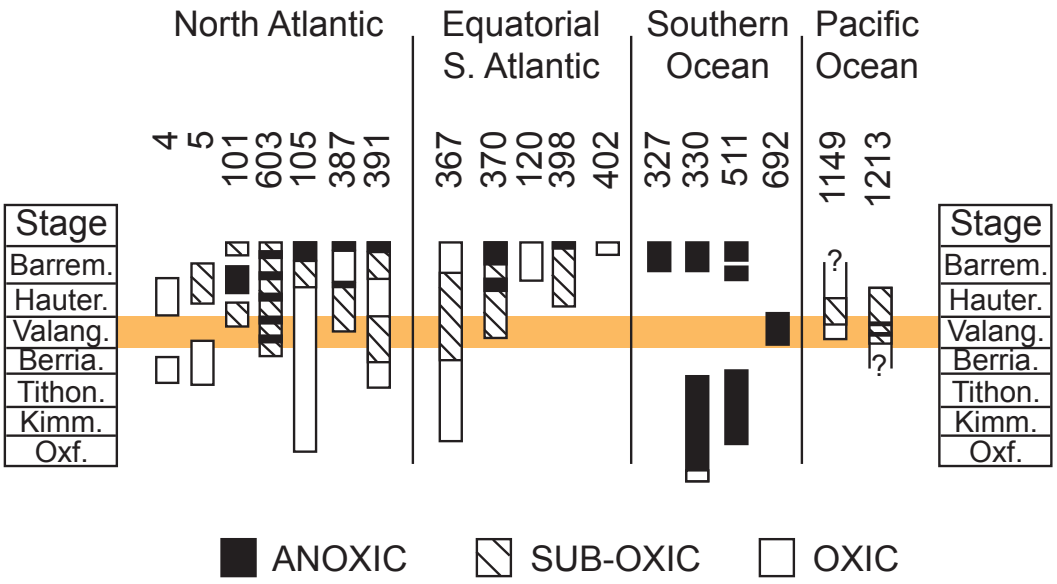

Fig. C1.8: Distribution of anoxic, suboxic and oxic conditions in bottom waters of the North Atlantic, Southern Ocean and Pacific interpreted from TOC contents, and sedimentary and paleontologic features of the sediments for the Late Jurassic and the Early Cretaceous (modified after Mutterlose and Wise, 1990).

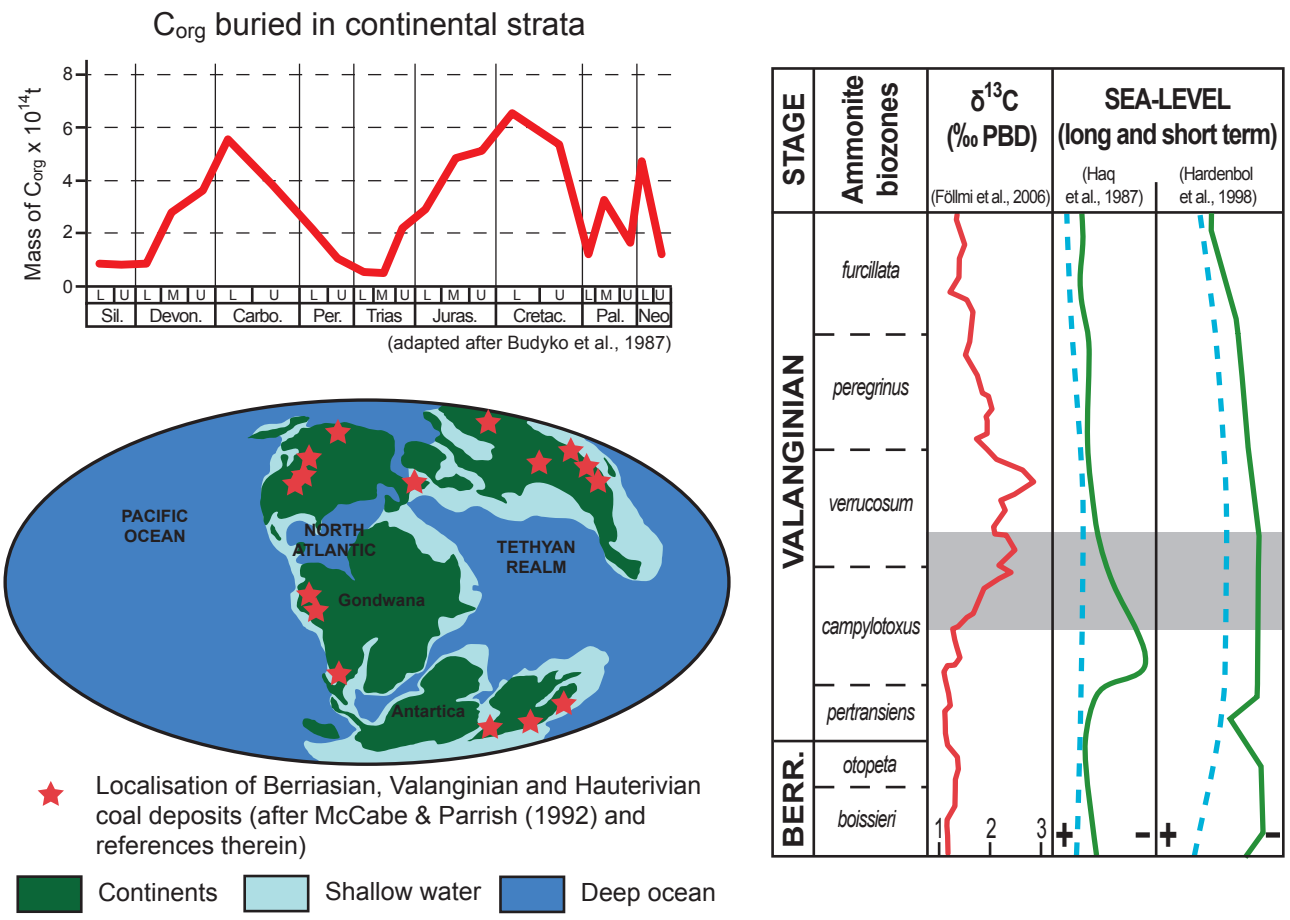

Fig. C1.9: Two global sea-level curves for the Valanginian (after Haq et al., 1987; Hardenbol et al., 1998) and organic-carbon accumulation in continental strata trough the Phanerozoic (Budyko et al., 1987). Localisation of basins with Early Cretaceous (Berriasian, Valanginian, and Hauterivian) coals (after McCabe and Totman Parrish, 1992 and references therein).

C1.6 The Valanginian carbon-isotope excursion

The Valanginian $\delta^{13}C$ excursion has been recognized in sections from the northern and central Tethyan realm, western North Atlantic, Gulf of Mexico and western and central Pacific, including pelagic, hemipelagic and shallow-water settings (Lini et al., 1992; Föllmi et al., 1994; Kuhnt et al., 1997; Hennig et al., 1999; Erba et al., 2004). It was furthermore identified in organic material derived from continental settings (Gröcke et al., 2005). This wide coverage suggests that the excursion reflects palaeoenvironmental changes important enough to affect the carbon cycle on a global scale. Traditionally, an increase in $\delta^{13}C$ in marine carbonate is interpreted as the consequence of an increase in primary productivity (sink of light carbon) associated with an increase in OM preservation (Scholle and Arthur, 1980; Arthur et al., 1987). OM preserved in sediments of the North Atlantic, Weddell Sea and at least part of the Pacific Ocean suggests conditions favourable to the enhanced preservation of organic matter in these basins. To evaluate the importance of the organic carbon sinks in these areas, we calculate the corresponding TOC mass-accumulation rates. For our calculations, we used an average shale density of 2.4 g/cm^3 (Attewell and Farmer, 1976). At Shatsky Rise, the sedimentation rate is estimated to have varied between 1.23 and 1.62 cm/kyr; with an average TOC value of 3.2 wt%, corresponding to a C_{org} accumulation rate of 94 to 124 mg/cm^2/kyr. Mort et al. (2007) obtained C_{org} accumulation rates varying between 2000 and 3000 mg/cm^2/kyr during the end-Cenomanian OAE2 in the section of Pueblo. In the actual high productivity zone along the Peru margin, the organic carbon burial rate varies between 1000 and 4500 mg/cm^2/kyr (Böning et al., 2004). This reveals moderate rates of organic-carbon burial at Shatsky Rise. For the sites in the Gulf of Mexico and Weddell Sea, stratigraphic time control is not sufficient to permit a meaningful calculation of C_{org} accumulation rates. Nevertheless, the Gulf of Mexico (North Atlantic) and the Weddell Sea appear

to have recorded anoxic conditions, which were more extended in time (Meyers, 1987; Barker et al., 1990). Mutterlose and Wise (1990) show that in the North Atlantic, prevailing redox conditions were suboxic with anoxic "pulses" rather than fully anoxic (Fig. C1.8). In contrast, the Weddell Sea site has an average TOC value of 8.60 wt% for the "Neocomian" sediments (Barker et al., 1990), which suggests long-lasting anoxic conditions in this marginal basin. The North Atlantic and the Weddell Sea are the only sites known for the Valanginian, where oxygen-depleted conditions may have persisted for longer time periods. This does not mean that high carbon burial rates did not occur at other sites or in other basins, but so far we are not aware of any published evidence for this.

Given the restriction of enhanced organic carbon burial to marginal basins of the Atlantic, additional mechanisms may have to be invoked in order to explain the positive $\delta^{13}C$ shift. We propose enhanced production and storage of organic matter on the continent (sink of light carbon), in association with the demise of shallow-water carbonate platforms (sink of heavy carbon; Weissert et al., 1998) as an alternative mechanism. The Early Cretaceous corresponds - together with the Carboniferous-Permian and the Paleocene-Eocene - to one of the three majors periods of coal deposition in Earth's history (Budyko et al., 1987; Haszeldine, 1989). Budyko et al. (1987) estimates the total amount of C_{org} trapped in the continental sediments during the Late Jurassic and the Early Cretaceous as high as 11.5×10^{20} g (Fig. 9). This corresponds to an average accumulation of ~1.9×10^{19} g C_{org}/My for the Early Cretaceous, which is 20% higher than the average rate proposed for the Phanerozoic (Budyko et al., 1987). For the Berriasian-Hauterivian period, coal depositions are known from USA, Russia, China, India, Indonesia, Australia and Canada (Fig. C1.9; Ziegler et al., 1987; McCabe and Totman Parrish, 1992). These deposits are commonly associated with sea-level rise and the spreading of epicontinental seas, followed by the development of dense vegetation covers in shallow coastal settings with a humid climate (Fig. C1.9; Ziegler et al. 1987; Haszeldine, 1989; McCabe and Totman Parrish, 1992). Published TOC and HI/OI data from Valanginian marine sediments and the data on organic matter obtained in this study suggest a continental component in preserved OM and this also in distal pelagic settings. This hints at the capacity of the Valanginian terrestrial cover to produce a surplus in terrestrial C_{org}, which was consequently exported into the oceans. In addition to this, the Valanginian records an estimated reduction of 13% of global carbonate production rates due to an important platform-drowning phase (Weissert et al., 1998). Changes in shallow-water carbonate production have been shown to influence the carbonate carbon stable-isotope signature (e.g., Weissert et al., 1998). The amount of increased continental C_{org} deposition (> 0.6×10^{19} g C_{org}/My) assumed here is lower than the amount of decreased C_{carb} deposition (~2.8×10^{19} g C_{carb}/My; Weissert et al., 1998). Since terrestrial C3 plants have a strongly negative carbon-isotope signature, a positive change in terrestrial C_{org} depositional rates may, however, still strongly influence the carbon-isotope signature on a global scale (Föllmi et al., 2005; Diester-Haass et al., 2009).

C1.7 Conclusions

In this study, we explore the extent of oceanic anoxic conditions during the Valanginian positive carbon-isotope excursion and the mechanisms leading to concomitant change in the global carbon cycle. We present new geochemical and OM data from a bathymetric transect in the western Tethys (sections at Malleval, Vergol and Angles in eastern France, Alvier in eastern Switzerland, and Breggia and Capriolo in southern Switzerland and northern Italy, respectively), which are complemented by analyses on sections at Wawal (Poland) and Shatsky Rise (northwestern Pacific). Preserved OM is generally of mixed marine-terrestrial origin and characteristic of a rather well-oxygenated marine environment (HI/OI, TOC/N, palynofacies), even in the deepest, distal-most pelagic sections (Capriolo, Breggia). No correlative enrichments have been observed in the stratigraphic distributions of the RSTE U, V, Co and Mo, which is taken as a further indication of oxic bottom-water conditions prevailing in the western Tethys during the Valanginian $\delta^{13}C$ excursion. In the cm-thin Vocontian "Barrande" layers of the Vergol section, we observe consistent enrichments in RSTE, which are indicative of anoxic conditions. These layers represent the only evidence of anoxic bottom waters in the western Tethys. The "Barrande layers", however, clearly predate the $\delta^{13}C$ positive shift.

Mn records show an increase in all sections, which is coeval with the increase of $\delta^{13}C$ values. This is explained by enhanced continental influx in Mn, combined with

increased Mn redox-recycling. Outside the Tethyan realm, we identify the presence of dysoxic to anoxic conditions in the restricted basins in the North Atlantic (DSDP Leg 77, Site 535) and Weddell Sea (ODP Leg 113, Site 692). Also at Shatsky Rise (northwestern Pacific Ocean; ODP Leg 192, Site 1213), conditions were intermittently anoxic. The resulting C_{org} burial rates for this and the other investigated sites, however, may not be sufficient to explain the shift in $\delta^{13}C$. We suggest therefore additional mechanisms in the form of decreasing shallow-marine carbonate production and increased storage of organic matter on the continent, which may have been implied in steering the global $\delta^{13}C$ record towards more positive values during the Valanginian.

Environmental change during the Valanginian stage resembles present-day environmental change more closely than any other OAE during the Mesozoic, especially because of the limitation of oceanic anoxic conditions to marginal seas, rather than covering entire oceanic basins. As such the Valanginian may provide a natural analogue to the presently observed perturbations in the global carbon cycle, rapid spreading of dysaerobic conditions in marginal seas close to heavily populated regions (so-called “dead zones”; Diaz et al., 2008), contemporaneous disappearance of tropical to subtropical reefs (Hughes et al., 2003), and spreading of vegetation covers in alpine and subpolar regions (Grace et al., 2002).

Acknowledgements

We would like to thank Stéphane Bodin, Alexis Godet and Melody Stein for their assistance during the sampling of the different sections and their advice in the field. We also thank Tiffany Monnier and André Villard for their help in the laboratory. We acknowledge the constructive reviews of three anonymous reviewers and of EPSL editor Peggy Delaney, which all helped to improve this publication. Funding for this research was provided by the Swiss National Science Foundation (grants 200021-109514 and 200020-121600). We used samples provided by the Ocean Drilling Program (ODP). ODP is sponsored by the U.S. National Science Foundation (NSF) and participating countries under management of Joint Oceanographic Institutions (JOI), Inc.

References

Algeo, T. J. and Maynard, J. B., 2004. Trace-element behavior and redox facies in core shales of Upper Pennsylvanian Kansas-type cyclothems. Chemical Geology 206, 289-318.

Arthur, M. A., Schlanger, S. O. and Jenkyns, H., C., 1987. The Cenomanian-Turonian oceanic anoxic event: Palaeoceanographic controls on organic matter production and preservation. *In*: Brooks, J. and Fleet, A. J. (eds) Marine Petroleum Source Rocks. Geological Society of London, Special Publication, 26, 401-420.

Attewell, P. B. and Farmer, I. W., 1976. Principles of engineering geology. Chapman and Hall.

Barker, P. F., Kennett, J. P., et al., 1990, Proceedings of the Ocean Drilling Program, Scientific Results 113, 1033pp.

Baudin, F., Busnardo, R., Beltran, C., de Rafelis, M., Renard, M., Charollais, J. and Clavel, B., 2006. Enregistrement de l’événement anoxique Faraoni (Hauterivien supérieur) dans le domaine ultrahelvétique. Revue de Paléobiologie, 25, 2, 525-535.

Bersezio, R., Erba, E., Gorza, M. and Riva, A., 2002. Berriasian-Aptian black shales of the Maiolica Formation (Lombardian Basin, Southern Alps, Northern Italy): local to global events. Palaeogeography, Palaeoclimatology, Palaeoecology 180, 253-275.

Blanc, E., 1996. Transect plate-forme/bassin dans les séries carbonatées du Berriasien supérieur et du Valanginien inférieur (domaines jurassien et nord-vocontien). Chronostratigraphie et transferts des sédiments. Géologie Alpine Mémoire 25, 312 p.

Bodin, S., Godet, A., Matera, V., Steinmann, P., Vermeulen, J., Gardin, S., Adatte, T., Coccioni, R. and Föllmi, K. B., 2006. Enrichment of redox-sensitive trace metals (U, V, Mo, As) associated with the late Hauterivian Faraoni oceanic anoxic event. International Journal of Earth Sciences, 96, 327-341, DOI 10.1007/s00531-006-0091-9.

Böning, P., Brumsack, H.-J., Böttcher, M. E., Schnetger, B., Kriete, C., Kallmeyer, J. and Borchers, S. L., 2004. Geochemistry of Peruvian near-surface sediments. Geochimica et Cosmochimica Acta 68(21), 4429-4451.

Bralower, T. J., Premoli-Silva, I. and Malone, M. J., 2002. New evidence for abrupt climate change in

the Cretaceous and Paleogene: An Ocean Drilling Program expedition to Shatsky Rise, northwest Pacific. GSA Today, 12(11), 4-10.

Briegel, U., 1972. Geologie der östlichen Alviergruppe (Helvetische Decken der Ostschweiz) unter besonderer Berücksichtigung der Drusberg- und Schrattenkalkformation (Unterkreide). Eclogae geol. Helv. 65, 425-483.

Brumsack, H.-J., 2006. The trace metal content of recent organic carbon-rich sediments: Implications for Cretaceous black shales formation. Palaeogeography, Palaeoclimatology, Palaeoecology 232, 344-361.

Budyko, M. I., Ronov, A. B. and Yanshin, A. L., 1987. History of the Earth's Atmosphere. Springer-Verlag.

Calvert, S. E. and Pedersen, T. F., 1993. Geochemistry of recent oxic and anoxic marine sediments: Implications for the geological record. Marine Geology 113, 67-88.

Channel, J. E. T., Bralower, T. J. and Grandesso, P., 1987. Biostratigraphie correlation of Mesozoic polarity chrons CM1 to CM23 at Capriolo and Xausa (Southern Alps, Italy). Earth and Planetary Science Letters 85, 203-221.

Channel, J. E. T. and Erba, E., 1992. Early Cretaceous polarity chrons CM0 to CM11 recorded in northern Italian land sections near Brescia. Earth and Planetary Science Letters 108(4), 161-192.

Channel, J. E. T., Erba, E. and Lini, A., 1993. Magnetostratigraphic calibration of the Late Valanginian carbon isotope event in pelagic limestones from Northern Italy and Switzerland. Earth and Planetary Science Letters 118, 145-166.

Claypool, G. E. and Baysinger, J. P., 1980. Analysis of Organic matter in sediment cores from the Morrocan Basin, Deep Sea Drilling Project Sites 415 and 416, Init. Rep. Deep Sea Drill. Proj. 50, 605-608.

Deconinck, J.-F., 1987.Identification de l'origine détritique ou diagénétique des assemblages argileux: le cas des alternances marnes-calcaires du Crétacé inférieur subalpin. Bulletin de la Société géologique de France 8 (t.III), 139-145.

Diaz, J., Ingall, E.D., Benitez Nelson, C., Paterson, D., de Jonde, M.D., McNulty, I., Brandes, J.A., 2008. Marine polyphosphate: a key player in geologic phophorus sequestration. Science, 320, 652-655.

Diester-Haass, L., Billups, K., Gröcke, D. R., François, L., Lefebvre, V., and Emeis, K. C., 2009. Mid-Miocene paleoproductivity in the Atlantic Ocean and implications for the global carbon cycle, Paleoceanography 24, PA1209, doi:10.1029/2008PA001605.

Duchamp-Alphonse, S., 2006. Changements paleoenvironnementaux et production carbonatée hémipélagique de la marge nord-ouest tethysienne durant le Valanginien. Unpublished PhD thesis, 304 p.

Duchamp-Alphonse, S., Gardin, S., Fiet, N., Bartolini, A., Blamart, D. and Pagel, M., 2007. Fertilization of the northwestern Tethys (Vocontian basin, SE France) during the Valanginian carbon isotope perturbation: Evidence from calcareous nanofossils and trace element data. Palaeogeography, Palaeoclimatology, Palaeoecology 243, 132-151.

Erba, E., 2004. Calcareous nannofossils and Mesozoic oceanic anoxic events. Marine Micropaleontology 52, 85-106.

Erba, E., Bartolini, A., and Larson, R. L., 2004. Valanginian Weissert oceanic anoxic event. Geology 32, 149-152.

Espitalié, J., Deroo, G. and Marquis, F., 1985. La pyrolyse Rock-Eval et ses applications. Revue de l'Institut Français du Pétrole 40, 563-579.

Föllmi, K. B., 1995. 160 m.y. record of marine sedimentary phosphorus burial : Coupling of climate and continental wearthering under greenhouse and icehouse conditions. Geology 23, 859-862.

Föllmi, K. B., Badertscher, C., de Kaenel, E., Stille, P., John, C., Adatte, T. and Steinmann, P., 2005. Phosphogenesis and organic-carbon preservation in the Miocene Monterey Formation at Naples Beach, California – the Monterey hypothesis revisited. Geological Society of America Bulletin 117, 589-619.

Föllmi, K. B., Godet, A., Bodin, S. and Linder, P., 2006. Interactions between environmental change and shallow water carbonate buildup along the nothern Tethyan margin and their impact on the Early Cretaceous carbon isotope record. Paleoceanography 21, PA4211, doi:10.1029/2006PA001313.

Föllmi, K. B., Weissert, H., Bisping, M. and Funk, H., 1994. Phosphogenesis, carbon-isotope stratigraphy, and carbonate-platform evolution

along the Lower Cretaceous northern Tethyan margin. Geological Society of America Bulletin 106, 729-746.

Force, E.R., Cannon, W.F., 1988. Depositional model for shallow-marine manganese depositis around black shale basins. Economic Geology, 83, 93-117.

Frakes, L. and Bolton, B., 1992. Effects of ocean chemistry, sea level, and climate on the formation of primary manganese ore deposits. Economic geology 87, 1207-1217.

Godet, A., Bodin, S., Adatte, T. and Föllmi, K. B., 2008. Platform-induced clay-mineral fractionation along a northern Tethyan basin-platform transect: implications for the interpretation of Early Cretaceous climate change (Late Hauterivian-Early Barremian), Cretaceous Research, 29, 5-6, 830-847.

Grace, J., Berninger, F., Nagy, L., 2002. Impacts of climate change on the tree line. Annals of Botany, 90, 537-544.

Gröcke, D. R., Price, G. D., Robinson, S.A., Baraboshkin, E. Y., Mutterlose, J. and Ruffell, A. H., 2005. The Upper Valanginian (Early Cretaceous) positive carbon–isotope event recorded in terrestrial plants. Earth and Planetary Science Letters 240, 495-509.

Habib, D., 1983. In: Orlofsky, S., Sheridan, F.M., Gradstein, L.A., Barnard, D.M., Bliefnick, D., Habib, D. et al. (Eds.), Sedimentation-rate-dependent distribution of organic matter in the North Atlantic Jurassic-Cretaceous: Init. Rep. Deep Sea Drill. Proj., vol. 76, 781-794.

Haq, B. U., Hardendol, J. and Vail, P. R., 1987. Chronology of fluctuating sea levels since the Triassic. Science 235, 1156-1166.

Hardenbol, J., Thierry, J., Farley, M. B., de Graciansky, P.-C., Vail, P. R., 1998. Mesozoic and Cenozoic sequence chronostratigraphic framework of European basins, in: P.-C. de Graciansky, J. Hardenbol, T. Jacquin, P.R. Vail (Eds.), Mesozoic and Cenozoic sequence stratigraphy of European basins, Special Publication, Society for Sedimentary Geology 60, 3-13.

Haszeldine, R. S., 1989. Coal reviewed: depositional controls, modern analogues and ancient climates. In Whaetely, M. K. G. and Pickering, K. T. (Eds.), Deltas: Sites and Traps for Fossil Fuels. Geological Society Special Publication 41, 289-308.

Hennig, S., 2003. Geochimical and sedimentological evidence for environmental changes in the Valanginian (Early Cretaceous) of the Tethys region. Unpublished PhD thesis, ETH Zürich, 267 p.

Hennig, S., Weissert, H. and Bulot, L. G., 1999. C-isotope stratigraphy, a calibration tool between ammonite- and magnetostratigraphy: the Valanginian-Hauterivian transition. Geologica Carpathica 50, 91-96.

Herbin, J.P., Deroo, G., Roucaché, J., 1983. In: Buffer, R.T., Schlager W., et al., (Eds.), Organic geochemistry of lower Cretaceous sediments from Site 535, leg 77, Florida Straits: Init. Rep. deep Sea Drill. Proj. vol. 77, 459-474.

Herbin,J. P., Masure, E. and Roucaché, J., 1987. Cretaceous formations from the lower continental rise off Cape Hatteras; organic geochemistry, dinoflagellate cysts, and the Cenomanian/Turonian boundary event at sites 603 (Leg 93) and 105 (Leg 11), in: J.H. Blakeslee, E. Whalen (Eds.), Init. Rep. Deep Sea Drill. Proj. 93(1-2) (1987) 1139–1162.

Hughes, T.P., Baird, A.H., Bellwood, D.R., Card, M., Connolly, S.R., Folke, C., Grosberg, R., Hoegh-Guldberg, O., Jackson, J.B.C., Kleypas, J., Lough, J.M., Marshall, P., Nyström, M., Palumbi, S.R., Pandolfi, J.M., Rosen, B., Roughgarden, J., 2003. Climate Change, Human Impacts, and the Resilience of Coral Reefs, Science, 301, 929-933.

Jenkyns, H. C., 1980. Cretaceous anoxic events: from continents to oceans. Jounal of the geological Society of London 137, 171-188.

Jenkyns, H. C., Gale, A. S. and Corfield, R. M., 1994. Carbon- and oxygen-isotope stratigraphy of the English Chalk and Italian Scaglia and its palaeoclimatic significance. Geol. Mag. 131, 1-34.

Kolonic, S., Wagner, T., Forster, A., Sinnighe Damsté, J. S., Walsworth-Bell, B., Erba, E., Turgeon, S., Brumsack, H.-J., Chellai, E. H., Tsikos, H., Kuhnt, W. and Kuypers, M. M. M., 2005. Black shale deposition on the northwest African Shelf during the Cenomanian/Turonian oceanic anoxic event: Climate coupling and global organic carbon burial. Paleoceanography 20, PA1006.

Katz, B. J., 1983. Organic geochemical character of some deep sea drilling project cores from legs 76 and 44. in: S. Orlofsky (Ed.), Sheridan, F.M.

,Gradstein, L.A., Barnard, D.M., Bliefnick, D., Habib, et al., Init. Rep. Deep Sea Drill. Proj. 76 (1983) 463–468.

Kuhn, O., Weissert, H., Föllmi, K. B. and Hennig, S., 2005. Altered carbon cycling and trace-metal enrichment during the late Valanginian and early Hauterivian. Eclogae geol. Helv. 98, 333-344.

Kuhnt, W., Nederbragt, A. and Leine, L., 1997. Cyclicity of Cenomanian-Turonian organic-carbon-rich sediments in the Tarfaya Atlantic Coastal Basin (Morocco), Cretaceous Research, 18, 4, 587-601.

Kuypers, M. M. M., Lourens, L. J., Rijpstra, W. I. C., Pancost, R. D., Nijenhuis, I. A. and Sinninghe Damsté, J. S., 2004. Orbital forcing of organic carbon burial in the proto-North Atlantic during oceanic anoxic event 2. Earth and Planetary Science Letters, 228, 465-482.

Langrock, M., Stein, R., Lipinski, M. and Brumsack, H.-J., 2003. Late Jurassic to Early Cretaceous black shale formation and paleoenvironment in high northern latitudes: Examples from the Norwegian-Greenland Seaway. Paleoceanography 18, DOI: 10.1029/2002PA000867.

Langrock, U. and Stein, R., 2004. Origin of marine petroleum source rocks from the Late Jurassic to Early Cretaceous Norwegian Greenland Seaway—evidence for stagnation and upwelling. Marine and Petroleum Geology 21, 157-176.

Leckie, R. M., Bralower, T. J. and Cashman, R., 2002. Oceanic anoxic events and plankton evolution: Biotic response to tectonic forcing during the mid-Cretaceous. Paleoceanography 17, 1-29.

Lesniak, P. M., Lacka, B., Krajewski, K. P., Zawidski, P. and Hladikova, J., 2003. Extreme sulfur isotopic fractionation between sulfate of carbonate fluorapatite and authegenic pyrite in the Neocomian sequence at the Wawal, Central Poland. Chemical Geology 200, 325-337.

Lini, A., Weissert, H. and Erba, E., 1992. The Valanginian carbon isotope event : a first episode of greenhouse climate condition during the Cretaceous. Terra Nova 4, 374-384.

Lipinski, M., Warning, B. and Brumsack, H.-J., 2003. Trace metal signatures of Jurassic/Cretaceous black shales from the Norwegian Shelf and the Barents Sea. Palaeogeography, Palaeoclimatology, Palaeoecology 190, 459-475.

McArthur, J. M., Janssen, N. M. M., Reboulet, S., Leng, M. J., Thirlwall, M. F. and Van de Schootbrugge, B., 2007. Palaeo-temperatures, polar ice-volume, and isotope stratigraphy (Mg/Ca, $\delta^{18}O$, $\delta^{13}C$, $^{87}Sr/^{86}Sr$): the Early Cretaceous (Berriasian, Valanginian, Hauterivian). Palaeogeography, Palaeoclimatology, Palaeoecology 202, 252-272.

McCabe, P. J. and Totman Parrish, J., 1992. Tectonic and climatic controls on the distribution and quality of Cretaceous coals. In McCabe, P. J. and Totman Parrish, J. (Editors), Controls on the Distribution and Quality of Cretaceous Coals. Geological Society of America, Special Publication 267, 1-16.

Meyers, P. A., 1987. Organic-carbon content of sediments and rocks from Deep Sea Drilling Project Sites 603, 604 and 605, Western margin of the North Atlantic. Init. Reports of the DSDP 93, 1187-1194.

Morford, J. L. and Emerson, S. R., 1999. The geochemistry of redox sensitive trace metal in sediments. Geochimica et Cosmochimica Acta 63, 1735-1750.

Mort, M., Adatte, T., Föllmi, K. B., Keller, G., Steinmann, P., Matera, V., Berner, Z. and Stüben, D., 2007. Phosphorus and the roles of productivity and nutrient recycling during oceanic event 2. Geology 35, 483-486.

Müller, P. J. and Suess, E., 1979. Productivity, sedimentation rate, and sedimentary organic matter in the ocean. I. Organic carbon preservation. Deep-Sea Research 26, 1347-1362.

Mutterlose, J., Brumsack, H.-J., Flögel, S., Hay, W. W., Klein, C., Langrock, U., Lipinski, M., Ricken, W., Söding, E., Stein, R. and Swientek, O., 2003. The Greenland-Norwegian Seaway: A key area for understanding Late Jurassic to Early Cretaceous paleoenvironments. Paleoceanography 18, DOI 10.1029/2001PA000625.

Mutterlose, J. and Wise S. W., 1990. Lower Cretaceous nannofossil biostratigraphy of ODP leg 113 holes 692B and 693A, continental slope off east Antractica, Weddell Sea. In Barker, P. F., Kennett, J. P., et al., Proceedings of the Ocean Drilling Program, Scientific Results 113, 325-351.

O'Connell, S. B., 1990. Sedimentary facies and depositional environment of the lower Cretaceous East Antarctic margin: Sites 692 and 693. In Barker, P. F., Kennett, J. P., et al., Proceedings of the Ocean Drilling Program, Scientific Results

113, 71-88.

Ogg, J.G, Ogg, G., Gradstein, F.M., 2008. The concise geological time scale. Cambridge University Press, 177 pp.

Peters, K. E., Kontorovich, A. E., Moldowan, J. M., Andrusevich, V. E., Huizinga, B. J., Demaison, G. J. and Stasova, O. F.,1993. Geochemistry of selected oils and rocks from the central portion of the West Siberian Basin, Russia. The American Association of Petroleum Geologists Bulletin 77, 863-887.

Price, G. D., 1999. The evidence and implications of polar ice during the Mesozoic. Earth-Science Reviews 48, 183-210.

Price, G. D., Ruffell, A. H., Jones, C. E., Kalin, R. M. and Mutterlose, J., 2000. Isotopic evidence for temperature variation during the early Cretaceous (late Ryazanian-mid-Hauterivian). Journal of the Geological Society of London 157, 335-343.

Reboulet, S. and Atrops, F., 1999. Comments and proposals about the Valanginian-Lower Hauterivian ammonite zonation of south-eastern France. Eclogae geol. Helv. 92, 183-197.

Reboulet, S., Mattioli, E., Pittet, B., Baudin, F., Olivero, D. and Proux, O., 2003. Ammonoid and nannoplankton abundance in Valanginian (early Cretaceous) limestone-marl successions from the southeast France Basin: carbonate dilution or productivity? Palaeogeography, Palaeoclimatology, Palaeoecology 201, 113-139.

Redfield, A. C., 1958. The biological control of chemical factors in the environment. American Scientist 46, 205 – 222.

Schlager, W., 1981. The paradox of drowned reefs and carbonate platforms. Bulletin of the Geological Society of America 92, 197-211.

Schlanger, S. O. and Jenkyns, H. C., 1976. Cretacous oceanic anoxic event: causes and consequences. Geolgie en Mijnbouw 55, 179-188.

Scholle, P. A. and Arthur, M. A., 1980. Carbon isotope fluctuations in Cretaceous pelagic limestone: potential stratigraphic and petroleum exploration tool. American Association of Petroleum Geologist Bulletin, 64, 67-87.

Smith, G.A., Smith D. G. and Funnel B. M., 1994. Atlas of Mesozoic and Cenozoic coastlines. Cambridge Univ. Press, London.

Stein, R., 1991. Accumulation of organic carbon in marine sediments. Lecture notes in Earth Science, Springer, 217 pp.

Stein, R. and Rullkötter, J., 1988. Organofacies reconstruction and lipid geochemistry of sediments from the Galicia margin, Northeast Atlantic (ODP leg 103). In Boillot, G., Winterer, E. L., et al., Proceedings of the Ocean Drilling Program, Scientific Results 103, 567-585.

Tribovillard, N., Algeo, T. J., Lyons, T. W. and Riboulleau, A., 2006. Trace metals as paleoredox and paleoproductivity proxies: An update. Chemical Geology 232, 12-32.

Tribovillard, N., Riboulleau, A., Lyons, T. and Baudin, F., 2004. Enhanced trapping of molybdenum by sulfurized marine organic matter of marine origin in Mesozoic limestones and shales. Chemical Geology 213, 385-401.

Turgeon, S. and Brumsack, H.-J., 2006. Anoxic vs dysoxic events reflected in sediment geochemistry during the Cenomanian-Turonian Boundary Event (Cretaceous) in the Umbria-Marche Basin of central Italy. Chemical Geology 234, 321-339.

Tyson, R. V., 1995. Sedimentary organic matter. Chapman and Hall ed., London, 615 pp.

Van de Schootbrugge, B., Kuhn, O., Adatte, T., Steinmann, P. and Föllmi, K. B., 2003. Decoupling of P and C_{org} burial following Early Cretaceous (Valanginian/Hauterivian) platform drowning along the NW Tethyan margin. Palaeogeography, Palaeoclimatology, Palaeoecology 199, 315-331.

Van Hinte, J. E., Wise, S. W., Biart, B. N., Covington, J. M., Dunn, D. A., Haggerty, J. A., Johns, M. W., Meyers, P. A., Moullade, M. R., Muza, J. P., Ogg, J. G., Okamura, M., Sarti, M. and von Rad, U., 1987. Site 603, DSDP Shipborad Scientific party. *In* Van Hinte, Wise S. W. et al., Init. Rept. DSDP: Washington (US Govt. Printing Office), 93, 25-276.

Vyssotski, A. V., Vyssotski, V. N. and Nezhdanov, A. A., 2006. Evolution of the West Siberian Basin. Marine and Petroleum Geology, 23, 93-126.

Weissert, H. J., 1979. Die Paläozeanographie der südwestlichen Tethys in der Unterkreide. Mitteilungen aus dem geologischen Institut der ETH und Universität Zürich 226, 174 pp.

Weissert, H., Lini, A., Föllmi, K. and Kuhn, O., 1998. Correlation of early Cretaceous carbon isotope stratigraphy and plate-form drowning event: a possible link? Palaeogeography, Palaeoclimatology, Palaeoecology 137, 189-203.

Westermann, S., 2010. Trace-element and phosphorus contents in sediments associated with Cretaceous anoxic events. Unpublished Ph.D. thesis, University of Lausanne, 223 pp.

Ziegler, A. M., Raymond, A. L., Gierlowski, T. C., Horrell, M. A., Rowley, D. B. and Lottes, A. L., 1987. Coal, Climate and terrestrial productivity: the present and the early Cretaceous compared. Geological Society Special Publication 32, 22-49.

Appendix A: TOC/N ratios in the samples of Capriolo and Wawal.

	Sample ID	N %	C %	TOC %	TOC/N[1]
Capriolo	CA 31	0.07	0.76	1.32	17.81
	CA 35	0.08	2.28	0.68	8.23
	CA 45	0.08	1.96	1.62	20.04
	CA 61	0.05	0.81	0.50	9.50
	CA 93	0.17	3.93	1.48	8.85
	CA 96	0.09	3.54	0.96	10.49
	CA 122	0.18	1.42	0.58	3.28
Wawal	e29471	0.11	3.47	1.66	15.81
	e29472	2.76	6.96	1.28	0.46
	e29473	2.03	5.25	0.77	0.38
	e29474	0.05	0.99	0.65	12.50
	e29475	0.11	3.53	2.94	27.22
	e23477	0.04	0.67	0.28	7.18
	e23478	0.07	2.29	2.41	34.43

[1] TOC/N are expressed as molar ratios

Appendix B: Redox-sensitive trace-element contents in the Valanginian samples for the studied sections. The grey bands indicate the organic-riched samples.

Sample ID	Core	U	V	Co	As	Mo	Zn	Cu	Cr	Fe	Mn	Al
SR 50	015R	1.24	47.37	13.37	11.24	4.25	76.61	167.98	52.24	25918.21	104.21	6372.85
SR 51	015R	0.29	5.34	1.09	0.79	0.28	20.97	14.54	5.06	1440.12	3.69	684.31
SR 52	015R	0.27	3.57	0.73	0.54	0.16	6.63	8.18	3.29	896.04	2.10	349.36
SR 53	019R	0.29	4.20	1.24	0.63	0.14	7.87	11.90	2.92	1046.50	2.33	314.27
SR 54	019R	0.18	4.19	0.71	0.79	0.21	33.37	13.15	4.42	1759.94	4.78	596.66
SR 55	019R	1.03	32.25	4.25	2.20	0.75	69.93	95.45	20.12	19683.53	561.07	4888.29
SR 56	019R	1.19	26.77	3.21	2.14	0.54	82.47	106.93	19.31	10558.44	462.98	2239.89
SR 57	019R	1.12	40.31	4.07	2.22	0.90	53.15	110.91	22.17	13928.33	504.11	3923.66
SR 58	019R	1.70	64.26	9.41	23.89	4.08	134.13	141.61	57.30	58376.65	281.49	1885.12
SR 59	019R	0.69	41.54	4.95	7.35	2.12	132.57	61.60	25.45	27954.31	518.88	1399.73

All the values are expressed in ppm.

Appendix C: data base for samples for Leg 198 site 1213B.

Leg	Site	Core	Section	Sample ID	Interval
198	1213B	015R	01W	SG001773950	08-09
		015R	01W	SG001773951	12-13
		015R	01W	SG001773952	15-16
198	1213B	019R	01W	SG001773953	20-21
		019R	01W	SG001773954	100-101
		019R	01W	SG001773955	105-106
		019R	01W	SG001773956	108-109
		019R	01W	SG001773957	110-111
		019R	01W	SG001773958	114-115
		019R	01W	SG001773959	117-118

-C2-
Paleoceanographic Change along a Tethyan Shelf-Basin Transect during the Valanginian Carbon-Isotope Excursion

Stéphane Westermann[1], Virginie Matera[2], Thierry Adatte[1], Nicolas Fiet[3,4], Dominik Fleitmann[5] and Karl B. Föllmi[1]

[1]Institute of geology and paleontology, University of Lausanne, Anthropôle, 1015 Lausanne, Switzerland.
[2]Institute of geology, University of Neuchâtel, Emile Argand 11, CP 158, 2009 Neuchâtel, Switzerland.
[3]UMR 8148 – I.D.E.S., Bât. 504, University of Paris XI Orsay, 91405 Orsay Cedex, France.
[4]AREVA, 33 rue La Fayette, 75009 Paris, France.
[5]Institute of Geological Sciences, University of Bern, Baltzerstrasse 1-3, 3012 Bern, Switzerland.

Manuscript in preparation for publication in Swiss Journal of Geosciences.

Abstract

The Early Cretaceous Valanginian stage is marked by a pronounced positive shift in the marine carbonate $\delta^{13}C$ record, which has commonly been interpreted as the expression of a global anoxic event. Here we evaluate paleoenvironmental and paleoclimatic change during this episode by investigating both bulk-rock and clay mineralogies, as well as phosphorus contents in a selection of five sections along a shelf/basin transect in the western Tethys (Capriolo, N Italy; Breggia, S Switzerland; Vergol, SE France; Alvier, E Switzerland; and Malleval, E France).Our results suggest a stepwise climatic evolution during the Valanginian in the western Tethys. In the Early Valanginian period preceding the $\delta^{13}C$ shift (*Pertransiens* to *Campylotoxus* zone), western tethyan shelf sediments are characterized both by the presence of kaolinite in their clay-mineral assemblages, as well as increasing or relatively high Phosphorus Accumulation Rates (PAR) and Detrital Index (DI) values. This is interpreted as an indication of warmer and more humid climate conditions on the southern European margin, which was associated with higher continental runoff and higher nutrient levels along the northern Tethyan margin. The northern Tethyan margin carbonate platform drowned as a consequence of these changing conditions. The increase in nutrient levels did, however, not lead to the development of widespread dys- to anaerobic conditions in the western Tethyan pelagic realm (low C/P ratios in Capriolo). The only indication fro a series of short-lasted dysaerobic to anaerobic episodes in the western Tethys is given by the presence of thin and organic-rich "Barrande layers" in Vergol. During the $\delta^{13}C$ shift, a general decrease in DI and PAR values is observed, which goes along with the complete disappearance of kaolinite on the shelf. These changes indicate a change toward dryer climate conditions. The period corresponding to the second part of the $\delta^{13}C$ excursion (*Verrucosum* zone) is characterized by stable or increasing DI and PAR, which may indicate a trend to stable or slightly more humid conditions.

***Keywords**: Valanginian, phosphorus accumulation rate (PAR), detrital index, clay minrelogy, oceanic anoxic event (OAE)*

C2.1 Introduction

The Early Cretaceous recorded pronounced episodes of paleoceanographic and paleoenvironmental change, which were associated with perturbations in the global carbon cycle. These episodes are characterized by distinct changes in ocean chemistry, nutrient stocks and climate in general, and provide excellent subjects for the study of geosphere-biosphere interactions and their consequences for general environmental

and climate evolution (Schlanger and Jenkyns, 1976; Föllmi,1995; Leckie et al., 2002).

The Valanginian includes the oldest Cretaceous episode of major environmental change (Fig. C2.1), which is characterized by a positive excursion of ~1.5‰ in the marine carbonate $\delta^{13}C$ record (Lini et al., 1992; Föllmi et al., 1994; Weissert et al., 1998; Hennig, 2003; Erba et al., 2004). This shift is associated with rapid change in nannofossil evolution and a crisis in shallow-water carbonate ecosystems (Lini et al., 1992; Erba et al., 2004; Duchamp-Alphonse et al., 2007). In the northern Tethyan Helvetic realm, these changes are coeval with demise of the northern tethyan carbonate platform (Föllmi et al., 1994, 2006). The Valanginian episode is considered to include the first oceanic anoxic event (OAE) of the Cretaceous ("Weissert event"; Erba et al., 2004).

The character of environmental change, which drove the Valanginian $\delta^{13}C$ shift remains unclear. For example, Lini et al., (1992) and Weissert et al. (1998) inferred a rapid increase in atmospheric CO_2 due to the formation of the Paraña-Etendeka basaltic plateau, and Föllmi et al. (1994, 2006) invoked an increase in the availability of phosphorus - an essential element in driving primary productivity. Further aspects of Valanginian environmental change remain equally unclear. This includes, for instance, the importance of glaciation during the Valanginian (Price, 1999; Price et al, 2000; McArthur et al, 2007).

Climate change may be deduced from temporal variations in clay and bulk rock mineralogy (Ruffell and Blattern, 1990; Ruffell et al, 2002; Godet et al., 2008). Clay minerals are good indicators of the intensity of geochemical continental weathering processes since climate change influences average temperature, humidity and seasonality (Ruffell, et al., 2002). Upper Tithonian-Berriasian sediments from the Jura Mountains contain relatively high amounts of kaolinite, whereas the Late Valanginian-Hauterivian period is characterized by high smectite contents in the clay fraction (Ruffell et al., 2002). This change suggests that the Late Valanginian-Hauterivian experienced colder and more seasonally contrasted conditions (Persoz, 1982; Adatte and Rumley, 1989).

Global oceanic Phosphorus Accumulation Rates (PAR), estimated from sediments analyzed in the framework of the Deep Sea Drilling Project (DSDP) and Ocean Drilling Program (ODP) (Föllmi, 1995), indicate a long-term increasing trend during the Late Berriasian and Valanginian. Phosphorus (P) is an important and often limiting element in primary productivity (Ingall and Jahnke, 1994; Tyrrell, 1999). The P cycle is closely

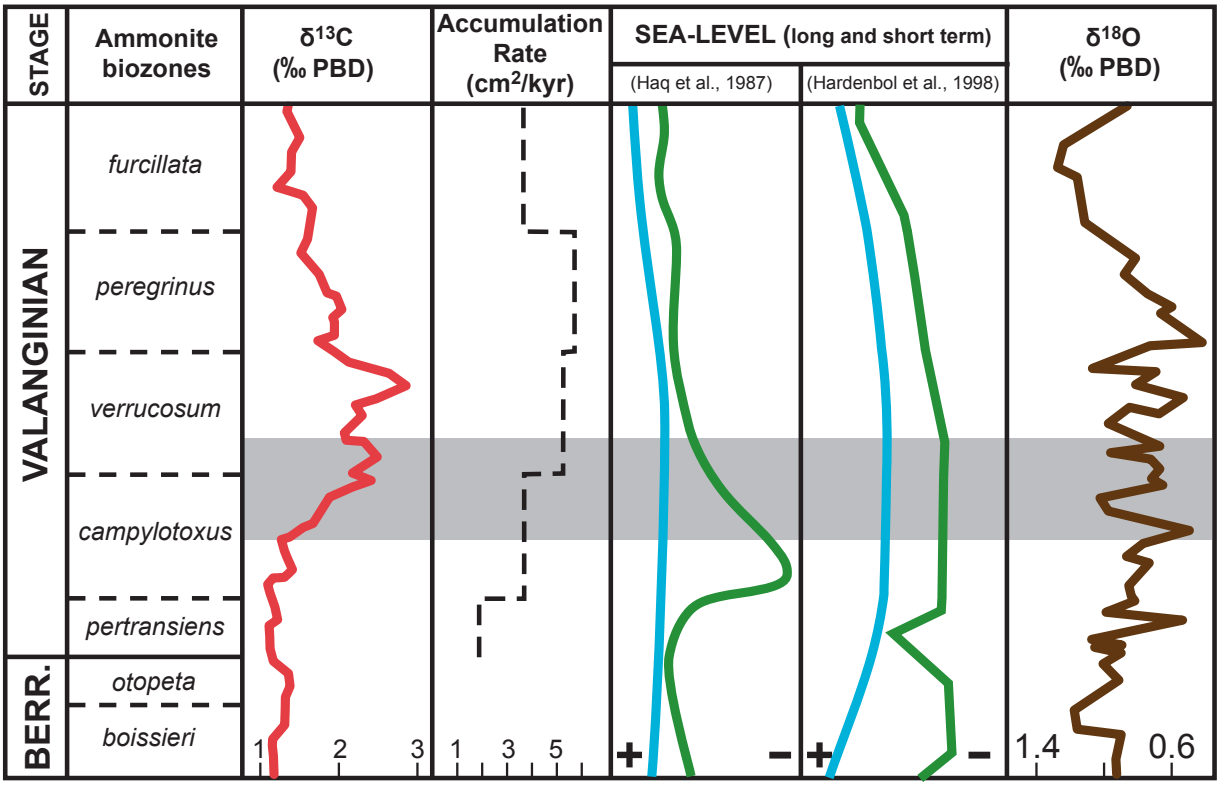

Fig. C2.1: Trends in the evolution of the whole-rock $\delta^{13}C$ record (Föllmi et al., 2006), sediment accumulation record (calculated form the Angles section, Duchamp-Alphonse, 2006), sea-level change (Haq et al., 1987; Hardenbol et al., 1998) and a simplified whole-rock and belemnite $\delta^{18}O$ record during the Valanginian (McArthur et al, 2007), calibrated in time against the paleomagnetic record and ammonite biostratigraphy (Ogg et al., 2008).

linked to the carbon cycle by two processes: (1) by continental weathering during which atmospheric CO_2 is transformed into HCO_3^- and P is mobilized; and (2) by photosynthesis, which is often limited by P as a nutrient (Föllmi et al., 2004; Bodin et al., 2006). A detailed reconstruction of regional change in the P cycle during this critical period may help to improve our understanding of the mechanisms leading to the changes in the carbon cycle indicated by the positive $\delta^{13}C$ excursion.

In this study, five pelagic or hemi-pelagic sections (Fig. C2.2) located in Capriolo (northern Italy), Breggia (southern Switzerland), Vergol (southeastern France), Alvier (eastern Switzerland) and Malleval (eastern France) were analyzed to evaluate the paleoclimatic evolution and depositional environment by tracing temporal change in clay and bulk-rock mineralogy and to estimate the nutrient levels in the western Tethys by quantifying total P content and related PAR.

C2.2 Geological settings

C2.2.1 The central Tethyan realm

We selected two sections of the Lombardian Basin (Capriolo and Breggia) in order to characterize the distal, pelagic environment. The Capriolo section is situated in an abandoned quarry near the village of Capriolo (northern Italy, Lini et al., 1992). The Breggia section outcrops in the Mt Generoso half graben close to the Breggia River (southern Switzerland, Ct Ticino; Bersezio et al, 2002). Both sections consist of a monotone limestone succession belonging to the Maiolica formation (Late Tithonian to Early Aptian; Lini et al., 1992). A good temporal framework is provided by carbon isotope stratigraphy, nannofossil biostratigraphy and magnetostratigraphy (Weissert et al., 1985; Channel et al., 1987; Channel and Erba, 1992; Lini et al., 1992; Channel et al., 1993; Bersezio et al., 2002).

C2.2.2 The northern Tethyan margin

We selected the section of Vergol because of the presence of the so-called “Barrande” layers (Reboulet et al., 2003), which correspond to centimetric organic-rich layers (B1, B2 B3 and B4). The “Barrande” layers are the only organic-rich sediments of Valanginian age known in the Vocontian Trough. The section outcrops along a secondary road between Montbrun-Les-Bains and Vergol (SE France). It is located in the central part of Vocontian Trough (Reboulet et al., 2003). This section is characterized by marl-limestone alternations. The biostratigraphy is based on ammonoids and well constrained for the Valanginian (Reboulet and Atrops, 1999; Reboulet et al., 2003). In our study, we focus on a two-meter interval, within the *Campylotoxus* zone, including all “Barrande” layers.

C2.2.3 The northern Tethyan shelf

To characterize the shelf environment of the northern Tethyan margin, the sections of Alvier (eastern Switzerland, Ct. St. Gall) and Malleval (Vercors, eastern France) were sampled. The Alvier section, located along a cliff near Sargans and Buchs, corresponds to the outer part of the shelf. This section is composed by a monotone limestone and marly-limestone succession. The base of the section belongs to the Diphyoides Formation (Valanginian) and the top to the Kieselkalk formation (Hauterivian; Briegel, 1972). The stratigraphic framework is given by the $\delta^{13}C$ curve (Föllmi et al., 1994).

The section of Malleval is located along a road between Malleval and the inn of Lombardière (Vercors) and consists of a sparitic limestone succession. The first part belongs to the “calcaires des Ecouges” Formation (thick limestone beds dated as late Berriasian; Blanc 1996). We focused on sediments corresponding to the *Campylotoxus* and *Verrucosum* zones (Blanc, 1996).

C2.3 Methods

C2.3.1 X-ray diffraction

X-ray diffraction analyses were performed to identify and quantify the bulk-rock and clay mineral assemblages. The mineralogical composition is determined by using a semi-quantifying method described by Kübler (1987) and Adatte et al (1996). About 800 mg of powdered sample were pressed in a powder holder and analyzed by a SCINTAG XRD 2000 diffractometer with a 5% error for grain minerals. For the clay-mineral analysis, samples were decarbonated by 10% HCl during 20 minutes. After having been washed, the insoluble residue was centrifuged in order to separate two granulometric fractions (< 2μm and 2-16 μm) (see Adatte et al., 1996 and references therein for more information).

For the bulk rock composition, the different minerals recognized and quantified are calcite, phyllosilicates, quartz, Na plagioclase (albite) and K feldspar (microcline). Poorly crystallized minerals (goethite for

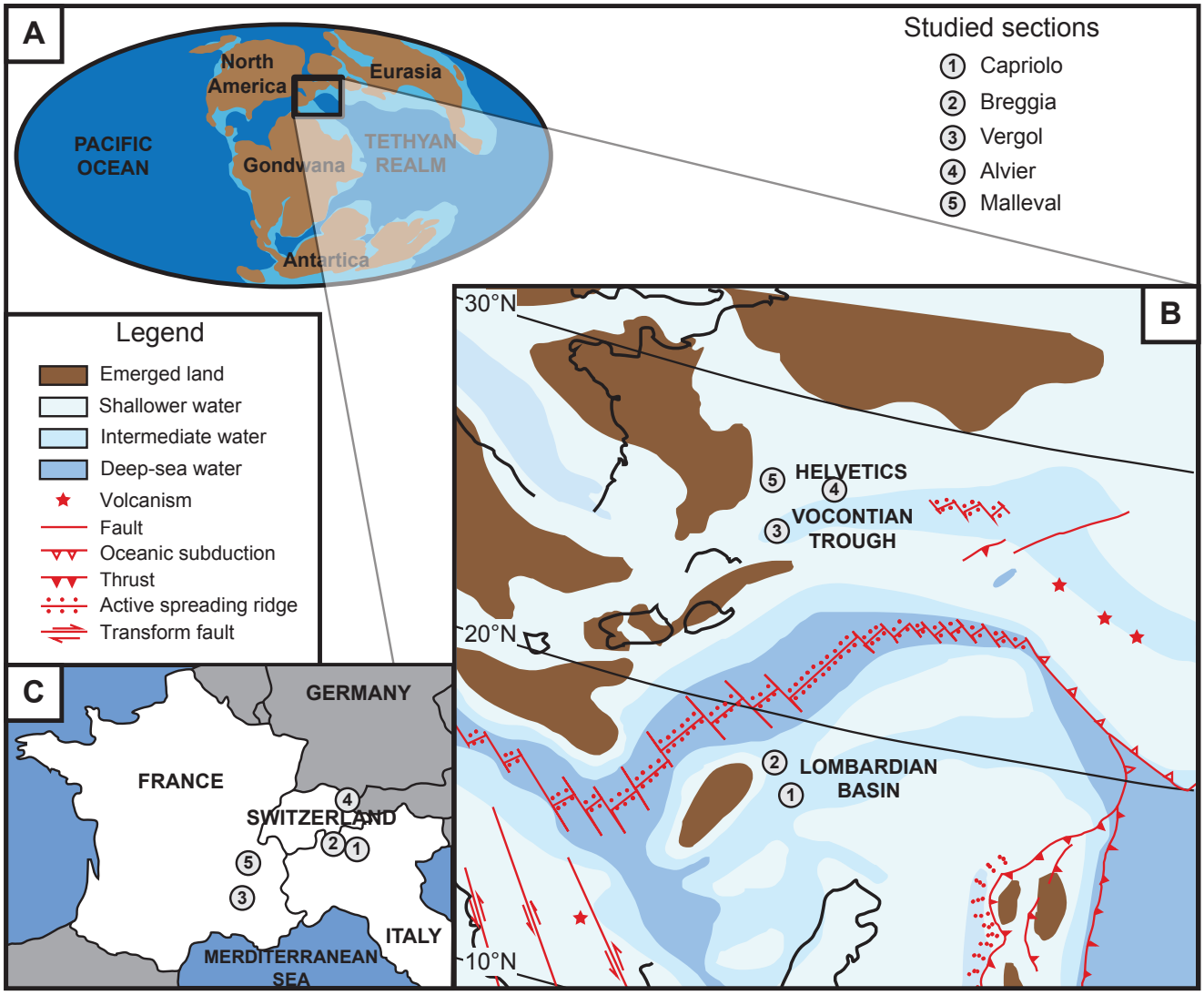

Fig. C2.2: A. Valanginian paleogeography map of the world (modified after Smith et al., 1994). B. Map of the western Tethys in the Early Cretaceous (redrawn after Hennig et al., 1999). C. Localisation of the five studied sections.

example), ankerite and dolomite were not quantified due to the low intensity of their respective peak and were included in the non-quantified component of the sample. A detrital index (DI) was calculated by dividing the sum of quartz, phyllosilicates, Na plagioclase, K feldspar intensities by calcite, assuming that quartz is of detrital origin. With regard to the clay-mineral assemblages, we identified mica, kaolinite, smectite, chlorite, illite/smectite irregular (R0) and ordered (rectorite, R1) for this study.

C2.3.2 Phosphorus contents

Total P analyses were performed on bulk rock samples. 1 ml of 1 M $MgNO_3$ was added to 100mg of powder and left in an oven at 130°C during 2 hours to oxidize the organic matter. Then, the samples were heated at 550°C during 2 hours. After cooling, 10 mL of HCL (1N) was added in order to liberate the P from the sediment matrix and the solutions were placed in a shaker during 16 hours. The solutions were filtered (0.45µm) and analyzed using the ascorbic acid method (Eaten et al., 1995). For this process, the solutions were diluted ten times and mixed with 100 µL molybdate mixing reagent to form phosphomolybdic acid. 100 µL of ascorbic acid was added to the solution to reduce the acid and produce a blue colour to the solution, which intensity is dependent on the P concentration.

Total P analyses were performed on bulk rock using a UV/Vis spectrophotometer (Perking Elmer UV/Vis Spectrophotometer Lamba 10, λ=865nm) with a mean precision of 5%.

To avoid the effect of condensation, total P contents were converted in Phosphorus Accumulation Rates (PAR) expressed in mg/cm²/ka.

PAR (mg/cm²/kyr)=[P](mg/g) x Sedimentation rate (cm/kyr) x Rock density

Capriolo

Sample ID	Feldspars-K	Plagioclase	Calcite	Unquantified
CA 19	0.00	1.04	94.45	1.45
CA 23	0.19	0.00	97.45	0.84
CA 27	0.43	0.07	79.41	12.53
CA 40	0.00	0.00	87.58	7.11
CA 49	0.27	0.10	88.18	6.80
CA 52	0.00	0.00	81.34	14.50
CA 58	0.57	0.24	85.30	6.62
CA 60	0.00	0.11	93.45	0.24
CA 70	0.09	0.24	87.44	5.05
CA 74	0.00	0.11	93.23	1.26
CA 83	0.09	0.07	94.21	0.22
CA 91	0.00	0.00	96.34	0.10
CA 94	0.11	0.00	63.56	31.62
CA 99	0.13	0.03	83.45	11.94
CA 101	0.43	0.27	82.69	13.52
CA 106	0.00	0.00	94.10	0.35
CA 109	0.18	0.10	91.67	1.06
CA 113	0.42	0.22	95.72	0.08
CA 116	0.51	0.10	87.45	8.25
CA 118	0.09	0.10	85.92	6.86
CA 122	0.13	0.29	78.56	11.20
CA 123	0.24	0.15	88.77	1.36
CA 125	0.00	0.00	78.90	17.85
CA 128	0.22	0.31	91.97	2.02
CA 130	0.18	0.52	85.43	3.40
CA 134	0.50	0.64	78.01	15.86
CA 136	0.09	0.33	79.87	12.37
CA 138	0.56	0.00	81.65	7.35
CA 142	0.18	0.49	94.82	1.58
CA 146	0.00	0.00	92.14	0.05
CA 148	0.43	0.30	83.77	9.91
CA 149	0.27	0.21	90.18	0.58
CA 151	0.00	0.15	91.24	3.96
CA 153	0.00	0.00	60.13	36.69
CA 154	0.29	0.22	71.60	24.84
CA 155	0.00	0.00	91.86	1.01
CA 157	0.00	0.16	93.27	0.06
CA 159	0.09	0.14	92.56	0.27
CA 161	0.00	0.15	93.16	0.34
CA 165	0.00	0.21	91.45	0.56

Breggia

Sample ID	Feldspars-K	Plagioclase	Calcite	Unquantified
BgV 1	0.00	0.12	88.34	1.21
BgV 3	0.10	0.00	92.89	0.21
BgV 5	0.00	0.23	87.01	1.87
BgV 8	0.00	0.00	91.99	0.57
BgV 11	0.00	0.00	89.12	1.97
BgV 14	0.25	0.00	75.34	8.56
BgV 16	0.00	0.11	85.54	6.81
BgV 17	0.00	0.00	93.78	0.12
BgV 18	0.16	0.00	88.13	0.11
BgV 20	0.10	0.00	89.17	2.06
BgV 21	0.00	0.34	88.54	0.23
BgV 23	0.19	0.14	82.44	0.78
BgV 25	0.49	0.71	85.09	1.31
BgV 27	0.27	0.00	91.45	0.37
BgV 29	0.09	0.25	85.89	6.13
BgV 31	0.17	0.09	84.14	1.23
BgV 33	0.06	0.21	89.56	0.64
BgV 34	0.18	0.37	90.43	0.97
BgV 35	0.12	0.77	85.43	0.39
BgV 38	0.11	0.25	94.83	0.53
BgV 40	0.04	0.23	89.34	4.67
BgV 45	0.54	0.00	92.98	2.56
BgV 47	0.00	0.00	93.04	1.49
BgV 48	0.10	0.00	93.76	0.15
BgV 49	0.11	0.52	84.89	0.86
BgV 50	0.00	0.08	90.43	1.76
BgV 51	0.00	0.44	91.67	0.07
BgV 53	0.00	0.00	94.43	0.87
BgV 55	0.00	0.00	91.36	0.11
BgV 57	0.00	0.00	90.76	2.12
BgV 58	0.05	0.00	92.04	0.14
BgV 60	0.00	0.08	94.53	0.68

Alvier

Sample ID	Feldspars-K	Plagioclase	Calcite	Unquantified
Al 54	0.00	5.79	68.98	1.47
Al 56	0.00	1.17	79.34	0.62
Al 59	0.00	1.68	72.65	0.82
Al 62	0.00	2.34	70.14	3.83
Al 66	0.00	4.63	78.12	1.29
Al 69	0.13	1.72	71.23	15.31
Al 70	0.00	2.63	83.00	0.77
Al 72	0.00	2.13	75.32	11.84
Al 75	0.00	2.54	76.03	1.24
Al 77	0.00	0.31	81.17	0.40
Al 81	0.00	1.07	76.03	0.63
Al 85	0.15	0.78	79.94	0.28
Al 88	0.00	1.47	77.54	7.43
Al 89	0.00	1.51	72.00	0.17
Al 90	0.00	1.96	78.34	3.21
Al 92	0.00	0.90	77.45	7.55
Al 93	0.00	2.17	83.88	1.50
Al 95	0.00	2.00	82.07	0.47
Al 97	0.00	1.77	76.99	5.23
Al 99	0.00	1.61	80.40	4.57
Al 102	0.00	1.04	76.05	0.59
Al 105	0.00	0.56	88.44	4.88
Al 107	0.00	1.79	80.43	5.68
Al 109	0.00	1.60	73.08	0.98
Al 110	0.12	1.86	77.09	5.97
Al 113	0.00	3.19	74.32	1.32
Al 118	0.00	0.88	70.56	1.24
Al 120	0.00	1.34	67.43	11.49
Al 122	0.11	1.23	70.32	0.57
Al 125	0.09	1.07	79.26	0.63
Al 127	0.00	1.16	71.34	0.43

Vergol

Sample ID	Feldspars-K	Plagioclase	Calcite	Unquantified
Ve 1	0.28	0.53	72.71	1.12
Ve 2	0.72	0.26	60.97	6.42
Ve 3	0.00	0.22	58.58	14.37
Ve 4	0.18	0.49	70.34	1.67
Ve 5	0.41	0.35	75.85	4.84
Ve 6	0.10	0.93	60.26	2.65
Ve 7	0.47	0.58	37.93	13.40
Ve 8	0.34	0.56	51.65	13.26
Ve 9	0.98	0.76	39.32	16.96
Ve 10	0.28	0.76	52.37	13.24
Ve 11	0.00	0.00	43.77	20.50
Ve 12	0.00	0.00	75.12	1.31
Ve 13	0.14	0.51	64.34	3.40
Ve 15	0.00	0.13	84.32	1.26
Ve 16	0.00	0.00	75.59	1.47
Ve 17	0.34	0.53	47.09	9.15
Ve 18	0.39	0.21	72.45	1.79
Ve 19	0.00	0.00	90.77	1.16

Table C2.1: Feldspars, plagioclase, calcites and unquantified contents (in relative %) for the five studied sections.

Malleval

Sample ID	Feldspars-K	Plagioclase	Calcite	Unquantified
MAm 21	0.00	0.00	83.56	14.62
MAm 22	0.00	0.00	78.99	1.55
MAm 23	0.00	0.00	96.02	2.09
MAm 24	0.00	0.00	91.43	1.35
MAm 25	0.00	0.00	98.02	1.21
MAm 26	0.00	0.00	97.44	0.40
MAm 27	0.00	0.00	88.56	8.07
MAm 28	0.00	0.00	88.71	7.52
MAm 29	0.00	0.00	96.57	0.68
MAm 30	0.00	0.00	97.91	0.65
MAm 31	0.00	0.00	95.21	0.49
MAm 32	0.00	0.00	98.56	0.30
MAm 33	0.00	0.00	94.23	2.79
MAm 34	0.00	0.00	91.65	0.52
MAm 35	0.00	0.00	89.38	0.42
MAm 36	0.00	0.00	79.95	10.12
MAs 1	0.00	0.00	90.42	1.25
MAs 2	0.00	0.00	68.76	23.42
MAm 37	0.00	0.00	79.27	15.15
MAs 4	0.00	0.00	81.34	10.33
MAs 5	0.00	0.00	91.95	2.28
MAs 6	0.00	0.00	93.56	2.89
MAs 7	0.00	0.00	93.67	1.41
MAs 8	0.00	0.00	94.51	1.01
MAs 9	0.00	0.00	96.01	3.00
MAs 10	0.00	0.00	97.03	0.45
MAs 11	0.00	0.00	83.51	5.12
MAs 12	0.00	0.00	93.45	6.30
MAs 13	0.00	0.00	92.71	0.66
MAs 14	0.00	0.00	93.10	3.40
MAs 15	0.00	0.00	97.32	1.11
MAs 16	0.00	0.00	99.03	0.39
MAs 17	0.00	0.00	92.66	1.81
MAs 18	0.00	0.00	93.29	0.95
MAs 19	0.00	0.00	99.03	0.36
MAs 20	0.00	0.00	94.12	1.95
MAs 21	0.00	0.00	94.41	0.15
MAs 22	0.00	0.00	92.52	1.20
MAs 23	0.00	0.00	98.67	0.52
MAs 24	0.00	0.00	96.43	0.17
MAs 25	0.00	0.00	99.04	0.14
MAs 26	0.00	0.00	92.76	4.73
MAs 27	0.00	4.16	87.00	1.44
MAs 28	0.00	0.00	98.43	0.67
MAs 29	0.00	0.00	94.67	1.82
MAs 30	0.00	0.00	88.61	4.60
MAs 31	0.00	0.00	86.50	4.84
MAs 32	0.00	0.00	93.75	3.24
MAs 33	0.00	0.00	89.45	1.64
MAs 34	0.00	0.00	88.77	1.99
MAs 35	0.00	0.00	89.68	2.60
MAs 36	0.00	0.00	89.65	1.11
MAs 37	0.00	2.49	81.54	8.10
MAs 38	0.00	0.00	87.99	6.72
MAs 39	0.00	0.00	90.91	1.26
MAs 40	0.00	0.00	86.29	1.08
MAs 41 b	0.00	0.00	89.73	1.81
MAs 41	0.00	0.00	88.23	1.06
MAs 43 b	0.00	0.00	93.23	4.51
MAs 42	0.00	0.00	95.76	3.26
MAs 43	0.00	0.00	92.65	0.04
MAs 48 b	0.00	0.00	87.34	0.93
MAs 49 b	0.00	0.00	97.67	1.39
MAs 50 b	0.00	0.00	96.93	1.12
MAs 51 b	0.00	0.00	95.23	0.64
MAs 52 b	0.00	0.00	94.43	0.94
MAs 53 b	0.00	0.00	95.00	0.10
MAs 54 b	0.00	0.00	93.75	1.95
MAs 55 b	0.00	0.00	96.61	0.04
MAs 56 b	0.00	0.00	87.81	0.62
MAs 57 b	0.00	0.00	97.78	1.36

Table C2.1 (continued): Feldspars, plagioclase, calcites and unquantified contents (in relative %) for the five studied sections.

Rock density is depending on the lithology. We used a rock density equal to 2.5, 2.4 and 2.3 g/cm^3 for limestone, shale and marl, respectively (Attewell and Farmer, 1976). The sedimentation rate was reconstructed by using the $\delta^{13}C$ curve calibrated on ammonite biostratigraphy (Föllmi et al., 2006) and magnetostratigraphy (Ogg et al., 2008).

C2.3.3 Carbon and oxygen isotopes.

Carbon- and oxygen-isotope analyses were performed on powdered bulk-rock samples at the stable-isotope laboratory of the Universities of Orsay (Paris XI, France) and Bern (Switzerland), using a Finnigan Detla V Advantage mass spectrometer. The results were calibrated to the PDB scale with the standard deviation of 0.06% for $\delta^{13}C$ and of 0.07 % for $\delta^{18}O$.

C2.4 Results

C2.4.1 Mineralogy

Our bulk-rock RXD analyses show the absence of major variations in calcite contents in the sediments corresponding to the $\delta^{13}C$ positive shift in all sections. In the sections of Capriolo and Breggia, the relative proportion of detrital minerals is low; a long-term evolution is, however, distinguished. In Capriolo, the quartz content fluctuates around 2% in sediments below the $\delta^{13}C$ shift, and increases to 6% in the sedimentary interval of the positive $\delta^{13}C$ excursion (Fig. C2.3). This increase is coeval with an increase in feldspar and plagioclase contents (Table C2.1). In the Breggia section, the quartz content remains more or less constant with an average value of approximately 4% along the entire section, except for an interval at 5 m below the carbon-isotopic shift, where a peak of 15% is observed. Plagioclase and feldspar contents show low initial values and an increase in sediments corresponding to the positive $\delta^{13}C$ excursion. In the Vergol section (Fig. C2.3), quartz, phyllosilicates, feldspar and plagioclase decrease slightly along the studied interval, except for within the “Barrande layers”. In the more proximal environment, the proportion of detrital minerals is generally higher. The Alvier section shows a long-term decrease in the quartz content in sediments below the positive $\delta^{13}C$ shift, reaching a minimum at the onset of the $\delta^{13}C$ shift in sediments of the *Campylotoxus* zone. Subsequently, quartz values increase and remain high during the Valanginian positive excursion. In the section of Malleval, two

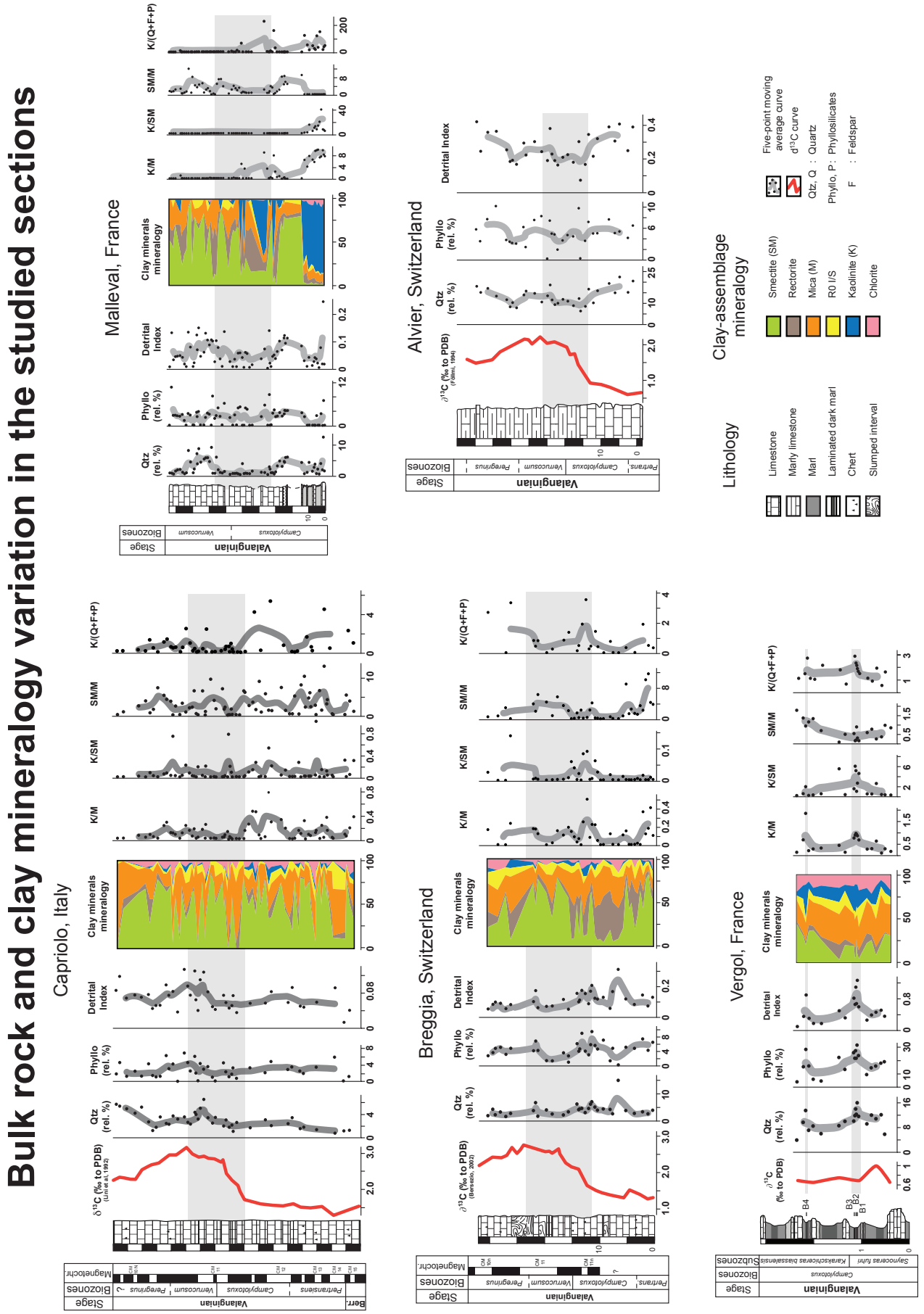

Fig. C2.3 : Bulk-rock and clay mineralogy of the studied sections. The detrital index (DI) corresponds to the ratio between the sum of quartz, feldspar, plagioclase and phyllosilicate and the calcite contents. The grey band indicates the stratigraphic position of the onset of the shift.

increases in quartz content are observed, the first in the *Campylotoxus* zone and the second at the base of the *Verrucosum* zone. This second increase is preceded by a peak in plagioclase contents reaching a value of 4%.

From these results, we calculated the detrital index (DI) for each section (Fig. C2.3). A common evolution of the DI is distinguished for all studied sections and described as followed:

- Below the positive $\delta^{13}C$ shift, in the *Campylotoxus* zone, DI shows high values, except for the Capriolo section, where DI values are rather constant and fluctuate between 0.04 and 0.12.
- The onset of the $\delta^{13}C$ shift is characterized by minimal DI values in all sections, except in Breggia, where an increase in DI is observed.
- During the shift, DI increases and reaches a maximum in the *Verrucosum* zone except for the Breggia section, where DI remains low.

In the insoluble residue of the <2μm fraction of the sediments from Capriolo, Breggia, Vergol and Malleval, mica, kaolinite, smectite, chlorite, rectorite and R0 I/S were identified. The Alvier section shows a burial and tectonic overprint for the clay fraction composition, with the transformation of the smectite into chlorite. In the pelagic sections of Capriolo and Breggia, clay mineral assemblages are dominated by smectite and mica. Kaolinite contents show rather low values along the sections, fluctuating between 5 and 10%. The evolution of the kaolinite/mica, kaolinite/smectite and kaolinite/(Qz+Fk+Pl) ratios (Fig. C2.3) suggests intervals with higher kaolinite contents relative to the other clay minerals in sediments of the *Campylotoxus* zone, just below the $\delta^{13}C$ shift. In sediments at the onset of the positive $\delta^{13}C$ excursion, at the transition of the *Campylotoxus* and *Verrucosum* zones, the relative abundance of kaolinite decreases and remains rather low during the shift. The sections of Vergol and Malleval show higher variations in the clay mineralogy. In Malleval, sediments corresponding to the *Campylotoxus* zone exhibit two maxima in kaolinite contents: one at the base of the section and a second in sediments of the late *Campylotoxus* zone (Fig. C2.3). An increase in smectite is observed in the interval of minimal kaolinite contents in the sediments corresponding to the *Verrucosum* zone.

In Vergol, the samples corresponding to the “Barrande” layers show an enrichment in kaolinite and appear to lack smectite. At the end of the section, an increase in smectite is observed (Fig. C2.3).

C2.4.3 Total Phosphorus Accumulation Rates and C/P ratio

In the section of Capriolo, the PAR values vary between 0.09 and 0.73 mg/cm^2/kyr (Fig. C2.4). In the lower part of the section (before the onset of the $\delta^{13}C$ shift), PAR values increase slightly. Within the *Verrucosum* zone, PAR values reach a maximum and start a long-term decrease. For the sections of Breggia and Alvier, PAR values show similarities with the global P trend (Föllmi, 1995). In sediments of the *Campylotoxus* zone, before the onset of the $\delta^{13}C$ shift, PAR values increase and reach a maximum of ~0.45 and ~2.75 mg/cm^2/kyr, respectively (Fig. C2.4). Consequently, in the section of Breggia, PAR values show a rapid decrease followed by a second increase. At Alvier, in sediments close to the transition of the *Campylotoxus* and *Verrucosum* zone, PAR start to decrease and reach a minimum in sediments belonging to the middle of the *Verrucosum* zone. PAR values increase again in sediments corresponding to the end of the positive $\delta^{13}C$ excursion (Fig. C2.4). In the Vergol section, a decreasing trend is observed between the bank 86 and 87. Within the “Barrande” layers B1, B2 and B3, PAR values reach a minimum of 1,84 mg P/cm^2/kyr. Between beds 87 and 88, PAR values increase and decrease again at layer B4. For the section of Malleval, the time model does not allow for the calculation of PAR, and therefore total P contents (P_{tot}) are shown instead (Fig. C2.5). P_{tot} content shows a maximum value of 285 ppm followed by a decreasing trend in the first part of the section, within the *Campylotoxus* zone. In sediments close to the transition of the *Campylotoxus* and the *Verrucosum* zone, corresponding to the onset of $\delta^{13}C$ excursion, P_{tot} decreases and remains low with a minimum of 26 ppm. At the end of the section, P content shows an increase (175 ppm) in sediments of the *Verrucosum* zone, corresponding to the second part of the $\delta^{13}C$ shift.

We also determined C_{org}/P_{tot} ratios in the marl levels of Capriolo and Vergol to evaluate the degree of organic P (P_{org}) retention and temporal variation therein during the Valanginian. The ratio is deduced from TOC data (Westermann et al., submitted) and the P content measured in this study. Following Anderson et al. (2001), $C_{org}/P_{reactive}$ is a more robust measure of the early diagenetic loss of P to the ocean ($P_{reactive}=P_{oxide\text{-}associated}+P_{authigenic}+P_{org}$) than C_{org}/P_{org} due to the possible

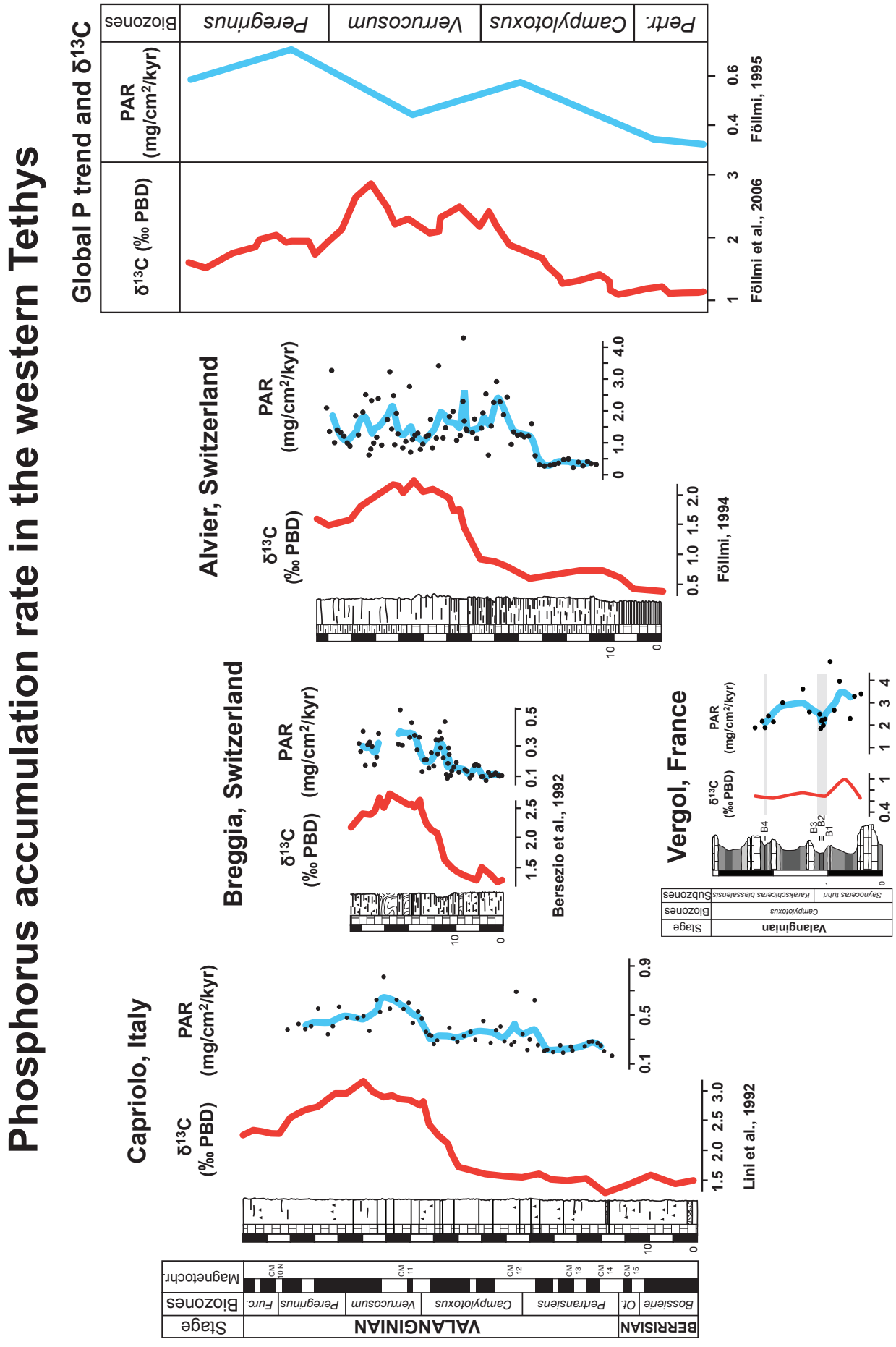

Fig. C2.4: Phosphorus accumulation rates (PAR) and δ13C curves of the sections of Capriolo, Breggia, Vergol and Alvier. The sedimentation rate was calculated using the duration of the ammonite biozones (Ogg. et al., 2008).

diagenetic transfer of organic P into an authigenic P phase. Here, we used total P (P_{tot}= $P_{reactive}$+$P_{detrtitic}$), thereby assuming that detrital P is minimal. Indeed, overall quantities of detrital minerals other than clay are minimal in both sections. The here calculated C/P ratio represents therefore a minimal estimate. In the Capriolo section (Fig. C2.6), C_{org}/P_{tot} ratios show two excursions toward values between 70 and 90, whereas the background level is around 30. The first increase is situated 15 m below the positive excursion in $\delta^{13}C$. The second maximum is coeval with the onset of the shift. In the section of Vergol (Fig. C2.5), the C_{org}/P_{tot} ratios are distinctly higher around the "Barrande" layers (with a threefold spike tracing B1, B2 and B3 and a maximum value of 592). A further peak close to 560 is distinguished at the B4 layer.

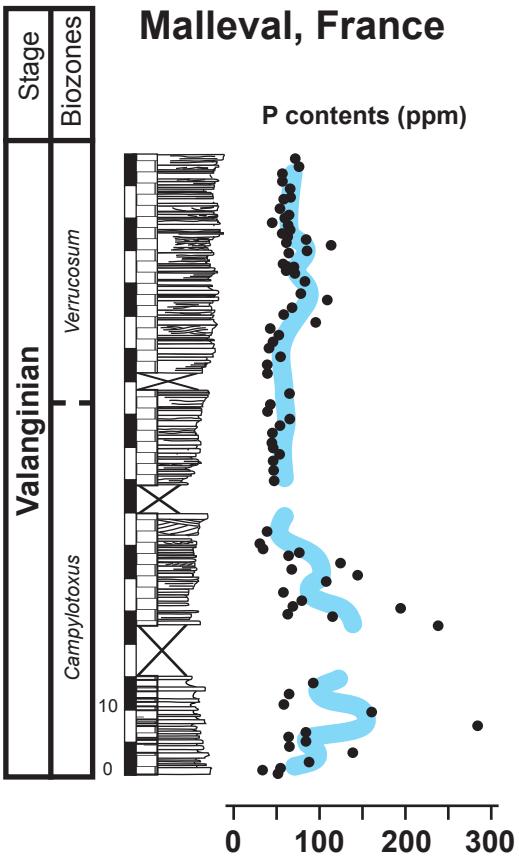

Fig. C2.5: Phosphorus contents in the section of Malleval.

C2.5 Discussion

C2.5.1 Mineralogy as paleoenvironmental index

Bulk-rock and clay mineralogy, and their deduced DI and clay-minerals ratios, provide an environmental and climate index. The DI is used as an indicator of the relative importance of detrital input. Variations in sea level and in the intensity of continental runoff are the major processes involved in detrital input into the marine environment (Adatte et al., 2001). The mineralogical composition of clay minerals formed in terrestrial soils is mainly determined by the mineralogical composition of the lithological substratum and the prevailing climate. The major clay minerals are kaolinite and smectite. Kaolinite preferentially forms under tropical or subtropical conditions (i.e. under humid and warm climate conditions), whereas smectite forms under dry climate conditions with a strong seasonality, or

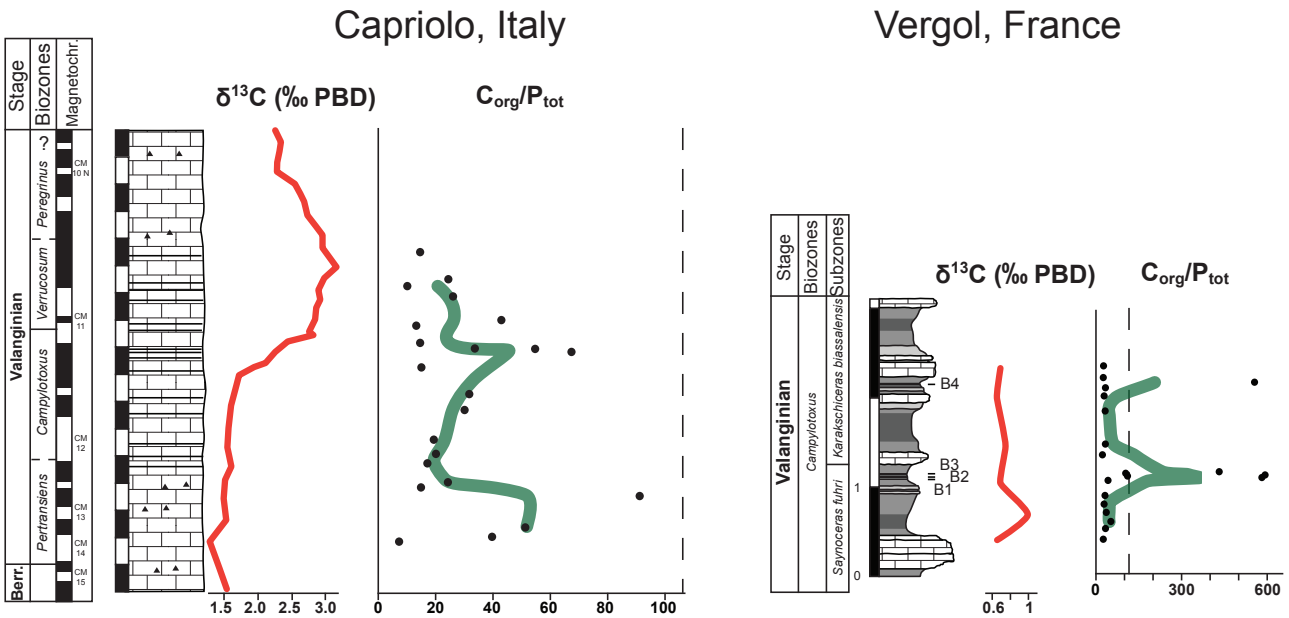

Fig. C2.6: C_{org}/P_{tot} ratios (expressed in mol/mol) in the section of Capriolo and Vergol. The dashed line indicates the position of the Redfield ratio (106:1; Redfield, 1958).

from the alteration of basalts (Chambley, 1989). Once formed, clay minerals have the potential to be eroded and transported to the ocean, where their composition in marine sediments is influenced by sea-level variations, fractionation processes during transport, diagenetic processes in the depositional environment and differential settling pattern of kaolinite versus smectite in the water column (Adatte and Rumbley, 1989; Chambley, 1989; Kübler and Jaboyedoff, 2000; Godet et al., 2008). These processes may perturb the original environmental signal. The diagenetic overprint is dependent on the original composition, the degree of burial and the tectonic history. In the studied sections, the clay-mineral assemblage shows rather high contents of smectite and kaolinite compared to R0 I/S, indicating low to medium diagenetic overprint (Deconinck and Chambley, 1983). Moreover, the rather good correlation of the long-term variations between the studied sections indicates original paleoenvironmental trends rather than a diagenetically overprinted evolution of the different mineral assemblages. An exception is given with Alvier section, where tectonic overprint altered the original clay composition.

The eustatic sea-level change curve is not well constrained for the Valanginian. In the Early Valanginian, an important decrease in sea level has been proposed by Haq et al. (1987). The time interval of the positive $\delta^{13}C$ excursion may correspond to a period of sea-level rise (Haq et al., 1987) or stillstand (Hardenbol et al., 1998). In the case we would correlate the general evolution in DI with sea-level change as proposed by Haq et al. (1987), the increase in DI observed before and in the second half of the positive $\delta^{13}C$ excursion would correspond to sea-level fall and sea-level rise.

In the Capriolo and Breggia sections, the proportion of detrital minerals is low and, in some cases, close to the quantification limits because of the distal position of the two sections. Temporal changes in mineralogical contents observed in these sections are therefore difficult to discuss in terms of climate change. The higher DI values near the onset of the $\delta^{13}C$ shift in the Breggia section are also seen in the more proximal settings represented by the section of Alvier and Malleval, where sediments of the *Campylotoxus* zone are generally characterized by rather high DI values. These values may have resulted from higher continental input into the Tethyan. The *Campylotoxus* zone may have witnessed an increase in deeper-water temperature based on the belemnite $\delta^{18}O$ record (van de Schootbrugge et al., 2001; McArthur et al., 2007). With regard to the clay-mineral composition, this interval corresponds to generally higher kaolinite contents (up to 80 % in the shelf section of Malleval, Fig. C2.7). The increased presence of kaolinite may indicate a warm and/or more humid climate, under which well-drained continental areas may have undergone intense biogeochemical weathering leading to the genesis of bauxite and kaolinite (e.g. Chambley, 1989; Weaver, 1989; Thiry et al. 1999). On the Helvetic carbonate platform, this period (from the *Pertransiens* to *Campylotoxus* zone) is characterized by heterozoan carbonate production (Föllmi et al., 2007), most likely due to higher nutrient levels in the water column. In the Jura Mountains, the Early Valanginian corresponds to the deposition of the “Calcaire roux” (Baumberger, 1903), which are composed of black to reddish-brown oolitic and bioclastic limestone containing limonite. This formation also shows higher kaolinite contents in the clay-mineral composition (Fahrni, 2004).

In sediments correlated to the period near and during the onset of the positive $\delta^{13}C$ excursion, a general decrease in detrital input is observed in the western Tethyan realm (Fig. C2.7). In Malleval, this relative diminution is coeval with the disappearance of kaolinite in the clay-mineral fraction. This change in the clay-mineral composition is also observed in the Jura Mountains (Fahrni, 2004) and the Vocontian trough (Duchamps-Alphonse, 2006). These trends are compatible with a change towards cooler and less humid conditions during the onset of the $\delta^{13}C$ positive excursion.

Subsequently, in sediments corresponding to the end of the positive $\delta^{13}C$ excursion (*Verrucosum* zone), a renewed increase in detrital input is observed, whereas kaolinite contents remain low (Fig. C2.7). This increase in terrestrial input might be the expression of a more mechanical-driven erosion on the continent related to a more strongly seasonally-contrasted climate. The observed change is also coeval with a increase in belemnite stable oxygen-isotopes, which might indicate a trend towards cooler bottom-water temperatures (Duchamp-Alphonse et al., 2007; McArthur et al., 2007).

C.2.5.2 Phosphorus as a proxy for global change

C2.5.2.1 Phosphorus accumulation rates

The flux of dissolved P is mainly controlled by continental runoff (Föllmi, 1996; Delaney, 1998; Compton et al., 2000). The transfer of P into the sediments occurs by sedimentation of organic P, P adsorbed on

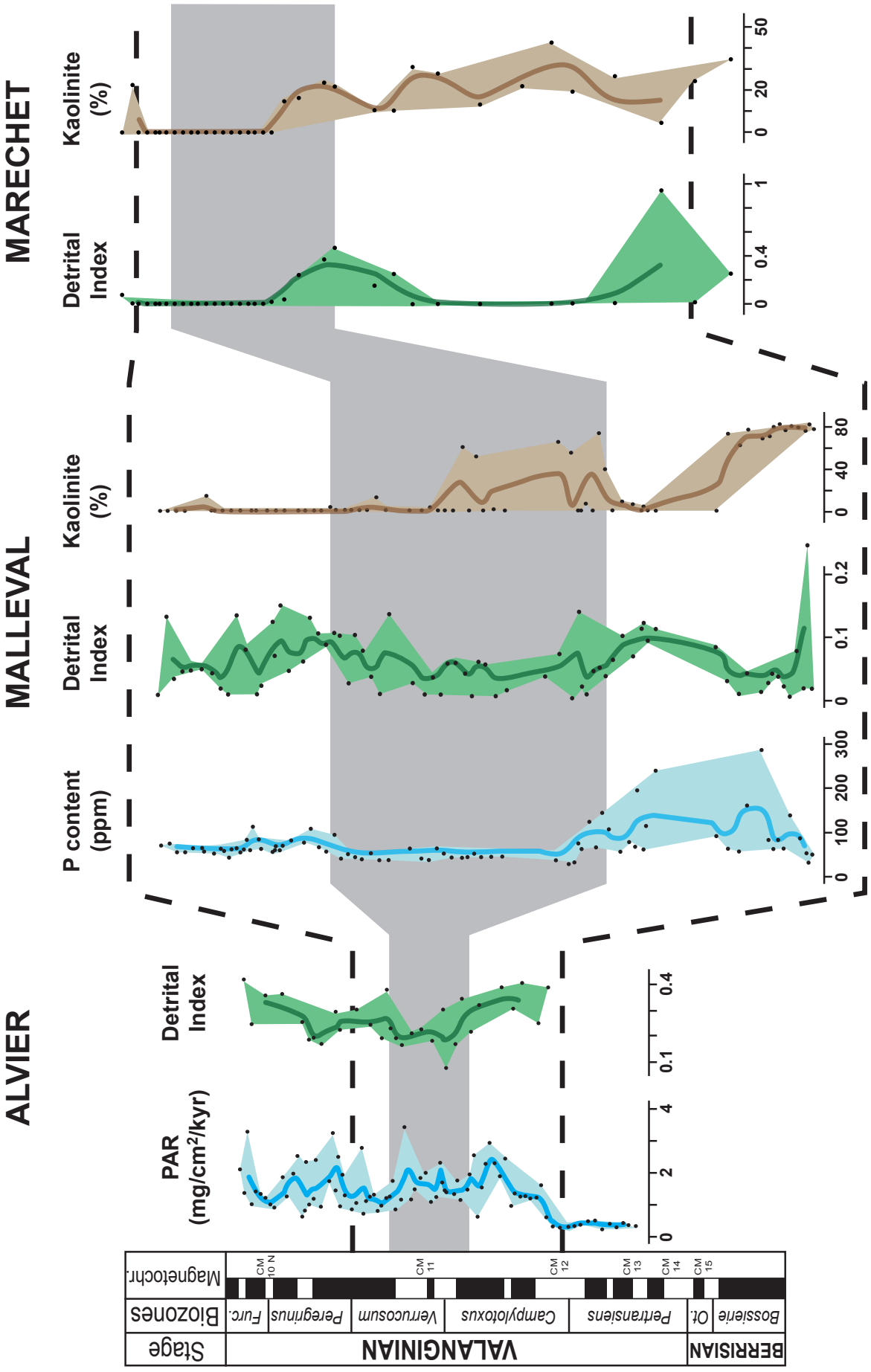

Fig. C2.7: Evolution of DI (green curve) and kaolinite content (brown curve) along the sections of Alvier, Malleval and Maréchet (Fahri, 2004). The Grey band shows the stratigraphic position of the $\delta^{13}C$ positive excursion.

surface-reactive particles, P in fish debris or by direct precipitation (Ruttenberg, 1993; Filippelli and Delaney, 1996; Föllmi, 1996). During early diagenesis, a part of the P trapped into the sediments may be removed and transferred back into the bottom waters. Early diagenetic P regeneration is redox dependent and becomes more efficient in oxygen-depleted bottom waters (Ingall and Jahnke, 1994; Van Cappellen and Ingall, 1996; Colman and Holland, 2000; Emeis et al., 2000; Tamburini et al. 2002; Bodin et al., 2006, Mort et al, 2007). A temporal decrease in P accumulation may therefore indicate a decrease in continental runoff and/or an expansion of anoxic bottom-water conditions.

In the western Tethyan realm, our results indicate that P influx was mainly driven by continental runoff, as is shown by the rather good correlation between PAR values and DI evolution (except for pre-excursion sediments in the Breggia section). The more distal settings (Capriolo and Breggia) seem to record a more global signal than Malleval and Alvier. P deposits increase worldwide during the Early Cretaceous as is shown by the global long-term trend established from the Deep Sea Drilling Project (DSDP) and Ocean Drilling Program (ODP) (Föllmi, 1995) and from the NW Tethyan margin (van de Schootbrugge et al., 2003). From these data, a two- to threefold increase is observed for the time interval between the Berriasian and Early Hauterivian (from 0.2 to 0.8 mg/cm^2/kyr). Since the trends in Capriolo and Breggia are similar in shape and magnitude, the underlying mechanisms of P accumulation and enrichment should be global (e.g. van de Schootbrugge et al., 2003). General longer-term changes in the marine P cycle (longer than several times the assumed actual marine residence time of approximately 10 kyrs for P) are related to changes in the P delivery rate from the continent (Froelich et al., 1982; Föllmi, 1995; Filippelli, 2008).

Valanginian eustatic sea-level rise has been documented from the NW Tethyan margin and the Russian platform (Sahagian et al., 1996; Hardenbol et al., 1998). One of the effects of the transgression was the establishment of a gateway between the Tethys and the Boreal realm trough the Polish Furrow (Price et al., 2000; Van de Schootbrugge et al., 2000). With this, cooler and possibly nutrien-enriched waters may have entered the Tethys, thereby adding to the general changes in P burial observed in the Tethyan sediments (van de Schootbrugge et al., 2003).

For the Vergol section, the trends of P depletion observed within the “Barrande” layers are decoupled from the detrital influx and are probably due to redox dependent behaviour of P.

In the more proximal settings, P enrichments are also correlated with an increase in DI. But when compared to the global P trend, it appears that P behaviour has been more strongly influenced by regional variations in runoff and climate. The diminution in PAR and P contents is coeval with changes in the clay-mineral composition, and especially with the disappearance of kaolinite.

C2.5.2.2 The C/P molar ratio

As shown by many studies, C/P molar ratios are good indicators of the degradation of organic matter and the relative loss of organic P under oxygen-depleted conditions (Ingall et al., 1993; Ingall and Jahnke, 1994, 1997; Van Cappellen and Ingall, 1996; Anderson et al., 2001; Slomp et al., 2004, Bodin et al., 2006; Mort et al., 2007). Bodin et al. (2006) observed that the C_{org}/P_{tot} represents a minimal value of the effective quantity of organic P that was transferred into authigenic phases. In Capriolo, C_{org}/P_{tot} values are generally lower than the Redfield ratio (106:1; Redfield, 1958). This may indicate that the P_{tot} measured is a composite of the P_{org} and $P_{authigenic+detritic}$. Moreover, TOC values are quite low in Capriolo (mean value close to 0.50 wt %). This may be linked to a late-stage diagenetic alteration coupled with the preferential loss of organic carbon under oxic/dysoxic conditions. During the onset of the carbon positive $\delta^{13}C$ shift, an increase in C/P ratio is observed. This increase is coeval with a diminution in PAR values, which may indicate a shift to a more oxygen-depleted conditions followed by a return to normal conditions.

At Vergol, pre- and post- Barrande sediments show lower C_{org}/P_{tot} ratio than the Redfield ratio, whereas the organic-rich layers have higher C_{org}/P_{tot} ratios (592 for the B3 layer). This and the decrease in PAR values suggest that during early diagenesis of the organic-rich layers, P was preferentially mobilized (relative to C) and transferred back into the bottom water. This change in the P trend may indicate that the organic layers have been deposited under more strongly oxygen-depleted conditions than the sediments surrounding the “Barrande” layers.

C2.5.3 Climate and environmental change through the Valanginian

The studied sections provide evidence for climate and environmental change in the western Tethyan realm

before, during and following the Valanginian positive $\delta^{13}C$ shift. The overall change both in P contents and accumulation rates as well as in the detrital indices reveals the importance of material transfer from the continent into the western Tethys and changes therein prior and during the positive $\delta^{13}C$ excursion. This observation finds its confirmation in reports on increases in overall detrital, iron and Mn flux rates during the Valanginian (Weissert et al., 1991; Kuhn et al., 2005; Westermann et al., 2010). Mechanisms by which the material flux from continents is enhanced, include the spreading of warm and humid conditions, the generation of relief by mountain building processes, enhanced glaciation or sea level rise. Indications of orogenetic episodes during the Early Cretaceous are sparse and the importance of glacial activity during the Valanginian is controversially discussed (Price, 1999; McArthur et al., 2007). The combination of increases in P, Fe and Mn and the pattern in kaolinite distribution suggest that climate warming is most likely the prime factor for enhancing continental weathering processes prior to the positive $\delta^{13}C$ excursion (Lini et al., 1992). Whole-rock and belemnite stable-oxygen isotope records point indeed to a warmer climate during the Early Valanginian, which was followed by a stable or cooler climate after the maximum in the $\delta^{13}C$ record (Duchamp-Alphonse et al., 2007; McArthur et al., 2007).

An enhanced P flux during the Valanginian has been implied as a factor driving the demise of the northern Tethyan carbonate platform (Föllmi et al., 1994, 2006; Duchamp-Alphonse et al., 2007). It may have generally led to an increase in primary productivity. This circumstance did, however, not result in the installation of widespread dys- to anaerobic conditions in the western Tethys; for reasons, which are likely related to the efficiency of oxygen replenishment of intermediate and deeper waters. The only evidence for a series of short-lasted dysaerobic to anaerobic episodes in the western Tethys is given by the “Barrande layers” in Vergol (high TOC/P_{tot} ratios and low PAR values), which predate the Valanginian positive $\delta^{13}C$ excursion.

C2.6 Conclusions

An analysis of the bulk-rock and clay mineralogy combined with P content has been performed on five mid-latitude sections of Valanginian age arranged along the shelf-basin transect through the northern and central part of the western Tethys, in order to trace paleoenvironmental and paleoclimatic changes prior and during the positive $\delta^{13}C$ shift.

Our results show an evolution in climate conditions in at least two steps: in the Early Valanginian, prior to the positive $\delta^{13}C$ shift, the sediments are characterized by the presence of kaolinite in the clay-mineral fraction and by higher continental detrital input (higher DI values). This suggests the prevalence of warmer and more humid climatic conditions in the western Tethyan realm. The change towards a more humid climate has already been observed in the Late Berriasian (Ruffell & Rawson, 1994; Price et al., 1999; Schnyder et al., 2006). The more humid climate in the early part of the Valanginian may have resulted in an intensification of the water cycle (Price et al., 1999) and thus in an acceleration of continental runoff and increase of terrestrially-derived material in more proximal settings. The resulting increase in the nutrient level has been implied as a factor driving the demise of the northern Tethyan carbonate platform (Föllmi et al., 1994, 2006; Duchamp-Alphonse et al., 2007). It may have generally led to an increase in primary productivity. This circumstance did, however, not result in the development of widespread dys- to anaerobic conditions in the western Tethys (low C/P ratios in Capriolo); for reasons, which are likely related to the efficiency of oxygen replenishment in intermediate and deeper waters. The only indication for a series of short-lasted dysaerobic to anaerobic episodes in the western Tethys is given by the “Barrande layers” in Vergol. Immediately prior and during the positive $\delta^{13}C$ excursion a decrease in the DI coeval with a decrease in kaolinite contents is observed, which is most likely related to a change towards drier conditions. In the following, during the second part of the $\delta^{13}C$ excursion (*Verrucosum* zone), the Capriolo and Breggia sections show a general increase in detrital influx but low kaolinite contents. This change is related to stronger seasonality, which was also observed in other parts of the Tethys (Duchamp-Alphonse et al., 2007). This climate evolution deduced from the bulk-rock and clay mineralogy is coherent with recent $\delta^{18}O$ studies (McArthur et al., 2007). Whole-rock and belemnite stable-oxygen isotope records point indeed to a warmer climate during the Early Valanginian, which was followed by a stable or cooler climate after the maximum in the $\delta^{13}C$ record (McArthur et al., 2007).

Acknowledgements

We thank Stéphane Bodin, Alexis Godet and Melody Stein for their assistance in the field and Tiffany Monnier and André Villard for their technical support.

Funding for this research was provided by the Swiss National Science Foundation (Grant 200021-109514, 200020-121600 and PP002-110554/1 to D. F.).

References

Adatte, T. and Rumley, G., 1989. Sedimentology and mineralogy of the Valanginian and Hauterivian in the stratotypic region (Jura mountains, Switzerland). *In*: Wiedmann J., (*Ed.*) Cretaceous of the western Tethys: proceedings of the 3rd International Cretaceous Symposium, Tübingen, 1987. E., Schweitzerbart'sche Verlagsbuchhandlung, Stuttgart, pp. 329-351.

Adatte, T., Remane, J., Stinnesbeck, W., López-Oliva, J. G. and Hubberten, H., 2001. Correlation of a Valanginian stable isotopic excursion in Northeastern Mexico with the European Tethys. *In*: Bartolini, C., Buffler, R. T. and Cantú-Chapa, A. (*Eds*). The Western Gulfe of Mexico basin, AAPG Memoir 75, 371-388.

Adatte, T., Stinnesbeck, W. and Keller, G., 1996. Lithostratigraphic and mineralogic correlations of near K/T boundary in NE Mexico: Implications for origin and nature of deposition. *In*: Ryder, G., Fastovsky, D. and Gartner, S. (*Eds*). The Cretaceous-Tertiary Event and Other Catastrophes in Earth History, Geological Society of America Special Paper 307, 211-226.

Anderson, L.D., Delaney, M.L. and Faul, K.L., 2001. Carbon to phosphorus ratios in sediments: implications for nutrient cycling. Global Biogeochemical Cycles 15, 65–79.

Attewell, P. B. and Farmer, I. W., 1976. Principles of engineering geology. Chapman and Hall.

Baumberger, E., 1903. Fauna der Kreide im westschweizerischen Jura: 1. Teil Stratigraphische Einleitung. Abh. der Schweizerischen Paläontologischen Gesellschaft, 30, 30 pp.

Bersezio, R., Erba, E., Gorza, M. and Riva, A., 2002. Berriasian-Aptian black shales of the Maiolica Formation (Lombardian Basin, Southern Alps, Northern Italy): local to global events. Palaeogeography, Palaeoclimatology, Palaeoecology 180, 253-275.

Blanc, E., 1996. Transect Plate-forme/Bassin dans les séries carbonatées du Berriasien supérieur et du Valanginien inférieur (domaines jurassien et nord-vocontien). Chronostratigraphie et transferts des sédiments. Mémoire H.S. Géologie alpine 25, 312 p.

Bodin, S., Godet, A., Föllmi, K. B., Vermeulen, J., Arnaud, H., Strasser, A., Fiet, N. and Adatte, T., 2006. The late Hauterivian Faraoni oceanic anoxic event in the western Tethys : Evidence from phosphorus burial rates. Palaeogeography, Palaeoclimatology, Palaeoecology 235, 245-264.

Briegel, U., 1972. Geologie der östlichen Alviergruppe (Helvetische Decken der Ostschweiz) unter besonderer Berücksichtigung der Drusberg- und Schrattenkalkformation (Unterkreide). Eclogae Geologicae Helvetiae 65, 425-483.

Chamley, H., 1989. Clay sedimentology. Springer Verlag, Berlin, 623 pp.

Channel, J. E. T., Bralower, T. J. and Grandesso, P., 1987. Biostratigraphic correlation of Mesozoic polarity chrons CM1 to CM23 at Capriolo and Xausa (Southern Alps, Italy). Earth and Planetary Science Letters 85, 203-221.

Channel, J. E. T. and Erba, E., 1992. Early Cretaceous polarity chrons CM0 to CM11 recorded in northern Italian land sections near Brescia. Earth and Planetary Science Letters 108, 161-192.

Channel, J. E. T., Erba, E. and Lini, A., 1993. Magnetostratigraphic calibration of the Late Valanginian carbon isotope event in pelagic limestones from Northern Italy and Switzerland. Earth and Planetary Science Letters 118, 145-166.

Colman, A.S. and Holland, H.D., 2000. The global diagenetic flux of phosphorus from marine sediments to the oceans; redox sensitivity and the control of atmospheric oxygen levels. *In*: Glenn, C.R., Prévôt-Lucas, L., Lucas, J. (*Eds*.), Marine Authigenesis; From Global to Microbial, SEPM Special Publication, vol. 66, pp. 53–75.

Compton, J., Mallinson, D., Glenn, C.R., Filippelli, G., Föllmi, K., Shields, G. and Zanin, Y., 2000. Variations in the global phosphorus cycle. *In*: Glenn, C.R., Prevot-Lucas, L., Lucas, J. (*Eds*), Marine Authigenesis; From Global to Microbial. Special Publication Society for Sedimentary Geology 66, pp. 21-33.

Deconinck, J.-F. and Chamley, H., 1983. Héritage et diagenèse des minéraux argileux dans les alternances marno-calcaires du Crétacé inférieur du domaine subalpin. Comptes Rendus de l'Académie des Sciences de Paris 297, 589–594.

Delaney, M.L., 1998. Phosphorus accumulation in marine sediments and the oceanic phosphorus cycle. Glob. Geochem. Cycles 12, 563-572.

Duchamp-Alphonse, S., Gardin, S., Fiet, N., Bartolini, A., Blamart, D. and Pagel, M., 2007. Fertilization of the northwestern Tethys (Vocontian basin, SE France) during the Valanginian carbon isotope perturbation: Evidence from calcareous nanofossils and trace element data. Palaeogeography, Palaeoclimatology, Palaeoecology 243, 132-151.

Eaton, A.D., Clesceri, L.S. and Greenberg, A.E., 1995. Standard Methods for the Examination of Water and Waste Water, vol. IXI, pp. 4.113-4.114.

Emeis, K.-C., Stuck, U., Leipe, T., Pollehne, F., Kunzendorf, H. and Christiansen, C., 2000. Changes in the C, N, P burial rates in some Baltic Sea sediments over the last 150 years__relevance to P regeneration rates and the phosphorus cycle. Marine Geology 167, 43-59.

Erba, E., Bartolini, A. and Larson, R. L., 2004. Valanginian Weissert oceanic anoxic event. Geology 32, 149-152.

Farhni, Y., 2004. Etude sédimentologique,miéralogique, micropaléontologique et géochimique de series valangiennes dans le Jura central. Master thesis, 100p.

Filippelli, G. M., 2008. The global phosphorus cycle: Past, present, and futur. Elements 4, 89-95.

Filippelli, G. M. and Delaney, M. L., 1996. Phosphorus geochemistry of equatorial Pacific sediments. Geochimica et Cosmochimica Acta 60, 1479-1495.

Föllmi, K. B., 1995. 160 m.y. record of marine sedimentary phosphorus burial: Coupling of climate and continental wearthering under greenhouse and icehouse conditions. Geology 23, 859-862.

Föllmi, K.B., 1996. The phosphorus cycle, phosphogenesis and marine phosphate-rich deposits. Earth Sci. Rev. 40, 55-124.

Föllmi, K. B., Bodin, S., Godet, A., Linder, P. and van de Schootbrugge, B., 2007. Unlocking paleo-environmental information from Early Cretaceous shelf sediments in the Helvetic Alps: stratigraphy is the key! Swiss journal of geosciences, 100, 349-369.

Föllmi, K. B., Godet, A., Bodin, S. and Linder, P., 2006. Interactions between environmental change and shallow water carbonate buildup along the nothern Tethyan margin and their impact on the Early Cretaceous carbon isotope record. Paleoceanography 21(PA4211, doi:10.1029/2006PA001313), 1-16.

Föllmi, K. B., Weissert, H., Bisping, M. and Funk, H., 1994. Phosphogenesis, carbon-isotope stratigraphy, and carbonate-platform evolution along the Lower Cretaceous northern Tethyan margin. Geological Society of America Bulletin, 106, 729-746.

Froelich, P. N., Bender, M. L., Luedtke, N. A., Heath, G. R. and DeVries, T., 1982. The marine phosphorus cycle. American Journal of Science 282, 474-511.

Godet, A., Bodin, S., Adatte, T. and Föllmi, K. B., 2008. Platform-induced clay-mineral fractionation along a northern Tethyan basin-platform transect: implications for the interpretation of Early Cretaceous climate change (Late Hauterivian-Early Aptian). Cretaceous Research 29, 830-847.

Haq, B. U., Hardendol, J. and Vail, P. R., 1987. Chronology of fluctuating sea levels since the Triassic. Science 235, 1156-1166.

Hardendol, J., Thierry, J., Farley, M. B., Jacquin, T., De Graciansky, P.-C. and Vail, P. R., 1998. Mesozoic and Cenozoic chronostratigraphic framework of European basins. *In*: de Graciansky, P.C, Hardenbol, J. , Jaquin, T. and P.R. Vail, P. R. (*Eds*). Mesozoic and Cenozoic Sequence Stratigraphy of European Basins, SEPM special publication 60, 3-13.

Hennig, S., 2003. Geochimical and sedimentological evidence for environmental changes in the Valanginian (Early Cretaceous) of the Tethys region. Unpublished PhD. thesis, ETH Zürich, 267p.

Ingall, E. D., Bustin, R. M. and Van Cappellen, P., 1993. Influence of water column anoxia on the burial and preservation of carbon and phosphorus in marine shales. Geochimica et Cosmochimica Acta 57, 303-316.

Ingall, E. D. and Jahnke, R., 1994. Evidence for enhanced phosphorus regeneration from marine sediments overlain by oxygen depleted waters. Geochimica et Cosmochimica Acta 58, 2571-2575.

Ingall, E. D. and Jahnke, R., 1997. Influence of water-column anoxia on the elemental fractionation of carbon and phosphorus during sediment diagenesis. Marine Geology 139, 219-229.

Kübler, B., 1987. Cristallinité de l'illite: méthodes normalisées de préparation, méthode normalisée de mesure, méthode automatique normalisée de mesure. Cahiers de l'Institut de Géologie, Université de Neuchâtel, Suisse Série ADX n° 2.

Kübler, B. and Jaboyedoff, M., 2000. Illite cristallinity. C. R. Académie des sciences, Paris, Sciences de la terre et des planètes 331, 75-89.

Kuhn, O., Weissert, H., Föllmi, K. B. and Hennig, S., 2005. Altered carbon cycling and trace-metal enrichment during the late Valanginian and early Hauterivian. Eclogae geol. Helv. 98, 333-344.

Kuhnt, W., Nederbragt, A. and Leine, L., 1997. Cyclicity of Cenomanian-Turonian organic-carbon-rich sediments in the Tarfaya Atlantic Coastal Basin (Morocco). Cretaceous Research 18, 587-601.

Leckie, R. M., Bralower, T. J. and Cashman, R., 2002. Oceanic anoxic events and plankton evolution: Biotic response to tectonic forcing during the mid-Cretaceous. Paleoceanography, 17, doi: 10.1029/2001PA000623.

Lini, A., Weissert, H. and Erba, E., 1992. The Valanginian carbon isotope event : a first episode of greenhouse climate conditions during the Cretaceous. Terra Nova 4, 374-384.

McArthur, J. M., Janssen, N. M. M., Reboulet, S., Leng, M. J., Thirlwall, M. F. and van de Schootbrugge, B., 2007. Palaeo-temperatures, polar ice-volume, and isotope stratigraphy (Mg/Ca, $\delta^{18}O$, $\delta^{13}C$, $^{87}Sr/^{86}Sr$): the Early Cretaceous (Berriasian, Valanginian, Hauterivian). Palaeogeography, Palaeoclimatology, Palaeoecology 202, 252-272.

Mort, M., Adatte, T., Föllmi, K. B., Keller, G., Steinmann, P., Matera, V., Berner, Z. and Stüben, D., 2007. Phosphorus and the roles of productivity and nutrient recycling during oceanic event 2. Geology 35, 483-486.

Ogg, J. G., Ogg., G. and Gradstein, F. M., 2008. The concise geological time scale. Cambridge University Press, 177 pp.

Persoz, F., 1982. Inventaire minéralogique, diagenèse des argiles et minéralostratigraphie des séries jurassiques et crétacées inférieures du Plateau suisse et de la bordure sud-est du Jura entre les lacs d'Annecy et de Constance. Matériaux pour la Carte Géologique de la Suisse Nouvelle Série 155, 1–52.

Poulsen, C.J., Seidov, D., Barron, E.J. and Peterson, W.H., 1998. The impact of paleogeographic evolution on the surface oceanic circulation and the marine environment within the mid-Cretaceous Tethys. Paleoceanography 13, 546-559.

Price, G. D., 1999. The evidence and implications of polar ice during the Mesozoic. Earth-Science Reviews 48, 183-210.

Price, G. D., Ruffell, A. H., Jones, C. E., Kalin, R. M. and Mutterlose, J., 2000. Isotopic evidence for temperature variation during the early Cretaceous (late Ryazanian-mid-Hauterivian). Journal of the Geological society of London 157, 335-343.

Reboulet, S. and Atrops, F. 1999. Comments and proposals about the Valanginian-Lower Hauterivian ammonite zonation of south-eastern France. Eclogae geol. Helv. 92, 183-197.

Reboulet, S., Mattioli, E., Pittet, B., Baudin, F., Olivero, D. and Proux, O., 2003. Ammonoid and nannoplankton abundance in Valanginian (early Cretaceous) limestone-marl successions from the southeast France Basin: carbonate dilution or productivity? Palaeogeography, Palaeoclimatology, Palaeoecology 201, 113-139.

Redfield, A. C., 1958. The biological control of chemical factors in the environment. American Scientist 46, 205 – 222.

Ruffell, A. H. and Batten, D. J., 1990. The Barremian-Aptian arid phase in western Europe. Palaeogeography, Palaeoclimatology, Palaeoecology 80, 197-212.

Ruffell, A., Mc Kinley, J. and Worden, R., 2002. Comparison of clay mineral stratigraphy to other proxy palaeoclimate indicators in the Mesozoic of NW Europe. Philosophical Transactions of the Royal Society of London 360, 675–693.

Ruttenberg, K.C. and Berner, R.A., 1993. Authigenic apatite formation and burial in sediments from non-upwelling, continental margin environments. Geochimica et Cosmochimica Acta 57, 991-1007.

Sahagian, D., Pinous, O., Olferiev, A. and Zakharov, V., 1996. Eustatic curve for the middle Jurassic-Cretaceous based on Russian Platform and Siberian Stratigraphy: Zonal resolution. AAPG Bull. 80, 1433-1458.

Schlanger, S. O. and Jenkyns, H. C., 1976. Cretacous oceanic anoxic event : causes and

consequences. Geologie en Mijnbouw 55, 179-188.

Schnyder, J., Ruffell, A. H., Deconinck, J.-F. and Baudin, F., 2006. Conjunctive use of spectral gamma-ray logs and clay mineralogy in defining late Jurassic–early Cretaceous palaeoclimate change (Dorset, U.K.). Palaeogeography, Palaeoclimatology, Palaeoecology 229, 303-320.

Slomp, C. P., Thomson, J. and De Lange, G. J., 2004. Controls on phosphorus regeneration and burial during formation of eastern Mediterranean sapropels. Marine Geology 203, 141-159.

Tamburini, F., Huon, S., Steinmann, P., Grousset, F.E., Adatte, T. and Föllmi, K.B., 2002. Dysaerobic conditions during Heinrich events 4 and 5: evidence from phosphorus distribution in a North Atlantic deep-sea core. Geochimica et Cosmochimica Acta 66, 4069– 4083.

Thiry, M., Simon-Coinçon, S. and Schmitt, J.-M., 1999. Paléoaltérations kaoliniques: signification climatique et signature dans la colonne sédimentaire. Comptes Rendus de l'Académie des Sciences de Paris. Sciences de la Terre et des Planètes 329, 853–863.

Tyrrell, T., 1999. The relative influences of nitrogen and phosphorus on oceanic primary production. Nature 400, 525-531.

Van Cappellen, P. and Ingall, E. D., 1994. Benthic phosphorus regeneration, net primary production, and ocean anoxia: A model of the coupled marine biogeochemical cycles of carbon and phosphorus. Paleoceanography 9, 677-692.

Van de Schootbrugge, B., 2001. Influence of paleo-environmental changes during the Hauterivian (early Cretaceous) on carbonate deposition along the northern margin of the Tethys: Evidence from geochemical records (C, O, and Sr-isotopes, P, Fe, Mn). Unpublished PhD. thesis University of Neuchâtel, 291 p.

Van de Schootbrugge, B., Föllmi, K. B., Bulot, L. and Burns, S., 2000. Paleoceanographic changes during the early Cretaceous (Valanginian-Hauterivian) : evidence from oxygen and carbon stable isotopes. Earth and Planetary Science Letters 181, 15-31.

Van de Schootbrugge, B., Kuhn, O., Adatte, T., Steinmann, P. and Föllmi, K. B., 2003. Decoupling of P and Corg burial following Early Cretaceous (Valangian/Hauterivian) platform drowning along the NW Tethyan margin. Paleogeography, Paleoclimatology, Paleoecology 199, 315-331.

Weaver, C.E., 1989. Clays, Muds, and Shales. Developments in Sedimentology, 44. Elsevier Science Publishers B.V., Amsterdam, 819 pp.

Weissert, H. and Bréhéret, J.-G., 1991. A carbonate carbon-isotope record from Aptian-Albian sediments of the Vocontian trough (SE France). Bulletin de la Société géologique de France 162(6), 1133-1140.

Weissert, H., Lini, A., Föllmi, K. and Kuhn, O., 1998. Correlation of early Cretaceous carbon isotope stratigraphy and platform drowning events: a possible link? Palaeogeography, Palaeoclimatology, Palaeoecology 137, 189-203.

Westermann, S., Föllmi, K. B., Adatte, T., Matera, V., Schnyder, J., Fleitmann, D., Fiet, N., Ploch, I. and Duchamp-Alphonse, S., 2010. The Valanginian $\delta^{13}C$ may not be an expression of a global oceanic anoxic event. Earth and Planetary Science Letters, 290, 118-131.

CHAPTER D:
The Early Aptian oceanic anoxic event (OAE 1a) in the Western Tethys

The Gorgo a Cerbara section, Italy

The redox-sensitive trace-element and the phosphorus contents are investigated in this paper in order to improve our understanding of mechanisms leading to widespread organic-rich sediments in the early Aptian by testing the proposed model for global anoxic event.

-D-

The Evolution of Redox Conditions during the Early Aptian Oceanic Anoxic Event (OAE 1a) in the Western Tethys

Stéphane Westermann[1], Melody Stein[1], Virginie Matera[2], Thierry Adatte[1], Nicolas Fiet[3,4], Dominik Fleitmann[5] and Karl B. Föllmi[1]

[1]Institute of geology and paleontology, University of Lausanne, Anthropôle, 1015 Lausanne, Switzerland.
[2]Institute of geology, University of Neuchâtel, Emile Argand 11, CP 158, 2009 Neuchâtel, Switzerland.
[3]UMR 8148 – I.D.E.S., Bât. 504, University of Paris XI Orsay, 91405 Orsay Cedex, France.
[4]AREVA, 33 rue La Fayette, 75009 Paris, France.
[5]Institute of Geological Sciences, University of Bern, Baltzerstrasse 1-3, 3012 Bern, Switzerland.

Manuscript in preparation for publication in Palaeogeography, Palaeoclimatology, Palaeoecology.

Abstract

The early Aptian OAE, labelled OAE 1a, corresponds to one of the most studied anoxic events within the Cretaceous. This event is characterized by a positive excursion in the $\delta^{13}C$ carbonate and organic carbon records, which is preceded by a pronounced negative spike right at its onset. In this study, we investigate phosphorus (P), redox-sensitive trace-element (RSTE) and organic matter contents in sections through Lower Aptian sediments along a basin-shelf transect in the western Tethys in order to improve our understanding of paleoceanographic change leading to and during this event. We selected three representative sections: Gorgo a Cerbara (central Italy) in the Umbria Marche basin, Glaise (SE France) located in the Vocontian Trough and Cassis/La Bédoule (SE France) located along the Provencal platform.

In Glaise and Cassis/La Bédoule, the general trend in P shows an increase at the onset of the Early Aptian event followed by a decrease in the Goguel interval. This suggests an increase in the marine P inventory near the onset of OAE 1a, followed by a return to lower values through the first part of OAE 1A, which may have been related to a weakened capacity to retain P in the sedimentary reservoir due to bottom-water oxygen depletion, and a renewed increase in the transfer rates of P into the sediments. This pattern is contrasted by the data of Gorgo a Cerbara which also show P-enrichments near the top of the Selli level. These P-enriched levels corresponds to sediments with the maximum of total organic carbon (TOC) and the highest C_{org}/P_{tot} ratios (up to 200). RSTE exhibit comparable variation in the section of Gorgo a Cerbara. Al-normalised U, V, Mo, Co, As contents show low background levels, which are contrasted by two subsequent maxima near the top of the Selli level. Conversely, in the sections of Glaise and Cassis/La Bédoule, no significant enrichments have been observed in sediments equivalent to the Selli level. These data seem to indicate anoxic conditions in the basin, which were most intense during the second half of OAE 1a. In shallower-water environments, conditions may have been less reducing.

Keywords*: Early Aptian; OAE 1a; Redox-sensitive trace elements; Phosphorus; Marine organic carbon; western Tethys*

D.1 Introduction

Oceanic anoxic events (OAEs) are documented by the deposition of laminated, organic-rich, sediments in marine environments, which were temporary depleted in oxygen. These episodes interrupted normal pelagic sedimentation pattern and were accompanied by strong perturbations in the carbon cycle (Schlanger and Jenkyns, 1976; Scholle and Arthur, 1980). They occur in unusual density in Cretaceous oceans and are one of the most intriguing features of this period. The mechanisms leading to the installation of the Cretaceous

OAE's are still under debate and various triggering mechanisms have been proposed: a prominent feature of many scenarios are episodes of intensified volcanism, which may have triggered a phase of global warming, a corresponding increase in continental weathering rates, which itself induced an increase in nutrient supply to the oceans (Jenkyns, 1999, 2003; Mort et al., 2007). In general, two end-member models have been proposed to explain the occurrence of widespread black-shale deposits in the Cretaceous: the expanded oxygen minimum zone (OMZ) model and the stagnant ocean model. The expanded OMZ model is a productivity-driven model, in which pelagic organic-rich sediments are the result of increased primary productivity in the photic zone of the ocean, which again has been related to an increase in nutrient flux, both by the enhanced supply of volcanically derived trace metals and by increased weathering rates on the continent (Larson, 1991; Larson and Erba, 1999; Hasegawa, 2003). The enhanced supply of organic matter to the deeper part of the ocean causes an expansion of the OMZ. The stagnant ocean model corresponds to a preservation-driven model, which is based on sluggish circulation pattern and a resulting highly stratified water column and diminishing oxygen concentrations in deeper waters (Bralower and Thierstein, 1984; Rullkötter, 2000). These circumstances are thought to enhance organic matter preservation in the deeper water sediments.

The Early Aptian oceanic anoxic event (OAE 1a) is one of the most significant and widespread black shale events of the Cretaceous (e.g. Arthur et al., 1990; Jenkyns, 1999; Robinson et al., 2004; Tejada et al., 2009). OAE 1a is characterized by a positive carbon isotope excursion (approximately +2 ‰), which is preceded by a short negative peak coinciding with the onset of the anoxic event (Menegatti et al., 1998; Weissert et al., 1998; Weissert and Erba, 2004; Méhay et al., 2009). The negative $\delta^{13}C$ spike has been interpreted as an indicator of the enhanced release of light carbon to the biosphere (Menegatti et al., 1998;

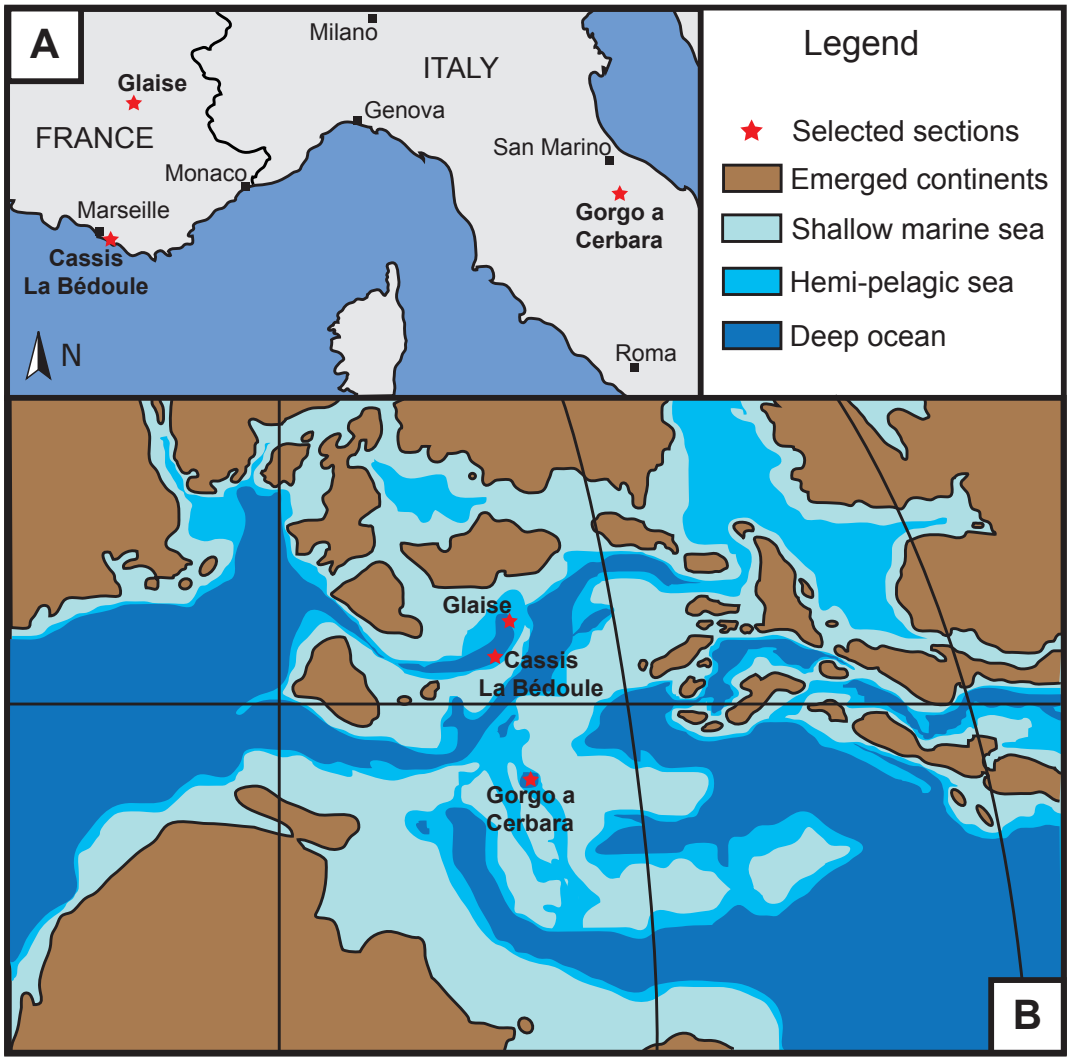

Fig. D.1: A. Localisation of the sections analysed in this study. B. Aptian paleogeographic map of the western Tethys (Redrawn after Scotese et al., 2001).

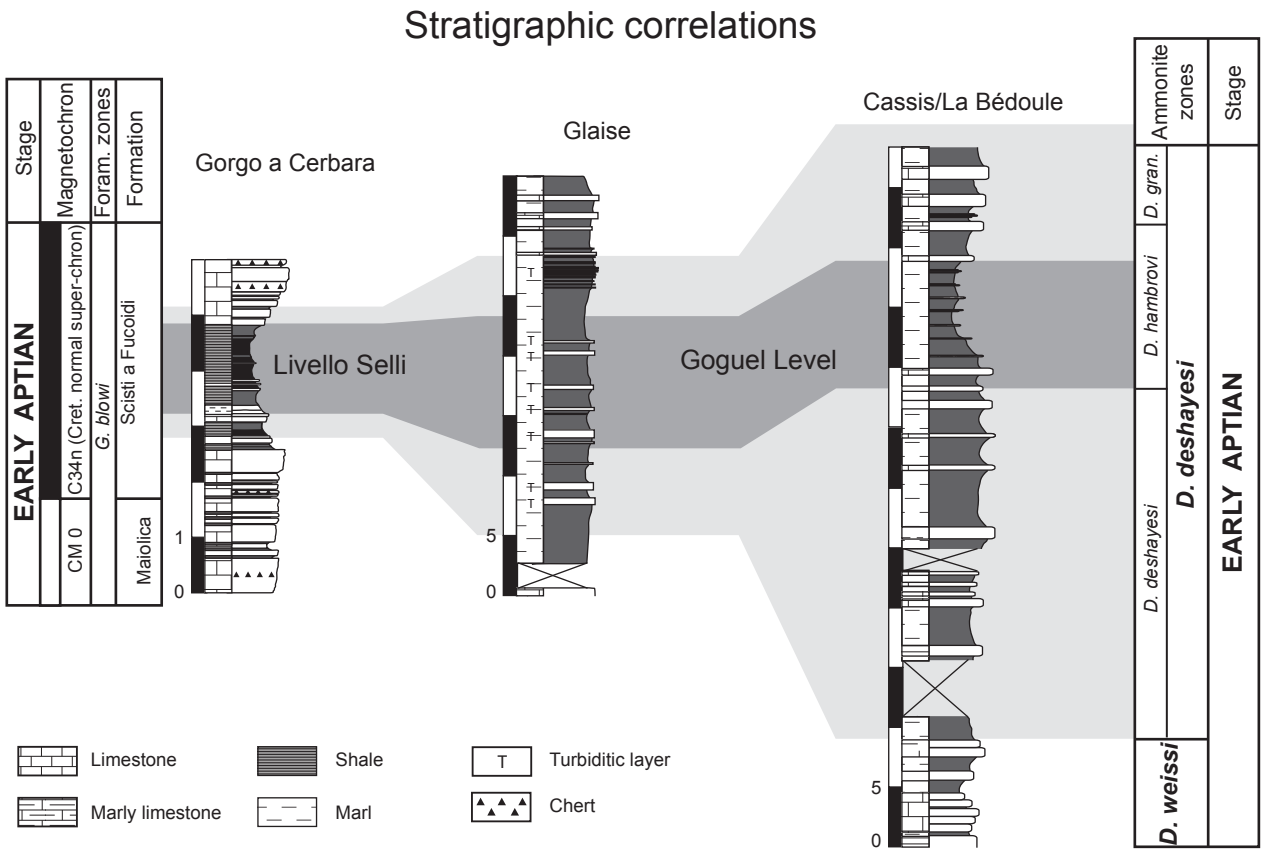

Fig. D.2: Lithology and stratigraphic correlation of the section of Gorgo a Cerbara (Coccioni et al., 1992), Glaise (Bréhéret, 1997) and Cassis/La Bédoule (Moullade et al., 1998). The light–grey and dark-grey bands indicate respectively the stratigraphic extent of OAE 1a and the Selli Level or its equivalents.

Jahren et al., 2001; Méhay et al., 2009). The Early Aptian OAE 1a is preceded by the abrupt decrease in $^{86}Sr/^{87}Sr$ isotopes values, and by a major demise of shallow-water carbonate platforms (Föllmi et al., 2006) and nannoconids (the "nannoconid crisis", Erba, 1994 and 2004). All these events occurred during the *Deshayesites dehayesi* ammonite zone, or near the base of the *Leupoldina cabri* foraminiferal biozone. The formation of the Ontong-Java flood-basalt plateau in the western Pacific has been identified as a potential trigger of OAE 1a (Erba, 1994; Leckie et al, 2002; Weissert and Erba, 2004; Méhay et al., 2009; Tejada et al., 2009; Misumi et al., in press).

Different definitions exist for the stratigraphic extent of OAE 1a. Some authors define the onset of OAE 1a at the base of the positive $\delta^{13}C$ excursion or at the negative peak (Menegatti et al., 1998; Méhay et al., 2009). Other authors (Bralower et al., 1999; Bellanca et al., 2002; Danelian et al., 2004; Tejada et al. 2009) propose an onset during the decrease of $\delta^{13}C$ based on significant change in marine flora and fauna. This complicates interpretation of paleoceanographic variations from different sections in terms of global change.

In this study, we evaluate changes in the redox conditions during OAE 1a and the lateral persistence of anoxic conditions in the western Tethys by investigating the distribution of redox-sensitive trace-elements (RSTE) along a shelf/basin transect. We also measured total phosphorus (P) and organic-carbon (TOC) contents to trace temporal changes in the marine P inventory and organic carbon preservation rates. This will help us to test the expanded OMZ versus the stagnant ocean model.

D.2 Geological settings

Three pelagic or hemi-pelagic sections were selected within the former western Tethyan realm according to their paleogeographic and the presence of the Livello Selli and its equivalents (Fig. D.1).

D.2.1 Gorgo a Cerbara, Italy

The section of Gorgo a Cerbara is located in central Italy, 4 km east of Piobbico (Cecca et al., 1995). This section starts in the Maiolica formation (Late Tithonian to Early Aptian) and ends in the Marne a Fucoidi formation (Early Aptian to Late Albian) (Coccioni et al., 1992). Gorgo a

Cerbara represents the type section for the Livello Selli and has been proposed as the stratotype for the Aptian stage (Erba et al., 1996). The lower part is composed of white to grey limestone (Maiolica Formation), which is intercalated with siliceous layers and contains marly and shaly, organic-rich intervals. The upper part of the section (Marne a Fucoidi Formation) consists of a greenish to reddish alternation of decimetric limestone and marly limestone with marly intervals. This formation begins with a 1.5 meter-thick dark interval of organic-rich shale: the Livello Selli.

D.2.2 Glaise l'Ermitage, France

The section of Glaise is situated 4 km north of Veyves (near Gap, SE France) in the Vocontian Trough. During Cretaceous time, this area was characterized by hemipelagic sedimentation leading to the deposition of the Aptian-Albian "Marnes Bleues" formation. The Glaise section consists of a marl succession interrupted by centimetric turbiditic layers. The Goguel level, time equivalent of the Livello Selli, is subdivided in six laminated layers annotated as Go 1 to Go 6 (Bréhéret, 1997). The section ends with the occurrence of marly limestone beds.

D.2.3 The section of Cassis/La Bédoule

The section of Cassis/La Bédoule (SE France) is a composite section representing the historical stratotype of the Bedoulian (Early Aptian; Moullade, 1998). It outcrops near the Cassis/La Bédoule railway station. The lower part of the composite section is located in an abandoned quarry and adjacent forest and consists of a marly whitish to grayish limestone succession with marly intervals.-The upper part of this hemipelagic section outcrops behind a camping area. This latter interval is constituted by a rather thick and well-preserved marly succession. The top becomes more calcareous with the occurrence of thick limestone banks.

D.3 Methods

D.3.1 Stable isotopes

Carbon- and oxygen-isotope analyses were performed on powdered bulk-rock samples of the section of Gorgo a Cerbara and Glaise, at the stable-isotope laboratory of the Universities of Orsay (Paris XI, France) and Bern (Switzerland), using a VG SIRA 10 triple collector and a Finnigan Delta V Advantage mass spectrometer, respectively. The results were calibrated to the PDB scale with the standard deviation of 0.05 % for $\delta^{13}C$ and of 0.07 % for $\delta^{18}O$.

D.3.2 Organic-matter characterization

Analysis of total organic carbon (TOC) and maturity (hydrogen and oxygen indices: HI and OI respectively) were conduced using a Rock Eval^{TM}6 with an instrumental precision <2% (Espitalié et al., 1985). HI and OI indices are used in a Van Krevelen diagram type to characterize and classify the organic matter (Espitalié et al., 1985). Two standards (IFP 160000 and VP143h) are used to calibrate the measurements.

D.3.3 Phosphorus

Total P contents were measured on bulk rock samples using a UV/Vis spectrophotometer (Perking Elmer UV/Vis Spectrophotometer Lambda 10, λ=865nm) with a mean precision of 5%. 100 mg of crushed sediments was weighted into a sterile glass bottle. 1 ml of 1 M $MgNO_3$ was added to the powder and then ashed in a furnace at 550°C during 2 hours. After cooling, 10 mL of HCL (1N) was added to the sediment in order to liberate the P from the matrix. After 16 h shaking, samples were filtered (0.45µm) and analyzed using the ascorbic acid method (Eaten et al., 1995). For this process, the solutions were diluted ten times and mixed with 100 µL molybdate mixing reagent to form phosphomolybdic acid. 100 µL of ascorbic acid was added to the solution to reduce the acid and produce a blue colour to the solution, which intensity is dependent on the P concentration.

P speciation analyses were performed on samples from the Gorgo a Cerbara section in order to quantify chances in the abundance of the different phases before, during and after the anoxic event. The sequential extraction procedure follows the SEDEX method developed by Ruttenberg (1992) and modified by Anderson and Delaney (2000) and allows to distinguish between authigenic, detrital, and organic P (P_{auth}, P_{det} and P_{org}). As for total P, the solutions were diluted ten times and measurements were conducted with a Perkin Elmer UV/Vis spectrophotometer Lambda 10, with a precision better as 5%.

D.3.4 Redox-sensitive trace elements

Redox-sensitive trace element (RSTE) analyses were performed on bulk-rock samples using a total acid digestion protocol (modified after Böning et al., 2004). 50 mg of sample powder were treated with 1mL of suprapur

Gorgo a Cerbara

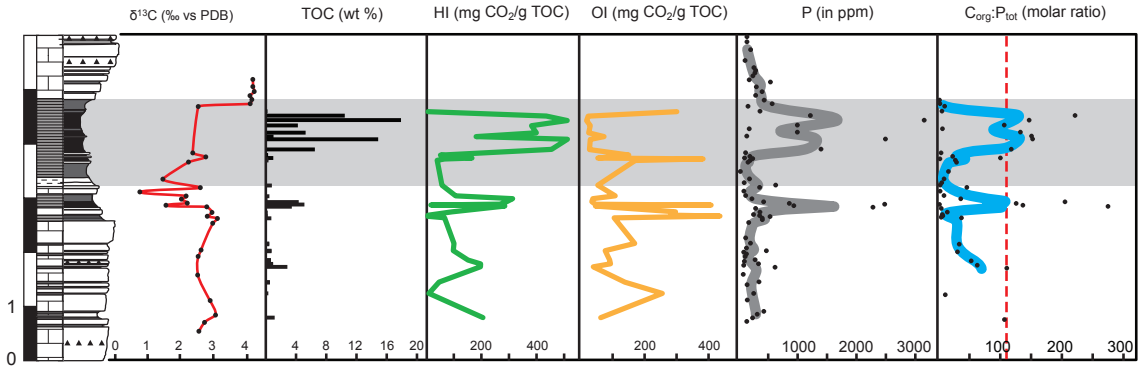

Glaise

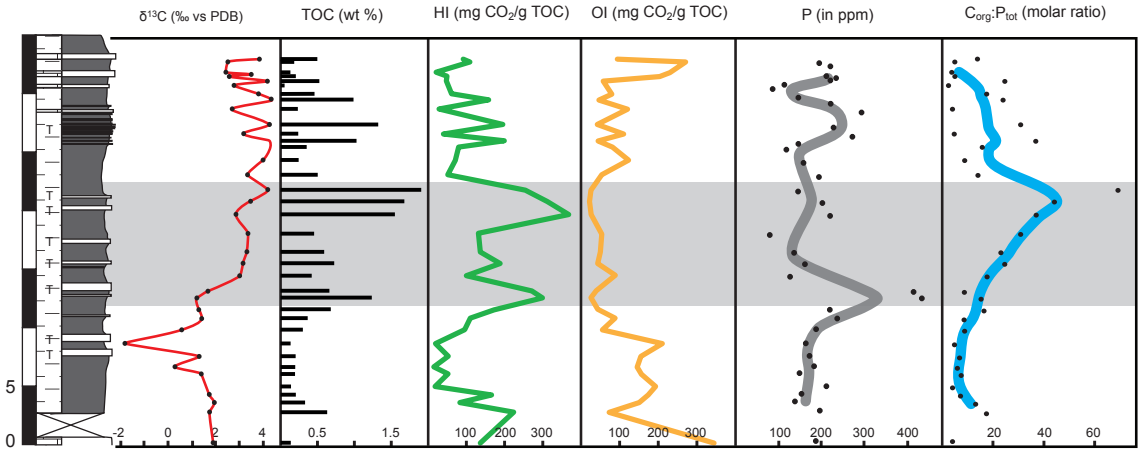

Cassis/La Bédoule

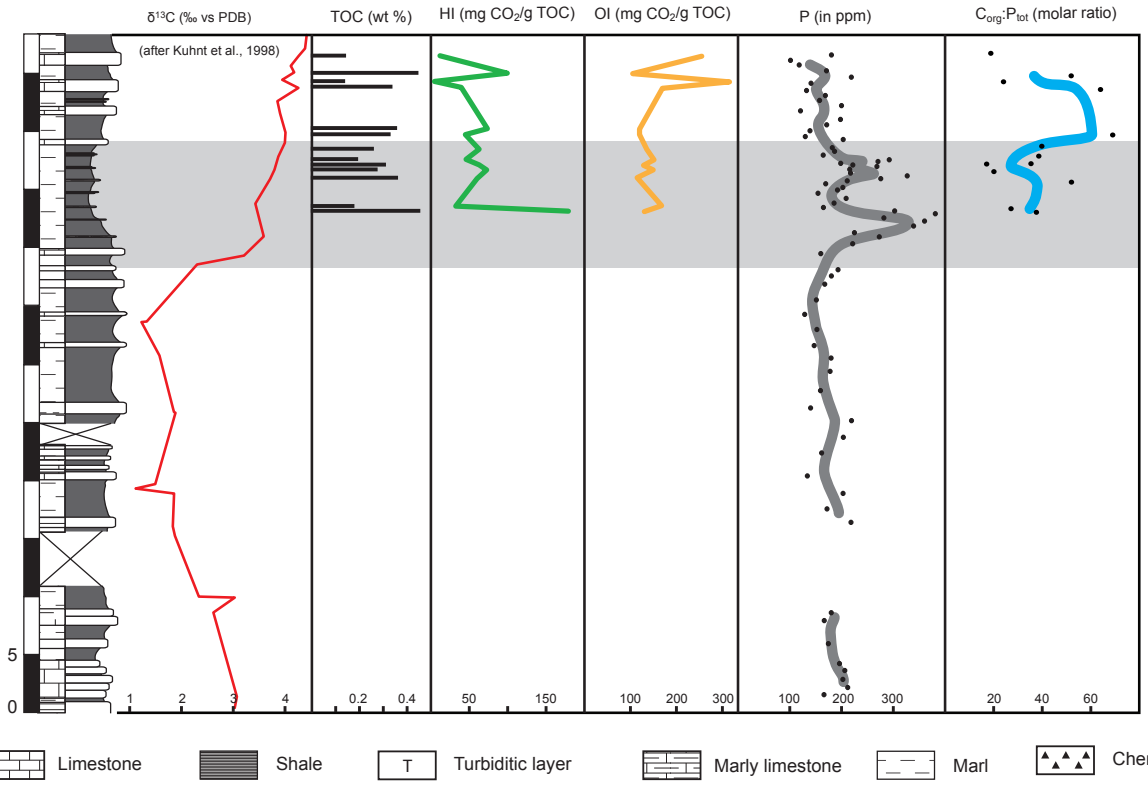

Fig. D.3: $\delta^{13}C$, total C_{org} and phosphorus contents. TOC is expressed in wt%, hydrogen indices (HI) in mg HC/g TOC, oxygen indices (OI) in mg CO_2/g TOC and P contents in ppm. C_{org}/P_{tot} ratios (expressed in mol/mol) are calculated for samples with a TOC > 0.1 wt%.

nitric acid (HNO_3) overnight in a 20 mL PFA digestion vessel (Savilex©) to oxidize organic matter. After that, a mixture composed of 3 mL of suprapur fluoridric acid (HF) and 3 mL of HNO_3 were added and the vessels were heated for 6h at 120°C on a hot plate with racks to heat samples in a uniform way. After digestion acids were evaporated and residues were redissolved and fumed off three times with 3 mL of half-concentrated chloridic acid (HCl 6N). After the third evaporation, residues were dissolved in 1 mL of suprapur HNO_3 and diluted to 50 mL with ultrapure water. RSTE contents were measured by a quadrupole ICP MS (ELAN 6100, Perkin Elmer) using a semi-quantitative mode (totalQuant™). The calibration is based on two certified reference materials (CRM): LKSD-1 lake sediment and NIST-1640 natural water. We studied the contents of U, V, Co, Mo, As, Mn, Cr, Ni, Cu, Zn and Fe. The mean recovery rates (n=12 digestions) and quantification limit for the analysed RSTE were determined by using LKSD-1 CRM and are 103% and 5×10^{-4} ppb for U, 90% and 2.9×10^{-1} ppb for V, 105% and 8×10^{-2} ppb for Co, 110% and 2×10^{-2} ppb for As, 89% and 1.4×10^{-1} ppb for Mo and 111% and 1.82 ppb for Mn.

RSTE concentrations are normalized to the aluminium content (Al) to correct for variable dilution by terrigenous input (Calvert and Pedersen, 1993; Morford et al., 2001). For most sedimentary deposits, Al is considered as an indicator of the alumosilicate fraction of the sediments, with very little ability to be diagenetically removed (Morford and Emerson, 1999; Morford et al., 2001; Piper and Perkins, 2004). We report all RSTE concentrations as Al-normalized having units of 10^{-3}.

D.4 Results

D.4.1 Stable carbon isotopes

Bulk-rock carbon-isotope data are shown in Fig. D.3. The base of the Gorgo a Cerbara section is characterised by a small maximum in $\delta^{13}C$ of ~3‰. Following this maximum, a decrease to 2.4‰ is observed in the upper part of the Maiolica Formation, which is followed by a gentle increase and a maximal value of 3.1‰ near the boundary between the Maiolica and Scisti a Fucoidi Formations. Thereafter, the $\delta^{13}C$ record exhibits a rapid and stepwise diminution, reaching a minimum of 0.7‰ in the limestone interval just below the Livello Selli. Within the Livello Selli a two-step increase is observed in $\delta^{13}C$ values towards ~2.8‰, followed by a more constant trend. The top of the Selli interval is characterized by a rapid increase towards a maximum of 4.1‰.

In Glaise, the $\delta^{13}C$ record shows a decreasing trend in the first part of the section (base to 8m), which appears accelerated in its latter part, before reaching the minimal value of -2‰. Subsequently, following a first sharp recovery to 1.8‰, $\delta^{13}C$ values gradually increase to 4‰, through the Goguel Level. The top of the section shows relatively constant carbon-isotope values fluctuating between 3 and 4‰.

The whole-rock stable carbon-isotope record for the Cassis/La Bédoule section has been published by Kuhnt et al., 1999), and only strategic intervals were remeasured, in order to correlate our section and sampling with the published section (Moullade, 1999; Kuhnt et al., 1999).

D.4.2 Organic carbon and organic matter composition

TOC contents were analysed in marly layers throughout the three studied sections. In samples with very low TOC values (< 0.1 – 0.3 wt%), HI and OI parameters are difficult to interpret (Espitalier et al., 1985). We therefore present the results for the samples with TOC values ≥ 0.1 wt%, but will only discuss the results for TOC values ≥ 0.3 wt%.

In the Gorgo a Cerbara section, TOC contents show three distinct maxima. A first increase in TOC values (2.77 wt%) is observed near the transition of the Maiolica to the Scisti a Fucoidi Formation (at about 1m below the Livello Selli). A second peak in TOC values (5.05 wt%) occurs in sediments corresponding to the negative spike in $\delta^{13}C$. In Livello Selli, the samples show higher TOC contents with an average value of 5.62 wt%. A two-step increase is observed upward through this interval with a first maximum in TOC values of 14.94 wt% at 4m and a second of 18.01 wt% at the top of the Livello Selli. The organic-rich samples are characterised by high HI (400-500 mg HC/g TOC) and low OI (20-30 mg HC/g TOC) throughout the section, indicating Type-II organic matter.

In the section of Glaise, TOC contents fluctuate throughout the measured interval. A stepwise increase is observed from the base to the top of Goguel level. In the lower part of the section (0-12m), TOC contents are rather low with values around 0.30 wt%. A maximum is observed at the base of the Goguel level interval with a TOC value of 1.27 wt%. A second peak in TOC values (1.94 wt%) in TOC content characterizes the end of this interval, corresponding to the end of the $\delta^{13}C$ shift. Above the Goguel level (at 27.5m), a third maximum in

TOC contents reaching 1.11 wt% is observed. A scatter plot between HI and OI shows a Type-II organic matter dominant with the highest TOC values associated with higher HI's and lower OI's. The samples with the lowest TOC content plot in the field of Type-III.

For Cassis/La Bédoule, marly intervals were only measured in the higher part of the section (from 35m to the top). In the lower part of the section, the marl intervals present a high degree of alteration and were not analyzed. TOC values are quite low in comparison to the Gorgo a Cerbara and Glaise sections. The average value is around 0.26 wt%. HI values are low and plot within the Type-III area.

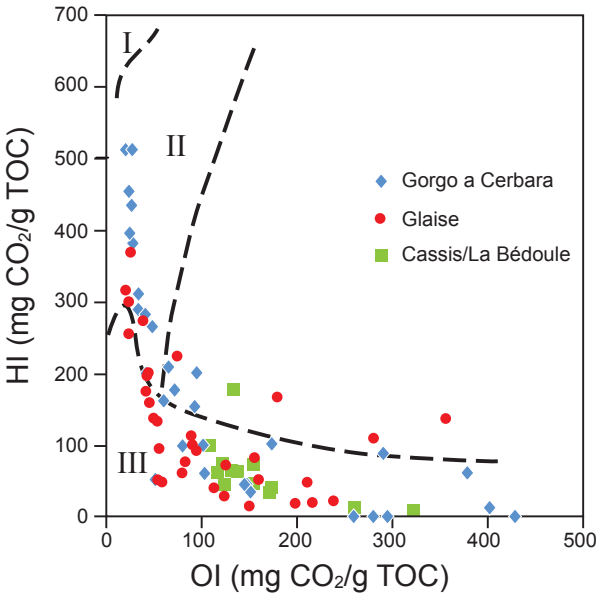

Fig. D.4: HI/OI diagram characterizing the quality of organic matter for the studied sections.

D.4.3 Phosphorus contents and C/P ratio

D.4.3.1 Total phosphorus contents

Total P contents and their variations across the studied sections are presented in Fig. D.3. In the section of Gorgo a Cerbara, P contents show a relatively high background average value (up to 450 ppm) superimposed by three sharp peaks. A first increase is observed in the lowest part of the measured section, with a relative maximum of 627 ppm at ~1.9 m, which is followed by a return to lower values. In the following, a well-defined peak with a maximum of 2488 ppm occurs in sediments coeval with the onset of the negative $\delta^{13}C$ spike. A second, lower peak in P contents (636 ppm) follows immediately, in sediments corresponding to the base of the Livello Selli. Within the Livello Selli, P values increase again and reach two subsequent maxima of 3497 and 3142 ppm, respectively. Thereafter, P contents decrease to pre-Selli values.

For the sections of Glaise and Cassis/La Bédoule, the measured P contents show comparable temporal variations. In sediments below the negative excursion in $\delta^{13}C$, P contents remain low with values fluctuating around 150-200 ppm. Subsequently, in sediments immediately above the negative spike, P values show a peak reaching a first maximum of 433 and 384 ppm for Glaise and Cassis/La Bédoule, respectively, which is followed by a decrease in both sections. A second increase in P contents is observed in sediments corresponding to the upper part of the Goguel level in both sections.

D.4.3.2 Phosphorus speciation

No significant differences were observed in the behaviour of the P species in the Gorgo a Cerbara section (Fig. D.5). The first part of the section is characterized by relatively low average values, ranging around 205, 111 and 29 ppm for authigenic-P (P_{auth}), detrital-P (P_{det}) and organic-P (P_{org}), respectively. At the base the Livelo Selli, P_{auth} shows a maximum of ~410 ppm followed by a return to lower values. The top of this interval is marked by two peaks for each P species reaching 912, 816 and 80 ppm for P_{auth}, P_{det} and P_{org}, respectively.

The P_{det} phase may represent a particularly well-crystallized authigenic phase, rather than a true detrital phase (e.g., Filippelli and Delaney, 1996; Föllmi et al., 2005). Given the good correlation between P_{auth} and P_{det} and the absence of detrital phosphatic grains in thin section, it is assumed here that the majority of P_{det} effectively embodies recrystallized P_{auth}, and was bioavailable as such.

D.4.3.3 C/P ratios

We determined C_{org}/P_{tot} ratios in the section of Gorgo a Cerbara and Glaise to evaluate the degree of organic P (P_{org}) retention in the sediments and temporal variations therein throughout the Livello Selli and Goguel Level. For Cassis/La Bédoule, data are only available for the upper part of the section corresponding to the equivalent of the Goguel level. As indicated by Anderson et al. (2001), $C_{org}/P_{reactive}$ is a more robust measure of the degree of P lost in the ocean than C_{org}/P_{org}, due to the possible diagenetic transfer of P_{org} into the authigenic P phase. Here, we used total P (P_{tot}= $P_{reactive}$+$P_{detrtitic}$), thereby assuming that detrital P is minimal. In the Gorgo a Cerbara section (Fig. D.3), C_{org}/P_{tot} ratios show a low background value (45) interrupted by excursions toward substantially higher values. A first maximum of

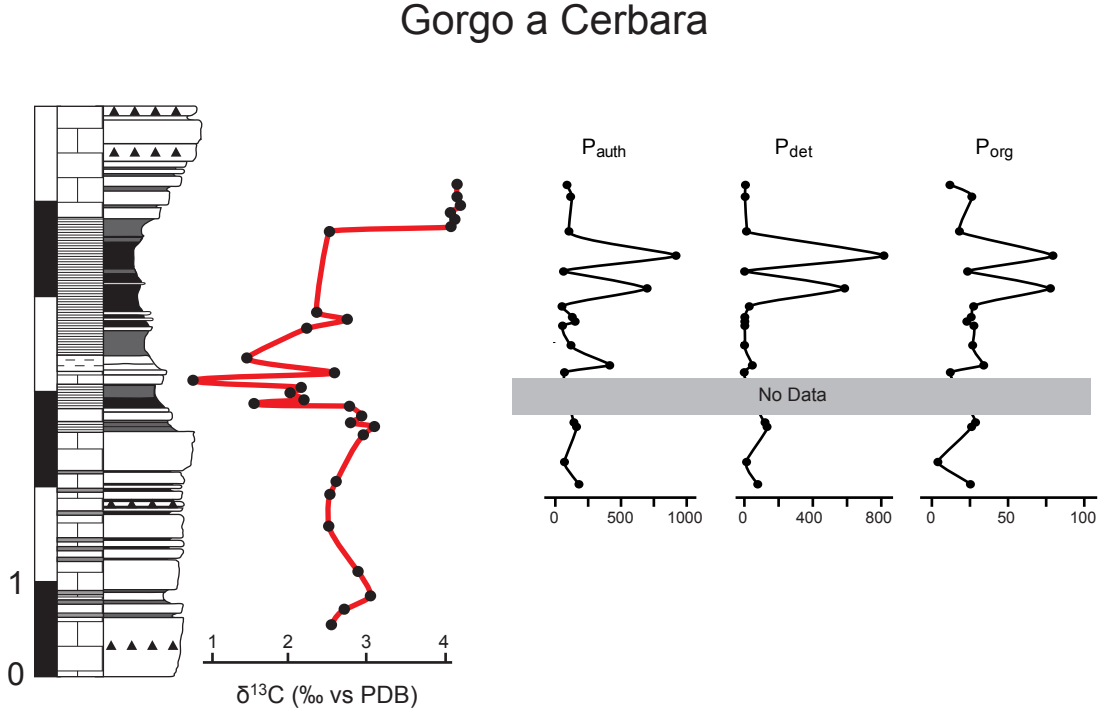

Fig. D.5: P contents for authigenic minerals (P_{auth}), terrigenous material (P_{det}) and organic matter (P_{org}) for the Gorgo a Cerbara section.

275 is observed at 1.9m above the base of the section. A second, less pronounced excursion in the C_{org}/P_{tot} values (205) is noticed in sediments immediately below the negative $\delta^{13}C$ spike. Within the Livello Selli, C_{org}/P_{tot} ratios rise toward high values ranging between 120 and 220. In the section of Glaise and in Cassis/La Bédoule, C_{org}/P_{tot} show lower values, with a background average value of 10 and 25, respectively. In both sections, the upper part of the Goguel level is marked by a shift toward higher values in C_{org}/P_{tot} ratios.

D.4.4 Redox-sensitive trace elements

The data of the RSTE studied here (U, V, Co, As, Mo, Cr, Ni, Cu, Zn, Fe and Mn) are shown in Fig. D.6. For the sections of Gorgo a Cerbara and Glaise, the RSTE distributions were investigated along the entire section, whereas for the section of Cassis/La Bédoule, we focused on the RSTE variations within the Goguel equivalent.

In the Gorgo a Cerbara section, the majority of RSTE shows comparable trends, with a low background value interrupted by three intervals of higher contents. The first interval, located at ~ 1m below the negative $\delta^{13}C$ spike, is characterized by moderate to high enrichments in all RSTE (except V and Mo) compared to average shale values. The anomaly is especially well developed in U contents ranging up to ten times the background value. The other elements (Co, As, Cr, Ni, Cu, Zn and Fe) show weaker enrichments with contents ranging from 1.5 to 5 times the background levels. A second interval of RSTE enrichments (except for Mo) is observed in the sediments corresponding to the negative $\delta^{13}C$ excursion. However, within this interval, U and V display only a moderate increase with values two to four times higher than the background levels. The Livello Selli itself is marked by two sharp peaks in all RSTE. They rise to the highest values along the entire measured section, and especially Mo shows enrichments from 50 to 150 times the background level. Contrary to the other elements, Mn displays rather high values in the first part of the section, with values ranging from five to nine times the average shale value. At the onset of the negative $\delta^{13}C$ excursion, the Mn content decreases abruptly and remain low in the Livello Selli. At the top of the section, Mn shows again an increase.

In the Glaise section, RSTE values are quite low compared to the section at Gorgo a Cerbara. U, V, Co, Cr, Ni, Cu, Zn and Fe contents show similar variations, with moderate enrichments in sediments of the Goguel level. The onset of the positive $\delta^{13}C$ excursion is marked by the highest RSTE contents with concentrations ranging from 1.6 to six times the background values. Contrary to the other studied elements, no enrichments in As and Mo contents are observed along the section, which fluctuate more or less around the average shale values. The Mn content remains also constant and shows relatively low values compared to the average shale content.

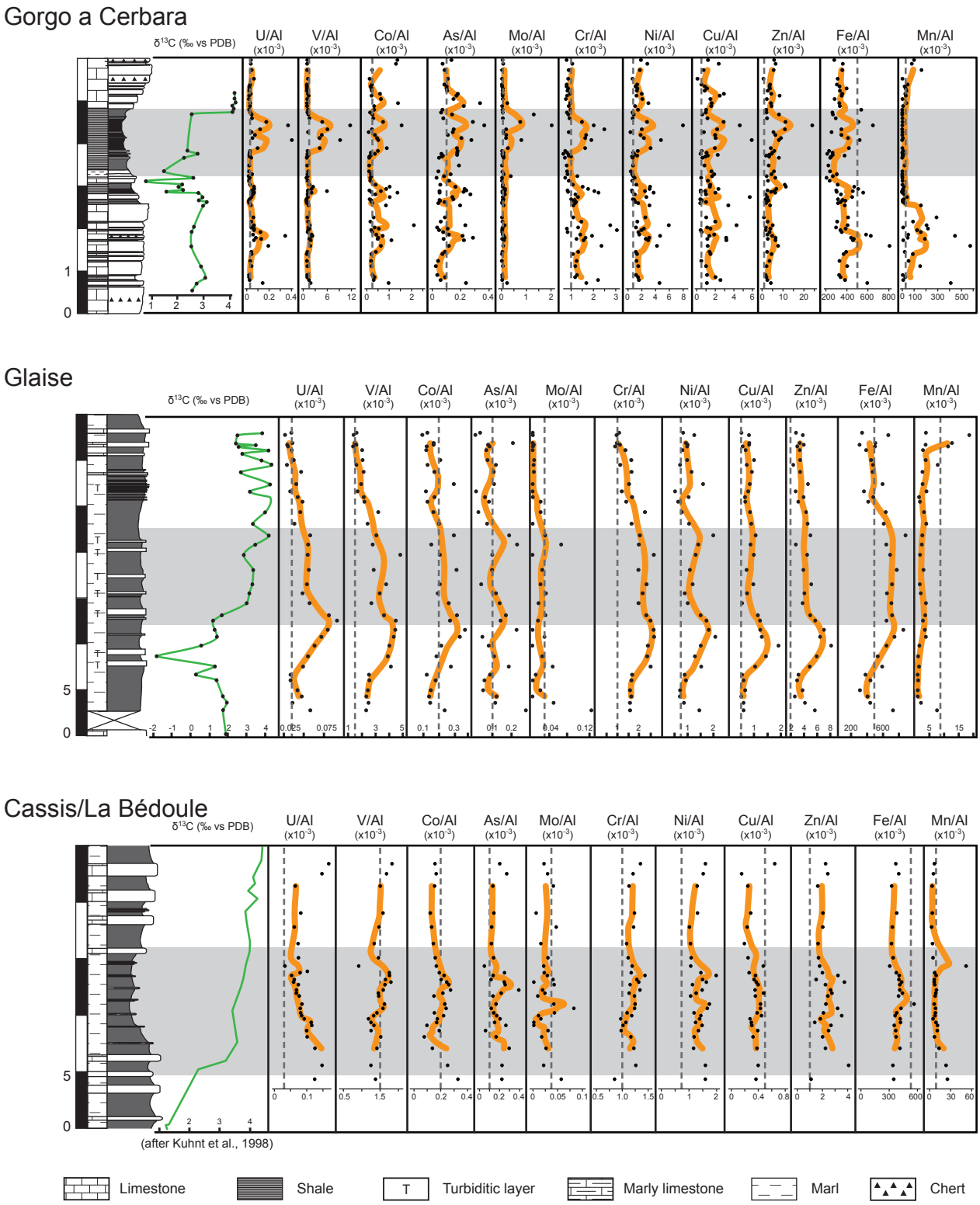

Fig. D.6: Redox-sensitive trace elements (RSTE) for the sections of Gorgo a Cerbara, Glaise and Cassis/ La Bédoule. Data are persented as Al-normalized having units of 10^{-3} expressed. The grey band indicates the position of the Livello Selli or its equivalent for each section. The average shale values (dash lines) are taken form Wedepohl (1971).

At Cassis/La Bédoule, the values for the average RSTE contents are quite low (Fig. D.6). No major enrichments are observed along the studied part of the section. U shows a decreasing trend reaching values around the background average shale value. V and Co remain quite constant and fluctuate around the average shale value, respectively. Cr, Ni, Cu, Zn and Fe show higher values in the first part of the Goguel equivalent and remain more or less constant at the top of the section.

D.5. Discussion

D.5.1 Carbon isotope stratigraphy

OAE 1a is marked by a globally recognized positive excursion in marine $\delta^{13}C_{carb}$ and $\delta^{13}C_{org}$ records, which is preceded by a negative shift (Menegatti et al., 1998; Bralower et al., 1999; Hochuli et al., 1999; Luciani et al., 2001; de Gea et al., 2003; Wissler et al., 2003; Heimhofer et al., 2004; Herrle et al., 2004; Dumistrescu and Brassell, 2006; Méhay et al., 2009). The evolution of the $\delta^{13}C_{carb}$ record recognized in Cismon, Italy and Roter Sattel, Switzerland (Menegatti et al., 1998), is characterized by a decreasing trend (C2) towards a minimum (C3) in sediments underlying the Selli level or its equivalent. Subsequently, the $\delta^{13}C$ record shows an abrupt step-like positive excursion (C4) at the base of the Livello Selli, which is followed by rather constant values (C5), a second step-like increase (C6) towards the top of the Selli interval and a plateau of high $\delta^{13}C$ values (C7). A decrease in $\delta^{13}C$ values (C8) marks the end of the anoxic event.

The characteristic features of the OAE 1a $\delta^{13}C$ record are observed in the sections of Gorgo a Cerbara and Glaise, where a marked decrease in the $\delta^{13}C$ record in sediments underneath the Livello Selli and Goguel level occurs (Fig. D.7) followed by a negative spike comparable to the one observed at Cismon and Roter Sattel (Menegatti et al., 1998), even if at Glaise the amplitude of the $\delta^{13}C$ negative spike is higher, at around ~4‰. The Cassis/La Bédoule section exhibits the negative $\delta^{13}C$ excursion in unprecedented detail (Kuhnt et al., 1998), which is here characterized by a double negative spike enveloping a minor, ~1‰ positive excursion (Fig. D.7).

Amplitudes comparable to the one observed in Glaise have been found in other studies, and were explained by a massive release of ^{13}C-depleted carbon either from the dissociation of CH_4-containing clathrates or from thermal metamorphism of C_{org}-rich sediments (Jahren et al., 2001; van Breugel et al., 2007; Ando et al., 2008). Recently, Méhay et al. (2009) used high-resolution bulk-rock and n-alkane-based $\delta^{13}C$ records from Cismon to propose an abrupt increase in volcanic CO_2 release due to the formation of the Ontong-Java Plateau as a trigger of the negative $\delta^{13}C$ excursion.

The subsequent positive excursion in the $\delta^{13}C$ record (C4), characterizing the onset of the Livello Selli, is well developed in all three sections and comparable to the ones observed in Cismon and Roter Sattel. The

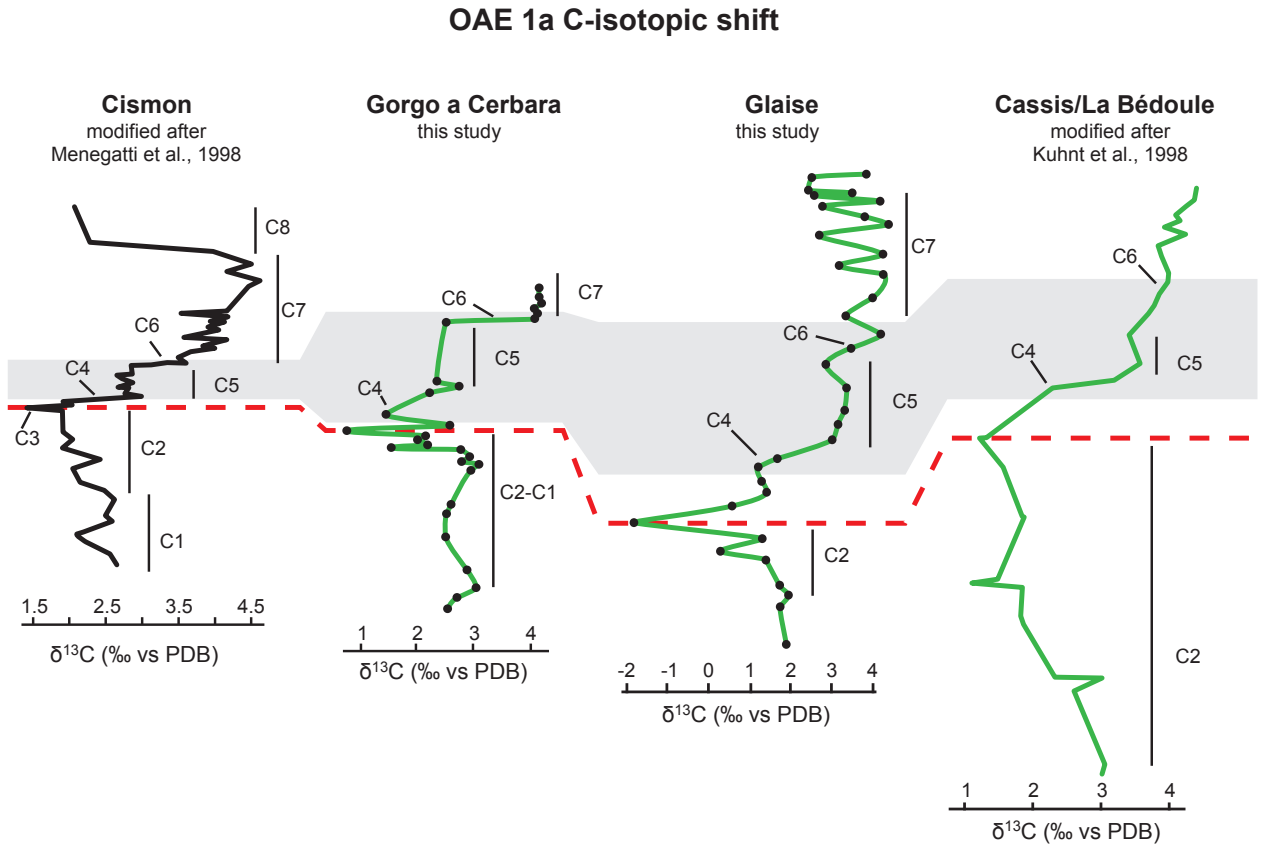

Fig. D.7: Stratigraphic correlations for the early Aptian OAE 1a between the sections of Gorgo a Cerbara, Glaise, Cassis/La Bédoule and Cismon. The grey band indicateThe dash line indicates the position of the negative peak in $\delta^{13}C$.

C5 plateau in the $\delta^{13}C$ record occurs in all sections even if the sparse occurrence of carbonate in the Gorgo a Cerbara section precludes to determine and differentiate between the C5 and C6 segments with precision. The uniformity in the C5 segment of the $\delta^{13}C$ record has been interpreted as an episode of stability in the marine carbon-isotope budget (Menegatti et al., 1998; Dumitrescu and Brassell, 2006). The higher $\delta^{13}C$ values observed in the sections of Gorgo a Cerbara and Glaise at the top of the Livello Selli and the Goguel level correspond to the plateau C7.

D.5.2 Origin and accumulation pattern of organic carbon

Information on the thermal evolution of preserved organic matter (OM) is obtained by Rock-Eval analyses of the maximum temperature needed to crack preserved OM during pyrolysis (T_{max}). For Type-II OM, T_{max} values higher than 435°C indicate a high degree of maturity and alteration (Espitalier et al., 1985). At Gorgo a Cerbara, organic-rich samples display T_{max} values between 410 and 420°C indicating rather good OM preservation (Fig. D.8). For the samples of Glaise, T_{max} values fluctuate between 430 and 440°C suggesting a higher degree of burial and thermal alteration and/or a matrix effect. This is particularly true for low TOC values (Espitalié et al., 1985). Samples with higher TOC contents show lower T_{max} values, which plot in the field of immature OM in a HI/T_{max} diagram indicating a relatively high degree of OM preservation (Fig. D.8). The samples of Cassis/La Bédoule show T_{max} values around 425°C. This indicates that its preserved OM experienced minor burial and thermal alteration.

The characteristics of OM are different in each of the three sections and probably reflect the different paleoenvironmental regime existing at each locality. In the Gorgo a Cerbara section, preserved OM shows an explicit marine origin (Type-II field in the HI/OI diagram with high HI and low OI) as shown by previous studies (Baudin et al., 1998 and references therein). Three intervals, corresponding to dark and laminated sediments, show high OM preservation rates with TOC values reaching a maximum of 18.01 wt% at the top of the Livello Selli. In Glaise the preserved OM appears to have a marine origin, despite its more pronounced alteration as suggested by HI/OI and HI/T_{max} diagrams (Figs. D.4 and D.8). This is shown by the positive correlation of higher HI values with higher TOC contents. The higher TOC are observed in centimetric darker layers of the Goguel level. The Cassis/La Bédoule section shows low TOC values, characterized by low HI and low OI suggesting a terrestrial origin of OM. However, the characteristics of OM observed in Cassis/La Bédoule (low HI with a mean TOC value of 0.3 wt%) show similarities with modern oxic pelagic environments (Tyson, 1995) and are indicative of the low preservation potential, as was already suggested by Bréhéret (1997).

In Gorgo a Cerbara, a significant increase in TOC contents is observed at the end of the $\delta^{13}C$ positive excursion indicating optimal OM preservation rates near the end in the deposition of the Livello Selli (Fig. D.3). This increase in TOC is correlated to the occurrence of well-laminated levels and may have been related to a switch to more reducing conditions. At the onset of the anoxic event, bottom waters carried sufficient oxygen to effectively breakdown organic matter. Steady high OM flux rates due to increased primary productivity caused gradual depletion of bottom-water oxygen, thereby leading to enhanced OM preservation. This scenario may, to a lesser extent, also be inferred to Glaise. The correlation between HI and TOC observed along the section provides good evidence for this.

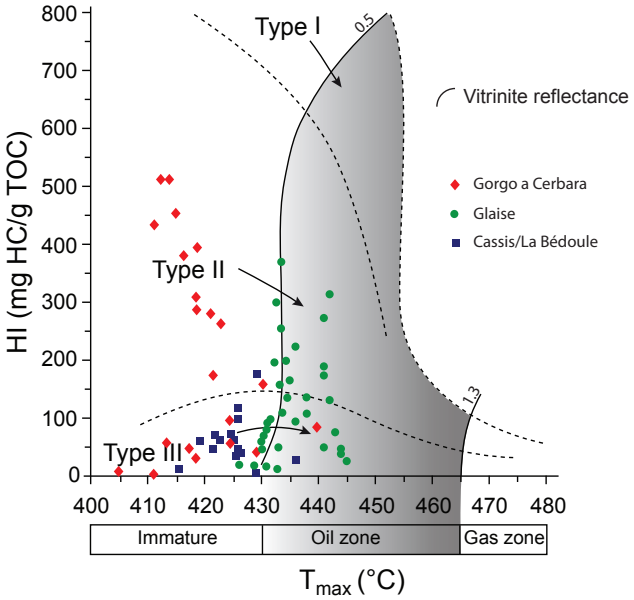

Fig. D.8: HI/T_{max} diagram for preserved organic matter (OM) in the studied sections. OM shows a good degree of immaturity for the sections Gorgo a Cerbara and Cassis/La Bédoule and indicates a predominantly marine origin. In Glaise a phase of higher degree of thermal alteration is observed.

D.5.3 Variations in paleoredox conditions during OAE 1a

The distribution of RSTE in sediments and sedimentary rocks has been used to characterize redox conditions in modern and ancient marine sediments (Calvert and Pedersen, 1993; Jones and Manning, 1994; Wignall, 1994; Crusius et al., 1996; Morford et al., 2001; Algeo and Maynard, 2004; Algeo and Lyons, 2006; Bodin et al., 2006; Riquier et al., 2006; Tribovillard et al., 2006). RSTE enrichments and ratios are useful proxies in determining if bottom-water conditions during sediment deposition were oxidizing or reducing. The behaviour of these elements is linked to the capacity of organic matter to scavenge RSTE during its passage through the water column and to their preservation in the sedimentary reservoir as a function of redox conditions. Here we use a suite of elements (U, V, Co, As and Mo; Algeo et al., 2004; Tribovillard et al., 2006).

In the Gorgo a Cerbara section, two episodes of moderate to significant increases in U, V, Co and As contents are recognized in sediments below the Livello Selli (at 1.5 m below the onset of the $\delta^{13}C$ positive shift and coeval with the decrease in $\delta^{13}C$ values), which coincide with centimetric, organic–rich laminae (Fig. D.6). These horizons show a relatively good correlation between TOC and RSTE accumulations, which is interpreted as indicative of an anoxic depositional environment (Algeo and Maynard, 2004; Tribovillard et al., 2006). These pre-Selli peaks have not been observed in the Glaise section and might result from regional changes in bottom-water oxygen conditions. Within the Livello Selli itself, RSTE show two phases of marked enrichment (Fig. D.6). The enrichments of U, V, Co, As and Mo in this interval are intercorrelated and correlate also with TOC values, which show maxima within these levels (Fig. D.9). These relations are taken to be indicative of an anoxic depositional environment (Algeo and Maynard, 2004; Tribovillard et al, 2006). For two samples showing the highest TOC values along the section, a weak TOC-RSTE covariation is observed (Fig. D.9). This provides evidence for more severe reducing conditions, which were probably close to the anoxic/euxinic threshold (Algeo and Maynard, 2004; Tribovillard et al., 2006).

The sections of Glaise and Cassis/La Bédoule show low to moderate RSTE enrichments within the Goguel level and its equivalent. A general increase in RSTE observed in sediment corresponding to the onset of the $\delta^{13}C$ positive shift may be used as an indication of a trend towards dysaerobic conditions in the Goguel level in Glaise. Throughout the Goguel level, the RSTE do not show significant enrichments. However, within this interval, the RSTE show slightly higher values than the average shale value, except for Mo. This, related with the higher TOC values in the Goguel level, may indicate that dysoxic rather than anoxic conditions were prevailing in this shallower setting of the western Tethys. At Cassis/La Bédoule, the absence of RSTE enrichments in the sediments equivalent to the Goguel level and their general low values are in favour of oxic conditions during the OAE 1a interval.

Further evidence for differences in oxygen levels during OAE 1a in the western Tethyan bottom waters is provided by the C/P molar ratios. C/P molar ratios are indicators of the degree of OM degradation and the relative loss of organic P under oxygen-depleted conditions (Ingall et al., 1993; Ingall and Jahnke, 1994, 1997; Van Cappellen and Ingall, 1996; Slomp et al., 2004, Bodin et al., 2006; Mort et al., 2007). In comparison to the C_{org}/P_{org} ratio the C_{org}/P_{tot} ratio is a more faithful indicator of the importance of the recycling of P_{org} into authigenic P phases relative to the amount that is transferred back into the bottom waters (Anderson and Delaney, 2000). At Gorgo a Cerbara, organic-lean sediments show lower C_{org}/P_{tot} ratio than the Redfield ratio (106:1; Redfield, 1958), whereas the organic-rich intervals have higher C_{org}/P_{tot} ratios (up to 200 for the Livello Selli), indicating the preferential P release from sediments. These values are similar to those observed for Furlo, Italy, during OAE 2 (Mort et al., 2007). In the sections of Glaise and Cassis/La Bédoule, C_{org}/P_{tot} values are lower than the Redfield ratio. In sediments near the top of the Goguel level or its equivalent (segment C6 of the $\delta^{13}C$ curve), an increase in the C_{org}/P_{tot} ratio is observed. This increase is coeval with a diminution in total P contents, which may indicate a shift to more oxygen-depleted conditions, which is followed by a return to normal conditions.

To summarize, the RSTE distributions and the C_{org}/P_{tot} ratios in the analysed sections indicate that the OAE 1a interval was characterized by anoxic to euxinic conditions in the deeper, more distal part of the western Tethys. Nevertheless, in Gorgo a Cerbara, the anaerobic conditions were not homogeneous during the entire Livello Selli and show intermittent returns to less reducing conditions. In the shallower sections, RSTE contents and C_{org}/P_{tot} ratios suggest less severe reducing conditions, characterized by rather dysoxic than truly anoxic conditions.

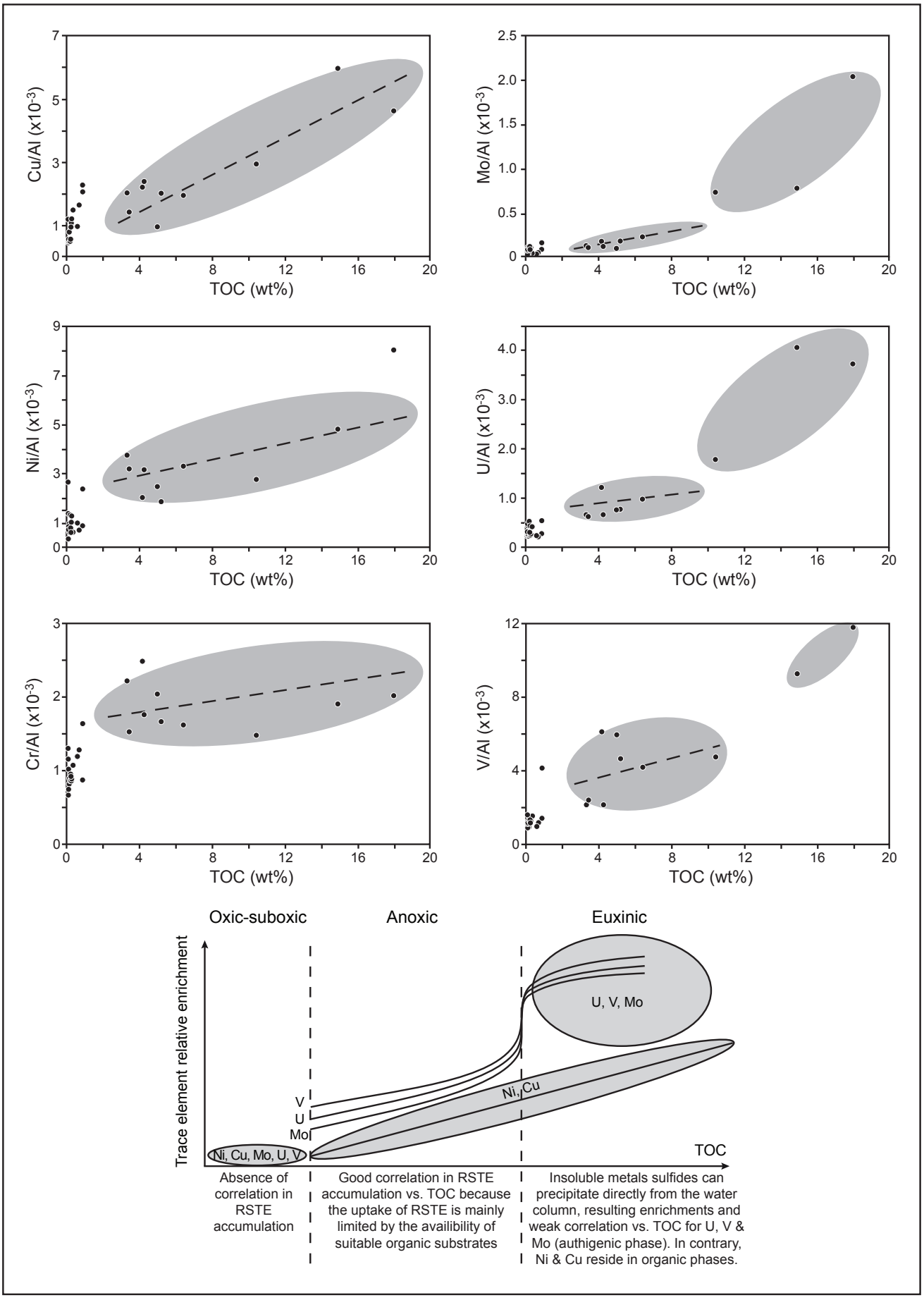

Fig. D.9: A.TOC-RSTE relationships for the Gorgo a Cerbara section. RSTE concentration are Al-normalized (x10^{-3}). B. Theoretical model of RSTE enrichment under dysoxic, anoxic and euxinic conditions (adapted from Tribovillard et al., 2006).

D.5.4 Productivity conditions

Ni, Cu and Zn are usually enriched in anoxic sediments (Brumsack, 1989; Calvert and Pedersen, 1993). Algeo and Maynard (2004) and Tribovillard et al. (2006) showed that these elements are transferred into the sediment mainly in association with OM and they are retained in the sediment within sulphides (usually in solid solution with pyrite), and this even in the case of complete OM remineralization. As such, Ni, Cu and Zn are considered to be reliable tracers of OM delivery to the sediment (Algeo and Maynard, 2004; Tribovillard et al., 2006). In the Gorgo a Cerbara section, the black-shale interval shows positive peaks in Ni/Al, Cu/Al and Zn/Al ratios (Fig. D.6). This may indicate periods of increased OM influx to the sediments. Higher Ni, Cu and Zn contents are also observed for the organic-rich horizons pre-dating the Livello Selli.

In the section of Glaise, sediments from the Goguel level appear to have experienced less reducing conditions, which were dysoxic rather than anoxic if compared to the Gorgo a Cerbara RSTE values. In moderate reducing sediments, these elements may partially be recycled from the sediment to the overlying water due to the absence of sulphides (Tribovillard et al., 2006). This might explain the lower values observed at Glaise and Cassis/La Bédoule. Despite the overall less-reducing conditions, the discrete centimetric layers with higher TOC values within the Goguel level contain higher Ni, Cu and Zn values, which is evidence for several short episodes of increased OM flux rates during the deposition of the Goguel level (Fig. D.6).

D.5.5 Changes in phosphorus input as a potential trigger of ocean productivity?

Phosphorus is an important and often limiting element in ocean primary productivity. The only significant source of P to the ocean is via rivers (continental weathering) and atmospheric transport (Föllmi, 1996; Delaney, 1998; Compton et al., 2000). The transfer of P into the sediments occurs by sedimentation of organic P, P adsorbed on surface-reactive particles, P in fish debris or by direct precipitation (Ruttenberg, 1993; Filippelli and Delaney, 1996; Föllmi, 1996). The efficiency of P storage in the sedimentary reservoir is redox dependent. P regeneration becomes more important in oxygen-depleted bottom waters (Ingall and Jahnke, 1994; Van Cappellen and Ingall, 1996; Colman and Holland, 2000; Emeis et al., 2000; Tamburini et al. 2002; Bodin et al., 2006; Mort et al., 2007). As such, a generalized increase in P contents may indicate either an increase in P delivery to the ocean and/or an increase in bottom-water oxygenation.

At Gorgo a Cerbara, P contents show higher values in organic-rich layers pre-dating OAE 1a and in the upper part of the Livello Selli. Surprisingly enough, these intervals bear evidence of strongly reducing anoxic conditions, shown by high TOC values, enrichments in RSTE and by high C/P ratios. The P speciation analysis shows that all P species increase within these horizons and that P_{auth} is the main component. Given the high C_{org}/P_{tot} ratios and the high P_{auth} values within these layers, a part of the remobilized P appears to have been trapped in the sediments in the form of authigenic P and was as such prevented from returning to the water column. The presence of benthic microbial mats, postulated by Gorin et al. (2009) may provide an explanation in that they may have trapped a quantity of remobilized-P during the early diagenesis and prevent it from being transferred back to the bottom waters.

In the sections of Glaise and Cassis/La Bédoule, P contents show an increase at the onset of the Goguel level and its equivalent, just above the $\delta^{13}C$ negative excursion (segment C3). The Goguel level itself is then marked by lower values, followed by an increase at the end of the positive excursion in C-isotopes. General longer-term changes in the marine P cycle (longer than several times the assumed actual marine residence time of approximately 10 kyrs for P) are related to changes in the P delivery rate from the continent (Froelich et al., 1982; Föllmi, 1995; Filippelli, 2008). The general increase in P accumulation characterizing the onset of the early Aptian anoxic event suggests an increase in nutrient input, probably related to a change in continental weathering. In the Hybla Formation of northwestern Sicily, observations based on Ba and P contents suggest increase in fluvial input just before the deposition of organic-rich facies (Bellanca et al., 2002). On the northern Tethyan carbonate platform, the change in nutrient supply results in the shift from a photozoan mode into a mixed heterozoan-demise mode (Föllmi et al., 2006; Föllmi and Gainon, 2008). The higher nutrient levels may have led to a general increase in primary productivity. The increase in surface production is monitored by the increase in $\delta^{13}C$ values and results in the installation of widespread dys- to anaerobic conditions in the western Tethys (RSTE enrichments and higher C/P ratios). The decrease and the partly low P values observed during the first part of OAE 1a interval may then be related to the higher

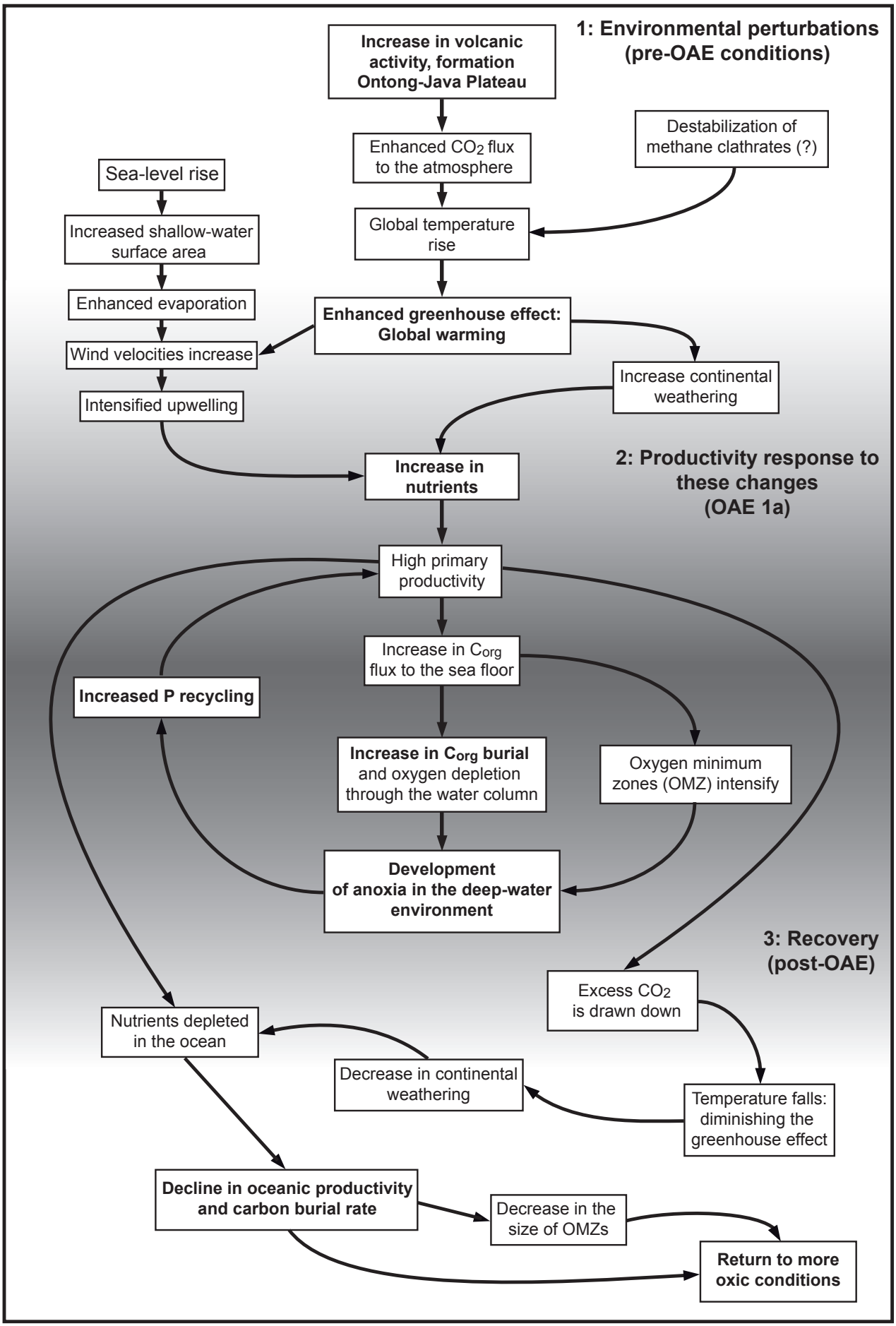

Fig. D.10: Conceptual model to explain the installation of widespread anoxia during the Early Aptian positive C-isotope shift. See text for explanation.

recycling rate of P from the sediment to the water column and would have act as a positive feedback loop on surface productivity. The return to higher P values near the end of the OAE 1a may be related to more efficient authigenic P capture induced by the presence of microbial mats, followed by a return to more oxygenated conditions.

D.6 Depositional and paleoenvironmental conditions

In taking into account the observed link between change in nutrient supply, OM productivity and accumulation and change in redox conditions accompanying the early Aptian OAE 1a, we propose the following model (Fig. D.10):

(1) The negative $\delta^{13}C$ excursion marking the onset of OAE 1a corresponds to a large variation in the carbon isotope ratio of carbonate and organic carbon. As explained above, these negative values have been linked to episodes of increased volcanic activity on the OJP (Larson and Erba, 1999; Méhay et al., 2009; Tejada et al., 2009; Misumi et al., in press), from the dissociation of CH_4 clathrate hydrates or from thermal metamorphism of C_{org}-rich sediments (Jahren et al., 2001; van Breugel et al., 2007; Ando et al., 2008). All processes invoked to explain these low $\delta^{13}C$ values imply an abrupt release of greenhouse gases. The Early Aptian corresponds to a "hot spike", showing an increase in pCO_2 based on *Ginkgo* stomatal index (Retallack, 2009). This led to a major rise in global temperature, which is also indicated by a decreasing trend in the $\delta^{18}O$ records in the Late Barremian to Early Aptian (Menegatti et al., 1998; Weissert and Erba, 2004). The intensified greenhouse conditions may have accelerated the hydrological cycle resulting in increased continental weathering and hence in altered nutrient and sediment fluxes from the continents to the ocean (Weissert, 1990; Föllmi, 1995). These climate modifications may have promoted intensified nutrient recycling form the deep and intermediate water column in upwelling zones. This is shown by the global increase in P accumulation rate observed at the onset of the OAE 1a interval (Föllmi, 1995).

(2) The increased nutrient supply induced higher primary surface productivity rates and a depletion of light carbon in the marine reservoir as indicated by the increase in the $\delta^{13}C$ record. Enhanced productivity was sufficiently sustained to cause the gradual consumption of bottom-water oxygen via eutrophisation processes and the ineffective breakdown of organic matter. This intensified the oxygen-minimum zone and marked the beginning of the OAE 1a. With the decrease in oxygen concentrations through the water column, P recycling became more efficient and acted as a positive feedback loop on oceanic productivity. As outlined in the model of Robinson et al. (2004), black-shale accumulation can be seen as the last step an ocean will go though when reacting to a perturbation of its "steady state". A critical threshold is passed when the production of C_{org} exceeds the rate in which it is oxidized. This seems to be the case for the early Aptian anoxic event, as indicated by the shift observed between increasing $\delta^{13}C$ values and OM accumulation. The consumption of bottom water oxygen by OM oxidation led to the development of reducing conditions. However, our data indicate that oxygen depletion is a function of the paleogeography and was less severe in shallower water. On the other hand, in basinal settings, we observe well-developed anoxic conditions (higher TOC contents, enrichment in RSTE, high C/P ratios values) characterized by at least two anoxic-to-euxinic phases separated by a return to less oxygen-depleted conditions. Similar observations based on changes in green sulphur bacteria biomarkers indicate episodic photic-zone euxinia during deposition of the Livello Selli (Pancost et al., 2004). These rapid changes in redox conditions are difficult to explain when using a preservation-driven model with stronger ocean stratification and may rather be related to a fluctuating oxygen-minimum zone.

(3) The end of OAE 1a is characterized by a return to more oxic conditions. Sustained productivity may have led to a drawdown of excess CO_2 and triggered the termination of the climate perturbation. This is shown by the increasing trend in $\delta^{18}O$ (Menegatti et al., 1998; Weissert and Erba, 2004) and changes in palynological assemblages (Hochuli et al., 1999). The decrease in CO_2 would have lead to cooler temperatures and less intense biochemical weathering processes on the continents.

D.7 Conclusions

In this study, we explore paleoceanographic change during the Early Aptian carbon-isotope excursion and the mechanisms leading to this major perturbation in the carbon cycle along a basin/shelf transect in the western Tethys. We present new geochemical and OM data from three selected sections (Gorgo a Cerbara in Central Italy, Glaise in eastern France, and Cassis/La Bédoule, in southern France).

Our results show that the expression of the OAE 1a is different in the different paleogeographic settings studied here. The onset of OAE 1a is marked by an increase in P contents, followed by low values during the positive $\delta^{13}C$ shift. The good correlation with the global P accumulation curve indicate that these change are global in nature and related to a general increase in nutrient supply at the onset of OAE 1a. This change in nutrient levels may have been related to global climate change triggered by perturbations in the carbon cycle. RSTE distributions indicate anoxic to euxinic conditions in the deeper-water environments and dysoxic to oxic conditions in the shallower water areas. In the Gorgo a Cerbara section, two phases of RSTE enrichment and higher C/P ratios were recorded in the Livello Selli showing at least two phases of anoxic conditions with intermittent return to more oxygenated conditions. These rapid changes in redox conditions may be related to a fluctuating OMZ and suggest that oceanic productivity has played a key role in bottom-water oxygen depletion during OAE 1a.

Acknowledgments

We would like to thank Jean-Pierre Masse for having guided us through the Cassis/La Bédoule composite section, Stéphane Bodin and Alexis Godet for their help in the field, Tiffany Monnier for laboratory assistance and André Villard for the preparation of thin sections. We also thank Haydon Mort for advise on the phosphorus analysis and for his general comments and suggestions. This research is supported by the Swiss National Science Foundation (Grants 200021-109514/1, 200020-121600 and 200020-113640).

References

Algeo, T. J., Lyons, T., 2006. Mo–total organic carbon covariation in modern anoxic marine environments: Implications for analysis of paleoredox and paleohydrographic conditions. Paleoceanography 21(PA1016).

Algeo, T. J., Maynard, J. B., 2004. Trace-element behavior and redox facies in core shales of Upper Pennsylvanian Kansas-type cyclothems. Chemical Geology 206, 289-318.

Anderson, D. L., Delaney, M. L., 2000. Sequential extraction and analysis of phosphorus in marine sediments: streamliming of the SEDEX procedure, Limnology and Oceanography 45, 509-515.

Ando, A., Kaiho, K., Kawahata, H., Kakegawa, T., 2008. Timing and magnitude of early Aptian extreme warming: unravelling primary $\delta^{18}O$ variation in indurated pelagic carbonates at Deep Sea Drilling Project Site 463, central Pacific Ocean. Palaeogeography, Palaeoclimatology, Palaeoecology 260, 463–476.

Arthur, M.A., Jenkyns, H.C., Brumsack, H.-J., Schlanger, S. O., 1990. Stratgraphy, geochemistry, and paleoceanography of organic-carbon rich Cretaceous sequences, *in* R. N. Ginsburg and B. Beaudoin: Cretaceous Research, Events and Rhythms, Kluwer Acad., Norwell, 75-119.

Baudin, F., Fiet, N., Coccioni, R., Galeotti, S., 1998. Organic matter characterisation of the Selli Level (Umbria-Marche Basin, central Italy). Cretaceous Research 19, 701-714.

Bellanca, A., Erba, E., Neri, R., Premoli Silva, I., Sprovieri, M., Tremolada, F., Verga, D., 2002. Palaeoceanographic significance of the Tethyan 'Livello Selli' (Early Aptian) from the Hybla Formation, northwestern Sicily: biostratigraphy and high-resolution chemostratigraphic records. Palaeogeography, Palaeoclimatology, Palaeoecology 185, 175-196.

Bodin, S., Godet, A., Föllmi, K. B., Vermeulen, J., Arnaud, H., Strasser, A., Fiet, N., Adatte, T., 2006. The late Hauterivian Faraoni oceanic anoxic event in the western Tethys: Evidence from phosphorus burial rates. Palaeogeography, Palaeoclimatology, Palaeoecology 235, 245-264.

Bodin, S., Godet, A., Matera, V., Steinmann, P.,

Vermeulen, J., Gardin, S., Adatte, T., Coccioni, R., Föllmi, K. B., 2006. Enrichment of redox-sensitive trace metals (U, V, Mo, As) associated with the late Hauterivian Faraoni oceanic anoxic event. International Journal of Earth Sciences 96, 327-341.

Böning, P., Brumsack, H.-J., Böttcher, M. E., Schetger, B., Kriete, C., Kallmeyer, J. Borchers, S. L., 2004. Geochemistry of Peruvian near-surface sediments. Geochimica et Cosmochimica Acta 68, 4429-4451.

Bralower, T.J., Thierstein, H.R., 1984. Low productivity and slow deep-water circulation in mid-Cretaceous oceans. Geology 12, 614-618.

Bréhéret, J.-G., 1997. L'Aptien et l'Albien de la Fosse vocontienne (des bordures au bassin). Evolution de la sédimentation et enseignements sur les événements anoxiques. Société géologique du Nord, 614 p.

Brumsack, H.J., 1989. Geochemistry of recent TOC-rich sediments from the Gulf of California and the Black Sea. Geologische Rundschau 78, 851–882.

Calvert, S. E., Pedersen, T. F., 1993. Geochemistry of recent oxic and anoxic marine sediments: Implications for the geological record. Marine Geology 113, 67-88.

Cecca, F., Faraoni, P., Marini, A., Pallini, G., 1995. Fieldtrip across the representative sections for the Upper Hauterivian-Barremian ammonite biostragraphy in the Maiolica exposed at Monte Nerone, Monte Petrano and Monte Catria (Umbira-Marche Apennines). Memorie Descriptive delia Carta Geologica d'Italia 51, 187-211.

Coccioni, R., Erba, E., Premoli-Silva, I., 1992. Barremian-Aptian calcareous plankton biostratigraphy from the Gorgo a Cerbara section (Marche, central Italy) and implications for plankton evolution. Cretaceous Research 13, 517-537.

Colman, A.S., Holland, H.D., 2000. The global diagenetic flux of phosphorus from marine sediments to the oceans; redox sensitivity and the control of atmospheric oxygen levels. *In*: Glenn, C.R., Prévôt-Lucas, L., Lucas, J. (*Eds*.), Marine Authigenesis; From Global to Microbial, SEPM Special Publication, vol. 66, 53–75.

Compton, J., Mallinson, D., Glenn, C.R., Filippelli, G., Föllmi, K., Shields, G., Zanin, Y., 2000. Variations in the global phosphorus cycle. *In*: Glenn, C.R., Prevot-Lucas, L., Lucas, J. (*Eds*), Marine Authigenesis; From Global to Microbial. Special Publication Society for Sedimentary Geology 66, 21-33.

Crusius, J., Calvert, S. E., Pedersen, T. F., Sage, D., 1996. Rhenium and molybdenum enrichments in sediments as indicators of oxic, suboxic and sulfidic conditions of deposition Earth and Planetary Science Letters 145, 65-78.

Danelian, T., Tsikos, H., Gardin, S., Baudin, F., Bellier, J. P., Emmanual, L., 2004. Global and regional palaeoceanographic changes as recorded in the mid-Cretaceous (Aptian-Albian) sequence of the Ionian zone (NW Greece), Journal of Geological Society of London 161, 703-709.

De Gea, G. A., Castro, J. M., Aguado, R., Ruiz-Ortiz, P. A., Company, M., 2003. Lower Aptian carbon isotope stratigraphy from a distal carbonate shelf setting: the Cau section, Prebetic zone, SE spain. Palaeogeography, Palaeoclimatology, Palaeoecology 200, 207-219.

Delaney, M.L., 1998. Phosphorus accumulation in marine sediments and the oceanic phosphorus cycle. Global Geochemical Cycles 12, 563-572.

Dumitrescu, M., Brassel, S.C., 2006. Compositional and isotopic characteristics of organic matter for the early Aptian Oceanic Anoxic Event at Shatsky Rise, ODP Leg 198. Palaeogeography, Palaeoclimatology, Palaeoecology 235, 168-191.

Eaton, A.D., Clesceri, L.S., Greenberg, A.E., 1995. Standard Methods for the Examination of Water and Waste Water, 19th ed., American Public Health Association, Washington, DC.

Emeis, K.-C., Stuck, U., Leipe, T., Pollehne, F., Kunzendorf, H., Christiansen, C., 2000. Changes in the C, N, P burial rates in some Baltic Sea sediments over the last 150 years: relevance to P regeneration rates and the phosphorus cycle. Marine Geology 167, 43-59.

Erba, E., 1994. Nannofossils and superplumes: the early Aptian "Nannoconid crisis". Paleoceanography 9, 483-501.

Erba, E., 2004. Calcareous nannofossils and Mesozoic oceanic anoxic events. Marine micropaleontology 52, 85-106.

E. Erba, The Aptian Stage (with contributions by Aguado, R., Avram, E., Baraboschkin, E.J.,

Bergen, J.A., Bralower, T.J., Cecca, F., Channel, J.E.T., Coccioni, R., Company, M., Delanoy, G., Erbacher, J., Herbert, T.D., Hoedemaeker, P., Kakabadze, M., Leereveld, H., Lini, A., Mikahailova, I.A., Mutterlose, J., Ogg, J.G., Premoli Silva, I., Rawson, P.F., Von Salis, K., Weissert, H.), Bulletin de l'Institut Royal des Sciences Naturelles de Belgique, Sciences de la Terre (66-Supp.), 31-43.

Espitalié, J., Deroo, G., Marquis, F., 1985. La pyrolyse Rock-Eval et ses applications. Revue de l'Institut Français du Pérole 40, 563-579.

Filippelli, G.M., 2008. The global phosphorus cycle: Past, present, and futur. Elements, 4, 89-95.

Filippelli, G.M. and Delaney, M.L., 1996. Phosphorus geochemistry of equatorial Pacific sediments. Geochimica et Cosmochimica Acta 60, 1479-1495.

Föllmi, K. B., 1995. 160 m.y. record of marine sedimentary phosphorus burial: Coupling of climate and continental weathering under greenhouse and icehouse conditions. Geology 23, 859-862.

Föllmi, K.B., 1996. The phosphorus cycle, phosphogenesis and marine phosphate-rich deposits. Earth Science Review 40, 55-124.

Föllmi, K. B., Badertscher, C., de Kaenel, E., Stille, P., John, C. M., Adatte, T., Steinmann, P., 2005. Phosphogenesis and organic-carbon preservation in the Miocene Monterey Formation at Naples Beach, California. The Monterey hypothesis revisited. Bulletin of the Geological Society of America 117, 589-619.

Föllmi, K.B., Godet, A., Bodin, S., Linder, P., 2006. Interactions between environmental change and shallow-water carbonate build-up along the northern Tethyan margin and their impact on the early Cretaceous carbon-isotope record. Paleoceanography 21, doi:10.1029/2006PA001313.

Föllmi, K.B., Gainon, F., 2008. Demise of the northern Tethyan Urgonian carbonate platform and subsequent transition towards pelagic conditions: The sedimentary record of the Col de la Plaine Morte area, central Switzerland. Sedimentary geology 205, 142-159.

Froelich, P.N., Bender, M. L., Luedtke, N. A., Heath, G. R., DeVries, T., 1982. The marine phosphorus cycle. American Journal of Science 282, 474-511.

Gorin, G., Fiet, N., Pacton, M., 2009. Benthic microbia mats: a possible major component of organic matter accumulation in the lower Aptian oceanic anoxic event. Terra Nova 21, 21-27.

Hasegawa, T., 2003. Cretaceous terrestrial paleoenvironments of northeastern Asia suugested from carbon isotope stratigraphy: Increased atmospheric pCO_2-induced climate. Journal of Asian Earth Sciences 21, 849-859.

Hay, W. W., Wold, C. N., 1997. The effect of changes of the mean salinity on ocean circulation, Mineralia Slovaca 29, 243-244.

Heimhofer, U., Hochuli, P. A., Herrle, J. O., Andersen, N., Weissert, H., 2004. Absence of major vegetation and palaeoatmospheric pCO_2 changes associated with oceanic anoxic event 1a (Early Aptian, SE France). Earth and Planetary Science Letters 223, 303-318.

Herrle, J. O., Kössler, P., Friedrich, O., Erlenkeuser, H., Hembelen, C., 2004. High-resolution carbon isotope records of the Aptian to Lower Albian from SE France and the Mazagan Plateau (DSDP Site 545): a stratigraphic tool for paleoceanographic and paleobiologic reconstruction. Earth and Planetary Science Letters 218, 148-161.

Hochuli, P. A., Menegatti, A. P., Weissert, H., Riva, A., Erba, E., Premoli-Silva, I., 1999. Episodes of high productivity and cooling in the early Aptian Alpine Tethys. Geology 27, 657-660.

Ingall, E. D., Bustin, R. M., Van Cappellen, P., 1993. Influence of water column anoxia on the burial and preservation of carbon and phosphorus in marine shales. Geochimica et Cosmochimica Acta 57, 303-316.

Ingall, E. D., Jahnke, R., 1994. Evidence for enhanced phosphorus regeneration from marine sediments overlain by oxygen depleted waters. Geochimica et Cosmochimica Acta 58, 2571-2575.

Ingall, E. D., Jahnke, R., 1997. Influence of water-column anoxia on the elemental fractionation of carbon and phosphorus during sediment diagenesis. Marine Geology 139, 219-229.

Jahren, A.H., Arens, N.C., Sarmiento, G., Guerrero, J., Amundson, R., 2001. Terrestrial record of methane hydrate dissociation in the early Cretaceous. Geology 29, 159–162.

Jenkyns, H. C., 2003. Evidence for rapid climate change in the Mesozoic-Palaeogene greenhouse world.

Philosphical Transaction of the Royal Society of London. A 361, 1885-1916.

Jenkyns, H. C., Wilson, P. A., 1999. Stratigraphy, paleoceanography, and evolution of Cretaceous pacific guyots: Relics from a greenhouse earth. American Journal of Science 299, 341-392.

Jones, B., Manning, A. C., 1994. Comparison of geochemical indices used for the interpretation of palaeoredox conditions in ancient mudstones. Chemical Geology 111, 111-129.

Kuhnt, W., Moullade, M., Masse, J. P., H. Erlenkeuser, H., 1998. Carbon isotope stratigraphy of the lower Aptian historical stratotype at Cassis-La Bédoule (S.E. France), Geologie Mediterranéenne 25, 63-79.

Larson, R. L., 1991. Geological consequences of superplumes. Geology 19, 963-966.

Larson, R. L., Erba, E., 1999. Onset of the mid-Cretaceous in the Barremian-Aptian igneous event and the biological sedimentary, and geochemical response. Paleoceanography 14, 663-678.

Leckie, R. M., Bralower, T. J., Cashman, R., 2002. Oceanic anoxic events and plankton evolution: Biotic response to tectonic forcing during the mid-Cretaceous. Paleoceanography 17, 1-29.

Luciani, V., Cobianchi, M., Jenkyns, H. C., 2001. Biotic and geochemical response to anoxic evetns : the Aptian pelagic succession of the Gargano Promontory (southern Italy). Geological Magazine 138, 277-298.

Mehay, S., Keller, C.E., Bernasconi, S.M., Weissert, H., Erba, E., Bottini, C., Hochuli, P.A., 2009. A volcanic CO_2 pulse triggered the Cretaceous oceanic anoxiv event 1a and a biocalcification crisis. Geology 37, 819-822.

Menegatti, A. P., Weissert, H., Brown, R. S., Tyson, R. V., Farrimond, P., Strasser, A., Caron, M., 1998. High-resolution $\delta^{13}C$ stratigraphy through the early Aptian "Livello Selli" of the Alpine Tethys. Paleoceanography 13, 530-545.

Misumi, K., Yamanaka, Y., Tajika, E. Numerical simulation of atmospheric and oceanic biogeochemical cycles to an episodic CO_2 release event: Implications for the cause of mid-Cretaceous Ocean Anoxic Event-1a. Earth and Planetary Science Letters, *in press*.

Morford, J. L., Emerson, S. R., 1999. The geochemistry of redox sensitive trace metal in sediments. Geochimica et Cosmochimica Acta 63, 1735-1750.

Morford, J. L., Ruffell, A. D., Emerson, S. R., 2001. Trace metal evidence for changes in the redox environment associated with the transition from terrigenous clay to diatomaceous sediment, Saanich Inlet, BC. Marine Geology 174, 355-369.

Mort, M., Adatte, T., Föllmi, K. B., Keller, G., Steinmann, P., Matera, V., Berner, Z., Stüben, D., 2007. Phosphorus and the roles of productivity and nutrient recycling during oceanic event 2. Geology 35, 483-486.

Moullade, M., Masse, J.-P., Tronchetti, G., Kuhnt, W., Ropolo, P., Bergen, J. A., Masure, E., Renard, M., 1998. Le stratotype historique de l'Aptien inférieur (région de Cassis-La Bédoule, SE France) : synthèse stratigraphique. Géologie Méditerranéenne 25, 289-298.

Pancost, R. D., Crawford, N., Magness, S., Turner, A., Jenkyns, H. C., Maxwell, J. R., 2004. Further evidence for the development of photic-zone euxinic conditions during Mesozoic oceanic anoxic events. Journal of the geological Society of London 161, 353-364.

Piper, D.Z., Perkins, R.B., 2004. A modern vs. Permian black shale - the hydrography, primary productivity, and water-column chemistry of deposition. Chemical Geology 206, 177–197.

Redfield, A. C., 1958. The biological control of chemical factors in the environment. American Scientist 46, 205 – 222.

Retallack, G. J., 2009. Greenhouse crises of the past 300 millions years. GSA Bulletin 121, 1441-1455.

Riquier, L., Tribovillard, N., Averbuch, O., Devleeschouwer, X., Riboulleau, A., 2006. The late Frasnian Kellwasser horizons of the Harz Mountains (Germany): Two oxygen-deficient periods resulting from different mechanisms. Chemical Geology 233, 137-155.

Robinson, S. A., Williams, T., Bown, P. R., 2004. Fluctuations in biosiliceous production and the generation of Early Cretaceous oceanic anoxic events in the Pacific Ocean (Shatsky Rise, Ocean Drilling Program Leg 198). Paleoceanography 19 (PA4024, doi:10.1029/2004PA001010).

Rullkötter, R., 2000. Organic matter: The driving force for early diagenesis. *In*: Schulz, H. D. and Zabel, M. (Eds), Marine Geochemistry. Springer, 129-

172.

Ruttenberg, K.C., 1992, Development of a sequential extraction method for different forms of phosphorus in marine sediments: Limnology and Oceanography, 37, 1460-1482.

Ruttenberg, K.C., Berner, R.A., 1993. Authigenic apatite formation and burial in sediments from non-upwelling, continental margin environments. Geochimica et Cosmochimica Acta 57, 991-1007.

Schlanger, S. O. and Jenkyns, H. C., 1976. Cretacous oceanic anoxic event: causes and consequences. Geolgie en Mijnbouw 55, 179-188.

Scholle, P. A. and Arthur, M. A., 1980. Carbon isotope fluctuations in Cretaceous pelagic limestone: potential stratigraphic and petroleum exploration tool. American Association of Petroleum Geology Bulletin 64, 67-87.

Slomp, C. P., Thomson, J., De Lange, G. J., 2004. Controls on phosphorus regeneration and burial during formation of eastern Mediterranean sapropels. Marine Geology 203, 141-159.

Tamburini, F., Huon, S., Steinmann, P., Grousset, F.E., Adatte, T., Föllmi, K.B., 2002. Dysaerobic conditions during Heinrich events 4 and 5: evidence from phosphorus distribution in a North Atlantic deep-sea core. Geochimica et Cosmochimica Acta 66, 4069– 4083.

Tejada, M.L.G., Suzuki, K., Kuroda, J., Coccioni, R., Mahoney, J.J., Ohkouchi, N., Sakamoto, T., Tatsumi, Y. 2009. Ontong Java plateau eruption as a trigger for the early Aptian oceanic anoxic event. Geology 37, 855-858.

Tribovillard, N., Algeo, T. J., Lyons, T. W., Riboulleau, A., 2006. Trace metals as paleoredox and paleoproductivity proxies : An update. Chemical Geology 232, 12-32.

Tyson, R. V., 1995. Sedimentary organic matter. Chapman and Hall ed., London, 615 pp.

Van Breugel, Y., Schouten, S., Tsikos, H., Erba, E., Price, G. D., Sinninghe Damsté, J. S., 2007. Synchronous negative carbon isotpe shifts in marine and terrestrial biomarkers at the onset of the early Aptian oceanic anoxic event 1a: Evidence for the release of 13C-depleted carbon into the atmosphere. Paleoceanography 22 (PA2010, doi:10.1029/2006PA001341), 1-13.

Van Cappellen, P., Ingall, E. D., 1996. Redox stabilization of the atmosphere and oceans by phosphorus-limited marine productivity. Science 271, 493-496.

Weissert, H., 1990. Siliciclastics in the early cretaceous tethys and North Atlantic oceans: Documents of periodic greenhouse climate conditions. Memorie Società Geologica Italiana 44, 59-69.

Weissert, H., Erba, E., 2004. Volcanism, CO_2 and palaeoclimate: a Late Jurassic-Early Cretaceous carbon and oxygen isotope record. Journal of the geological Society of London 161, 695-702.

Weissert, H., Lini, A., Föllmi, K., Kuhn, O., 1998. Correlation of early Cretaceous carbon isotope stratigraphy and platform drowning event: a possible link? Palaeogeography, Palaeoclimatology, Palaeoecology 137, 189-203.

Wignall, P. B., 1994. Black Shales. Oxford Monographs on Geology and Geophysics 30, 1-127.

Wissler, L., Funk, H., Weissert, H., 2003. Response of Early Cretaceous carbonate platforms to changes in atmospheric carbon dioxide levels. Palaeogeography, Palaeoclimatology, Palaeoecology 200, 187-205.

CHAPTER E:
The end-Cenomanian Oceanic Anoxic Event (OAE 2) in the Helvetic Alps

The Chrummflueschlucht section, Switzerland

In the northern Tethyan margin (helvetic zone), sediments coeval with OAE 2 are rather exceptional in that organic carbon-rich layers have not been observed. This goal of study was to verify if changes in nutrient level and oxic conditions can be geochemically traced. An expanded section through the OAE-2 time interval at Chrummflueschlucht (E of Euthal, Canton of Schwyz) has been selected and was investigated.

-E-

The Expression of the End-Cenomanian Oceanic Anoxic Event (OAE 2) in the Helvetic Alps

Stéphane Westermann[1], Nicolas Fiet[3,4], Dominik Fleitmann[5], Virginie Matera[2], Thierry Adatte[1], and Karl B. Föllmi[1]

[1]Institute of geology and paleontology, University of Lausanne, Anthropôle, 1015 Lausanne, Switzerland.
[2]Institute of geology, University of Neuchâtel, Emile Argand 11, CP 158, 2009 Neuchâtel, Switzerland.
[3]UMR 8148 – I.D.E.S., Bât. 504, University of Paris XI Orsay, 91405 Orsay Cedex, France.
[4]AREVA, 33 rue La Fayette, 75009 Paris, France.
[5]Institute of Geological Sciences, University of Bern, Baltzerstrasse 1-3, 3012 Bern, Switzerland.

Accepted for publication with major revisions in Cretaceous Research.

Abstract

Upper Cenomanian hemipelagic sediments from the northern Alpine Helvetic fold-and-thrust belt (northern Tethyan margin) coeval with Oceanic Anoxic Event (OAE) 2 are characterized by the temporal persistence of micrite sedimentation and lack of organic carbon-rich layers. We studied an expanded section in the Chrummflueschlucht (E of Euthal, Ct Schwyz), which envelops the OAE 2 time interval, and investigated its biostratigraphy (planktonic foraminifera), bulk rock stable carbon- and oxygen-isotope, total phosphorus (P) and redox-sensitive trace-element (RSTE) contents. Our goal is to identify the paleoceanographic and paleoenvironmental conditions during OAE 2 in this part of the northern Tethyan margin, and more specifically to trace eventual changes in nutrient levels and oxic conditions.

Using thin sections, we were able to determine - with some remaining uncertainties - the different planktonic foraminiferal biozones characteristic of the Cenomanian-Turonian boundary interval (*Rotalipora cushmani*, *Whiteinella archeocretacea* and *Helvetoglobotruncana helvetica* zones). In the lower part of the section (*R. cushmani* zone), the whole-rock $\delta^{13}C$ record shows a long-term increase. Within sediments attributed to the *W. archeocretacea* zone, the values reach a maximum of 3.30‰. Consequently the values decrease and increase again to arrive at a plateau with high $\delta^{13}C$ values of around 3.10‰. At the top of the section, in sediments belonging to the *H. helvetica* zone, the $\delta^{13}C$ record decreases to post-OAE values (approximately 2.25‰). The extinction of *R. cushmani* is observed just above the positive $\delta^{13}C$ shift characterizing OAE 2.

The average contents of RSTE (U, V, As, Co, Mo and Mn) remain low throughout the section and appreciable RSTE enrichments have not been observed for the sedimentary interval corresponding to OAE 2. No correlation is noted with stratigraphic trends in RSTE contents in organic-rich deeper-water sections is observed. P contents display small variations along the section with a long-term decreasing trend towards the top. Superimposed on this trend, P values reach a maximum in sediments at the onset of the $\delta^{13}C$ positive excursion within the *R. cushmani* zone. This is coeval with the onset of the anoxic event. In the interval corresponding to OAE 2, P values remain low and show a small increase at the end of the positive shift in the $\delta^{13}C$ record (in the *H. helvetica* zone).

Our results show that the Chrummflueschlucht section corresponds to one of the most complete sections for the Cenomanian-Turonian boundary interval known from the Helvetic realm even if a small hiatus may be present between $\delta^{13}C$ peaks 1 and 2. The evolution of P contents suggests an increase in input of this nutritive element at the onset of OAE2. However, the trends in RSTE contents show that the Helvetic realm has not been affected by strongly depleted oxygen conditions during OAE 2, despite its hemipelagic position.

Keywords: OAE 2; Cenomanian-Turonian boundary; Palaeoceanography; Redox-sensitive trace elements; Phosphorus; Helvetic Realm; Alps; Switzerland.

E.1 Introduction

According to the original definition by Schlanger and Jenkyns (1976), oceanic anoxic events (OAEs) represent exceptional episodes in Earth's history, which are marked by widespread dysoxic to anoxic conditions in the world oceans. These events results in the extensive deposition of organic-rich sediments and changes in the dynamics of the global carbon cycle leading, for instance, to changes in the relative importance of inorganic and organic-carbon reservoirs. The driving mechanisms behind OAEs are still under debate. In the case of the formation of Cretaceous black shales, different models have been proposed including - either alone or in combination – large-scale increases in primary productivity, world-wide expansion of oxygen-minimum zones and the intensification of water-column stratification (Schlanger and Jenkyns, 1976; Bralower and Thierstein, 1984; Pederson and Calvert, 1990; Jenkyns, 2003; Pancost et al., 2004). Recently, the stratigraphic distribution of redox-sensitive trace-elements (RSTE) such as U, V, As, Mo and Co has been explored in OAE-related sediments throughout the Mesozoic, in order to trace the temporal and spatial evolution in oxygen contents (Algeo and Maynard, 2004; Bodin et al., 2006; Brumsack, 2006; Algeo and Maynard, 2008). In addition, the evolution in phosphorus (P) contents and accumulation rates has been employed to trace both changes in the marine P cycle and their impact on primary productivity rates, as well as the influence of anoxic bottom-water conditions on the capacity of the sedimentary reservoir to retain P (Ingall and Van Cappellen, 1990; Van Cappellen and Ingall, 1994; Mort et al., 2007). These two approaches represent valuable tools in unravelling the paleoceanographic and paleoenvironmental conditions during OAEs (e.g., Turgeon and Brumsack, 2006).

The Late Cenomanian sedimentary record encompasses one of the best-studied OAEs, which is labelled OAE 2 or Bonarelli event (Schlanger and Jenkyns, 1976; Jenkyns, 1980; Schlanger et al., 1987; Jenkyns et al., 1994; Strasser et al., 2001; Leckie et al., 2002; Caron et al., 2006; Mort et al., 2007; Voigt et al., 2007). Major climatic and paleoceanographic changes have been associated this event (Jenkyns et al., 1994; Huber et al., 2002; Norris et al., 2002; Forster et al., 2007). The onset of OAE 2 is characterized by an important positive excursion in the $\delta^{13}C$ carbonate whole-rock record of approximately 2.5‰ (Erbacher et al. 1996,Jarvis et al., 2006; Voigt et al., 2006). OAE 2 is also marked by an extinction event and turnover in planktonic foraminifera, radiolaria and nannofossils assemblages (Keller et al., 2001; Leckie et al., 2002; Erba, 2004), a sea level rise (Haq et al., 1987) and a decrease in the $^{87}Sr/^{86}Sr$ ratio (Jones and Jenkyns, 2001). Recently, Mort et al. (2007) showed that the onset of OAE 2 correlates with a generalized increase in P-accumulation rates, which may have triggered an overall increase in sea surface-water productivity.

The northern Alpine Helvetic thrust-and-fold belt representing the central part of the northern Tethyan margin remains an underexplored area with regards to OAE 2, in spite of the presence of pelagic sediments. This maybe related to the fact that organic-rich sediments and any other obvious change in the lithological and mineralogical composition are lacking in the corresponding formation (Seewen Formation; Bolli, 1944; Föllmi & Ouwehand, 1987; Delamette, 1988). This is in contrast to more distal shelf areas on the northern Tethyan margin, which are presently locked up in Ultrahelvetic units, and from which organic-rich sediments related to OAE 2 have been described (Strasser et al., 2001; Wagreich et al., 2008).

We selected a well-preserved and relatively expanded section in the Chrummflueschlucht (central Switzerland), in order to study paleoenvironmental change during OAE 2 in a hemipelagic environment, which does not appear to have been affected by oxygen-depleted conditions. We carried out a bio- and chemostratigraphic study to obtain an age control on

the section and to evaluate eventual biotic effects and changes in primary productivity. We investigated P and RSTE contents to trace eventual changes in nutrient levels and oxygen contents. Finally, we correlate our results with published data from the sections of Pueblo, Colorado (GSSP for Cenomanian-Turonian boundary, Keller et al., 2004), Wünstorf (Voigt et al., 2008) and Eastbourne, southern England (Paul et al., 1999).

E.2 Geological setting and lithology

The Chrummflueschlucht section is located along a forest road northeast of Einsiedeln (Ct Schwyz, central Switzerland; 8°50'E, 47°05'N; Fig. E.1). The base of the section consists of a sandy and glauconitic limestone, which corresponds to the Kamm Bed – the top lithostratigraphic unit of the Garschella Formation and the latest Albian to middle Cenomanian in age (Fig. E.2; Föllmi & Ouwehand, 1987). The remainder of the section is composed of (hemi-)pelagic carbonate of Cenomanian and Turonian age, which belongs to the Seewen formation. The carbonate is consistently micritic and rich in calcispheres, inoceramid prisms and planktonic foraminifera, which underlines its hemipelagic position. The Seewen carbonate

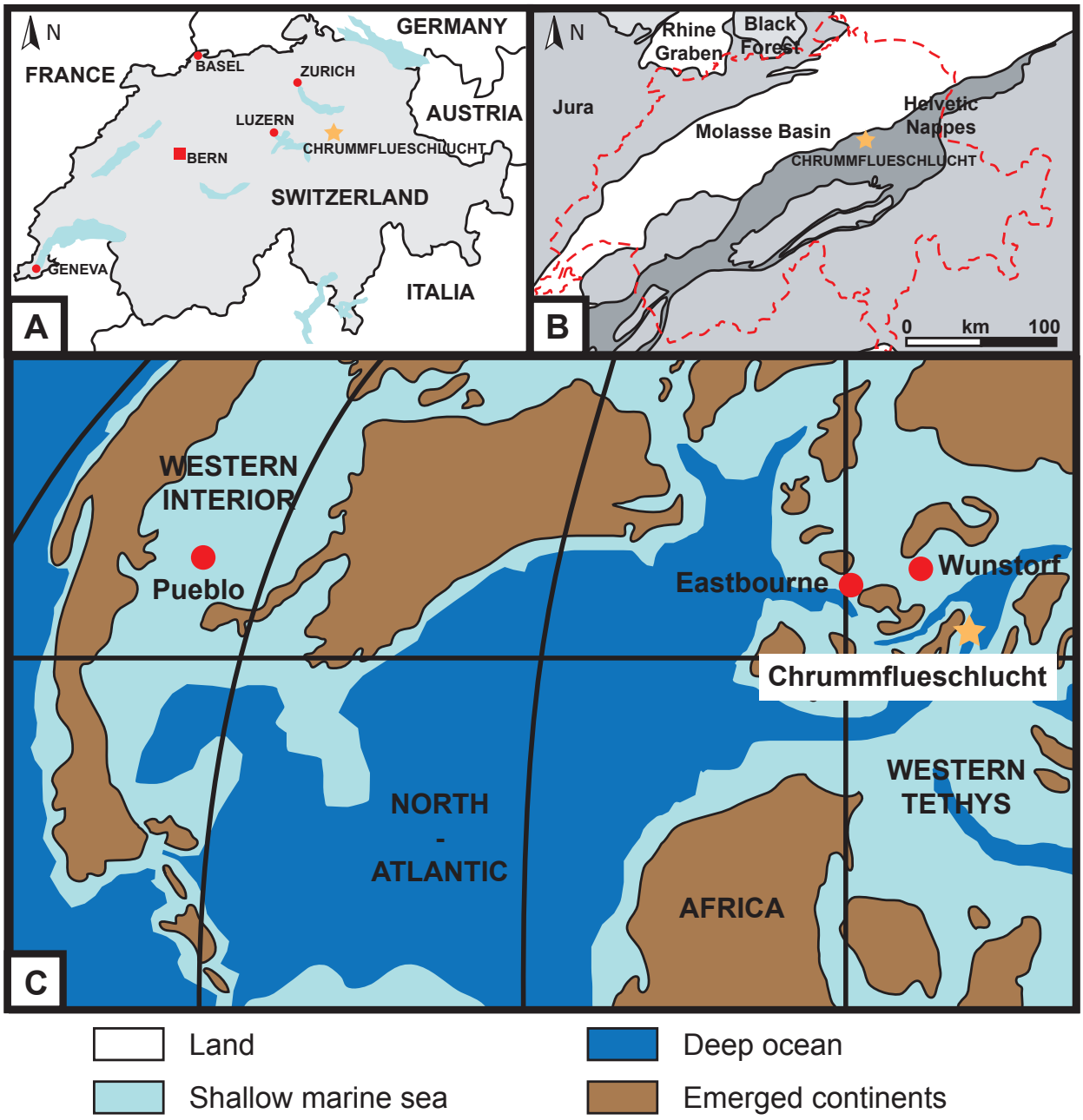

Fig. E.1: A. Localisation of the Chrummflueschlucht section. B. Tectonic map of Switzerland with indication of the Helvetic realm (after Bodin et al., 2006).C. Late Cenomanian (93 Ma) paleogeographic map of the western Tethys (redrawn after Scotese et al., 2001).

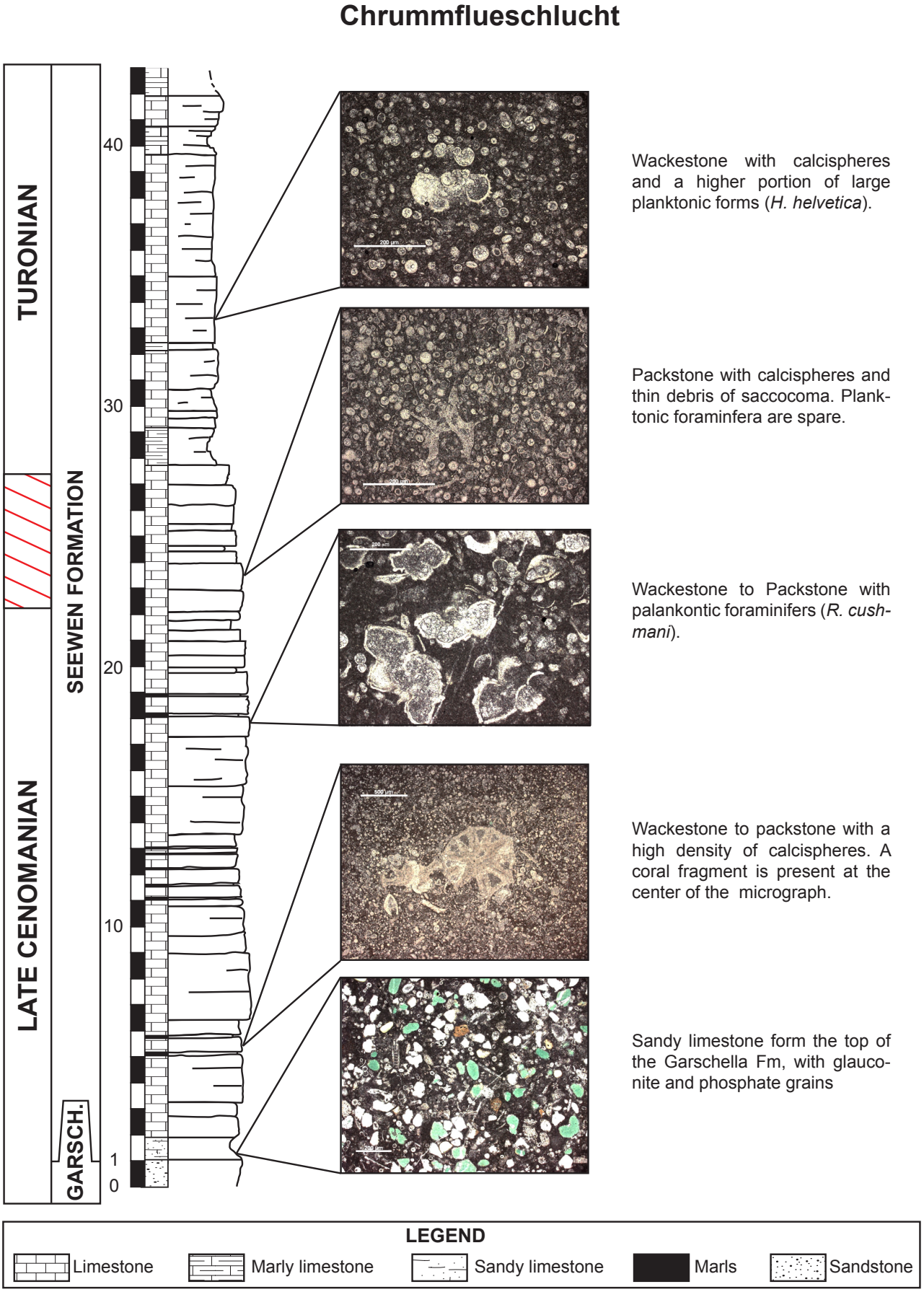

Fig. E.2: Lithological and microfacies of the Chrummflueschlucht section.

succession measured and sampled for this study is lithostratigraphically divided into three parts. The first part is composed of mostly massive limestone beds (2-18m; Fig. E.2), which consist of wackestone rich in planktonic foraminifera and pelagic crinoid remains. The second part of the section (18-30m; Fig. E.2) is characterized by max. 95 cm thick limestone beds, which become marlier towards the top and show a transition from wackestone to packstone with smaller planktonic foraminifera at the base of this part. At the base of this part, we observe the occurrence of radiolaria and bryozoan debris. We also note the presence of *Thalassinoides* at the base of sample Ch 27 (20.2 m; Fig. E.2). The last and uppermost part of the section (30m to the top; Fig. E.2) corresponds to a succession of marly carbonate, consisting of wackestone with large planktonic foraminifera.

E.3 Methods

The biostratigraphy of the Chrummflueschlucht section is based on planktonic foraminifera, which were determined using thin sections of 102 samples in total. For the critical zones, especially for the transition of the *Rotalipora cushmani to Whiteinella archeocretacea* zones, up to six thin-section replicates have been observed per sample.

The analysis of the bulk-rock mineralogy was carried out by X-ray diffraction (Scintag XRD 2000 Diffractometer) based on procedures described by Kübler (1983) and Adatte et al. (1996). This semi-quantitative method is based on non-oriented powder samples with a precision of 5-10% for phyllosilicates and 5% for grain minerals.

Carbon- and oxygen-isotope analyses were performed on powdered bulk-rock samples at the stable-isotope laboratory of the Universities of Orsay (Paris XI, France) and Bern (Switzerland), using VG SIRA 10 triple collector and a Finnigan Detla V Advantage mass spectrometer, respectively. The results were calibrated to the PDB scale with the standard deviation of 0.05 % for $\delta^{13}C$ and of 0.07 % for $\delta^{18}O$.

Total P analysis was performed on bulk-rock samples, following the procedure described in Bodin et al. (2006). The concentration of PO_4, expressed in ppm, is obtained by calibration with known standard solutions, using a UV/Vis photospectrometer (Perking Elmer UV/Vis Photospectrometer Lamba 10, λ = 865nm) with a mean precision of 5%.

The determination of Al, Fe and redox-sensitive trace elements was performed on bulk rock following the procedure described in Bodin et al. (2006). The samples were attacked by suprapur nitric acid and elements contents were determined by a quadrupole ICP-MS (ELAN 6100, Perkin Elmer), using a quantitative mode with a mean precision of 1-2% depending on the element under consideration. The dissolution percentages determined after filtration were about 95% of initial sample weight in the studied section. Moreover, no correlation was observed between the concentration of the different analysed samples and the dissolution percentage obtained during the digestion procedure (Fig. E.3). This shows that the studied elements are present in the soluble biogenic and authigenic phases and are not due to partial leaching of the detrital insoluble fraction.

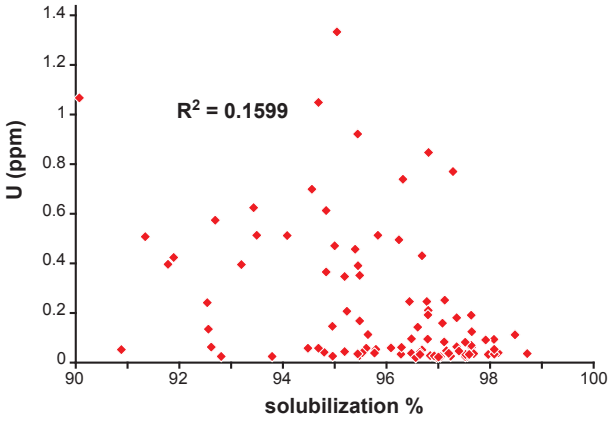

Fig. E.3: U contents in ppm versus the percentage of dissolution of the samples attacked by suprapur nitric acid in the section of Chrummflueschlucht.

E.4 Data

E.4.1 Biostratigraphy

The temporal framework is given by the stratigraphic distribution of planktonic foraminifera. The index species of the Cenomanian-Turonian boundary interval were all observed and three assemblages were distinguished with some remaining uncertainties.

The first assemblage (from the base to the first ~18 meters of the section) is characterised by the presence of *Rotalipora* species, including the Late Cenomanian index species *R. cushmani*. The first occurrence of the index species is situated 7 m above the base of the section and coeval with the last occurrence of *R. reicheli*. The latest Cenomanian species *Whiteinella archeocretacea* appears at 15.9 m, about 1.5m below

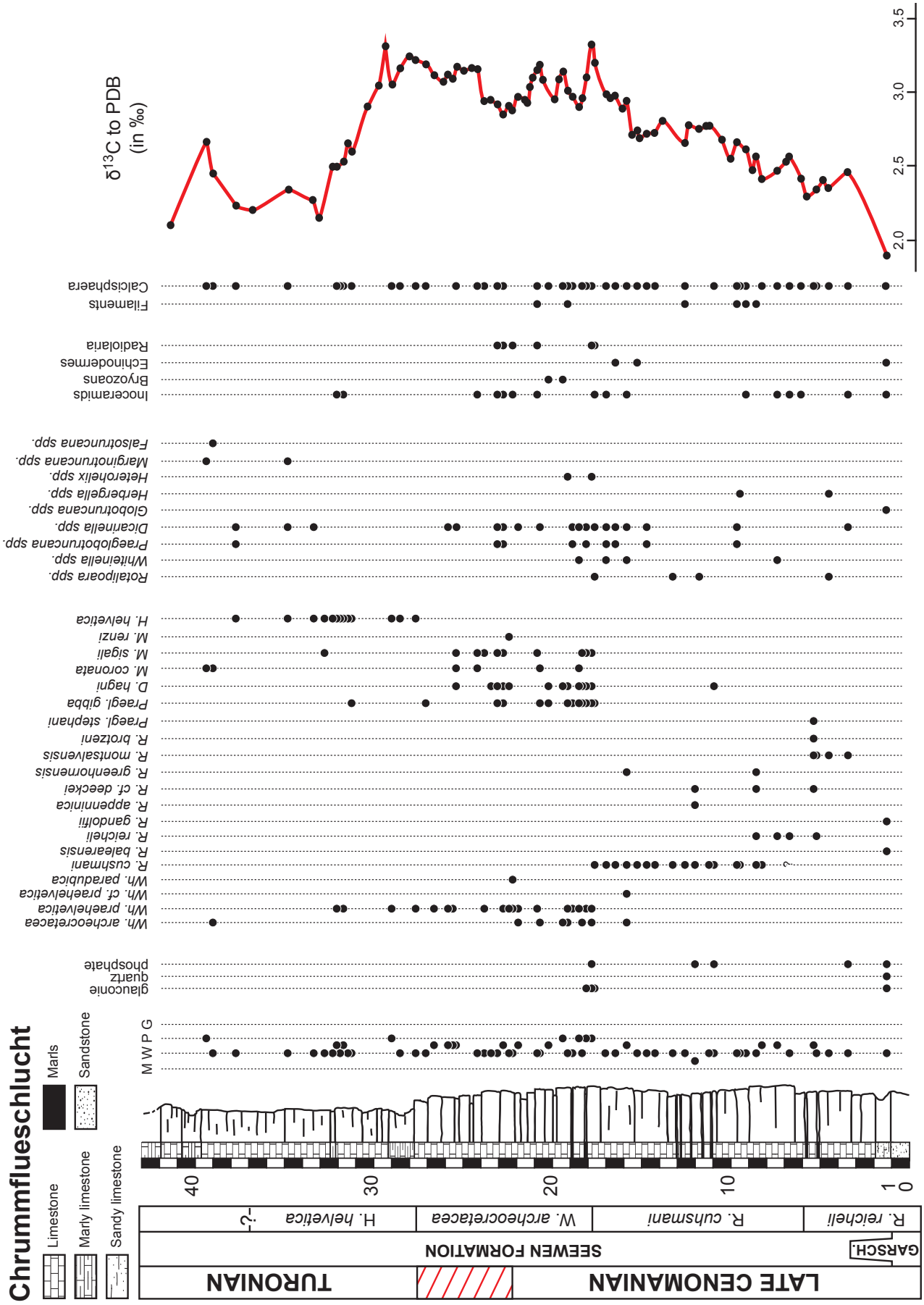

Fig E.4: Stratigraphic occurrences of planktonic and benthic foraminifera, other microfossils and macrofossil fragments. The biozonation is based on the distribution of planktonic foraminifera, the evolution of the $\delta^{13}C$ curve and biostratigraphic and chemostratigraphic correlation with the Pueblo GSSP section.

the last occurrence of *R. cushmani*, near the onset of the $\delta^{13}C$ positive excursion, as is also observed in the section at Pueblo, Colorado, U.S.A. (Keller et al., 2001). In Pueblo, however, the extinction of *R. cushmani* occurred later, compared to the $\delta^{13}C$ record -between peaks 1 and 2 (Keller et al., 2001). This assemblage ends with the disappearance of *R. cushmani* (at 17.9m). The observed assemblage is characteristic of the total-range *R. cushmani* biozone, dated as Late Cenomanian (Fig. E.4).

The second assemblage is marked by the disappearance of keeled planktonic forms (*R. cushmani*). It is characterised by the common presence of bulbous forms like *W. archeocretacea*, *W. praehelvetica* or *W. paradubica* and by *Dicarinella* specimens (*D. hagni*). This part of the section defines the *W. archeocretacea* biozone. The presence of *Praeglobotruncana gibba* (17.9-40m) within this biozone indicates that the Cenomanian-Turonian boundary is situated in this zone. This assemblage also contains low-oxygen tolerant *Heterohelix spp*. Within this zone, we observe the first *Marginotruncanids* (Fig. E.4), which are represented by small forms.

The upper part of the section is marked by the return of keeled forms and by the appearance of the index species *Helvetoglobotruncana helvetica* (at 27.7m). This assemblage corresponds to the *H. helvetica* biozone. At the top of the section, the samples display a dominance of large keeled forms and *Falsotruncana sp*. (Late Turonian, Caron et al., 1981).

E.4.2 Stable carbon- and oxygen-isotope data

Bulk-rock stable-isotope ($\delta^{18}O$ and $\delta^{13}C$) data profiles across the section are presented in Fig. E.5. The reliability of $\delta^{18}O$ and $\delta^{13}C$ data in bulk-rock sediments is largely dependent upon the degree of diagenesis, which primarily affects oxygen-isotope values by lowering the $^{18}O/^{16}O$ ratio in sediments (e.g., Schrag et al., 1995). By cross-plotting all $\delta^{18}O$ and $\delta^{13}C$ values, no significant correlation has been observed for the Chrummflueschlucht section (Fig. E.5, R^2= 0.0572), suggesting that the stable-isotope values are less affected by late diagenetic processes.

The bulk-rock $\delta^{13}C$ curve shows a progressively increasing trend in the first part of the section (from the base to 10m) with values ranging from 2.0 to 2.7‰ (VPDB). In sediments corresponding to the upper part of the *R. cushmani* zone (10-15.5m), $\delta^{13}C$ values are quite stable and fluctuate around 2.7‰. Thereafter, the $\delta^{13}C$ exhibits a first relative maximum of 3.3‰ (16-17m), following the disappearance of *R. cushmani*, within sediments attributed to the *W. archeocretacea* zone. For the rest of the paper, we will consider this peak as the onset of the positive excursion. Consequently the values decrease and increase again to arrive at a plateau (24-30m) with high $\delta^{13}C$ values of around 3.1‰. At the top of the section, in sediments belonging to the *H. helvetica* zone, the $\delta^{13}C$ record decreases to post-OAE values (approximately 2.25‰).

The bulk-rock oxygen-isotope data record a smooth and progressive decline in values from -2.6 to -3.4‰ in the first part of the section (from the base to 12m). In the following part of the section, in sediments close to the transition of the *R. cushmani* and *W. archeocretacea* zones, the $\delta^{18}O$ record shows relative stable values (around approximately -2.7‰) followed by a negative spike (minimum at -3.6‰) in sediments at the base of the *W. archeocretacea* zone (at about 18m). Thereafter, $\delta^{18}O$ values exhibit an increasing trend and remain quite high in the remainder of the section.

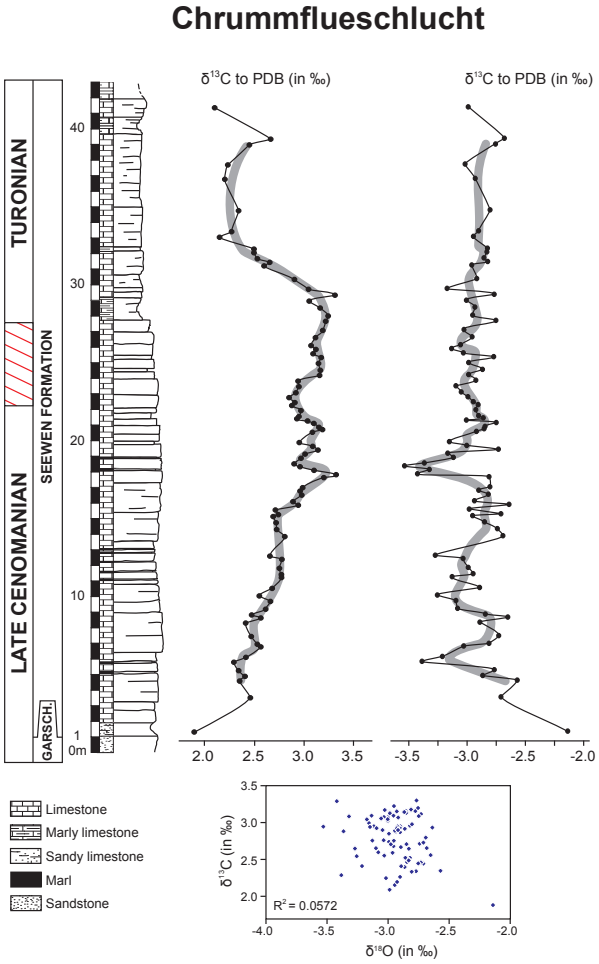

Fig. E.5: $\delta^{13}C$ and $\delta^{18}O$ curves for the Chrummflueschlucht section. The lack of significant correlation between the $\delta^{13}C$ and $\delta^{18}O$ records and the absolute $\delta^{18}O$ values indicate that late diagenetic processes did not affect the stable-isotope record too strongly.

E.4.3 Bulk-rock mineralogy

At Chrummflueschlucht, the sediments consist essentially of calcite, with minor inclusions of quartz and phyllosilicates (Fig. E.6). The relative proportion of calcite ranges between 85 and 97% with an upward-increasing trend. Quartz and phyllosilicates show low values, from the detection limit to 11% for quartz and to 5% for phyllosilicates, respectively. These minerals exhibit a first maximum at the base of the section in the glauconite-rich Kamm Bed. Two further enrichments are observed in sediments at the onset of the positive $\delta^{13}C$ shift (at about 15m) and below the $\delta^{13}C$ plateau (21-23m), respectively. K-feldspar and Na-plagioclase occur only sporadically throughout the section.

We determine a detrital index [DI = Calcite/(Quartz + Phyllosilicates + K-Feldspar + Na-Plagioclase)] to observe changes in detrital influx. The DI shows highest values at the onset of the $\delta^{13}C$ shift and within the trough between the peaks and the plateau. DI, phyllosilicates and the unquantified minerals show similar trends, suggesting that most of the unquantifieds have a detrital origin, with a high component of phyllosilicates.

E.4.4 Total phosphorus contents

Total P contents range from 117 to 1097 ppm (Fig. E.7). P accumulation rates were not calculated because of uncertainties in the attribution of absolute ages. In the first 15m of the section, in sediments attributed to the *R. cushmani* zone, P contents display small variations superimposed on a long-term decreasing trend with values reaching from ~500 to ~150 ppm. In the following, the P trend exhibits a positive spike, reaching a maximum of 1097 ppm in sediments representing the transition of the *R. cushmani* and *W. archeocretacea* zones, coeval with the first positive peak in $\delta^{13}C$. After this first peak in $\delta^{13}C$, P values remain quite low, fluctuating between 150 and 200 ppm. In sediments corresponding to the end of the positive shift in $\delta^{13}C$ (within the *H. helvetica zone*) a smooth increase is observed (290 ppm), coeval with the decrease in the $\delta^{13}C$ record.

E.4.5 Redox-sensitive trace elements

We investigated the stratigraphic behaviour of the following redox-sensitive trace-elements: U, V, Co, Mo, As, Mn and Fe. We describe the behaviour of U, V, Co, Mo and As in more detail, as they are commonly used to interpret changes in paleoredox conditions (Algeo & Maynard, 2004; Tribovillard et al., 2006; Algeo & Lyons, 2006). The contents of these RSTE are presented in Fig. E.7. They show no comparable variations throughout the Chrummflueschlucht section. The average values for U, V, As, Co and Mo correspond to approximately 0.5, 2.3, 0.6, 2.3 and 0.7 ppm, respectively. In the first part of the section (from the base to 12m), U and V contents show higher values ranging around 0.8 and 2.5-3 ppm respectively. Consequently, U and V contents decrease in sediments attributed to the *R. cushmani* zone and remain low along the rest of the section, showing higher fluctuations in the first 20 meters of the section, with values between the detection limits and 3 ppm. In the second part of the section, As shows rather low and constant values. Co displays an intermediate behaviour between V and As. The lower part of the Co trend shows variations similar to As (with values between 1 and 6 ppm). In the second part of the section (from 20m to the top), Co contents shows rather low values with a slightly increase at ~32m. Mo contents remain quite constant along the entire section and deviate towards higher values only in the interval coeval with the decrease in $\delta^{13}C$ values. Mn shows values between 125 and 920 ppm. Mn concentrations exhibit a long-term decreasing trend in the first part of the section reaching a minimum of about 200 ppm in sediments concomitant with the plateau in $\delta^{13}C$. In the following, Mn values increase again to pre-OAE values. Fe distribution along the section shows a decreasing trend from the base of the section to the 20 first meters. Then, Fe contents increase slightly and at ~32m, Fe values display an increase towards 8000 ppm. Al contents are well correlated to the evolution of phyllosilicates, except for the interval corresponding to the $\delta^{13}C$ plateau. Al contents show higher values in the 10 first meters of the section, followed by a small decrease at ~15m. Thereafter, Al values increase slowly and show a peak at ~32m.

E.5 Discussion

E.5.1 Stable isotopes, biostratigraphy and chronology of the OAE 2

The OAE 2 is characterized by a globally recognized positive excursion in $\delta^{13}C$ (Schlanger & Jenkyns, 1976; Jenkyns, 1980; Jenkyns et al., 1994; Leckie et al., 2002; Tsikos et al., 2004; Jarvis et al., 2006; Voigt et al., 2006, 2007; Mort et al., 2007). The typical shape of the end-Cenomanian positive excursion, as observed in the GSSP section at Pueblo, Colorado (Sageman et al., 2006), in Eastbourne, England (Jarvis et al., 2006)

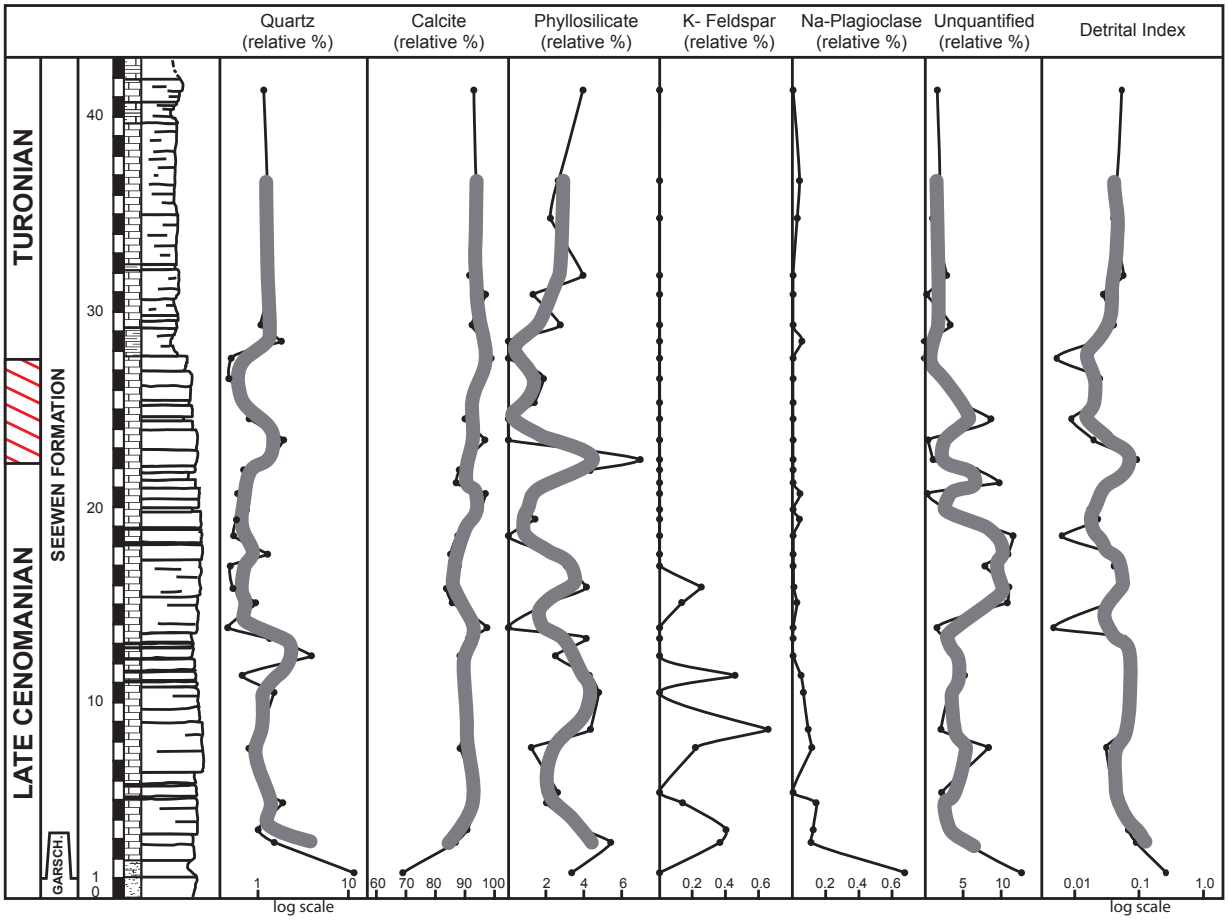

Fig. E.6: Bulk-rock analysis of the Chrummflueschlucht section. Grey lines correspond to three-point average curves for the contents of quartz, calcite, phyllosilicates, unquantifieds and for the detrital index (see text). High detrital influx rates are explained by more humid climate and increased continental runoff.

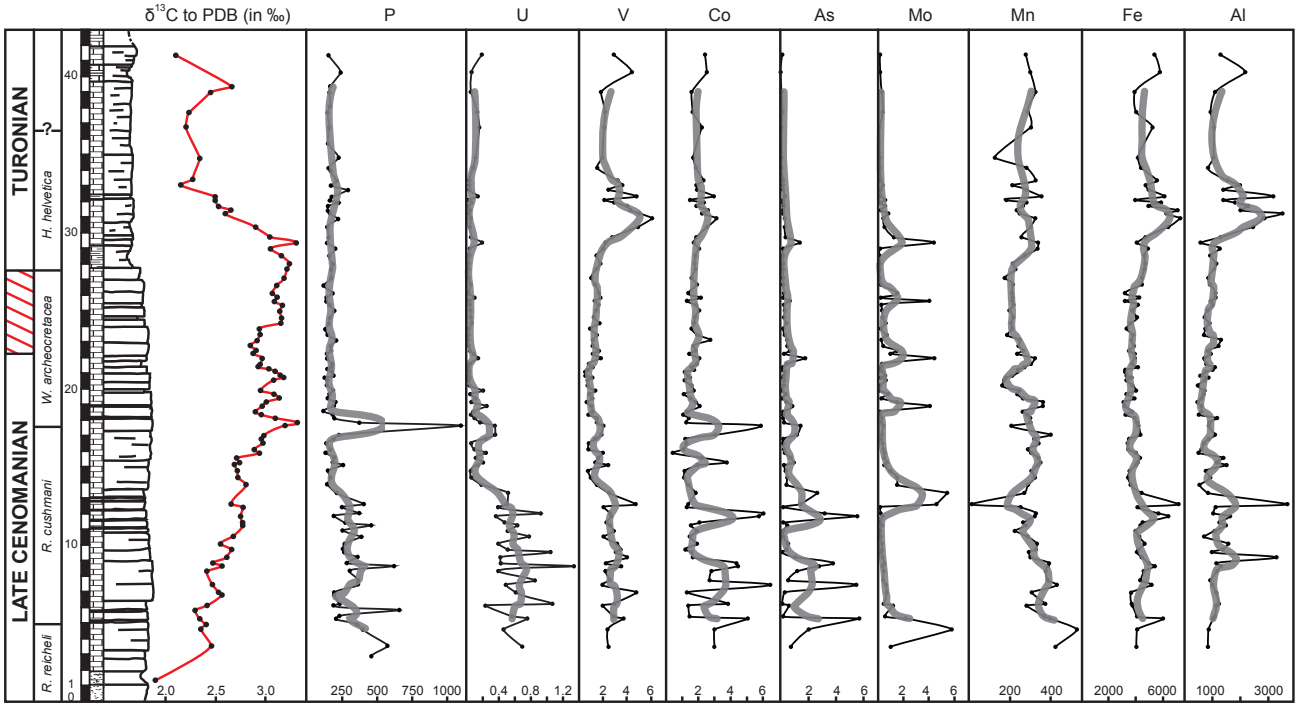

Fig E.7: Phosphorus, redox-sensitive trace elements and aluminium distributions (in ppm) for the Chrummflueschlucht section. Grey lines correspond to five-point average curves for each element.

and in Wünstrof (Voigt et al., 2008), is characterized by a rapid increase in $\delta^{13}C$ reaching a first peak (peak 1), followed by a minor decrease, a second peak (peak 2) and a prolonged plateau (Fig. E.8).

The characteristic increase in $\delta^{13}C$ values is also observed in the section of Chrummflueschlucht. However the OAE 2 is preceded by a gradual increase in the $\delta^{13}C$ (0-11m). The amplitude of the positive $\delta^{13}C$ excursion in the Helvetic realm is also lower than at Pueblo (approximately 1‰), but is well comparable to the generalized curves published by Erbacher et al. (1996), Leckie et al. (2002), and Jarvis et al. (2006). In the Chrummflueschlucht section, *W. archeocretacea* first appears in sediments at the onset of the $\delta^{13}C$ positive shift, just below the last occurrence of *R. greenhornensis.* This is comparable to the section of Pueblo and indicates that the onset of OAE 2 has been recorded in the Chrummflueschlucht section without any hiatus (Fig. E.8). *R. cushmani* disappears, however, approximately 50 cm below the first peak in $\delta^{13}C$, whereas at Pueblo, the last occurrence of this index species coincides with peak 1 (Keller & Pardo, 2004). In addition, in sediments corresponding to the first peak in $\delta^{13}C$ values of the Chrummflueschlucht section, we observe the presence of glauconite and phosphatic grains. The early disappearance of *R. cushmani* relative to the evolution in the $\delta^{13}C$ curve in comparison to the Pueblo and Eastbourne sections (Fig. E.8) may be related to a small hiatus and the presence of reworked sediments which are frequent in the Seewen formation (Föllmi & Ouwehand, 1987). This would imply that the first peak in the $\delta^{13}C$ record at Chrummflueschlucht corresponds to the peaks 1 and 2 measured at Pueblo (Fig. E.8). The stratigraphic position of the Heterohelix-dominated assemblages in relation to the $\delta^{13}C$ curve remains problematic: for Keller et al. (2001), it is situated above the peak 2, whereas, following Caron et al. (2006), the Heterohelix shift is located between the peak 1 and 2 in the $\delta^{13}C$ curve.

The following plateau in C-isotope values is comparable to that in the Pueblo section, suggesting that the Chrummflueschlucht preserves a relatively complete succession representing the Cenomanian-Turorian boundary and the Early Turonian. *H. helvetica* appears early in the sediments of the Chrummflueschlucht section, within the plateau of $\delta^{13}C$ values, whereas at Pueblo, the first occurrence of *H. helvetica* is situated in sediments corresponding to the subsequent negative excursion in the $\delta^{13}C$ record. This difference in the chronological position of the base of the *H. helvetica* biozone has also been observed in other basins (Keller & Pardo, 2004; Grosheny et al., 2006; Ifrim & Stinnesbeck, 2008). Keller & Pardo (2004) related this to diachronism in the appearance of this index species and/or to the difficulty to determine the evolutionary transition from *W. praehelvetica* to *H. helvetica*.

The similarity in the $\delta^{13}C$ excursions between the Chrummflueschlucht and Pueblo sections, with as only deviation a probable merger of peaks 1 and 2, shows that the Chrummflueschlucht section records the onset and the end of OAE 2. It also indicates that the Chrummflueschlucht section constitutes one of the most complete sections in the Helvetic thrust-and-fold belt for the Late Cenomanian – Early Turonian known so far.

E.5.2 Planktonic foraminifera as environmental proxies

The microfossil assemblages in the Chrummflueschlucht section show distinct differences in their morphologies through time, which are probably related to different living conditions. Two groups are distinguished: the first group is characterized by large keeled forms, with complex morphologies and inferred long reproduction cycles. Representatives of this group are interpreted as K-strategists (Caron, 1983). They date from the *R. cushmani* and the *H. helvetica* zone, which are periods characterized by well-oxygenated water with low nutrient levels allowing a specific diversification and the development of more sophisticated morphotypes. The second group is composed of bulbous forms with small and simple morphologies (e.g., *Whiteinella* and *Heterohelix*), which mainly lived in the upper-water column with high nutrient levels (Hart, 1989; Petters, 1980; Jarvis et al., 1988; Leckie et al., 1998; Keller and Pardo, 2004). They are interpreted as r-strategists and date from the *W. archeocretacea* zone. The change in the morphology and ecology of planktonic foraminifera observed in the Chrummflueschlucht section occurred during the period of the positive $\delta^{13}C$ excursion and are interpreted as the consequence of a change in the oxygenation state of the water column. The disappearance of complex forms with long reproduction cycles (rotaliporoids) and the presence of low-oxygen tolerant heterohelicids at the onset and during the positive excursion suggest the presence of oxygen-depleted conditions in the deeper part of the water column (Leckie 1987; Leckie et al., 1998; Keller & Pardo, 2004) and point out changes in surface water

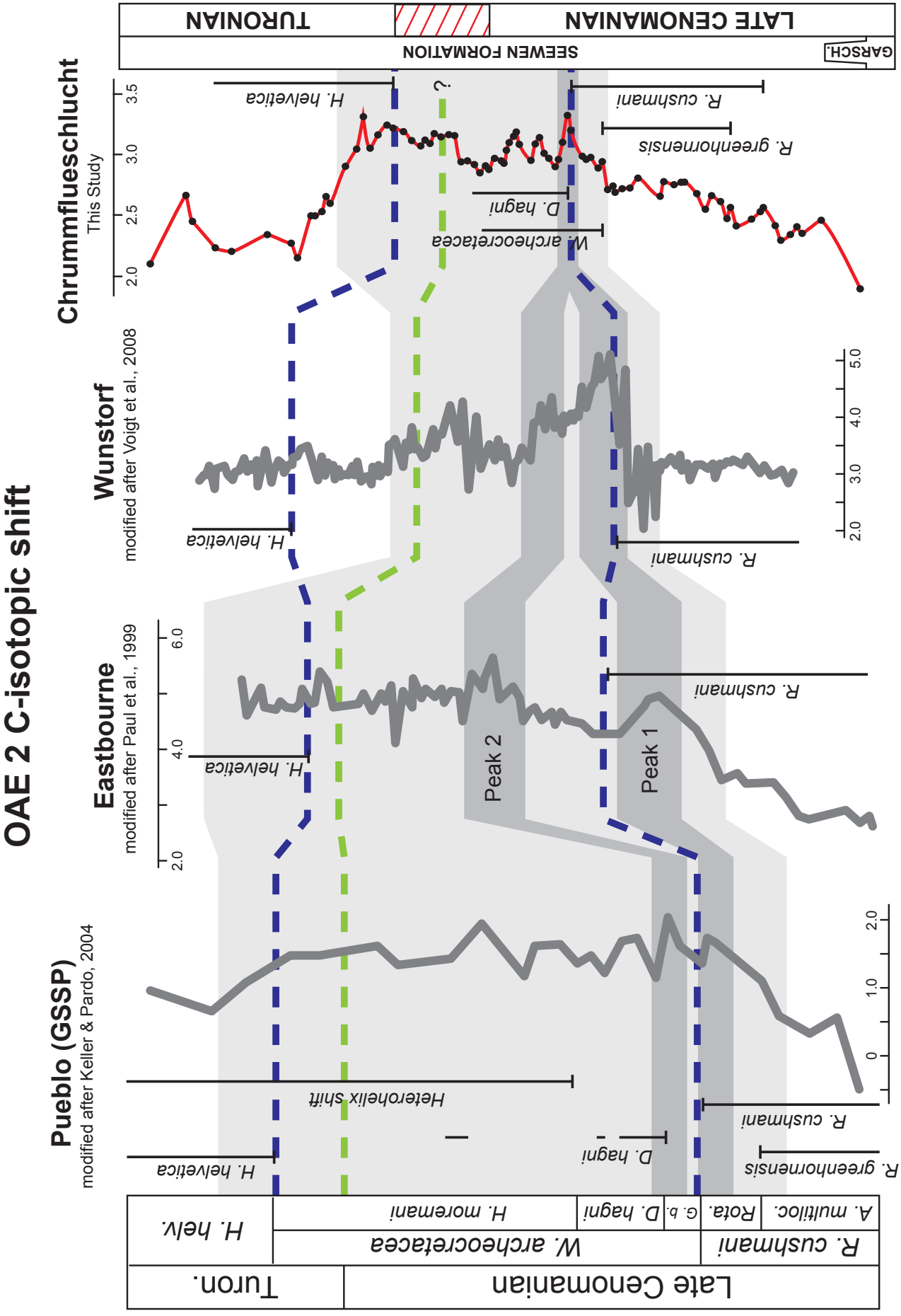

Fig E.8: Stratigraphic correlations for the end-Cenomanian OAE 2 (light grey) between the sections of Chrummflueschlucht, Pueblo, Eastbourne and Wunstorf. The dark grey bands indicate the position of the peak 1 and 2.

fertility, probably related to the modification of upwelling systems (Premoli Silva, et al., 1999).

At Chrummflueschlucht, the change in the morphology of planktonic foraminifera is comparable to that observed in many other sections of the western Tethys (Keller et al., 2001; Grosheny et al., 2006; Wagreich et al., 2008). This indicates that also in the Helvetic realm, dissolved oxygen contents in the water column diminished during the onset of the positive $\delta^{13}C$ excursion in the *W. archeocretacea* zone. However, the presence of small forms of *Marginotruncana* in the *W. archeocretacea* zone is in favour of the presence of only slightly diminished oxygen levels, rather than fully anoxic conditions in this part of the northern Tethyan shelf margin.

E.5.3 Paleoenvironmental conditions in the Helvetic realm during OAE 2

The bulk-rock mineralogical composition and especially the detrital index (DI) provide valuable information on environmental and climatic change. Low DI values indicate higher rates of continental runoff, whereas high values characterize low continental runoff. In the Chrummflueschlucht section, the onset of the positive $\delta^{13}C$ excursion is marked by an increase in detrital influx (low DI values). This interval is also characterized by a positive correlation of the stratigraphic trends in DI, P and Al contents. This suggests a coupling between runoff and P delivery. The higher DI and P values may indicate the presence of higher nutrient levels in this time interval. The increase in P content has been observed in many sections of the Tethys and the North Atlantic indicating a change in continental runoff and nutrient influx and/or intensification in upwelling during the Late Cenomanian (Mort et al., 2007). This inferred change in nutrient input may have triggered an increase in primary productivity and a concomitant increase in $\delta^{13}C$ values (Ingall et al., 1993; Van Cappellen & Ingall, 1994; Föllmi, 1995; Mort et al., 2007). Organic-rich sediments are, however, lacking in the Chrummflueschlucht section. Black shales related to OAE2 have been found in the Ultrahelvetic Zone (Strasser et al., 2001; Wagreich et al., 2008) indicating increased organic-matter production and/or better preservation in deeper, distal parts of the northern Tethyan shelf.

Following the first maximum in the $\delta^{13}C$ curve, P contents are less well correlated with Al contents and DI variations: Al and DI values increase in sediments attributed to the *W. archeocretacea* zone, whereas P contents remain low. The sedimentary interval with low P values shows an increase in abundance of *W. archeocretacea* and the presence of heterohelicids,

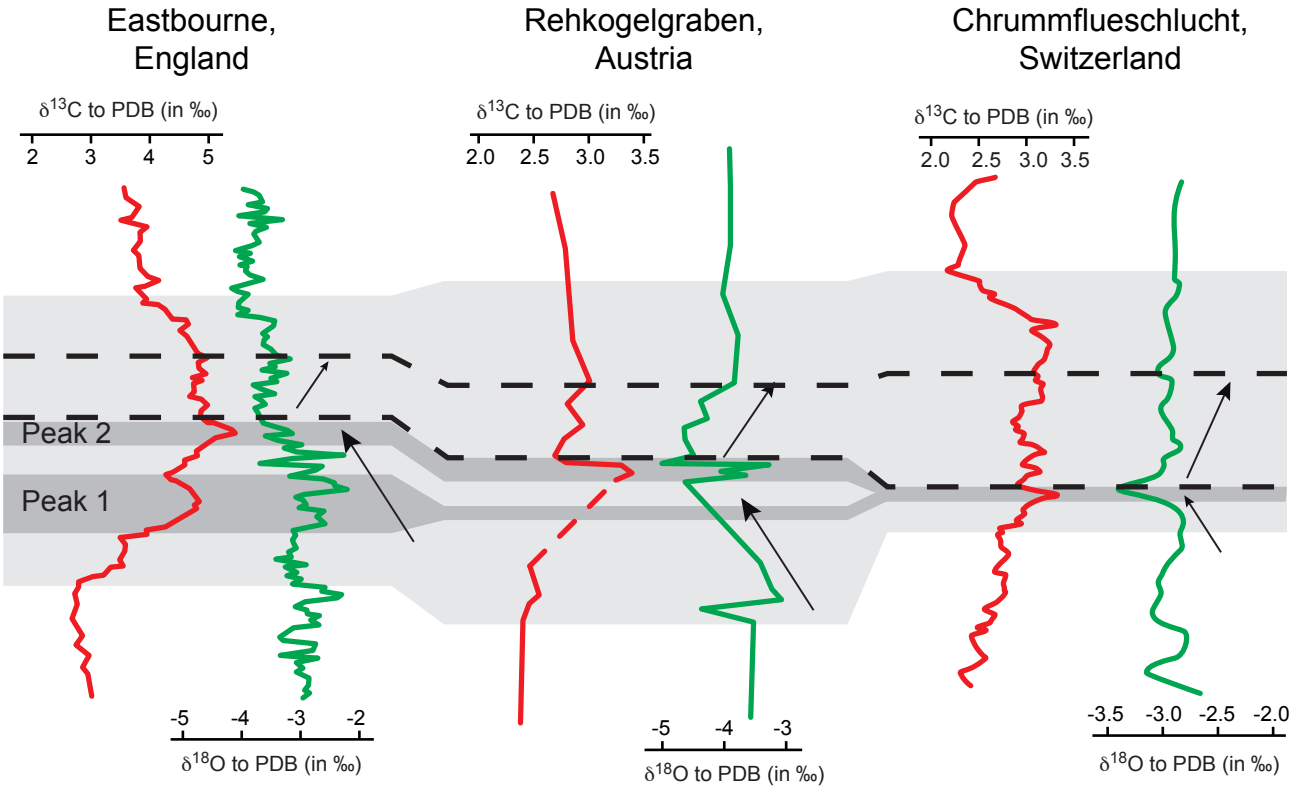

Fig E.9: Change in $\delta^{18}O$ through the end-Cenomanian OAE 2 in the sections of Eastbourne (Tsikos et al., 2004), Rehkogelgraben (Wagreich et al., 2008) and Chrummflueschlucht. Dark grey bands indicate the position of the Peak 1 and 2.

which are tolerant to low-oxygen conditions. This suggests that P behaviour may have been influenced by redox variations in the water column and at the water/sediment interface (Mort et al., 2007).

Changes in detrital influx are partly associated with high values in the $\delta^{18}O$ record. The observed pattern in oxygen isotopes recorded at Chrummflueschlucht is comparable to the published curves of the sections at Eastbourne and Gubbio (Jenkyns et al., 1994; Tsikos et al., 2004) and also with the section of Rehkogelgraben in the Ultrahelvetic unit (Wagreich et al., 2008). Oxygen isotopes in carbonates are more affected by diagenesis compared to carbon isotopes, but the good correlation between Chrummflueschlucht and other sections of the northern Tethys indicates that the long-term variations in the $\delta^{18}O$ signal represent a consistent trend (Fig. E.9). The fluctuations in the $\delta^{18}O$ record suggest changes in temperature and/or freshwater influx during OAE2. In the sections of Rehkogelgraben and Eastbourne, a long decreasing trend in $\delta^{18}O$, preceding the onset of $\delta^{13}C$ excursion, is also observed. This is consistent with a generally warmer climate before OAE 2 (Jenkyns et al., 1994; Tsikos et al., 2004; Wagreich et al., 2008). At Chrummflueschlucht, the good correlation between trends in the DI and $\delta^{18}O$ records goes along with a paleoclimatic interpretation of the latter record. The decreasing trend in $\delta^{18}O$ values before the onset of the OAE 2 is associated with a warmer climate with higher rates in continental runoff. The onset of the shift is marked by a plateau of higher oxygen-isotope values, indicating a possible cooling trend and/or an input of fresh water at the onset of the shift. This plateau is followed by a negative shift in $\delta^{18}O$ coeval with the first maximum in the $\delta^{13}C$ and an increase in detrital input. This may be linked to an increase in continental runoff associated with a return to warmer and more humid climate (Fig. E.10). The second part of the positive shift shows an increasing trend in the $\delta^{18}O$ record is associated with low detrital input, suggesting a change in the hydrological cycle related to a possible cooling and more contrasted climate.

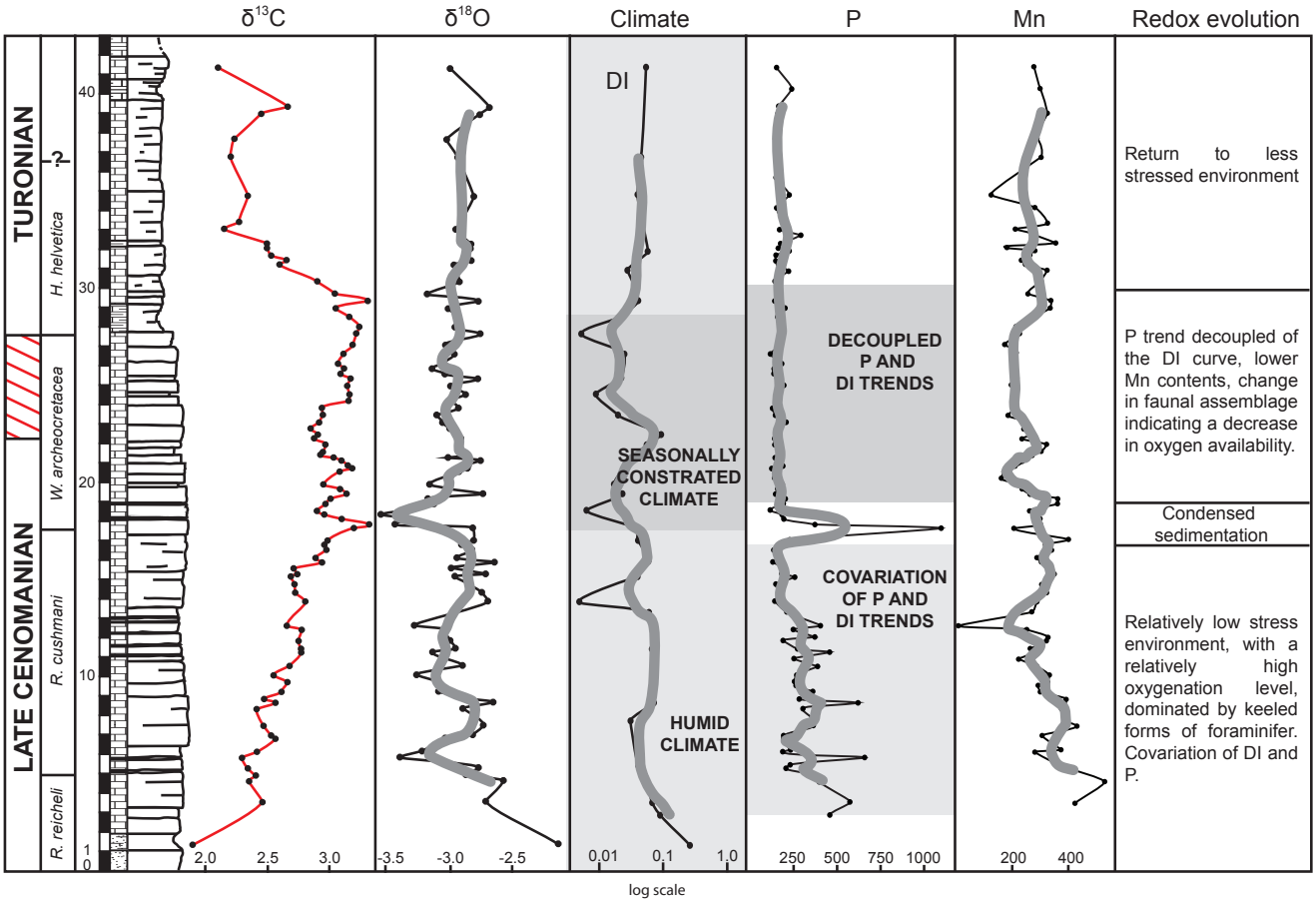

Fig E.10: Summary of paleoenvironmental proxies including $\delta^{13}C$ and $\delta^{18}O$ (in ‰ to PDB), climate change (as deducted from the stratigraphic trends in the mineralogy and P contents) and redox variations (from faunal assemblage and TM contents) across OAE 2 in the Helvetic realm.

E.5.4 Redox conditions in the Helvetic realm during OAE 2

The behaviour of P in relation with the change in planktonic foraminiferal assemblages suggests a change towards oxygen-depleted conditions in the western Tethys. Mort et al. (2007) suggested a direct dependency between the evolution of redox conditions and P accumulation rates during OAE2, with lowered P retention rates during dysoxic/anoxic conditions. The higher P contents in sediments at the onset of the $\delta^{13}C$ positive excursion, followed by lower P values during the $\delta^{13}C$ excursion decoupled from detrital proxies are in good agreement with this hypothesis.

Mn contents show a long-term decrease, which may be in favour of oxygen-depleted conditions. Mn is generally not used as a paleoredox proxy due to its high mobility in reducing sediments (Tribovillard et al., 2006). However, a negative correlation is frequently observed between Mn trapping and the development of anoxic conditions (Frakes & Bolton, 1992; Brumsack, 1986; Kuhn et al., 2005; Tribovillard et al., 2006). At Chrummflueschlucht, the positive shift in $\delta^{13}C$ is coeval with a decrease in Mn contents. This, together with the decoupling of the trends in the contents of P and detrital proxies and the presence of the low-oxygen-tolerant species *Heterohelix* may indicate the beginning of oxygen depletion in the water column. In the Pueblo section, enrichments in Co and Mo indicate strong oxygen depletion in the Western interior basin (Snow et al., 2005). However, the suite of RSTE (U, V, Mo, Co, As) shows no correlable enrichments along the section of Chrummflueschlucht (Fig. E.7). The higher values of U corresponds to higher values in DI, and the trend in V contents is similar to the Al trend indicating that these RSTE enrichments are principally of detrital origin. This provides evidence for the absence of well-developed anoxic conditions at this site of the Helvetic realm (Tribovillard et al., 2006). However, one has to bear in mind that the onset of the $\delta^{13}C$ positive shift may be related to a possible reduction in sediment accumulation in the Chrummflueschlucht section, which as such may represent a loss of information on the time period directly after the onset of OAE2. The presence of *Marginotruncana* during the plateau is another argument against full-fletched anoxic conditions.

E.6 Depositional model and conclusions

The Chrummflueschlucht section provides a good opportunity to reconstruct the effects of the end-Cenomanian OAE2 in the hemipelagic environment of the Helvetic realm. The $\delta^{13}C$ positive excursion and the accompanying characteristic overturn in planktonic foraminifera are documented in high detail.

The presence of keeled foraminifera and the moderate P and detrital contents indicate a relatively low stress environment during the *R. reicheli* zone and most of the *R. cushmani* zone. At the onset of the $\delta^{13}C$ positive excursion near the limit between the *R. cushmani* and the *W. archeocretacea* zones, the P record shows a rapid spike linked to the presence of glauconitic and phosphatic grains. This probably corresponds to a phase of reworked sediments, which may have been linked to the end-Cenomanian sea-level rise (Haq et al., 1987), and results in an early disappearance of *R. cushmani* in comparison to the Pueblo GSSP section.

At the base of the *W. archeocretacea* zone, the positive $\delta^{13}C$ excursion coincides with the presence of Heterohelicidae, low P contents decoupled of the detrital input and a decrease in Mn contents. This reflects increasing dysaerobic conditions and an increasingly stressed environment. The absence of organic-rich sediments and obvious RSTE enrichments, and the presence of small *Marginotruncana* species suggest, however, that full-fletched anoxic conditions did not develop in the hemipelagic zone of the northern Tethyan margin.

The plateau of high $\delta^{13}C$ values during the remainder of the *W. archeocretacea* zone and the following negative excursion towards normal values suggest that this part of the Chrummflueschlucht section is quite complete. The first occurrence of *H. helvetica* in the Chrummfluechlucht section predates the one at Pueblo, as was also observed in other parts of the world (Keller et al., 2001; Grosheny et al., 2006; Caron et al., 2006).

The hemipelagic character of the section, the dominance of planktonic foraminifera and the presence of important quantities of calcispheres along the section indicate that the section was situated in the deeper part of the shelf. The chemical redox proxies place the section, however, well above the core of the oxygen-minimum zone (OMZ), which probably fluctuated and expanded onto the shelf during OAE2. The paleoecological and geochemical proxies observed at Chrummflueschlucht suggest that anoxic conditions never reached this part of the northern Tethyan, southern European and that the observed fluctuations in redox conditions from fully oxic to slightly disaerobic conditions appear less compatible with a stagnant ocean model.

Acknowledgments

We would like to thank Stéphane Bodin for his their help in the field, Tiffany Monnier for laboratory assistance and André Villard for the preparation of thin sections. We also thank Haydon Mort for advise on the phosphorus analysis and for his general comments and suggestions. A special thank goes to Michèle Caron for the determination of planktonic foraminifera and for her advice on the ecology of planktonic foraminifera and on an earlier draft of the manuscript.

This research is supported by the Swiss National Science Foundation (Grants 200021-109514/1 and 200020-113640).

References

Adatte, T., Stinnesbeck, W. & Keller, G. 1996: Lithostratigraphic and mineralogic correlations of near K/T boundary sediments in northeastern Mexico: Implicartions for origin and nature deposition. *In*: Ryder, G., Fastovsky, D. & Gartner, S., (*Eds*). The Cretaceous-Tertiary Event and Other Catastrophes in Earth History. Boulder, Colorado, Geological Society of America Special Paper, 307, 211-226.

Algeo, T. J. & Lyons, T. 2006: Mo–total organic carbon covariation in modern anoxic marine environments: Implications for analysis of paleoredox and paleohydrographic conditions. Paleoceanography 21, doi: 10.1029/2004PA001112.

Algeo, T. J., & Maynard, J. B. 2004: Trace-element behaviour and redox facies in core shales of Upper Pennsylvanian Kansas-type cyclothems. Chemical Geology 206, 289-318.

Algeo, T. J. & Maynard, J. B. 2008: Trace metal covariation as a guide to water-mass conditions in ancient anoxic marine environments. Geosphere 4, 872-887, doi: 10.1130/GES00174.1.

Bodin, S., Godet, A., Föllmi, K. B., Vermeulen, J., Arnaud, H., Strasser, A., Fiet, N. & Adatte, T. 2006: The late Hauterivian Faraoni oceanic anoxic event in the western Tethys : Evidence from phosphorus burial rates. Palaeogeography, Palaeoclimatology, Palaeoecology 235, 245-264.

Bodin, S., Godet, A., Matera, V., Steinmann, P., Vermeulen, J., Gardin, S., Adatte, T., Coccioni, R. & Föllmi, K. B. 2006: Enrichment of redox-sensitive trace metals (U, V, Mo, As) associated with the late Hauterivian Faraoni oceanic anoxic event. International Journal of Earth Sciences 96, 327-341, doi: 10.1007/s00531-006-0091-9.

Bolli, H. 1944: Zur Stratigraphie der Oberen Kreide in den höheren helvetischen Decken. Eclogae geologicae helvetiae, 37, 2, 218-328.

Brumsack, H.-J. 1986: The inorganic geochemistry of Cretaceous black shales (DSDP Leg 41) in comparison to modern upwelling sediments from the Gulf of California. Geological Society, London, Special Publication, 21, 447-462.

Brumsack, H.-J. 2006: The trace metal content of recent organic carbon-rich sediments : Implications for Cretaceous black shales formation. Palaeogeography, Palaeoclimatology, Palaeoecology 232, 344-361.

Bralower, T. J. & Thierstein, H. R. 1984: Low productivity and slow deep-water circulation in mid-Cretaceous oceans. Geology 12, 614-618.

Caron, M. 1981: Un nouveau genre de foraminifère planctonique du Crétacé : Falsotruncana nov. gen. Eclogae geologicae helvetiae, 74, 65-73.

Caron, M. 1983: La spéciation chez les foraminifères planctiques: une réponse adaptée aux contraintes de l'environnement. Zitteliana 10, 671–676.

Caron, M., Dall'Agnolo, S., Accarie, H., Barrera, E., Kauffman, E. G., Amédro, F. & Robaszynski, F. 2006: High-resolution stratigraphy of the Cenomanian-Turonian boundary interval at Pueblo (USA) and wadi Balhoul (Tunisia): stable isotope and bio-events correlation. GEOBIOS 39, 171-200.

Delamette, M. 1988: L'evolution du domaine helvétique (entre Bauges et Morcles) de l'Aptien supérieur au Turonien: series condensées, phosphorites et circulations océaniques. Publicatio du Départemtn de la géologie et paleontology, Université Genève, 5, 316 pp.

Elrick, M., Molina-Garza, R., Duncan, R. & Snow, L. 2009: C-isotope stratigraphy and paleoenvironmental changes across OAE2 (mid-Cretaceous) from shallow-water platform carbonates of southern Mexico. Earth and Planetary Science Letters 277, 295-306, doi:10.1016/j.epsl.2008.10.020.

Erba, E. 2004: Calcareous nannofossils and

Mesozoic oceanic anoxic events. Marine micropaleontology 52, 85-106.

Erbacher, J., Thurow, J. & Littke, R. 1996: Evolution patterns of radiolaria and organic matter variations: A new approach to identify sea-level changes in mid-Cretaceous pelagic environments. Geology 24, 499-502.

Föllmi, K. B. 1995: 160 m.y. record of marine sedimentary phosphorus burial : Coupling of climate and continental wearthering under greenhouse and icehouse conditions. Geology 23, 859-862.

Föllmi, K. B., Ouwehand, P. J. 1987: Garschalla-Formation und Götzis-Schichten (Aptian-Coniacian): Neue stratigraphische Daten aus dem Helvetikum der Ostschweiz und des Vorarlbergs. Eclogae geologicae Helvetiae 80, 141-191.

Föllmi, K. B., Bodin, S., Godet, A., Linder, P. & Van de Schootbrugge, B. 2007: Unlocking paleo-environmental information from Early Cretaceous shelf sediments in the Helvetic Alps: stratigraphy is the key! Swiss Journal of Geosciences 100, 349-369, doi: 10.1007/s00015-007-1236-y.

Föllmi, K., Gertsch, B., Renevey, J.-P., De Kaenel, E. & Stille, P. 2008: Stratigraphy and sedimentology of phosphate-rich sediments in Malta and south-eastern Silicy (latest Oligocene to early Late Miocene). Sedimentology 55, 1029-1051, doi: 10.1111/j.1365-3091.2007.00935.x.

Forster, A., Schouten, S., Moriya, K., Wilson, P. A. & Sinninghe Damsté, J. S. 2007: Tropical warming and intermittent cooling duirng the Cenomanian/Turonian oceanic anoxic event 2: Sea surface temparture records from the equtorial Atlantic. Paleoceanography 22, PA1219, doi:10.1029/2006PA001349.

Frakes, L. & Bolton, B. 1992: Effects of ocean chemistry, sea level, and climate on the formation of primary manganese ore deposits: Economic Geology 87, 1207-1217, doi: 10.2113/gsecongeo.87.5.1207.

Gertsch, B., Keller, G., Adatte, T., Berner, Z., Kassab, A. S., Tantawy, A. A. A., El-Sabbagh, A. M. & Stueben, D. 2008: Cenomanian-Turonian transition in a shallow water sequence of the Sinai, Egypt. International Journal of Earth Sciences, doi: 10.1007/s00531-008-0374-4.

Grosheny, D., Beaudoin, B., Morel, L. & Desmares, D. 2006: High-resolution biotratigraphy and chemostratigraphy of the Cenomanian/Turonian boundary event in the Vocontian Basin, southeast France. Cretaceous Research 27, 629-640.

Haq, B. U., Hardenbol, J. & Vail, P. R. 1987: Chronology of fluctuating sea levels since the Triassic. Science 235, 1156-1166.

Hardenbol, J., Thierry, J., Farley, M. B., Jacquin, T., De Graciansky, P.-C., and Vail, P. R. 1998: Mesozoic and Cenozoic chronostratigraphic framework of European basins: SEPM special publication 60, 3-13.

Hart, M. B. & Leary, P. N. 1989: The stratigraphic and palaeogeographic setting of the late Cenomanian “anoxic” event. Jounal of the geological Society of London 146, 252-254, doi: 10.1038/286252a0.

Huber B. T., Norris R. D. & McLeod K. G. 2002: Deep-sea paleotemperature record of extreme warmth during the Cretaceous. Geology 30, 123–126, doi:10.1130/0091-7613(2002)030\0123:DSPROE[2.0.CO;2.

Ifrim, C. & Stinnesbeck, W. 2008: Cenomanian-Turonian high-resolution biostratigraphy of north-eastern Mexico and its correlation with the GSSP and Europe: Cretaceous Research, In press.

Ingall, E. D., Bustin, R. M. & Van Cappellen, P. 1993: Influence of water column anoxia on the burial and preservation of carbon and phosphorus in marine shales. Geochimica et Cosmochimica Acta 57, 303-316.

Jarvis I., Carson G. A., Cooper M. K. E., Hart M. B., Leary P. N., Tocher B. A. Horne, D. & Rosenfeld A. 1988: Microfossil assemblages and the Cenomanian–Turonian (late Cretaceous) oceanic anoxic event. Cretaceous Research 9, 3–103, doi: 10.1016/0195-6671(88)90003-1.

Jarvis, I., Gale, A. S., Jenkyns, H. C. & Pearce, M. A. 2006: Secular variation in the Late Cretaceous carbon isotopes: a new d13C carbonate reference curve for the Cenomanian-Campanian (99.6-70.6Ma). Geological Magazine 143, 561-608.

Jenkyns, H. C. 1980: Cretaceous anoxic events : from continents to oceans. Jounal of the geological Society of London 137, 171-188.

Jenkyns, H. C. 2003, Evidence for rapid climate change in the Mesozoic-Palaeogene greenhouse

world. Phil. Trans. R. Soc. Lond. A 361, 1885-1916.

Jenkyns, H. C., Gale, A. S. & Corfield, R. M. 1994: Carbon- and oxygen-isotope stratigraphy of the English Chalk and Italian Scaglia and its palaeoclimatic significance: Geological Magazine 131, 1-34.

Jones, C. E. & Jenkyns, H. C. 2001: Seawater strontium isotopes, oceanic anoxic events, and seafloor hydrothermal activity in the Jurassic and Cretaceous: American Journal of Science 301, 112-149.

Keller, G., Adatte, T., Berner, Z., Chellai, E. H. & Stueben, D. 2008: Oceanic events and biotic effects of the Cenomanian-Turonian anoxic event, Tarfaya Basin, Morocco. Cretaceous Research 29, 976-994, doi:10.1016/j.cretres.2008.05.020.

Keller, G., Han, Q., Adatte, T., and Burn, S. J. 2001: Palaeoenvironment of the Cenomanian-Turonian transition at Eastbourne, England. Cretaceous Research 22, 391-422.

Keller, G. & Pardo, A. 2004: Age and paleoenvironment of the Cenomanian-Turonian global stratotype section and point at Pueblo, Colorado. Marine micropaleontology 51, 95-128, doi:10.1016/j.marmicro.2003.08.004.

Kolonic, S., Wagner, T., Forster, A., Sinnighe Damsté, J. S., Walsworth-Bell, B., Erba, E., Turgeon, S., Brumbsack, H.-J., Chellai, E. H., Tsikos, H., Kuhnt, W. & Kuypers, M. M. M. 2005: Black shale deposition on the northwest African Shelf during the Cenomanian/Turonian oceanic anoxic event: Climate coupling and global organic carbon burial. Paleoceanography 20, PA1006, doi: 10.1029/2003PA000950.

Kübler, B. 1983: Dosage quantitative des minéraux majeurs des roches sédimentaires par diffractionX. Cahier de l'Institut de Géologie, Université de Neuchâtel, Suisse. Série ADX, 2.

Kuhn, O., Weissert, H., Föllmi, K. B., and Hennig, S. 2005: Altered carbon cycling and trace-metal enrichment during the late Valanginian and early Hauterivian. Eclogae geol. Helv. 98, 333-344.

Leckie R. M. 1987: Paleoecology of the mid-Cretaceous planktic foraminifera: a comparison of open ocean and epicontinental sea assemblages. Micropaleontology 33, 164–176. doi: 10.2307/1485491.

Leckie, R. M., Bralower, T. J. & Cashman, R. 2002: Oceanic anoxic events and plankton evolution: Biotic response to tectonic forcing during the mid-Cretaceous: Paleoceanography17, PA 1041, doi:10.1029/2001PA000623.

Leckie R.M. , Yuretich R. F., West L. O. L., Finkelstein D., Schmidt M. 1998: Paleoceanography of the southwestern Interior Sea during the time of the Cenomanian–Turonian boundary (late Cretaceous).Dean WE, Arthur MA (eds) Concepts in sedimentology and paleontolgy, vol 6 SEPM, USA, 101–126.

Mort, M., Adatte, T., Föllmi, K. B., Keller, G., Steinmann, P., Matera, V., Berner, Z. & Stüben, D. 2007: Phosphorus and the roles of productivity and nutrient recycling during oceanic event 2. Geology 35, 483-486.

Norris R.D., Bice K. L., Magno E. A. & Wilson P. A. 2002: Jiggling the tropical thermostat in the Cretaceous hothouse. Geology 30, 299–302.

Pancost, R. D., Crawford, N., Magness, S., Turner, A., Jenkyns, H. C., and Maxwell, J. R. 2004: Further evidence for the development of photic-zone euxinic conditions during mesozoic oceanic anoxic events: Jounal of the geological Society of London 161, 353-364.

Paul, C. R. C., Lamoldad, S. F., Mitchell, S. F., Vaziri, M. R., Gorostidib, A. & Marshall, J. D. 1999: The Cenomanian-Turonian boundary at Eastbourne (Sussex, UK): a proposed European reference section. Palaeogeography, Palaeoclimatology, Palaeoecology, 150, 1-2, 83-121.

Pederson, T.F. & Calvert, S. E. 1990: Anoxia vs. Producivty : what controls the formation of organic carbon-rich sediments and sedimentary rock ? Bulletin of the American Association of Petroleum geologists 74, 454-466.

Petters, S. W. 1980: Foraminiferal paleoecology of Nigerian late Cretaceous epeiric seas. Ann. Mus. Hist. Nat. 6, 82-133.

Philip, J. M. & Airaud-Crumiere, C. 1991: The demise of the rudistbearing carbonate platforms at the Cenomanian/Turonian boundary: a global control. Coral Reefs 10, 115–125.

Premoli-Silva, I., Erba, I., Salvini, G., Locatelli, C. & Verga, D. 1999: Biotic changes in Cretaceous oceanic anoxic events of the Tethys. Journal of

Foraminiferal research, 29, 352-370.

Sageman, B. B., Meyers, S. R. & Arthur, M. A. 2006: Orbital time scale and new C-isotope record for Cenomanian-Turonian boundary stratotype. Geology 34, 125-128.

Schlanger, S. O. & Jenkyns, H. C. 1976: Cretacous oceanic anoxic event : causes and consequences. Geologie en Mijnbouw 55, 179-188.

Schlanger S. O., Arthur M. A., Jenkyns H. C. & Scholle P.A. 1987: The Cenomanian-Turonian Oceanic Anoxic Event, I. Stratigraphy and distribution of organic carbon-rich beds and the marine d13C excursion. Geological Society, London, Special Publications 26; 371-399; doi: 10.1144/GSL. SP.1987.026.01.24

Schrag, D. P., Depaolo, D. J. & Richter, F. M. 1995: Reconstructing past sea surface temperatures: Correcting for diagenesis of bulk marine carbonate. Geochimica et Cosmochimica Acta 59, 2265-2278.

Snow, L. J., Duncan, R. A. & Bralower, T. J. 1995: Trace element abundances in the Rock Canyon Anticline, Pueblo, Colorado, marine sedimentary section and their relationship to Caribbean plateau construction and ocean anoxic event 2. Paleoceanography, 20, PA3005, doi:10.1029/2004PA001093.

Strasser, A., Caron, M. & Gjermeni, M. 2001: The Aptian, Albian and Cenomanian of Roter Sattel, Romandes Prealps, Switzerland: a high-resolution record of oceanographic changes. Cretaceous Research 22, 173-199.

Tribovillard, N., Algeo, T. J., Lyons, T. W. & Riboulleau, A. 2006: Trace metals as paleoredox and paleoproductivity proxies : An update. Chemical Geology 232, 12-32.

Tsikos, H., Jenkyns, H. C., Walsworth-Bell, B., Petrizzo, M. R., Forster, A., Kolonic, S., Erba, E., Premoli Silva, I., Baas, M., Wagner, T. & Sinninghe Damsté, J. S. 2004: Carbon-isotope stratigraphy recorded by the Cenomanian–Turonian Oceanic Anoxic Event: correlation and implications based on three key localities. Journal of the geological Society of London 161, 711-719.

Turgeon, S. & Brumsack, H.-J. 2006: Anoxic vs dysoxic events reflected in sediment geochemistry during the Cenomanian-Turonian Boundary Event (Cretaceous) in the Umbria-Marche Basin of central Italy. Chemical Geology 234, 321-339.

Van Cappellen, P. & Ingall, E. D. 1994: Benthic phosphorus regeneration, net primary production, and ocean anoxia: A model of the coupled marine biogeochemical cycles of carbon and phosphorus: Paleoceanography 9, 677-692.

Voigt, S., Aurag, A., Leis, F. & Kaplan, U. 2007: Late Cenomanian to Middle Turonian high-resolution carbon isotope stratigraphy: New data from the Münsterland Cretaceous Basin, Germany. Earth and Planetary Science Lettres 235, 1-2, 196-210, doi:10.1016/j.epsl.2006.10.026.

Voigt, S., Gale, A. S. & Voigt, T. 2006: Sea-level change, carbon cycling and palaeoclimate during the Late Cenomanian of northwest Europe; an integrated palaeoenvironmental analysis. Cretaceous Research 27, 6, 836-858, doi:10.1016/j.cretres.2006.04.005.

Voigt, S., Erbacher, J., Mutterlose, J., Weiss, W., Westerhold, T., Wiese, F., Wilmsen, M. & Wonik, T. 2008: The Cenomanian-Turonian of the Wunstorf section (North Germany): global stragraphic reference section and new orbital time scale for oceanic anoxic event 2. Newsletters on Stratigraphy, 43, 1, 65-89.

Wagreich, M., Bojar, A.-V., Sachsenhofer, R. F., Neuhuber, S. & Egger, H. 2008: Calcareous nannoplanktonic foraminiferal, and carbonate carbon isotope stratigraphy of the Cenomanian-Turonian boundary section in the Ultrahelvetic zone (Eastern Alps, Upper Austria). Cretaceous Research 29, 965-975, doi:10.1016/ j.cretres.2008.05.017.

CHAPTER F:
Conclusions and outlook

The Bonarelli level at Furlo, Italy

-F-

General Conclusions

This project has introduced a new angle to the debate surrounding the causes and consequences of Cretaceous oceanic anoxic events. Changes in the ocean redox state have been investigated during three major perturbations of the global carbon cycle and new data sets have been obtained both on the temporal and lateral evolution, as well as the intensity of redox conditions of OAEs. The findings of these studies are open to multiple interpretations. Regardless of the interpretations adopted, the research highlights can be summarized as followed. Please refer to each individual chapter for a more extensive conclusion on each point.

F.1 Main Conclusions

F.1.1 The Valanginian positive $\delta^{13}C$ excursion

The Valanginian $\delta^{13}C$ excursion, considered to represent the first OAE of the Cretaceous, is associated with organic-rich sediments in only a few localities. In the western Tethys, TOC contents and palynologic observations reveal characteristics of oxic pelagic settings. This has been confirmed by the absence of major excursions in the stratigraphic distribution of RSTE during the $\delta^{13}C$ shift. In the Vocontian Trough, only the “Barrande” layers show evidence for anoxia (laminations, higher TOC values, RSTE enrichments). These centimetric layers predate, however, the positive $\delta^{13}C$ positive excursion and appear to be related to regional rather than global redox variations. Published TOC data from other parts of the Valanginian ocean indicate that dys- to anaerobic zones were restricted to marginal seas of the opening Atlantic, the Southern Ocean and eventually also the Pacific. P and mineralogical contents suggest a stepwise climatic evolution during the Valanginian, with a humid and warm climate before the $\delta^{13}C$ shift, which has led to an increase in continental runoff. During the $\delta^{13}C$ shift, a decrease in detrital input and P contents suggests a climatic change toward more arid conditions.

F.1.2 The Early Aptian OAE 1a

The onset of the Early Aptian OAE 1a is marked by a general increase in P contents, which is followed by a rapid decrease suggesting an increase in nutrient input at the beginning of OAE 1a. The return to lower values during the anoxic event, associated with an increase in RSTE contents, may be related to the weakened capacity to retain P in the sedimentary reservoir due to bottom-water oxygen depletion. This general pattern is contrasted by the data from Gorgo a Cerbara, which also show higher P contents at the top of OAE interval. Along the studied transect, the different pattern in RSTE contents may be related to differences in their paleogeographic seting. In the basinal setting, the RSTE distribution indicates well-developed anoxic conditions during OAE 1a, whereas in the shallower-water environments, conditions were oxic to suboxic, rather than anoxic. Moreover, in the deeper part of the

Tethys, two distinct phases of RSTE enrichments and higher C:P ratios have been observed, which reveal at least two phases of anoxic conditions with intermittent return to more oxygenated conditions. These rapid changes in redox conditions may be related to a fluctuating OMZ and suggest that oceanic productivity has played a key role in bottom-water oxygen depletion during OAE 1a.

F.1.3 The end-Cenomanian OAE 2 in the Helvetic Realm

For the end-Cenomanian period, we investigated paleoceanographic and paleoenvironmental conditions during OAE 2 on the northern Tethyan margin. The Chrummflueschlucht section (E of Euthal, Ct Schwyz) provides a good opportunity to reconstruct the effects of OAE 2 in the hemipelagic environment of the Helvetic realm. The positive $\delta^{13}C$ excursion and the accompanying characteristic overturn in planktonic foraminifera are documented in high detail and show that this section corresponds to one of the most complete sections for the Cenomanian-Turonian boundary interval known from the Helvetic realm. Contrary to deeper-water, organic-rich, sections, RSTE contents at Chrummflueschlucht remain low throughout the section and appreciable RSTE enrichments have not been observed for the sedimentary interval corresponding to OAE 2. P contents display small variations along the section with a long-term decreasing trend towards the top. Superimposed on this trend, P values reach a maximum in sediments at the onset of the $\delta^{13}C$ positive excursion within the *R. cushmani* zone. This is coeval with the onset of the anoxic event. In the interval corresponding to OAE 2, P values remain low and show a small increase at the end of the positive shift in the $\delta^{13}C$ record. The evolution of P contents suggests an increase in the input of this nutrient at the onset of OAE 2. However, the trends in RSTE contents show that the Helvetic realm has not been affected by a strong depletion in oxygen conditions during OAE 2, despite its hemipelagic position.

F.1.4 Comparison of partial and total extraction methods used in RSTE analysis

A further goal of this project was to submit the samples to different types of acid attack and different methods in order to standardize the analytical processes. We submitted samples of the Early Aptian OAE to a method of total extraction (a combined $HF/HNO_3/HCl$ acid digestion) and compared the results with the data we obtained by the HNO_3 digestion. The RSTE contents and stratigraphic trends obtained by HNO_3 digestion for the sections of Gorgo a Cerbara and Glaise, which are characterized by euxinic to dysoxic conditions, are well correlated with the Al-normalized data obtained by the total extraction method. In Cassis/ La Bédoule, the correlation is less clear, likely because of the absence of RSTE enrichments along the section. These results suggest that partial digestion by HNO_3 viably trace all RSTE enrichment intervals within the OAE-1a sediments. The HNO_3 extraction method provides therefore a valuable alternative for accessing changes in paleoredox conditions in the OAE-1a related sediments. This is especially valid for RSTE, which precipitate in the sediment as an authigenic phase under anoxic conditions (U, V, Mo). Overall, the partial digestion method provides a good approximation of RSTE contents in the analysed OAE-1a-related sediments, especially if stratigraphic variations are evaluated.

F.2 New insights into the understanding of the global carbon cycle

The results of the investigation of paleoceanographic change during the three periods studied in this project point to similarities but also to differences between these events and lead to new insights in the comprehension of the dynamics of such perturbations of the global carbon cycle.

F.2.1 Changes in continental weathering and importance of the nutrient cycle

With this work, data of the studied sections point out the importance of terrestrial input as a triggering mechanism of perturbations in the global carbon cycle. For each studied time interval, the sections from the western Tethyan realm exhibit changes in detrital input and higher P contents at the onset of the positive $\delta^{13}C$ excursion. The observed trends in P accumulation show good agreement with the global phosphorus accumulation rate curve indicating a rather global signal (Föllmi, 1995; Föllmi et al., 2007). A period of elevated P accumulation during the start of the positive excursion of OAE 2 was already observed by Mort (2007). The increases in P supply are probably linked to changes in continental weathering, as is indicated by

the correlation between P accumulation and the detrital index observed in the Tethyan realm. These changes in nutrient availability are also coeval with changes in platform growth (Föllmi et al., 2007). Indeed, in the Early Cretaceous, the Helvetic carbonate platform passed through two different types of carbonate production: a photozoan mode characterized by the growth of patch reefs (presence of corals, green algae) and a rimmed morphology; and a heterozoan mode dominated by crinoidal biostromes, bivalves, echinoids and brachiopods and a ramp morphology, which was repeatedly interrupted by drowning episodes (Föllmi et al., 2007). The onset of each phase of heterozoan carbonate production is correlated with a major positive change in the isotopic carbon budget and an increase in oceanic P burial rates. These changes in nutrient supply are accompanied by enhanced primary productivity as is indicated by generally higher TOC values, even if for the Valanginian the increase in productivity is less well documented by organic-rich sediments. All these changes occurred before or just at the onset of the positive C-isotopic shift, the development of anoxic conditions and widespread black-shale deposition. As proposed by Robinson et al. (2004), an OAE may correspond to the final stage of global change, through which the ocean system went (and will go) through as a reaction to climatic and environmental perturbations of its “steady state”.

F.2.2 The role of oceanic anoxia in the global C cycle

The positive $\delta^{13}C$ excursions characterizing OAEs are commonly explained by an increase in oceanic primary productivity, which provides an enhanced sink of light ^{12}C by the accompanying increase in C_{org} burial. Understanding changes in primary productivity, the resulting anoxic conditions and their lateral and temporal persistence, and the role of anoxic conditions in amplifying organic carbon burial are all critical questions for our understanding of OAEs. The study of the evolution of redox conditions undertaken with this research project brought new insights in the comprehension of the development of anoxia and its influence on the oceanic $\delta^{13}C$ signature.

A first important finding of our research lies in the fact that we provide the first solid data base to prove that in the Tethyan realm, anoxic conditions have not been important during the Valanginian positive carbon-isotope excursion, and that black-shale deposition was limited during this time interval. Consequently, other mechanisms have to be involved to explain the shift towards heavier $\delta^{13}C$ values, such as increased C_{org} burial on continents or carbonate-platform drowning. Thus, the increase in $\delta^{13}C$ values during the Valanginian is not necessarily linked to the development of widespread anoxic conditions. Therefore, the new data suggests a re-evaluation of the contribution of sources and sinks in the global carbon cycle, which are different to those traditionally proposed. This highlights the need of a better quantification of the different carbon sources and sinks, and also of the establishment of numerical models of global carbon perturbations to better constrain to what extent changes in each source and/or sink may influence the carbon budget.

A second point of this work is the observation of variable intensities in anoxic conditions during OAEs as a function of the paleogeography. The data obtained on TOC, C_{org}/P_{tot} ratios and RSTE distributions show the presence of less severely reducing conditions in shallower parts of the ocean. For OAE 1a and OAE 2, which are characterized by a similar positive shift in C-isotopic values and considered as the two most important OAEs of the Cretaceous, sedimentary archives preserve characteristics of rather well oxygenated conditions in shallower parts of the ocean. On the other hand, in basinal settings, the temporal evolution of anoxia is characterized by several distinct phases of severe anoxic conditions, which are separated by phases during which a return to less reducing conditions occurred (chapter 4 and Turgeon & Brumsack, 2006). These results bring to the forefront new elements of response to the still ongoing controversy, in which two models for the origin and development of OAEs are opposed: a preservation-driven model, the stagnant-ocean model (e.g., Simons et al., 1998; Pancost et al., 2004) versus a productivity-driven model, the expanded oxygen-minimum-zone model (e.g., Jenkyns, 2003). The distribution of the anoxic areas and the rapid changes in redox conditions are rather in favour of a dynamic model in which both production and preservation play a crucial role. The onset of the anoxic event, characterized by the positive $\delta^{13}C$ shift, is driven by an increase in organic matter productivity. Then, the occurrence of anoxic/euxinic conditions occurs when the rate of organic matter production exceeds the rate in which it is oxidized. By increasing the degree of oxygen depletion in the water column, a switch toward a preservation-dominated

system may occur, which sustains organic matter burial even if the rates in primary production decrease (Robinson et al., 2004; Mort, 2007).

F.3 Outlook

Some questions still remain open at the end of this PhD thesis. Although the results obtained here help for better constrain changes in redox conditions during OAEs, it also calls for further studies. Some points may be considered.

Firstly, this work shows the necessity to obtain a precise stratigraphic framework for each section in order to better correlate changes in each carbon reservoir and obtain an estimation of the kinetics of change within them. This will also help to acquire quantifications for each reservoir and provide a good framework for the next step in our comprehension of OAEs: the numerical modelling of the global carbon cycle. Modelling change in the carbon cycle through anoxic events will give us the opportunity to better constrain the influence of change in each reservoir on the global carbon cycle and thus determine the threshold conditions at which the ocean system switches into an "OAE". This appears essential as we attempt to predict the impact of anthropogenic global change and associated climate change.

Another issue focuses on the triggering mechanisms. In fact, in this work, we highlight the importance of changes in nutrient delivery to the ocean, which is mainly due to increases in continental weathering linked to higher pCO_2 and global warming. Many authors showed the existence of positive relations between the formation of major large igneous provinces (LIPs) and the occurrences of OAEs (Courtillot & Renne, 2003; Jenkyns, 2003). Recently, Méhay et al. (2009) show that the negative spike in the $\delta^{13}C$ record preceding the early Aptian OAE 1a is related to the stepwise release of light volcanic carbon. However, despite the correlation between the stratigraphic position of LIPs and the positive $\delta^{13}C$ excursions, only one OAE is preceded by a negative peak. This leads to new questions: Why does a negative peak in $\delta^{13}C$ not precede all OAEs? Can the release of volcanogenic CO_2 occur without changing the atmospheric composition of $\delta^{13}C$?

Further, RSTEs provide a limited overview of redox conditions in that they indicate only the regional oxygenation state. In order to obtain an idea of the global extent of marine anoxia, RSTE abundances have to be investigated in different basins. At the other end of the scale, the perturbations of the carbon cycle that are characteristic of OAEs correspond to a global signal, as they are recorded worldwide with comparable amplitudes for each anoxic event. To better define the relationship between the onset and the duration of reducing conditions and the major perturbation of the carbon cycle, the next step would be to obtain a global view of the extent of marine anoxia during these anoxic events. Recently new proxies, such as molybdenum isotopes, have been developed in order to characterize global change in ocean chemistry (Anbar, 2004; Siebert et al., 2006; Anbar & Rouxel, 2007; Archer & Vance, 2008; Voegelin et al., 2009; Dahl et al., 2010).

References

Anbar, A. D. [2004] Molybdenum Stable Isotopes: Observations, Interpretations and Directions. Reviews in Mineralogy and Geochemistry, 55, 429-454.

Anbar, A. D. and Rouxel, O. [2007]. Metal stable isotopes in paleoceanography. Annual Review of Earth and Planetary sciences, 35, 717-746.

Archer, C. and Vance, D. [2008]. The isotopic signature of the global riverine molybdenum flux and anoxia in the ancient oceans. Nature Geoscience, 1, 597-600.

Courtillot, V. E. and Renne, P. R. [2003]. On the ages of flood basalt events. Comptes Rendus Geosciences, 335, 113-140.

Dahl, T. W., Anbar, A. D., Gordon, G. W., Rosing, M. T., Frei, R. and Canfield, D. E. [2010]. The behavior of molybdenum and its isotopes across the chemocline and in the sediments of sulfidic lake Cadagno, Switzerland. Geochimica et Cosmochimica Acta, 74, 144-163.

Föllmi, K., Bodin, S., Godet, A., Linder, P. and Van de Schootbrugge, B. [2007]. Unlocking paleo-environmental information from Early Cretaceous shelf sediments in the Helvetic Alps: stratigraphy is the key! Swiss journal of geosciences, 100, 349-369.

Föllmi, K. B. [1995]. 160 m.y. record of marine sedimentary phosphorus burial : Coupling of climate and contiental wearthering under greenhouse and icehouse conditions. Geology, 23, 859-862.

Jenkyns, H. C. [2003]. Evidence for rapid climate change

in the Mesozoic-Palaeogene greenhouse world. Phil. Trans. R. Soc. Lond., A 361, 1885-1916.

Méhay, S., Keller, C. E., M., B. S., Weissert, H., Erba, E., Bottini, C. and Hochuli, P. A. [2009]. A volcanic CO_2 pulse triggered the Cretaceous Oceanic Anoxic Event 1a and a biocalcification crisis Geology, 37, 819-822.

Mort, H. [2007]. Biogeochemical Changes during the Cenomanian-Turonian Oceanic Anoxic Event (OAE 2).

Mort, M., Adatte, T., Föllmi, K. B., Keller, G., Steinmann, P., Matera, V., Berner, Z. and Stüben, D. [2007] Phosphorus and the roles of productivity and nutrient recycling during oceanic event 2. Geology, 35, 483-486.

Pancost, R. D., Crawford, N., Magness, S., Turner, A., Jenkyns, H. C. and Maxwell, J. R. [2004]. Further evidence for the development of photic-zone euxinic conditions during mesozoic oceanic anoxic events. Jounal of the geological Society of London, 161, 353-364.

Robinson, S. A., Williams, T. and Bown, P. R. [2004]. Fluctuations in biosiliceous production and the generation of Early Cretaceous oceanic anoxic events in the Pacific Ocean (Shatsky Rise, Ocean Drilling Program Leg 198). Paleoceanography, 19, PA4024, doi:10.1029/2004PA001010.

Siebert, C., McManus, J., Bice, A., Poulson, R. L. and Berelson, W. M. [2006]. Molybdenum isotope signatures in continental margin marine sediments. Earth and Planetary Science Letters, 241, 723-733.

Simons, D. J. H. & Kenig, F., [1998]. Photic zone anoxia in the Cenomanian-Turonian of the western Interior Seaway, USA. Geological Society of America, Annual Meeting, 1998 Abstract Volume, 30/7, 220.

Turgeon, S. and Brumsack, H.-J. [2006]. Anoxic vs dysoxic events reflected in sediment geochemistry during the Cenomanian-Turonian Boundary Event (Cretaceous) in the Umbria-Marche Basin of central Italy. Chemical Geology, 234, 321-339.

Voegelin, A. R., Nägler, T. F., Samankassou, E. and Villa, I. M. [2009]. Molybdenum isotopic composition of modern and Carboniferous carbonates. Chemical Geology, 265, 488-498.

CHAPTER G:

Appendix 1: Affiliated paper

View from the Pilatus, Switzerland

-G-

Early Cretaceous (late Berriasian to early Aptian) Palaeoceanographic Change along the Northwestern Tethys Margin (Vocontiona Trough, southestern France): $\delta^{13}C$, $\delta^{18}O$ and Sr-isotope Belemnite and Whole-rock Records

Stéphane Bodin[1, 2], Nicolas Fiet[3], Alexis Godet[1,4], Virginie Matera[1], Stéphane Westermann[1, 8], Arnaud Clément[5], Nico M.M. Janssen[6], Peter Stille[7], Karl B. Föllmi[1, 8]

[1]Institut de Géologie et d'Hydrogeéologie, Université de Neuchâtel, Rue Emile Argand 11, CP 158, 2009 Neuchâtel, Switzerland

[2]North Africa Research Group, School of Earth, Atmospheric and Environmental Sciences, University of Manchester, Williamson Building, Oxford Road, Manchester, M13 9PL, United Kingdom

[3]UMR 8148–I.D.E.S., Baˆt. 504, University of Paris XI Orsay, 91405 Orsay Cedex, France

[4]Neftex Petroleum Consultants Ltd, 115BD Milton Park, Abingdon, OX14 4SA, United Kingdom

[5]5b rue de Camargue, la Cigalière, 05000 Gap, France

[6]Geertekerkhof 14bis, 3511XC Utrecht, The Netherlands

[7]EOST-Centre de Géochimie de la Surface, CNRS-UMR 7517, Université Louis Pasteur, 67084 Strasbourg, France

[8]Institut de Géologie et Paléontologie, Faculté des Géosciences et de l'Environnement, Université de Lausanne, Quartier UNIL-Dorigny, Baˆtiment Anthropole 4171, 1015 Lausanne, Switzerland

Published in Cretaceous Research, 2009, volume 30, pages 1247-1262.

Abstract

Stable carbon, oxygen, and strontium isotope records were obtained from uppermost Hauterivian to lowermost Aptian belemnite rostra, which were collected in well-dated sections from the Vocontian Trough (southeastern France). This data set complements previously published belemnite-isotope records from the uppermost Berriasian-Hauterivian interval from the same basin. The belemnite carbon and oxygen isotope record is compared to the carbonate bulk-rock isotope record from the same sections, and from additional Italian sections. With regards to their long-term trends, both belemnite and wholerock $\delta^{18}O$ records are well correlated, except for the uppermost Hauterivian-lower Barremian interval, within which they deviate. This discrepancy is interpreted to be linked to the latest Hauterivian Faraoni oceanic anoxic event and its early Barremian aftermath. The Faraoni level is characterized by enhanced sea-water stratification, probably induced by the onset of a warmer and more humid climate along the northern Tethyan margin. The early Barremian was characterized by stronger vertical sea-water mixing reflected by a decrease in density contrast between sea-surface and deeper waters. The belemnite oxygen isotope record shows a more stable evolution with smaller fluctuations than its bulk-rock counterpart, which indicates that deeper water masses were not as much subjected to density fluctuations as seasurface water. The comparison of belemnite and bulk-rock carbon isotope records allows observing the impact of regional influence exerted by platform carbonate ooze shedding on the carbon cycle. Discrepancies in the two records are observed during time of photozoan carbonate platform growth. The strontium isotopic record shows a gradual

increase from the uppermost Berriasian to the uppermost lower Barremian followed by a rapid decrease until the uppermost Barremian and a renewed small increase within the lowermost Aptian. The major inflection point in the uppermost lower Barremian appears to predate the onset in the formation of the Ontong-Java volcanic plateau.

Keywords: Belemnites, Carbon stable isotopes, Oxygen stable isotopes, Strontium isotopes, Early Cretaceous, Faraoni oceanic anoxic event.

G.1 Introduction

The Early Cretaceous witnessed numerous episodes of palaeoceanographic and palaeoenvironmental change, which are, for instance, documented by the Valanginian positive shift in the stable carbon-isotope record (e.g. Lini et al., 1992; Weissert et al., 1998; Erba et al., 2004; Duchamp-Alphonse et al., 2007), the latest Hauterivian Faraoni oceanic anoxic event (e.g. Baudin, 2005; Bodin et al., 2006a, 2007), or the onset and development of the Urgonian photozoan carbonate platform along the northern Tethyan margin during the late Barremian-earliest Aptian (e.g. Arnaud et al., 1998; Bodin et al., 2006b, 2006c; Fo¨ llmi et al., 2006, 2007). All these episodes are linked to important changes in ocean chemistry, nutrient stocks, and temperature, and it is therefore important to improve our knowledge on these very aspects within this interval. One aspect, which is still discussed is the importance of water stratification and coupled with that the capacity of ocean waters to mix and vertically exchange (e.g. Hay, 2002; Friedrich et al., 2008). We therefore performed stable carbon- and oxygen-isotope analyses on well-preserved belemnite rostra from the Vocontian Basin (SE France), in order to obtain a deeper-water signal, and compared our records to whole-rock carbonate records from the same region– which are considered as a near surface-water signal.

Belemnite isotopic proxies approach within the Lower Cretaceous has revealed itself as a valuable tool, which helps to improve our understanding of oceanic water-column characteristics and palaeoceanographic conditions in general (e.g. Van de Schootbrugge et al., 2000; McArthur et al., 2004, 2007b, Mutterlose et al., 2009). Comparison of sea surface to deep-water carbon and oxygen isotopic signals has been performed by numerous studies within the Upper Cretaceous-Cenozoic interval using benthic and pelagic foraminifera. This method has given valuable palaeoceanographic information on various subjects such as, for example, methane hydrate instability during the Holocene (Kennett et al., 2000), upwelling intensity in the Arabian Sea during the latest Neogene (Naidu, 2004), palaeoproductivity across the Cretaceous-Tertiary boundary (Stott and Kennett, 1989), or the influence on warm saline deep water on the Cenomanian-Turonian oceanic anoxic event (Friedrich et al., 2008).

Furthermore, we systematically analyzed the belemnites for their strontium-isotope signals, in order to establish a high-resolution record, which is well calibrated against Tethyan ammonite biostratigraphy. The strontium-isotope record is informative with regards to the relative importance of volcanic episodes versus continental runoff (e.g. Hodell et al., 1991; Jones et al., 1994, McArthur et al., 2004).

G.2 Material

The geochemical results used here are derived from our own investigations and from previously published studies on hemipelagic sections from the Vocontian Trough (SE France; Fig. G1.1). Additional bulk rock isotope data were gathered from Emmanuel and Renard (1993), Duchamp-Alphonse et al. 2007), Van de Schootbrugge et al. (2000), Godet et al. (2006) and Wissler et al. (2002) for the uppermost Berriasian, Valanginian-lowermost Hauterivian, Hauterivian, upper Hauterivian-Barremian, and Barremian, respectively. Additional belemnite isotope data were compiled from McArthur et al. (2007b) and Van de Schootbrugge et al. (2000) for the uppermost Berriasian-upper Hauterivian and Valanginian-Hauterivian, respectively.

70 belemnites were collected in uppermost Hauterivian to lowermost Aptian sedimentary rocks of the Vocontian Trough (see Table G.1 for a detailed list of sampled belemnites). 64 new belemnite results presented here stem from the Angles section, which is the stratotype section for the Barremian stage (e.g. Vermeulen, 2002) and is situated near St. André -les-Alpes (see Bodin et al., 2006a, for a more precise location). Additional

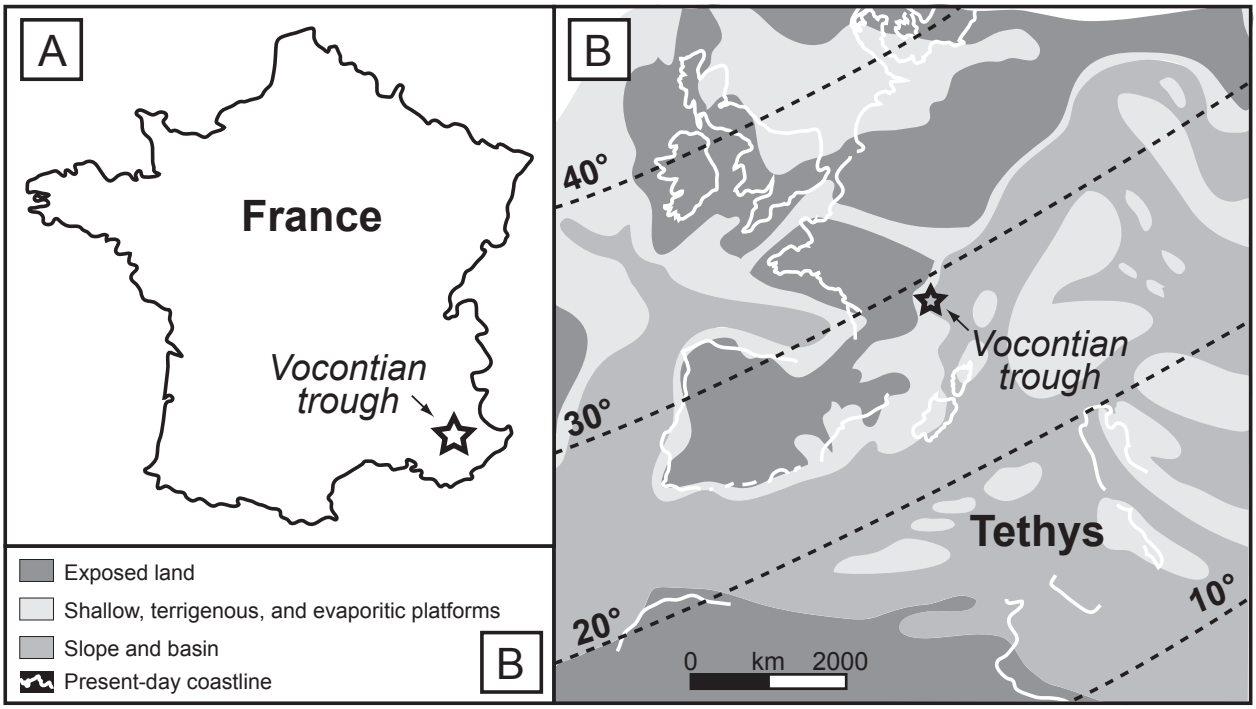

Fig. G.1: A, Map of France showing the actual position of the Vocontian Trough. B, Early Aptian paleomap of the western Tethyan realm showing the original location of the Vocontian Trough (after Masse et al., 1993b).

results were obtained from other sections, close to Angles (Saut-du-Loup, Clos de Barral, and Combe Lambert; Delanoy, 1998; Vermeulen, 2002). These additional sections provided the possibility to sample specific horizons, which correlate to levels which in the Angles section are presently not well exposed or barren in belemnites.

During the Early Cretaceous, the Vocontian Trough was surrounded to the north, west, and south by the northern Tethyan carbonate platform and open in an eastward direction to the Tethys (Masse, 1993). It was situated at a palaeolatitude of 20-30° N, in the northwestern part of the Tethys.

The sections of the Vocontian basin sampled here are composed of hemipelagic marl-limestone alternations, which are well dated by ammonite biostratigraphy (e.g. Bulot et al., 1992; Bulot and Thieuloy, 1994; Delanoy, 1998; Vermeulen, 2002; Duchamp-Alphonse et al., 2007).

G.3 Methods

The procedure for belemnite sample preparation used here follows the one described by McArthur et al. (2007b). Belemnites were first cleaned in an ultrasonic bath, and consequently the exterior layer, the apical region, and the alveolus were removed. The remains were cleaned in a 10% HCl solution for one minute, dried and crushed into small pieces of approximately 1 mm diameter, which were once again cleaned within a sieve with a 10 % HCl solution and ultra-pure water. After drying, non-opaque pieces, showing growth bands, were selected by hand picking. Final powders were obtained by hand crushing in an agate mortar.

In order to complete our carbonate bulk-rock record for the lowermost Aptian in the Vocontian Trough, we also measured the Combe-Lambert section in detail (see Delanoy, 1998, for sedimentological and biostratigraphical aspects of this section). We sampled each separate limestone bed and, where appropriate, intervening marl levels (Fig. G1.2). The carbonate samples were cut with a circular saw in order to eliminate weathered surfaces and recrystallised areas or veins. Rock powder was obtained by using a mechanic agate crusher.

$\delta^{18}O$ and $\delta^{13}C$ ratios from belemnites and bulk rock were analyzed at the Stable Isotope Laboratory of the Hydrology department (UMR 8148-IDES), University of Paris Sud (Orsay, France), using a VG SIRA 10 triple collector instrument. The powdered carbonate samples were reacted with anhydrous orthophosphoric acid at 25°C. Using internal carbonate standards, the reference material NBS 19 as well as replicate analyses of samples, the reproducibility of C and O analyses was better than ± 0.05 ‰ and ± 0.08 ‰, respectively

Stage	Sample N°	Specimen type	Ammonite zone	$\delta^{13}C$ *VPDB (‰)*	$\delta^{18}O$ *VPDB (‰)*	Mg *(ppm)*	Mn *(ppm)*	Fe *(ppm)*	Ca *(%)*	Sr *(ppm)*	Mg/Ca *(mmol/mol)*	Sr/Ca *(mmol/mol)*
Hauterivian	AN 1b	*Hibolithes sp.*	*B. balearis*	0.04	-0.26	3379	1.40	343	39.58	1317	14.07	1.52
Hauterivian	AN 2b	*Hibolithes sp.*	*B. balearis*	0.28	-0.42	3647	1.29	350	40.02	1386	15.03	1.58
Hauterivian	AN 7b	*Hibolithes sp.*	*B. balearis*	0.42	-0.40	3301	1.15	310	39.01	1387	13.96	1.63
Hauterivian	AN 18b	*Hibolithes sp.*	*B. balearis*	0.06	-0.02	2830	0.82	305	37.94	1319	12.30	1.59
Hauterivian	AN 22b	*Hibolithes sp.*	*B. balearis*	0.39	-0.39	2930	1.72	310	36.28	1266	13.32	1.60
Hauterivian	AN 37b	*Hibolithes sp.*	*S. angulicostatum*	0.37	-0.56	3379	10.66	322	36.79	1101	15.15	1.37
Hauterivian	AN 41 b	*Hibolithes gr. subfusiformis*	*S. angulicostatum*	0.12	-0.15	3151	1.93	212	35.82	1283	14.51	1.64
Hauterivian	AN 43b	*Hibolithes gr. subfusiformis*	*S. angulicostatum*	0.32	-0.24	3018	0.89	142	36.65	1386	13.58	1.73
Hauterivian	AN 43b bis	*Hibolithes gr. subfusiformis*	*S. angulicostatum*	-0.42	-0.20	3076	7.42	306	36.15	1195	14.03	1.51
Hauterivian	AN 53.2b	*Hibolithes gr. subfusiformis*	*S. angulicostatum*	0.09	-0.03	3213	2.15	150	37.87	1334	13.99	1.61
Hauterivian	AN 54.1b	*Hibolithes sp.*	*P. mortilleti*	0.09	0.08	3304	1.64	189	35.83	1358	15.21	1.73
Hauterivian	AN 54.2b	*Hibolithes sp.*	*P. mortilleti*	0.80	-0.23	3298	17.13	187	32.24	1058	16.86	1.50
Hauterivian	AN 71b	*Hibolithes sp.*	*P. mortilleti*	0.18	-0.48	3459	2.26	177	39.00	1348	14.63	1.58
Barremian	AN 73b	*Hibolithes sp.*	*A. kiliani*	0.52	-0.04	2379	1.19	297	37.15	1217	10.56	1.50
Barremian	AN 74b	*Hibolithes sp.*	*A. kiliani*	0.40	-0.28	3451	1.99	217	38.93	1410	14.62	1.66
Barremian	AN 75b	*Hibolithes gr. jaculiformis*	*A. kiliani*	0.40	-0.21	2877	0.89	184	33.78	1246	14.04	1.69
Barremian	AN 76b	*Hibolithes sp.*	*A. kiliani*	0.46	-0.75	3493	4.31	316	36.48	1249	15.79	1.57
Barremian	AN 77b	*Hibolithes sp.*	*A. kiliani*	0.54	-0.23	3231	0.96	283	35.31	1286	15.09	1.67
Barremian	AN 77.2b	*Hibolithes sp.*	*A. kiliani*	0.38	-0.22	3270	6.85	196	38.22	1262	14.11	1.51
Barremian	AN 78b	*Hibolithes sp.*	*A. kiliani*	0.35	-0.44	4025	1.84	175	40.53	1440	16.38	1.63
Barremian	AN 79b	*Hibolithes sp.*	*A. kiliani*	0.28	-0.50	3387	1.83	190	40.38	1339	13.83	1.52
Barremian	AN 80b	*Hibolithes sp.*	*A. kiliani*	0.31	-0.29	3391	1.36	155	38.62	1332	14.48	1.58
Barremian	AN 84b	*Hibolithes sp.*	*A. kiliani*	-0.04	-0.33	3209	1.27	167	38.66	1327	13.69	1.57
Barremian	AN 85b	*Hibolithes sp.*	*A. kiliani*	0.41	-0.51	3870	1.65	179	39.23	1412	16.27	1.65
Barremian	AN 87b	*Hibolithes sp.*	*A. kiliani*	0.02	-0.63	3334	3.88	201	39.02	1446	14.09	1.70
Barremian	AN 88b	*Hibolithes sp.*	*A. kiliani*	0.50	-0.55	3762	6.85	230	39.03	1410	15.89	1.65
Barremian	AN 89b	*Hibolithes sp.*	*A. kiliani*	0.18	-0.39	2490	8.71	197	38.79	1215	10.59	1.43
Barremian	AN 92b	*Hibolithes sp.*	*A. kiliani*	0.43	-0.34	3807	9.20	183	37.59	1392	16.70	1.69
Barremian	AN 94b	*Hibolithes sp.*	*K. nicklesi*	0.70	-0.50	3539	2.01	119	37.88	1308	15.41	1.58
Barremian	AN 102b	*Hibolithes sp.*	*K. nicklesi*	0.46	-0.68	2526	1.87	241	40.40	1217	10.31	1.38
Barremian	AN 103b	*Hibolithes sp.*	*K. nicklesi*	0.60	-0.44	3239	1.54	249	41.46	1492	12.88	1.65
Barremian	AN 103 b2	*Hibolithes sp.*	*K. nicklesi*	0.10	-0.53	3788	1.45	177	38.08	1485	16.40	1.78
Barremian	AN 104b	*Hibolithes sp.*	*K. nicklesi*	0.52	-0.78	3301	1.49	222	38.68	1371	14.07	1.62
Barremian	AN 110.1b	*"Mesohibolites" sp.*	*N. pulchella*	0.38	-0.70	3147	1.77	189	37.16	1255	13.96	1.54
Barremian	AN 110.4b	*Hibolithes gr. jaculiformis*	*N. pulchella*	0.55	-0.40	4023	1.53	150	35.38	1199	18.75	1.55
Barremian	AN 111.1b	Unspecified	*N. pulchella*	-0.34	-1.28	4082	22.54	230	40.36	1409	16.68	1.60
Barremian	AN 111.4b	*"Mesohibolites" sp.*	*N. pulchella*	0.69	-0.52	3042	1.82	202	32.54	1068	15.42	1.50
Barremian	AN 112	Unspecified	*N. pulchella*	0.17	-1.64	4233	6.08	252	40.68	1340	17.16	1.51
Barremian	AN 112.7b	*"Mesohibolites" sp.*	*K. compressissima*	0.53	-0.35	2963	10.20	257	35.93	1239	13.60	1.58
Barremian	AN 119b	Unspecified	*K. compressissima*	0.61	-2.68	3257	26.36	304	41.18	1308	13.04	1.45
Barremian	AN 121b	*"Mesohibolithes" sp.*	*K. compressissima*	-0.31	-0.71	4144	23.58	237	40.64	1395	16.82	1.57
Barremian	AN 125	*Duvalia sp. ?*	*C. darsi*	-0.29	-0.34	3287	10.53	226	43.36	1304	12.50	1.38
Barremian	AN 125b	Unspecified	*C. darsi*	0.65	-0.26	4203	1.40	236	41.50	1404	16.70	1.55
Barremian	AN 136b	*"Mesohibolites" sp.*	*C. darsi*	-0.08	-0.31	4208	3.09	218	41.75	1415	16.62	1.55
Barremian	AN 139.1	*Mesohibolitidae indet.*	*C. darsi*	0.11	-0.60	3023	3.92	286	33.94	1401	14.69	1.89
Barremian	AN 143b	*"Mesohibolites" gr. minaret*	*H. uhligi*	1.96	-2.41	2354	83.03	1105	38.44	1005	10.10	1.20
Barremian	AN 144b	*Duvalia sp. ?*	*H. uhligi*	0.31	-0.19	4943	2.11	170	42.14	1498	19.34	1.63
Barremian	AN 151.3b	*Mesohibolites sp.*	*H. sayni*	0.37	-0.54	3608	7.52	260	39.65	1290	15.00	1.49
Barremian	AN 155.2b	*Mesohibolites sp.*	*H. sayni*	-0.55	-0.85	4047	19.77	356	40.43	1283	16.50	1.45
Barremian	AN 158	Unspecified	*H. sayni*	0.44	-0.27	3386	3.62	209	37.02	1185	15.08	1.46
Barremian	AN 158b	*Mesohibolites sp.*	*H. sayni*	1.07	-0.62	3348	2.85	254	40.39	1344	13.67	1.52
Barremian	AN 160.3b	*Mesohibolites sp.*	*G. sartousiana*	0.53	-0.59	4340	27.08	191	39.49	1213	18.12	1.40
Barremian	AN 161.1b	*Mesohibolites sp.*	*G. sartousiana*	0.61	-0.70	3737	7.92	178	40.00	1408	15.41	1.61
Barremian	AN 161.2b	*Mesohibolites sp.*	*G. sartousiana*	1.23	-0.26	3139	2.65	185	40.35	1258	12.83	1.43
Barremian	AN 161.3b	*Mesohibolites sp.*	*G. sartousiana*	0.17	-0.53	3512	3.51	162	40.76	1319	14.21	1.48
Barremian	AN 161.3b	Unspecified	*G. sartousiana*	1.24	-0.24	3407	0.78	220	43.10	1434	13.03	1.52
Barremian	AN 162b	*Mesohibolites sp.*	*G. sartousiana*	0.44	-0.32	3337	4.23	170	40.32	1341	13.65	1.52
Barremian	AN 165b	*Mesohibolites sp.*	*H. feraudianus*	1.69	-0.41	3486	0.77	145	39.40	1402	14.59	1.63
Barremian	AN 165b bis	*Mesohibolites sp.*	*H. feraudianus*	1.66	-0.51	3413	2.57	241	40.44	1445	13.91	1.63
Barremian	AN 165b ter	*Mesohibolites sp.*	*H. feraudianus*	1.32	-0.62	4294	31.41	308	43.12	1591	16.42	1.69
Barremian	AN 172.2b	*Neohibolites sp.*	*I. giraudi*	0.72	0.02	1879	2.53	271	41.03	1191	7.55	1.33
Barremian	AN 173b	*Neohibolites sp.*	*I. giraudi*	1.29	-0.58	2378	49.73	519	43.71	1232	8.97	1.29
Barremian	AN 185b	*Mesohibolites sp. (imm.)*	*M. sarasini*	1.52	-1.80	2133	1.92	269	34.44	1072	10.21	1.42
Aptian	AN 202	*Mesohibolites sp.*	*D. oglanlensis*	-0.19	-0.67	2764	1.84	177	33.50	1129	13.61	1.54
Barremian	SDL 362b	*Neohibolites sp.*	*I. giraudi*	1.28	-0.23	2006	2.50	233	41.77	1236	7.92	1.35
Barremian	SDL 365	*Mesohibolites sp.*	*I. giraudi*	1.97	-1.83	2504	13.63	355	36.34	1086	11.36	1.37
Barremian	SDL 366b	*Mesohibolites sp.*	*I. giraudi*	1.24	-0.31	3492	15.82	263	41.78	1351	13.79	1.48
Barremian	SDL 373b	*Mesohibolites sp.*	*M. sarasini*	-0.11	-0.65	3419	2.01	250	41.58	1432	13.56	1.58
Aptian	COM 109b	*Mesohibolites sp.*	*D. weissi*	0.93	-0.74	4144	16.39	274	39.96	1448	17.10	1.66
Barremian	CB 134.4b	*"Mesohibolites" sp.*	*N. pulchella*	-0.10	-0.49	3682	1.36	189	40.69	1414	14.92	1.59

Table G.1: Isotopic and chemical data for belemnites from uppermost Hauterivian to Barremian strata of the Vocontian Trough. Most belemnites were collected in the Angles section. The sample number corresponds to the official bed numbering adopted in this section (cf. Vermeulen, 2002). The grey band highlights belemnites that are considered to be diagenetically altered and were therefore not used in the discussion (see text for more details).

Abbreviation to section numbering: AN: Angles; SDL: Saut-du-Loup; COM: Combe-Lambert; CB: Clos de Barral.

(Fig. G.3).

Mg, Sr, Mn, Fe, and Ca concentrations in belemnites were analyzed using the quadrupole ICP-MS (Elan 6100, Perkin Elmer) of the Geological Institute, University of Neuchâtel. A portion of approximately 25 mg was transferred into an Eppendorf tube and 10 ml 0.6 M nitric acid (suprapur, Merck) was added. A 1/10 dilution was then performed prior to analysis. See Bodin et al. (2007) for a more detailed analytical procedure. In order to compare the belemnite and bulk-rock carbon and oxygen stable-isotope records, a mean value of $\delta^{13}C$ and $\delta^{18}O$ was calculated for each ammonite zone (or subzone where relevant). The difference between the mean belemnite and bulk-rock values per ammonite zone is expressed in $\Delta\delta^{13}C$ and $\Delta\delta^{18}O$.

Strontium-isotope analyses were performed on 26

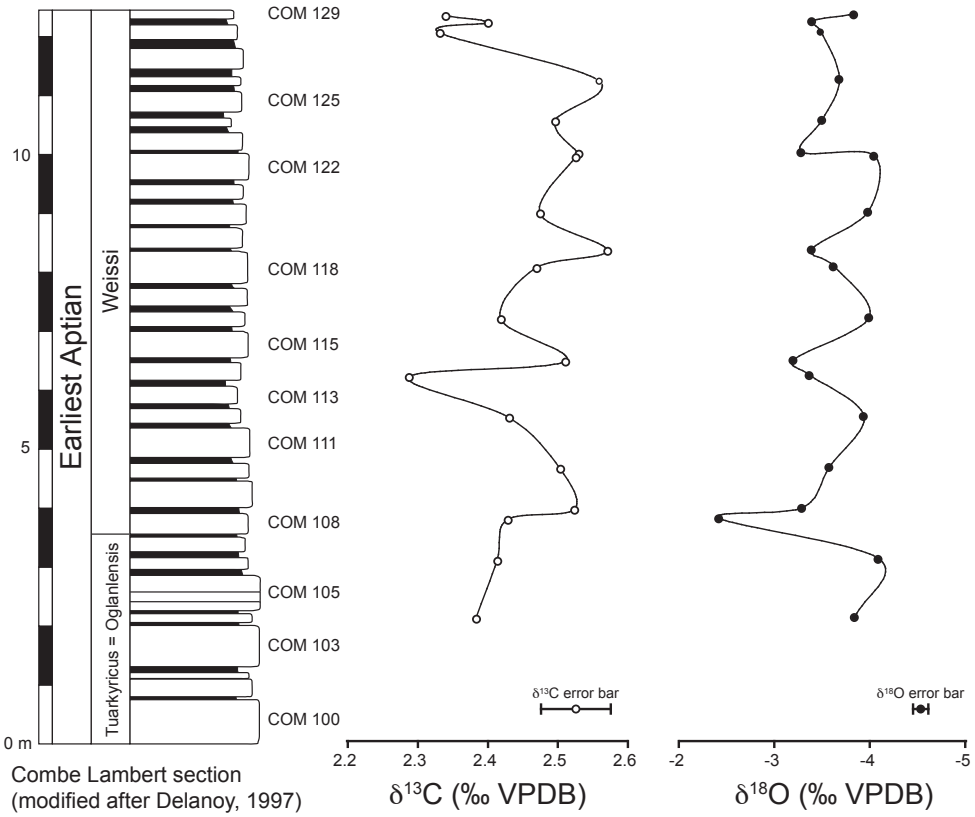

Fig. G.2: Basal part of the Combe-Lambert section (drawn after Delanoy, 1998). Isotopic results of carbonate bulk-rock analyses expressed in VPDB.

selected belemnites at the Centre de Géochimie de la Surface (CNRS) in Strasbourg (France). The procedure used is similar to the one described by Stille et al. (1994). Powdered samples were treated with 0.5 M acetic acid in order to remove Sr-rich calcite overgrowths and rinsed with distilled water prior to dissolution in 6 N HCl. Chemical separations were performed using ammonium citrate and 4.0 and 6.0 M HCl as eluent through AG 50W-X12 (200-400) ion exchange resin in 1 ml quartz columns for Sr and bulk rare-earth element separation. The blank at the time of analysis was < 1 ng for Sr. Sr was measured using triple Re filament assemblies and single oxidized Ta filaments. Sr isotope measurements were performed on a fully automatic VG Sector mass spectrometer with a 6 cups multicollector. The ratio $^{86}Sr/^{88}Sr = 0.1194$ was used for fractionation correction. Within the measuring interval, the NBS 987 Sr standard yielded $^{86}Sr/^{88}Sr = 0.710258\pm5$ (±S.D., n=9). 80-100 ratios for Sr were collected to achieve adequate precision.

G.4 Results

G.4.1 Carbon isotopes

The belemnite carbon isotope ($\delta^{13}C_{bel}$) record obtained here shows a twofold division in the overall trend (Table G.1 and Figs. G.3-G.4). From the *B. balearis* to the *H. sayni* ammonite zones, the $\delta^{13}C_{bel}$ values are relatively stable and vary between 0 and 0.5 ‰. A subsequent positive shift is observed in belemnites of the *H. feraudianus* ammonite zone with values rising to approximately 1.6 ‰, which is followed by a decrease to a level of approximately - 0.2 ‰ in belemnites of the *D. oglanlensis* ammonite zone. Finally the $\delta^{13}C_{bel}$ record increases again in belemnites of the lowermost Aptian toward the *D. weissi* ammonite zone. The $\delta^{13}C_{bel}$ value in the *H. feraudianus* zone is the maximum value recorded in belemnites for the entire Valanginian to Barremian interval in the Vocontian Trough. Moreover, there is a very good continuity of $\delta^{13}C_{bel}$ values between this study and the results of van de Schootbrugge et al. (2000) and McArthur et al. (2007b). The compilation of belemnite and bulk-rock data from the uppermost Berriasian to the lowermost Aptian shows that the long-term $\delta^{13}C$ trends are

well comparable (Fig. G.4). Belemnite carbon-isotope values are, however, always lower than those for bulk rock.

$\Delta\delta^{13}C$ values corresponding to the absolute difference between mean $\delta^{13}C_{bulk}$ and $\delta^{13}C_{bel}$ values per ammonite zone show a well-contrasted trend within the uppermost

Berriasian – lowermost Aptian interval. A first important positive shift, reaching 2.6 ‰, is recorded in the *S. boissieri* zone. It is followed by a negative shift at the Berriasian-Valanginian transition and a plateau (ca. 1.8 ‰) within the lower Valanginian. The upper Valanginian is characterized by a decreasing trend reaching approximately 1.2 ‰ in the *T. callidiscus* zone. Less pronounced positive shifts (with an amplitude of 0.2 to 0.8 ‰) are also recorded around the *A. radiatus*, in the *P. ligatus*, in the *S. angulicostatum*, in the *N. pulchella* and around the *H. sayni* zones. The *H. feraudianus* zone is characterized by a distinct negative shift reaching approximately 0.5 ‰. Finally a positive shift reaching approximately 2.5 ‰ is recorded in the *D. oglanlensis* zone and is followed by a negative shift within the *D. weissi* zone.

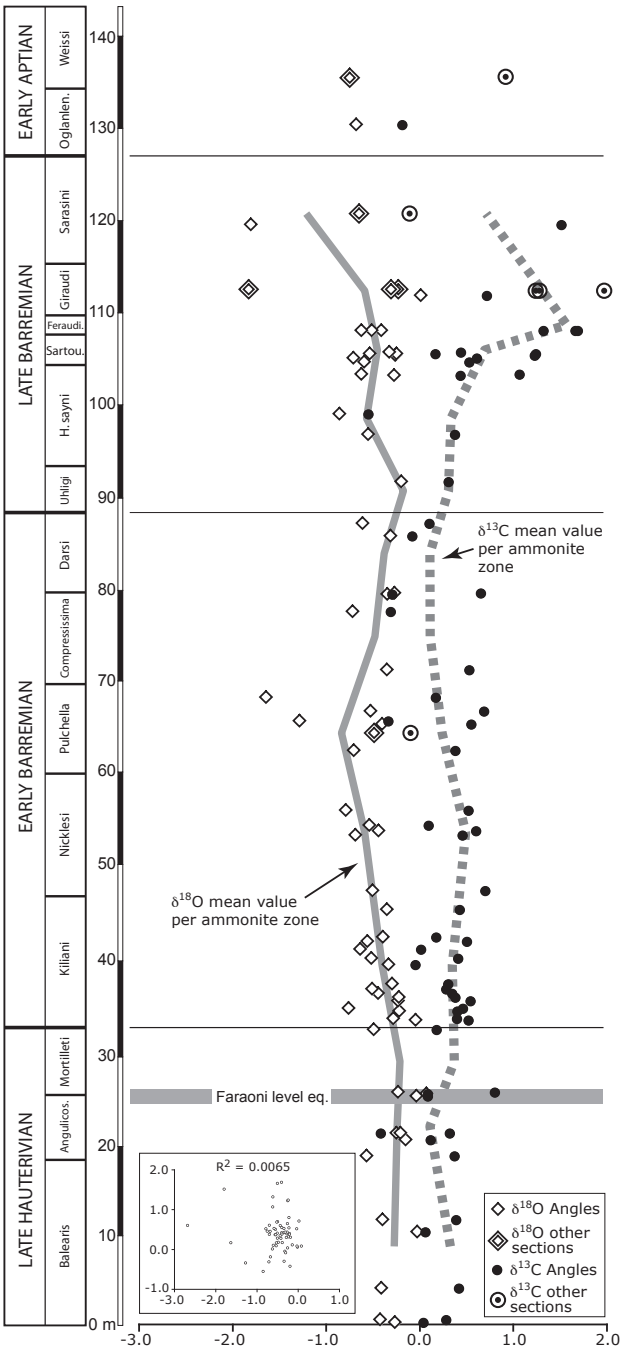

Fig. G.3: Raw data of the belemnite $\delta^{13}C$ and $\delta^{18}O$ records. Note that no correlation is observed between these two proxies. For both carbon and oxygen isotope records, a mean value is calculated per ammonite zone from all data resulting from this study, except within the lower Aptian, where only one belemnite has been collected in each of the two ammonite zones.

G.4.2 Oxygen isotopes

With regards to their oxygen isotope values ($\delta^{18}O_{bel}$), the belemnites from this study (Table G.1 and Figs. G.3, G.5) show a stable trend of around -0.3 ‰ within the uppermost Hauterivian, which is followed by a progressive decrease and a minimum of -0.85 ‰ reached in the *N. pulchella* zone. In belemnites from the *K. compressissima* to the *H. uhligi* zone, $\delta^{18}O_{bel}$ values are again increasing, reaching -0.2 ‰. This trend is calculated by excluding diagenetically altered belemnite and the belemnite sample AN 119b, which shows a highly negative oxygen isotope (see discussion). A second negative shift is documented within the *M. sarasini* zone (-1.2 ‰). As for the $\delta^{13}C$ results, there is a very good continuity of $\delta^{18}O_{bel}$ values between the here-presented results and the data presented by van de Schootbrugge et al. (2000) and McArthur et al. (2007b). Moreover, McArthur et al. (2004) also noted a

negative shift in the $\delta^{18}O_{bel}$ record of the upper lower Barremian of Speeton (England, Boreal realm, Fig. G.6). As shown in Fig. G.7, no correlation is observed between $\delta^{18}O$ and $\delta^{13}C$ values in belemnite rostra for *Hibolithes* and *Mesohibolites* genera (see discussion). The compilation of $\delta^{18}O$ belemnite and bulk-rock records shows a good correlation for the uppermost Berriasian-Hauterivian and the upper Barremian-lowermost Aptian data set. Within the lower Barremian, the $\delta^{18}O_{bel}$ and $\delta^{18}O_{bulk}$ records appear decoupled: the $\delta^{18}O_{bel}$ negative shift is mirrored by a positive $\delta^{18}O_{bulk}$ shift. Correlation between both records improves again from the H. sayni zone onward.

$\Delta\delta^{18}O$ values corresponding to the absolute difference between $\delta^{18}O_{bulk}$ and $\delta^{18}O_{bel}$ values, show a very contrasted trend within the Valanginian – Barremian interval. Minimum values are recorded around the Berriasian-Valanginian boundary interval, and for the *C. loryi, P. ligatus, N. pulchella, M. sarasini,* and *D. weissi* ammonite zones. Maximum values are recorded in the *S. verrucosum, L. nodosoplicatum, S. angulicostatum, H. uhligi*, and *D. oglanlensis* ammonite zones (Fig.

G.5).

G.4.3 Mn, Fe, Mg, Sr and Ca contents

Chemical results from the herein analyzed belemnites are listed in Table G.1. The Mn record shows values between 0.77 and 83.05 ppm with an average value of 7.82 ppm. Fe contents are comprised between 119 and 1105 ppm with an average value of 247 ppm. Two samples (AN 143b and AN 173b) show high values above 50 ppm for Mn and 500 ppm for Fe.

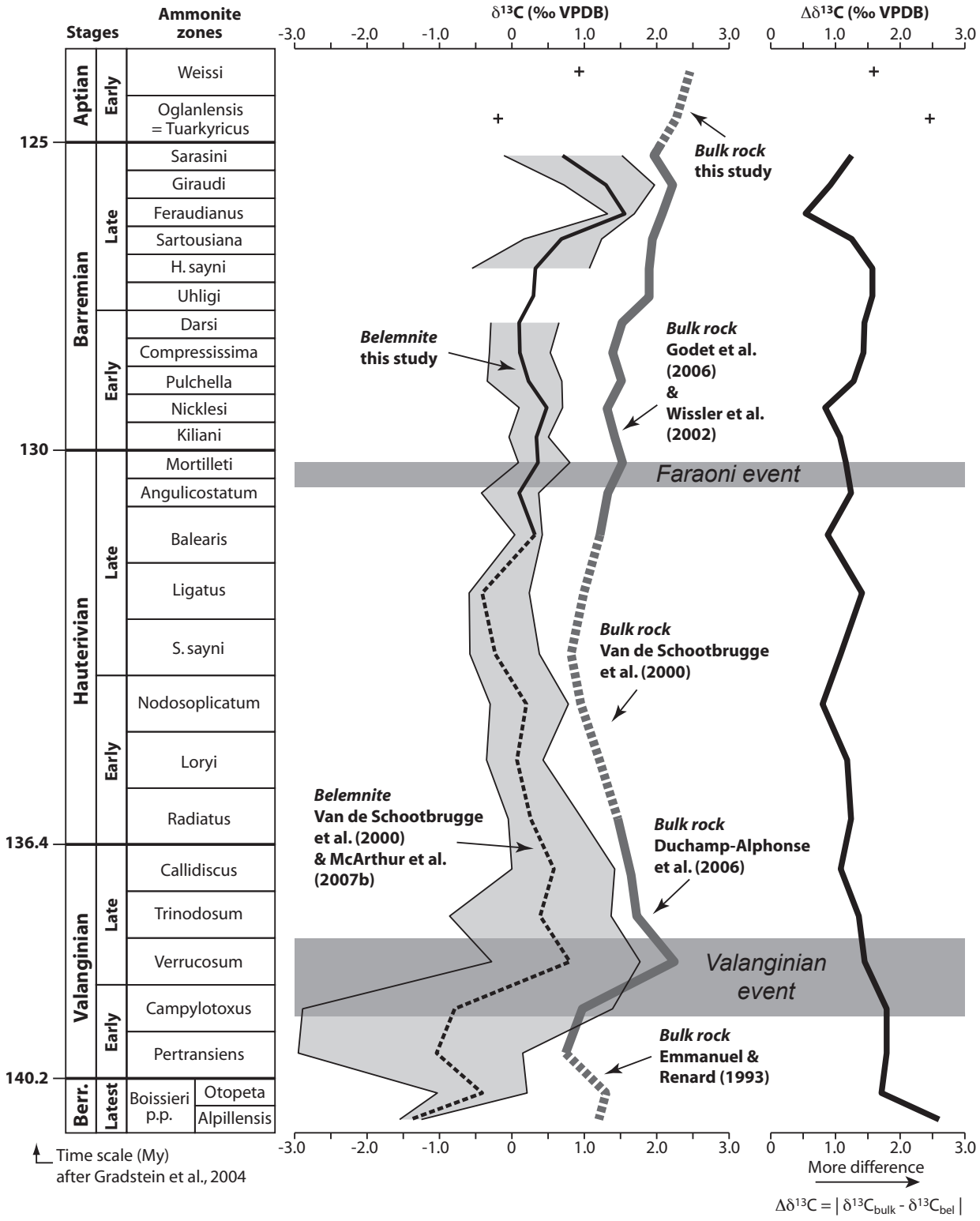

Fig. G.4: Evolution of the bulk-rock and belemnite carbon isotope records averaged per ammonite zone from the uppermost Berriasian to the uppermost Barremian. The two lowermost Aptian crosses highlight the value of the two belemnites analyzed within this interval. The $\Delta\delta^{13}C$ index corresponds to the absolute difference between $\delta^{13}C_{bulk}$ and $\delta^{13}C_{bel}$ per ammonite zone. Dark grey shading bands mark the position of the Valanginian and Faraoni events.

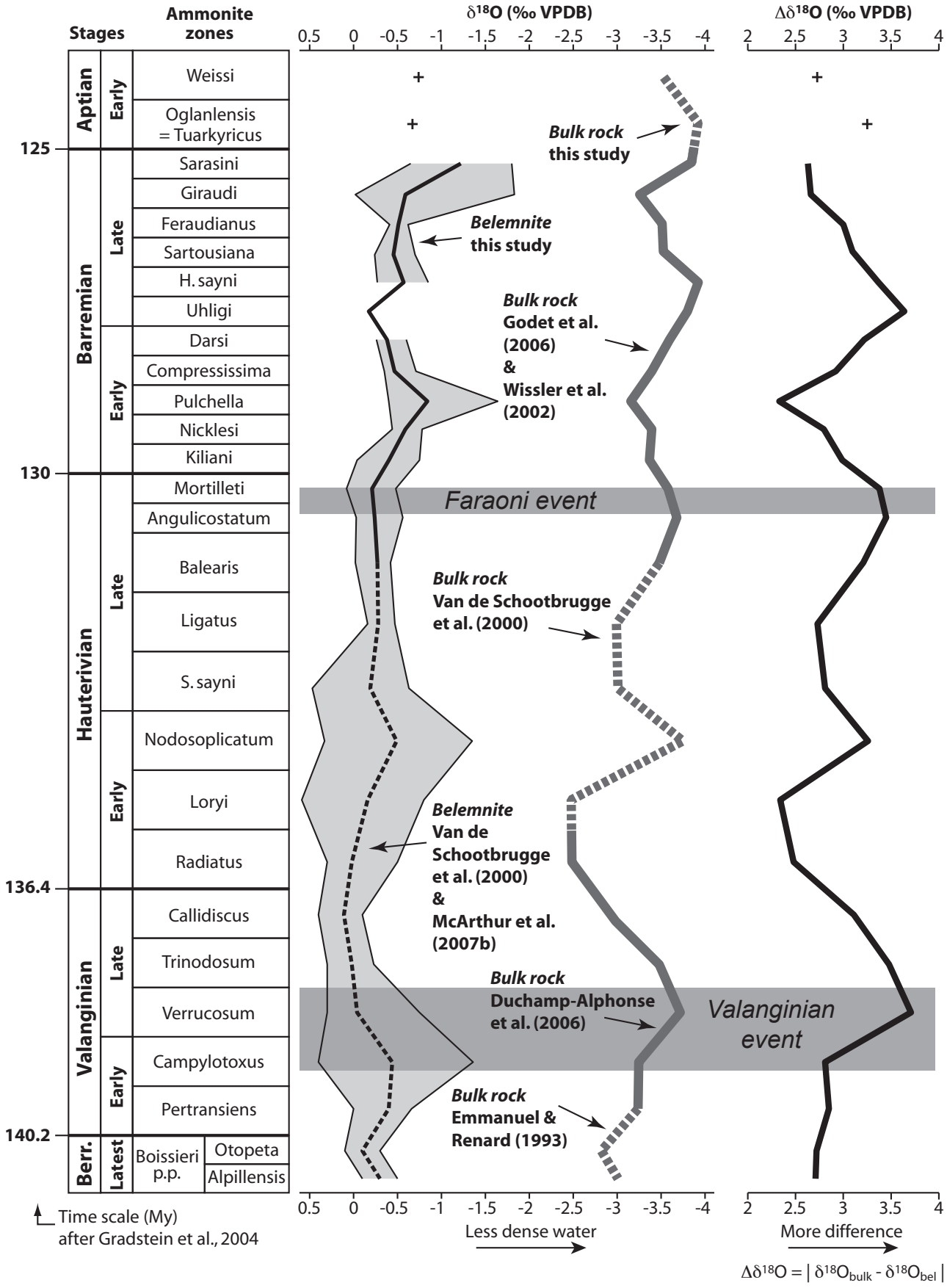

Fig. G.5: Evolution of the bulk-rock and belemnite oxygen isotope records averaged per ammonite zone, with minimal and maximal values envelope, from the uppermost Berriasian to the uppermost Barremian. The two lowermost Aptian crosses highlight the value of the two belemnites analyzed within this interval. The $\Delta\delta^{18}O$ index corresponds to the absolute difference between $\delta^{18}O_{bulk}$ and $\delta^{18}O_{bel}$ per ammonite zone. Grey shading bands mark the position of the Valanginian and Faraoni events.

Mg values range between 1878 and 4943 ppm with an average value of 3351 ppm. Sr values vary between 1005 and 1591 ppm with an average value of 1315 ppm. These values are in good agreement with those from van de Schootbrugge et al. (2000), who studied Valanginian-Hauterivian belemnites from the Vocontian Trough.

Cross plots of Mg/Ca and Sr/Ca ratios to $\delta^{18}O$ values show a very poor correlation for both *Hibolithes* and *Mesohibolites* genera (Fig. G.7). Due to the low number of specimens from both *Duvalia* and *Neohibolites* genera, we were not able to apply this test for these genera.

G.4.4 Strontium isotopes

Within the Hauterivian (Fig. G.8 and Table G.2), the belemnite $^{87}Sr/^{86}Sr$ record shows a rapid increase, and a maximum is reached in the lower Barremian (mean value of 0.707504 in the *K. compressissima* zone). In the following, the strontium-isotope curve shifts gently toward less radiogenic values (mean value of 0.707422 in the *M. sarasini* zone) before slightly increasing again in the uppermost Barremian. The evolution and the numerical values of the belemnite $^{87}Sr/^{86}Sr$ record are coherent with previous studies carried out on bulk rock, brachiopods and belemnites from the Hauterivian – lower Aptian interval (e.g. Jones et al., 1994; Jones and Jenkyns, 2001; McArthur et al., 2004, 2007b).

G.5 Discussion

G.5.1 Belemnite preservation and reliability

According to previous publications on Lower Cretaceous belemnite geochemistry (Ditchfield, 1997; Podlaha et al., 1998; van de Schootbrugge et al., 2000; McArthur et al., 2004, 2007b; Dutton et al., 2007; Mutterlose et al., 2009; and references therein), the following criteria have been proposed to check sample preservation: visually well-preserved belemnites (i.e. non-opaque pieces, showing growth bands), isotopic and element composition that replicate well, low concentrations of Fe and Mn, concentrations of Sr and Mg typical of well-preserved belemnites, no positive covariance between oxygen and carbon isotope values, and carbon isotopes values lighter and oxygen isotopes heavier than the bulk-rock values. According to McArthur et al. (2007a), absence of cloudiness in belemnite calcite argues for well-preserved material suitable for palaeoceanographic studies. Sr and Mg concentrations are considered to

Section	Sample	Stage	Ammonite zone	$^{87}Sr/^{86}Sr$	2σ
Angles	AN1b	Late Hauterivian	*Balearis*	0.707466	0.000013
Angles	AN 53.2b	Late Hauterivian	*Mortilleti*	0.707466	0.000012
Angles	AN 71b	Early Barremian	*Kiliani*	0.707470	0.000011
Angles	AN76b	Early Barremian	*Kiliani*	0.707495	0.000012
Angles	AN85b	Early Barremian	*Kiliani*	0.707473	0.000015
Angles	AN92b	Early Barremian	*Kiliani*	0.707400	0.000018
Angles	AN103b	Early Barremian	*Nicklesi*	0.707500	0.000011
Angles	AN104b	Early Barremian	*Nicklesi*	0.707513	0.000011
Angles	AN111.1b	Early Barremian	*Pulchella*	0.707498	0.000014
Angles	AN 112	Early Barremian	*Pulchella*	0.707478	0.000013
Angles	AN 112.7b	Early Barremian	*Compressissima*	0.707483	0.000011
Angles	AN 121b	Early Barremian	*Compressissima*	0.707524	0.000013
Angles	AN 125b	Early Barremian	*Darsi*	0.707479	0.000013
Angles	AN 136b	Early Barremian	*Darsi*	0.707496	0.000012
Angles	AN 144b	Early Barremian	*Uhligi*	0.707485	0.000010
Angles	AN 151.3b	Late Barremian	*Sayni*	0.707486	0.000012
Angles	AN158b	Late Barremian	*Sayni*	0.707475	0.000013
Angles	AN161.1b	Late Barremian	*Sartousiana*	0.707475	0.000010
Angles	AN162b	Late Barremian	*Sartousiana*	0.707457	0.000014
Angles	AN165b	Late Barremian	*Feraudianus*	0.707460	0.000012
Saut du Loup	SDL362b	Late Barremian	*Giraudi*	0.707457	0.000010
Saut du Loup	SDL366b	Late Barremian	*Giraudi*	0.707448	0.000013
Saut du Loup	SDL373b	Late Barremian	*Sarasini*	0.707418	0.000013
Angles	AN 185b	Late Barremian	*Sarasini*	0.707425	0.000012
Angles	AN 202	Early Aptian	*Oglanlensis*	0.707433	0.000011
Combe Lambert	COM109b	Early Aptian	*Weissi*	0.707433	0.000013

Table G.2: Strontium isotope data from upper Hauterivian to lowermost Aptian belemnites of the Vocontian trough.

be a good indicator of diagenetic overprint in calcite (e.g. Veizer, 1983; Steuber, 1999). Cut-off values for Mn and Fe are rather arbitrary and vary depending on the author (e.g. Ditchfield, 1997). Mutterlose et al. (2009) considered a threshold value of 100 ppm for Mn to be critical for diagenesis, as well as Sr concentration below 1000 ppm. McArthur et al. (2007a) in their fig. 9 showed moreover that there is no firm correlation between Mn and Fe concentration values and eye check sample preservation. Some of their samples, that are considered by eye check under thin section as altered show low values of these elements concentrations and vice versa. We decided to set the limit for Fe, Mn and Sr at 500 ppm, 50 ppm and 1000 ppm, respectively. Belemnite samples with higher concentrations of Fe and Mn, or lower concentration of Sr, (i.e. AN 143b and AN 173b) were considered as diagenetically altered and excluded from our discussion. The belemnite AN 119b is as well excluded from further consideration in this study because it has a very light $\delta^{18}O$ signature compared to the other belemnite samples around this interval. As this belemnite could not be identified to the genus level, we decided to exclude it from the mean value calculation, taking into account that this discrepancy could be linked to peculiar genus-species fractionation.

All other samples match the above listed criteria. We assume, for this reason, that they have retained their original isotopic and elemental compositions. Moreover, both the fact that our results match well with those obtained by van de Schootbrugge et al. (2000) and McArthur et al. (2007b) for uppermost Hauterivian belemnites from the Vocontian Trough, as well as the fact that we are able to correlate the herein observed trends with those observed by McArthur et al. (2004) for the Boreal realm (cf. Fig. G1.6), is an additional indication for the reliability of the here-presented belemnite isotope records.

Our belemnite isotope records are quite “noisy” (Fig. G.3). A similar spread in values was already noted by Podlaha et al. (1998) and McArthur et al. (2007a, 2007b). We exclude diagenetic alteration as a source

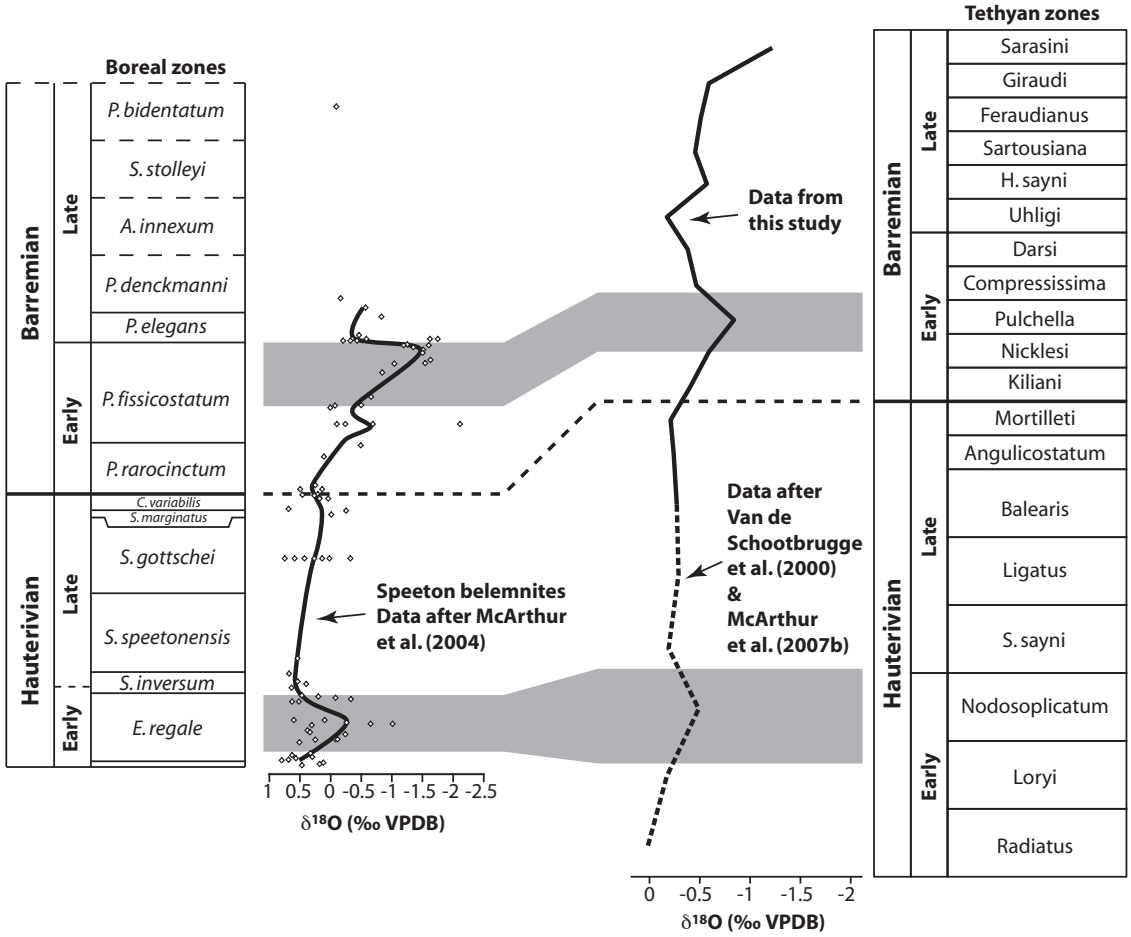

Fig. G.6: Comparison of Hauterivian – lowermost Aptian long-term trends in belemnite oxygen isotope records from the Vocontian Trough (Tethyan realm, France, this study) and the Speeton area (Boreal realm, England, after McArthur et al., 2004). The two major negative shift of the lower Hauterivian and lower Barremian are highlighted by grey shading bands. The similarity of the long-term trend between the two records underlines the reliability of the use of the $\delta^{18}O_{bel}$ record and the weak impact of diagenesis on the here-used belemnites.

of the noise because all belemnites used here were checked for their diagenetic state. Following McArthur et al. (2007b) (see also Rexfort and Mutterlose, 2006), this noise may be related to the fact that belemnites closely record environmental signals and short-term (i.e., seasonal) changes therein and that therefore the belemnite isotope values are not as averaged as those obtained from carbonate bulk rock (see McArthur et al., 2007b, for an in-depth discussion of this point). The same spread of value is as well observed for multi-species isotope analyses for benthic foraminifera (e.g. Friedrich et al., 2008). For belemnite, this spread of values can also be related to intra-rostral fractionation, gender effect species difference and range of belemnite habitats (McArthur et al., 2007a).

The here analyzed belemnites belong principally to two different genera: *Hibolithes* and *Mesohibolites* (Table G.1). All sampled belemnites in uppermost Hauterivian – lowermost Barremian rocks (*B. balearis* to *K. nicklesi* ammonite zone) belong to the *Hibolithes* genera. A rapid transition in the belemnite assemblage, with occurrence of both *Hibolithes* and "*Mesohibolites*," takes place within the uppermost lower Barremian. Upper Barremian - lowermost Aptian samples are dominated by *Mesohibolites*, with few occurrences of *Neohibolites*. This threefold division in our sampling reflects belemnite association changes for this interval (e.g. Janssen and Fözy, 2005). No genera-related difference of the stable isotope signal can be observed between these three zones. We therefore exclude any

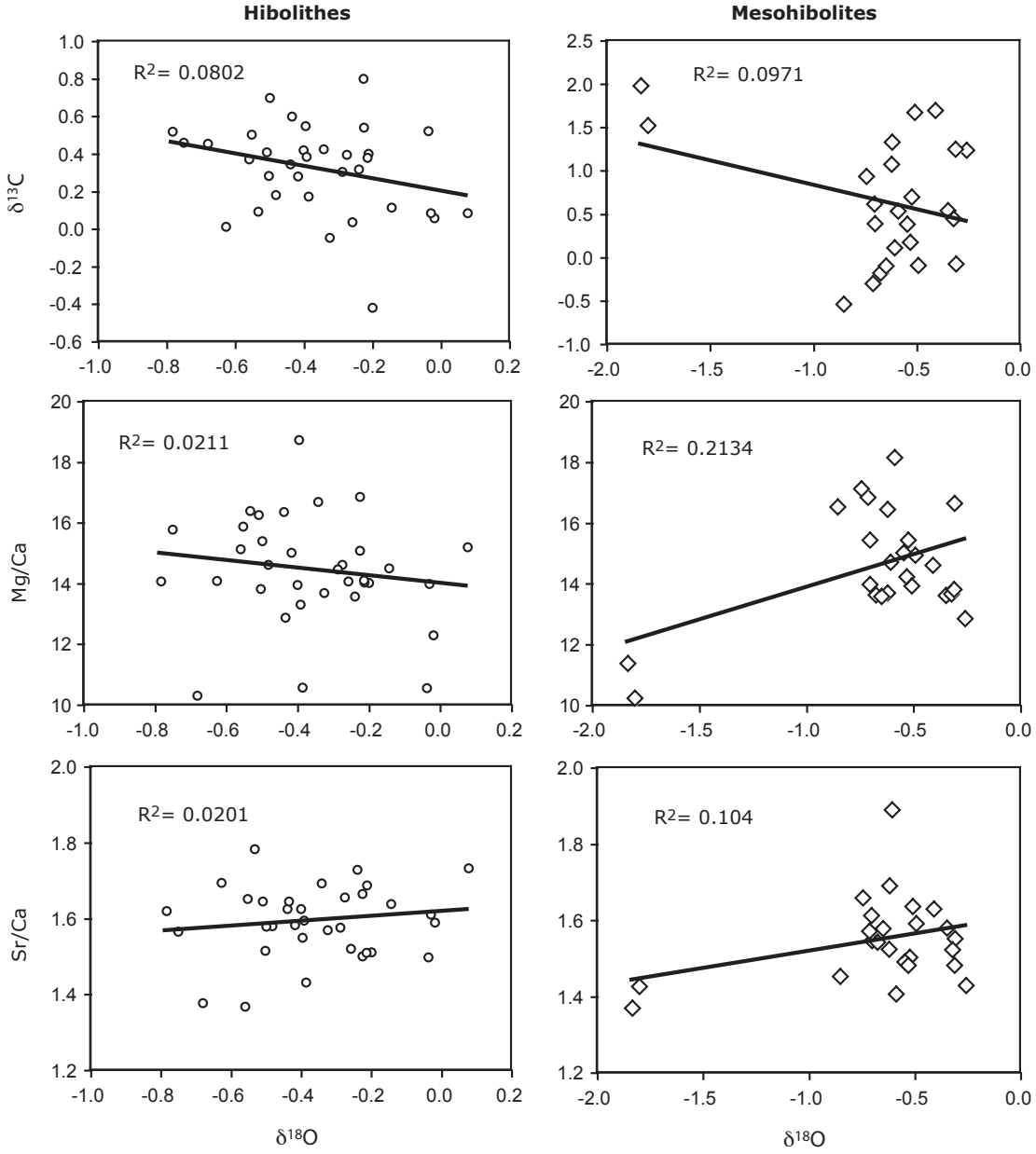

Fig. G.7: Correlation of $\delta^{13}C$, Mg/Ca and Sr/Ca to $\delta^{18}O$ in the belemnite genera Hibolithes and Mesohibolites. When excluding the two Mesohibolites samples showing low $\delta^{18}O$ values, the R^2 value changes to 0.1508, 0.1778 and 0.0339 for the comparison with $\delta^{13}C$, Mg/Ca and Sr/Ca, respectively.

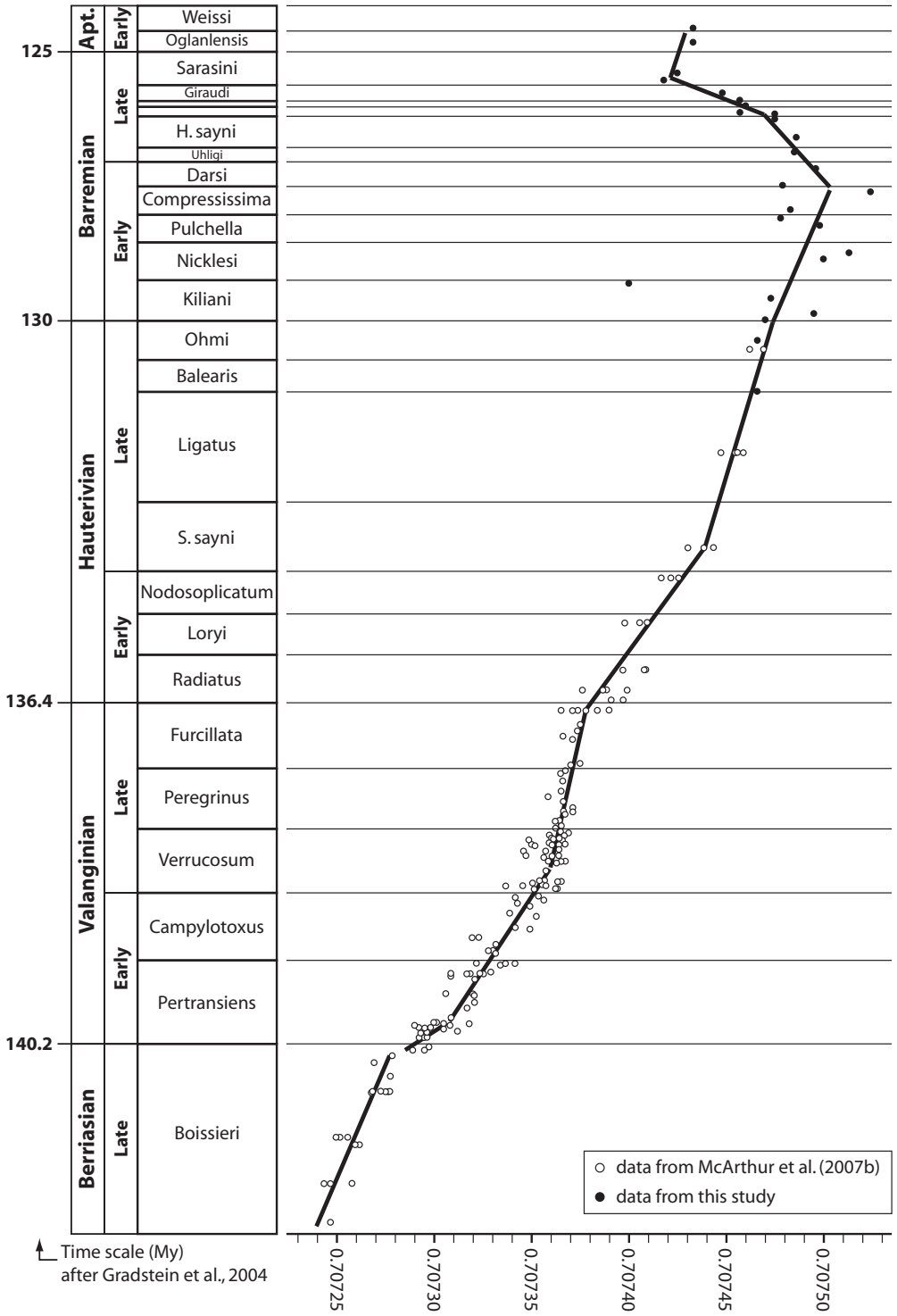

Fig. G.8: Evolution of the belemnite 87Sr/86Sr record within the upper Berriasian – lowermost Aptian. Berriasian, Valanginian, and the large majority of Hauterivian data are from McArthur et al. (2007), whereas the Barremian and lowermost Aptian data represent own data.

significant differential fractionation process between these genera that would affect the reliability of our sampling.

G.5.2 Bulk-rock diagenesis

Following Godet et al. (2008), the clay-mineral distribution in the Angles section shows that this region has suffered from minor diagenetic impact. This is also shown by the slight negative offset in $\delta^{18}O$ values from this region compared to other Vocontian sections situated further away from the "nappe de Dignes" (van de Schootbrugge et al., 2000). Godet et al. (2006) have, however, also shown that this slight diagenetic effect was not sufficient enough to totally reset the trends in the original $\delta^{18}O$ record and that the long-term trends are preserved and comparable to others regions. We

refrain, however, from calculating palaeotemperatures from our $\delta^{18}O$ dataset because of this slight diagenetic overprint, and also because oxygen stable isotopes may change as a function of seawater salinity.

With the exception of the lower Barremian (see the following for a discussion of this point), the oxygen isotope trends observed in bulk-rock and belemnite are comparable and differ only with regards to their exact value and amplitude. Moreover, a comparison between the Vocontian $\delta^{18}O$ bulk-rock trend with the one compiled by Weissert and Erba (2004) for the southern Tethyan margin shows a good correlation between these two palaeogeographic domains (Fig. G.9). These observations indicate that the here-compiled Vocontian bulk-rock $\delta^{18}O$ signal can be interpreted as a palaeoenvironmental and palaeoclimatic signal.

G.5.3 Belemnite vs. bulk rock record

In the Vocontian Trough, carbonate bulk rock is mostly composed of a mixture of calcareous nannoplankton and exported carbonate platform ooze (e.g. Van de Schootbrugge et al., 2000; Reboulet et al., 2003). The here recorded $\delta^{18}O$ signal of carbonate bulk rock may thus be related to density values of near sea-surface water. On the other hand, belemnites are thought to have had a nektonic or nektobenthonic life style and may have inhabited deeper water settings (e.g. van de Schootbrugge et al., 2000; Rexfort and Mutterlose, 2006; Dutton et al., 2007; McArthur et al., 2007a; Wierzbowski and Joachimski, 2007). According to Mitchell (2005), the normal habitat for belemnites was the deeper area of the shelf. Mutterlose et al. (2009) estimate that they have lived as active swimmers in subsurface water of 50m to 150m depth. The interpretation of belemnite lifestyle is moreover supported by their $\delta^{18}O$ and $\delta^{13}C$ values, which are systematically heavier and lighter, respectively, and thus representative of denser deeper water.

G.5.4 Purported hiatus in the Angles section?

Wissler et al. (2002) were the first to publish a Barremian - lowermost Aptian bulk-rock carbon isotope record from the Angles section. They correlated the Angles record with the Cismon Apticore drilling record (Erba et al., 1999) and concluded that: “up to 50% of the Barremian stage is missing in the selected reference section” (i.e. the Angles section) and that: “the gap occurs most probably within the *giraudi* ammonite zone.” This interpretation is based on their observation that the upper Barremian sediments of Cismon show one short-lived carbon-isotope positive peak which is not present in the Angles section.

This conclusion is debatable for several reasons. Firstly, if up to 50% of the Barremian stage would be missing in the Angles section, it is very difficult to imagine how this hiatus can be accommodated by less than the time equivalent to one single ammonite zone (*I. giraudi* zone), whereas the entire Barremian stage is presently subdivided in 11 ammonite zones (e.g. Vermeulen, 2002). The sedimentary equivalent of this purported hiatus should be present elsewhere, in more complete sections, and should be manifested by a more complete ammonite biostratigraphy. Such a difference in ammonite biostratigraphy has, to our knowledge, never been reported. On the contrary, following the extensive work on ammonite biostratigraphy by French specialists (e.g. Vermeulen, 2002), it appears that the Angles section represents a very complete section with regards to Barremian ammonite zones and sub-zones. The ammonite biozonation derived from this stratotype section is generally used in the Tethyan realm (e.g. Vermeulen, 2002) and is now, almost entirely, accepted as the reference ammonite biozonation for the Barremian by the Kilian group (e.g. Reboulet et al., 2006).

Secondly, no major break is observed in the sedimentary record of the Angles section and also the lower upper Barremian segment of the strontium isotopic curve based on belemnites of the Angles section (Fig. G1.8) is continuous, which would not be expected in the case of a significant hiatus.

Thirdly, following the work of Bodin et al. (2006c), it appears that the carbon-isotope correlation proposed by Wissler et al. (2002) is debatable. Following new ammonite findings in the Alvier region (Switzerland), where the same short-lived positive shift in the carbon-isotope record was reported by Wissler et al. (2003), this latter shift may now be dated as earliest late Barremian (most probably *H. sayni* zone), and not as belonging to the *I. giraudi* zone as postulated by Wissler et al. (2002).

The absence of this first, short-lived, upper Barremian positive isotopic shift in the Angles section is, to our point of view, not necessarily related with a stratigraphical hiatus. It may rather be due to the peculiar position of the Vocontian Trough during the Early Cretaceous. This peripheral basin was surrounded to the north, west and south by an extensive carbonate platform (Föllmi et al., 2006), and this particular position rendered it

very sensitive to carbonate platform shedding. Thus, following Föllmi et al. (2006), the bulk-rock carbon-isotope signal in the Vocontian is the result of a mix between both global palaeoceanographic signals and local signals depending on the intensity and quality of platform carbonate shedding (cf. also Reboulet et al., 2003) and therefore not necessarily entirely correlatable with coeval records from the southern Tethys.

G.5.5 Palaeoceanographic changes

G.5.5.1 Changes in water density

The value of $\delta^{18}O$ in seawater ($\delta^{18}O_{sw}$) is a function of water density (which depends on water temperature and salinity) and ice volume (e.g. Fisher and Arthur, 2002; Miller et al., 2005; McArthur et al., 2007b). Salinity is influenced by evaporation, water masses mixing and fresh water input. There is a negative correlation between temperature and $\delta^{18}O$, and a positive correlation between salinity and $\delta^{18}O$ (e.g. Delaygue et al., 2001). As a result, a positive correlation is observed between $\delta^{18}O$ and water density. Assuming constant ice volume, depleted $\delta^{18}O$ values may thus be representative of less dense water while heavier $\delta^{18}O$ values may represent denser water. Moreover, because the $\Delta\delta^{18}O$ index is the result of a subtraction between surface and deeper water masses for a given time, it may also be independent of changes in ice volume. The here presented $\delta^{18}O_{bulk}$ and $\delta^{18}O_{bel}$ records are a compilation derived from one single basin for this time interval, and as such we are able to preclude the potentially blurring effect related to the accumulation of records from different basins with different environmental and depositional histories.

A remarkable feature of the $\delta^{18}O_{bulk}$ curve is that both the Valanginian and Faraoni events are mirrored by minimal $\delta^{18}O_{bulk}$ values. This indicates that these events were associated with less dense surface water. Similar trends are seen for the so-called “mid”-Hauterivian episode (van de Schootbrugge et al., 2003), the lower upper Barremian, and the uppermost Barremian intervals (Fig. G.5). It can also be noted here that the Valanginian event is followed by a significant increase in $\delta^{18}O_{bulk}$ values, reaching the heaviest values observed in this study within the lowermost Hauterivian.

Another remarkable feature is the fact that the belemnite record is more flat and stable than the bulk-rock one. This may indicate that deeper waters were less subjected to density fluctuations than superficial waters. This is also observed in the $\Delta\delta^{18}O$ index, which – except for the lower Barremian - follows the bulk-rock $\delta^{18}O$ trend. This signifies that along the northern Tethyan margin surface waters were more easily perturbed by changes in temperature and salinity, whereas deeper waters remained more stable. This seems logical for density-stratified water bodies.

G.5.5.2 $\delta^{18}O$ versus Mg/Ca ratios

In previous studies, the Mg/Ca ratio of many modern, as well as past calcifying groups has been used as a proxy for seawater temperatures (e.g. Rosenthal et al., 1997; Lear et al., 2000, 2002; Steuber and Rauch, 2005). Mg/Ca ratios from belemnites have also been used to trace palaeotemperature variations during the Mesozoic (e.g. Bailey et al., 2003; Rosales et al., 2004a, 2004b; McArthur et al., 2004, 2007b). McArthur et al. (2004) however showed that the Mg/Ca record in *Hibolithes* provides a very poor correlation with the $\delta^{18}O_{bel}$ record, contrary to other belemnite genera. The here-obtained results lead us to the same conclusion (Fig. G.7). A similar conclusion can as well be drawn for Mesohibolites.

Consequently, due to the absence of correlation between the Mg/Ca and $\delta^{18}O$ records in *Hibolithes* and *Mesohibolites*, we refrain from using the Mg/Ca record from the here studied belemnites as a palaeotemperature proxy. The very poor or absent correlation of Mg/Ca and $\delta^{18}O$ records in *Hibolithes* and *Mesohibolites* genera, which appears in contrast to other belemnite genera, could be linked to an unidentified fractionation mechanism of Mg by these genera (e.g. McArthur et al., 2000, 2004, 2007a; Bailey et al., 2003; Rosales et al., 2004a, b). Further studies are needed to examine this discrepancy.

G.5.5.3 Changes in the carbon cycle

In a classical view, the bulk-rock $\delta^{13}C$ signal is used to trace phytoplankton productivity (e.g. Weissert, 1989). High phytoplankton productivity will lead to ^{13}C-enriched surface waters that are imaged by the $\delta^{13}C$ record of calcareous shells of planktonic organisms, which compose the pelagic carbonate bulk rock. As a result, high phytoplankton productivity will induce a higher difference in the $\delta^{13}C$ records of surface and deeper waters, reflecting the magnitude of isotopically light carbon export to deeper waters (Broecker and Peng, 1982; Fisher and Arthur, 2002). This difference may as such be traced by the $\Delta\delta^{13}C$ index.

The belemnite and bulk-rock $\delta^{13}C$ records show a good correlation within the Valanginian to lower Barremian interval, and both records mirror the Valanginian positive

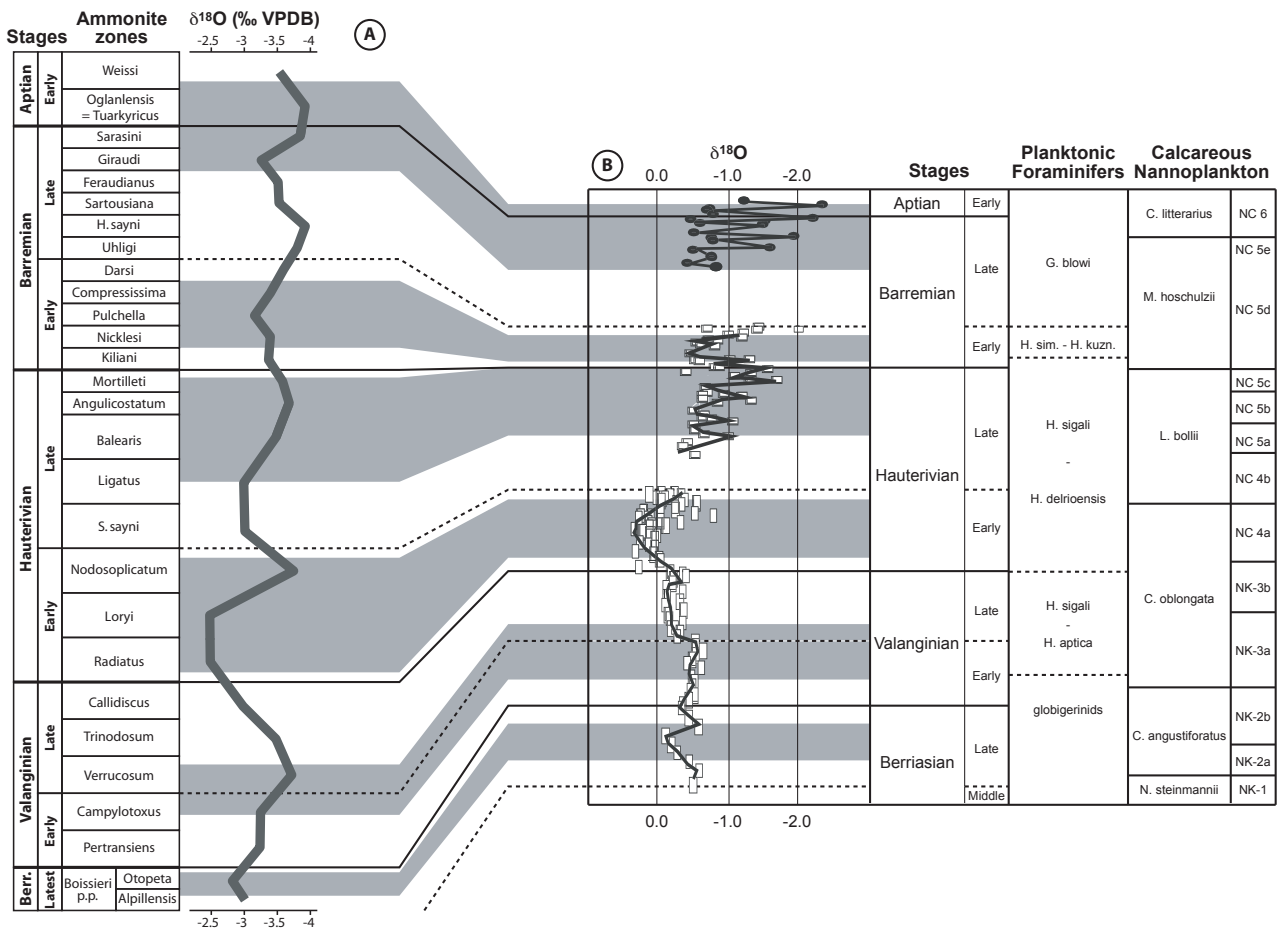

Fig. G.9: Comparison between the here-compiled Vocontian bulk-rock δ18O signal [a] and the record compiled by Weissert and Erba (2004), which represents the southern Tethyan margin [b] (original data of Weissert et al. (1985), Lini et al. (1992) and Menegatti et al. (1998)).
Correlation of planktonic foraminifera and calcareous nannoplankton biozones with regards to ammonite biozonation is after Channell et al. (1995).

excursion, with an onset observed in sediments and belemnites of the *B. campylotoxus* zone. The $\Delta\delta^{13}C$ index shows, however, no peculiar shift which may be interpreted as a major increase in phytoplankton productivity. Small positive shifts or relative high values are observed within the lower Valanginian, the *P. ligatus* zone, the uppermost Hauterivian, and the middle lower Barremian. The close correlation of the belemnite and bulk-rock carbon isotope records within the Valanginian to early Barremian time interval, and the resulting lack of larger excursions in the $\Delta\delta^{13}C$ index is interpreted as the result of an interference between global changes in the oceanic carbon cycle and the quality and quantity of carbon exported from the adjacent northern Tethyan carbonate platform. This platform functioned in a heterozoan mode (i.e. mainly composed of crinoids and bryozoans), which was repetitively interrupted by drowning events during this time interval. It is therefore possible that - especially during the drowning episodes - the carbon isotope signal became buffered due to the increased export of dissolved inorganic carbon (Godet et al., 2006; Föllmi et al., 2006). This mechanism may explain why the Valanginian and latest Hauterivian Faraoni event are not mirrored by important shifts in the $\Delta\delta^{13}C$ index.

The uppermost Berriasian and the upper Barremian-lowermost Aptian intervals are characterized by important negative and positive shifts in $\Delta\delta^{13}C$ values. In the Tethyan realm, both intervals are not identified as intervals of enhanced primary productivity on a larger scale and widespread oceanic anoxic conditions have not been described from these time intervals. It is thus difficult to explain the shifts in $\Delta\delta^{13}C$ by such phenomena. These two intervals, however, correspond to the onset and the development of photozoan-dominated carbonate platforms and an impact of platform ooze shedding may thus be evoked to explain these peculiar $\Delta\delta^{13}C$ signals. Photozoan carbonate platforms may have exported carbonate aragonite ooze, which may have influenced the carbon-isotope

signature in a positive direction, and this especially in deeper waters (Godet et al., 2006; Föllmi et al., 2006).

G.5.6 The late Hauterivian Faraoni anoxic event and its aftermath

According to the reconstruction of phosphorus burial rates around the Faraoni Level, Bodin et al. (2006a) have proposed a model in which the increased influx of nutrients from the continent, in tandem with an operating Tethyan-Boreal connection and stronger upwelling along the northern Tethyan margin, have lead to increased nutrient contents in the Tethyan realm. The bulk rock and belemnite $\delta^{18}O$ records, however, suggest that the Faraoni event is characterized by less dense sea-surface water and an enhanced density contrast between surface and deeper waters (Fig. G.5). This implies that vertical water exchange was restrained during the Faraoni event and upwelling was less likely.

Of particular interest is the fact that, just prior to the Faraoni Level, within the *B. balearis* zone, a major climate shift to warm and humid conditions has been reported along the northern Tethyan margin (Godet et al., 2008). This change may have induced an increase in fluvial input into the Tethys, and following the model of Meyers (2006), increased fluvial input may have been responsible for an increase in salinity stratification of water masses. Moreover, the onset of a warmer and more humid climate may have implied an increase in nutrient input into the ocean through intensified biogeochemical continental weathering. The resulting combination of enhanced primary productivity and restricted vertical water exchange may have promoted an expanded and intensified oxygen minimum zone. The rain of organic matter associated with enhanced productivity and the presence of a well-developed oxygen minimum zone promoted the formation of an “anoxic blanket” at the seafloor, thereby creating optimal conditions for the preservation of organic-rich sediments (e.g. Coccioni et al., 1998; Baudin, 2005; Bodin et al., 2006a). This mechanism, coupled with enhanced nutrient input from the continent, the influx of colder and possibly nutrient-enriched water from the Boreal realm, and an intensified phosphorus reflux from anoxic sediments (Bodin et al., 2006a), may have triggered the Faraoni oceanic anoxic event (Fig. G.10).

Following this scenario, we may also be able to better understand the early Barremian episode, which is characterized by an important negative shift in $\delta^{18}O_{bel}$ values, more positive $\delta^{18}O_{bulk}$ values and less important $\Delta\delta^{18}O$ values. A comparable negative shift in $\delta^{18}O_{bel}$ values has also been reported from England by McArthur et al. (2004) (Fig. G.6) and may thus correspond to an event, which can be traced at a European scale. This interval cannot be associated with enhanced upwelling because the $\delta^{18}O_{bel}$ signal indicates that the deeper waters were associated with less dense water, which is incompatible with an upwelling scenario. It can however be associated with increased vertical water mixing, as is indicated by the low $\Delta\delta^{18}O$ index for the lower Barremian. We postulate a connection between this episode and the preceding Faraoni event and hypothesize that the early Barremian event was the result of the mixing of the buoyant surface layer that evolved just prior to the Faraoni event with deeper water layers. The enhanced vertical water mass exchange may also have induced enhanced surface productivity as is reported by the $\Delta\delta^{13}C$ record. The enhanced deposition of organic matter reported in the Tethyan realm during the early Barremian (Bréhéret, 1994; Erba et al., 1999; Bersezio et al., 2002) may thus be related to this episode. Following this scenario, the Faraoni event did not only affect the oceanic carbon cycle during the latest Hauterivian, but also during the early Barremian, during the aftermath of this oceanic anoxic event.

G.5.7 The Early Cretaceous strontium isotope record

The belemnite strontium isotope record shows a rather steady evolution towards heavier and less radiogenic values throughout the Lower Cretaceous until the upper lower Barremian (top *K. compressissima* Zone), which is followed by a trend towards lower, more radiogenic values until the uppermost Barremian (base *C. sarasini* Zone). The remainder of the Barremian and lowermost Aptian are again characterized by a trend towards heavier values. The presence of this first inflection point in the $^{87}Sr/^{86}Sr$ record was known since Jones et al. (1994) (see also Jones and Jenkyns (2001)), but its exact age was so far unclear compared to Tethyan ammonite biostratigraphy. In the Boreal realm, this inflection point is located in the lower *P. elegans* zone (McArthur et al., 1994). Here we are able to confine its age to *K compressissima - C. darsi* zone transition in the Tethyan realm. According to presently used timescales (Gradstein et al., 2004; e.g. also Sprovieri et al., 2006) this age may predate the onset of the formation of the Ontong-Java Plateau, which is presently set around

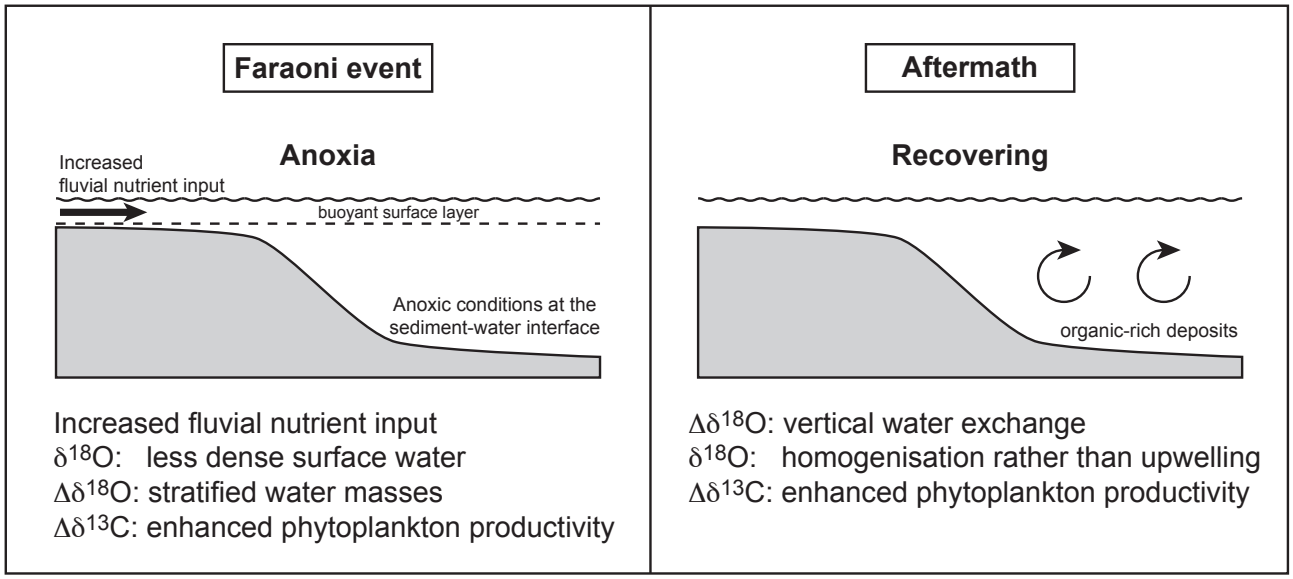

Fig. G.10: Synthetic model resuming palae-oceanographic change within the uppermost Hauterivian – lower Barremian interval (Faraoni event and its aftermath) as deducted from this study.

125-120 Ma (e.g. Taylor, 2006). Following Bodin et al. (2006a) cyclostratigraphic scheme of the Angles section, this inflection point predates the Barremian-Aptian boundary by ca. 2.8 My. Other correlations to the formation of large igneous provinces are not obvious, either. This confirms the observation of McArthur et al. (2004) that changes in $^{87}Sr/^{86}Sr$ values during the Early Cretaceous were principally driven by mid-oceanic ridge production changes.

The second inflection point and the following positive trend in the uppermost upper Barremian seems to correspond to a small plateau in the overall gradient towards lower values within most of the Aptian (Jones et al., 1994; Jones and Jenkyns, 2001).

G.6 Conclusions

Belemnite and bulk-rock oxygen isotope records from the Vocontian Basin are well correlated throughout the uppermost Berriasian – lowermost Aptian, with the exception of the lower Barremian where an important negative shift in belemnite oxygen isotopes is mirrored by a positive shift in the bulk-rock record. The systematic offset between the two records is related to the nektobenthonic life style of belemnites, which thus represent a deeper water setting, whereas the hemipelagic carbonate bulk rock is composed of a mixture of plankton remains and periplatform ooze, which both are representative of near sea-surface water. The bulk-rock $\delta^{18}O$ record shows intervals of less dense surface water within the lower Valanginian, the lower lower to lower upper Hauterivian, the uppermost Hauterivian, the lower upper Barremian, and the uppermost Barremian. Dense surface waters were recorded within the lower Hauterivian. The belemnite oxygen isotope record for the Lower Cretaceous is more stable and less subjected to large excursions than the bulk-rock record and the difference between the two records – the $\Delta\delta^{18}O$ record is largely an image of the bulk-rock record, with the exception of the lower Barremian. This behaviour is interpreted as an indication that deeper waters were less subjected to density fluctuations than superficial waters.

The belemnite and bulk-rock stable carbon isotope records are also systematically offset, which is the result of productivity- and depth-dependent uptake of ^{12}C and ^{13}C in carbonates. Both records mirror quite well, with the exception of the intervals of the uppermost Berriasian and the upper Barremian to lower Aptian. The difference between the two records expressed by the $\Delta\delta^{13}C$ record can therefore not be interpreted as a function of differences in primary productivity rates. A strong interference between pelagic primary productivity and carbon derived from the adjacent carbonate platform is thought to have influenced both $\delta^{13}C$ and the resulting $\Delta\delta^{13}C$ records.

The strontium isotopic curve shows a gradual increase from the uppermost Berriasian to the uppermost lower Barremian (compressissima-darsi zone), which is followed by a rapid decrease until the sarasini zone. It is followed by a renewed small increase within the lowermost Aptian. The upper lower Barremian inflection point seems too early to be correlated with the onset of

the Ontong-Java volcanic phase.

With regards to the Faraoni oceanic anoxic event (latest Hauterivian), the $\Delta\delta^{18}O$ record points to an increased difference in densities between deeper and surface waters, which is interpreted here as the result of increased seawater stratification. This was probably initiated by the onset of a warmer and more humid climate on land and the resulting enhanced fluvial input into the ocean, which may ultimately have been responsible of bottom-water anoxia (Fig. G.10). The northern Tethys became better mixed again during the early Barremian, and this may have favored the deposition of numerous organic-matter enriched horizons reported in the Tethyan realm from this time interval.

Acknowledgments

We thank Thierry Adatte for stimulating discussions, Jean Vermeulen and Jaap Klein for their help in the field, Bas van de Schootbrugge for advice on the procedure of belemnite preparation and Tiffany Monnier for her help during the laboratory work. Financial support from the Swiss National Science Foundation (project 2100-067807/1 and 200020-105206/1) is gratefully acknowledged. Constructive reviews by anonymous reviewers improved the manuscript substantially.

References

Arnaud, H., Arnaud-Vanneau, A., Blanc-Aletru, M.C., Adatte, T., Argot, M., Delanoy, G., Thieuloy, J.-P., Vermeulen, J., Virgone, A., Virlouvet, B. Wermeille, S., 1998. Répartition stratigraphique des orbitolinidés de la plate-forme urgonienne subalpine et jurassienne (SE de la France). Géologie Alpine 74, 3-89.

Bailey, T.R., Rosenthal, Y., McArthur, J.M., Van de Schootbrugge, B. Thirlwall, M.F., 2003. Paleoceanographic changes of the Late Pliensbachian - Early Toarcian interval: a possible link to the genesis of an Oceanic Anoxic Event. Earth and Planetary Science Letters 212, 307-320.

Baudin, F., 2005. A Late Hauterivian short-lived anoxic event in the Mediterranean Tethys: the “Faraoni Event”. Comptes Rendus Geoscience 337, 1532-1540.

Bersezio, R., Erba, E., Gorza, M. Riva, A., 2002. Berriasian-Aptian black shales of the Maiolica formation (Lombardian Basin, Southern Alps, Northern Italy): local to global events. Palaeogeography, Palaeoclimatology, Palaeoecology 180, 253-275.

Bodin, S., Godet, A., Föllmi, K.B., Vermeulen, J., Arnaud, H., Strasser, A., Fiet, N. Adatte, T., 2006a. The Late Hauterivian Faraoni oceanic anoxic event in the western Tethys: Evidence from phosphorus burial rates. Palaeogeography, Palaeoclimatology, Palaeoecology 235, 245-264.

Bodin, S., Godet, A., Matera, V., Steinmann, P., Vermeulen, J., Gardin, S., Adatte, T., Coccioni, R. Föllmi, K.B., 2007. Enrichment of redox-sensitive trace metals (U, V, Mo, As) associated with the late Hauterivian Faraoni oceanic anoxic event. International Journal of Earth Sciences (Geol. Rundsch.) 96, 327-341.

Bodin, S., Godet, A., Vermeulen, J., Linder, P. Föllmi, K.B., 2006b. Biostratigraphy, sedimentology and sequence stratigraphy of the latest Hauterivian - early Barremian drowning episode of the Northern Tethyan margin (Altmann Member, Helvetic nappes, Switzerland). Eclogae geologicae Helvetiae 99, 157-174.

Bodin, S., Vermeulen, J., Godet, A. Föllmi, K.B., 2006c. New data on the age of the installation of Urgonian-type carbonates along the northern Tethyan margin: Biostratigraphy of the Chopf Member (Helvetic Alps, eastern Switzerland). Comptes Rendus Geoscience 338, 727-733.

Bréhéret, J.-G., 1994, The Mid-Cretaceous organic-rich sediments from the Vocontian zone of the French Southeast basin. In: A. Mascle (ed.), Hydrocarbon and Petroleum Geology of France. Special Publication of the European Association of Petroleum Geoscientists, 4, pp. 295-320.

Broecker, W.S. Peng, T.-H., 1982, Tracers in the sea. Lamont-Doherty Geological Observatory, Columbia University, Palisades, New-York, Eldigio Press, pp. 690.

Bulot, L.G. Thieuloy, J.-P., 1994. Les biohorizons du Valanginien du Sud-Est de la France: un outil fondamental pour les corrélations au sein de la Téthys occidentale. Géologie Alpine. Memoire HS 20, 15-41.

Bulot, L.G., Thieuloy, J.-P., Blanc, E. Klein, J., 1992. Le

cadre stratigraphique du Valanginien supérieur et de l'Hauterivien du Sud-Est de la France; définition des biochronozones et caractérisation de nouveaux biohorizons. Géologie Alpine 68, 13-56.

Channell, J.E.T., Erba, E., Nakanishi, M. Tamaki, K., 1995, Late Jurassic - Early Cretaceous time scales and oceanic magnetic anomaly block models. In: W. A. Berggren, D. V. Kent, M.-P. Aubry and J. Hardenbol (eds.), Geochronology time scales and global stratigraphic correlation. SEPM Special Publication, pp. 51-63.

Coccioni, R., Baudin, F., Cecca, F., Chiari, M., Galeotti, S., Gardin, S. Salvini, G., 1998. Integrated stratigraphic, palaeontological, and geochemical analysis of the uppermost Hauterivian Faraoni Level in the Fiume Bosso section, Umbria-Marche Apennines, Italy. Cretaceous Research 19, 1-23.

Delanoy, G., 1998. Biostratigraphie des faunes d'ammonites à la limite Barrémien-Aptien dans la région d'Angles-Barrême-Castellane. Etude particulière de la famille des Heteroceratina Spath, 1922 (Ancyloceratina, Ammonoidea). Annales du Muséum d'Histoire Naturelle de Nice (Nice) tome XII, 1-270.

Delaygue, G., Bard, E., Rollion, C., Jouzel, J., Stiévenard, M., Duplessy, J.-C. Ganssen, G., 2001. Oxygen isotope/salinity relationship in the northern Indian Ocean. Journal of Geophysical Research 106, 4565-4574.

Ditchfield, P.W., 1997. High northern palaeolatitude Jurassic-Cretaceous palaeotemperature variation: new data from Kong Karls Land, Svalbard. Palaeogeography, Palaeoclimatology, Palaeoecology 130, 163-175.

Duchamp-Alphonse, S., Gardin, S., Fiet, N., Bartolini, A., Blamart, D. Pagel, M., 2007. Fertilization of the northwestern Tethys (Vocontian basin, SE France) during the Valanginian carbon isotope perturbation: Evidence from calcareous nannofossils and trace element data. Palaeogeography, Palaeoclimatology, Palaeoecology 243, 132-151.

Dutton, A., Huber, B.T., Lohmann, K.C. Zinsmeister, W.J., 2007. High-resolution stable isotope profiles of a Dimitobelid belemnite: Implications for paleodepth habitat and Late Maastrichtian climate seasonality. Palaios 22, 642-650.

Emmanuel, L. Renard, M., 1993. Carbonate geochemistry (Mn, δ13C, δ18O) of the late Tithonian-Berriasian pelagic limestones of the Vocontian trough (SE France). Bull. Cent. Rech. Explor. Prod. Elf Aquitaine 17, 205-221.

Erba, E., Bartolini, A. Larson, R.L., 2004. Valanginian Weissert oceanic anoxic event. Geology 32, 149-152.

Erba, E., Channell, J.E.T., Claps, M., Jones, C.E., Larson, R.L., Opdyke, B., Premoli-Silva, I., Riva, A., Salvini, G. Torriceli, S., 1999. Integrated stratigraphy of the Cismon APTICORE (Southern Alps, Italy): A "reference section" for the Barremian-Aptian interval at low latitudes. Journal of Foraminiferal Research 29, 371-391.

Fisher, C.G. Arthur, M.A., 2002. Water mass characteristics in the Cenomanian US Western Interior seaway as indicated by stable isotopes of calcareous organisms. Palaeogeography, Palaeoclimatology, Palaeoecology 188, 189-213.

Föllmi, K.B., Bodin, S., Godet, A., Linder, P. Van de Schootbrugge, B., 2007. Unlocking paleo-environmental information from Early Cretaceous shelf sediments in the Helvetic Alps: stratigraphy is the key! Swiss Journal of Geosciences 100, 349-369.

Föllmi, K.B., Godet, A., Bodin, S. Linder, P., 2006. Interactions between environmental change and shallow-water carbonate build-up along the northern Tethyan margin and their impact on the Early Cretaceous carbon-isotope record. Paleoceanography 21, PA4211.

Friedrich, O., Erbacher, J., Moriya, K., Wilson, P.A. Kuhnert, H., 2008. Warm saline intermediate waters in the Cretaceous tropical Atlantic Ocean. Nature Geoscience 1, 453-457.

Godet, A., Bodin, S., Adatte, T. Föllmi, K.B., 2008. Platform-induced clay-mineral fractionation along a northern Tethyan basin-platform transect: implications for the interpretation of Early Cretaceous climate change (late Hauterivian-early Aptian). Cretaceous Research 29, 830-847.

Godet, A., Bodin, S., Föllmi, K.B., Vermeulen, J., Gardin, S., Fiet, N., Adatte, T., Berner, Z., Stüben, D. Van de Schootbrugge, B., 2006. Evolution of the marine stable carbon-isotope record during the Early Cretaceous: A focus on the late Hauterivian

and Barremian in the Tethyan realm. Earth and Planetary Science Letters 242, 254-271.

Gradstein, F.M., Agterberg, F.P., Ogg, J.G., Hardenbol, J., Van Veen, P., Thierry, J. Huang, Z., 1994. A Mesozoic time scale. Journal of Geophysic Research 99, 24051-24074.

Hay, W.W., 2002. A new view of Cretaceous paleoceanography. In: J. Michalik (ed.). Tethyan/ Boreal Cretaceous correlation. Publishing House of Slovak Academy of Science, Bratislava, pp. 11-37.

Hodell, D.A., Mueller, P.A. Garrido, J.R., 1991. Variations in the strontium isotopic composition of seawater during the Neogene. Geology 19, 24-27.

Janssen, N.M.M., Főzy, I., 2005. Neocomian belemnites and ammonites from the Bersekhegy (Gerecse Mountains, Hungary), part II: Barremian. Fragmenta Palaeontologica Hungarica 23, 59-86.

Jones, C.E. Jenkyns, H.C., 2001. Seawater strontium isotopes, oceanic anoxic events, and seafloor hydrothermal activity in the Jurassic and Cretaceous. American Journal of Science 301, 112-149.

Jones, C.E., Jenkyns, H.C., Coe, A.L. Hesselbo, S.P., 1994. Sr isotopic variation in Jurassic and Cretaceous seawater. Geochimica et Cosmochimica Acta 58, 3061-3074.

Kennett, J.P., Cannariato, K.G., Hendy, I.L. Behl, R.J., 2000. Carbon isotopic evidence for methane hydrate instability during Quaternary interstadials. Science 288, 128-133.

Lear, C.H., Elderfield, H. Wilson, P.A., 2000. Cenozoic deep-sea temperature and global ice volume from Mg/Ca in benthic foraminiferal calcite. Science 287, 269-272.

Lear, C.H., Rosenthal, Y. Slowey, N., 2002. Benthic foraminiferal Mg/Ca-paleothermometry: a revised core-top calibration. Geochimica et Cosmochimica Acta 66, 3375-3387.

Lini, A., Weissert, H. Erba, E., 1992. The Valanginian carbon isotope event: a first episode of greenhouse climate conditions during the Cretaceous. Terra Nova 4, 374-384.

Masse, J.-P., 1993, Valanginian-Early Aptian Carbonate Platforms from Provence, Southeastern France, In: Simo J.A.T., Scott R.W. and Masse J.-P. (eds.), Cretaceous carbonates platforms. AAPG Memoir. American Association of Petroleum Geologists. Tulsa, OK, United States, pp. 363-374.

Masse, J.P., Bellion, Y., Benkhelil, J., Ricou, L.E., Dercourt, J. Guiraud, R., 1993, Early Aptian (114 to 111 Ma), In: J. Dercourt, L. E. Ricou and B. Vrielynck (eds.), Atlas, Tethys, Palaeoenvironmental Maps. BEICIP-FRANLAB, Rueil-Malmaison.

McArthur, J.M., Donovan, D.T., Thirlwall, M.F., Fouke, B.W. Mattey, D., 2000. Strontium isotope profile of the early Toarcian (Jurassic) oceanic anoxic event, the duration of ammonite biozones, and belemnite palaeotemperatures. Earth and Planetary Science Letters 179, 269-285.

McArthur, J.M., Doyle, P., Leng, M.J., Reeves, K., Williams, C.T., Garcia-Sanchez, R. Howarth, R.J., 2007a. Testing palaeo-environmental proxies in Jurassic belemnites: Mg/Ca, Sr/Ca, Na/Ca, δ18O and δ13C. Palaeogeography, Palaeoclimatology, Palaeoecology 252, 464-480.

McArthur, J.M., Janssen, N.M.M., Reboulet, S., Leng, M.J., Thirlwall, M.F. Van de Schootbrugge, B., 2007b. Palaeo-temperatures, polar ice-volume, and isotope stratigraphy (Mg/Ca, δ18O, δ13C, 87Sr/86Sr): the Early Cretaceous (Berriasian, Valanginian, Hauterivian). Palaeogeography, Palaeoclimatology, Palaeoecology 248, 391-430.

McArthur, J.M., Mutterlose, J., Price, G.D., Rawson, P.F., Ruffell, A. Thirlwall, M.F., 2004. Belemnites of Valanginian, Hauterivian and Barremian age: Sr-isotope stratigraphy, composition (87Sr/86Sr, δ13C, δ18O, Na, Sr, Mg), and palaeo-oceanography. Palaeogeography, Palaeoclimatology, Palaeoecology 202, 253-272.

Menegatti, A.P., Weissert, H., Brown, R.S., Tyson, R.V., Farrimond, P., Strasser, A. Caron, M., 1998. High-resolution δ13C stratigraphy through the early Aptian “Livello Selli” of the Alpine Tethys. Paleoceanography 13, 530-545.

Meyers, P.A., 2006. Paleoceanographic and paleoclimatic similarities between Mediterranean sapropels and Cretaceous black shales. Palaeogeography, Palaeoclimatology, Palaeoecology 235, 305-320.

Miller, K.G., Wright, J.D. Browning, J.V., 2005. Visions of ice sheets in a greenhouse world. Marine

Geology 217, 215-231.

Mitchell, S.F., 2005. Eight belemnite biohorizons in the Cenomanian of northwest Europe and their importance. Geological Journal 40, 363-382.

Mutterlose, J., Pauly, S. Steuber, T., 2009. Temperature controlled deposition of Early Cretaceous (Barremian–early Aptian) black shales in an epicontinental sea. Palaeogeography, Palaeoclimatology, Palaeoecology 273, 330-345.

Naidu, P.D., 2004. Isotopic evidences of past upwelling intensity in the Arabian Sea. Global and Planetary Change 40, 285-293.

Podlaha, O.G., Mutterlose, J. Veizer, J., 1998. Preservation of δ18O and δ13C in belemnite rostra from the Jurassic/Early Cretaceous successions. American Journal of Science 298, 324-347.

Reboulet, S., Hoedemaeker, P.J., Aguirre-Urreta, M.B., Alsen, P., Atrops, F., Baraboshkin, E., Company, M., Delanoy, G., Dutour, Y., Klein, J., Latil, J.-L., Lukeneder, A., Mitta, V., Mourgues, F.A., Ploch, I., Raisossadat, N., Ropolo, P., Sandoval, J., Tavera, J.M., Vasicek, Z. Vermeulen, J., 2006. Report on the 2nd international meeting of the IUGS lower Cretaceous ammonite working groug, the “Kilian Group” (Neuchâtel, Switzerland, 8 September 2005). Cretaceous Research 27, 712-715.

Reboulet, S., Mattioli, E., Pittet, B., Baudin, F., Olivero, D. Proux, O., 2003. Ammonoid and nannoplankton abundance in Valanginian (Early Cretaceous) limestone-marl successions from the southeast France Basin: carbonate dilution or productivity? Palaeogeography, Palaeoclimatology, Palaeoecology 201, 113-139.

Rexfort, A. Mutterlose, J., 2006. Stable isotope records from Sepia officinalis - a key to understanding the ecology of belemnites? Earth and Planetary Science Letters 247, 212-221.

Rosales, I., Quesada, S. Robles, S., 2004a. Paleotemperature variations of Early Jurassic seawater recorded in geochemical trends of belemnites from the Basque-Cantabrian basin, northern Spain. Palaeogeography, Palaeoclimatology, Palaeoecology 203, 253-275.

Rosales, I., Robles, S. Quesada, S., 2004b. Elemental and oxygen isotope composition of Early Jurassic belemnites: salinity vs. temperature signals. Journal of Sedimentary Research 74, 343-355.

Rosenthal, Y., Boyle, E.A. Slowey, N., 1997. Temperature control on the incorporation of magnesium, strontium, fluorine, and cadmium into benthic foraminiferal shells from Little Bahama Bank: Prospects for thermocline paleoceanography. Geochimica et Cosmochimica Acta 61, 3633-3643.

Sprovieri, M., Coccioni, R., Lirer, F., Pelosi, N. Lozar, F., 2006. Orbital tuning of a lower Cretaceous composite record (Maiolica Formation, central Italy). Paleoceanography 21, PA4212.

Steuber, T., 1999. Isotopic and chemical intra-shell variations in low-Mg calcite of rudist bivalves (Mollusca-Hippuritacea): disequilibrium fractionations and late Cretaceous seasonality. International Journal of Earth Sciences (Geol. Rundsch.) 88, 551-570.

Steuber, T. Rauch, M., 2005. Evolution of the Mg/Ca ratio of Cretaceous seawater: Implications from the composition of biological low-Mg calcite. Marine Geology 217, 199-213.

Stille, P., Riggs, S., Clauer, N., Ames, D., Crowson, R. Snyder, S., 1994. Sr and Nd isotopic analysis of phosphorite sedimentation through one Miocene high-frequency depositional cycle on the North Carolina continental shelf. Marine Geology 117, 253-273.

Stott, L.D. Kennett, J.P., 1989. New constraints on early Tertiary palaeoproductivity from carbon isotopes in foraminifera. Nature 342, 526-529.

Taylor, B., 2006. The single largest oceanic plateau: Ontong Java-Manihiki-Hikurangi. Earth and Planetary Science Letters 241, 372-380.

Van de Schootbrugge, B., Föllmi, K.B., Bulot, L.G. Burns, S.J., 2000. Paleoceanographic changes during the Early Cretaceous (Valanginian-Hauterivian): evidence from oxygen and carbon stable isotopes. Earth and Planetary Science Letters 181, 15-31.

Van de Schootbrugge, B., Kuhn, O., Adatte, T., Steinmann, P. Föllmi, K.B., 2003. Decoupling of P- and Corg-burial following Early Cretaceous (Valanginian-Hauterivian) platform drowning along the NW Tethyan margin. Palaeogeography, Palaeoclimatology, Palaeoecology 199, 315-331.

Veizer, J., 1983. Trace elements and isotopes in sedimentary carbonates. Reviews in Mineralogy

11, 265-299.

Vermeulen, J., 2002, Etude stratigraphique et paléontologique de la famille des Pulchelliidae (ammonoidea, Ammonitina, Endemoceratacea). In: Laboratoire de Géologie de l'Université I de Grenoble (ed.), Géologie Alpine. Grenoble, France, pp. 333.

Weissert, H., 1989. C-isotope stratigraphy, a monitor of paleoenvironmental change: a case study from the Early Cretaceous. Surveys in Geophysics 10, 1-61.

Weissert, H. Erba, E., 2004. Volcanism, CO2 and palaeoclimate; a Late Jurassic-Early Cretaceous carbon and oxygen isotope record. Journal of the Geological Society of London 161, 695-702.

Weissert, H., Lini, A., Föllmi, K.B. Kuhn, O., 1998. Correlation of Early Cretaceous carbon isotope stratigraphy and platform drowning events: a possible link? Palaeogeography, Palaeoclimatology, Palaeoecology 137, 189-203.

Weissert, H., McKenzie, J.A. Channell, J.E.T., 1985, Natural variations in the carbon cycle during the Early Cretaceous, In: E. T. Sundquist and W. S. Broecker (eds.), The carbon cycle and atmospheric CO2: Natural variations Archean to Present. Geophysical Monograph, American Geophysical Union, pp. 531-545.

Wierzbowski, H. Joachimski, M., 2007. Reconstruction of late Bajocian–Bathonian marine palaeoenvironments using carbon and oxygen isotope ratios of calcareous fossils from the Polish Jura Chain (central Poland). Palaeogeography, Palaeoclimatology, Palaeoecology 254, 523-540.

Wissler, L., Funk, H. Weissert, H., 2003. Response of Early Cretaceous carbonate platforms to changes in atmospheric carbon dioxide levels. Palaeogeography, Palaeoclimatology, Palaeoecology 200, 187-205.

Wissler, L., Weissert, H., Masse, J.-P. Bulot, L.G., 2002. Chemostratigraphic correlation of Barremian and lower Aptian ammonite zones and magnetic reversals. International Journal of Earth Sciences (Geol. Rundsch.) 91, 272-279.

Appendix 2: Raw Data

Matterhorn, Switzerland

ICP-MS Data

Alvier section, Switzerland

GEA N°	Sample ID	depth (m)	% sol	Al	Ca	Ti	V	Cr	Mn	Fe
33503	Al 1	113.60	71.06	704.17	215330.25	163.09	3.49	3.88	58.19	3440.89
33505	Al 3	112.05	58.51	1742.42	218695.14	181.89	4.54	4.86	83.20	6550.78
33509	Al 6	108.95	78.00	618.67	280441.15	276.12	6.00	4.23	88.05	4227.38
33512	Al 9	107.15	78.71	192.96	291810.48	309.05	2.36	2.16	85.07	2583.73
33514	Al 11	105.30	65.63	921.40	228422.02	173.61	2.78	2.37	73.70	4055.20
33515	Al 12	103.95	56.99	1306.17	190127.90	149.84	3.36	2.93	59.05	5242.71
33518	Al 15	101.95	68.61	1484.26	249912.42	199.98	4.12	3.33	83.90	4422.71
33521	Al 18	99.95	73.66	965.44	255339.30	186.29	3.87	2.74	75.18	3443.94
33523	Al 20	97.95	75.68	1125.02	267693.32	254.11	3.81	3.50	78.40	3719.36
33526	Al 23	95.40	79.41	2107.53	284179.43	335.32	6.80	5.84	95.79	4887.21
33530	Al 27	92.50	72.02	1049.44	258915.68	178.36	3.42	3.13	102.94	4352.95
33533	Al 30	90.05	81.62	1651.80	298634.67	299.89	4.43	3.57	131.67	4876.89
33536	Al 33	86.70	77.66	2083.00	280382.03	315.75	5.26	5.24	122.73	5391.92
33537	Al 34	85.60	76.41	2332.73	267239.36	232.55	5.91	5.15	107.93	5597.55
33538	Al 35	84.80	70.30	4888.37	320957.67	333.41	9.70	10.50	139.48	7934.68
33539	Al 36	83.50	79.50	1249.84	301676.28	209.96	3.39	1.64	110.29	3459.62
33540	Al 37	82.55	81.22	2087.16	341337.09	0.00	4.45	4.66	133.95	4040.95
33542	Al 39	81.00	78.57	1749.75	271078.04	224.86	3.99	2.85	99.78	4795.33
33544	Al 41	79.10	74.70	3559.52	349304.95	272.23	6.37	9.25	151.16	7060.11
33546	Al 43	77.05	67.13	3746.36	239942.26	187.19	7.40	7.91	97.56	9502.24
33548	Al 45	74.75	81.69	2944.25	384737.32	372.95	7.66	7.39	188.94	7599.73
33550	Al 47	72.90	73.98	4294.63	256118.73	192.99	7.83	9.33	136.55	11594.74
33553	Al 50	71.60	83.49	3796.55	356882.70	339.21	8.93	10.74	192.48	9249.90
33555	Al 52	70.30	78.68	3833.05	279356.31	229.00	5.75	7.84	153.95	8359.38
33558	Al 55	68.45	57.37	8028.22	239595.81	133.69	14.35	18.29	147.67	15240.02
33560	Al 57	66.75	81.15	3138.66	288829.51	237.37	5.94	8.57	171.75	8066.48
33563	Al 60	64.75	82.07	2929.05	371117.58	368.33	6.96	11.05	227.83	7770.37
33565	Al 62	63.00	75.72	2936.22	277383.27	197.13	4.95	6.40	193.01	6127.30
33567	Al 64	61.50	78.32	4887.46	329345.19	319.70	10.99	13.86	270.60	11692.00
33569	Al 66	60.25	83.35	2124.59	308530.03	261.92	5.35	4.43	241.08	6442.18
33571	Al 68	59.70	64.20	6217.81	274017.27	216.30	11.54	13.43	238.59	14610.95
33573	Al 70	58.60	83.27	2541.52	298220.38	249.42	6.15	5.93	237.32	7007.28
33575	Al 72	57.60	84.14	3225.38	384238.80	355.23	6.76	8.44	344.74	7672.51
33576	Al 73	56.40	78.38	2985.16	270770.55	214.76	6.74	6.88	201.99	7171.64
33579	Al 76	55.15	65.23	5582.02	278058.63	0.00	8.82	10.21	198.78	10433.71
33581	Al 78	54.60	68.72	3629.62	239673.58	188.25	5.98	7.81	165.39	8448.24
33584	Al 81	52.60	82.02	4005.94	366343.49	377.92	7.75	9.49	251.06	10634.67
33588	Al 85	50.70	81.62	4041.37	356237.53	359.43	7.28	8.52	312.99	11382.50
33589	Al 86	50.10	82.53	2402.42	360314.81	326.33	7.17	12.17	273.13	7926.24
33590	Al 87	49.60	84.33	1881.78	378396.33	356.57	5.13	9.53	262.50	6424.63
33591	Al 88	49.00	79.66	4102.70	353088.26	0.00	7.00	14.87	329.36	10140.75
33592	Al 89	48.35	77.92	4375.55	338594.53	331.51	6.92	10.28	371.40	10511.79
33593	Al 90	47.85	81.40	5166.74	351806.12	342.22	8.28	9.14	336.37	14189.05
33594	Al 91	47.40	77.80	5457.89	348837.40	330.66	8.14	10.88	352.29	11454.53
33595	Al 92	47.20	82.54	3611.14	356152.85	0.00	4.71	5.60	327.74	8422.31
33596	Al 93	46.25	84.65	1956.28	374586.72	364.47	5.40	8.97	328.04	7057.16
33597	Al 94	45.80	67.67	5034.52	293300.28	249.54	7.31	11.71	248.97	11397.84
33598	Al 95	44.85	83.18	3121.24	378368.52	368.73	5.64	9.26	322.35	8973.65
33599	Al 96	44.40	78.49	2105.93	339489.45	320.55	3.43	6.64	291.81	5714.11
33600	Al 97	43.55	79.80	3932.30	341813.28	325.80	8.40	9.84	311.11	9572.20
33601	Al 98	42.65	82.59	4235.78	337903.46	359.59	7.88	10.80	338.59	11327.15
33602	Al 99	42.00	83.55	2687.98	365608.00	391.93	4.88	8.75	326.93	8641.77
33603	Al 100	41.30	84.21	4029.27	381069.65	359.08	5.72	8.93	289.02	10205.47
33604	Al 101	40.75	72.13	6665.58	311101.48	308.18	8.77	12.48	252.06	17803.58
33605	Al 102	40.50	77.78	6756.20	333639.07	337.71	11.30	15.36	276.68	17677.43
33606	Al 103	39.90	77.64	5719.87	306817.75	290.29	9.68	12.13	249.62	15120.91
33607	Al 104	40.70	75.69	6180.24	327559.39	321.17	11.35	21.12	298.49	15714.24
33608	Al 105	40.20	85.91	4994.46	383559.31	324.98	9.89	12.26	361.59	12599.83
33610	Al 107	38.90	85.76	4883.08	386445.04	327.90	11.96	10.66	326.16	13510.72
33611	Al 108	38.45	58.62	6265.24	259183.76	194.23	10.46	11.59	212.23	14172.76
33612	Al 109	38.00	78.39	3562.67	341083.59	0.00	7.30	7.82	250.33	8967.67
33613	Al 110	36.95	75.92	4315.98	311643.38	296.61	8.93	10.74	244.79	13224.99
33614	Al 111	36.70	68.10	6176.66	297950.74	214.15	11.44	13.11	220.48	14526.46
33615	Al 112	36.10	80.54	3750.78	338492.55	326.10	8.23	9.62	282.60	9867.11
33616	Al 113	35.50	66.92	6891.15	277818.37	277.62	18.28	23.61	224.36	17555.90
33617	Al 114	35.00	74.31	5083.01	310616.97	254.43	11.16	13.94	243.69	12341.49
33618	Al 115	34.40	57.11	7234.49	215892.43	154.72	16.18	19.45	152.60	20430.97
33619	Al 116	33.85	77.23	3609.82	305874.43	338.41	9.90	16.58	177.05	12030.36
33620	Al 117	33.20	73.72	3365.57	282808.44	308.51	8.46	11.78	150.82	10996.64
33621	Al 118	32.40	73.71	3480.22	265569.17	200.12	7.37	10.23	113.50	8633.95
33622	Al 119	31.70	74.49	2999.29	273715.47	213.35	6.73	9.60	109.92	7487.54
33626	Al 123	28.80	58.33	2602.01	251675.11	152.34	5.76	5.29	87.93	7560.55
33630	Al 127	25.85	71.73	1967.56	269550.96	213.45	4.42	4.54	84.23	4936.27
33632	Al 129	23.95	71.01	2470.17	323626.11	0.00	4.69	7.30	116.37	6808.15
33636	Al 133	20.00	69.26	2262.86	259359.14	180.16	4.19	5.16	79.31	5402.15
33638	Al 135	18.00	74.47	2498.83	330492.17	329.85	5.75	7.75	115.14	6397.73
33642	Al 139	14.30	77.22	2314.68	292426.75	221.25	4.90	5.35	114.97	4213.18
33644	Al 141	12.35	84.27	3599.50	324185.77	274.27	6.38	9.06	179.43	7837.40
33646	Al 143	10.35	83.44	1617.09	306335.95	268.18	5.29	5.43	155.85	4519.40
33648	Al 145	8.30	81.92	1730.30	306294.99	237.03	4.03	4.08	174.64	4205.51
33650	Al 147	6.25	81.64	1143.37	365927.16	386.78	2.34	5.49	163.02	4101.90
33652	Al 149	4.30	84.38	1008.87	318499.26	261.40	3.00	3.35	148.46	3124.11
33654	Al 151	2.30	90.19	1558.75	335661.33	239.90	4.42	3.98	164.07	4014.60
33656	Al 153	0.00	73.09	1992.89	386071.29	334.85	7.36	7.59	178.12	5604.10

N. B.: All the data presented here are expressed in ppm and have been obtained using a HNO_3 acid extraction.

Alvier section, Switzerland (continued)

GEA N°	Sample ID	Co	Ni	Cu	Zn	As	Mo	Cd	Ba	U
33503	Al 1	0.72	8.23	2.06	110.56	1.23	0.36	0.40	3.28	0.49
33505	Al 3	2.28	19.38	4.41	23.07	2.42	0.60	0.07	7.61	0.24
33509	Al 6	1.16	13.30	1.68	32.80	1.28	0.38	0.08	7.82	1.94
33512	Al 9	0.82	13.45	1.07	13.65	0.63	0.43	0.07	3.96	0.54
33514	Al 11	1.16	9.89	1.45	5.85	1.16	0.43	0.00	4.56	0.22
33515	Al 12	0.88	12.08	3.05	13.31	2.17	0.43	0.00	3.79	0.20
33518	Al 15	1.29	12.59	2.22	12.55	0.95	0.12	0.00	4.87	0.33
33521	Al 18	1.18	10.77	2.84	16.57	0.66	0.08	0.02	3.48	0.17
33523	Al 20	1.33	13.61	2.19	23.51	1.22	0.55	0.00	7.37	0.42
33526	Al 23	1.69	17.64	3.32	11.95	1.38	0.82	0.00	10.60	0.43
33530	Al 27	1.19	14.26	1.97	20.13	2.14	0.31	0.00	7.09	0.41
33533	Al 30	1.64	16.92	2.75	25.59	0.55	0.06	0.02	9.37	0.16
33536	Al 33	1.73	13.45	3.64	25.80	1.23	0.00	0.00	6.55	0.24
33537	Al 34	1.51	18.40	5.33	21.09	0.88	0.07	0.00	7.97	0.23
33538	Al 35	4.88	34.75	10.88	59.06	2.60	0.44	0.00	15.54	0.33
33539	Al 36	1.08	14.62	2.71	18.35	0.60	0.00	0.10	7.71	0.30
33540	Al 37	1.13	17.28	2.86	11.94	0.35	0.06	0.00	12.01	0.31
33542	Al 39	2.16	15.49	4.49	21.34	1.03	0.14	0.00	8.79	0.14
33544	Al 41	3.07	20.90	6.09	37.63	1.91	0.37	0.00	11.79	0.30
33546	Al 43	5.40	27.09	18.25	60.70	2.64	0.25	0.09	10.76	0.39
33548	Al 45	1.91	23.88	3.98	28.70	0.47	0.08	0.00	12.06	0.49
33550	Al 47	6.07	25.70	10.28	56.11	2.35	0.21	0.00	11.72	0.28
33553	Al 50	3.16	23.25	6.06	49.49	0.71	0.37	0.06	34.43	0.31
33555	Al 52	1.56	21.54	5.40	22.47	0.43	0.30	0.00	12.87	0.21
33558	Al 55	5.04	40.81	14.02	90.25	1.65	0.25	0.11	13.33	0.49
33560	Al 57	1.76	21.74	5.61	35.05	1.06	0.11	0.00	10.46	0.27
33563	Al 60	1.43	26.91	5.23	27.04	0.17	0.09	0.00	13.79	0.30
33565	Al 62	1.70	18.86	5.45	16.95	0.41	0.00	0.05	10.72	0.37
33567	Al 64	3.03	33.91	8.68	49.88	0.96	0.30	0.10	25.70	0.40
33569	Al 66	1.34	20.23	3.20	19.64	0.16	0.00	0.00	9.41	0.23
33571	Al 68	5.59	44.52	16.26	51.18	2.65	0.00	0.13	13.76	0.37
33573	Al 70	2.93	19.17	5.70	36.49	0.94	0.00	0.00	13.02	0.16
33575	Al 72	2.21	26.70	5.18	53.53	0.92	0.00	0.00	29.67	0.31
33576	Al 73	2.05	21.29	10.47	18.63	0.19	0.00	0.00	11.77	0.28
33579	Al 76	3.65	26.22	10.03	56.98	1.41	0.06	0.00	15.97	0.36
33581	Al 78	3.25	24.77	7.97	39.93	0.49	0.00	0.10	9.87	0.25
33584	Al 81	3.04	28.43	9.32	36.35	0.44	0.23	0.04	9.74	0.23
33588	Al 85	3.36	28.97	8.10	25.41	0.73	0.12	0.00	8.16	0.24
33589	Al 86	2.35	23.01	5.51	25.12	0.19	0.00	0.00	9.23	0.31
33590	Al 87	1.63	19.59	4.32	19.56	0.40	0.44	0.00	9.42	0.20
33591	Al 88	3.96	30.93	5.35	35.33	0.95	0.01	0.00	14.12	0.20
33592	Al 89	5.54	31.99	8.93	66.45	1.31	0.00	0.00	16.06	0.48
33593	Al 90	5.67	33.66	5.22	37.86	0.80	0.13	0.00	11.31	0.34
33594	Al 91	5.41	31.14	8.19	38.99	1.90	0.00	0.00	14.74	0.27
33595	Al 92	2.22	20.11	2.96	19.51	0.92	0.00	0.00	9.88	0.36
33596	Al 93	2.64	21.19	6.74	15.90	0.44	0.00	0.00	10.56	0.30
33597	Al 94	6.00	29.09	11.37	50.72	2.55	0.13	0.00	9.29	0.35
33598	Al 95	3.07	21.38	5.21	29.15	0.52	0.00	0.00	10.25	0.20
33599	Al 96	3.54	21.70	6.01	35.90	1.52	0.03	0.00	16.08	0.51
33600	Al 97	3.13	30.63	7.56	28.68	0.54	0.00	0.00	10.98	0.73
33601	Al 98	3.58	27.70	7.21	32.09	1.00	0.00	0.00	16.27	0.50
33602	Al 99	3.06	23.77	3.91	26.95	0.66	0.00	0.00	9.36	0.41
33603	Al 100	4.02	24.63	5.87	42.10	1.48	0.00	0.00	9.84	0.24
33604	Al 101	5.09	32.06	8.59	44.26	2.12	0.06	0.00	8.37	0.21
33605	Al 102	4.22	27.96	9.16	32.27	0.80	0.00	0.00	11.06	0.41
33606	Al 103	2.51	27.35	6.74	38.12	0.00	0.08	0.00	10.25	0.35
33607	Al 104	6.02	33.71	12.74	39.49	1.32	0.14	0.00	21.55	1.02
33608	Al 105	2.51	31.77	7.13	29.61	0.20	0.00	0.00	12.28	0.38
33610	Al 107	2.98	23.90	7.67	33.90	0.58	0.12	0.00	9.18	0.90
33611	Al 108	6.27	30.54	11.78	64.55	2.51	0.18	0.00	13.62	0.73
33612	Al 109	3.12	22.89	4.28	34.79	1.54	0.29	0.00	22.04	0.81
33613	Al 110	4.60	22.07	6.00	45.98	2.31	0.15	0.04	10.73	0.38
33614	Al 111	4.49	25.14	6.76	68.49	2.13	0.02	0.25	10.44	0.78
33615	Al 112	2.75	24.88	3.59	25.51	0.72	0.00	0.00	7.59	0.49
33616	Al 113	5.13	29.33	5.80	31.83	2.28	0.07	0.00	19.85	0.67
33617	Al 114	3.89	23.51	5.01	45.15	1.58	0.10	0.00	13.25	0.69
33618	Al 115	5.94	29.86	11.08	63.65	3.24	0.00	0.00	12.86	0.52
33619	Al 116	4.18	24.60	5.24	25.60	3.51	0.09	0.00	6.52	1.03
33620	Al 117	3.10	22.45	4.55	29.88	1.07	0.00	0.00	6.90	0.64
33621	Al 118	2.68	15.79	3.68	26.57	1.36	0.43	0.06	8.42	0.51
33622	Al 119	2.56	14.57	10.22	28.18	1.62	0.00	0.00	6.22	0.53
33626	Al 123	1.78	24.06	4.69	30.70	2.53	0.00	0.00	6.46	0.28
33630	Al 127	1.56	10.42	3.54	13.43	0.92	0.15	0.00	5.33	0.34
33632	Al 129	2.13	17.45	4.21	22.40	1.12	0.00	0.00	5.03	0.23
33636	Al 133	1.58	14.32	2.74	19.06	0.61	0.03	0.00	4.67	0.24
33638	Al 135	1.75	16.69	4.01	15.51	0.79	0.05	0.00	6.08	0.33
33642	Al 139	1.06	14.28	1.82	17.94	0.56	0.04	0.02	7.18	0.28
33644	Al 141	2.80	22.65	5.20	29.05	1.20	0.16	0.00	10.93	0.40
33646	Al 143	2.08	11.93	2.51	17.16	0.49	0.00	0.00	5.38	0.31
33648	Al 145	1.88	12.74	1.95	18.52	0.32	0.00	0.00	6.07	0.22
33650	Al 147	1.71	17.49	3.17	13.15	0.32	0.01	0.00	3.20	0.28
33652	Al 149	1.47	11.32	3.32	9.79	0.28	0.17	0.05	4.19	0.23
33654	Al 151	1.44	11.43	1.46	12.94	0.23	0.00	0.00	3.87	0.19
33656	Al 153	2.12	20.51	5.75	32.34	0.60	0.00	0.00	5.33	2.01

Breggia section, Switzerland

GEA N°	Sample ID	Depth (m)	% Sol	Al	Ca	Ti	V	Cr	Mn	Fe
34619	BgV 1	0.15	93.07	1228.62	380138.06	363.77	2.60	3.35	422.90	2302.53
34620	BgV 2	0.63	92.44	696.45	351686.77	307.55	1.44	1.64	443.43	1986.30
34621	BgV 3	1.00	91.65	1000.00	328707.10	321.09	1.98	1.18	393.62	2062.84
34622	BgV 4	1.50	90.97	834.27	321012.44	303.49	1.78	0.35	392.19	1902.65
34623	BgV 5	2.00	93.35	907.03	322488.41	293.13	1.84	0.00	409.42	1849.87
34624	BgV 6	2.50	92.87	541.74	316022.24	313.55	1.24	0.17	384.59	1576.45
34625	BgV 7	3.00	93.75	527.74	308084.67	278.90	1.27	0.00	363.51	1489.68
34626	BgV 8	3.50	95.48	411.01	309617.68	318.66	1.01	0.09	366.60	1489.37
34627	BgV 9	4.10	92.79	873.60	293384.22	291.00	1.77	0.00	323.87	2973.53
34628	BgV 10	4.53	92.45	1635.04	424846.37	422.21	2.43	2.59	532.02	2644.10
34629	BgV 11	5.08	92.33	1169.18	396029.00	352.75	1.86	2.71	453.65	2319.89
34630	BgV 12	5.65	93.92	1165.90	409340.20	354.06	1.96	2.45	453.79	2310.65
34631	BgV 13	5.98	92.87	1020.23	386964.02	310.25	1.83	2.27	456.26	1998.44
34632	BgV 14	6.50	69.92	1206.13	280774.75	169.34	2.08	1.73	286.93	1695.10
34633	BgV 15	6.93	94.61	738.77	392699.92	369.83	1.83	2.35	485.06	2113.61
34634	BgV 16	7.50	93.41	1054.29	389266.64	332.98	1.78	2.54	468.38	2305.62
34635	BgV 17	7.95	90.92	1331.56	380152.32	305.75	2.37	2.99	421.12	2251.87
34636	BgV 18	9.20	89.90	1963.15	378776.68	327.32	3.35	3.48	462.86	2837.81
34637	BgV 19	9.75	78.66	4183.88	315666.79	230.72	6.16	5.07	396.59	3684.81
34638	BgV 20	10.25	87.82	1956.33	367443.84	332.10	3.18	3.00	538.63	3601.18
34639	BgV 21	10.75	88.24	1783.75	363632.38	330.55	2.62	4.53	552.97	3345.72
34640	BgV 22	11.00	49.98	1218.67	194100.03	110.37	2.18	0.97	268.39	1990.31
34641	BgV 23	11.30	87.01	2295.73	351465.07	269.62	2.93	4.23	496.89	3294.53
34642	BgV 24	11.40	83.98	3097.05	319746.63	275.74	3.77	3.85	510.62	4133.03
34643	BgV 25	11.50	88.07	1647.11	350027.43	307.27	2.29	2.53	601.94	2740.46
34644	BgV 26	11.68	48.52	1524.03	165499.72	135.44	1.98	0.73	231.06	2152.35
34645	BgV 27	11.90	90.62	1419.72	364326.23	340.39	2.18	0.82	556.71	2743.41
34646	BgV 28	12.15	88.03	2818.97	383925.64	308.62	4.43	3.71	546.01	4232.61
34647	BgV 29	12.50	91.13	1142.06	394098.87	322.25	2.13	2.78	565.33	3187.41
34648	BgV 30	12.90	44.04	1445.82	173109.73	97.25	2.40	1.27	185.58	2277.54
34649	BgV 31	13.05	91.04	1209.82	390980.42	340.63	1.91	2.58	552.02	2842.16
34650	BgV 32	13.25	87.29	1865.42	382506.96	287.12	3.07	3.47	616.56	3147.86
34651	BgV 33	13.50	89.76	1479.03	365040.45	248.49	2.30	1.87	509.27	2996.14
34652	BgV 34	13.65	90.56	1211.70	389426.88	320.43	2.63	2.49	527.43	2829.48
34653	BgV 35	14.00	88.78	1607.30	370486.64	302.66	2.36	2.83	541.70	2923.59
34654	BgV 36	14.50	95.17	712.35	404529.79	369.20	1.35	1.22	690.79	2521.16
34655	BgV 37	15.00	92.69	1409.22	437716.69	320.69	2.45	3.16	698.19	2897.00
34656	BgV 38	15.50	92.71	930.36	457572.27	340.45	2.00	2.39	769.47	2710.79
34657	BgV 39	16.00	93.25	883.83	429952.82	372.70	1.55	2.78	777.73	2506.83
34658	BgV 40	16.45	91.57	1113.36	427926.74	361.63	2.54	2.80	681.62	2676.88
34659	BgV 41	16.95	60.86	756.52	256286.07	173.38	1.16	2.00	303.98	1745.76
34661	BgV 43	17.55	24.83	1768.15	406171.82	311.90	2.73	3.27	494.03	3330.86
34662	BgV 44	18.00	92.92	1095.81	415187.36	5.15	1.55	1.59	487.79	2921.43
34663	BgV 45	18.50	89.98	3235.93	378918.37	292.36	4.88	5.93	378.83	3944.52
34664	BgV 46	19.10	85.61	1667.01	404042.10	321.89	2.58	3.03	527.12	3452.01
34665	BgV 47	19.55	91.59	1950.12	404955.33	397.55	3.60	4.24	510.78	3547.55
34666	BgV 48	21.13	92.69	1357.64	426130.11	388.78	2.19	2.12	601.10	3781.49
34667	BgV 49	21.55	84.37	2877.42	372764.71	234.23	3.51	3.84	440.98	3843.54
34668	BgV 50	21.93	90.80	1890.05	423336.40	386.67	2.92	4.24	556.83	4491.07
34669	BgV 51	26.10	92.97	560.12	260183.48	200.64	1.11	0.00	262.20	1507.22
34670	BgV 52	26.50	66.63	494.17	186599.51	0.00	1.22	0.00	198.77	1308.44
34671	BgV 53	26.95	94.27	483.60	298206.62	190.22	1.27	0.00	281.12	1711.85
34672	BgV 54	27.48	93.28	681.07	289843.33	218.10	1.81	0.00	287.89	1755.51
34673	BgV 55	27.98	91.92	887.28	285423.48	206.04	1.28	0.00	286.38	1851.46
34674	BgV 56	28.35	92.43	2171.06	414286.14	284.70	3.54	3.29	401.28	3203.37
34675	BgV 57	28.88	92.03	1299.79	426621.45	267.71	2.37	2.60	384.85	2610.19
34676	BgV 58	29.38	90.06	1965.19	416922.56	257.93	2.39	3.27	420.78	2902.21
34677	BgV 59	29.85	93.76	1223.23	432532.25	243.08	1.72	2.15	412.77	2699.45
34678	BgV 60	30.25	93.88	1405.71	429018.33	256.78	1.74	2.40	429.46	2513.03

Breggia section, Switzerland (continued)

GEA N°	Sample ID	Depth (m)	Co	Ni	Cu	Zn	As	Mo	Ba	U
34619	BgV 1	0.15	2.56	22.38	4.49	12.95	0.00	0.27	11.30	0.29
34620	BgV 2	0.63	3.31	25.98	4.00	14.82	0.57	0.06	9.21	0.18
34621	BgV 3	1.00	2.85	27.83	4.17	12.34	0.32	0.16	10.15	0.29
34622	BgV 4	1.50	2.16	25.51	8.10	8.73	0.13	0.11	10.00	0.15
34623	BgV 5	2.00	2.23	23.22	5.06	13.47	0.12	0.05	12.55	0.18
34624	BgV 6	2.50	2.32	23.30	2.18	6.24	0.19	0.00	10.32	0.16
34625	BgV 7	3.00	2.86	20.41	4.09	2.17	0.20	0.07	10.11	0.20
34626	BgV 8	3.50	1.43	20.05	3.22	6.52	0.00	0.00	8.16	0.08
34627	BgV 9	4.10	4.61	27.73	4.40	10.95	0.79	0.32	11.81	0.29
34628	BgV 10	4.53	3.85	32.55	2.51	5.23	0.16	0.28	15.15	0.33
34629	BgV 11	5.08	2.29	27.60	5.63	10.66	0.00	0.03	13.88	0.44
34630	BgV 12	5.65	3.50	27.41	4.57	18.36	1.07	0.03	13.84	0.55
34631	BgV 13	5.98	2.66	30.86	2.78	5.73	0.44	0.12	11.95	0.14
34632	BgV 14	6.50	2.10	19.03	2.64	7.68	0.00	0.00	12.33	0.25
34633	BgV 15	6.93	2.67	25.97	6.55	8.75	0.33	0.04	11.99	0.56
34634	BgV 16	7.50	2.65	27.60	5.59	10.58	1.29	0.00	17.79	0.41
34635	BgV 17	7.95	2.54	28.94	7.32	5.52	0.42	0.00	26.59	0.34
34636	BgV 18	9.20	3.03	25.48	6.19	14.93	0.00	0.00	19.88	0.33
34637	BgV 19	9.75	5.08	25.88	13.71	22.12	1.50	0.23	37.18	0.46
34638	BgV 20	10.25	5.65	31.24	10.77	23.54	0.65	0.08	27.08	0.14
34639	BgV 21	10.75	5.89	35.58	11.19	21.36	0.56	0.00	25.44	0.34
34640	BgV 22	11.00	5.12	18.66	9.65	28.63	0.00	0.00	11.26	0.30
34641	BgV 23	11.30	4.80	28.03	10.26	18.37	0.00	0.19	27.49	0.40
34642	BgV 24	11.40	6.87	35.98	14.19	23.86	0.08	0.00	21.00	0.26
34643	BgV 25	11.50	4.24	30.41	9.18	21.28	0.25	0.05	17.39	0.21
34644	BgV 26	11.68	4.35	15.06	7.92	40.42	0.24	0.00	13.92	0.15
34645	BgV 27	11.90	3.52	30.95	8.00	7.18	0.08	0.00	18.52	0.27
34646	BgV 28	12.15	4.66	31.27	10.29	16.88	1.71	0.23	31.53	0.43
34647	BgV 29	12.50	4.59	35.53	6.87	16.70	0.97	0.00	22.02	0.20
34648	BgV 30	12.90	4.44	16.43	14.95	7.33	1.02	0.14	14.88	0.27
34649	BgV 31	13.05	3.14	27.88	6.30	10.40	0.89	0.05	20.39	0.58
34650	BgV 32	13.25	3.51	30.23	8.63	14.73	1.14	0.00	20.29	0.25
34651	BgV 33	13.50	3.12	28.65	6.96	4.65	0.36	0.09	21.06	0.45
34652	BgV 34	13.65	3.27	28.63	7.40	15.60	0.43	0.00	14.95	0.42
34653	BgV 35	14.00	3.60	28.47	8.60	7.47	0.52	0.03	16.72	0.32
34654	BgV 36	14.50	2.11	28.43	3.21	13.71	0.76	0.09	12.00	0.42
34655	BgV 37	15.00	2.98	31.99	5.29	3.32	0.58	0.43	13.65	0.54
34656	BgV 38	15.50	2.71	33.13	4.64	12.02	0.00	0.20	12.10	0.38
34657	BgV 39	16.00	3.26	29.15	5.69	15.07	0.44	0.00	14.12	0.51
34658	BgV 40	16.45	2.85	34.11	5.74	17.49	0.36	0.00	17.71	0.44
34659	BgV 41	16.95	1.33	17.24	4.56	22.64	0.28	0.00	8.11	0.22
34661	BgV 43	17.55	3.97	33.13	10.69	23.86	0.09	0.00	65.74	0.36
34662	BgV 44	18.00	2.65	28.97	3.19	11.04	0.19	0.00	12.54	0.25
34663	BgV 45	18.50	3.97	30.26	14.07	22.11	0.26	0.00	28.55	0.73
34664	BgV 46	19.10	2.88	30.64	6.34	18.37	0.35	0.00	41.09	0.39
34665	BgV 47	19.55	3.72	39.13	6.30	10.68	1.02	0.13	21.43	0.70
34666	BgV 48	21.13	2.57	30.44	6.59	4.94	0.70	0.00	15.98	0.30
34667	BgV 49	21.55	5.02	36.71	13.40	15.61	0.85	0.14	25.24	0.41
34668	BgV 50	21.93	4.31	36.75	14.05	20.04	1.56	0.00	16.17	0.35
34669	BgV 51	26.10	1.73	23.33	3.98	4.87	0.69	0.00	8.13	0.10
34670	BgV 52	26.50	2.01	19.66	7.54	13.98	0.50	0.00	12.58	0.11
34671	BgV 53	26.95	2.28	26.30	21.90	9.07	0.83	0.00	8.10	0.22
34672	BgV 54	27.48	2.79	29.48	16.64	17.13	0.36	0.00	30.31	0.11
34673	BgV 55	27.98	2.36	29.64	3.97	7.79	0.47	0.00	15.19	0.08
34674	BgV 56	28.35	3.27	46.22	11.78	25.91	0.84	0.48	20.70	0.24
34675	BgV 57	28.88	2.77	40.74	9.42	12.12	0.70	0.00	12.98	0.14
34676	BgV 58	29.38	2.89	37.25	6.17	16.57	0.00	0.00	21.39	0.09
34677	BgV 59	29.85	3.38	41.62	5.49	5.15	0.12	0.00	63.66	0.09
34678	BgV 60	30.25	3.04	35.28	4.17	10.32	0.48	0.00	12.53	0.09

Cassis/La Bédoule section, France

N° GEA	N° Client	depth (m)	% sol	Al	Ca	V	Cr	Mn	Fe
28438	BE 119	55.70	55.70	1048.14	208406.45	3.15	2.55	116.32	1252.67
28439	BE 120	56.28	56.28	1671.91	300840.73	5.48	4.69	161.08	2254.42
28440	BE 121	56.86	56.86	1097.78	273645.05	3.36	3.41	144.60	2261.50
28441	BE 122	57.44	57.44	851.84	283245.17	2.79	3.98	155.67	2422.81
28442	BE 123	58.02	58.02	658.13	263753.96	2.75	3.87	147.60	1619.71
28443	BE 125	60.00	60.00	553.48	262978.60	2.11	2.48	139.04	1133.14
28444	BE 127	61.86	61.86	558.34	255605.75	2.21	2.17	133.40	1496.65
28445	BE 128	62.79	62.79	1010.94	244404.27	2.65	3.93	116.34	1677.53
28446	BE 129	63.95	63.95	1881.39	246613.02	4.17	5.38	195.17	5243.69
28449	BE 135	70.81	70.81	1335.30	232324.82	3.24	3.61	121.54	2101.73
28451	BE 136b	72.79	72.79	1959.76	275742.97	5.09	4.45	111.04	2640.69
28452	BE 137	74.19	74.19	1568.82	318029.72	3.29	3.82	132.54	3945.12
28456	BE 140	80.47	80.47	726.31	288103.45	2.20	3.15	122.69	1521.28
28458	BE 142	82.79	82.79	1260.20	314618.72	3.58	3.71	126.41	2231.89
28460	BE 144	85.58	85.58	1449.20	302030.45	4.34	4.93	124.80	1693.69
28461	BE 145	87.09	87.09	1574.90	291226.07	3.76	4.02	115.91	2821.83
28462	BE 145top	88.37	88.37	1263.00	317593.60	2.90	3.66	127.68	2177.96
28463	BE 147	91.16	91.16	1414.49	286754.16	3.94	6.53	349.05	2551.92
28464	BE 147*	91.79	88.14	2699.86	328598.77	5.20	5.46	403.66	4153.57
28465	BE 148	92.32	92.32	1078.45	268844.26	2.88	4.02	310.44	1825.27
28466	BE 149	92.72	90.02	1227.46	341916.18	2.60	3.97	284.13	2540.47
28467	BE 150	93.04	93.04	780.95	314655.55	1.62	2.44	291.50	1473.05
28468	BE 151	93.39	86.42	1817.87	316537.31	4.23	3.97	194.73	3718.99
28469	BE 152a	93.66	93.66	1828.99	252799.07	4.54	5.38	179.42	3286.70
28470	BE 152a1	93.91	79.31	2276.98	273063.94	3.76	4.66	154.24	4792.18
28471	BE 152a2	94.56	86.27	2167.26	310479.20	4.54	4.29	183.80	4955.96
28472	BE 152a3	94.82	83.95	1742.49	310170.53	3.59	3.98	176.75	3946.75
28473	BE 152b1	95.12	66.51	1893.29	289943.10	3.15	3.67	161.74	5563.73
28474	BE 152b2	95.42	66.93	2847.27	269481.97	3.98	5.06	147.02	7329.45
28475	BE 152b3	95.72	83.65	2072.01	300099.00	4.12	3.48	168.36	4336.75
28476	BE 152 top	95.98	95.98	2115.41	232390.73	4.23	5.66	141.71	4826.40
28477	BE 153a1	96.33	73.65	5211.43	268205.74	8.14	10.25	145.36	7808.24
28478	BE 153a2	96.63	74.21	2849.80	274038.43	3.90	5.68	144.76	5845.92
28479	BE 153a3	96.88	96.88	2173.07	240055.40	4.67	5.56	143.53	5432.91
28480	BE 153b1	97.18	76.72	2314.14	275005.04	3.74	4.47	140.76	7756.10
28481	BE 153b2	97.48	69.58	3273.23	244707.06	2.71	4.44	143.80	5854.66
28482	BE 153b3	97.88	67.23	3914.13	231293.21	3.65	5.52	144.73	7291.09
28483	BE 153b4	98.30	98.30	2241.36	226153.61	3.82	4.14	145.84	3864.57
28484	BE 154a	98.69	73.66	2530.40	269187.15	3.44	4.02	156.80	5310.17
28485	BE 154b	98.99	81.57	3434.78	233671.79	4.29	5.39	139.63	6950.80
28486	BE 155a	99.29	77.16	3358.17	235023.48	4.47	6.29	129.04	5784.06
28487	BE 155b	99.59	69.97	3830.82	247087.98	5.00	7.25	137.37	5586.81
28488	BE 156a	99.68	78.04	3635.28	274552.39	6.76	8.09	149.52	5349.32
28489	BE 156b	99.97	73.61	2102.85	267904.36	3.66	5.18	128.76	4234.04
28490	BE 156c	100.15	64.49	2802.52	221025.15	3.83	5.26	103.52	6267.84
28491	BE 156d	100.31	69.70	1996.99	236556.75	2.76	3.48	95.77	4633.35
28492	BE 156e	100.54	77.43	1993.93	263920.91	3.08	4.25	121.48	3798.59
28493	BE 157a	100.75	82.55	1809.90	135731.14	2.81	3.75	56.15	2799.31
28494	BE 157b	101.03	74.59	1531.08	258064.60	2.78	3.39	110.06	3021.74
28495	BE 157c	101.28	69.17	2232.39	233302.75	4.57	4.69	91.78	4569.08
28496	BE 157d	101.68	64.51	2683.61	219415.47	4.67	4.84	85.20	4554.53
28497	BE 158a	102.18	61.13	3345.83	201110.80	6.18	8.15	75.87	5289.53
28498	BE 158b	102.76	60.90	2602.94	194519.86	4.53	5.25	69.66	4431.30
28499	BE 159a	103.02	67.45	4028.10	233658.44	8.16	9.92	86.53	5619.43
28500	BE 159b	103.56	56.33	2829.50	196805.08	5.70	6.84	63.28	5995.72
28501	BE 160	103.96	69.89	2295.90	224439.27	5.83	6.06	77.06	3492.69
28502	BE 161a	104.35	64.34	2953.05	222529.55	6.62	6.93	66.28	5861.31
28503	BE 161b	104.73	70.78	1457.48	244734.25	3.58	4.13	78.54	3225.72
28504	BE 161c	105.27	74.34	2201.28	251902.54	4.31	4.46	76.56	3836.24
28505	BE 162a	105.63	67.21	1759.16	207602.81	5.69	5.37	54.93	3136.46
28506	BE 162b	106.29	75.99	1141.62	215509.25	3.53	4.38	64.34	2280.77
28507	BE 163a	106.76	64.21	3627.24	213621.22	7.23	7.60	62.52	5904.93
28508	BE 163b	107.00	70.22	3091.41	220554.53	6.80	7.46	67.97	4294.24
28509	BE 164a	107.59	69.86	2372.13	199201.38	8.57	6.05	56.64	3931.55
28510	BE 164b	107.86	75.76	1473.65	238161.18	6.28	4.67	65.62	2551.52
2851	BE 164c	108.31	68.86	1343.91	220288.97	4.93	4.58	57.77	2641.63

Cassis/La Bédoule section, France (continued)

N° GEA	N° Client	Co	Ni	Cu	Zn	As	Mo	Cd	Ba
28438	BE 119	0.97	8.38	2.04	9.11	0.82	0.21	0.07	4.17
28439	BE 120	1.80	17.57	3.31	17.43	1.54	0.57	0.16	5.92
28440	BE 121	1.58	16.40	2.83	15.56	1.79	0.32	0.09	4.54
28441	BE 122	1.74	18.63	2.27	13.26	1.79	0.26	0.14	4.28
28442	BE 123	1.34	13.83	1.95	17.06	1.11	0.16	0.09	3.71
28443	BE 125	1.21	10.73	1.62	8.33	0.48	0.09	0.06	3.33
28444	BE 127	1.60	12.71	2.03	6.72	0.96	0.25	0.07	4.46
28445	BE 128	2.00	16.01	2.47	12.81	1.02	0.31	0.09	4.26
28446	BE 129	3.99	19.64	5.53	21.41	2.92	0.16	0.07	16.98
28449	BE 135	1.67	13.54	3.46	20.71	1.40	0.22	0.08	5.08
28451	BE 136b	1.74	14.43	4.12	20.94	2.22	0.30	0.08	6.39
28452	BE 137	1.30	14.37	3.65	16.85	2.27	0.70	0.09	5.60
28456	BE 140	0.90	16.12	1.85	10.56	0.85	0.31	0.03	3.20
28458	BE 142	1.20	13.72	4.60	17.48	1.55	0.47	0.11	4.89
28460	BE 144	1.24	12.65	2.66	10.36	1.68	0.89	0.05	4.92
28461	BE 145	2.05	15.69	4.00	14.37	1.74	0.78	0.00	5.44
28462	BE 145top	1.11	14.56	2.95	16.28	1.41	0.50	0.07	5.08
28463	BE 147	1.49	13.84	3.10	22.86	1.98	0.33	0.31	5.54
28464	BE 147*	5.32	26.33	5.85	22.51	3.89	0.45	0.00	7.12
28465	BE 148	1.20	11.01	1.51	7.98	0.83	0.20	0.00	4.04
28466	BE 149	3.52	17.79	3.45	16.35	1.42	0.13	0.00	5.37
28467	BE 150	0.73	9.72	3.80	7.18	0.61	0.04	0.02	3.74
28468	BE 151	2.33	19.95	4.03	18.49	2.69	0.00	0.00	6.86
28469	BE 152a	1.74	16.68	2.59	12.70	1.94	0.09	0.01	5.63
28470	BE 152a1	1.82	24.80	6.22	29.07	2.97	0.20	0.00	8.19
28471	BE 152a2	2.56	19.02	5.88	31.86	2.12	0.00	0.00	6.42
28472	BE 152a3	1.50	15.17	4.76	18.81	2.39	0.00	0.00	7.84
28473	BE 152b1	2.95	26.82	7.09	30.51	3.75	0.30	0.00	7.51
28474	BE 152b2	3.82	38.91	6.74	31.19	4.00	0.21	0.00	9.62
28475	BE 152b3	3.31	24.16	4.79	19.27	1.50	0.00	0.00	8.08
28476	BE 152 top	2.50	20.01	4.44	18.69	2.57	0.25	0.01	10.52
28477	BE 153a1	4.92	35.37	7.74	27.71	4.38	0.43	0.00	12.33
28478	BE 153a2	3.81	23.77	7.39	22.96	2.56	0.36	0.00	6.39
28479	BE 153a3	2.94	17.73	4.07	23.21	2.76	0.28	0.03	6.61
28480	BE 153b1	3.54	22.52	6.89	31.29	3.33	0.42	0.00	7.92
28481	BE 153b2	4.51	21.70	9.11	30.79	1.53	0.32	0.00	9.13
28482	BE 153b3	4.74	23.30	9.73	31.28	3.58	0.00	0.00	10.49
28483	BE 153b4	2.90	18.92	4.35	15.85	2.40	0.00	0.02	7.19
28484	BE 154a	4.51	25.57	7.26	18.81	4.08	0.29	0.00	8.35
28485	BE 154b	6.42	30.29	9.17	39.61	5.19	0.46	0.00	11.07
28486	BE 155a	5.22	26.69	7.37	30.78	3.10	0.37	0.00	9.19
28487	BE 155b	5.00	26.79	9.01	37.95	3.55	0.27	0.00	10.18
28488	BE 156a	3.92	28.03	5.39	39.60	3.78	0.58	0.00	9.44
28489	BE 156b	3.94	31.00	6.11	27.70	3.86	0.15	0.00	7.60
28490	BE 156c	4.55	35.85	8.95	43.23	4.26	0.14	0.04	10.22
28491	BE 156d	3.47	26.45	6.68	30.74	3.29	0.05	0.09	7.10
28492	BE 156e	3.15	18.19	4.18	22.39	2.70	0.14	0.00	7.81
28493	BE 157a	1.87	16.65	2.94	19.77	1.63	0.12	0.04	5.44
28494	BE 157b	2.17	17.36	4.38	25.85	1.53	0.00	0.00	6.95
28495	BE 157c	3.35	29.89	7.84	39.19	3.05	0.28	0.04	8.07
28496	BE 157d	2.71	24.19	6.57	52.89	3.00	0.00	0.17	8.75
28497	BE 158a	3.73	24.02	7.46	48.99	3.85	0.26	0.10	9.03
28498	BE 158b	2.75	24.76	6.55	41.82	2.67	0.33	0.10	8.48
28499	BE 159a	2.51	23.24	5.70	40.51	2.22	0.01	0.00	11.19
28500	BE 159b	3.63	34.46	8.55	56.35	3.56	0.00	0.00	9.92
28501	BE 160	1.89	21.28	3.94	25.02	2.04	0.35	0.19	7.98
28502	BE 161a	2.82	40.47	6.98	37.85	2.91	0.14	0.12	9.91
28503	BE 161b	1.03	14.71	3.39	12.61	1.13	0.08	0.04	6.09
28504	BE 161c	2.36	22.02	5.34	30.52	1.41	0.28	0.00	9.16
28505	BE 162a	0.98	15.93	3.84	19.95	2.02	0.06	0.07	7.47
28506	BE 162b	0.99	13.16	2.47	15.42	1.08	0.09	0.01	5.55
28507	BE 163a	4.02	42.64	9.14	37.42	3.15	0.22	0.00	11.60
28508	BE 163b	2.28	21.17	4.65	26.99	1.73	0.17	0.09	9.16
28509	BE 164a	1.80	18.88	3.78	29.47	3.61	0.65	0.13	7.74
28510	BE 164b	0.91	12.10	3.45	10.74	1.35	0.04	0.07	6.36
28511	BE 164c	1.22	14.85	4.27	19.00	1.16	0.11	0.09	6.40

Capriolo section, Italy

GEA N°	Sample ID	depth (m)	% Sol	Al	Ca	V	Cr	Mn	Fe
28271	CA 1	0.20	95.29	1465.88	283450.66	2.80	3.50	305.95	6573.04
28273	CA 3	1.65	95.96	909.43	300040.71	1.48	2.31	336.42	1755.91
28275	CA 5	3.44	94.73	869.13	288152.26	1.37	1.03	363.49	1496.50
28277	CA 7	5.11	93.11	944.19	277992.46	1.48	1.90	532.40	1864.16
28279	CA 9	6.94	94.03	984.66	270204.13	1.57	1.44	345.70	1583.58
28281	CA 11	8.72	95.80	577.18	290193.23	0.92	0.84	452.62	1255.09
28283	CA 13	10.92	96.40	433.32	285699.60	0.84	0.75	776.48	1116.24
28285	CA 15	12.40	94.95	812.44	285152.96	2.12	0.93	911.56	1586.84
28287	CA 16	12.95	96.96	794.20	271292.75	1.74	0.92	437.72	1281.10
28289	CA 18	14.00	95.81	550.27	265698.81	1.19	0.93	467.84	1208.38
28291	CA 20	15.52	95.99	693.46	274324.52	2.01	1.20	540.32	1254.96
28293	CA 22	15.74	96.92	809.57	296696.89	2.49	1.81	782.84	1530.82
28296	CA 25	16.39	96.88	486.66	278547.33	1.05	1.25	732.34	1261.95
28297	CA 26	17.24	97.56	405.09	270358.73	0.93	1.07	985.33	1135.60
28298	CA 27	18.95	97.25	422.29	276464.66	0.92	0.64	2669.52	1153.72
28301	CA 30	19.75	96.97	380.90	296454.57	0.79	0.65	2361.07	1091.49
28303	CA 32	20.36	95.84	680.69	257997.58	1.47	1.32	1994.94	1194.15
28305	CA 34	21.56	96.81	664.95	296245.39	2.76	0.99	2525.45	2233.29
28307	CA 36	22.22	96.75	543.36	283161.04	1.66	1.19	1239.05	1323.86
28309	CA 38	23.40	95.60	685.12	277565.62	1.65	1.57	557.65	1415.28
28311	CA 40	25.39	96.77	397.55	278974.56	0.96	1.45	420.69	1195.01
28313	CA 42	26.04	96.00	611.67	269424.05	1.35	1.31	360.57	1346.78
28315	CA 44	27.76	96.56	380.66	282942.09	1.01	1.37	332.88	1279.66
28317	CA 46	28.21	94.79	656.02	273399.43	1.29	1.37	313.59	1494.64
28320	CA 49	29.80	95.36	629.24	281257.60	1.33	1.05	323.47	1664.42
28323	CA 52	31.05	95.72	856.26	287870.68	1.88	1.68	343.52	1680.56
28325	CA 54	31.78	96.08	813.26	306976.19	1.79	1.65	400.32	1510.02
28327	CA 56	33.05	94.56	601.99	295727.97	1.36	2.11	359.43	1458.04
28329	CA 58	33.74	85.87	1951.93	259033.63	4.13	4.69	284.53	2961.02
28331	CA 60	35.24	95.40	399.04	291053.34	0.82	0.91	365.39	1255.59
28333	CA 62	36.29	96.79	291.84	306893.16	0.68	1.42	359.26	1151.46
28335	CA 64	37.79	96.24	394.57	295698.45	0.92	1.78	356.15	1290.62
28336	CA 65	38.00	84.35	2169.45	262405.41	4.32	4.50	286.42	3143.85
28337	CA 66	38.64	96.23	375.06	302630.75	0.93	1.34	372.68	1264.40
28339	CA 68	40.24	94.51	718.16	295032.83	1.50	1.85	414.90	1681.89
28341	CA 70	40.88	94.28	861.22	283887.65	2.03	2.06	385.14	1460.55
28343	CA 72	41.97	93.92	808.51	278512.43	1.72	1.79	338.01	1563.32
28345	CA 74	43.27	94.11	712.35	279263.18	1.60	2.27	369.60	1459.22
28347	CA 76	44.10	94.16	713.57	279229.50	1.94	2.35	334.07	1553.87
28349	CA 78	45.27	93.33	1040.79	284743.90	2.43	2.43	367.62	1680.61
28352	CA 81	47.47	96.05	413.93	292421.23	1.20	1.31	384.24	1613.70
28354	CA 83	48.47	95.12	549.48	284522.98	1.28	1.50	367.69	1388.83
28356	CA 85	49.83	94.37	592.56	283611.07	1.50	1.75	406.45	1391.77
28358	CA 87	50.96	94.52	813.20	281216.15	1.52	1.86	422.16	1488.76
28360	CA 89	51.66	94.97	809.53	297814.72	1.47	1.68	439.83	1673.24
28362	CA 91	53.13	93.85	480.63	302038.39	0.97	1.22	514.75	1502.18
28366	CA 94	54.41	94.24	669.74	293811.64	1.38	1.58	594.19	1505.44
28371	CA 99	54.96	94.84	475.96	301410.39	1.19	1.46	489.89	1317.71
28373	CA 101	55.74	95.07	519.67	300599.28	1.20	1.86	564.84	1237.14
28376	CA 104	56.27	94.05	791.48	283550.99	1.92	1.57	602.00	1575.92
28378	CA 106	56.83	94.28	524.23	295670.49	1.19	1.43	511.97	1462.38
28381	CA 109	57.88	93.96	734.16	289353.47	1.61	2.41	429.24	1702.33
28382	CA 110	58.58	92.69	944.55	271545.93	1.75	2.20	472.33	1774.53
28385	CA 113	59.83	91.15	1370.94	319343.91	2.28	3.43	495.46	2092.73
28388	CA 116	60.66	92.45	917.05	312732.14	1.80	3.19	456.54	1983.48
28390	CA 118	61.63	91.22	1158.33	302650.79	2.18	3.98	465.28	2407.31
28392	CA 120	62.93	93.72	1043.67	313268.64	2.04	2.87	436.54	2354.70
28395	CA 123	64.54	90.42	1309.36	300631.20	2.26	3.61	467.37	2551.50
28397	CA 125	65.99	88.60	1887.60	324268.51	3.11	4.61	608.63	3742.14
28400	CA 128	66.77	93.71	872.84	346083.90	1.66	2.97	505.52	2265.46
28402	CA 130	67.29	89.67	1533.85	331747.69	2.55	4.15	509.37	2917.06
28406	CA 134	69.24	94.17	811.33	346869.78	1.38	2.12	450.92	2053.52
28408	CA 136	70.29	92.23	1344.05	318797.01	2.21	2.73	388.51	2210.64
28410	CA 138	71.50	93.72	751.48	334915.30	1.55	2.06	355.84	1897.96
28414	CA 142	73.72	93.15	742.05	320759.52	1.36	2.30	392.44	2089.06
28418	CA 146	75.45	91.15	1462.15	317467.26	2.24	2.72	378.15	2685.98
28420	CA 148	76.85	92.64	1007.26	330696.23	1.86	2.71	358.38	2291.94
28421	CA 149	77.70	94.29	820.80	322550.88	1.58	2.07	338.22	2065.59
28423	CA 151	79.78	93.40	1141.84	316457.11	1.91	2.36	342.22	2207.17
28425	CA 153	81.38	93.92	585.34	325418.18	1.05	1.15	309.93	1726.36
28426	CA 154	82.39	95.37	673.66	351752.18	1.22	1.37	316.70	1858.59
28427	CA 155	83.79	94.27	1474.40	333795.19	2.68	3.05	321.84	2335.74
28429	CA 157	86.30	92.13	1071.75	340770.90	2.12	2.69	388.18	2492.25
28431	CA 159	88.63	91.77	1274.70	329307.65	2.12	3.05	439.16	2547.42
28433	CA 161	91.36	90.36	1210.55	327058.48	2.41	2.61	413.76	2409.22
28437	CA 165	94.76	92.21	952.91	329041.62	1.88	2.18	432.39	2167.92

Capriolo section, Italy (continued)

GEA N°	Sample ID	Co	Ni	Cu	Zn	As	Mo	Cd	Ba
28271	CA 1	2.21	13.36	5.77	18.96	2.53	0.35	0.15	23.88
28273	CA 3	1.36	13.73	2.90	12.83	0.00	0.17	0.11	6.26
28275	CA 5	1.73	12.77	3.88	15.76	0.15	0.00	0.07	32.28
28277	CA 7	2.42	14.36	3.51	9.34	0.18	0.23	0.07	9.64
28279	CA 9	1.37	12.71	3.52	12.78	0.00	0.00	0.08	12.26
28281	CA 11	1.15	12.86	2.47	18.93	0.00	0.07	0.16	3.92
28283	CA 13	1.59	13.29	2.22	16.01	0.00	0.00	0.11	3.49
28285	CA 15	1.41	13.43	3.37	11.22	0.18	0.04	0.06	5.68
28287	CA 16	1.18	11.83	2.35	9.47	0.03	0.11	0.02	4.96
28289	CA 18	1.43	10.73	3.90	11.48	0.00	0.00	0.06	4.56
28291	CA 20	0.98	10.76	2.54	5.70	0.00	0.03	0.00	5.03
28293	CA 22	1.89	13.28	3.55	13.61	0.08	0.00	0.12	5.95
28296	CA 25	1.34	10.99	3.06	7.83	0.03	0.00	0.05	20.43
28297	CA 26	0.77	13.10	2.89	3.13	0.00	0.00	0.00	3.81
28298	CA 27	1.13	13.68	2.28	15.44	0.00	0.05	0.03	5.16
28301	CA 30	1.41	18.09	1.72	7.59	0.27	0.15	0.03	5.56
28303	CA 32	1.94	15.98	3.46	13.41	0.15	0.00	0.00	6.09
28305	CA 34	6.84	29.93	7.64	17.31	0.42	0.23	0.02	4.27
28307	CA 36	2.02	15.33	3.19	5.94	0.18	0.02	0.03	4.90
28309	CA 38	1.49	13.93	2.77	10.26	0.00	0.00	0.00	4.89
28311	CA 40	1.71	13.60	3.63	13.58	0.00	0.06	0.05	3.33
28313	CA 42	1.49	14.33	3.50	12.37	0.00	0.00	0.07	3.45
28315	CA 44	1.76	14.42	2.07	5.12	0.00	0.01	0.02	2.92
28317	CA 46	1.83	14.90	3.47	6.50	0.00	0.00	0.07	4.38
28320	CA 49	2.02	15.54	2.60	8.76	0.00	0.05	0.06	5.1
28323	CA 52	2.00	14.98	4.29	24.95	0.17	0.00	0.11	4.75
28325	CA 54	1.74	14.08	3.11	8.44	0.23	0.29	0.00	5.51
28327	CA 56	1.65	14.95	3.79	12.56	0.00	0.13	0.03	4.87
28329	CA 58	4.36	20.82	12.12	20.29	0.23	0.01	0.08	9.94
28331	CA 60	1.47	14.32	2.22	8.33	0.03	0.01	0.05	4.35
28333	CA 62	1.57	13.91	1.57	7.71	0.09	0.00	0.00	3.91
28335	CA 64	1.76	12.35	3.32	4.99	0.25	0.00	0.00	4.75
28336	CA 65	6.54	25.04	16.22	23.66	0.70	0.01	0.19	11.20
28337	CA 66	1.84	14.24	2.27	8.37	0.28	0.00	0.05	4.73
28339	CA 68	1.74	13.18	3.27	11.45	0.19	0.00	0.00	5.71
28341	CA 70	1.51	14.20	3.84	16.05	0.46	0.28	0.00	6.84
28343	CA 72	2.25	13.47	2.68	11.60	0.13	0.03	0.00	5.85
28345	CA 74	1.90	16.35	3.82	7.93	0.31	0.03	0.06	6.20
28347	CA 76	1.92	13.87	3.50	6.76	0.18	0.00	0.00	7.24
28349	CA 78	2.06	13.33	3.01	9.05	0.06	0.00	0.00	7.90
28352	CA 81	3.45	18.41	3.59	8.64	0.39	0.00	0.00	7.03
28354	CA 83	1.22	16.41	3.97	9.17	0.12	0.00	0.02	7.19
28356	CA 85	3.29	17.54	2.80	5.95	0.16	0.00	0.00	7.66
28358	CA 87	1.37	15.37	1.79	11.13	0.25	0.00	0.02	7.88
28360	CA 89	1.99	14.67	2.56	13.35	0.35	0.39	0.00	11.05
28362	CA 91	1.46	15.35	2.63	10.23	0.35	0.07	0.00	7.32
28366	CA 94	2.39	14.85	4.92	10.42	0.09	0.07	0.00	6.67
28371	CA 99	2.02	16.17	3.53	6.05	0.00	0.01	0.00	6.22
28373	CA 101	1.80	13.87	2.60	6.85	0.23	0.01	0.00	5.82
28376	CA 104	1.90	15.08	2.93	7.13	0.09	0.04	0.00	6.95
28378	CA 106	2.29	17.93	2.32	14.40	0.29	0.06	0.00	18.22
28381	CA 109	1.96	15.89	2.37	2.83	0.24	0.05	0.00	5.97
28382	CA 110	1.99	16.71	2.15	12.11	0.09	0.00	0.00	7.39
28385	CA 113	2.79	21.07	3.87	26.57	0.00	0.10	0.03	9.70
28388	CA 116	1.12	22.09	10.36	22.12	0.38	0.00	0.01	14.31
28390	CA 118	2.04	18.68	2.91	13.92	0.00	0.00	0.02	10.51
28392	CA 120	1.47	21.15	5.77	16.20	0.47	0.00	0.00	12.93
28395	CA 123	1.58	17.96	4.52	8.33	0.23	0.00	0.03	14.99
28397	CA 125	2.13	21.59	4.07	13.12	0.45	0.00	0.02	31.44
28400	CA 128	2.10	18.78	3.47	16.19	0.00	0.00	0.05	20.23
28402	CA 130	2.04	21.62	6.24	10.72	0.60	0.00	0.00	18.70
28406	CA 134	1.70	21.24	5.45	6.65	0.23	0.00	0.02	16.45
28408	CA 136	1.58	16.57	3.34	22.57	0.00	0.39	0.09	18.76
28410	CA 138	1.90	18.39	2.96	11.58	0.08	0.13	0.00	17.58
28414	CA 142	1.61	19.25	3.24	13.39	0.40	0.00	0.00	18.10
28418	CA 146	1.87	16.95	6.03	12.37	0.43	0.00	0.02	14.74
28420	CA 148	2.04	18.41	4.02	8.91	0.00	0.00	0.00	16.07
28421	CA 149	1.45	17.31	2.71	5.54	0.27	0.00	0.05	10.26
28423	CA 151	1.39	18.99	1.70	8.68	0.00	0.00	0.06	10.77
28425	CA 153	1.39	17.45	4.19	15.35	0.00	0.56	0.07	8.72
28426	CA 154	1.73	23.18	2.84	6.31	0.19	0.00	0.00	6.05
28427	CA 155	1.43	18.87	4.64	8.39	0.08	0.36	0.04	8.47
28429	CA 157	1.80	19.54	3.97	7.91	0.00	0.14	0.09	11.00
28431	CA 159	1.75	17.50	3.97	11.63	0.00	0.00	0.05	9.42
28433	CA 161	2.99	19.32	6.97	15.95	0.00	0.00	0.07	12.13
28437	CA 165	1.99	17.25	8.72	9.70	0.20	0.00	0.00	10.28

Chrummflueschlucht section, Switzerland

N° GEA	Sample ID	depth(m)	% Sol	Al	Cd	Fe	Mn	Zn	Cu	Ni
30006	Ch 1	1.32	84.23	2925.46	0.22	8729.95	918.41	28.42	3.97	36.65
30008	Ch 3	3.51	94.56	864.12	0.08	4100.08	425.79	12.17	3.88	34.21
32225	Ch 1 B	4.55	95.39	867.89	0.12	4148.36	531.87	9.53	3.96	19.83
32226	Ch 2 B	5.15	96.31	1038.52	0.22	5979.26	396.50	14.94	3.41	20.58
30010	Ch 5	5.30	92.69	1116.12	0.07	4157.96	371.95	9.12	5.49	34.93
32227	Ch 3 B	6.10	92.53	1126.09	0.07	3785.50	282.10	1.20	4.54	17.11
30012	Ch 7	6.12	90.02	1225.79	0.12	3881.94	374.77	20.92	7.31	34.92
32228	Ch 4 B	6.80	94.83	1145.32	0.06	3665.59	307.70	1.55	3.59	18.43
32229	Ch 5 B	7.40	96.24	1005.01	0.13	5224.38	430.18	26.75	3.45	25.61
30014	Ch 9	7.54	96.81	922.82	0.12	4371.56	390.03	30.67	3.36	33.28
32230	Ch 6 B	8.45	95.45	1174.50	0.03	4622.60	378.42	5.91	3.08	21.44
30015	Ch 10	8.51	95.04	1333.57	0.17	5443.28	389.89	22.72	2.77	36.96
32231	Ch 7 B	8.75	96.68	1171.04	0.05	5164.21	391.98	-0.88	2.20	22.23
32232	Ch 8 B	9.00	91.88	3284.35	0.12	4468.79	302.34	13.47	7.32	19.93
30016	Ch 11	9.40	94.69	989.32	0.05	4075.51	293.33	11.82	4.09	32.34
32233	Ch 9 B	9.75	93.49	1376.59	0.06	4254.13	328.55	7.52	4.58	18.39
32234	Ch 10 B	9.95	93.19	1582.27	0.07	4646.30	334.89	8.06	4.19	20.75
30017	Ch 12	10.37	97.28	709.83	0.09	4315.84	289.61	27.63	3.71	35.62
30018	Ch 13	10.75	94.08	1082.10	0.05	4013.88	224.46	5.86	3.96	35.15
32235	Ch 11 B	11.00	93.43	1479.64	0.07	4294.93	277.93	2.71	4.19	19.84
30019	Ch 14	11.27	95.00	1246.88	0.02	4340.01	264.16	4.51	2.23	35.63
32236	Ch 12 B	11.67	94.83	1624.24	0.18	6398.41	323.05	28.70	3.51	24.39
30020	Ch 15	11.87	95.44	1035.93	0.12	5658.66	329.66	19.10	4.24	38.94
30021	Ch 16	12.31	91.78	1116.53	0.09	4155.39	250.46	9.64	3.57	32.98
32237	Ch 13 B	12.56	91.34	3679.47	0.12	4197.47	9.02	7.05	7.55	18.64
30023	Ch 18	13.33	95.83	851.18	0.21	4465.58	268.68	3.20	2.94	36.66
30024	Ch 19	13.86	97.35	538.73	0.08	3648.41	290.14	2.74	1.87	35.29
32238	Ch 14 B	14.33	94.48	912.42	0.12	3476.37	321.39	4.12	2.97	16.83
32239	Ch 15 B	14.75	96.68	768.59	0.07	3585.73	301.84	-1.08	2.15	17.21
30025	Ch 20	15.15	94.96	1508.71	0.09	4070.01	342.81	4.90	2.48	36.09
32240	Ch 16 B	15.25	95.23	1157.56	0.04	4094.17	351.30	10.55	2.85	23.27
32241	Ch 17 B	15.70	95.64	1386.42	0.03	4314.30	341.87	0.75	2.64	19.13
30026	Ch 21	15.91	96.78	504.06	0.04	3996.55	303.60	3.55	13.19	37.80
32242	Ch 18 B	16.20	96.48	608.60	0.11	3459.33	289.27	3.65	18.74	17.43
32243	Ch 19 B	16.55	96.09	696.95	0.07	3469.40	341.78	-3.87	2.03	17.10
32244	Ch 20 B	16.85	96.45	869.68	0.08	3642.91	320.53	-0.23	1.62	17.98
30027	Ch 22	17.05	95.48	1101.10	0.08	4379.81	397.49	4.06	2.15	39.73
30028	Ch 23	17.73	95.19	856.06	0.14	4182.78	203.41	21.03	6.28	39.14
32245	Ch 21 B	18.15	95.48	870.98	0.08	4127.54	300.75	4.51	4.49	17.18
32246	Ch 22 B	18.35	98.08	1147.04	0.13	3955.71	300.70	12.36	5.87	17.85
32247	Ch 23 B	18.50	97.36	511.03	0.09	3328.76	279.46	6.69	3.57	16.74
30029	Ch 24	18.56	97.12	579.82	0.06	3765.23	262.73	6.19	3.31	35.88
32248	Ch 24 B	19.10	97.13	607.46	0.13	3219.93	363.17	11.76	10.35	17.72
32249	Ch 25 B	19.25	97.64	459.94	0.04	3164.06	364.71	2.56	8.62	17.09
30030	Ch 25	19.39	98.48	598.71	0.15	3890.53	262.74	14.22	4.26	37.18
32250	Ch 26 B	19.87	98.16	685.00	0.09	3335.71	230.99	2.25	3.65	16.60
30031	Ch 26	19.92	96.81	716.02	0.07	4027.27	245.46	7.74	4.08	36.70
30032	Ch 27	20.23	96.28	478.53	0.11	3792.78	162.82	20.55	4.20	36.02
32251	Ch 27 B	20.55	94.96	727.69	0.13	3375.28	171.22	4.11	2.89	18.12
30033	Ch 28	20.76	98.72	863.95	0.16	3718.51	179.95	11.85	2.91	38.63
32252	Ch 28 B	21.09	97.68	572.99	0.11	3339.05	208.83	13.32	15.73	18.80
32253	Ch 29 B	21.35	97.56	761.03	0.11	3213.83	240.71	10.49	4.91	18.94
30034	Ch 29	21.29	97.96	1008.01	0.12	4172.06	239.61	4.93	2.38	36.87
32254	Ch 30 B	21.65	97.24	1076.58	0.13	3646.75	269.88	9.42	3.60	20.00
30035	Ch 30	21.59	97.04	755.77	0.13	3994.86	302.67	18.60	4.93	14.53
30036	Ch 31	21.97	96.60	699.57	0.15	3937.13	323.05	6.17	3.17	36.37
32255	Ch 31 B	22.50	97.64	931.46	0.16	3485.66	234.62	21.66	5.97	19.59
30037	Ch 32	22.75	95.61	839.10	0.14	3891.51	262.88	13.58	3.79	37.01
32256	Ch 32 B	23.10	96.85	1193.52	0.19	3725.21	243.82	19.63	4.68	20.29
32257	Ch 33 B	23.43	95.48	1284.99	0.14	3848.66	247.10	19.51	13.20	22.53
30038	Ch 33	23.56	95.19	705.57	0.09	3716.76	185.60	22.78	3.31	32.79
32258	Ch 34 B	24.12	97.52	741.09	0.12	3355.90	212.97	8.77	2.63	19.53
30039	Ch 34	24.24	96.29	883.77	0.08	3655.97	207.23	13.49	2.42	33.58
30040	Ch 35	24.55	97.16	720.52	0.12	4103.90	218.07	19.12	4.29	48.05
30041	Ch 36	25.08	96.64	837.32	0.12	3773.52	197.16	36.03	5.89	36.31
30042	Ch 37	25.38	96.48	1019.12	0.12	4158.22	216.86	12.99	3.22	38.70
32259	Ch 35 B	25.95	97.92	931.94	0.15	3179.39	211.88	2.88	3.01	18.05
30043	Ch 38	25.83	97.52	1123.70	0.07	4278.17	209.52	12.44	2.49	38.12
32260	Ch 36 B	26.54	97.60	1069.08	0.09	3284.20	209.01	4.13	3.13	18.18
30044	Ch 39	26.67	97.40	913.69	0.15	4468.43	215.74	13.29	3.80	40.09
30045	Ch 40	27.12	96.56	861.34	0.12	4485.89	175.16	12.68	2.18	40.00
30046	Ch 41	27.73	96.97	1068.42	0.09	4648.89	227.05	10.60	4.83	38.66
30047	Ch 42	28.03	96.92	1125.97	0.09	4690.84	213.96	11.79	1.95	37.82
30048	Ch 43	28.56	98.08	930.71	0.10	4660.08	273.75	8.02	3.42	35.85
30049	Ch 44	29.02	95.53	1261.55	0.09	4897.83	338.63	17.52	2.69	37.73
30050	Ch 45	29.39	97.64	575.22	0.09	4085.34	337.93	12.64	2.52	36.11
30051	Ch 46	29.70	95.79	1288.67	0.11	4747.01	257.15	11.20	2.14	35.80
30052	Ch 47	30.38	94.80	2456.59	0.16	6379.71	304.48	20.44	2.58	38.43
30053	Ch 48	30.91	90.87	2861.26	0.10	7281.34	324.61	16.42	3.18	38.57
32261	Ch 37 B	31.09	92.80	3501.17	0.14	6239.41	247.00	7.17	2.38	19.92
30054	Ch 49	31.44	95.77	2013.45	0.12	7073.68	231.69	11.81	2.29	37.52
32262	Ch 38 B	31.65	93.79	2280.29	0.11	4965.83	263.30	21.68	5.70	19.69
30055	Ch 50	31.89	94.68	1808.49	0.09	5915.94	277.60	11.74	2.08	37.48
32263	Ch 39 B	32.02	97.01	1404.00	0.08	3951.89	181.83	8.62	2.19	18.57
30056	Ch 51	32.35	92.55	3181.57	0.10	6215.00	358.10	22.53	3.81	39.38
30057	Ch 52	32.73	97.20	1388.81	0.04	4960.40	275.21	7.16	1.98	35.43
32264	Ch 40 B	33.20	96.65	1982.25	0.13	4756.57	211.19	4.20	3.03	20.94
30058	Ch 53	33.41	95.44	1547.52	0.13	5563.79	327.22	11.79	2.30	37.33
30059	Ch 54	34.17	97.52	834.45	0.09	4393.00	279.18	1.57	1.68	34.56
30060	Ch 55	34.85	96.80	1034.31	0.13	4207.93	126.82	7.13	2.35	36.08
30062	Ch 57	36.82	97.08	1048.30	0.11	5271.26	306.63	7.64	2.00	16.19
32265	Ch 41 B	38.01	97.64	934.57	0.06	4033.71	285.26	4.70	2.69	18.66
32266	Ch 42 B	39.02	98.08	1104.42	0.03	3960.53	328.72	2.95	3.75	18.83
30065	Ch 60	40.23	92.61	2204.79	0.48	5736.67	302.46	53.41	11.25	36.11
30066	Ch 61	41.36	96.80	1235.38	0.01	5378.03	273.50	20.05	1.96	33.63

Chrummflueschlucht section, Switzerland (continued)

N° GEA	Sample ID	Cr	As	U	V	Mo	Co	Ba
30006	Ch 1	7.78	2.53	7.33	13.62	2.09	5.69	10.33
30008	Ch 3	0.97	0.72	0.70	2.52	1.01	3.01	14.54
32225	Ch 1 B	3.04	1.99	0.46	2.48	5.80	3.02	14.18
32226	Ch 2 B	3.02	5.73	0.74	3.78	2.16	5.10	21.92
30010	Ch 5	0.98	0.25	0.57	3.04	0.57	1.42	11.31
32227	Ch 3 B	3.24	0.62	0.24	2.12	1.20	1.40	12.57
30012	Ch 7	1.16	0.11	1.07	3.03	0.47	3.83	13.20
32228	Ch 4 B	3.73	0.28	0.61	4.85	0.70	1.28	15.72
32229	Ch 5 B	3.39	5.49	0.49	2.06	0.62	6.48	12.43
30014	Ch 9	0.84	0.56	0.85	2.66	0.44	2.71	10.35
32230	Ch 6 B	3.55	1.22	0.39	2.29	0.49	2.84	13.95
30015	Ch 10	0.74	2.77	1.33	3.60	0.37	4.48	9.93
32231	Ch 7 B	3.31	3.83	0.43	2.33	0.51	4.39	12.05
32232	Ch 8 B	8.22	1.07	0.42	4.05	0.40	1.62	21.12
30016	Ch 11	0.43	-0.12	1.05	3.16	0.24	1.57	13.31
32233	Ch 9 B	4.14	0.44	0.51	3.56	0.30	1.19	33.16
32234	Ch 10 B	4.25	0.54	0.39	3.23	0.31	1.91	17.00
30017	Ch 12	0.26	-0.18	0.77	2.14	0.21	1.44	10.25
30018	Ch 13	1.00	-0.10	0.51	2.98	0.19	1.83	14.55
32235	Ch 11 B	3.88	0.44	0.62	2.74	0.33	1.52	19.36
30019	Ch 14	0.77	0.11	0.47	2.38	0.20	2.02	14.95
32236	Ch 12 B	3.85	5.57	0.36	2.75	0.38	5.78	19.96
30020	Ch 15	0.07	3.22	0.92	2.65	0.25	6.08	12.66
30021	Ch 16	0.92	-0.14	0.40	2.16	0.20	1.29	16.02
32237	Ch 13 B	4.13	1.45	0.51	4.79	4.59	1.38	19.93
30023	Ch 18	1.84	2.67	0.51	2.62	5.43	1.82	15.83
30024	Ch 19	1.57	0.43	0.18	1.60	1.51	1.37	13.30
32238	Ch 14 B	1.85	0.48	0.06	1.08	1.54	1.11	13.43
32239	Ch 15 B	1.89	0.36	0.05	0.89	0.97	1.11	12.48
30025	Ch 20	1.73	0.29	0.15	2.52	0.53	1.97	12.29
32240	Ch 16 B	2.03	0.99	0.21	1.47	0.71	3.79	16.13
32241	Ch 17 B	2.04	0.66	0.11	1.71	0.51	2.21	16.29
30026	Ch 21	1.73	0.31	0.24	2.07	0.52	0.37	10.41
32242	Ch 18 B	1.91	0.21	0.10	0.89	0.39	1.06	13.47
32243	Ch 19 B	2.02	0.19	0.06	0.93	0.37	1.21	10.43
32244	Ch 20 B	2.04	0.24	0.25	1.47	0.27	1.18	12.14
30027	Ch 22	2.17	1.19	0.35	1.98	0.31	3.05	11.02
30028	Ch 23	1.07	1.40	0.35	2.12	0.41	5.92	17.70
32245	Ch 21 B	1.98	0.22	0.17	1.56	0.28	1.19	12.08
32246	Ch 22 B	2.11	0.17	0.09	1.53	0.28	1.37	14.20
32247	Ch 23 B	1.63	0.17	0.06	0.87	0.19	1.02	45.85
30029	Ch 24	1.19	0.08	0.08	1.26	0.18	1.27	10.13
32248	Ch 24 B	1.52	0.88	0.25	1.12	4.06	2.04	14.09
32249	Ch 25 B	1.47	0.48	0.06	0.74	1.50	1.85	10.45
30030	Ch 25	2.34	0.01	0.11	1.23	0.28	1.55	9.62
32250	Ch 26 B	1.45	0.37	0.04	0.94	0.81	1.04	10.60
30031	Ch 26	1.76	0.00	0.21	1.46	0.14	1.70	13.37
30032	Ch 27	2.21	0.24	0.03	0.80	0.15	1.53	9.56
32251	Ch 27 B	1.56	0.32	0.03	0.86	0.66	1.14	12.67
30033	Ch 28	1.91	0.05	0.04	1.21	0.21	1.46	9.66
32252	Ch 28 B	2.05	0.35	0.04	0.65	0.56	1.26	8.34
32253	Ch 29 B	2.05	0.32	0.02	0.79	0.37	1.17	9.85
30034	Ch 29	1.38	-0.03	0.03	1.26	0.16	1.71	9.24
32254	Ch 30 B	2.78	0.42	0.03	1.16	0.33	1.57	11.25
30035	Ch 30	1.38	0.17	0.02	0.95	0.27	1.96	9.22
30036	Ch 31	1.02	1.77	0.14	1.93	4.42	2.07	9.47
32255	Ch 31 B	2.97	0.24	0.07	1.22	0.97	1.40	9.51
30037	Ch 32	0.94	0.67	0.06	1.72	1.49	1.83	11.18
32256	Ch 32 B	2.77	0.44	0.03	1.21	0.41	1.63	10.31
32257	Ch 33 B	2.80	0.47	0.03	1.22	0.31	2.73	12.96
30038	Ch 33	0.82	0.32	0.04	1.54	0.69	1.89	9.06
32258	Ch 34 B	2.63	0.20	0.02	1.00	0.21	1.50	9.59
30039	Ch 34	1.25	0.40	0.06	1.80	0.64	1.72	7.54
30040	Ch 35	0.87	0.26	0.05	1.34	0.41	1.78	8.69
30041	Ch 36	1.32	0.33	0.04	1.53	0.34	2.04	8.88
30042	Ch 37	1.77	0.24	0.04	1.70	0.28	1.81	8.61
32259	Ch 35 B	1.35	0.68	0.09	1.40	4.05	1.25	10.10
30043	Ch 38	0.83	0.21	0.03	1.85	0.19	2.16	10.19
32260	Ch 36 B	1.69	0.27	0.03	1.70	1.49	1.36	10.69
30044	Ch 39	1.47	0.13	0.05	1.42	0.20	1.94	8.65
30045	Ch 40	0.95	0.23	0.02	1.13	0.13	1.60	9.00
30046	Ch 41	1.35	0.07	0.02	1.56	0.12	1.80	10.73
30047	Ch 42	1.28	0.05	0.03	1.90	0.18	1.74	8.59
30048	Ch 43	1.51	-0.05	0.03	1.57	0.11	1.80	9.31
30049	Ch 44	1.55	0.10	0.04	2.11	0.19	2.04	11.81
30050	Ch 45	0.57	1.41	0.19	2.32	4.43	1.71	9.04
30051	Ch 46	1.09	0.37	0.05	2.80	1.26	1.90	35.64
30052	Ch 47	1.85	0.31	0.04	4.99	0.54	2.58	12.68
30053	Ch 48	3.10	0.35	0.05	6.16	0.42	3.10	16.90
32261	Ch 37 B	2.78	0.27	0.02	5.09	0.81	2.21	14.47
30054	Ch 49	1.46	0.29	0.04	4.36	0.34	2.59	12.56
32262	Ch 38 B	2.43	0.32	0.02	4.13	0.60	1.84	12.38
30055	Ch 50	2.19	0.27	0.06	3.05	0.24	2.34	14.26
32263	Ch 39 B	1.99	0.16	0.02	2.22	0.57	1.46	29.81
30056	Ch 51	2.76	0.37	0.13	4.88	0.25	2.97	23.04
30057	Ch 52	1.54	0.13	0.04	2.54	0.21	1.93	13.73
32264	Ch 40 B	2.75	0.16	0.03	3.69	0.40	1.87	18.15
30058	Ch 53	1.73	0.17	0.03	3.30	0.20	2.31	19.16
30059	Ch 54	0.94	0.01	0.08	1.63	0.13	1.79	10.31
30060	Ch 55	1.61	0.09	0.09	2.02	0.17	1.67	9.56
30062	Ch 57	1.80	0.04	0.16	2.21	0.12	2.24	13.82
32265	Ch 41 B	1.79	0.10	0.12	2.25	0.38	1.65	11.91
32266	Ch 42 B	2.13	0.10	0.05	1.96	0.31	1.58	20.22
30065	Ch 60	3.01	-0.03	0.06	4.46	0.11	2.55	19.02
30066	Ch 61	1.91	0.09	0.19	2.89	0.14	2.43	14.57

Gorgo a Cerbara section, Italy

GEA N°	Sample ID	depth (m)	% Sol	Al	Cd	Fe	Mn	Zn	Cu
31730	GC 110	19.69	91.03	1210.67	0.24	2870.41	1574.09	12.80	7.12
31731	GC 111	19.76	63.69	5630.80	0.43	6533.71	303.57	76.57	98.32
31732	GC 112	19.83	70.99	3370.57	0.17	3854.39	623.57	35.56	51.33
31733	GC 113	19.90	52.54	5410.75	0.15	4663.81	279.93	53.50	60.10
31734	GC 114	20.09	85.65	1961.74	0.17	3261.79	1411.22	15.72	9.04
31735	GC 115	20.22	78.93	1842.98	0.18	2771.36	835.76	35.37	9.60
31736	GC 116	20.38	83.61	2623.15	0.18	3464.31	1256.76	20.29	23.04
31737	GC 117	20.43	64.08	4417.20	0.18	6465.68	731.71	38.80	49.52
31738	GC 118	20.57	92.35	678.85	0.11	2884.97	1708.81	17.55	5.97
31739	GC 119	20.69	58.84	4718.55	1.29	10632.97	471.73	247.91	139.84
31740	GC 120	20.72	91.24	1731.87	0.13	3403.56	1382.36	21.40	8.57
31741	GC 121	20.76	78.77	2326.09	0.41	5386.72	827.62	98.13	60.96
31742	GC 122	20.81	92.72	687.65	0.11	2634.34	1379.42	16.37	8.05
31743	GC 123	20.84	80.34	2268.21	0.42	8656.88	880.32	39.48	35.38
31744	GC 124	20.90	86.62	1521.99	0.18	2924.25	1389.03	20.23	6.66
31745	GC 125	20.95	85.61	1537.30	0.15	2936.47	1315.84	21.10	7.44
31746	GC 126	20.97	88.84	893.27	0.24	2643.18	1443.47	15.64	14.40
31747	GC 127	21.00	52.83	11424.51	0.62	6942.01	510.05	60.92	57.12
31748	GC 128	21.05	87.82	1196.90	0.19	2809.13	1322.18	16.60	32.73
31749	GC 129	21.14	82.46	2460.39	0.19	3272.94	1148.57	17.50	27.07
31750	GC 130	21.22	86.57	943.94	0.16	2596.50	1644.53	15.67	8.83
31751	GC 131	21.49	81.18	1359.01	0.42	3149.98	1364.56	39.06	34.49
31752	GC 132	21.54	59.89	4547.91	0.06	4683.65	666.92	28.22	16.20
31753	GC 133	21.56	48.54	9549.78	0.11	6634.82	258.46	48.47	51.22
31754	GC 134	21.59	41.02	10934.36	0.18	8898.74	287.31	59.64	30.95
31755	GC 135	21.61	43.62	5092.65	0.32	7312.65	340.37	93.82	27.45
31756	GC 136	21.63	47.74	6328.52	0.28	5953.45	513.69	59.53	19.52
31757	GC 137	21.67	63.43	3526.60	0.46	6148.63	757.88	51.59	121.31
31758	GC 138	21.74	44.83	2179.86	0.21	3834.36	558.18	32.28	23.78
31759	GC 139	21.78	61.75	4426.42	0.71	12290.08	505.81	199.07	69.20
31760	GC 140	21.80	16.78	16484.58	0.55	10400.08	174.84	206.82	46.45
31761	GC 141	21.81	24.69	14018.62	2.24	19437.20	161.86	281.09	67.39
31762	GC 142	21.83	20.01	14516.21	0.52	9563.69	157.51	153.54	37.64
31763	GC 143	21.86	45.55	7653.04	1.65	16524.46	296.64	267.13	110.97
31764	GC 144	21.91	45.67	6442.45	2.55	12935.68	317.14	415.28	59.38
31765	GC 145	21.96	50.22	3341.23	0.87	5252.16	386.82	166.11	45.18
31766	GC 146	22.06	12.74	12599.52	0.25	6331.49	29.98	49.98	67.06
31767	GC 147	22.13	13.86	2886.80	0.04	1547.50	58.49	19.25	10.02
31768	GC 148	22.17	15.91	21559.86	0.19	9797.78	48.70	60.89	112.82
31769	GC 149	22.22	16.16	7711.20	0.23	8350.73	37.13	56.65	101.87
31770	GC 150	22.28	16.61	3826.07	0.03	3283.20	16.34	20.46	41.54
31771	GC 151	22.41	13.22	12347.04	0.21	5536.62	29.63	64.32	45.94
31772	GC 152	22.58	24.60	1979.59	0.05	1974.33	206.75	21.01	10.29
31773	GC 153	22.61	12.61	15277.14	0.15	8212.85	41.15	72.48	55.08
31774	GC 154	22.63	7.17	20643.64	0.16	15912.72	45.09	94.95	69.34
31775	GC 155	22.66	17.08	8115.73	0.27	10718.09	43.60	151.92	162.46
31776	GC 156	22.68	7.00	1927.91	0.07	2516.13	90.49	29.19	12.09
31777	GC 157	22.75	9.91	6057.00	0.20	9255.00	50.91	111.04	78.30
31778	GC 158	22.81	7.43	1829.61	0.08	2759.03	150.46	33.83	15.73
31779	GC 159	22.88	25.31	7150.20	2.06	18450.54	49.60	190.04	119.62
31780	GC 160	23.05	35.86	6429.03	3.10	19149.31	47.88	202.83	285.02
31781	GC 161	23.12	16.93	2978.35	0.47	7569.76	64.87	61.26	64.66
31782	GC 162	23.19	20.68	9235.11	4.09	16421.53	48.43	304.38	162.34
31783	GC 163	23.26	20.31	9235.11	4.09	16421.53	48.43	304.38	162.34
31784	GC 164	23.33	21.56	7702.55	3.40	12788.51	34.50	202.64	136.14
31785	GC 165	23.41	36.73	20056.99	20.29	33440.13	57.93	1305.52	312.22
31786	GC 166	23.52	31.75	23059.96	7.78	30375.81	50.37	637.59	237.17
31787	GC 167	23.60	13.69	18530.52	1.07	11519.61	48.90	151.31	133.76
31788	GC 168	23.69	7.37	4621.34	0.34	4757.19	50.20	67.74	26.78
31789	GC 169	23.74	19.38	8327.20	0.30	8702.21	147.91	84.73	86.58
31790	GC 170	23.79	16.70	23662.72	0.11	13257.39	102.17	77.38	107.96
31791	GC 171	23.88	50.62	5270.38	0.10	7337.49	718.37	55.58	91.41
31792	GC 172	23.95	35.61	7542.16	0.08	9103.50	452.18	56.73	95.29
31793	GC 173	24.03	56.34	3574.36	0.09	4283.72	828.62	42.20	52.21
31794	GC 174	24.12	25.98	17055.57	0.26	10482.90	264.89	95.37	144.33
31795	GC 175	24.17	57.73	3972.22	0.51	5235.87	785.82	212.50	72.17
31796	GC 176	24.24	56.28	2312.52	0.08	3627.82	770.83	11.08	19.08
31797	GC 177	24.29	54.57	4319.65	0.07	6835.19	831.74	24.55	32.16
31798	GC 178	24.34	52.30	3835.77	0.09	4670.83	666.91	27.46	33.05
31799	GC 179	24.40	56.79	2400.32	0.07	3213.32	785.28	15.10	11.06
31800	GC 180	24.52	75.82	1193.36	0.37	3146.30	1547.67	13.68	11.24
31801	GC 181	24.72	71.90	4487.54	0.16	4548.18	1467.24	25.58	44.26
31802	GC 182	24.86	55.36	1579.22	0.05	2310.89	963.57	12.27	11.86
31803	GC 183	24.97	68.53	2105.13	0.14	3160.69	1521.05	14.84	16.81

Gorgo a Cerbara section, Italy (continued)

GEA N°	Sample ID	Ni	Cr	As	U	V	Mo	Co
31730	GC 110	26.54	1.81	1.13	0.67	3.32	3.81	3.63
31731	GC 111	56.87	26.46	6.30	0.78	9.71	7.13	9.01
31732	GC 112	41.43	6.10	2.16	0.32	3.93	2.16	7.49
31733	GC 113	56.60	13.16	2.08	0.46	4.24	1.40	9.57
31734	GC 114	19.57	3.39	0.58	0.24	3.17	1.57	1.69
31735	GC 115	21.00	3.76	0.81	0.27	2.42	0.70	1.68
31736	GC 116	22.37	3.52	0.66	0.41	2.68	0.94	2.27
31737	GC 117	37.92	10.28	2.84	0.66	4.91	0.79	12.27
31738	GC 118	21.39	1.02	0.37	0.64	1.21	0.67	2.01
31739	GC 119	126.33	16.77	12.00	1.65	10.13	1.32	44.10
31740	GC 120	23.91	2.22	0.42	0.96	4.16	0.45	3.45
31741	GC 121	57.55	8.07	4.63	1.09	5.43	0.89	8.02
31742	GC 122	20.85	0.78	0.38	1.40	1.86	0.31	2.13
31743	GC 123	30.97	5.12	1.88	0.81	6.93	0.59	6.70
31744	GC 124	20.50	1.71	1.07	1.33	2.20	0.23	1.93
31745	GC 125	21.17	2.54	0.39	0.64	2.60	0.28	1.52
31746	GC 126	21.26	0.54	0.51	0.41	1.93	0.17	3.36
31747	GC 127	55.61	23.77	4.80	1.54	12.07	6.16	15.27
31748	GC 128	42.72	1.37	1.19	0.45	2.66	0.32	14.42
31749	GC 129	21.01	5.97	1.19	0.40	4.94	1.96	1.60
31750	GC 130	21.11	1.41	0.83	0.27	2.10	1.01	1.35
31751	GC 131	33.07	1.85	1.85	0.24	2.67	0.81	7.16
31752	GC 132	47.74	7.54	2.48	0.34	3.62	0.46	6.24
31753	GC 133	43.69	13.06	1.95	0.41	3.70	0.50	7.89
31754	GC 134	43.24	11.70	3.69	0.44	3.22	0.43	8.22
31755	GC 135	41.49	8.91	2.45	0.38	2.73	0.45	7.35
31756	GC 136	30.72	8.61	1.83	0.62	2.85	0.25	3.82
31757	GC 137	58.68	7.70	6.62	0.89	6.77	6.47	20.95
31758	GC 138	20.50	4.22	3.15	0.77	3.54	1.89	7.46
31759	GC 139	121.62	16.56	9.97	1.39	12.76	2.21	45.17
31760	GC 140	50.35	14.61	3.67	2.29	7.17	0.93	16.78
31761	GC 141	174.67	39.46	16.07	3.77	64.80	2.51	44.29
31762	GC 142	44.35	12.42	3.40	2.32	6.22	0.86	9.03
31763	GC 143	152.38	26.23	12.02	2.22	19.69	2.20	41.38
31764	GC 144	131.11	18.40	10.72	1.45	18.78	1.80	42.37
31765	GC 145	39.65	6.25	3.56	0.53	5.80	0.63	10.89
31766	GC 146	34.33	12.16	2.01	0.49	7.10	0.79	9.26
31767	GC 147	13.17	2.22	1.21	0.12	3.00	0.11	2.61
31768	GC 148	41.44	36.73	1.46	0.52	13.08	0.71	11.40
31769	GC 149	26.40	8.77	2.95	1.69	6.25	6.15	8.50
31770	GC 150	10.19	4.40	1.88	0.22	5.42	0.70	2.35
31771	GC 151	30.66	10.40	1.27	0.28	5.94	0.63	4.86
31772	GC 152	8.31	0.97	1.19	0.08	2.87	0.09	1.20
31773	GC 153	30.42	14.88	1.91	0.41	8.14	0.92	6.08
31774	GC 154	71.78	20.37	3.43	0.49	15.98	2.19	10.16
31775	GC 155	61.33	15.29	4.61	0.79	12.84	4.67	12.40
31776	GC 156	21.74	0.20	3.68	0.16	3.84	1.49	7.75
31777	GC 157	49.73	8.37	3.83	0.50	7.71	2.29	12.75
31778	GC 158	28.64	-0.07	3.67	0.25	3.27	1.14	10.91
31779	GC 159	189.76	29.15	13.65	5.00	51.77	8.22	55.15
31780	GC 160	237.67	30.89	18.60	20.25	140.02	21.24	26.00
31781	GC 161	57.80	3.20	5.12	0.66	16.18	2.11	12.88
31782	GC 162	150.98	28.27	10.91	3.98	55.69	5.06	31.01
31783	GC 163	150.98	28.27	10.91	3.98	55.69	5.06	31.01
31784	GC 164	121.09	50.54	9.99	5.57	88.74	4.37	14.20
31785	GC 165	522.82	54.21	35.71	24.32	275.46	70.84	105.80
31786	GC 166	226.28	45.93	28.70	12.82	112.37	25.83	56.47
31787	GC 167	63.77	21.52	10.19	2.30	14.03	7.51	27.32
31788	GC 168	27.94	8.62	5.87	0.66	8.08	2.25	8.38
31789	GC 169	52.71	19.17	4.92	1.22	8.93	1.62	11.32
31790	GC 170	143.02	29.48	6.50	0.93	11.77	1.38	30.48
31791	GC 171	61.55	10.30	5.56	0.45	8.10	0.77	16.72
31792	GC 172	58.36	15.03	12.65	0.58	7.54	0.52	17.41
31793	GC 173	75.88	9.37	7.59	0.34	4.76	0.29	31.83
31794	GC 174	193.68	14.50	12.70	0.52	5.03	0.39	57.79
31795	GC 175	36.95	5.98	3.98	0.24	6.21	0.05	5.15
31796	GC 176	30.72	4.42	2.08	0.18	2.14	0.13	3.87
31797	GC 177	40.29	7.66	2.63	0.30	4.21	0.12	5.02
31798	GC 178	37.24	5.85	3.16	0.26	2.93	0.00	4.61
31799	GC 179	25.77	4.35	1.12	0.19	2.76	0.00	3.48
31800	GC 180	26.06	3.34	3.91	0.60	4.00	5.91	2.55
31801	GC 181	56.03	5.45	1.71	0.36	5.25	1.52	23.29
31802	GC 182	23.33	2.36	1.41	0.16	2.97	0.59	12.46
31803	GC 183	27.30	4.47	1.00	0.20	3.35	0.40	3.75

Glaise section, France

N° GEA	Sample ID	Depth (m)	% Sol	Al	Ca	V	Cr	Mn	Fe	Co
29408	GL 1	0.12	85.99	2791.40	301684.52	8.63	5.75	242.62	6358.36	1.99
29409	GL 2	2.75	44.97	6018.56	142373.29	17.03	9.82	261.35	20980.61	8.68
29410	GL 3	3.56	16.55	7617.92	36798.81	16.03	13.74	112.49	18329.68	9.62
29411	GL 4	4.25	11.37	8350.87	13041.46	16.14	17.99	59.93	19104.32	10.03
29412	GL 5	4.88	11.18	9016.50	2683.99	18.52	19.43	52.14	14835.87	12.85
29413	GL 6	6.00	15.77	9201.68	8428.91	19.89	18.19	66.18	21833.66	12.74
29414	GL 7	6.62	8.33	8658.33	4904.14	15.04	17.99	43.57	16628.60	8.09
29415	GL 8	7.50	9.38	8626.35	8762.13	16.18	17.33	49.03	14963.39	12.37
29416	GL 9	8.62	8.28	8210.04	6733.43	14.83	15.94	38.12	12847.78	7.85
29417	GL 10	9.81	11.95	10255.05	7143.50	19.82	21.93	43.10	14004.33	9.36
29418	GL 11	10.75	18.97	8059.88	44882.30	17.12	17.77	130.56	15416.16	11.94
29419	GL 12	11.50	19.24	10322.38	37838.91	28.44	23.18	106.59	20870.38	14.31
29420	GL 13	12.50	15.43	9309.64	26890.59	24.22	20.91	94.51	15120.27	10.73
29421	GL 14	13.06	28.20	11069.18	59318.09	24.60	22.66	111.24	17538.96	10.31
29422	GL 15	14.38	25.19	8903.98	62604.90	12.49	16.80	143.72	18911.33	10.14
29423	GL 16	15.44	20.76	8048.57	35669.34	14.51	14.34	74.42	17797.42	9.23
29424	GL 17	16.44	17.01	8259.37	28543.30	17.70	18.36	61.97	20000.53	8.77
29425	GL 18	18.00	24.99	10578.25	66314.79	18.59	19.87	112.16	22788.31	13.36
29426	GL 19	19.63	18.13	10727.89	35397.94	29.57	22.98	63.41	18057.69	8.47
29427	GL 20	20.75	24.32	7495.26	63296.39	13.57	15.76	82.16	19418.13	6.79
29428	GL 21	21.75	19.30	7379.51	36088.37	11.35	12.00	91.64	24676.46	13.75
29429	GL 22	23.00	31.43	6580.34	97107.05	9.26	11.82	150.71	16264.74	7.01
29430	GL 23	24.25	26.40	8307.37	79126.39	13.63	16.19	93.70	13592.05	4.07
29431	GL 24	25.38	8.03	6306.88	64986.94	10.93	10.98	87.25	14425.80	7.44
29432	GL 25	25.88	24.17	7010.82	59297.58	12.77	14.36	71.84	17309.01	8.66
29433	GL 26	26.50	38.32	6299.70	122587.65	10.22	13.39	216.64	13090.66	6.27
29434	GL 27	27.31	33.28	7101.76	92078.33	11.82	12.35	137.06	21946.60	14.10
29435	GL 28	28.62	55.80	8650.50	195878.90	22.15	17.92	346.91	15840.12	6.37
29436	GL 29	29.38	36.28	7057.70	111498.91	13.98	14.41	112.24	13495.94	8.88
29437	GL 30	29.90	37.72	6016.63	123919.76	10.83	12.55	166.60	12002.10	9.10
29438	GL 31	30.62	99.32	189.11	345721.25	3.14	3.74	260.44	7130.52	3.53
29439	GL 32	31.00	35.20	7442.95	104496.16	13.85	14.05	129.73	11012.33	6.55
29440	GL 33	31.38	73.07	5807.97	240211.67	13.78	9.88	346.48	12304.06	4.35
29441	GL 34	31.56	49.70	5008.43	165484.20	9.16	9.25	191.03	8877.57	9.87
29442	GL 35	31.75	73.23	5200.30	246181.36	14.11	8.68	362.36	11330.26	5.40
29443	GL 36	32.62	77.52	5268.32	255931.63	14.79	9.53	412.34	12728.81	2.70
29444	GL 37	32.87	50.52	8446.94	167540.11	18.40	16.73	210.90	13016.76	7.73

Vergol section, France

N° GEA	Sample ID	Depth (m)	% Sol	Al	Ca	V	Cr	Mn	Fe	Co
38450	Ve 0	0.40	82.57	4473.50	308425.07	10.51	9.23	175.71	8237.40	3.02
38451	Ve 1	0.52	70.23	3921.94	247411.20	8.93	8.32	150.18	10230.04	4.28
38452	Ve 2	0.60	62.97	4306.82	208942.32	9.41	7.94	137.00	10479.86	4.12
38453	Ve 3	0.69	60.93	4235.25	201066.15	9.10	7.20	134.68	11791.35	5.22
38454	Ve 4	0.79	69.58	4438.59	241131.62	9.90	8.86	156.04	9736.44	3.74
38455	Ve 5	0.88	71.62	4369.14	251057.26	10.34	8.51	160.09	9640.06	3.12
38456	Ve 6	1.05	64.21	4465.05	208361.67	12.26	8.43	133.30	14329.11	5.60
38457	Ve 7	1.08	49.16	4384.78	144944.97	12.45	10.48	75.79	17210.52	8.79
38458	Ve 8	1.10	53.90	5472.67	165830.12	14.76	11.02	104.36	15336.40	5.90
38459	Ve 9	1.11	52.10	4319.68	158795.29	23.45	21.74	91.58	17804.80	9.18
38460	Ve 10	1.13	55.71	5409.51	192925.75	15.29	12.60	115.77	14639.65	7.18
38461	Ve 11	1.15	54.20	5584.67	161191.18	15.67	14.28	88.62	17089.38	12.69
38462	Ve 12	1.33	85.28	2885.64	312914.51	7.63	6.35	206.87	6254.43	2.38
38463	Ve 13	1.46	63.69	6084.96	217830.28	13.19	13.70	156.21	10548.31	4.72
38464	Ve 14	1.82	66.35	5017.74	228191.74	10.39	10.67	196.13	9694.04	5.15
38465	Ve 15	1.99	79.48	3423.81	285257.89	7.92	7.96	192.97	7562.65	2.44
38466	Ve 16	2.08	72.02	4622.09	249920.94	9.57	9.53	170.68	8719.67	4.32
38467	Ve 17	2.14	57.52	5975.55	169634.15	12.89	15.87	75.61	14413.09	12.86
38468	Ve 18	2.19	72.89	6619.04	253631.03	14.94	13.14	180.27	9730.67	3.69
38469	Ve 19	2.32	86.46	3241.35	312310.80	7.91	6.06	222.82	7517.14	2.40

Glaise section, France (continued)

N° GEA	Sample ID	Ni	Cu	Zn	As	Mo	Cd	Ba	U
29408	GL 1	20.03	7.15	40.34	1.29	0.62	0.00	81.52	1.09
29409	GL 2	40.89	18.78	212.63	6.79	2.46	0.10	164.80	0.91
29410	GL 3	37.48	25.50	148.66	4.99	0.19	0.05	120.69	0.40
29411	GL 4	43.58	33.96	122.10	3.69	0.00	0.00	119.89	0.29
29412	GL 5	36.04	49.23	175.69	4.67	0.46	0.00	329.47	0.15
29413	GL 6	55.55	45.19	120.99	5.48	0.17	0.00	67.33	0.22
29414	GL 7	41.23	38.69	174.81	4.44	0.18	0.00	414.51	0.15
29415	GL 8	48.51	46.03	137.21	5.66	0.17	0.14	76.50	0.09
29416	GL 9	38.31	69.15	161.55	3.07	0.14	0.09	106.13	0.16
29417	GL 10	41.91	73.93	243.36	3.68	0.29	0.08	421.67	0.24
29418	GL 11	63.70	44.94	133.74	4.05	0.16	0.00	157.15	0.43
29419	GL 12	71.99	41.97	151.49	10.03	0.18	0.08	272.86	0.57
29420	GL 13	68.60	52.80	125.14	4.80	0.24	0.00	112.06	0.99
29421	GL 14	44.10	31.40	80.13	6.60	0.00	0.09	108.71	0.76
29422	GL 15	31.37	23.16	75.56	3.71	0.00	0.00	147.78	0.31
29423	GL 16	38.68	32.68	88.13	7.14	0.41	0.00	196.20	0.43
29424	GL 17	47.57	41.50	111.52	5.28	0.19	0.00	161.09	0.31
29425	GL 18	48.22	28.13	122.91	6.74	0.45	0.00	249.44	0.47
29426	GL 19	53.47	43.06	62.08	5.58	0.39	0.00	141.67	0.61
29427	GL 20	58.29	34.22	81.07	5.52	0.66	0.19	57.25	0.61
29428	GL 21	75.28	41.38	65.08	9.78	1.06	0.00	84.97	0.39
29429	GL 22	33.24	35.72	104.03	2.31	0.20	0.00	268.56	0.55
29430	GL 23	27.64	28.20	73.18	1.70	0.04	0.04	191.05	0.34
29431	GL 24	32.02	35.18	85.12	3.92	0.27	0.00	207.69	0.40
29432	GL 25	55.09	34.68	98.06	3.54	0.20	0.00	72.86	0.34
29433	GL 26	31.67	46.25	83.05	1.07	0.00	0.07	83.23	0.38
29434	GL 27	79.74	54.15	132.25	7.17	0.00	0.09	76.56	0.65
29435	GL 28	33.46	25.96	69.89	3.07	0.26	0.04	128.35	0.74
29436	GL 29	53.21	44.22	137.87	3.85	0.16	0.25	153.60	0.61
29437	GL 30	38.58	50.66	120.34	3.57	0.00	0.18	82.33	0.52
29438	GL 31	29.92	0.88	31.04	13.22	0.23	0.08	65.35	0.53
29439	GL 32	36.60	37.80	71.29	2.11	0.04	0.00	95.92	0.41
29440	GL 33	27.87	19.19	73.92	0.95	0.00	0.11	147.41	0.48
29441	GL 34	49.83	42.58	199.23	2.88	0.15	0.41	143.13	0.84
29442	GL 35	34.13	29.83	61.98	1.95	0.12	0.12	83.29	0.72
29443	GL 36	27.01	22.26	124.40	1.58	0.08	3.50	398.06	0.52
29444	GL 37	46.29	36.32	105.82	3.15	0.22	0.17	173.88	0.63

Vergol section, France (continued)

N° GEA	Sample ID	Ni	Cu	Zn	As	Mo	Cd	Ba	U
38450	Ve 0	17.70	5.96	38.49	0.74	0.16	0.00	39.88	0.58
38451	Ve 1	24.62	11.33	46.95	2.58	0.14	0.08	31.70	1.15
38452	Ve 2	26.30	12.62	48.94	1.97	0.13	0.05	23.99	1.16
38453	Ve 3	25.63	13.66	52.70	2.76	0.17	0.04	28.28	0.62
38454	Ve 4	19.96	10.63	42.25	1.51	0.10	0.02	26.77	0.72
38455	Ve 5	19.30	7.86	43.26	1.46	0.23	0.04	25.90	0.66
38456	Ve 6	32.66	12.78	49.32	3.68	1.97	0.07	29.96	0.76
38457	Ve 7	74.40	24.77	150.06	8.51	1.93	0.34	32.69	1.54
38458	Ve 8	53.37	19.22	53.55	8.53	1.44	0.12	27.79	1.34
38459	Ve 9	85.07	31.17	144.81	11.47	1.44	0.54	43.53	1.90
38460	Ve 10	54.61	18.53	50.13	6.30	1.99	0.07	33.09	1.45
38461	Ve 11	87.64	30.27	111.50	10.57	1.40	0.31	32.09	1.97
38462	Ve 12	17.93	5.37	18.52	0.74	0.03	0.00	22.99	0.57
38463	Ve 13	27.78	13.53	44.16	1.53	0.09	0.00	30.90	1.12
38464	Ve 14	27.26	14.34	76.16	1.57	0.11	0.09	27.68	1.07
38465	Ve 15	20.49	7.41	31.40	0.92	0.00	0.00	37.92	0.65
38466	Ve 16	22.36	12.99	48.03	1.60	0.15	0.04	29.33	0.82
38467	Ve 17	77.26	28.34	76.28	8.62	0.10	0.07	71.75	1.21
38468	Ve 18	25.25	12.02	46.12	1.50	0.17	0.00	42.56	0.90
38469	Ve 19	17.18	4.22	27.72	0.73	0.11	0.00	24.83	0.50

Malleval section, France

GEA N°	Sample ID	Depth (m)	% Sol	Al	Ca	V	Cr	Mn	Fe	Co
29346	MAm 21	2.50	97.72	549.17	376215.51	19.46	6.04	37.94	2595.27	0.94
29347	MAm 22	3.10	96.24	241.93	379197.55	9.52	6.13	40.63	1939.51	0.84
29348	MAm 23	3.35	97.00	283.52	377850.92	10.59	8.48	37.25	1399.73	0.94
29349	MAm 24	4.30	93.76	453.25	360016.90	5.44	7.53	39.20	2158.55	1.00
29350	MAm 25	5.75	98.60	250.57	374151.16	4.70	4.85	47.46	1616.30	0.75
29351	MAm 26	6.65	97.76	260.70	369870.30	5.10	5.59	49.41	1885.42	0.79
29352	MAm 27	7.50	97.68	300.01	366073.37	5.78	6.69	51.97	2202.06	0.67
29353	MAm 28	8.20	94.40	582.49	361262.75	7.23	7.13	61.93	4456.57	1.28
29354	MAm 29	8.95	97.84	749.56	361275.49	5.77	4.76	55.09	3702.23	0.86
29355	MAm 30	9.90	96.80	784.76	370843.39	7.11	4.74	61.26	3514.69	0.98
29356	MAm 31	12.00	96.24	412.06	380386.62	15.67	6.68	57.52	4396.73	0.88
29357	MAm 32	13.20	97.56	324.60	370519.29	13.97	6.49	57.79	4226.01	0.78
29358	MAm 33	14.90	97.76	278.89	369989.06	8.51	4.94	59.20	3805.77	0.92
29359	MAm 34	16.60	91.45	1057.74	347421.84	3.48	3.86	105.85	3012.83	1.19
29360	MAm 35	25.30	89.04	687.03	349197.42	3.60	2.92	138.32	3585.26	1.02
29361	MAm 36	27.20	86.42	877.77	328788.34	4.04	3.48	132.72	3441.57	1.56
29363	MAs 1	27.60	91.46	1031.55	344851.15	4.25	3.88	102.91	3315.77	1.09
29364	MAs 2	28.55	85.86	1589.34	344700.91	5.41	4.46	133.47	4142.18	0.96
29362	MAm 37	28.80	91.88	731.09	369115.97	4.90	3.93	113.78	3262.43	1.15
39365	MAs 3	29.65	90.00	645.01	358275.43	4.27	3.69	120.20	3519.89	1.20
29366	MAs 4	30.95	93.20	564.65	353866.39	4.55	4.35	104.86	3961.33	1.41
29367	MAs 5	32.60	94.65	345.14	377028.05	3.47	2.57	100.10	2516.69	0.95
29368	MAs 6	33.50	98.84	308.17	380368.60	9.94	5.03	90.71	2088.19	0.77
29369	MAs 7	34.45	99.16	171.69	386354.29	10.17	5.52	91.40	2528.16	0.73
29370	MAs 8	35.40	97.00	330.15	379215.02	4.83	3.40	102.09	2528.99	0.80
29371	MAs 9	36.30	97.25	388.11	382876.44	5.98	3.35	106.97	2672.87	0.66
29372	MAs 10	36.95	93.88	815.95	360339.14	5.08	2.66	120.72	2912.87	1.30
29373	MAs 11	37.50	98.84	407.14	376952.50	6.42	2.86	77.18	2913.10	0.87
29374	MAs 12	38.40	98.96	157.45	385277.62	10.26	6.17	78.02	1417.68	0.78
29375	MAs 13	40.20	99.16	218.85	382529.19	12.48	6.10	85.47	2148.87	0.73
29376	MAs 14	41.70	98.68	117.89	387866.81	8.15	2.63	80.66	5958.09	1.05
29377	MAs 15	47.70	97.03	400.59	379404.98	6.19	3.57	131.48	1515.89	0.59
29378	MAs 16	49.30	97.52	294.94	379345.16	6.71	4.52	96.96	1584.35	0.63
29379	MAs 17	50.75	98.48	227.34	381604.37	7.08	6.16	94.86	1382.18	0.69
29380	MAs 18	51.80	97.66	378.21	370751.20	11.80	5.47	97.46	3169.92	0.87
29381	MAs 19	52.75	99.40	241.80	380619.39	8.08	4.08	109.19	2422.25	0.80
29382	MAs 20	53.60	98.08	319.95	386454.29	12.88	4.27	110.25	3000.31	0.77
29383	MAs 21	55.00	99.08	217.69	384037.41	8.30	4.29	114.36	2756.99	0.94
29384	MAs 22	56.20	98.48	251.84	381240.52	11.03	4.50	100.28	2941.12	0.84
29385	MAs 23	57.15	98.52	212.26	377791.04	8.05	4.96	111.26	2676.15	0.73
29386	MAs 24	58.25	97.80	316.46	383485.49	10.65	6.84	95.18	2350.16	0.78
29387	MAs 25	59.40	98.32	243.73	377674.22	9.23	4.31	108.88	2891.63	0.99
29388	MAs 26	61.10	98.88	210.35	380250.78	6.18	4.83	120.87	2414.98	0.82
29389	MAs 27	64.55	95.92	399.50	364547.84	4.74	3.81	143.65	3226.59	0.85
29390	MAs 28	65.85	98.72	195.68	386389.49	8.97	5.85	111.95	2531.91	0.83
29391	MAs 29	67.00	98.20	296.62	395917.53	7.81	3.43	110.51	2201.11	1.10
29392	MAs 30	68.30	97.88	170.82	376674.55	3.73	3.75	234.61	2178.17	0.86
29393	MAs 31	69.40	97.44	215.06	393662.12	6.73	6.74	208.65	2707.75	0.83
29394	MAs 32	70.45	98.08	197.87	390911.19	3.39	2.29	221.97	1833.09	0.69
29395	MAs 33	71.50	98.56	172.39	396922.37	6.67	3.44	197.79	2365.65	0.81
29396	MAs 34	72.40	94.48	323.55	380163.60	4.33	2.73	177.48	3158.57	1.02
29397	MAs 35	73.55	92.05	432.32	364762.43	6.92	5.01	175.79	2691.53	0.68
29398	MAs 36	74.65	89.50	497.79	364665.59	10.05	7.86	196.90	5356.10	1.16
29399	MAs 37	75.80	89.72	555.93	361472.51	11.08	5.52	194.92	1775.38	0.67
29400	MAs 38	76.90	89.78	692.91	350061.92	10.27	5.27	242.31	5262.36	1.61
29401	MAs 39	78.20	88.68	528.81	324144.96	9.14	5.34	266.35	5907.72	1.15
29402	MAs 40	79.40	93.57	239.58	359491.59	7.36	3.18	163.81	3850.45	0.78
30705	MAs 40 b	79.40	88.89	505.12	340666.52	8.86	6.30	186.65	5571.19	1.12
30706	MAs 41 b	80.30	90.60	571.16	349615.38	9.16	6.58	194.64	4706.85	1.18
30707	MAs 42 b	80.40	89.74	484.30	347129.73	10.37	7.27	208.75	5332.33	1.66
29403	MAs 41	80.60	89.05	440.94	348687.00	9.67	6.72	208.81	5794.09	1.55
30708	MAs 43 b	82.15	96.17	192.68	380260.66	6.23	5.36	160.89	3844.17	0.90
29404	MAs 42	82.65	96.85	170.36	374186.14	6.63	3.73	169.46	5543.90	1.02
30709	MAs 44 b	83.40	97.12	187.61	387525.28	5.62	4.95	143.64	2026.91	0.82
30710	MAs 45 b	83.70	96.53	346.84	372364.31	7.48	6.59	129.50	3091.78	0.71
29405	MAs 43	84.35	91.79	410.92	357135.05	5.75	2.44	122.07	2906.71	0.96
30711	MAs 46 b	84.60	96.68	228.99	373019.45	4.05	4.10	169.73	2112.27	1.00
30712	MAs 47 b	85.15	95.20	290.65	359751.37	6.31	4.34	117.48	3571.99	1.28
30713	MAs 48 b	85.55	91.68	385.78	359239.82	5.51	5.15	117.27	2268.16	0.68
30714	MAs 49 b	86.85	96.80	356.09	377275.83	5.17	4.42	129.66	2396.22	0.78
30715	MAs 50 b	87.90	96.60	461.98	381098.65	4.54	3.18	138.29	2727.42	0.87
29406	MAs 44	88.20	96.84	267.86	382789.07	7.83	8.42	154.41	3329.25	0.76
30716	MAs 51 b	89.10	98.28	171.40	343449.36	5.40	4.70	130.73	3251.01	0.79
30717	MAs 52 b	90.65	96.65	254.93	388887.03	10.40	5.68	175[illegible]1	2154.21	0.76
29407	MAs 45	91.10	94.29	225.12	374535.42	7.07	5.54	158.85	4568.14	1.09
30718	MAs 53 b	92.20	97.84	210.77	384416.47	8.86	6.10	183.01	3435.25	1.85
30719	MAs 54 b	93.30	99.72	210.44	386463.77	5.68	3.21	179.46	2669.36	0.91
30720	MAs 55 b	94.60	100.04	156.96	382302.44	7.23	4.09	156[illegible]1	2180.92	0.81
30721	MAs 56 b	95.60	97.80	236.29	385063.42	5.67	3.82	222.56	2550.68	1.54
30722	MAs 57 b	96.90	98.40	201.19	383779.38	6.69	4.28	199.76	2160.84	0.81

Malleval section, France (continued)

GEA N°	Sample ID	Ni	Cu	Zn	As	Mo	Cd	Ba	U
29346	MAm 21	10.60	0.22	4.39	6.19	0.58	0.02	2.19	0.87
29347	MAm 22	11.90	0.00	0.75	2.80	0.49	0.04	1.73	1.37
29348	MAm 23	13.67	0.19	0.35	3.27	0.25	0.02	1.63	2.45
29349	MAm 24	12.14	0.59	4.58	2.44	1.18	0.05	2.06	1.12
29350	MAm 25	13.59	0.85	3.87	2.46	0.57	0.00	1.70	1.43
29351	MAm 26	24.61	0.00	2.17	3.07	0.73	0.00	1.71	1.46
29352	MAm 27	13.44	0.00	3.55	3.04	0.89	0.02	1.73	2.12
29353	MAm 28	12.61	0.16	5.60	5.47	0.26	0.03	2.77	0.87
29354	MAm 29	11.73	0.28	1.95	3.87	0.37	0.01	2.48	0.75
29355	MAm 30	11.35	0.80	9.33	4.92	0.47	0.15	2.99	0.58
29356	MAm 31	10.96	0.40	1.26	8.33	0.1	0.02	2.58	0.81
29357	MAm 32	9.71	0.31	6.26	8.93	0.05	0.04	2.11	0.83
29358	MAm 33	11.19	0.08	5.54	7.47	0.13	0.02	1.74	0.68
29359	MAm 34	19.76	0.15	10.94	2.36	0.53	0.03	3.11	0.68
29360	MAm 35	27.81	0.26	8.47	3.13	0.02	0.00	2.47	0.48
29361	MAm 36	9.94	0.14	23.60	3.90	0.03	0.05	3.20	0.48
29363	MAs 1	10.92	1.09	6.35	3.36	0.45	0.03	3.46	0.83
29364	MAs 2	11.07	3.48	14.88	3.91	0.49	0.06	3.91	0.55
29362	MAm 37	11.33	0.30	6.72	5.34	0.31	0.06	3.01	1.52
39365	MAs 3	13.26	3.68	9.23	3.88	0.25	0.00	1.94	0.53
29366	MAs 4	11.20	0.64	8.25	4.43	0.58	0.00	2.97	0.90
29367	MAs 5	11.99	0.00	2.66	3.41	0.20	0.00	1.93	0.43
29368	MAs 6	29.13	0.00	4.03	3.72	0.08	0.00	1.60	0.47
29369	MAs 7	12.20	0.00	6.05	3.73	0.09	0.00	1.39	0.64
29370	MAs 8	12.24	0.00	1.67	5.25	0.12	0.00	1.81	0.70
29371	MAs 9	11.76	0.19	3.06	4.70	0.23	0.00	1.56	0.75
29372	MAs 10	9.56	0.26	3.72	5.17	0.02	0.00	2.61	0.49
29373	MAs 11	12.43	0.11	2.55	6.22	0.37	0.01	1.75	0.58
29374	MAs 12	13.83	0.04	3.47	1.71	0.12	0.01	1.23	0.47
29375	MAs 13	13.50	0.09	5.11	4.13	0.14	0.03	2.22	0.85
29376	MAs 14	16.62	0.26	7.86	28.21	1.18	0.03	2.24	2.69
29377	MAs 15	11.53	1.37	3.27	3.22	0.11	0.00	1.76	0.53
29378	MAs 16	12.38	0.34	5.53	2.84	0.03	0.00	1.58	0.54
29379	MAs 17	13.15	0.51	1.31	2.97	0.02	0.01	1.49	0.54
29380	MAs 18	14.13	0.07	5.42	4.81	0.07	0.05	1.98	0.71
29381	MAs 19	12.21	0.26	9.33	3.35	0.00	0.00	3.03	0.40
29382	MAs 20	13.30	0.06	0.74	5.14	0.23	0.02	2.23	0.83
29383	MAs 21	12.77	0.00	0.53	4.05	0.11	0.01	2.72	0.37
29384	MAs 22	13.98	0.03	0.93	6.34	0.05	0.02	2.17	0.50
29385	MAs 23	12.67	0.00	1.27	2.40	0.07	0.00	2.91	0.36
29386	MAs 24	13.03	0.00	3.26	3.60	0.25	0.02	1.89	0.99
29387	MAs 25	13.43	0.00	1.96	6.57	0.14	0.00	2.63	0.66
29388	MAs 26	13.22	0.00	2.19	6.23	0.06	0.00	2.80	0.41
29389	MAs 27	12.98	0.00	2.42	5.43	0.21	0.02	2.43	0.69
29390	MAs 28	12.27	0.94	0.19	4.33	0.02	0.01	1.82	0.67
29391	MAs 29	15.13	0.00	0.89	3.40	0.36	0.00	1.35	0.68
29392	MAs 30	12.00	0.00	1.94	5.04	0.23	0.03	1.57	0.57
29393	MAs 31	13.24	0.02	2.55	5.60	0.00	0.01	1.68	0.77
29394	MAs 32	14.80	0.05	3.09	2.49	0.15	0.02	1.60	0.45
29395	MAs 33	15.23	0.00	4.71	4.96	0.04	0.01	1.34	0.69
29396	MAs 34	14.50	0.02	0.39	9.38	0.06	0.00	1.54	0.91
29397	MAs 35	12.48	0.25	3.06	5.78	0.04	0.02	2.24	1.64
29398	MAs 36	14.26	0.08	7.50	8.61	0.16	0.04	3.22	1.19
29399	MAs 37	13.64	0.00	0.63	0.75	0.05	0.02	2.12	5.22
29400	MAs 38	13.99	0.10	1.27	10.56	0.80	0.04	3.01	1.88
29401	MAs 39	11.28	0.00	1.88	11.68	0.17	0.01	6.31	0.90
29402	MAs 40	12.13	0.00	21.39	1.77	0.09	0.13	1.97	1.56
30705	MAs 40 b	12.63	0.13	0.61	7.28	0.04	0.04	2.14	0.77
30706	MAs 41 b	12.83	0.25	2.86	6.90	0.56	0.01	2.26	1.08
30707	MAs 42 b	15.45	0.46	8.02	10.84	0.35	0.00	3.05	3.06
29403	MAs 41	16.81	0.11	8.22	13.28	0.37	0.02	2.45	2.84
30708	MAs 43 b	13.26	1.74	4.37	7.40	0.24	0.03	1.38	2.20
29404	MAs 42	12.49	0.00	0.58	3.54	0.18	0.00	4.47	1.31
30709	MAs 44 b	14.02	0.02	0.00	3.56	0.20	0.00	1.87	1.22
30710	MAs 45 b	13.00	3.61	9.94	3.76	0.20	0.00	2.18	0.80
29405	MAs 43	13.06	0.00	5.86	5.48	0.51	0.14	1.93	1.69
30711	MAs 46 b	14.06	11.51	4.40	3.06	0.30	0.02	3.79	1.09
30712	MAs 47 b	16.03	2.80	4.68	12.91	0.70	0.00	2.10	2.44
30713	MAs 48 b	14.06	0.27	1.64	2.63	0.12	0.00	2.27	1.09
30714	MAs 49 b	13.44	5.15	7.27	2.37	0.21	0.01	2.92	0.84
30715	MAs 50 b	13.37	0.00	14.16	7.78	0.52	0.08	2.02	1.05
29406	MAs 44	13.40	0.00	1.71	4.27	0.13	0.08	2.17	1.03
30716	MAs 51 b	11.27	1.37	9.12	6.33	0.09	0.07	1.95	0.82
30717	MAs 52 b	15.53	3.29	4.73	2.20	0.07	0.00	2.59	0.96
29407	MAs 45	12.22	0.00	0.65	8.84	0.35	0.03	2.16	0.88
30718	MAs 53 b	14.46	2.15	3.26	6.36	0.31	0.01	1.88	1.50
30719	MAs 54 b	14.44	7.81	12.81	4.56	0.17	0.00	3.43	0.50
30720	MAs 55 b	15.08	4.94	2.66	3.50	0.11	0.02	2.31	0.82
30721	MAs 56 b	15.64	4.79	4.55	6.23	0.37	0.02	3.57	0.77
30722	MAs 57 b	15.28	7.52	8.63	2.80	0.23	0.03	2.51	1.33

Gorgo a Cerbara

Samples ID	Al	Ti	V	Cr	Co	Ni	Cu	As	Mo	U
GC 110	3933.9	538.5	7.3	6.6	3.9	18.1	4.4	0.9	0.9	0.6
GC 111	36016.6	1795.8	52.3	79.7	11.6	57.4	92.9	2.1	0.9	0.9
GC 112	27193.5	1356.8	28.9	32.2	9.5	40.0	55.6	2.5	0.5	0.6
GC 113	52161.3	2341.6	55.3	65.7	13.6	61.3	59.4	1.9	0.7	1.2
GC 114	9862.7	750.8	11.3	11.8	2.2	14.7	10.1	0.3	0.4	0.4
GC 115	16254.0	890.8	15.9	20.3	3.2	20.1	8.4	0.7	0.2	0.5
GC 116	14345.6	893.0	14.0	15.5	3.2	18.9	21.5	1.0	0.4	0.7
GC 117	35172.1	1732.6	38.9	46.4	14.8	41.0	49.5	3.2	1.0	1.6
GC 118	3309.7	603.4	5.8	7.8	2.1	13.9	3.9	0.4	0.2	0.6
GC 119	45162.6	2163.4	84.2	70.1	50.0	133.1	145.2	10.1	4.0	3.0
GC 120	8111.1	653.5	13.4	10.1	4.1	21.0	9.5	0.7	0.3	1.0
GC 121	17311.2	1064.9	29.3	28.7	9.1	53.6	55.0	5.0	2.0	1.4
GC 122	3322.6	581.7	7.8	6.4	2.4	15.4	4.6	0.7	0.3	1.2
GC 123	16794.3	969.7	35.2	23.7	7.3	28.0	31.8	1.9	0.6	1.0
GC 124	9645.4	711.9	10.7	8.2	2.5	14.8	5.2	0.7	0.2	1.2
GC 125	10389.0	664.7	13.6	31.8	2.2	20.6	4.7	0.5	0.3	0.7
GC 126	7338.5	615.2	11.1	5.9	3.9	17.0	11.0	0.8	0.2	0.5
GC 127	47687.5	2423.8	65.5	62.7	17.2	54.5	55.4	1.7	0.5	2.0
GC 128	7082.4	628.1	11.5	19.6	14.9	42.2	30.5	1.6	0.9	0.5
GC 129	12184.7	828.8	14.5	17.8	2.2	16.7	24.5	0.8	0.1	0.5
GC 130	5985.6	607.4	6.5	6.6	1.7	15.0	6.2	0.5	0.0	0.4
GC 131	8805.3	640.1	11.7	9.7	7.6	27.6	30.1	1.7	0.6	0.3
GC 132	33870.6	1624.4	33.0	39.1	8.7	49.2	13.9	2.7	0.5	0.9
GC 133	54448.6	2512.6	53.0	66.0	12.4	54.3	54.5	2.4	0.9	1.3
GC 134	64948.2	4403.5	59.0	67.1	14.0	54.2	33.8	5.6	1.0	1.6
GC 135	59933.5	2510.4	55.5	69.5	11.8	51.2	28.6	3.3	1.4	1.4
GC 136	53881.5	2364.3	47.9	53.9	7.7	38.1	20.5	2.7	0.5	1.4
GC 137	21026.0	1055.5	25.3	27.3	21.8	55.8	120.2	3.1	1.2	1.0
GC 138	21262.0	975.2	25.1	25.5	8.4	20.5	21.7	3.1	0.8	1.2
GC 139	32294.9	1564.6	68.5	71.6	44.7	121.1	64.8	8.7	4.4	2.2
GC 140	99792.7	6599.8	119.8	86.1	20.7	61.1	45.4	5.3	2.4	4.9
GC 141	74820.9	3231.2	443.7	152.9	48.4	184.3	70.6	16.6	8.0	5.7
GC 142	97775.4	6293.2	122.1	81.0	12.8	57.2	40.1	5.1	3.4	5.2
GC 143	47640.5	1915.2	100.2	84.1	42.3	149.8	112.3	11.4	6.3	3.1
GC 144	38949.2	1700.1	92.5	59.5	39.7	124.5	55.6	8.9	4.5	2.5
GC 145	28848.4	1374.9	43.9	31.2	11.6	36.1	42.7	4.7	1.6	1.2
GC 146	57071.6	2157.2	65.1	51.0	10.4	38.2	68.3	3.3	2.7	1.5
GC 147	17223.6	548.1	14.8	12.7	3.1	15.0	8.7	2.1	0.6	0.5
GC 148	73366.6	4023.2	85.1	93.8	13.8	51.1	120.2	2.4	3.0	1.6
GC 149	57138.6	2110.6	69.9	48.0	11.5	35.8	108.1	4.8	21.6	2.7
GC 150	26535.4	1038.1	33.2	21.7	3.0	11.6	42.5	3.5	1.9	0.7
GC 151	55660.4	2008.8	56.9	46.1	6.5	39.2	49.0	2.6	1.8	1.2
GC 152	12213.4	403.6	12.7	9.1	1.6	8.3	7.7	2.3	0.6	0.4
GC 153	62190.5	2322.1	71.2	60.1	8.0	38.7	57.5	3.0	3.7	1.6
GC 154	59450.4	3195.5	74.5	52.1	11.2	77.8	69.7	4.1	5.3	1.6
GC 155	54333.5	1985.2	76.9	47.7	10.4	48.2	123.5	4.0	4.8	1.5
GC 156	18754.8	579.3	21.3	12.4	6.8	15.9	8.4	3.3	0.8	0.5
GC 157	57985.0	3164.2	75.6	48.1	11.8	45.6	61.8	3.7	4.5	1.7
GC 158	18967.8	638.8	21.1	14.2	9.4	27.1	10.5	3.4	0.5	0.6
GC 159	47806.3	1921.0	198.2	78.1	43.6	157.5	93.5	8.3	11.5	4.7
GC 160	40705.2	1666.4	374.6	77.7	21.6	195.7	242.2	11.2	31.9	16.5
GC 161	21781.6	626.4	89.5	35.5	10.2	51.6	44.8	4.5	3.7	1.2
GC 162	61627.3	2446.7	284.5	103.1	23.4	114.9	123.9	6.9	11.9	4.7
GC 163	35344.6	1168.2	43.5	31.8	2.8	12.1	27.3	5.1	2.1	1.6
GC 164	43290.3	1660.8	262.1	107.7	10.4	87.6	95.8	6.5	7.9	5.2
GC 165	46196.5	1701.3	540.5	93.3	72.5	370.9	214.2	17.0	94.0	17.1
GC 166	57913.2	2060.4	272.6	86.0	42.8	160.9	169.5	16.6	42.9	10.2
GC 167	84216.0	2969.2	135.1	78.5	25.0	58.2	99.3	6.7	3.7	4.1
GC 168	32434.7	1031.8	42.5	28.4	8.4	26.8	19.7	4.5	42.5	1.5
GC 169	70760.8	2400.9	75.0	57.9	11.3	47.7	71.1	4.4	1.9	2.4
GC 170	80440.5	2721.9	91.9	78.1	27.7	116.5	83.1	5.9	2.8	2.0
GC 171	50813.1	1926.6	50.7	45.3	17.0	52.8	79.8	11.3	0.7	1.5
GC 172	21964.3	950.5	21.8	21.0	30.9	65.3	35.2	7.4	4.9	0.7
GC 173	85717.8	4422.5	83.7	65.9	55.1	179.1	128.0	13.0	1.1	1.8
GC 174	24729.1	1024.6	34.1	20.3	5.7	30.5	61.7	4.2	0.2	0.6
GC 175	24209.1	987.8	28.6	22.9	14.6	48.6	71.0	4.3		0.9
GC 176	20380.6	915.9	18.3	17.1	4.8	26.8	17.8	2.1	0.7	0.5
GC 177	24602.2	1074.2	23.7	21.5	5.6	34.0	27.6	2.5	0.7	0.6
GC 178	33175.2	1403.6	32.8	26.2	6.0	36.3	28.8	3.4	0.4	0.8
GC 179	16410.2	759.2	15.4	13.1	3.9	21.5	8.5	1.4		0.5
GC 180	21923.9	1174.3	25.3	19.3	3.1	14.9	2.4	2.4	0.2	1.5
GC 181	7955.4	537.4	7.9	7.2	2.1	13.7	6.0	0.7		0.4
GC 182	15260.6	871.2	15.6	16.0	20.0	42.7	36.5	1.1	0.8	0.6
GC 183	8913.0	522.3	8.9	7.2	12.3	16.7	10.9	1.2	0.4	0.4

N. B.: The data presented here are expressed in ppm and have been obtained using a total HF/HNO_3 acid extraction.

Glaise

Samples ID	Al	Ti	V	Cr	Co	Ni	Cu	As	Mo	U
GL 2	34489.5	2777.5	79.9	55.3	8.5	49.9	20.8	9.4	4.2	2.0
GL 3	63014.4	5375.4	156.5	101.2	9.4	55.0	37.6	7.3	2.9	2.3
GL 4	68989.6	5581.0	161.5	113.9	9.9	49.6	35.0	8.4	0.0	3.3
GL 5	82578.4	6016.1	201.7	131.3	12.8	59.9	55.3	4.2	1.4	3.5
GL 6	69940.6	5859.0	178.8	116.6	13.0	66.2	42.2	4.1		2.4
GL 7	68858.6	5872.8	173.8	116.4	8.8	61.8	38.9	6.1	0.5	2.3
GL 8	40875.1	5246.5	168.8	103.6	11.8	62.9	42.5	7.6	1.8	2.0
GL 9	43415.3	4990.1	169.5	103.2	8.4	55.9	62.8	4.8	0.9	2.4
GL 10	39571.0	4530.1	159.2	96.0	8.9	59.7	75.9	3.2		2.5
GL 11	35009.5	3897.5	151.6	94.6	12.2	72.6	45.2	1.7	0.9	2.5
GL 12	35877.0	3932.6	159.6	95.8	13.8	65.2	44.3	8.2		2.9
GL 13	38097.5	3976.0	170.9	96.6	10.8	65.5	46.8	5.5	0.5	3.5
GL 14	33333.3	3832.3	120.7	78.0	11.0	50.1	38.0	5.7	1.0	2.7
GL 15	35458.1	3479.5	95.6	70.6	9.8	36.1	19.6	4.9	0.5	2.0
GL 16	42854.3	4086.1	141.6	93.2	8.6	38.6	31.5	5.1	1.3	2.1
GL 17	44010.2	4246.2	166.2	103.8	9.4	52.7	42.7	1.8	0.8	2.4
GL 18	40251.0	3725.6	114.6	79.7	13.1	44.3	28.7	3.9	0.9	2.3
GL 19	33731.4	3549.9	162.5	90.6	7.2	44.5	33.5	3.3		1.9
GL 20	41532.5	3253.6	116.2	82.8	6.6	59.2	35.8	9.5	2.7	2.3
GL 21	38898.2	3537.5	119.3	79.9	12.0	77.5	41.2	7.3	1.1	2.3
GL 22	37653.1	2956.2	91.4	62.7	7.9	40.2	33.7	2.7		1.5
GL 23	32548.9	3460.6	104.2	74.1	5.6	25.7	27.7	0.9	0.6	1.5
GL 24	57762.0	3708.1	126.1	82.6	7.6	37.3	38.7	4.8	1.1	2.8
GL 25	57502.6	3803.8	123.3	97.0	10.3	60.4	38.0	3.6		2.5
GL 26	56872.6	3016.3	95.6	69.0	6.9	30.5	44.1	0.9		1.9
GL 27	53219.8	3212.2	103.7	82.6	16.4	85.4	44.6	5.8		2.2
GL 28	51227.2	3254.3	109.3	84.9	9.2	60.4	47.1	5.5	0.1	2.4
GL 29	45018.7	2199.8	71.7	51.5	6.0	32.3	32.7	5.4	0.1	1.3
GL 30	50323.2	3243.3	103.5	82.9	11.0	50.1	50.1	3.9	0.2	1.9
GL 32	55197.5	3337.2	111.2	76.4	7.0	45.1	37.9	3.9		2.0
GL 33	33661.2	1399.0	45.5	30.8	4.3	33.5	19.1	2.9		1.0
GL 34	57113.2	2499.0	91.3	64.8	10.0	57.7	46.5	4.5	0.1	1.7
GL 35	31571.8	1341.8	47.1	31.7	5.5	30.2	26.0	6.5		1.1
GL 36	23928.7	1044.2	33.5	23.8	2.4	30.3	19.3	0.3		0.7
GL 37	52516.4	2421.1	84.2	57.4	6.9	44.2	27.6	1.9		1.8

Cassis/La Bédoule

Samples ID	Al	Ti	V	Cr	Co	Ni	Cu	As	Mo	U
BE 147*	16800.5	1014.7	23.2	14.3	5.5	27.0	6.2	3.8	1.0	2.1
BE 149	12204.3	787.3	15.4	15.2	3.1	19.7	4.8	2.7	0.3	1.8
BE 151	16555.5	946.4	23.7	20.1	2.3	19.5	6.2	4.9	0.4	2.1
BE 152a1	25409.5	1397.6	38.6	29.6	2.0	30.3	8.4	4.2	0.4	2.5
BE 152a2	18174.4	1061.2	23.2	17.9	3.5	25.1	7.1	1.0	0.5	1.8
BE 152a3	18212.3	1062.5	24.2	18.7	1.8	26.9	5.7	4.9		2.1
BE 152b1	20781.7	1144.7	26.5	22.3	3.5	26.5	6.2	3.1		2.4
BE 152b2	26698.7	1337.6	31.9	26.1	4.7	37.0	7.5	5.2	0.4	2.4
BE 152b3	18481.1	1084.4	24.8	21.6	4.1	26.4	8.1	3.1	0.2	1.5
BE 153a1	29129.1	1465.1	41.5	32.0	4.5	34.7	11.3	4.2	1.3	2.3
BE 153a2	23734.0	1452.6	37.6	29.0	5.7	39.6	10.1	2.8	2.0	1.9
BE 153b1	20924.3	1413.4	34.1	25.9	4.8	36.7	9.0	3.3	0.9	1.7
BE 153b2	27695.8	1695.3	40.9	34.2	4.2	29.1	9.8	3.9	0.3	2.1
BE 153b3	27866.0	1745.7	40.6	31.6	6.1	35.4	13.4	6.0	0.7	1.9
BE 154a	22150.0	1262.7	35.4	29.6	6.1	32.9	7.8	8.8	0.4	1.6
BE 154b	26643.1	1578.8	43.7	30.6	6.9	30.2	10.4	6.8	1.1	1.6
BE 155a	25518.5	1565.8	46.0	33.4	6.3	41.7	9.2	6.3		1.6
BE 155b	24146.9	1445.2	40.0	30.9	5.0	36.0	8.2	2.8	1.0	1.3
BE 156a	18477.4	1151.7	32.3	26.3	4.2	36.8	6.5	2.5	0.5	1.5
BE 156b	21396.6	1288.7	37.5	25.1	4.1	30.7	5.6	5.3	0.5	2.2
BE 156e	15317.4	852.9	14.1	18.2	2.6	16.4	7.3	0.7	0.3	0.5
BE 157c	27686.9	1466.9	40.3	30.6	4.4	30.0	6.9	3.9	0.8	2.1
BE158a	28779.3	1593.2	38.8	31.1	4.2	30.5	5.7	3.4	0.5	2.1
BE 159b	36205.3	1809.1	53.8	44.0	4.8	37.2	8.6	4.4	1.7	2.2
BE 161a	27780.5	1441.5	44.1	34.1	3.4	36.4	8.1	4.0	0.2	2.3
BE 163a	31204.3	1566.6	47.2	35.2	4.8	41.1	7.7	4.2	1.3	2.0
BE 164a	15480.8	1026.8	26.1	18.7	2.6	23.5	2.4	4.3	0.5	2.3
BE 164c	11219.6	826.7	20.6	15.1	1.8	18.0	7.2	2.3	0.3	1.9

N. B.: The data presented here are expressed in ppm and have been obtained using a total HF/HNO_3 acid extraction.

Phosphorus Data

Alvier section, Switzerland

GEA N°	Sample ID	Depth (m)	P (mg/g)	P (ppm)	Sed. Rate	P (MAR)
33503	Al 1	113.60	0.23	229.52		
33504	Al 2	113.10	0.23	228.22		
33505	Al 3	112.05	0.26	259.04		
33506	Al 4 b	111.30	0.26	257.75		
33507	Al 4	111.03	0.16	156.25		
33508	Al 5	110.35	0.14	143.46		
33509	Al 6	108.95	0.18	184.64		
33510	Al 7	108.40	0.34	343.32		
33511	Al 8	108.00	0.32	317.64		
33512	Al 9	107.15	0.14	139.83		
33513	Al 10	106.05	0.17	165.78		
33514	Al 11	105.30	0.14	135.22		
33515	Al 12	103.95	0.19	185.52		
33516	Al 13	103.20	0.20	195.14		
33517	Al 14	102.65	0.19	185.52		
33518	Al 15	101.95	0.13	133.69		
33519	Al 16	101.50	0.11	105.06		
33520	Al 17	100.77	0.13	129.42		
33521	Al 18	99.95	0.20	198.01		
33522	Al 19	99.05	0.16	163.38		
33523	Al 20	97.95	0.17	171.78		
33524	Al 21	97.10	0.16	163.05		
33525	Al 22	96.25	0.33	329.67		
33526	Al 23	95.40	0.14	143.45		
33527	Al 24	94.60	0.22	221.55		
33528	Al 25	93.30	0.34	337.45		
33529	Al 26	92.85	0.27	267.32		
33530	Al 27	92.50	0.69	692.07		
33531	Al 28	91.65	0.15	152.22		
33532	Al 29	90.65	0.22	221.98		
33533	Al 30	90.05	0.25	249.58	1.49	0.93
33534	Al 31	89.50	0.28	280.39	1.49	1.04
33535	Al 32	88.85	0.22	219.34	1.49	0.82
33536	Al 33	86.70	0.24	241.45	1.49	0.90
33537	Al 34	85.60	0.35	352.90	1.49	1.31
33538	Al 35	84.80	0.42	418.27	1.49	1.56
33539	Al 36	83.50	0.17	171.53	1.49	0.64
33540	Al 37	82.55	0.18	175.87	1.49	0.66
33541	Al 38	82.10	0.19	192.26	1.49	0.72
33542	Al 39	81.00	0.23	233.48	1.49	0.87
33543	Al 40	80.00	0.17	172.37	1.49	0.64
33544	Al 41	79.10	0.32	323.64	1.49	1.21
33545	Al 42	78.10	0.29	289.20	1.49	1.08
33546	Al 43	77.05	0.55	552.93	1.49	2.06
33547	Al 44	76.00	0.26	262.07	1.49	0.98
33548	Al 45	74.75	0.21	212.16	1.49	0.79
33549	Al 46	74.25	0.23	231.79	1.49	0.86
33550	Al 47	72.90	0.60	600.18	1.49	2.24
33551	Al 48	73.00	0.84	844.47	1.49	3.15
33552	Al 49	72.50	0.36	360.01	1.49	1.34
33553	Al 50	71.60	0.26	263.29	1.64	1.08
33554	Al 51	71.25	0.80	801.85	1.64	3.30
33555	Al 52	70.30	0.28	279.69	1.64	1.15
33556	Al 53	69.50	0.51	512.49	1.64	2.11
33557	Al 54	68.85	0.33	327.45	1.64	1.35
33558	Al 55	68.45	0.80	798.27	1.64	3.28
33559	Al 56	67.75	0.24	238.30	1.64	0.98
33560	Al 57	66.75	0.32	322.36	1.64	1.33
33561	Al 58	66.10	0.31	306.80	1.64	1.26
33562	Al 59	65.35	0.28	281.91	1.64	1.16
33563	Al 60	64.75	0.24	236.68	1.64	0.97
33564	Al 61	64.10	0.22	216.60	1.64	0.89
33565	Al 62	63.00	0.45	448.50	1.64	1.84
33566	Al 63	62.50	0.30	304.93	1.64	1.25
33567	Al 64	61.50	0.47	473.92	1.64	1.95
33568	Al 65	60.90	0.61	612.32	1.64	2.52
33569	Al 66	60.25	0.15	154.73	1.64	0.64
33570	Al 67	59.85	0.20	195.25	1.64	0.80
33571	Al 68	59.70	0.57	565.75	1.64	2.33
33572	Al 69	59.30	0.24	235.05	1.64	0.97
33573	Al 70	58.60	0.27	274.52	1.64	1.13
33574	Al 71	58.45	0.58	580.29	1.64	2.39
33575	Al 72	57.60	0.22	223.09	1.64	0.92
33576	Al 73	56.40	0.35	345.75	2.01	1.74
33577	Al 74	55.95	0.64	642.26	2.01	3.23
33578	Al 75	55.55	0.28	282.94	2.01	1.42
33579	Al 76	55.15	0.50	495.06	2.01	2.49
33580	Al 77	54.90	0.18	183.73	2.01	0.93
33581	Al 78	54.60	0.38	381.71	2.01	1.92
33582	Al 79	54.25	0.26	256.28	2.01	1.29
33583	Al 80	53.25	0.17	170.92	2.01	0.86
33584	Al 81	52.60	0.20	203.35	2.01	1.02
33585	Al 82	51.85	0.55	550.76	2.01	2.77
33586	Al 83	51.60	0.14	141.32	2.01	0.71
33587	Al 84	51.30	0.22	218.11	2.01	1.10
33588	Al 85	50.70	0.25	250.34	2.01	1.26
33589	Al 86	50.10	0.26	264.96	2.01	1.33
33590	Al 87	49.60	0.16	158.82	2.01	0.80
33591	Al 88	49.00	0.19	190.94	2.01	0.96
33592	Al 89	48.35	0.24	238.09	2.01	1.20
33593	Al 90	47.85	0.25	254.47	2.01	1.28
33594	Al 91	47.40	0.35	347.11	2.01	1.75
33595	Al 92	47.20	0.17	168.73	2.01	0.85
33596	Al 93	46.25	0.23	231.09	2.01	1.16
33597	Al 94	45.80	0.69	687.81	2.01	3.46
33598	Al 95	44.85	0.23	227.20	2.01	1.14
33599	Al 96	44.40	0.29	290.50	2.01	1.46
33600	Al 97	43.55	0.37	365.29	2.01	1.84
33601	Al 98	42.65	0.39	393.12	2.01	1.98
33602	Al 99	42.00	0.20	199.55	2.19	1.09
33603	Al 100	41.30	0.23	225.32	2.19	1.23
33604	Al 101	40.75	0.42	423.89	2.19	2.32
33607	Al 104	40.70	0.79	790.44	2.19	4.32
33605	Al 102	40.50	0.31	309.79	2.19	1.69
33608	Al 105	40.20	0.26	260.26	2.19	1.42
33606	Al 103	39.90	0.25	249.98	2.19	1.37
33610	Al 107	38.90	0.24	237.72	2.19	1.30
33611	Al 108	38.45	0.32	316.74	2.19	1.73
33612	Al 109	38.00	0.21	208.72	2.19	1.14
33613	Al 110	36.95	0.27	265.65	2.19	1.45
33614	Al 111	36.70	0.36	355.31	2.19	1.94
33615	Al 112	36.10	0.46	464.66	2.19	2.54
33616	Al 113	35.50	0.12	116.55	2.19	0.64
33617	Al 114	35.00	0.28	278.12	2.19	1.52
33618	Al 115	34.40	0.42	417.38	2.19	2.28
33619	Al 116	33.85	0.54	539.07	2.19	2.95
33620	Al 117	33.20	0.42	422.25	2.19	2.31
33621	Al 118	32.40	0.34	341.51	2.19	1.87
33622	Al 119	31.70	0.45	446.08	2.19	2.44
33623	Al 120	30.80	0.18	177.05	2.19	0.97
33624	Al 121	30.30	0.25	247.91	2.19	1.36
33625	Al 122	29.50	0.23	228.62	2.19	1.25
33626	Al 123	28.80	0.23	230.78	2.19	1.26
33627	Al 124	28.10	0.22	217.61	2.19	1.19
33628	Al 125	27.25	0.22	221.67	2.19	1.21
33629	Al 126	26.60	0.29	289.48	2.19	1.58
33630	Al 127	25.85	0.10	104.85	2.19	0.57
33631	Al 128	25.00	0.21	206.72	0.61	0.32
33632	Al 129	23.95	0.16	159.59	0.61	0.24
33633	Al 130	22.80	0.19	190.71	0.61	0.29
33634	Al 131	21.90	0.21	213.18	0.61	0.33
33635	Al 132	21.10	0.22	224.82	0.61	0.34
33636	Al 133	20.00	0.30	296.24	0.61	0.45
33637	Al 134	19.00	0.31	311.18	0.61	0.47
33638	Al 135	18.00	0.14	144.45	0.61	0.22
33639	Al 136	16.95	0.26	259.77	0.61	0.40
33640	Al 137	16.00	0.19	187.82	0.61	0.29
33641	Al 138	15.00	0.26	263.97	0.61	0.40
33642	Al 139	14.30	0.23	229.21	0.61	0.35
33643	Al 140	13.20	0.22	222.58	0.61	0.34
33644	Al 141	12.35	0.25	250.82		
33645	Al 142	11.40	0.17	166.54		
33646	Al 143	10.35	0.19	193.72		
33647	Al 144	9.35	0.30	298.69		
33648	Al 145	8.30	0.30	299.38		
33649	Al 146	7.30	0.23	225.38		
33650	Al 147	6.25	0.14	143.87		
33651	Al 148	5.15	0.28	277.03		
33652	Al 149	4.30	0.20	204.21		
33653	Al 150	3.40	0.50	503.97		
33654	Al 151	2.30	0.25	253.16		
33655	Al 152	1.50	0.26	259.50		
33656	Al 153	0.00	0.23	230.70		

N. B.: Sed. Rate = Sedimentation rate, expressed in cm/kyr

Breggia section, Switzerland

GEA N°	Sample ID	Depth (m)	P (mg/g)	P(ppm)	Sed. Rate	P (MAR)
34619	BgV 1	0.15	0.07	71.40	0.57	0.10
34620	BgV 2	0.63	0.07	69.52	0.57	0.10
34621	BgV 3	1.00	0.07	72.73	0.57	0.10
34622	BgV 4	1.50	0.09	86.15	0.57	0.12
34623	BgV 5	2.00	0.08	75.09	0.57	0.11
34624	BgV 6	2.50	0.07	70.56	0.57	0.10
34625	BgV 7	3.00	0.09	86.32	0.57	0.12
34626	BgV 8	3.50	0.05	53.85	0.57	0.08
34627	BgV 9	4.10	0.07	69.87	0.57	0.10
34628	BgV 10	4.53	0.07	68.70	0.57	0.10
34629	BgV 11	5.08	0.11	112.56	0.57	0.16
34630	BgV 12	5.65	0.12	117.35	0.57	0.17
34631	BgV 13	5.98	0.11	113.75	0.57	0.16
34632	BgV 14	6.50	0.07	73.56	0.57	0.11
34633	BgV 15	6.93	0.07	65.17	0.57	0.09
34634	BgV 16	7.50	0.09	91.79	0.57	0.13
34635	BgV 17	7.95	0.10	96.40	0.57	0.14
34636	BgV 18	9.20	0.09	87.58	0.57	0.13
34637	BgV 19	9.75	0.13	127.34	0.57	0.18
34638	BgV 20	10.25	0.11	109.03	0.57	0.16
34639	BgV 21	10.75	0.09	92.51	0.57	0.13
34640	BgV 22	11.00	0.07	72.96	0.57	0.10
34641	BgV 23	11.30	0.16	160.97	0.57	0.23
34642	BgV 24	11.40	0.19	187.49	0.57	0.27
34643	BgV 25	11.50	0.13	125.50	0.57	0.18
34644	BgV 26	11.68	0.06	62.69	0.57	0.09
34645	BgV 27	11.90	0.08	78.68	0.57	0.11
34646	BgV 28	12.15	0.16	162.08	1.04	0.42
34647	BgV 29	12.50	0.08	80.28	1.04	0.21
34648	BgV 30	12.90	0.12	124.16	1.04	0.32
34649	BgV 31	13.05	0.10	103.90	1.04	0.27
34650	BgV 32	13.25	0.14	139.17	1.04	0.36
34651	BgV 33	13.50	0.12	121.02	1.04	0.32
34652	BgV 34	13.65	0.09	89.40	1.04	0.23
34653	BgV 35	14.00	0.12	120.29	1.04	0.31
34654	BgV 36	14.50	0.06	62.62	1.04	0.16
34655	BgV 37	15.00	0.09	93.22	1.04	0.24
34656	BgV 38	15.50	0.06	58.03	1.04	0.15
34657	BgV 39	16.00	0.08	77.09	1.04	0.20
34658	BgV 40	16.45	0.08	75.31	1.04	0.20
34659	BgV 41	16.95	0.05	50.41	1.04	0.13
34661	BgV 43	17.55	0.11	109.14	1.22	0.33
34662	BgV 44	18.00	0.08	83.74	1.22	0.26
34663	BgV 45	18.50	0.11	112.67	1.22	0.34
34664	BgV 46	19.10	0.14	137.95	1.22	0.42
34665	BgV 47	19.55	0.11	108.07	1.22	0.33
34666	BgV 48	21.13	0.09	92.77	1.22	0.28
34667	BgV 49	21.55	0.16	162.08	1.22	0.49
34668	BgV 50	21.93	0.10	96.13	1.22	0.29
34669	BgV 51	26.10	0.12	116.65	1.22	0.36
34670	BgV 52	26.50	0.07	70.77	1.22	0.22
34671	BgV 53	26.95	0.06	55.99	1.22	0.17
34672	BgV 54	27.48	0.09	91.31	1.22	0.28
34673	BgV 55	27.98	0.10	99.55	1.22	0.30
34674	BgV 56	28.35	0.09	94.96	1.22	0.29
34675	BgV 57	28.88	0.08	83.69	0.81	0.17
34676	BgV 58	29.38	0.18	180.66	0.81	0.37
34677	BgV 59	29.85	0.12	120.52	0.81	0.25
34678	BgV 60	30.25	0.15	145.05	0.81	0.30

Capriolo section, Italy

GEA N°	Sample ID	Depth (m)	P (mg/g)	P(ppm)	Sed. Rate	P (MAR)
28271	CA 1	0.20	0.12	123.90		
28273	CA 3	1.65	0.15	145.61		
28275	CA 5	3.44	0.14	137.47		
28277	CA 7	5.11	0.12	117.11		
28279	CA 9	6.94	0.14	136.11		
28281	CA 11	8.72	0.10	103.53		
28283	CA 13	10.92	0.08	81.82		
28285	CA 15	12.40	0.08	75.03		
28287	CA 16	12.95	0.08	84.53		
28289	CA 18	14.00	0.12	122.54		
28291	CA 20	15.52	0.08	80.46		
28293	CA 22	15.74	0.10	98.11		
28296	CA 25	16.39	0.08	75.03	1.05	0.16
28297	CA 26	17.24	0.07	65.53	1.05	0.17
28298	CA 27	18.95	0.08	79.10	1.05	0.21
28301	CA 30	19.75	0.10	96.75	1.05	0.25
28303	CA 32	20.36	0.10	103.53	1.05	0.27
28305	CA 34	21.56	0.11	110.32	1.05	0.29
28307	CA 36	22.22	0.11	107.61	1.05	0.28
28309	CA 38	23.40	0.09	92.68	1.05	0.24
28311	CA 40	25.39	0.08	81.82	1.05	0.22
28313	CA 42	26.04	0.09	92.68	1.05	0.24
28315	CA 44	27.76	0.08	75.03	1.05	0.20
28317	CA 46	28.21	0.10	98.11	1.05	0.26
28320	CA 49	29.80	0.08	76.39	1.05	0.20
28323	CA 52	31.05	0.08	83.17	1.05	0.22
28325	CA 54	31.78	0.08	79.10	1.05	0.21
28327	CA 56	33.05	0.08	79.10	1.40	0.28
28329	CA 58	33.74	0.19	191.77	1.40	0.67
28331	CA 60	35.24	0.09	92.68	1.40	0.32
28333	CA 62	36.29	0.07	68.24	1.40	0.24
28335	CA 64	37.79	0.11	106.25	1.40	0.37
28336	CA 65	38.00	0.21	213.48	1.40	0.75
28337	CA 66	38.64	0.09	87.25	1.40	0.31
28339	CA 68	40.24	0.08	80.46	1.40	0.28
28341	CA 70	40.88	0.09	88.60	1.40	0.31
28343	CA 72	41.97	0.13	126.61	1.40	0.44
28345	CA 74	43.27	0.12	117.11	1.40	0.41
28347	CA 76	44.10	0.08	84.53	1.40	0.30
28349	CA 78	45.27	0.14	140.18	1.40	0.49
28352	CA 81	47.47	0.09	91.32	1.40	0.32
28354	CA 83	48.47	0.11	111.68	1.40	0.39
28356	CA 85	49.83	0.10	102.18	1.40	0.36
28358	CA 87	50.96	0.09	87.25	1.40	0.31
28360	CA 89	51.66	0.10	95.39	1.40	0.33
28362	CA 91	53.13	0.12	122.54	1.40	0.43
28366	CA 94	54.41	0.09	91.32	1.40	0.32
28371	CA 99	54.96	0.08	81.82	1.40	0.29
28373	CA 101	55.74	0.10	95.39	1.40	0.33
28376	CA 104	56.27	0.10	96.75	1.40	0.34
28378	CA 106	56.83	0.07	69.60	1.40	0.24
28381	CA 109	57.88	0.09	89.96	2.26	0.51
28382	CA 110	58.58	0.10	100.82	2.26	0.57
28385	CA 113	59.83	0.08	83.17	2.26	0.47
28388	CA 116	60.66	0.11	114.39	2.26	0.65
28390	CA 118	61.63	0.10	104.89	2.26	0.59
28392	CA 120	62.93	0.12	118.47	2.26	0.67
28395	CA 123	64.54	0.10	104.89	2.26	0.59
28397	CA 125	65.99	0.15	153.76	2.26	0.87
28400	CA 128	66.77	0.10	100.82	2.26	0.57
28402	CA 130	67.29	0.12	118.47	2.26	0.67
28406	CA 134	69.24	0.07	70.96	2.26	0.40
28408	CA 136	70.29	0.09	94.03	2.26	0.53
28410	CA 138	71.50	0.09	89.96	2.26	0.51
28414	CA 142	73.72	0.11	108.96	1.52	0.41
28418	CA 146	75.45	0.13	129.33	1.52	0.49
28420	CA 148	76.85	0.09	94.03	1.52	0.36
28421	CA 149	77.70	0.08	79.10	1.52	0.30
28423	CA 151	79.78	0.13	126.61	1.52	0.48
28425	CA 153	81.38	0.09	94.03	1.52	0.36
28426	CA 154	82.39	0.09	88.60	1.52	0.34
28427	CA 155	83.79	0.10	98.11	1.52	0.37
28429	CA 157	86.30	0.09	87.25	1.52	0.33
28431	CA 159	88.63	0.12	122.54		
28433	CA 161	91.36	0.14	137.47		
28437	CA 165	94.76	0.14	142.90		

Chrummflueschlucht section, Switzerland

GEA N°	Sample ID	Depth (m)	P (mg/g)	P (ppm)
30006	Ch 1	1.32	2.63	2631.74
30007	Ch 2	2.79	0.46	459.21
30008	Ch3	3.51	0.57	574.91
32225	Ch 1 B	4.55	0.40	397.72
30009	Ch4	4.85	0.36	359.01
32226	Ch 2 B	5.15	0.21	207.80
30010	Ch 5	5.30	0.23	228.34
30011	Ch 6	5.75	0.66	660.59
32227	Ch 3 B	6.10	0.19	185.78
30012	Ch 7	6.12	0.23	231.24
30013	Ch 8	6.72	0.20	195.46
32228	Ch 4 B	6.80	0.19	194.91
32229	Ch 5 B	7.40	0.36	360.99
30014	Ch 9	7.54	0.36	361.91
32230	Ch 6 B	8.45	0.31	308.58
30015	Ch 10	8.51	0.62	619.19
32231	Ch 7 B	8.75	0.28	283.72
32232	Ch 8 B	9.00	0.36	358.80
30016	Ch 11	9.40	0.26	259.88
32233	Ch 9 B	9.75	0.26	257.38
32234	Ch 10 B	9.95	0.27	267.29
30017	Ch 12	10.37	0.39	387.12
30018	Ch 13	10.75	0.25	251.86
32235	Ch 11 B	11.00	0.46	455.22
30019	Ch 14	11.27	0.27	272.38
32236	Ch 12 B	11.67	0.20	195.16
30020	Ch 15	11.87	0.37	371.19
30021	Ch 16	12.31	0.25	246.82
32237	Ch 13 B	12.56	0.40	401.12
30023	Ch 18	13.33	0.21	209.70
30024	Ch 19	13.86	0.14	140.84
32238	Ch 14 B	14.33	0.17	166.10
32239	Ch 15 B	14.75	0.15	147.44
30025	Ch 20	15.15	0.26	256.88
32240	Ch 16 B	15.25	0.18	180.27
32241	Ch 17 B	15.70	0.19	190.51
30026	Ch 21	15.91	0.13	129.37
32242	Ch 18 B	16.20	0.17	165.97
32243	Ch 19 B	16.55	0.14	138.56
32244	Ch 20 B	16.85	0.19	185.61
30027	Ch 22	17.05	0.23	227.15
30028	Ch 23	17.65	1.10	1096.73
32245	Ch 21 B	18.15	0.37	371.30
32246	Ch 22 B	18.35	0.19	186.50
32247	Ch 23 B	18.50	0.18	182.58
30029	Ch 24	18.86	0.12	117.44
32248	Ch 24 B	19.10	0.19	192.66
32249	Ch 25 B	19.25	0.20	199.93
30030	Ch 25	19.67	0.15	147.15
32250	Ch 26 B	19.87	0.16	156.48
30031	Ch 26	20.07	0.17	170.15

GEA N°	Sample ID	Depth (m)	P (mg/g)	P (ppm)
30032	Ch 27	20.23	0.14	139.40
32251	Ch 27 B	20.55	0.14	139.14
30033	Ch 28	20.76	0.12	122.13
32252	Ch 28 B	21.09	0.18	181.47
32253	Ch 29 B	21.35	0.18	176.35
30034	Ch 29	21.59	0.15	146.02
32254	Ch 30 B	21.65	0.17	172.03
30035	Ch 30	21.87	0.18	176.35
30036	Ch 31	21.97	0.14	139.74
32255	Ch 31 B	22.50	0.14	139.23
30037	Ch 32	22.75	0.17	166.26
32256	Ch 32 B	23.10	0.17	166.95
32257	Ch 33 B	23.43	0.21	206.56
30038	Ch 33	23.76	0.14	143.39
32258	Ch 34 B	24.12	0.14	142.25
30039	Ch 34	24.34	0.15	151.40
30040	Ch 35	24.75	0.16	160.75
30041	Ch 36	25.18	0.19	191.45
30042	Ch 37	25.68	0.15	154.71
32259	Ch 35 B	25.95	0.14	139.06
30043	Ch 38	26.13	0.15	149.13
32260	Ch 36 B	26.54	0.18	178.59
30044	Ch 39	26.87	0.12	122.20
30045	Ch 40	27.12	0.17	169.95
30046	Ch 41	27.73	0.18	175.34
30047	Ch 42	28.03	0.18	182.94
30048	Ch 43	28.56	0.16	156.34
30049	Ch 44	29.02	0.20	199.96
30050	Ch 45	29.39	0.14	141.87
30051	Ch 46	29.70	0.15	153.95
30052	Ch 47	30.38	0.14	143.67
30053	Ch 48	30.91	0.22	217.27
32261	Ch 37 B	31.09	0.16	158.27
30054	Ch 49	31.44	0.16	155.01
32262	Ch 38 B	31.65	0.22	220.86
30055	Ch 50	31.89	0.17	165.06
32263	Ch 39 B	32.02	0.18	175.17
30056	Ch 51	32.35	0.29	290.41
30057	Ch 52	32.73	0.17	169.76
32264	Ch 40 B	33.20	0.21	210.03
30058	Ch 53	33.41	0.16	161.71
30059	Ch 54	34.17	0.15	152.09
30060	Ch 55	34.85	0.22	221.61
30061	Ch 56	35.68	0.15	146.37
30062	Ch 57	36.82	0.16	155.12
32265	Ch 41 B	38.01	0.14	144.63
30063	Ch 58	38.18	0.16	158.45
32266	Ch 42 B	39.02	0.16	161.09
30064	Ch 59	39.39	0.16	164.19
30065	Ch 60	40.23	0.24	240.73
30066	Ch 61	41.36	0.16	155.01

Gorgo a Cerbara section, Italy

GEA N°	Sample ID	Depth (m)	P (mg/g)	P (ppm)	Sed. Rate	P (MAR)
31730	GC 110	19.69	0.16	158.83	0.60	0.24
31731	GC 111	19.76	0.25	249.62	0.60	0.33
31732	GC 112	19.83	0.33	330.09	0.60	0.43
31733	GC 113	19.90	0.45	450.48	0.60	0.59
31734	GC 114	20.09	0.16	161.11	0.60	0.24
31735	GC 115	20.22	0.27	268.54	0.32	0.19
31736	GC 116	20.38	0.16	161.70	0.32	0.13
31737	GC 117	20.43	0.36	362.65	0.32	0.25
31738	GC 118	20.57	0.10	98.15	0.32	0.08
31739	GC 119	20.69	0.63	627.48	0.32	0.44
31740	GC 120	20.72	0.11	108.98	0.89	0.24
31741	GC 121	20.76	0.35	350.22	0.89	0.68
31742	GC 122	20.81	0.11	113.31	0.89	0.25
31743	GC 123	20.84	0.29	290.59	0.89	0.57
31744	GC 124	20.90	0.13	127.23	0.89	0.28
31745	GC 125	20.95	0.14	144.94	0.89	0.28
31746	GC 126	20.97	0.11	109.95	0.89	0.24
31747	GC 127	21.00	0.49	485.38	0.89	0.95
31748	GC 128	21.05	0.15	146.10	0.89	0.32
31749	GC 129	21.14	0.21	208.82	0.89	0.41
31750	GC 130	21.22	0.14	136.49	0.89	0.30
31751	GC 131	21.49	0.18	183.93	0.89	0.41
31752	GC 132	21.54	0.42	420.68	0.65	0.60
31753	GC 133	21.56	0.42	418.17	0.65	0.60
31754	GC 134	21.59	0.46	459.03	0.65	0.66
31755	GC 135	21.61	0.54	542.80	0.65	0.78
31756	GC 136	21.63	0.37	367.62	0.65	0.53
31757	GC 137	21.67	0.27	274.95	0.65	0.45
31758	GC 138	21.74	0.37	369.99	0.65	0.60
31759	GC 139	21.78	0.31	314.59	0.65	0.49
31760	GC 140	21.80	2.28	2278.57	0.65	3.57
31761	GC 141	21.81	0.95	950.72	0.65	1.49
31762	GC 142	21.83	2.49	2488.20	0.65	3.90
31763	GC 143	21.86	0.87	869.43	0.65	1.36
31764	GC 144	21.91	0.44	435.58	0.65	0.68
31765	GC 145	21.96	0.24	244.12	0.65	0.35
31766	GC 146	22.06	0.13	125.52	0.65	0.20
31767	GC 147	22.13	0.11	110.37	0.65	0.18
31768	GC 148	22.17	0.37	371.82	0.65	0.58
31769	GC 149	22.22	0.64	636.32	0.65	0.91
31770	GC 150	22.28	0.10	102.14	0.58	0.13
31771	GC 151	22.41	0.20	200.12	0.58	0.28
31772	GC 152	22.58	0.04	41.87	0.58	0.06
31773	GC 153	22.61	0.17	170.58	0.58	0.24
31774	GC 154	22.63	0.20	203.50	0.58	0.28
31775	GC 155	22.66	0.22	223.00	0.58	0.31
31776	GC 156	22.68	0.12	115.86	0.58	0.17
31777	GC 157	22.75	0.20	201.30	0.44	0.21
31778	GC 158	22.81	0.14	139.10	0.44	0.15
31779	GC 159	22.88	1.41	1405.56	0.44	1.50
31780	GC 160	23.05	2.50	2496.53	0.44	2.66
31781	GC 161	23.12	0.16	159.01	0.44	0.18
31782	GC 162	23.19	1.01	1010.43	0.44	1.08
31783	GC 163	23.26	0.20	196.58	0.44	0.21
31784	GC 164	23.33	1.00	1003.94	0.67	1.07
31785	GC 165	23.41	3.14	3141.71	0.67	5.03
31786	GC 166	23.52	1.22	1217.01	0.67	1.95
31787	GC 167	23.60	0.38	381.76	0.67	0.56
31788	GC 168	23.69	0.18	182.75	0.67	0.27
31789	GC 169	23.74	0.58	583.77	0.67	0.86
31790	GC 170	23.79	0.45	445.06	0.67	0.65
31791	GC 171	23.88	0.30	301.57	0.92	0.69
31792	GC 172	23.95	0.41	409.06	0.92	0.83
31793	GC 173	24.03	0.32	319.83	0.92	0.73
31794	GC 174	24.12	0.56	555.67	0.92	1.12
31795	GC 175	24.17	0.20	197.82	0.92	0.45
31796	GC 176	24.24	0.25	254.81	0.92	0.58
31797	GC 177	24.29	0.29	286.97	0.92	0.66
31798	GC 178	24.34	0.30	296.84	0.92	0.68
31799	GC 179	24.40	0.27	270.03	0.92	0.62
31800	GC 180	24.52	0.12	122.24	0.92	0.28
31801	GC 181	24.72	0.21	209.32	0.92	0.48
31802	GC 182	24.86	0.15	150.29		
31803	GC 183	24.97	0.15	150.69		

Gorog a Cerbara section, Switzerland
P speciation

No. GEA	Sample ID	Depth (m)	P_{exch} (mg/g)	P_{auth} (mg/g)	P_{det} (mg/g)	P_{org} (mg/g)	P_{Rtot} (mg/g)
31747	GC 127	21.00	0.03	0.17	0.08	0.03	0.49
31750	GC 130	21.22	0.00	0.07	0.01	0.00	0.14
31753	GC 133	21.56	0.00	0.16	0.13	0.03	0.42
31755	GC 135	21.61	0.00	0.14	0.12	0.03	0.54
31767	GC 147	22.13	0.00	0.06	0.00	0.01	0.11
31769	GC 149	22.22	0.00	0.41	0.04	0.03	0.64
31771	GC 151	22.41	0.00	0.12	0.01	0.03	0.20
31773	GC 153	22.61	0.01	0.06	0.01	0.03	0.17
31775	GC 155	22.66	0.00	0.15	0.01	0.02	0.22
31777	GC 157	22.75	0.00	0.13	0.01	0.03	0.20
31779	GC 159	22.88	0.58	0.05	0.03	0.03	1.41
31780	GC 160	23.05	0.00	0.69	0.58	0.08	2.50
31783	GC 163	23.26	0.01	0.06	0.00	0.02	0.20
31785	GC 165	23.41	0.01	0.91	0.82	0.08	3.14
31788	GC 168	23.69	0.00	0.10	0.01	0.02	0.18
31793	GC 173	24.03	0.00	0.11	0.01	0.03	0.32
31795	GC 175	24.17	0.00	0.08	0.02	0.01	0.20

Glaise section, France

GEA N°	Sample ID	Depth (m)	P (mg/g)	P (ppm)
29408	GL 1	0.12	0.19	186.61
29409	GL 2	2.75	0.20	196.80
29410	GL 3	3.56	0.14	138.24
29411	GL 4	4.25	0.15	153.51
29412	GL 5	4.88	0.21	212.07
29413	GL 6	6.00	0.15	149.69
29414	GL 7	6.62	0.18	184.07
29415	GL 8	7.50	0.17	171.34
29416	GL 9	8.62	0.16	163.70
29417	GL 10	9.81	0.19	186.61
29418	GL 11	10.75	0.24	236.26
29419	GL 12	11.50	0.22	218.44
29420	GL 13	12.50	0.43	433.58
29421	GL 14	13.06	0.41	414.49
29422	GL 15	14.38	0.13	126.78
29423	GL 16	15.44	0.16	161.15
29424	GL 17	16.44	0.14	136.96
29425	GL 18	18.00	0.08	79.68
29426	GL 19	19.63	0.22	219.71
29427	GL 20	20.75	0.20	201.89
29428	GL 21	21.75	0.15	145.88
29429	GL 22	23.00	0.19	194.25
29430	GL 23	24.25	0.16	158.61
29431	GL 24	25.38	0.12	119.14
29432	GL 25	25.88	0.15	147.15
29433	GL 26	26.50	0.27	273.18
29434	GL 27	27.31	0.23	228.62
29435	GL 28	28.62	0.29	293.55
29436	GL 29	29.38	0.22	220.98
29437	GL 30	29.90	0.15	147.15
29438	GL 31	30.62	0.09	87.32
29439	GL 32	31.00	0.11	114.05
29440	GL 33	31.38	0.22	220.98
29441	GL 34	31.56	0.23	233.71
29442	GL 35	31.75	0.21	212.07
29443	GL 36	32.62	0.22	220.98
29444	GL 37	32.87	0.20	195.52

Malleval section, France

GEA N°	Sample ID	Depth (m)	P (mg/g)	P (ppm)
29346	MAm 21	2.50	0.05	46.61
29347	MAm 22	3.10	0.03	29.57
29348	MAm 23	3.35	0.05	50.02
29349	MAm 24	4.30	0.08	84.11
29350	MAm 25	5.75	0.14	135.24
29351	MAm 26	6.65	0.06	60.25
29352	MAm 27	7.50	0.08	80.70
29353	MAm 28	8.20	0.06	56.84
29354	MAm 29	8.95	0.08	80.70
29355	MAm 30	9.90	0.29	285.24
29356	MAm 31	12.00	0.16	159.11
29357	MAm 32	13.20	0.05	53.43
29358	MAm 33	14.90	0.06	63.66
29359	MAm 34	16.60	0.09	94.34
29360	MAm 35	25.30	0.24	237.51
29361	MAm 36	27.20	0.11	111.38
29363	MAs 1	27.60	0.06	56.84
29364	MAs 2	28.55	0.19	193.20
29362	MAm 37	28.80	0.06	63.66
29365	MAs 3	29.65	0.07	73.88
29366	MAs 4	30.95	0.05	53.43
29367	MAs 5	32.60	0.10	104.56
29368	MAs 6	33.50	0.14	142.06
29369	MAs 7	34.45	0.06	63.66
29370	MAs 8	36.40	0.06	60.25
29371	MAs 9	36.30	0.12	121.61
29372	MAs 10	36.95	0.07	70.47
29373	MAs 11	37.50	0.03	29.57
29374	MAs 12	38.40	0.03	26.16
29375	MAs 13	40.20	0.04	36.38
29376	MAs 14	41.70	0.05	53.43
29377	MAs 15	47.70	0.04	43.20
29378	MAs 16	49.30	0.04	43.20
29379	MAs 17	50.75	0.04	36.38
29380	MAs 18	51.80	0.05	46.61
29381	MAs 19	52.75	0.04	43.20
29382	MAs 20	53.60	0.04	39.79
29383	MAs 21	55.00	0.04	39.79
29384	MAs 22	56.20	0.05	50.02
29385	MAs 23	57.15	0.06	60.25
29386	MAs 24	58.25	0.03	32.98
29387	MAs 25	59.40	0.04	36.38
29388	MAs 26	61.10	0.06	60.25
29389	MAs 27	64.55	0.03	32.98
29390	MAs 28	65.85	0.03	32.98
29391	MAs 29	67.00	0.05	46.61
29392	MAs 30	68.30	0.04	36.38
29393	MAs 31	69.40	0.04	39.79
29394	MAs 32	70.45	0.05	46.61
29395	MAs 33	71.50	0.04	36.38
29396	MAs 34	72.40	0.09	90.93
29397	MAs 35	73.55	0.05	53.43
29398	MAs 36	74.65	0.06	63.66
29399	MAs 37	75.80	0.10	104.56
29400	MAs 38	76.90	0.08	77.29
29401	MAs 39	78.20	0.07	73.88
29402	MAs 40	79.40	0.05	53.43
30706	MAs 41 b	80.30	0.06	60.31
30707	MAs 42 b	80.40	0.05	53.20
29403	MAs 41	80.60	0.08	80.70
30708	MAs 43 b	82.15	0.06	55.45
29404	MAs 42	82.65	0.08	80.70
30709	MAs 44 b	83.40	0.10	95.49
30710	MAs 45 b	83.70	0.05	53.91
29405	MAs 43	84.35	0.06	56.84
30711	MAs 46 b	84.60	0.05	54.77
30712	MAs 47 b	85.15	0.05	50.22
30713	MAs 48 b	85.55	0.06	57.31
30714	MAs 49 b	86.85	0.04	40.54
30715	MAs 50 b	87.90	0.05	52.33
29406	MAs 44	88.20	0.06	60.25
30716	MAs 51 b	89.10	0.05	48.04
30717	MAs 52 b	90.65	0.05	51.50
29407	MAs 45	91.10	0.06	63.66
30718	MAs 53 b	92.20	0.06	57.42
30719	MAs 54 b	93.30	0.05	50.06
30720	MAs 55 b	94.60	0.05	50.01
30721	MAs 56 b	95.60	0.07	65.75
30722	MAs 57 b	96.90	0.06	61.73

Vergol section, France

GEA N°	Sample ID	Depth (m)	P (mg/g)	P (ppm)	Sed. Rate	P (MAR)
38450	Ve 0	0.40	0.31	313.72	4.35	3.41
38451	Ve 1	0.52	0.33	330.18	4.35	3.31
38452	Ve 2	0.60	0.23	228.55	4.35	2.29
38453	Ve 3	0.69	0.42	420.26	4.35	4.21
38454	Ve 4	0.79	0.40	397.95	4.35	3.98
38455	Ve 5	0.88	0.27	267.97	4.35	2.68
38456	Ve 6	1.05	0.23	226.61	4.35	2.27
38457	Ve 7	1.08	0.19	189.16	4.35	1.98
38458	Ve 8	1.10	0.21	214.69	4.35	2.15
38459	Ve 9	1.11	0.21	211.58	4.35	2.21
38460	Ve 10	1.13	0.18	184.31	4.35	1.85
38461	Ve 11	1.15	0.24	239.36	4.35	2.50
38462	Ve 12	1.33	0.24	238.11	4.35	2.59
38463	Ve 13	1.46	0.36	361.97	4.35	3.62
38464	Ve 14	1.82	0.30	301.00	4.35	3.01
38465	Ve 15	1.99	0.21	214.50	4.35	2.15
38466	Ve 16	2.08	0.24	240.39	4.35	2.41
38467	Ve 17	2.14	0.18	180.62	4.35	1.89
38468	Ve 18	2.19	0.22	216.79	4.35	2.17
38469	Ve 19	2.32	0.17	172.53	4.35	1.88

Stable Isotopes Data

Alvier section, Switzerland

GEA N°	Sample ID	Depth (m)	d13C	d18O
33504	Al 2	113.10	0.43	-4.59
33511	Al 8	108.00	0.81	-4.54
33518	Al 15	101.95	0.90	-4.55
33528	Al 25	93.30	0.98	-4.40
33535	Al 32	88.85	1.21	-4.28
33545	Al 42	78.10	1.34	-4.29
33559	Al 56	67.75	1.63	-4.12
33569	Al 66	60.25	1.97	-4.07
33582	Al 79	54.25	2.19	-3.91
33589	Al 86	50.10	2.19	-4.12
33599	Al 96	44.40	2.08	-3.80
33610	Al 107	38.90	1.24	-3.73
33622	Al 119	31.70	0.77	-3.76
33630	Al 127	25.85	0.65	-3.88
33636	Al 133	20.00	0.69	-4.15
33642	Al 139	14.30	0.81	-4.24
33648	Al 145	8.30	0.64	-4.54
33653	Al 150	3.40	0.42	-5.26
33656	Al 153	0.00	0.39	-5.30

Breggia section, Switzerland

GEA N°	Sample ID	Depth (m)	d13C	d18O
34619	BgV 1	0.15	1.43	-1.97
34622	BgV 4	1.5	1.45	-2.00
34628	BgV 10	4.525	1.48	-1.81
34631	BgV 13	5.975	1.34	-1.83
34643	BgV 25	11.5	1.53	-1.82
34646	BgV 28	12.15	1.72	-2.01
34649	BgV 31	13.05	1.88	-2.04
34652	BgV 34	13.65	2.11	-2.19
34655	BgV 37	15	2.20	-1.90
34661	BgV 43	17.55	2.67	-1.54
34664	BgV 46	19.1	2.67	-1.98
34670	BgV 52	26.5	2.65	-2.30
34678	BgV 60	30.25	2.37	-1.31

Capriolo section, Italy

GEA N°	Sample ID	Depth (m)	d13C	d18O
28277	CA 7	5.11	1.375	-1.669
28285	CA 15	12.4	1.287	-2.255
28296	CA 25	16.39	1.434	-2.09
28307	CA 36	22.22	1.381	-1.855
28320	CA 49	29.8	1.493	-1.754
28327	CA 56	33.05	1.577	-1.893
28329	CA 58	33.74	1.499	-1.756
28333	CA 62	36.29	1.487	-2.045
28337	CA 66	38.64	1.484	-1.578
28343	CA 72	41.97	1.506	-1.853
28349	CA 78	45.27	1.498	-1.979
28358	CA 87	50.96	1.694	-1.996
28366	CA 94	54.41	2.277	-2.056
28376	CA 104	56.27	2.492	-1.972
28382	CA 110	58.58	2.758	-1.98
28392	CA 120	62.93	2.869	-2.061
28406	CA 136	70.29	3.184	-1.728
28420	CA 148	76.85	2.955	-1.878
28427	CA 155	83.79	2.633	-1.777
28437	CA 165	94.76	2.287	-2.171

Chrummflueschlucht section, Switzerland

GEA N°	Sample ID	Depth (m)	d13C	d18O
30006	Ch 1	1.32	1.887	-2.142
30008	Ch 3	3.51	2.453	-2.712
32225	Ch 1 B	4.55	2.355	-2.572
30009	Ch 4	4.85	2.406	-2.866
32226	Ch 2 B	5.15	2.348	-2.772
30011	Ch 6	5.75	2.295	-3.386
32227	Ch 3 B	6.10	2.417	-3.216
30013	Ch 8	6.72	2.560	-3.034
32228	Ch 4 B	6.80	2.53	-2.822
32229	Ch 5 B	7.40	2.468	-2.733
32230	Ch 6 B	8.45	2.416	-2.894
30015	Ch 10	8.51	2.567	-2.653
32231	Ch 7 B	8.75	2.473	-2.847
32232	Ch 8 B	9.00	2.606	-3.082
32233	Ch 9 B	9.75	2.66	-3.102
32234	Ch 10 B	9.95	2.552	-3.259
30017	Ch 12	10.37	2.675	-2.897
32235	Ch 11 B	11.00	2.765	-3.131
30019	Ch 14	11.27	2.764	-2.955
32236	Ch 12 B	11.67	2.748	-2.995
30021	Ch 16	12.31	2.769	-3.039
32237	Ch 13 B	12.56	2.657	-3.274
30024	Ch 19	13.86	2.805	-2.693
32238	Ch 14 B	14.33	2.723	-2.743
32239	Ch 15 B	14.75	2.716	-2.851
30025	Ch 20	15.15	2.689	-2.958
32240	Ch 16 B	15.25	2.737	-2.712
32241	Ch 17 B	15.70	2.713	-2.98
30026	Ch 21	15.91	2.942	-2.639
32242	Ch 18 B	16.20	2.883	-2.941
32243	Ch 19 B	16.55	2.967	-2.822
32244	Ch 20 B	16.85	2.958	-2.901
30027	Ch 22	17.05	2.987	-2.806
30028	Ch 23	17.65	3.187	-2.813
32245	Ch 21 B	18.15	3.299	-3.423
32246	Ch 22 B	18.35	3.093	-3.322
32247	Ch 23 B	18.50	2.954	-3.534
30029	Ch 24	18.86	2.890	-3.367
32248	Ch 24 B	19.10	2.959	-3.118
32249	Ch 25 B	19.25	3.003	-3.16
30030	Ch 25	19.67	3.125	-2.732
32250	Ch 26 B	19.87	3.082	-3.003
30031	Ch 26	20.07	2.951	-3.151
32251	Ch 27 B	20.55	3.078	-2.919
30033	Ch 28	20.76	3.167	-2.853
32252	Ch 28 B	21.09	3.142	-2.852
32253	Ch 29 B	21.35	3.097	-2.751
30034	Ch 29	21.59	3.032	-3.005
32254	Ch 30 B	21.65	2.924	-2.865
30035	Ch 30	21.87	2.938	-2.906
30036	Ch 31	21.97	2.957	-2.925
32255	Ch 31 B	22.50	2.877	-2.904
30037	Ch 32	22.75	2.899	-2.946
32256	Ch 32 B	23.10	2.858	-2.995
32257	Ch 33 B	23.43	2.908	-3.047
30038	Ch 33	23.76	2.934	-3.096
32258	Ch 34 B	24.12	2.931	-2.929
30039	Ch 34	24.34	3.147	-2.987
30040	Ch 35	24.75	3.152	-2.869
30041	Ch 36	25.18	3.136	-2.987
30042	Ch 37	25.68	3.165	-2.777
32259	Ch 35 B	25.95	3.084	-3.036
30043	Ch 38	26.13	3.104	-3.137
32260	Ch 36 B	26.54	3.065	-3.059
30044	Ch 39	26.87	3.103	-2.957
30045	Ch 40	27.12	3.181	-3.030
30046	Ch 41	27.73	3.208	-2.756
30047	Ch 42	28.03	3.233	-2.954
30048	Ch 43	28.56	3.162	-2.931
30049	Ch 44	29.02	3.054	-3.005
30050	Ch 45	29.39	3.311	-2.768
30051	Ch 46	29.70	3.052	-3.176
30052	Ch 47	30.38	2.908	-2.920
32261	Ch 37 B	31.09	2.598	-2.965
30054	Ch 49	31.44	2.655	-2.832
32262	Ch 38 B	31.65	2.531	-2.86
32263	Ch 39 B	32.02	2.497	-2.832
30056	Ch 51	32.35	2.495	-2.833
32264	Ch 40 B	33.20	2.16	-2.947
30058	Ch 53	33.41	2.270	-2.903
30060	Ch 55	34.85	2.341	-2.808
30062	Ch 57	36.82	2.202	-2.928
32265	Ch 41 B	38.01	2.254	-3.019
32266	Ch 42 B	39.02	2.454	-2.755
30064	Ch 59	39.39	2.664	-2.685
30066	Ch 61	41.36	2.096	-2.990

Gorgo a Cerbara section, Italy

GEA N°	Sample ID	Depth (m)	d13C	d18O
31748	GC 128	21.05	2.563	-1.789
31751	GC 131	21.49	2.931	-1.909
31753	GC 133	21.56	3.037	-2.317
31755	GC 135	21.61	2.765	-1.925
31757	GC 137	21.67	2.887	-2.531
31759	GC 139	21.78	2.732	-3.002
31761	GC 141	21.81	1.522	-0.263
31762	GC 142	21.83	2.140	-1.447
31764	GC 144	21.91	2.000	-3.115
31765	GC 145	21.96	2.105	-2.831
31766	GC 146	22.06	0.737	-1.659
31767	GC 147	22.13	2.531	-2.391
31770	GC 150	22.28	1.419	-2.614
31772	GC 152	22.58	2.194	-1.754
31776	GC 156	22.68	2.686	-1.925
31778	GC 158	22.81	2.341	-1.779
31788	GC 168	23.69	2.484	-2.176
31789	GC 169	23.74	4.043	-2.120
31790	GC 170	23.79	4.094	-2.364
31791	GC 171	23.88	4.057	-2.961
31792	GC 172	23.95	4.171	-2.396
31793	GC 173	24.03	4.124	-2.660
31795	GC 175	24.17	4.128	-1.841

Glaise section, France

GEA N°	Sample ID	Depth (m)	d13C	d18O
29408	GL 1	0.12	1.863	-2.536
29409	GL 2	2.75	1.736	-5.981
29410	GL 3	3.56	1.930	-3.197
29411	GL 4	4.25	1.722	-3.435
29413	GL 6	6.00	1.380	-3.329
29414	GL 7	6.62	0.280	-2.943
29415	GL 8	7.50	1.304	-3.431
29416	GL 9	8.62	-1.763	-4.535
29417	GL 10	9.81	0.574	-4.585
29418	GL 11	10.75	1.394	-3.399
29419	GL 12	11.50	1.272	-3.631
29420	GL 13	12.50	1.219	-3.390
29421	GL 14	13.06	1.671	-3.497
29422	GL 15	14.38	2.972	-3.306
29423	GL 16	15.44	3.108	-3.195
29424	GL 17	16.44	3.263	-2.800
29425	GL 18	18.00	3.316	-2.829
29426	GL 19	19.63	2.820	-3.443
29427	GL 20	20.75	3.418	-3.165
29428	GL 21	21.75	4.126	-2.977
29429	GL 22	23.00	3.287	-3.904
29430	GL 23	24.25	3.933	-3.384
29431	GL 24	25.38	4.227	-3.651
29432	GL 25	25.88	4.178	-3.331
29433	GL 26	26.50	3.120	-3.857
29434	GL 27	27.31	4.182	-3.437
29435	GL 28	28.62	2.660	-3.950
29436	GL 29	29.38	4.292	-3.341
29437	GL 30	29.90	3.748	-3.599
29438	GL 31	30.62	2.735	-3.107
29439	GL 32	31.00	4.106	-3.596
29440	GL 33	31.38	2.540	-3.520
29441	GL 34	31.56	3.436	-3.780
29442	GL 35	31.75	2.404	-3.610
29443	GL 36	32.62	2.476	-3.635
29444	GL 37	32.87	3.771	-3.682

Malleval section, France

GEA N°	Sample ID	Depth (m)	d13C	d18O
29407	MAs 45	91.10	0.551	-3.345
29406	MAs 44	88.20	0.548	-3.998
29405	MAs 43	84.35	-0.074	-4.589
29403	MAs 41	80.60	-0.173	-4.484
29401	MAs 39	78.20	0.267	-5.162
29399	MAs 37	75.80	-0.657	-4.833
29397	MAs 35	73.55	-0.617	-4.881
29395	MAs 33	71.50	0.748	-1.900
29393	MAs 31	69.40	0.668	-2.681
29391	MAs 29	67.00	0.128	-2.883
29389	MAs 27	64.55	0.324	-3.550
29388	MAs 26	61.10	0.160	-1.940
29387	MAs 25	59.40	-0.412	-2.267
29385	MAs 23	57.15	-0.939	-3.367
29383	MAs 21	55.00	0.202	-2.370
29381	MAs 19	52.75	0.046	-2.724
29379	MAs 17	50.75	-2.163	-4.280
29377	MAs 15	47.70	0.302	-2.044
29376	MAs 14	41.70	-0.770	-2.565
29375	MAs 13	40.20	0.639	-2.986
29374	MAs 12	38.40	-1.087	-3.978
29372	MAs 10	36.95	0.254	-2.408
29370	MAs 8	36.40	-1.078	-2.087
29368	MAs 6	33.50	-0.632	-2.115
29366	MAs 4	30.95	1.635	-2.355
29364	MAs 2	28.55	1.704	-1.936
29362	MAm 37	28.80	1.475	-2.371
29361	MAm 36	27.20	1.464	-2.283
29359	MAm 34	16.60	2.164	-1.946
29358	MAm 33	14.90	1.417	-2.624
29356	MAm 31	12.00	1.426	-2.518
29355	MAm 30	9.90	1.195	-2.316
29352	MAm 27	7.50	1.314	-2.592
29350	MAm 25	5.75	1.132	-1.982
29348	MAm 23	3.35	1.434	-2.748
29346	MAm 21	2.50	1.003	-2.493

Vergol section, France

GEA N°	Sample ID	Depth (m)	d13C	d18O
38450	Ve 0	0.40	0.648	-0.897
38453	Ve 3	0.69	0.997	-1.157
38456	Ve 6	1.05	0.687	-1.403
38463	Ve 13	1.46	0.747	-0.995
38465	Ve 15	1.99	0.65	-0.947
38469	Ve 19	2.32	0.691	-0.736

Rock Eval Data

Rock eval data for the Angles section

Sample ID	Depth (m)	PC [%]	RC [%]	TOC [%]	MINC [%]	HI [mg HC/g TOC]	OI [mg CO2/g TOC]	Tmax [°C]	S1 [mg HC/g]	S2a [mg HC/g]	S2b [mg HC/g]	S3
304	79.73	0.02	0.17	0.19	7.85	39.08	286.48	439	0.0000	0.0733	0	0.5373
328	86.55	0.08	0.28	0.35	7.30	224.86	87.76	442	0.0210	0.7964	0	0.3108
03F30	89.60	0.03	0.10	0.13	9.27	178.82	203.98	442	0.0105	0.2307	0	0.2632
03F28	92.40	0.06	0.23	0.29	9.15	204.72	130.71	442	0.0105	0.5982	0	0.3820
03F25	95.72	0.04	0.18	0.22	8.32	161.82	164.08	441	0.0105	0.3571	0	0.3621
03F23	97.60	0.04	0.20	0.25	8.33	162.77	133.73	442	0.0000	0.3995	0	0.3282
03F22	100.00	0.02	0.12	0.15	8.73	106.01	272.80	441	0.0000	0.1578	0	0.4061
03F21	102.07	0.04	0.22	0.27	6.29	150.82	145.55	439	0.0000	0.4001	0	0.3861
03F20	103.95	0.03	0.14	0.17	8.88	150.59	167.67	442	0.0105	0.2529	0	0.2816
03F19	105.36	0.04	0.17	0.20	7.48	144.34	189.77	440	0.0422	0.2952	0	0.3882
03F18	107.95	0.04	0.21	0.25	7.58	122.84	147.71	445	0.0211	0.3060	0	0.3680
03F14	112.90	0.04	0.20	0.24	7.56	161.62	132.06	442	0.0317	0.3907	0	0.3193
03F05	113.83	0.01	0.09	0.11	8.45	79.51	220.77	438	0.0106	0.0846	0	0.2348
03F04	115.00	0.03	0.19	0.22	7.29	124.97	129.65	440	0.0106	0.2750	0	0.2853
03F03	116.42	0.03	0.17	0.20	6.94	113.85	212.45	438	0.0000	0.2223	0	0.4148
03F02	117.12	0.03	0.16	0.19	7.59	137.33	174.76	440	0.0106	0.2648	0	0.3370
03F32	120.18	0.04	0.12	0.17	8.29	134.32	203.87	444	0.1696	0.2226	0	0.3379
03F36	128.41	0.02	0.14	0.16	7.52	87.05	195.62	439	0.0106	0.1379	0	0.3100
03F39	131.70	0.03	0.19	0.22	6.68	86.40	196.04	439	0.0106	0.1911	0	0.4336
03F40	135.23	0.02	0.11	0.14	6.32	93.59	297.84	437	0.0000	0.1275	0	0.4058
03F42	136.73	0.04	0.23	0.27	6.96	148.52	104.13	439	0.0213	0.4041	0	0.2833
03F45	139.06	0.08	0.33	0.41	6.84	216.22	61.66	439	0.0319	0.8939	0	0.2549
03F47	144.17	0.02	0.13	0.15	7.12	86.84	188.54	438	0.0107	0.1278	0	0.2775
03F50	146.99	0.02	0.22	0.24	6.87	57.33	148.44	438	0.0107	0.1386	0	0.3587
03F51	148.64	0.06	0.35	0.40	6.82	142.70	69.10	440	0.0107	0.5760	0	0.2789
03F53	149.81	0.04	0.27	0.32	7.42	143.90	78.44	440	0.0000	0.4590	0	0.2502
03F56	153.58	0.03	0.20	0.22	7.82	96.12	136.08	441	0.0000	0.2137	0	0.3025
03F59	154.52	0.03	0.32	0.35	6.00	75.75	117.39	437	0.0000	0.2673	0	0.4142
03F60	155.69	0.01	0.15	0.16	8.21	6.54	276.32	443	0.0000	0.0107	0	0.4523
03F61	158.04	0.03	0.41	0.44	7.83	75.57	50.78	440	0.0000	0.3319	0	0.2230

Rock eval data for the Breggia section

Sample ID	Depth (m)	PC [%]	RC [%]	TOC [%]	MINC [%]	HI [mg HC/g TOC]	OI [mg CO2/g TOC]	Tmax [°C]	S1 [mg HC/g]	S2a [mg HC/g]	S2b [mg HC/g]	S3
BgV 22	11.00	0.01	0.02	0.03	5.61	0.00	749.09	-22	0.0000	0.0000	0.0000	0.2054
BgV 24	11.40	0.01	0.03	0.04	9.40	0.00	500.11	-22	0.0000	0.0000	0.0000	0.1895
BgV 30	12.90	0.02	0.08	0.10	4.80	145.72	247.29	432	0.0000	0.1469	0.0000	0.2493
BgV 31	13.05	0.01	0.03	0.03	10.47	0.00	600.17	-22	0.0000	0.0000	0.0000	0.1957
BgV 35	14.00	0.00	0.02	0.03	10.37	0.00	603.20	-22	0.0000	0.0000	0.0000	0.1575
BgV 40	16.45	0.00	0.03	0.03	10.04	0.00	557.70	-22	0.0000	0.0000	0.0000	0.1794
BgV 43	17.55	0.01	0.03	0.03	10.02	0.00	758.17	-23	0.0000	0.0000	0.0000	0.2607
BgV 45	18.50	0.01	0.04	0.05	10.40	0.00	447.89	-23	0.0000	0.0000	0.0000	0.2226
BgV 46	19.10	0.01	0.02	0.03	10.13	0.00	775.10	-23	0.0000	0.0000	0.0000	0.2144
BgV 47	19.55	0.00	0.01	0.02	10.31	0.00	1057.39	-23	0.0000	0.0000	0.0000	0.1621

Rock eval data for the Capriolo section

Sample ID	Depth (m)	PC [%]	RC [%]	TOC [%]	MINC [%]	HI [mg HC/g TOC]	OI [mg CO2/g TOC]	Tmax [°C]	S1 [mg HC/g]	S2a [mg HC/g]	S2b [mg HC/g]	S3
CA 29	19.42	0.04	0.31	0.35	1.65	11.15	385.94	399	0.0097	0.0389	0.0000	1.3452
CA 35	22.12	0.14	0.54	0.68	8.91	231.95	49.79	428	0.0000	1.5845	0.0000	0.3401
CA 48	29.32	0.01	0.10	0.10	9.45	9.18	269.36	426	0.0000	0.0096	0.0000	0.2817
CA 50	30.40	0.01	0.10	0.12	10.12	16.63	313.05	430	0.0000	0.0192	0.0000	0.3607
CA 58	33.74	0.01	0.11	0.12	10.23	39.44	287.35	426	0.0000	0.0477	0.0000	0.3478
CA 61	35.38	0.12	0.38	0.50	7.70	255.39	90.06	430	0.0000	1.2853	0.0000	0.4532
CA 65	38.00	0.01	0.12	0.14	9.94	48.49	230.26	427	0.0000	0.0664	0.0000	0.3156
CA 75	43.52	0.03	0.19	0.22	9.96	118.27	164.44	436	0.0000	0.2650	0.0000	0.3685
CA 79	46.34	0.05	0.27	0.33	9.64	156.45	121.31	431	0.0000	0.5095	0.0000	0.3951
CA 93	54.12	0.45	1.03	1.48	7.36	341.00	41.00	430	0.1700	5.0400	0.0000	0.6100
CA 96	54.65	0.25	0.70	0.96	9.27	290.00	82.00	429	0.0100	2.7700	0.0000	0.7900
CA 98	54.71	0.27	0.82	1.09	7.90	268.00	69.00	430	0.0900	2.9200	0.0000	0.7500
CA 102	55.80	0.04	0.36	0.40	5.92	49.00	200.00	429	0.0100	0.2000	0.0000	0.8100
CA 111	59.08	0.03	0.15	0.18	9.75	131.00	238.00	430	0.0000	0.2400	0.0000	0.4300
CA 114	60.00	0.06	0.20	0.25	9.45	196.00	204.00	426	0.0000	0.5000	0.0000	0.5200
CA 122	64.37	0.09	0.49	0.58	7.90	123.00	215.00	412	0.0000	0.7200	0.0000	1.2600
CA 126	66.21	0.01	0.12	0.13	3.17	15.00	223.00	423	0.0000	0.0200	0.0000	0.3000
CA 131	67.55	0.03	0.20	0.22	9.39	86.00	195.00	429	0.0000	0.1900	0.0000	0.4400
CA 140	72.61	0.02	0.17	0.19	8.02	31.00	337.00	420	0.0000	0.0600	0.0000	0.6600

Rock eval data for the Gorgo a Cerbara section

Sample ID	Depth (m)	PC [%]	RC [%]	TOC [%]	MINC [%]	HI [mg HC/g TOC]	OI [mg CO2/g TOC]	Tmax [°C]	S1 [mg HC/g]	S2a [mg HC/g]	S2b [mg HC/g]	S3
GC 111	19.76	0.20	0.86	1.07	8.60	208.45	62.73	429	0.0000	2.2220	0.0000	0.6687
GC 117	20.43	0.03	0.41	0.44	8.92	44.58	141.98	422	0.0000	0.1968	0.0000	0.6267
GC 119	20.69	0.49	2.28	2.77	7.37	199.68	39.48	424	0.0109	5.5394	0.0000	1.0951
GC 121	20.76	0.16	0.69	0.85	9.94	200.38	92.12	430	0.0000	1.6997	0.0000	0.7814
GC 123	20.84	0.09	0.49	0.57	10.20	153.25	90.02	430	0.0000	0.8770	0.0000	0.5152
GC 127	21.00	0.06	0.55	0.62	5.73	98.42	77.34	427	0.0000	0.6058	0.0000	0.4760
GC 129	21.14	0.04	0.25	0.29	10.54	101.28	170.50	434	0.0000	0.2913	0.0000	0.4905
GC 133	21.56	0.06	0.57	0.63	5.25	60.11	100.32	425	0.1899	0.3798	0.0000	0.6339
GC 134	21.59	0.02	0.08	0.11	3.88	0.00	424.46	-23	0.1496	0.0000	0.0000	0.4574
GC 135	21.61	0.02	0.13	0.15	4.50	0.00	276.48	-24	0.1493	0.0000	0.0000	0.4213
GC 137	21.67	0.02	0.12	0.15	7.33	88.00	286.91	440	0.0000	0.1276	0.0000	0.4162
GC 139	21.78	0.82	2.54	3.36	6.58	281.84	38.45	421	0.0099	9.4767	0.0000	1.2930
GC 140	21.80	0.04	0.12	0.16	0.13	12.22	397.97	405	0.2176	0.0198	0.0000	0.6441
GC 141	21.81	1.18	3.87	5.05	0.52	264.76	45.75	423	0.0494	13.3665	0.0000	2.3098
GC 143	21.86	1.07	3.24	4.31	3.70	288.68	31.12	419	0.0393	12.4359	0.0000	1.3406
GC 144	21.91	0.92	2.54	3.47	4.17	310.47	31.35	419	0.0098	10.7618	0.0000	1.0867
GC 145	21.96	0.04	0.33	0.37	5.65	99.45	98.82	425	0.0000	0.3720	0.0000	0.3696
GC 148	22.17	0.04	0.66	0.70	0.03	51.51	48.85	417	0.0000	0.3615	0.0000	0.3428
GC 153	22.61	0.01	0.19	0.21	0.02	34.32	148.29	419	0.0000	0.0705	0.0000	0.3045
GC 154	22.63	0.04	0.19	0.23	0.04	60.85	374.65	414	0.0000	0.1397	0.0000	0.8605
GC 155	22.66	0.13	0.76	0.89	0.03	161.32	57.64	430	0.0000	1.4350	0.0000	0.5128
GC 157	22.75	0.02	0.18	0.20	0.02	44.88	144.41	429	0.0000	0.0883	0.0000	0.2841
GC 159	22.88	2.48	3.98	6.46	0.11	453.53	21.34	415	0.1362	29.3132	0.0000	1.3791
GC 160	23.05	6.49	8.45	14.94	0.16	511.75	24.80	414	0.5399	76.4758	0.0000	3.7055
GC 161	23.12	0.15	0.78	0.94	0.05	176.47	69.06	422	0.0000	1.6536	0.0000	0.6472
GC 162	23.19	1.76	3.47	5.23	0.09	395.17	22.17	419	0.1242	20.6478	0.0000	1.1585
GC 164	23.33	1.36	2.85	4.21	0.08	381.11	25.44	417	0.0189	16.0314	0.0000	1.0700
GC 165	23.41	7.77	10.24	18.01	0.12	511.58	17.89	413	0.4556	92.1375	0.0000	3.2218
GC 166	23.52	3.85	6.62	10.46	0.12	433.99	24.13	411	0.1198	45.4104	0.0000	2.5252
GC 167	23.60	0.01	0.11	0.12	0.04	0.00	291.30	411	0.0000	0.0000	0.0000	0.3542

Rock eval data for the Glaise section

Sample ID	Depth (m)	PC [%]	RC [%]	TOC [%]	MINC [%]	HI [mg HC/g TOC]	OI [mg CO2/g TOC]	Tmax [°C]	S1 [mg HC/g]	S2a [mg HC/g]	S2b [mg HC/g]	S3
GL 1	0.12	0.03	0.11	0.14	10.22	137.23	352.31	438	0.0000	0.1921	0.0000	0.4931
GL 2	2.75	0.14	0.52	0.65	4.62	224.09	72.03	436	0.0170	1.4601	0.0000	0.4693
GL 3	3.56	0.04	0.30	0.34	1.09	81.43	151.99	431	0.0289	0.2792	0.0000	0.5212
GL 4	4.25	0.04	0.17	0.21	0.49	166.16	176.41	435	0.0000	0.3498	0.0000	0.3713
GL 5	4.88	0.01	0.14	0.16	0.05	18.40	194.43	431	0.0386	0.0290	0.0000	0.3060
GL 6	6.00	0.02	0.20	0.22	0.25	51.20	157.00	433	0.0086	0.1115	0.0000	0.3418
GL 7	6.62	0.01	0.20	0.21	0.08	13.94	146.98	433	0.0097	0.0290	0.0000	0.3062
GL 8	7.50	0.02	0.20	0.22	0.25	51.20	157.00	433	0.0086	0.1115	0.0000	0.3418
GL 9	8.62	0.01	0.14	0.15	0.15	19.79	213.05	429	0.0097	0.0291	0.0000	0.3133
GL 10	9.81	0.03	0.30	0.33	0.14	95.70	52.70	436	0.0000	0.3117	0.0000	0.1716
GL 11	10.75	0.05	0.35	0.40	1.32	110.82	86.41	434	0.0097	0.4378	0.0000	0.3414
GL 12	11.50	0.11	0.58	0.69	1.02	174.45	39.69	441	0.0174	1.2093	0.0000	0.2751
GL 13	12.50	0.33	0.93	1.26	0.70	300.21	21.01	433	0.1463	3.7846	0.0000	0.2649
GL 14	13.06	0.17	0.52	0.68	1.61	273.26	36.08	441	0.0437	1.8708	0.0000	0.2470
GL 15	14.38	0.05	0.39	0.43	1.64	99.48	87.09	432	0.0098	0.4303	0.0000	0.3767
GL 16	15.44	0.13	0.63	0.76	0.91	190.29	40.04	441	0.0439	1.4407	0.0000	0.3032
GL 17	16.44	0.08	0.53	0.60	0.67	136.35	47.38	435	0.0294	0.8236	0.0000	0.2862
GL 18	18.00	0.06	0.41	0.47	1.74	132.18	51.30	442	0.0177	0.6267	0.0000	0.2432
GL 19	19.63	0.51	1.06	1.57	1.00	369.73	23.16	434	0.2654	5.7995	0.0000	0.3632
GL 20	20.75	0.47	1.24	1.71	1.88	314.00	17.84	442	0.2217	5.3657	0.0000	0.3048
GL 21	21.75	0.45	1.49	1.94	1.00	255.46	21.29	433	0.2858	4.9472	0.0000	0.4124
GL 22	23.00	0.03	0.49	0.52	2.93	50.99	50.47	441	0.0000	0.2673	0.0000	0.2646
GL 23	24.25	0.03	0.24	0.26	2.41	71.25	122.11	430	0.0099	0.1877	0.0000	0.3217
GL 24	25.38	0.03	0.33	0.36	2.00	77.07	79.83	443	0.0090	0.2776	0.0000	0.2875
GL 25	25.88	0.19	0.85	1.05	1.80	199.83	41.49	434	0.0693	2.0900	0.0000	0.4339
GL 26	26.50	0.02	0.23	0.25	4.67	39.96	110.15	444	0.0000	0.0990	0.0000	0.2728
GL 27	27.31	0.24	1.11	1.35	2.94	197.06	39.93	432	0.0596	2.6614	0.0000	0.5392
GL 28	28.62	0.01	0.22	0.23	6.97	27.67	121.03	445	0.0000	0.0633	0.0000	0.2767
GL 29	29.38	0.15	0.87	1.02	3.45	158.47	43.38	433	0.0498	1.6128	0.0000	0.4415
GL 30	29.90	0.04	0.46	0.49	4.37	60.98	76.96	430	0.0000	0.2996	0.0000	0.3781
GL 32	31.00	0.03	0.51	0.54	3.70	48.86	55.86	444	0.0091	0.2645	0.0000	0.3024
GL 33	31.38	0.02	0.19	0.21	10.27	47.77	207.69	430	0.0000	0.1001	0.0000	0.4350
GL 35	31.75	0.01	0.13	0.14	8.48	20.99	235.00	426	0.0000	0.0301	0.0000	0.3370
GL 36	32.62	0.03	0.17	0.20	9.38	109.07	276.67	438	0.0000	0.2199	0.0000	0.5579
GL 37	32.87	0.05	0.47	0.52	5.33	93.12	92.16	431	0.0000	0.4827	0.0000	0.4777

Rock eval data for the Cassis/La Bédoule section

Sample ID	Depth (m)	PC [%]	RC [%]	TOC [%]	MINC [%]	HI [mg HC/g TOC]	OI [mg CO2/g TOC]	Tmax [°C]	S1 [mg HC/g]	S2a [mg HC/g]	S2b [mg HC/g]	S3
BE 128	62.79	0.02	0.07	0.09	7.57	119.51	443.00	426	0.0000	0.1056	0.0000	0.3915
BE 139	78.84	0.01	0.11	0.12	9.67	29.24	346.24	436	0.0000	0.0360	0.0000	0.4266
BE 152b2	95.42	0.08	0.37	0.45	8.46	177.90	130.71	429	0.0000	0.8081	0.0000	0.5938
BE 152b3	95.72	0.01	0.17	0.18	9.84	34.99	168.37	425	0.0000	0.0630	0.0000	0.3030
BE 153b3	97.88	0.03	0.32	0.35	7.44	62.18	113.75	419	0.0000	0.2158	0.0000	0.3948
BE 154b	98.99	0.03	0.24	0.27	7.57	73.08	150.81	422	0.0000	0.1977	0.0000	0.4080
BE 155a	99.29	0.03	0.28	0.31	7.74	64.33	128.89	423	0.0000	0.1976	0.0000	0.3958
BE 156a	99.68	0.02	0.17	0.19	9.03	47.50	151.17	421	0.0000	0.0898	0.0000	0.2857
BE 157a	100.75	0.02	0.23	0.25	7.99	63.37	134.71	425	0.0000	0.1615	0.0000	0.3433
BE 157d	101.68	0.02	0.30	0.32	7.47	47.19	120.47	426	0.0000	0.1524	0.0000	0.3891
BE 158a	102.18	0.03	0.32	0.35	6.93	74.56	119.33	425	0.0000	0.2598	0.0000	0.4159
BE 162a	105.63	0.03	0.31	0.33	6.56	40.27	170.25	426	0.0000	0.1343	0.0000	0.5679
BE 162b	106.29	0.01	0.13	0.14	7.96	6.44	319.06	429	0.0000	0.0090	0.0000	0.4431
BE 163a	106.76	0.05	0.39	0.44	7.31	100.73	104.56	426	0.0000	0.4472	0.0000	0.4642
BE 164c	108.31	0.01	0.13	0.14	8.02	12.69	257.20	416	0.0000	0.0179	0.0000	0.3625

Rock eval data for the Shatsky Rise section

Sample ID	Depth (m)	PC [%]	RC [%]	TOC [%]	MINC [%]	HI [mg HC/g TOC]	OI [mg CO2/g TOC]	Tmax [°C]	S1 [mg HC/g]	S2a [mg HC/g]	S2b [mg HC/g]	S3
SG001773950	08-09	1.83	2.75	4.58	5.47	449.12	73.60	424	0.3694	20.5621	0.0000	3.3698
SG001773951	12-13	0.02	0.03	0.05	0.06	324.73	754.74	435	0.0000	0.1688	0.0000	0.3923
SG001773952	15-16	0.01	0.02	0.02	0.03	88.34	884.47	422	0.0000	0.0211	0.0000	0.2111
SG001773953	20-21	0.01	0.01	0.02	0.03	121.60	989.10	433	0.0000	0.0211	0.0000	0.1715
SG001773954	100-101	0.01	0.02	0.02	0.05	0.00	1120.60	438	0.0000	0.0000	0.0000	0.2641
SG001773955	105-106	0.02	0.01	0.03	7.93	0.00	2365.97	-22	0.0000	0.0000	0.0000	0.7276
SG001773956	108-109	0.03	0.03	0.06	7.61	82.73	1528.15	421	0.0000	0.0526	0.0000	0.9719
SG001773957	110-111	0.02	0.03	0.05	7.31	21.33	1574.21	420	0.0000	0.0105	0.0000	0.7764
SG001773958	114-115	0.98	2.94	3.92	7.07	277.23	64.08	426	0.1262	10.8710	0.0000	2.5127
SG001773959	117-118	0.23	0.88	1.11	9.90	202.05	136.44	423	0.0315	2.2383	0.0000	1.5115

Rock eval data for the Vergol section

Sample ID	Depth (m)	PC [%]	RC [%]	TOC [%]	MINC [%]	HI [mg HC/g TOC]	OI [mg CO2/g TOC]	Tmax [°C]	S1 [mg HC/g]	S2a [mg HC/g]	S2b [mg HC/g]	S3
Ve 0	0.40	0.03	0.16	0.18	10.80	92.22	246.76	433	0.0000	0.1692	0.0000	0.4527
Ve 1	0.52	0.08	0.25	0.33	8.42	260.20	121.33	434	0.0113	0.8557	0.0000	0.3990
Ve 2	0.60	0.14	0.22	0.37	7.21	423.81	114.52	435	0.0450	1.5623	0.0000	0.4221
Ve 3	0.69	0.14	0.34	0.47	6.71	298.84	125.56	432	0.0337	1.4136	0.0000	0.5939
Ve 4	0.79	0.09	0.23	0.32	8.47	258.94	207.07	433	0.0112	0.8175	0.0000	0.6538
Ve 5	0.88	0.07	0.16	0.22	8.71	288.16	171.39	436	0.0112	0.6484	0.0000	0.3856
Ve 6	1.05	0.07	0.22	0.29	7.25	242.62	163.59	436	0.0000	0.6918	0.0000	0.4665
Ve 7	1.08	1.38	2.89	4.28	4.78	361.06	30.02	427	0.7797	15.4373	0.0000	1.2837
Ve 8	1.10	0.25	0.61	0.86	5.85	313.74	80.28	436	0.0667	2.6905	0.0000	0.6885
Ve 9	1.11	1.39	3.47	4.86	4.65	319.97	30.57	427	0.7435	15.5477	0.0000	1.4856
Ve 10	1.13	0.19	0.50	0.69	6.02	291.06	99.85	432	0.0554	2.0050	0.0000	0.6878
Ve 11	1.15	1.16	2.85	4.01	5.11	321.68	30.82	427	0.7077	12.8926	0.0000	1.2353
Ve 12	1.33	0.03	0.08	0.11	10.43	163.70	489.89	434	0.0000	0.1876	0.0000	0.5615
Ve 13	1.46	0.10	0.24	0.34	7.29	263.65	254.41	436	0.0110	0.8923	0.0000	0.8611
Ve 14	1.82	0.09	0.19	0.28	7.61	308.14	179.52	437	0.0110	0.8577	0.0000	0.4997
Ve 15	1.99	0.03	0.13	0.17	10.04	172.40	199.18	442	0.0000	0.2854	0.0000	0.3297
Ve 16	2.08	0.05	0.18	0.23	8.69	231.68	149.46	435	0.0000	0.5368	0.0000	0.3463
Ve 17	2.14	1.47	2.43	3.89	5.60	426.10	18.26	428	0.8420	16.5893	0.0000	0.7110
Ve 18	2.19	0.04	0.11	0.15	8.60	180.19	350.22	432	0.0000	0.2620	0.0000	0.5092
Ve 19	2.32	0.01	0.07	0.09	10.90	50.33	405.55	430	0.0000	0.0436	0.0000	0.3512

Bulk Rock (including the detrital index) and Clay Minerals Analysis

Sample ID	Depth (m)	Phyllosilicates	Quartz	Feldspath-K	Plagioclase-Na	Calcite	Dolomite	Goethite	Ankérite	Indicies	Detrital Index
AI 54	68.85	5.66	18.09	0.00	5.79	68.98	0.00	0.00	0.00	1.47	0.43
AI 56	67.75	3.43	15.29	0.00	1.17	79.34	0.00	0.16	0.00	0.62	0.25
AI 59	65.35	7.59	17.19	0.00	1.68	72.65	0.00	0.08	0.00	0.82	0.36
AI 62	63.00	10.13	13.56	0.00	2.34	70.14	0.00	0.00	0.00	3.83	0.37
AI 66	60.25	3.68	11.84	0.00	4.63	78.12	0.00	0.45	0.00	1.29	0.26
AI 69	59.3	3.37	8.24	0.13	1.72	71.23	0.00	0.00	0.00	15.31	0.19
AI 70	58.6	3.15	10.45	0.00	2.63	83.00	0.00	0.00	0.00	0.77	0.20
AI 72	57.6	2.96	7.75	0.00	2.13	75.32	0.00	0.00	0.00	11.84	0.17
AI 75	55.55	6.16	14.03	0.00	2.54	76.03	0.00	0.00	0.00	1.24	0.30
AI 77	54.9	2.24	15.88	0.00	0.31	81.17	0.00	0.00	0.00	0.40	0.23
AI 81	52.6	7.49	14.78	0.00	1.07	76.03	0.00	0.00	0.00	0.63	0.31
AI 85	50.7	8.29	10.56	0.15	0.78	79.94	0.00	0.00	0.00	0.28	0.25
AI 88	49	0.00	13.56	0.00	1.47	77.54	0.00	0.00	0.00	7.43	0.19
AI 89	48.35	7.42	18.90	0.00	1.51	72.00	0.00	0.00	0.00	0.17	0.39
AI 90	47.85	4.90	11.38	0.00	1.96	78.34	0.00	0.21	0.00	3.21	0.23
AI 92	47.2	4.65	9.45	0.00	0.90	77.45	0.00	0.00	0.00	7.55	0.19
AI 93	46.25	1.75	10.06	0.00	2.17	83.88	0.00	0.64	0.00	1.50	0.17
AI 95	44.85	3.57	11.89	0.00	2.00	82.07	0.00	0.00	0.00	0.47	0.21
AI 97	43.55	4.56	11.23	0.00	1.77	76.99	0.00	0.00	0.22	5.23	0.23
AI 99	42	4.35	8.78	0.00	1.61	80.40	0.00	0.28	0.00	4.57	0.18
AI 102	40.5	9.87	12.45	0.00	1.04	76.05	0.00	0.00	0.00	0.59	0.31
AI 105	40.2	0.00	6.12	0.00	0.56	88.44	0.00	0.00	0.00	4.88	0.08
AI 107	38.9	3.46	8.49	0.00	1.79	80.43	0.00	0.00	0.14	5.68	0.17
AI 109	38	7.15	16.88	0.00	1.60	73.08	0.30	0.00	0.00	0.98	0.35
AI 110	36.95	4.87	10.09	0.12	1.86	77.09	0.00	0.00	0.00	5.97	0.22
AI 113	35.5	5.01	15.98	0.00	3.19	74.32	0.06	0.00	0.13	1.32	0.33
AI 118	32.4	7.62	19.45	0.00	0.88	70.56	0.00	0.00	0.25	1.24	0.40
AI 120	30.8	4.88	14.77	0.00	1.34	67.43	0.00	0.00	0.09	11.49	0.31
AI 122	29.5	5.23	22.54	0.11	1.23	70.32	0.00	0.00	0.00	0.57	0.41
AI 125	27.25	3.97	14.98	0.09	1.07	79.26	0.00	0.00	0.00	0.63	0.25
AI 127	25.85	6.42	20.65	0.00	1.16	71.34	0.00	0.00	0.00	0.43	0.40

Data of XRD analysis of bulk-rock samples from the section of Alvier.

Sample ID	Depth (m)	Phyllosilicates	Quartz	Feldspath-K	Plagioclase-Na	Calcite	Dolomite	Goethite	Ankérite	Indicies	Detrital Index
BgV 1	0.15	6.51	3.81	0.00	0.12	88.34	0.00	0.00	0.00	1.21	0.13
BgV 3	1.00	4.17	2.61	0.10	0.00	92.89	0.00	0.00	0.02	0.21	0.08
BgV 5	2.00	7.36	3.39	0.00	0.23	87.01	0.14	0.00	0.00	1.87	0.15
BgV 8	3.50	4.79	2.63	0.00	0.00	91.99	0.00	0.00	0.03	0.57	0.09
BgV 11	5.08	5.13	3.75	0.00	0.00	89.12	0.03	0.00	0.00	1.97	0.12
BgV 14	6.50	0.00	14.96	0.25	0.00	75.34	0.05	0.82	0.02	8.56	0.32
BgV 16	7.50	4.89	2.65	0.00	0.11	85.54	0.00	0.00	0.00	6.81	0.17
BgV 17	7.95	1.46	4.19	0.00	0.00	93.78	0.12	0.24	0.10	0.12	0.06
BgV 18	9.20	7.04	4.46	0.16	0.00	88.13	0.00	0.00	0.10	0.11	0.13
BgV 20	10.25	4.55	4.13	0.10	0.00	89.17	0.00	0.00	0.00	2.06	0.12
BgV 21	10.75	5.60	5.10	0.00	0.34	88.54	0.09	0.00	0.10	0.23	0.13
BgV 23	11.30	9.27	7.13	0.19	0.14	82.44	0.00	0.00	0.04	0.78	0.21
BgV 25	11.50	5.71	6.42	0.49	0.71	85.09	0.28	0.00	0.00	1.31	0.17
BgV 27	11.90	3.06	4.74	0.27	0.00	91.45	0.06	0.00	0.05	0.37	0.09
BgV 29	12.50	3.94	3.13	0.09	0.25	85.89	0.13	0.43	0.00	6.13	0.16
BgV 31	13.05	8.92	4.69	0.17	0.09	84.14	0.13	0.59	0.04	1.23	0.18
BgV 33	13.50	4.66	4.72	0.06	0.21	89.56	0.00	0.00	0.16	0.64	0.11
BgV 34	13.65	3.89	4.17	0.18	0.37	90.43	0.00	0.00	0.00	0.97	0.11
BgV 35	14.00	6.06	6.09	0.12	0.77	85.43	0.07	1.07	0.00	0.39	0.16
BgV 38	15.50	1.02	3.25	0.11	0.25	94.83	0.00	0.00	0.00	0.53	0.05
BgV 40	16.45	3.65	2.06	0.04	0.23	89.34	0.00	0.00	0.00	4.67	0.12
BgV 45	18.50	1.39	2.53	0.54	0.00	92.98	0.00	0.00	0.00	2.56	0.08
BgV 47	19.55	1.54	3.93	0.00	0.00	93.04	0.00	0.00	0.00	1.49	0.07
BgV 48	21.13	4.26	1.73	0.10	0.00	93.76	0.00	0.00	0.00	0.15	0.07
BgV 49	21.55	6.82	6.57	0.11	0.52	84.89	0.19	0.00	0.04	0.86	0.18
BgV 50	21.93	3.95	3.72	0.00	0.08	90.43	0.00	0.00	0.05	1.76	0.11
BgV 51	26.10	4.83	2.60	0.00	0.44	91.67	0.00	0.39	0.00	0.07	0.09
BgV 53	26.95	3.15	1.55	0.00	0.00	94.43	0.00	0.00	0.00	0.87	0.06
BgV 55	27.98	5.15	3.32	0.00	0.00	91.36	0.00	0.00	0.06	0.11	0.09
BgV 57	28.88	4.86	2.24	0.00	0.00	90.76	0.03	0.00	0.00	2.12	0.10
BgV 58	29.38	3.60	4.17	0.05	0.00	92.04	0.00	0.00	0.00	0.14	0.09
BgV 60	30.25	2.75	1.96	0.00	0.08	94.53	0.00	0.00	0.00	0.68	0.06

Data of XRD analysis of bulk-rock samples from the section of Breggia.

Sample ID	Depth (m)	Phyllosilicates	Quartz	Feldspath-K	Plagioclase-Na	Calcite	Dolomite	Goethite	Ankérite	Indicies	Detrital Index
CA 19	14.40	1.40	1.43	0.00	1.04	94.45	0.00	0.23	0.00	1.45	0.06
CA 23	16.10	0.00	1.30	0.19	0.00	97.45	0.16	0.00	0.06	0.84	0.02
CA 27	18.95	6.02	0.86	0.43	0.07	79.41	0.12	0.45	0.03	12.53	0.25
CA 35	22.12	6.95	4.23	0.41	1.11	74.67	0.00	0.00	0.00	12.62	0.34
CA 40	25.39	3.71	1.50	0.00	0.00	87.58	0.10	0.00	0.00	7.11	0.14
CA 48	29.32	2.75	5.90	0.25	0.32	76.40	0.00	0.00	0.00	14.29	0.31
CA 49	29.80	2.08	1.81	0.27	0.10	88.18	0.00	0.61	0.00	6.80	0.13
CA 52	31.05	2.69	1.47	0.00	0.00	81.34	0.00	0.00	0.00	14.50	0.23
CA 58	33.74	3.67	3.52	0.57	0.24	85.30	0.00	0.00	0.00	6.62	0.17
CA 60	35.24	3.05	2.37	0.00	0.11	93.45	0.00	0.78	0.00	0.24	0.06
CA 61	35.38	19.59	5.44	0.79	2.94	66.45	0.00	0.00	0.00	4.57	0.50
CA 65	38.00	6.29	3.92	0.00	0.69	89.03	0.00	0.00	0.00	0.06	0.12
CA 70	40.88	4.94	2.10	0.09	0.24	87.44	0.15	0.00	0.00	5.05	0.14
CA 74	43.27	2.18	3.14	0.00	0.11	93.23	0.08	0.00	0.00	1.26	0.07
CA 75	43.52	8.74	3.14	0.00	0.56	76.85	0.10	0.77	0.00	9.85	0.29
CA 79	46.34	8.34	2.93	0.40	0.76	86.43	0.00	0.00	0.04	0.91	0.15
CA 83	48.47	3.47	1.79	0.09	0.07	94.21	0.00	0.00	0.00	0.22	0.06
CA 88	51.21	10.00	3.15	0.12	0.38	70.98	0.00	0.00	0.00	15.37	0.41
CA 91	53.13	0.85	2.68	0.00	0.00	96.34	0.03	0.00	0.00	0.10	0.04
CA 93	54.12	13.06	7.31	0.68	1.20	64.70	0.00	0.00	0.02	13.04	0.55
CA 94	54.41	3.48	1.15	0.11	0.00	63.56	0.06	0.00	0.02	31.62	0.57
CA 96	54.65	8.73	4.27	0.30	0.79	78.79	0.00	0.00	0.00	7.13	0.27
CA 98	54.71	6.49	3.50	0.00	1.81	84.46	0.00	0.00	0.00	3.74	0.18
CA 99	54.96	2.02	2.24	0.13	0.03	83.45	0.15	0.00	0.03	11.94	0.20
CA 101	55.74	1.21	1.88	0.43	0.27	82.69	0.00	0.00	0.00	13.52	0.21
CA 102	55.80	9.87	6.75	0.83	1.22	64.56	0.04	0.00	0.08	16.64	0.55
CA 106	56.83	2.40	3.15	0.00	0.00	94.10	0.00	0.00	0.00	0.35	0.06
CA 107	56.91	9.78	3.23	0.09	0.29	85.16	0.00	0.00	0.09	1.35	0.17
CA 109	57.88	4.63	2.04	0.18	0.10	91.67	0.18	0.00	0.03	1.06	0.09
CA 113	59.83	0.00	3.56	0.42	0.22	95.72	0.00	0.00	0.00	0.08	0.04
CA 116	60.66	1.20	2.49	0.51	0.10	87.45	0.00	0.00	0.00	8.25	0.14
CA 118	61.63	3.63	3.40	0.09	0.10	85.92	0.00	0.00	0.00	6.86	0.16
CA 121	63.88	2.89	2.11	0.27	0.30	71.23	0.00	0.00	0.00	23.20	0.40
CA 122	64.37	3.14	6.58	0.13	0.29	78.56	0.00	0.00	0.03	11.20	0.27
CA 123	64.54	4.43	5.06	0.24	0.15	88.77	0.00	0.00	0.00	1.36	0.13
CA 125	65.99	0.00	3.25	0.00	0.00	78.90	0.00	0.00	0.00	17.85	0.27
CA 126	66.21	13.47	25.91	0.13	1.76	45.32	0.15	0.61	0.00	12.65	1.19
CA 128	66.77	2.09	3.37	0.22	0.31	91.97	0.00	0.00	0.02	2.02	0.09
CA 130	67.29	6.32	4.15	0.18	0.52	85.43	0.00	0.00	0.00	3.40	0.17
CA 131	67.55	12.79	7.47	0.25	0.59	77.45	0.00	0.00	0.00	1.45	0.29
CA 134	69.24	2.73	2.05	0.50	0.64	78.01	0.17	0.00	0.04	15.86	0.28
CA 136	70.29	4.79	2.56	0.09	0.33	79.87	0.00	0.00	0.00	12.37	0.25
CA 138	71.50	7.12	3.32	0.56	0.00	81.65	0.00	0.00	0.00	7.35	0.22
CA 140	72.61	9.34	8.65	0.28	0.29	80.65	0.00	0.00	0.00	0.78	0.24
CA 142	73.72	0.00	2.88	0.18	0.49	94.82	0.00	0.00	0.05	1.58	0.05
CA 145	75.05	11.08	6.85	0.64	3.02	78.03	0.00	0.00	0.00	0.38	0.28
CA 146	75.45	4.35	3.46	0.00	0.00	92.14	0.00	0.00	0.00	0.05	0.09
CA 148	76.85	3.24	2.35	0.43	0.30	83.77	0.00	0.00	0.00	9.91	0.19
CA 149	77.70	6.27	2.23	0.27	0.21	90.18	0.15	0.00	0.12	0.58	0.11
CA 151	79.78	1.34	3.32	0.00	0.15	91.24	0.00	0.00	0.00	3.96	0.10
CA 153	81.38	1.39	1.79	0.00	0.00	60.13	0.00	0.00	0.00	36.69	0.66
CA 154	82.39	1.55	1.22	0.29	0.22	71.60	0.28	0.00	0.00	24.84	0.39
CA 155	83.79	4.42	2.71	0.00	0.00	91.86	0.00	0.00	0.00	1.01	0.09
CA 157	86.30	1.44	5.07	0.00	0.16	93.27	0.00	0.00	0.00	0.06	0.07
CA 159	88.63	2.56	4.26	0.09	0.14	92.56	0.13	0.00	0.00	0.27	0.08
CA 161	91.36	1.34	5.01	0.00	0.15	93.16	0.00	0.00	0.00	0.34	0.07
CA 163	93.44	16.34	18.61	0.40	0.62	64.00	0.00	0.00	0.00	0.02	0.56
CA 165	94.76	2.01	5.77	0.00	0.21	91.45	0.00	0.00	0.00	0.56	0.09

Data of XRD analysis of bulk-rock samples from the section of Capriolo.

Sample ID	Depth (m)	Phyllosilicates	Quartz	Feldspath-K	Plagioclase-Na	Calcite	Dolomite	Goethite	Ankérite	Indicies	Detrital Index
Ch 1	1.32	3.37	11.34	0.00	3.43	69.12	0.00	0.00	0.00	12.74	0.26
Ch 2	2.79	5.43	1.49	0.37	0.59	86.90	0.00	0.00	0.00	5.22	0.09
Ch 3	3.51	4.03	1.01	0.41	0.65	90.88	0.00	0.00	0.00	3.02	0.07
Ch 4	4.85	2.02	1.90	0.14	0.70	92.77	0.00	0.00	0.00	2.47	0.05
Ch 5	5.30	2.60	1.15	0.00	0.00	93.99	0.00	0.00	0.00	2.26	0.04
Ch 9	7.54	1.23	0.77	0.20	0.61	88.72	0.00	0.00	0.00	8.47	0.03
Ch 10	8.51	4.33	1.04	0.66	0.53	91.14	0.00	0.00	0.00	2.30	0.07
Ch 12	10.37	4.76	1.51	0.00	0.37	89.88	0.00	0.00	0.00	3.48	0.07
Ch 14	11.27	4.31	0.68	0.46	0.30	89.02	0.00	0.00	0.00	5.22	0.06
Ch 16	12.31	2.51	3.93	0.00	0.11	88.77	0.00	0.00	0.00	4.68	0.07
Ch 18	13.33	4.16	1.35	0.00	0.00	91.52	0.00	0.00	0.17	2.79	0.06
Ch 19	13.86	0.00	0.46	0.00	0.00	97.55	0.12	0.00	0.10	1.76	0.00
Ch 20	15.15	2.23	0.93	0.14	0.15	85.77	0.00	0.00	0.00	10.78	0.04
Ch 21	15.91	4.18	0.53	0.25	0.00	84.05	0.00	0.00	0.00	10.99	0.06
Ch 22	17.05	3.06	0.50	0.00	0.00	88.18	0.41	0.00	0.00	7.85	0.04
Ch 23	17.73	2.24	1.28	0.00	0.00	85.45	0.16	0.00	0.00	10.86	0.04
Ch 24	18.56	0.00	0.54	0.00	0.00	87.92	0.00	0.00	0.00	11.54	0.01
Ch 25	19.39	1.38	0.57	0.00	0.27	92.90	0.00	0.00	0.00	4.89	0.02
Ch 26	19.92	0.93	0.73	0.00	0.00	95.37	0.00	0.00	0.00	2.97	0.02
Ch 28	20.76	1.49	0.60	0.00	0.29	97.12	0.15	0.00	0.00	0.35	0.02
Ch 29	21.29	2.24	0.76	0.00	0.00	87.29	0.00	0.00	0.00	9.71	0.03
Ch 31	21.97	4.25	0.69	0.00	0.00	88.34	0.00	0.00	0.00	6.72	0.06
Ch 32	22.50	6.99	1.33	0.00	0.00	90.34	0.00	0.00	0.10	1.24	0.09
Ch 33	23.56	0.00	1.93	0.00	0.00	97.12	0.35	0.00	0.00	0.59	0.02
Ch 35	24.55	0.00	0.79	0.00	0.00	90.43	0.00	0.00	0.03	8.75	0.01
Ch 37	25.38	1.39	0.76	0.00	0.00	93.09	0.17	0.00	0.00	4.60	0.02
Ch 39	26.67	1.86	0.47	0.00	0.00	94.99	0.17	0.00	0.00	2.51	0.02
Ch 41	27.73	0.00	0.51	0.00	0.00	99.12	0.00	0.00	0.00	0.37	0.01
Ch 43	28.56	0.00	1.82	0.00	0.34	97.55	0.00	0.00	0.00	0.29	0.02
Ch 45	29.39	2.75	1.07	0.00	0.00	92.66	0.22	0.00	0.00	3.30	0.04
Ch 48	30.91	1.29	1.30	0.00	0.00	97.03	0.08	0.00	0.00	0.29	0.03
Ch 50	31.89	3.95	1.26	0.00	0.00	91.77	0.00	0.00	0.00	3.02	0.06
Ch 55	34.85	2.23	1.29	0.00	0.18	95.00	0.18	0.00	0.00	1.12	0.04
Ch 57	36.82	2.65	1.28	0.00	0.24	94.03	0.00	0.00	0.00	1.80	0.04
Ch 61	41.36	3.98	1.15	0.00	0.00	93.23	0.00	0.00	0.00	1.64	0.05

Data of XRD analysis of bulk-rock samples from the section of Chrummflueschlucht.

Sample ID	Depth (m)	Phyllosilicates	Quartz	Feldspath-K	Plagioclase-Na	Calcite	Dolomite	Goethite	Ankérite	Indicies	Detrital Index
MAm 21	2.50	0.00	1.57	0.00	0.00	83.56	0.00	0.00	0.00	14.62	0.02
MAm 22	3.10	6.91	12.55	0.00	0.00	78.99	0.00	0.00	0.00	1.55	0.25
MAm 23	3.35	0.00	1.90	0.00	0.00	96.02	0.00	0.00	0.00	2.09	0.02
MAm 24	4.30	3.25	3.97	0.00	0.00	91.43	0.00	0.00	0.00	1.35	0.08
MAm 25	5.75	0.00	0.54	0.00	0.00	98.02	0.23	0.00	0.00	1.21	0.01
MAm 26	6.65	0.00	2.16	0.00	0.00	97.44	0.00	0.00	0.00	0.40	0.02
MAm 27	7.50	2.68	0.69	0.00	0.00	88.56	0.00	0.00	0.00	8.07	0.04
MAm 28	8.20	0.00	3.78	0.00	0.00	88.71	0.00	0.00	0.00	7.52	0.04
MAm 29	8.95	0.00	2.75	0.00	0.00	96.57	0.00	0.00	0.00	0.68	0.03
MAm 30	9.90	0.00	1.44	0.00	0.00	97.91	0.00	0.00	0.00	0.65	0.01
MAm 31	12.00	0.00	4.30	0.00	0.00	95.21	0.00	0.00	0.00	0.49	0.05
MAm 32	13.20	0.00	1.14	0.00	0.00	98.56	0.00	0.00	0.00	0.30	0.01
MAm 33	14.90	2.38	0.60	0.00	0.00	94.23	0.00	0.00	0.00	2.79	0.03
MAm 34	16.60	3.46	4.37	0.00	0.00	91.65	0.00	0.00	0.00	0.52	0.09
MAm 35	25.30	4.09	6.11	0.00	0.00	89.38	0.00	0.00	0.00	0.42	0.11
MAm 36	27.20	4.06	5.87	0.00	0.00	79.95	0.00	0.00	0.00	10.12	0.12
MAs 1	27.60	4.11	4.22	0.00	0.00	90.42	0.00	0.00	0.00	1.25	0.09
MAs 2	28.55	3.18	4.42	0.00	0.00	68.76	0.00	0.00	0.00	23.42	0.11
MAm 37	28.80	2.57	3.01	0.00	0.00	79.27	0.00	0.00	0.00	15.15	0.07
MAs 4	30.95	3.50	4.66	0.00	0.00	81.34	0.00	0.00	0.00	10.33	0.10
MAs 5	32.60	2.53	3.24	0.00	0.00	91.95	0.00	0.00	0.00	2.28	0.06
MAs 6	33.50	2.39	1.17	0.00	0.00	93.56	0.00	0.00	0.00	2.89	0.04
MAs 7	34.45	4.28	0.46	0.00	0.00	93.67	0.17	0.00	0.00	1.41	0.05
MAs 8	35.40	3.32	0.99	0.00	0.00	94.51	0.17	0.00	0.00	1.01	0.05
MAs 9	36.30	0.00	0.99	0.00	0.00	96.01	0.00	0.00	0.00	3.00	0.01
MAs 10	36.95	0.00	2.12	0.00	0.00	97.03	0.00	0.40	0.00	0.45	0.02
MAs 11	37.50	8.56	2.80	0.00	0.00	83.51	0.00	0.00	0.00	5.12	0.14
MAs 12	38.40	0.00	0.25	0.00	0.00	93.45	0.00	0.00	0.00	6.30	0.00
MAs 13	40.20	5.62	1.02	0.00	0.00	92.71	0.00	0.00	0.00	0.66	0.07
MAs 14	41.70	2.38	1.12	0.00	0.00	93.10	0.00	0.00	0.00	3.40	0.04
MAs 15	47.70	0.00	1.57	0.00	0.00	97.32	0.00	0.00	0.00	1.11	0.02
MAs 16	49.30	0.00	0.58	0.00	0.00	99.03	0.00	0.00	0.00	0.39	0.01
MAs 17	50.75	4.48	0.64	0.00	0.00	92.66	0.00	0.00	0.00	1.81	0.06
MAs 18	51.90	4.81	0.79	0.00	0.00	93.29	0.16	0.00	0.00	0.95	0.06
MAs 19	52.75	0.00	0.61	0.00	0.00	99.03	0.00	0.00	0.00	0.36	0.01
MAs 20	53.60	0.00	3.93	0.00	0.00	94.12	0.00	0.00	0.00	1.95	0.04
MAs 21	55.00	5.12	0.32	0.00	0.00	94.41	0.00	0.00	0.00	0.15	0.06
MAs 22	56.20	4.82	0.53	0.00	0.00	92.52	0.00	0.94	0.00	1.20	0.06
MAs 23	57.15	0.00	0.81	0.00	0.00	98.67	0.00	0.00	0.00	0.52	0.01
MAs 24	58.25	2.83	0.57	0.00	0.00	96.43	0.00	0.00	0.00	0.17	0.04
MAs 25	59.40	0.00	0.82	0.00	0.00	99.04	0.00	0.00	0.00	0.14	0.01
MAs 26	61.10	2.11	0.40	0.00	0.00	92.76	0.00	0.00	0.00	4.73	0.03
MAs 27	64.55	6.12	1.28	0.00	4.16	87.00	0.00	0.00	0.00	1.44	0.13
MAs 28	65.85	0.00	0.90	0.00	0.00	98.43	0.00	0.00	0.00	0.67	0.01
MAs 29	67.00	2.50	1.01	0.00	0.00	94.67	0.00	0.00	0.00	1.82	0.04
MAs 30	68.30	4.84	1.95	0.00	0.00	88.61	0.00	0.00	0.00	4.60	0.08
MAs 31	69.40	2.70	5.96	0.00	0.00	86.50	0.00	0.00	0.00	4.84	0.10
MAs 32	70.45	1.86	0.70	0.00	0.00	93.75	0.00	0.45	0.00	3.24	0.03
MAs 33	71.50	8.14	0.77	0.00	0.00	89.45	0.00	0.00	0.00	1.64	0.10
MAs 34	72.40	0.00	9.24	0.00	0.00	88.77	0.00	0.00	0.00	1.99	0.10
MAs 35	73.55	3.09	4.63	0.00	0.00	89.68	0.00	0.00	0.00	2.60	0.09
MAs 36	74.65	3.35	5.89	0.00	0.00	89.65	0.00	0.00	0.00	1.11	0.10
MAs 37	75.80	2.16	5.71	0.00	2.49	81.54	0.00	0.00	0.00	8.10	0.13
MAs 38	76.90	0.00	5.29	0.00	0.00	87.99	0.00	0.00	0.00	6.72	0.06
MAs 39	78.20	0.00	4.29	0.00	0.00	90.91	0.00	0.00	3.54	1.26	0.05
MAs 40	79.40	3.81	8.82	0.00	0.00	86.29	0.00	0.00	0.00	1.08	0.15
MAs 41 b	79.40	2.36	3.91	0.00	0.00	89.73	0.00	0.00	2.20	1.81	0.07
MAs 41	80.60	3.64	7.07	0.00	0.00	88.23	0.00	0.00	0.00	1.06	0.12
MAs 43 b	82.15	0.00	2.26	0.00	0.00	93.23	0.00	0.00	0.00	4.51	0.02
MAs 42	82.65	0.00	0.98	0.00	0.00	95.76	0.00	0.00	0.00	3.26	0.01
MAs 43	84.35	2.81	4.50	0.00	0.00	92.65	0.00	0.00	0.00	0.04	0.08
MAs 48 b	85.55	3.26	8.24	0.00	0.00	87.34	0.00	0.00	0.00	0.93	0.13
MAs 49 b	86.85	0.00	0.95	0.00	0.00	97.67	0.00	0.00	0.00	1.39	0.01
MAs 50 b	87.90	1.30	0.64	0.00	0.00	96.93	0.00	0.00	0.00	1.12	0.02
MAs 51 b	89.10	3.01	1.12	0.00	0.00	95.23	0.00	0.00	0.00	0.64	0.04
MAs 52 b	90.65	2.48	2.15	0.00	0.00	94.43	0.00	0.00	0.00	0.94	0.05
MAs 53 b	92.20	2.62	1.85	0.00	0.00	95.00	0.22	0.00	0.07	0.10	0.05
MAs 54 b	93.30	2.79	1.51	0.00	0.00	93.75	0.00	0.00	0.00	1.95	0.05
MAs 55 b	94.60	2.75	0.61	0.00	0.00	96.61	0.00	0.00	0.00	0.04	0.03
MAs 56 b	95.60	10.67	0.69	0.00	0.00	87.81	0.20	0.00	0.00	0.62	0.13
MAs 57 b	96.90	0.00	0.86	0.00	0.00	97.78	0.00	0.00	0.00	1.36	0.01

Data of XRD analysis of bulk-rock samples from the section of Malleval.

Sample ID	Depth (m)	Phyllosilicates	Quartz	Feldspath-K	Plagioclase-Na	Calcite	Dolomite	Pyrite	Ankérite	Indicies	Detrital Index
Ve 1	0.52	19.04	5.90	0.28	0.53	72.71	0.00	0.41	0.00	1.12	0.35
Ve 2	0.60	17.89	11.87	0.72	0.26	60.97	1.47	0.40	0.00	6.42	0.50
Ve 3	0.69	15.76	10.65	0.00	0.22	58.58	0.13	0.00	0.29	14.37	0.45
Ve 4	0.79	14.56	11.76	0.18	0.49	70.34	0.75	0.00	0.25	1.67	0.38
Ve 5	0.88	9.52	9.03	0.41	0.35	75.85	0.00	0.00	0.00	4.84	0.25
Ve 6	1.05	23.53	11.38	0.10	0.93	60.26	0.00	1.09	0.06	2.65	0.60
Ve 7	1.08	31.21	15.66	0.47	0.58	37.93	0.24	0.51	0.01	13.40	1.26
Ve 8	1.10	21.54	12.07	0.34	0.56	51.65	0.00	0.59	0.00	13.26	0.67
Ve 9	1.11	27.43	13.65	0.98	0.76	39.32	0.11	0.80	0.00	16.96	1.09
Ve 10	1.13	21.44	11.65	0.28	0.76	52.37	0.00	0.27	0.00	13.24	0.65
Ve 11	1.15	25.55	9.95	0.00	0.00	43.77	0.11	0.09	0.02	20.50	0.81
Ve 12	1.33	13.30	9.89	0.00	0.00	75.12	0.00	0.38	0.00	1.31	0.31
Ve 13	1.46	22.22	8.52	0.14	0.51	64.34	0.75	0.00	0.11	3.40	0.49
Ve 14	1.82	4.55	5.99	0.11	0.11	64.05	0.08	0.00	0.04	25.07	0.17
Ve 15	1.99	5.92	8.37	0.00	0.13	84.32	0.00	0.00	0.00	1.26	0.17
Ve 16	2.08	15.87	7.07	0.00	0.00	75.59	0.00	0.00	0.00	1.47	0.30
Ve 17	2.14	28.04	13.09	0.34	0.53	47.09	0.00	1.75	0.00	9.15	0.89
Ve 18	2.19	15.23	9.47	0.39	0.21	72.45	0.16	0.14	0.16	1.79	0.35
Ve 19	2.32	4.09	3.98	0.00	0.00	90.77	0.00	0.00	0.00	1.16	0.09

Data of XRD analysis of bulk-rock samples from the section of Vergol.

Sample ID	Depth (m)	Peak Intensity (cps)									
		Smectite 001	Rectorite	Micas 001	R0 I/S	Kaolinite 001	Chlortie 002	K001/M001	K001/SM001	SM001/M001
BgV 1	0.15	89.00	20.00	23.00	16.00	2.33	25.67	0.10	0.03	3.87
BgV 2	0.63	97.00	14.00	22.00	15.00	9.10	4.90	0.41	0.09	4.41
BgV 3	1.00	389.00	20.00	33.00	16.00	6.00	6.00	0.18	0.02	11.79
BgV 4	1.50	193.00	17.00	19.00	15.00	2.29	5.71	0.12	0.01	10.16
BgV 5	2.00	77.00	34.00	33.00	18.00	12.16	2.84	0.37	0.16	2.33
BgV 6	2.50	70.00	14.00	20.00	6.00	0.00	0.00	0.00	0.00	3.50
BgV 7	3.00	53.00	36.00	39.00	17.00	0.55	2.45	0.01	0.01	1.36
BgV 8	3.50	17.00	39.00	11.00	12.00	0.00	9.00	0.00	0.00	1.55
BgV 9	4.10	64.00	33.00	24.00	7.00	0.00	0.00	0.00	0.00	2.67
BgV 10	4.53	69.00	33.00	46.00	17.00	0.00	0.00	0.00	0.00	1.50
BgV 11	5.08	292.00	31.00	32.00	18.00	4.91	4.09	0.15	0.02	9.13
BgV 12	5.65	33.00	58.00	37.00	22.00	4.09	4.91	0.11	0.12	0.89
BgV 14	6.50	14.00	61.00	61.00	9.00	0.00	27.00	0.00	0.00	0.23
BgV 16	7.50	7.00	62.00	42.00	17.00	0.00	9.00	0.00	0.00	0.17
BgV 17	7.95	26.00	65.00	37.00	5.00	4.50	4.50	0.12	0.17	0.70
BgV 18	9.20	15.00	198.00	133.00	27.00	0.00	0.00	0.00	0.00	0.11
BgV 19	9.75	18.00	88.00	84.00	21.00	0.00	12.00	0.00	0.00	0.21
BgV 20	10.25	10.00	61.00	52.00	19.00	2.52	6.48	0.05	0.25	0.19
BgV 21	10.75	19.00	47.00	53.00	13.00	11.76	8.24	0.22	0.62	0.36
BgV 23	11.30	157.00	30.00	37.00	11.00	8.38	6.62	0.23	0.05	4.24
BgV 26	11.68	143.00	14.00	59.00	12.00	4.94	14.06	0.08	0.03	2.42
BgV 28	12.15	16.00	52.00	29.00	0.00	14.79	8.21	0.51	0.92	0.55
BgV 30	12.90	17.00	36.00	56.00	13.00	14.35	15.65	0.26	0.84	0.30
BgV 32	13.25	236.00	21.00	97.00	26.00	0.00	48.00	0.00	0.00	2.43
BgV 34	13.65	20.00	59.00	51.00	11.00	3.40	1.60	0.07	0.17	0.39
BgV 35	14.00	132.00	28.00	82.00	23.00	2.44	7.56	0.03	0.02	1.61
BgV 36	14.50	15.00	64.00	67.00	13.00	5.93	7.07	0.09	0.40	0.22
BgV 37	15.00	14.00	79.00	57.00	14.00	8.33	6.67	0.15	0.60	0.25
BgV 38	15.50	158.00	14.00	72.00	23.00	14.00	3.00	0.19	0.09	2.19
BgV 40	16.45	179.00	14.00	50.00	21.00	5.33	4.67	0.11	0.03	3.58
BgV 43	17.55	860.00	12.00	148.00	13.00	22.62	39.38	0.15	0.03	5.81
BgV 45	18.50	90.00	45.00	91.00	43.00	2.00	6.00	0.02	0.02	0.99
BgV 47	19.55	187.00	23.00	42.00	32.00	0.00	21.00	0.00	0.00	4.45
BgV 48	21.13	629.00	51.00	98.00	10.00	12.00	12.00	0.12	0.02	6.42
BgV 49	21.55	165.00	49.00	78.00	16.00	10.71	31.29	0.14	0.06	2.12
BgV 50	21.93	246.00	5.00	61.00	7.00	10.67	11.33	0.17	0.04	4.03
BgV 51	26.10	12.00	50.00	71.00	17.00	17.00	0.00	0.24	1.42	0.17
BgV 53	26.95	209.00	13.00	70.00	31.00	0.00	34.00	0.00	0.00	2.99
BgV 56	28.35	118.00	28.00	135.00	99.00	0.00	55.00	0.00	0.00	0.87
BgV 60	30.25	37.00	31.00	56.00	22.00	9.45	16.55	0.17	0.26	0.66

Peaks intensities for the minerals identified in the <2μm fraction of samples from the section of Breggia

Sample ID	Depth (m)	*Peak Intensity (cps)*								
		Smectite *001*	Rectorite	Micas *001*	R0 I/S	Kaolinite *001*	Chlortie *002*	K001/M001	K001/SM001	SM001/M001
Ve 0	0.40	119.00	0.00	141.00	32.00	31.37	67.63	0.22	0.26	0.84
Ve 1	0.52	346.00	17.00	351.00	126.00	116.23	98.77	0.33	0.34	0.99
Ve 2	0.60	137.00	49.00	381.00	68.00	54.37	40.63	0.14	0.40	0.36
Ve 3	0.69	54.00	60.00	215.00	112.00	141.27	82.73	0.66	2.62	0.25
Ve 4	0.79	113.00	26.00	146.00	11.00	52.35	94.65	0.36	0.46	0.77
Ve 5	0.88	164.00	86.00	277.00	25.00	86.28	110.72	0.31	0.53	0.59
Ve 6	1.05	16.00	38.00	104.00	91.00	74.69	68.31	0.72	4.67	0.15
Ve 7	1.08	91.00	75.00	304.00	57.00	241.35	90.65	0.79	2.65	0.30
Ve 8	1.10	250.00	33.00	277.00	117.00	259.89	119.11	0.94	1.04	0.90
Ve 9	1.11	37.00	76.00	196.00	22.00	194.13	60.87	0.99	5.25	0.19
Ve 10	1.13	42.00	103.00	271.00	89.00	252.73	92.27	0.93	6.02	0.15
Ve 11	1.15	181.00	14.00	342.00	33.00	278.80	122.20	0.82	1.54	0.53
Ve 12	1.33	229.00	82.00	458.00	191.00	80.33	130.67	0.18	0.35	0.50
Ve 13	1.46	23.00	133.00	269.00	107.00	127.56	112.44	0.47	5.55	0.09
Ve 14	1.82	164.00	22.00	233.00	54.00	85.75	77.25	0.37	0.52	0.70
Ve 15	1.99	466.00	58.00	348.00	94.00	114.22	185.78	0.33	0.25	1.34
Ve 16	2.08	464.00	91.00	395.00	145.00	105.38	94.62	0.27	0.23	1.17
Ve 17	2.14	100.00	22.00	106.00	27.00	194.34	54.66	1.83	1.94	0.94
Ve 18	2.19	595.00	64.00	431.00	344.00	302.81	231.19	0.70	0.51	1.38
Ve 19	2.32	622.00	46.00	347.00	72.00	64.67	268.33	0.19	0.10	1.79

Peaks intensities for the minerals identified in the <2µm fraction of samples from the section of Vergol.

Sample ID	Depth (m)	Peak Intensity (cps)									
		Smectite 001	Rectorite	Micas 001	R0 I/S	Kaolinite 001	Chlortie 002	K001/M001	K001/SM001	SM001/M001
CA 16	12.95	91.00	33.00	76.00	12.00	27.91	32.09	0.37	0.31	1.20
CA 19	14.40	131.00	29.00	34.00	18.00	6.00	41.00	0.18	0.05	3.85
CA 20	15.52	628.00	0.00	117.00	12.00	4.21	17.79	0.04	0.01	5.37
CA 23	16.10	46.00	32.00	208.00	82.00	14.29	44.71	0.07	0.31	0.22
CA 31	20.31	169.00	32.00	743.00	446.00	0.00	0.00	0.00	0.00	0.23
CA 32	20.36	39.00	23.00	90.00	18.00	1.09	0.91	0.01	0.03	0.43
CA 35	22.12	771.00	34.00	182.00	23.00	25.25	66.75	0.14	0.03	4.24
CA 36	22.22	239.00	30.00	76.00	26.00	26.64	10.36	0.35	0.11	3.14
CA 38	23.40	1444.00	14.00	111.00	12.00	1.90	36.10	0.02	0.00	13.01
CA 40	25.39	60.00	0.00	38.00	11.00	8.26	3.74	0.22	0.14	1.58
CA 42	26.04	558.00	12.00	85.00	14.00	0.00	0.00	0.00	0.00	6.56
CA 44	27.76	315.00	7.00	119.00	45.00	11.45	51.55	0.10	0.04	2.65
CA 45	27.69	91.00	0.00	552.00	150.00	71.99	345.01	0.13	0.79	0.16
CA 46	28.21	238.00	35.00	102.00	53.00	6.00	24.00	0.06	0.03	2.33
CA 48	29.32	726.00	18.00	121.00	39.00	8.28	46.72	0.07	0.01	6.00
CA 49	29.80	338.00	8.00	74.00	20.00	5.20	4.80	0.07	0.02	4.57
CA 50	30.40	566.00	9.00	246.00	22.00	0.00	0.00	0.00	0.00	2.30
CA 52	31.05	596.00	9.00	58.00	15.00	17.46	55.54	0.30	0.03	10.28
CA 54	31.78	938.00	24.00	117.00	61.00	11.07	15.93	0.09	0.01	8.02
CA 56	33.05	67.00	58.00	129.00	38.00	17.53	8.47	0.14	0.26	0.52
CA 58	33.74	1915.00	14.00	374.00	84.00	7.17	77.83	0.02	0.00	5.12
CA 60	35.24	26.00	37.00	48.00	16.00	0.00	0.00	0.00	0.00	0.54
CA 61	35.38	228.00	16.00	387.00	57.00	0.00	0.00	0.00	0.00	0.59
CA 64	37.79	134.00	14.00	93.00	17.00	16.70	31.30	0.18	0.12	1.44
CA 65	38.00	2697.00	0.00	367.00	238.00	118.34	156.66	0.32	0.04	7.35
CA 72	41.97	107.00	43.00	76.00	38.00	21.78	20.22	0.29	0.20	1.41
CA 74	43.27	83.00	18.00	55.00	20.00	42.43	23.57	0.77	0.51	1.51
CA 76	44.10	450.00	20.00	79.00	10.00	2.86	9.14	0.04	0.01	5.70
CA 78	45.27	110.00	10.00	108.00	6.00	0.00	0.00	0.00	0.00	1.02
CA 79	46.34	1469.00	27.00	164.00	66.00	11.14	23.86	0.07	0.01	8.96
CA 81	47.47	63.00	21.00	38.00	0.00	17.14	22.86	0.45	0.27	1.66
CA 83	48.47	142.00	20.00	41.00	8.00	19.00	0.00	0.46	0.13	3.46
CA 85	49.83	83.00	19.00	31.00	18.00	7.64	10.36	0.25	0.09	2.68
CA 87	50.96	693.00	0.00	113.00	59.00	15.56	67.44	0.14	0.02	6.13
CA 88	51.21	1529.00	0.00	235.00	73.00	0.00	0.00	0.00	0.00	6.51
CA 91	53.13	0.00	24.00	62.00	10.00	0.00	0.00	0.00	0.00	0.00

Peaks intensities for the minerals identified in the <2μm fraction of samples from the section of Capriolo.

Sample ID	Depth (m)	Peak Intensity (cps)								
		Smectite 001	Rectorite	Micas 001	R0 I/S	Kaolinite 001	Chlortie 002	K001/M001	K001/SM001	SM001/M001
CA 93	54.12	0.00	32.00	439.00	94.00	0.00	59.00	0.00	0.00	0.00
CA 94	54.41	180.00	9.00	103.00	9.00	0.05	1.95	0.00	0.00	1.75
CA 96	54.65	47.00	10.00	199.00	7.00	4.33	9.67	0.02	0.09	0.24
CA 99	54.96	22.00	36.00	94.00	0.00	4.14	37.86	0.04	0.19	0.23
CA 101	55.74	0.00	7.00	328.00	64.00	0.00	0.00	0.00	0.00	0.00
CA 102	55.80	13.00	27.00	83.00	20.00	9.64	35.36	0.12	0.74	0.16
CA 106	56.83	141.00	17.00	65.00	11.00	4.53	12.47	0.07	0.03	2.17
CA 107	56.91	638.00	16.00	359.00	184.00	13.27	114.73	0.04	0.02	1.78
CA 109	57.88	908.00	18.00	129.00	93.00	3.39	57.61	0.03	0.00	7.04
CA 114	60.00	242.00	22.00	133.00	87.00	0.00	0.00	0.00	0.00	1.82
CA 116	60.66	203.00	0.00	51.00	13.00	0.00	0.00	0.00	0.00	3.98
CA 118	61.63	643.00	18.00	68.00	31.00	0.00	0.00	0.00	0.00	9.46
CA 121	63.88	104.00	19.00	91.00	21.00	21.18	68.82	0.23	0.20	1.14
CA 122	64.37	200.00	90.00	1288.00	143.00	0.00	287.00	0.00	0.00	0.16
CA 123	64.54	575.00	0.00	89.00	65.00	13.20	10.80	0.15	0.02	6.46
CA 126	66.21	32.00	29.00	393.00	51.00	6.02	23.98	0.02	0.19	0.08
CA 128	66.77	52.00	0.00	83.00	0.00	0.00	0.00	0.00	0.00	0.63
CA 130	67.29	366.00	29.00	57.00	51.00	9.17	45.83	0.16	0.03	6.42
CA 131	67.55	913.00	0.00	401.00	47.00	14.77	26.23	0.04	0.02	2.28
CA 134	69.24	253.00	52.00	122.00	103.00	16.53	11.47	0.14	0.07	2.07
CA 136	70.29	101.00	21.00	102.00	35.00	22.15	19.85	0.22	0.22	0.99
CA 138	71.50	334.00	43.00	103.00	16.00	9.47	18.53	0.09	0.03	3.24
CA 140	72.61	79.00	44.00	614.00	53.00	0.00	0.00	0.00	0.00	0.13
CA 142	73.72	420.00	16.00	164.00	58.00	10.77	49.23	0.07	0.03	2.56
CA 145	75.05	93.00	35.00	733.00	155.00	67.24	372.76	0.09	0.72	0.13
CA 146	75.45	389.00	4.00	103.00	18.00	10.00	20.00	0.10	0.03	3.78
CA 148	76.85	488.00	44.00	115.00	10.00	31.16	68.84	0.27	0.06	4.24
CA 149	77.70	246.00	7.00	46.00	11.00	10.00	30.00	0.22	0.04	5.35
CA 151	79.78	430.00	44.00	59.00	10.00	0.00	0.00	0.00	0.00	7.29
CA 153	81.38	124.00	6.00	73.00	13.00	1.80	13.20	0.02	0.01	1.70
CA 154	82.39	46.00	45.00	57.00	0.00	3.50	9.50	0.06	0.08	0.81
CA 155	83.79	242.00	22.00	64.00	0.00	0.96	26.04	0.02	0.00	3.78
CA 157	86.30	199.00	11.00	77.00	14.00	3.64	13.36	0.05	0.02	2.58
CA 161	91.36	84.00	21.00	82.00	0.00	0.00	0.00	0.00	0.00	1.02
CA 163	93.44	18.00	10.00	349.00	13.00	0.00	0.00	0.00	0.00	0.05

Peaks intensities for the minerals identified in the <2μm fraction of samples from the section of Capriolo (continued).

Sample ID	Depth (m)	Peak Intensity (cps)								
		Smectite 001	Rectorite	Micas 001	R0 I/S	Kaolinite 001	Chlortie 002	K001/M001	K001/SM001	SM001/M001
MAm 21	2.50	24.00	14.00	125.00	19.00	964.61	84.39	7.72	494.77	0.19
MAm 22	3.10	0.00	25.00	194.00	13.00	1449.98	74.02	7.47	0.00	0.00
MAm 23	3.35	23.00	43.00	128.00	6.00	1058.23	116.77	8.27	632.64	0.18
MAm 24	4.30	18.00	62.00	246.00	46.00	2367.35	217.65	9.62	3889.03	0.07
MAm 25	5.75	16.00	55.00	211.00	32.00	1597.19	46.81	7.57	1954.56	0.08
MAm 26	6.65	31.00	59.00	243.00	39.00	1784.91	152.09	7.35	1329.47	0.13
MAm 27	7.50	48.00	59.00	173.00	22.00	1714.69	51.31	9.91	738.75	0.28
MAm 28	8.20	19.00	127.00	140.00	29.00	1360.08	15.92	9.71	1210.47	0.14
MAm 29	8.95	10.00	83.00	148.00	26.00	852.70	74.30	5.76	1018.12	0.07
MAm 30	9.90	61.00	83.00	221.00	135.00	1429.71	129.29	6.47	482.59	0.28
MAm 31	12.00	18.00	78.00	184.00	42.00	1431.32	86.68	7.78	1463.13	0.10
MAm 32	13.20	10.00	83.00	92.00	28.00	381.01	7.99	4.14	229.37	0.11
MAm 33	14.90	22.00	55.00	84.00	17.00	540.75	13.25	6.44	179.92	0.26
MAm 34	16.60	842.00	47.00	94.00	59.00	0.00	0.00	0.00	0.00	8.96
MAm 35	25.30	257.00	11.00	53.00	9.00	0.00	0.00	0.00	0.00	4.85
MAm 36	27.20	325.00	18.00	55.00	12.00	0.00	0.00	0.00	0.00	5.91
MAs 1	27.60	613.00	32.00	72.00	7.00	34.75	4.25	0.48	0.43	8.51
MAs 2	28.55	191.00	55.00	41.00	7.00	0.00	0.00	0.00	0.00	4.66
MAm 37	28.80	375.00	30.00	46.00	8.00	40.00	0.00	0.87	0.53	8.15
MAs 4	30.95	92.00	70.00	40.00	0.00	23.00	0.00	0.58	0.56	2.30
MAs 5	32.60	0.00	52.00	41.00	0.00	0.00	0.00	0.00	0.00	0.00
MAs 6	33.50	17.00	51.00	26.00	0.00	63.00	0.00	2.42	5.82	0.65
MAs 7	34.45	16.00	63.00	43.00	0.00	342.00	0.00	7.95	99.18	0.37
MAs 8	35.40	138.00	0.00	41.00	0.00	0.00	0.00	0.00	0.00	3.37
MAs 9	36.30	55.00	15.00	15.00	0.00	7.00	0.00	0.47	0.12	3.67
MAs 10	36.95	86.00	48.00	56.00	13.00	0.00	0.00	0.00	0.00	1.54
MAs 11	37.50	37.00	29.00	42.00	0.00	0.00	0.00	0.00	0.00	0.88
MAs 12	38.40	56.00	43.00	58.00	0.00	201.00	0.00	3.47	12.85	0.97
MAs 13	40.20	99.00	54.00	43.00	0.00	385.55	6.45	8.97	22.90	2.30
MAs 15	47.70	30.00	102.00	41.00	21.00	0.00	0.00	0.00	0.00	0.73
MAs 16	49.30	21.00	37.00	31.00	0.00	1.20	0.80	0.04	0.05	0.68
MAs 17	50.75	29.00	30.00	32.00	0.00	0.00	0.00	0.00	0.00	0.91
MAs 18	51.80	38.00	33.00	33.00	0.00	114.00	0.00	3.45	6.54	1.15
MAs 19	52.75	34.00	70.00	28.00	0.00	0.00	0.00	0.00	0.00	1.21
MAs 20	53.60	27.00	42.00	31.00	0.00	158.00	0.00	5.10	15.10	0.87
MAs 21	55.00	74.00	13.00	24.00	0.00	0.00	0.00	0.00	0.00	3.08
MAs 22	56.20	59.00	0.00	28.00	0.00	0.00	0.00	0.00	0.00	2.11

Peaks intensities for the minerals identified in the <2µm fraction of samples from the section of Malleval.

Sample ID	Depth (m)	Peak Intensity (cps)							
		Smectite 001	Rectorite	Micas 001	R0 I/S	Kaolinite 001	Chlortie 002	K001/M001	K001/SM001	SM001/M001
MAs 23	57.15	123.00	34.00	42.00	0.00	0.00	0.00	0.00	0.00	2.93
MAs 24	58.25	214.00	30.00	53.00	14.00	13.85	6.15	0.26	0.21	4.04
MAs 25	59.40	136.00	41.00	58.00	19.00	0.00	0.00	0.00	0.00	2.34
MAs 26	61.10	19.00	31.00	32.00	12.00	0.00	0.00	0.00	0.00	0.59
MAs 27	64.55	165.00	0.00	23.00	16.00	0.00	0.00	0.00	0.00	7.17
MAs 28	65.85	198.00	0.00	0.00	0.00	32.00	0.00	0.00	0.37	0.00
MAs 29	67.00	129.00	33.00	26.00	0.00	0.00	0.00	0.00	0.00	4.96
MAs 30	68.30	13.00	53.00	50.00	0.00	0.00	0.00	0.00	0.00	0.26
MAs 31	69.40	10.00	44.00	23.00	0.00	0.00	0.00	0.00	0.00	0.43
MAs 32	70.45	6.00	57.00	54.00	0.00	0.00	0.00	0.00	0.00	0.11
MAs 33	71.50	71.00	59.00	42.00	0.00	0.60	2.40	0.01	0.01	1.69
MAs 34	72.40	66.00	0.00	22.00	0.00	4.38	2.63	0.20	0.06	3.00
MAs 35	73.55	123.00	33.00	51.00	33.00	0.00	0.00	0.00	0.00	2.41
MAs 36	74.65	57.00	87.00	53.00	0.00	0.00	0.00	0.00	0.00	1.08
MAs 37	75.80	195.00	0.00	37.00	0.00	0.00	0.00	0.00	0.00	5.27
MAs 38	76.90	201.00	0.00	43.00	14.00	0.00	0.00	0.00	0.00	4.67
MAs 39	78.20	257.00	26.00	75.00	37.00	0.00	0.00	0.00	0.00	3.43
MAs 40	79.40	270.00	11.00	63.00	38.00	0.00	0.00	0.00	0.00	4.29
MAs 41	80.60	271.00	0.00	33.00	36.00	0.00	0.00	0.00	0.00	8.21
MAs 43 b	82.15	12.00	25.00	13.00	0.00	0.00	0.00	0.00	0.00	0.92
MAs 42	82.65	34.00	0.00	0.00	0.00	0.00	0.00	0.00	0.00	0.00
MAs 43	84.35	513.00	21.00	43.00	0.00	0.00	0.00	0.00	0.00	11.93
MAs 48 b	85.55	74.00	51.00	53.00	0.00	0.00	0.00	0.00	0.00	1.40
MAs 49 b	86.85	34.00	29.00	33.00	0.00	0.00	0.00	0.00	0.00	1.03
MAs 50 b	87.90	29.00	49.00	48.00	0.00	0.00	0.00	0.00	0.00	0.60
MAs 44	88.20	53.00	58.00	84.00	0.00	0.00	0.00	0.00	0.00	0.63
MAs 51 b	89.10	46.00	37.00	17.00	0.00	18.00	0.00	1.06	0.46	2.71
MAs 53 b	92.20	44.00	0.00	18.00	0.00	0.00	0.00	0.00	0.00	2.44
MAs 54 b	93.30	77.00	37.00	47.00	16.00	0.00	0.00	0.00	0.00	1.64
MAs 55 b	94.60	59.00	18.00	43.00	0.00	0.00	0.00	0.00	0.00	1.37
MAs 56 b	95.60	93.00	29.00	55.00	0.00	0.00	0.00	0.00	0.00	1.69

Peaks intensities for the minerals identified in the <2µm fraction of samples from the section of Malleval (continued).